TORSIONAL ANALYSIS OF CORE STRUCTURES IN TALL BUILDINGS

SHAWKY YOUSSIF TAWFIK

B.Sc., M.Sc., M.E.S.E.

A thesis presented for the degree of

Doctor of Philosophy

of the

University of Glasgow

1980

ProQuest LLC.
789 East Eisenhower Parkway
P.O. Box 1346
Ann Arbor, MI 48106 – 1346

ACKNOWLEDGEMENTS

The author is indebted to Professor A. Coull, Regius Professor of Civil Engineering, University of Glasgow, for his supervision, guidance, encouragement and invaluable advice during the course of study and in the preparation of the thesis.

The work was carried out in the University of Glasgow, and the author would like to thank Dr. P.D. Arthur for his valuable advice on various aspects of the experimental work, Dr. P. Bhatt, Dr. D.R. Green and Mr. H.M. Nelson for their interest and lengthy fruitful discussions.

The author is grateful to Professor I. Macleod, Paisley College of Technology for allowing the use of his program and for his comments.

Acknowledgement is due to the staffs of the Concrete and Structures Laboratories, in particular the help of Mr. J. Thomson and Mr. R. Thornton.

Thanks are due to Mrs. G. Stewart for her neat and diligent typing of the manuscript.

The author is grateful to his family for their encouragement and financial assistance, without which this work would not have been possible.

Last but not least to my brother Tawfik and all my comrades for their sacrifices, God may reward them.

ABSTRACT

A folded plate analysis of the behaviour of core structures subjected to torsional loading is presented. In this method the core is assumed to consist of vertical plates rigidly connected together along their edges, and by using the engineering theory of bending in conjunction with the continuous connection technique for panels containing openings, the core behaviour has been represented by a third order linear differential equation. The method has been shown to be applicable to any core which is totally open or partially closed with lintel beams. The general governing equation is expressed in terms of one unknown, the angle of rotation and a single non-dimensional stiffness parameter αH, the core relative stiffness. The influence of a stiffening element at the top and flexibility of the foundations have been included. Solutions of the governing equation for three standard load cases, a point torque at the top, a uniformly distributed torque and a triangularly distributed torque are given. A parameter study has been carried out to show the interactive effects of the three fundamental parameters on the primary core actions when subjected to the standard load cases. Design charts have been produced for the rapid evaluation of the core rotations and internal forces. Consideration has been given to core structures with stiffness variations throughout the height, special emphasis being given to the effects of a reduction of thickness of the walls at some level.

The method has been extended to deal with core structures undergoing post-elastic deformations by assuming that plastic hinges develop at the connections between the lintel beams and the adjacent walls when a limiting moment is reached. A study of the development of plasticity throughout the structure has been made and mathematical expressions for the core overall equilibrium condition at the various stages of plasticity are given.

A description is given of a series of associated experimental investigations carried out on perspex and micro-concrete models. The test results are compared with the theoretical values for both stresses and displacements.

CONTENTS

CHAPTER 1

INTRODUCTION

CHAPTER 1

INTRODUCTION

1.1 TALL BUILDINGS

Tall buildings are one of the features of the modern industrial city, dictated by reasons varying from a desire to express power or prestige, to a functional, economical or geographical necessity.

They may be used for commercial purposes to provide an economical means of accommodating the huge amount of office work involved with a big commercial company or the various departments of a light manufacturing one in one building which will result in smoothing the daily work and increase the efficiency with less cost in communication and transportation.

In some countries there is strong opposition to the use of tall buildings for residential purposes, for various social reasons. But the economical fact still stands, that tall residential buildings form one of the most economical means of providing large numbers of people with modern housing in big cities, considering the scarcity of land and the cost of expanding or creating new cities, with all their requirements of other services.

The arrangement and form of any tall building structure depends mainly on its function, height and the type of loading to which it may be subjected during its useful life.

In general three basic vertical structural units,

namely rigidly-jointed frames, shear walls and structural cores, may be used in a suitable combination to provide the required strength and stability of a tall building.

As the height of the building increases, the lateral loads as well as the gravity loads tend to control the design. For medium height buildings up to say about twenty storeys, a concrete rigid frame could be adequate in providing the required lateral stiffness. For tall buildings up to about forty storeys, a system of shear walls may be used to increase the stiffness of the structure whilst simultaneously serving as functional partitions and giving adequate fire resistance between specific areas. For taller buildings, a tube-in-tube or multiple frame-tube structure might be more economic and efficient in resisting lateral loads (1,2).

Due to functional and practical requirements of planning and constructing a multi-storey building, a group of shear walls are frequently jointed together to form a core which is used to accommodate lifts and other services.

These cores are usually considered to consist of thin-walled open section shear walls connected by floor slabs or lintel beams at each floor level to form a perforated box structure.

If the core axis does not coincide with the building axis, the core will be subjected to torsion as well as to shear and bending due to the applied uniform lateral loading. In the case of earthquakes, torsion occurs when the centres of mass and rigidity do not coincide. Torsion

may also occur due to asymmetry of the wind loading.

In the case of severe wind loading or earthquake action, a core structure may deform beyond its elastic limit and in this case failure will generally occur first at the connections between the lintel beams and the core walls, when the bending moment in the lintel beams reaches its ultimate value.

Although winds and earthquakes produce in reality dynamic loads on the structure, it has been common practice to replace them with an approximate equivalent static load and solve the problem as a static problem.

In this study the elastic and elasto-plastic behaviour of core structures subjected to torsional loading have been examined.

1.2 PREVIOUS RESEARCH

Over the past three decades, a considerable amount of research has been carried out to study the behaviour of tall buildings and to provide the design engineer with sufficient data to produce a safe and economic design. In the course of these studies, various methods have been established to analyse tall building structural assemblies.

Initially most of the work was concerned with the case of plane walls undergoing bending, but in the last two decades work has been carried out on core structures as a major component in resisting bending and torsional loading. The published research work may be categorized under four main methods of analysis, namely the Energy method, Vlasov's theory, the engineering theory of bending

and the Matrix formation method.

The Energy method was used by Jenkins and Harrison (3) to analyse core structures by assuming torsional displacements and rotations in the form of polynomials and applying the minimum potential energy theorem to determine the unknown constants in the series for displacements and rotations. The analytical results did not compare favourably with the experimental values from a perspex model.

In Vlasov's theory (4), it is assumed that no cross-sectional distortion may take place and the shear strain is constant through the thickness of each wall. This theory forms the basis for different approaches for the solution of core structures containing openings. Stafford Smith and Taranath (5,6) considered the warping displacements as a seventh degree of freedom of the section, and the effect of bracings was taken into account by adding their warping stiffness to the warping stiffness of the open section. In similar investigations by Heidebrecht and Stafford Smith (7) a braced open section was solved by taking into account the bracing effect by modifying the St. Venant constant of the section, and graphical-analytical solutions for a specific loading were given.

Based on the same theory, Khan and Stafford Smith (8), converted a braced open section to an equivalent closed section by introducing a continuous connection to allow the shear flow to circulate around the profile of the core. The procedure does not converge to the limiting case of an

open section. Rosman (9) studied the torsional behaviour of concrete shafts perforated with openings by combining Vlasov's theory with the continuous medium approach to develop expressions for the internal forces and rotations. A mathematical analogy between a torsionally loaded shaft and a laterally loaded shear wall was concluded.

Using the Engineering theory of bending Michael (10) considered a simple doubly-symmetric core to be composed of two equal separate channels and by applying closing forces to the beams, he derived a second order differential equation relating the bending moment in the walls and the applied torque. His results showed a good correlation with the experimental results obtained by Jenkins and Harrison (3). However the accuracy of the method decreases as the size of the openings decreases.

Similarly Tso and Biswas (11) analysed the same core by formulating the problem in terms of the direct equilibrium of forces, and considering the rotation as the unknown variable in the governing equation. In later work (12), the method was refined by taking the shearing strains and deformations of the channel walls into account.

Based on the same theorem and by considering the core to consist of vertical plates rigidly connected together along their edges and by using the continuous connection method and the folded plate approach, Coull (13) derived a third order equation for structures on fixed or flexible foundations.

Based on matrix formulation, core structures subjected

to torsional loading were investigated by using the transfer matrix method by Liauw (14,15), in which Vlasov's theory was used to evaluate the matrix parameters. A matrix was formed for each storey level and by matching the compatibility conditions between each two successive segments, starting from the base end conditions, a solution was obtained.

Using a similar approach, Goodno and Gere (16), solved the problem by assembling two-dimensional plane stress and plate bending finite elements into a three-dimensional finite element termed a super-element, and every storey of the core was represented by a single super-element. Core structures subjected to torsional loading have also been analysed by using an analogous wide-column frame structure proposed by Macleod and Hosny (17). Good agreement has been claimed when compared with three other examples analysed by the above three methods (3,6,13).

Most of the aforementioned work was limited to the elastic range of the core behaviour. Although the elasto-plastic behaviour of plane reinforced concrete coupled shear walls have been investigated theoretically (18,19) and experimentally (20,21,22), the only investigation to study post-elastic behaviour of core structures subjected to torsional loading was carried out by Irwin and Andrew (23) by testing a micro-concrete model, although an analytical solution to the problem was not considered.

1.3 SCHEME OF THE PRESENT WORK

The main object of the present research is to study the elastic and elasto-plastic behaviour of core structures in tall buildings, when subjected to torsional loading.

Using the folded plate and continuous connection techniques, the derivation and solution of a general governing equation for core structures have been achieved and demonstrated in Chapter 2.

In Chapters 3 and 4, the effects of any foundation flexibility and a top end restraint have been considered. Non-dimensional parameters have been introduced to include their effect on the elastic behaviour of core structures, and design curves have been drawn for a quick evaluation of the angle of rotation and the internal forces. A numerical example has been used to illustrate the relative influences of these parameters.

In Chapter 5, core structures with stiffness variations throughout the height have been considered. A mathematical solution has been achieved for the problem and the same numerical example has been used to illustrate the effect of reducing the thickness of the walls throughout the core height.

In Chapter 6, a theoretical approach to the analysis of core structures undergoing elasto-plastic deformations has been demonstrated, and investigation of the plasticity propagation throughout the core under various end conditions and applied torques was carried out.

The implementation of the above methods of analysis

in a computer program is given in Chapter 7, with illustration of the elasto-plastic behaviour of the numerical example.

Two series of experiments were carried out to substantiate the theoretical investigations. The first series was carried out on perspex models to study the elastic behaviour of stiffened and unstiffened core structures. The second series was carried out on reinforced concrete models to study the elasto-plastic behaviour of unstiffened structures. A description of the experiments, and a discussion of the results, are given in Chapter 8.

In the last chapter, the conclusions drawn from the above investigations and suggestions for future research are given.

CHAPTER 2

CORE STRUCTURES SUBJECTED TO TORSIONAL LOADING

GENERAL GOVERNING EQUATION

CHAPTER 2

CORE STRUCTURES SUBJECTED TO TORSIONAL LOADING

GENERAL GOVERNING EQUATION

2.1 NOTATION

The following symbols are used in this Chapter:-

A_n = cross-sectional area of wall 'n'

B = core breadth

D = core length

E = modulus of elasticity

G = shear modulus

H = overall core height

h = storey height

I_n = moment of inertia of wall 'n' about its local axis

I_c = moment of inertia of connecting beam

I_w = core warping moment of inertia

GJ = St. Venant torsional rigidity

M_n = in-plane bending moment in wall 'n'

N_n = normal force in wall 'n'

q_n = vertical shear flow along line n-n

S_n = horizontal shear force in wall 'n'

T = applied torque of any cross-section

T_w = core warping resistance

T_s = St. Venant torsional resistance

t = applied distributed torque

th_n = thickness of wall 'n'

x,y,z = co-ordinate system

u_n = displacement in x-direction of point 'n'

v_n = displacement in y-direction of point 'n'

w_n = displacement in z-direction of point 'n'

α = structural parameter

γ = non-dimensional structural parameter (= αH)

ξ = non-dimensional co-ordinate (= $\frac{x}{H}$)

β = connecting medium stiffness constant

2.2 INTRODUCTION

Core structures for tall buildings consist of assemblies of slender vertical wall elements connected together along their vertical edges, either continuously or through a series of connecting lintel beams at each floor level, to create an open box or cellular structure. These walls may be arranged to create any core structural layout, which serves to enclose lifts and other services, and to resist floor and wind loads.

Due to an eccentric disposition of wind loads or to an asymmetry of structural layout, the core is frequently subjected to torsional loading, which produces warping stresses as well as the usual bending, shear and normal stresses in the core walls. The magnitude of the warping stresses depends mainly on the shape and dimensions of the core, and on the loading and restraints to which the core is subjected.

By using the Engineer's theory of bending in conjunction with the continuous medium technique, it becomes possible to describe the torsional behaviour of the core structure by a third-order differential equation which may be solved for different types of loading and boundary conditions. In this chapter, a method of analysis for core structures of unsymmetrical, singly- and doubly-symmetrical cross-section has been presented and has been proved to be represented generally by a third order governing differential equation. Solutions for the governing equation are presented for three standard load cases.

2.3 ASSUMPTIONS

The assembly of various structural elements in a core produces a highly statically indeterminate structure. In order to simplify the analysis of the structure so that a closed-form solution may be obtained for the problem, the following assumptions are made:

1. The structural material is homogeneous, isotropic and linearly elastic.
2. The floor heights and the sizes of the core openings and the coupling beams are uniform within a specific zone of the structure, but they may vary from one zone to another.
3. The floor slabs behave as rigid diaphragms having infinite stiffness in their own plane but negligible stiffness out of plane. The diaphragm action constrains the core cross-sections to undergo only rigid body displacements in the horizontal plane.
4. The axial and shear deformations of the connecting beams and the shear deformations and out-of-plane bending of the walls can be neglected.
5. The walls adjacent to the connecting beams deflect equally; consequently, a point of contraflexure exists at the mid-span position of each beam.
6. The discrete set of connecting beams can be replaced by an equivalent uniform continuous medium with uniform stiffness distributed over the storey height. The discrete set of shear forces at the points of contra-flexure may then be replaced by a shear flow or

equivalent system of continuously distributed laminar shear forces per unit height of the connecting medium.

7. The reference co-ordinate axes are assumed to follow a left hand system with the origin at the centre of rotation, which is taken as the shear centre of the core at the base.
8. The external applied load may be expressed as a point load, or as a continuous function of the height, at any level.

2.4 DERIVATION OF THE GOVERNING EQUATION

In order to derive the governing differential equation for a core structure undergoing elastic deformations when subjected to torsional loading, a segment of height dx of each panel at any level is considered, with the internal forces applied to it as shown in Figs. 2.1 and 2.3.

The internal forces on a solid wall segment consist of the in-plane bending moment M, the axial force N, the horizontal shear force S, and the vertical shear flow q at the corners. In the case of a wall element which contains a number of continuous media, a vertical shear flow is assumed to be distributed throughout the height at the lines of contraflexure which divide the complete wall into a number of panels.

The position of the shear centre is determined for the open section disregarding the connecting beams, because of the assumption that the connecting beams are shallow lintel beams or floor slabs and the segments in which the

horizontal shear will flow around the perimeter will be relatively small. The method of locating the shear centre for common structural shapes is described in many text-books on Strength of Materials as well as in some published computer programs (24,25).

By considering the displacements which arise as a result of the core rotation about the shear centre, the equilibrium of the internal forces on each segment, and the compatibility conditions at the vertical lines of interaction of the various panels, the overall governing equation may be expressed in terms of a single function Θ, the angle of rotation about the shear centre. This general procedure can be followed in the analysis of various forms of core structures, producing in each case the same form of governing equation as demonstrated in the cases considered in the following sections, as well as some other cases discussed in Appendix A.

2.4.1 UNSYMMETRICAL CORE STRUCTURES

In the case of an unsymmetrical core structure as shown in Fig. 2.1, the origin O is assumed to coincide with the shear centre. The rigid body rotation about the vertical axis OX will consist of three basic displacements, displacement V in the y direction, W in the z direction, and angular rotation Θ, as shown in Fig. 2.2.

DISPLACEMENTS

In the displaced core shown in Fig. 2.1.II, the point 'CG' moves to the position 'CG_1' on an arc of a circle with

radius R where,

$$R = \sqrt{F^2 + (e + L)^2}$$

The horizontal displacements of point 'CG' in the z and y directions are,

$$W_G = (e + L)\theta - F\frac{\theta^2}{2} \qquad 2.4.1$$

$$V_G = -F\theta - (e + L)\frac{\theta^2}{2} \qquad 2.4.2$$

Since in the actual structure, the angle of rotation θ is very small, the terms of second order in θ can be neglected without significantly affecting the calculations.

The final displacements of the core cross-section can be achieved by adding the horizontal displacements W_G and V_G to the displacements due to the rotation θ. The final displacements of the significant points on the perimeter of the core as shown in Fig. 2.1.II become

$$W_1 = W_2 = W_5 = -(e + B)\theta$$

$$V_2 = V_3 = (n - F)\theta$$

$$W_3 = W_4 = -e\theta \qquad 2.4.3$$

$$V_4 = V_5 = -(m + F)\theta$$

where the displacements V and W are in the directions of the y and z axes respectively.

EQUILIBRIUM CONDITIONS

Considering the equilibrium of the internal forces for a segment of height dx from each panel as shown in

Fig. 2.3, the following relationships may be derived.

For panel 1

$$S_1 = \frac{dM_1}{dx} + q_2 \frac{d}{2} - q_1 \frac{(d + a)}{2} \qquad 2.4.4$$

$$q_1 + q_2 + \frac{dN_1}{dx} = 0 \qquad 2.4.5$$

For panel 2

$$S_2 = \frac{dM_2}{dx} - q_2 \frac{B}{2} - q_3 \frac{B}{2} \qquad 2.4.6$$

$$q_3 - q_2 + \frac{dN_2}{dx} = 0 \qquad 2.4.7$$

For panel 3

$$S_3 = \frac{dM_3}{dx} - q_3 \frac{D}{2} - q_4 \frac{D}{2} \qquad 2.4.8$$

$$q_4 - q_3 + \frac{dN_3}{dx} = 0 \qquad 2.4.9$$

For panel 4

$$S_4 = \frac{dM_4}{dx} + q_4 \frac{B}{4} + q_5 \frac{B}{2} \qquad 2.4.10$$

$$q_5 - q_4 + \frac{dN_4}{dx} = 0 \qquad 2.4.11$$

For panel 5

$$S_5 = \frac{dM_5}{dx} + q_5 \frac{C}{2} - q_1 \frac{(a + c)}{2} \qquad 2.4.12$$

$$\frac{dN_5}{dx} - q_1 - q_5 = 0 \qquad 2.4.13$$

By assuming that the walls behave as vertical slender cantilevers, the elastic moment-curvature relationships

for the given set of axes and positive directions of the displacements may be written for each panel respectively as follows:

$$M_1 = EI_1 \frac{d^2W_1}{dx^2} \qquad 2.4.14$$

$$M_2 = EI_2 \frac{d^2V_2}{dx^2} \qquad 2.4.15$$

$$M_3 = EI_3 \frac{d^2W_3}{dx^2} \qquad 2.4.16$$

$$M_4 = EI_4 \frac{d^2V_4}{dx} \qquad 2.4.17$$

$$M_5 = EI_5 \frac{d^2W_5}{dx^2} \qquad 2.4.18$$

COMPATIBILITY CONDITIONS

From the conditions of vertical strain compatibility along the lines of interaction between each two adjacent panels, the following relationships may be derived. Along line 1-1 at the mid-span positions of the connecting mediums

$$\int_o^x \frac{M_1}{EI_1} \frac{(d + a)}{2} dx + \int_o^x \frac{M_5}{EI_5} \frac{(a + c)}{2} dx -$$

$$- \int_o^x \frac{N_1}{EA_1} dx - \int_o^x \frac{N_5}{EA_5} dx - \frac{q_1}{\beta E} = 0 \qquad 2.4.19$$

where the stiffness constant of the connecting beams $\beta = \frac{12I_c}{a^3h}$ and I_c = the moment of inertia of a connecting beam.

Along line 2-2 between panel 1 and 2

$$\int_0^x \frac{M_1}{EI_1}\frac{d}{2}\,dx - \int_0^x \frac{M_2}{EI_2}\frac{B}{2}\,dx + \int_0^x \frac{N_1}{EA_1}\,dx - \int_0^x \frac{N_2}{EA_2} = 0 \qquad 2.4.20$$

Along line 3-3 between panel 2 and 3

$$\int_0^x \frac{M_2}{EI_2}\frac{B}{2}\,dx + \int_0^x \frac{M_3}{EI_3}\frac{D}{2}\,dx - \int_0^x \frac{N_2}{EA_2}\,dx - \int_0^x \frac{N_3}{EA_3}\,dx = 0 \qquad 2.4.21$$

Along line 4-4 between panel 3 and 4

$$\int_0^x \frac{M_3}{EI_1}\frac{D}{2}\,dx - \int_0^x \frac{M_4}{EI_4}\frac{B}{2}\,dx + \int_0^x \frac{N_3}{EA_3}\,dx - \int_0^x \frac{N_4}{EA_4}\,dx = 0 \qquad 2.4.22$$

Along line 5-5 between panel 4 and 5

$$\int_0^x \frac{M_4}{EI_4}\frac{B}{2}\,dx + \int_0^x \frac{M_5}{EI_5}\frac{C}{2}\,dx + \int_0^x \frac{N_5}{EA_5}\,dx - \int_0^x \frac{N_4}{EA_4}\,dx = 0 \qquad 2.4.23$$

INTERNAL FORCES

Substituting by the second derivatives of the displacements from equation 2.4.3 into equations 2.4(14, 15, 16, 17 and 18), the moment-curvature relationships of the core panels may be written in terms of θ as follows:

$$M_1 = -EI_1(e + B)\frac{d^2\theta}{dx^2}$$

$$M_2 = EI_2(n - F)\frac{d^2\theta}{dx^2}$$

$$M_3 = -EI_3\, e\,\frac{d^2\theta}{dx^2} \qquad 2.4.24$$

$$M_4 = - EI_4(m + F) \frac{d^2\theta}{dx^2}$$

$$M_5 = - EI_5(e + B) \frac{d^2\theta}{dx^2}$$

Substituting for the bending actions from the above equations into the compatibility conditions and solving with the aid of equations 2.4(5, 7, 9, 11 and 13), the axial forces in the core panels become,

$$N_1 = EA_1P \frac{d^2\theta}{dx^2}$$

$$N_2 = EA_2(C_2 + P) \frac{d^2\theta}{dx^2}$$

$$N_3 = EA_3(C_3 - C_2 - P) \frac{d^2\theta}{dx^2} \qquad 2.4.25$$

$$N_4 = EA_4(C_4 + C_3 - C_2 - P) \frac{d^2\theta}{dx^2}$$

$$N_5 = -EA_5(C_5 + C_2 - C_4 - C_3 - P) \frac{d^2\theta}{dx^2}$$

The vertical shear distribution will be given by,

$$q_1 = - E\beta P_1 \frac{d\theta}{dx}$$

$$q_2 = E\beta P_1 \frac{d\theta}{dx} - EP_2 \frac{d^3\theta}{dx^3}$$

$$q_3 = E\beta P_1 \frac{d\theta}{dx} - EP_3 \frac{d^3\theta}{dx^3} \qquad 2.4.26$$

$$q_4 = E\beta P_1 \frac{d\theta}{dx} - EP_4 \frac{d^3\theta}{dx^3}$$

$$q_5 = E\beta P_1 \frac{d\theta}{dx} - EP_5 \frac{d^3\theta}{dx^3}$$

where

$$C_1 = -(e + B)\ \frac{(d + 2a + C)}{2}$$

$$C_2 = -\ [(e + B)\ \frac{d}{2} + (n-F)\ \frac{B}{2}]$$

$$C_3 = (n-F)\ \frac{B}{2} - e\frac{D}{2}$$

$$C_4 = (m+F)\ \frac{B}{2} - e\frac{D}{2}$$

$$C_5 = -[(m+F)\ \frac{B}{2} + (e + B)\ \frac{C}{2}]$$

and

$$P = [A_2C_2 + A_3(C_3-C_2) + A_4(C_4 + C_3 - C_2) - A_5(C_5 + C_2 - C_4-C_3)]/$$

$$[A_1 + A_2 + A_3 + A_4 + A_5]$$

$$P_1 = (C_3 + C_4 - C_2 - C_1 - C_5)$$

$$P_2 = A_1P$$

$$P_3 = P_2 + A_2(C_2 + P)$$

$$P_4 = P_3 + A_3(C_3 - C_2 - P)$$

$$P_5 = P_4 + A_4(C_4 + C_3 - C_2 - P)$$

Substituting for the first derivatives of equation 2.4.25 and equation 2.4.26 in equations 2.4.(4, 6, 8, 10 and 12), will yield the horizontal shear forces as follows

$$S_1 = -E[I_1(e + B) + P_2\ \frac{d}{2}]\ \frac{d^3\theta}{dx^3} + E\beta P_1\ \frac{(2d+a)}{2}\ \frac{d\theta}{dx}$$

$$S_2 = E[I_2(n-F) + \frac{B}{2}(P_2 + P_3)]\ \frac{d^3\theta}{dx^3} - E\beta P_1 B\ \frac{d\theta}{dx}$$

$$S_3 = -E\left[I_3 e - \frac{D}{2}(P_3 + P_4)\right] \frac{d^3\theta}{dx^3} - E\beta P_1 D \frac{d\theta}{dx} \qquad 2.4.27$$

$$S_4 = -E\left[I_4(m+F) - \frac{B}{2}(P_4 + P_5)\right] \frac{d^3\theta}{dx^3} + E\beta P_1 B \frac{d\theta}{dx}$$

$$S_5 = -E\left[I_5(e + B) + \frac{C}{2} P_5\right] \frac{d^3\theta}{dx^3} + E\beta P_1 \frac{(2c+a)}{2} \frac{d\theta}{dx}$$

GOVERNING EQUATION

The internal torsional resistance of the core which consists of the warping resistance T_W and the St. Venant torsional resistance T_S, must equal the external applied torque T at the same level. The overall equilibrium of the core cross-section at any level, as shown in Fig. 2.4, is

$$T = T_W + T_S$$

where the core warping resistance T_W is given by

$$T_W = S_1(e + B) - S_2(n-F) + S_3 e + S_4(m+F) + S_5(e + B)$$

and assuming that the walls are slender in form, (26), the St. Venant torsional resistance is given by

$$T_S = GJ \frac{d\theta}{dx}$$

where

$$J = \sum \frac{L_n \, th_n^3}{3}$$

and

L_n = width of wall 'n'

th_n = thickness of wall 'n'

The overall equilibrium condition may then be written as,

$$T = S_1(e + B) - S_2(n-F) + S_3 e + S_4(m+F) + S_5(e +F) + \\ + GJ \frac{d\theta}{dx} \qquad 2.4.28$$

Substituting for the horizontal shear forces from equation 2.4.27 into the last equation yields

$$T = - EI_W \frac{d^3\theta}{dx^3} + GJ_o \frac{d\theta}{dx} \qquad 2.4.29$$

where I_W is the core warping inertia given by

$$I_W = I_1(e+B)^2 + I_2(n-F)^2 + I_3e^2 + I_4(m+F)^2 + I_5(e+B)^2$$

$$+ P_2(\frac{d}{2}(B+e) + \frac{B}{2}(n-F)) + P_3(\frac{B}{2}(n-F) - \frac{eD}{2})$$

$$- P_4(\frac{eD}{2} + \frac{B}{2}(m+F)) + P_5(\frac{C}{2}(e+B) - \frac{B}{2}(m+F))$$

and

$$J_o = J + 2 \frac{E}{G} \beta P_1 BD$$

Equation 2.4.29 is the governing differential equation of a core structure subjected to torsional loading and may be expressed in the form

$$\frac{d^3\theta}{dx^3} - \alpha^2 \frac{d\theta}{dx} = - \frac{T}{EI_W}$$

where $\alpha = \sqrt{\frac{GJ}{EI_W}}$

The parameter α is a characteristic torsional relative stiffness parameter which depends on the material properties, structural geometry of the core and the stiffness of the connecting beams.

2.4.2 SINGLY-SYMMETRIC CORE STRUCTURES

If the core contains only one axis of symmetry as shown in Fig. 2.5, the shear centre will lie on the axis of symmetry (y axis). The origin O is assumed to coincide

with the shear centre at distance e from the centre line of the back wall, and in this case

$F = 0$

$n = m = \frac{D}{2}$

$c = d$

$L = B/2$

DISPLACEMENTS

In this case only two basic displacements need be considered, the displacement in the z-direction, W_G, and the angular rotation θ. Substituting for the above dimensions into equations 2.4(1 and 3), the displacements of the various points become

$$W_G = (e + \frac{B}{2})\theta$$

$$W_1 = W_2 = W_5 = -(e + B)\theta$$

$$V_2 = V_3 = \frac{B}{2}\theta \qquad 2.4.30$$

$$W_3 = W_4 = -e\theta$$

$$V_4 = V_5 = -\frac{B}{2}\theta$$

EQUILIBRIUM CONDITIONS

From symmetry, panel 1 and panel 2 are similar to panel 3 and panel 4 respectively and the axial force in panel 3 equals zero. Thus only three panels are considered. The equilibrium conditions for panels 1, 2 and 3 are identical to equations 2.4(4, 5, 6, 7, 8 and 9) when substituting $N_3 = 0$. The moment-curvature relationships for the above panels are given in equations

2.4(14, 15, and 16).

COMPATIBILITY CONDITIONS

In this case the vertical strain compatibility condition along the line of contraflexure at the mid-span position of the connecting medium will be

$$\int_0^x \frac{M_1}{EI_1}(d+a)dx - 2 \int_0^x \frac{N_1}{EA_1} dx - \frac{q_1}{\beta E} = 0 \qquad 2.4.31$$

and the compatibility conditions along lines 2-2 and 3-3 are the same as given in equations 2.4.20 and 2.4.21.

INTERNAL FORCES

Solving the above equations yields

$$N_1 = EA_1 [\frac{d}{2}(B+e) + \frac{D}{2}(B-e)] \frac{d^2\theta}{dx^2}$$

$$N_2 = EA_2 \frac{D}{2}(\frac{B}{2} - e) \frac{d^2\theta}{dx^2}$$

$$N_3 = 0 \qquad 2.4.32$$

$$q_1 = - 2\beta EBD \frac{d\theta}{dx}$$

$$q_2 = -EA_1 [\frac{d}{2}(B+e) + \frac{D}{2}(B-e)] \frac{d^3\theta}{dx^3} + 2\beta EBD \frac{d\theta}{dx}$$

$$q_3 = -E[A_1(\frac{d}{2}(B+e) + \frac{D}{2}(B-e)) + A_2 \frac{D}{2}(\frac{B}{2} - e)] \frac{d^3\theta}{dx^3} + 2\beta EBD \frac{d\theta}{dx}$$

$$S_1 = -E(I_1(B+e) + A_1 \frac{d}{2}(\frac{d}{2}(B+e) + \frac{D}{2}(B-e)] \frac{d^3\theta}{dx^3} + \beta EBD^2 \frac{d\theta}{dx}$$

$$S_2 = E[I_2 \frac{D}{2} + A_1 B(\frac{d}{2}(B+e) + \frac{D}{2}(B-e)) + A_2 \frac{BD}{4}(\frac{B}{2} - e)]$$

$$\frac{d^3\theta}{dx^3} - 2\beta EB^2 D \frac{d\theta}{dx}$$

$$S_3 = -E[I_3 e - DA_1(\frac{d}{2}(B+e) + \frac{D}{2}(B-e)) - A_2 \frac{D^2}{2} (\frac{B}{2} - e)]$$

$$\frac{d^3\theta}{dx^3} - 2\beta EBD^2 \frac{d\theta}{dx}$$

GOVERNING EQUATION

The overall equilibrium condition for the core at any level is

$$T = 2S_1(B + e) + S_3 e - S_2 D + GJ \frac{d\theta}{dx}$$

which may be written in the general form,

$$-EI_W \frac{d^3\theta}{dx^3} + GJ_o \frac{d\theta}{dx} = T$$

where

$$I_W = 2I_1(B + e)^2 + I_2 \frac{D^2}{2} + I_3 e^2 + \frac{A_1}{2}(d(B + e) + D(B - e))^2 + A_2 \frac{D^2}{2} (\frac{B}{2} - e)^2$$

and

$$J_o = 4 \beta \frac{E}{G} B^2 D^2 + J$$

The expression for I_W is identical to that for evaluating the sectorial moment of inertia according to Vlasov's theory (4).

2.4.3 DOUBLY-SYMMETRICAL CORE STRUCTURE

In the case of core structures with doubly symmetrical cross-sections, such as that shown in Fig.2.6, the shear centre coincides with the centroid of the cross-section.

DISPLACEMENTS

The rigid body movement of the cross-section will consist of the angular rotation θ about the vertical axis O-X. The horizontal displacements of the various points at the perimeter will then be,

$$W_1 = W_2 = W_5 = -\frac{B}{2}\theta$$

$$V_2 = V_3 = \frac{D}{2}\theta$$

$$W_3 = W_4 = \frac{B}{2}\theta \qquad 2.4.33$$

$$V_4 = V_5 = -\frac{D}{2}\theta$$

EQUILIBRIUM CONDITIONS

In this case only two panels need be considered namely panels 1 and 2. The equilibrium conditions and moment-curvature relationships for the above panels are given respectively by equations 2.4(4, 5, 6, 7, 14 and 15).

COMPATIBILITY CONDITIONS

The two compatibility conditions along the line of contraflexure 1-1 and the corner line 2-2 are the same as those given in equations 2.4.31 and 2.4.20.

INTERNAL FORCES

In solving the above equations, the internal forces may be obtained as

$$N_1 = EA_1 \frac{B}{4}(d+D)\frac{d^2\theta}{dx^2}$$

$$N_2 = 0$$

$$q_1 = -\beta EBD \frac{d\theta}{dx}$$

$$q_2 = -EA_1 \frac{B}{4} (d+D) \frac{d^3\theta}{dx^3} + \beta EBD \frac{d\theta}{dx}$$

$$S_1 = -E \frac{B}{2}[I_1 + A_1 \frac{d}{4} (d+D)] \frac{d^3\theta}{dx^3} + \beta E \frac{BD^2}{2} \frac{d\theta}{dx} \qquad 2.4.34$$

$$S_2 = E[I_2 \frac{D}{2} + A_1 \frac{B^2}{4} (d+D)] \frac{d^3\theta}{dx^3} - \beta EB^2D \frac{d\theta}{dx}$$

GOVERNING EQUATION

The overall equilibrium condition for the core cross-section at any level is,

$$T = 2.B.S_1 - S_2D + GJ \frac{d\theta}{dx}$$

Substituting for S_1 and S_2, from equation 2.4.34, into the above equilibrium condition yields

$$T = -EI_W \frac{d^3\theta}{dx^3} + GJ_o \frac{d\theta}{dx}$$

where in this case

$$I_W = I_1B^2 + I_2 \frac{D^2}{2} + A_1 \frac{B^2}{4} (d + D)^2$$

$$J_o = 2 \frac{E}{G} \beta B^2 D^2 + J$$

2.5 SOLUTION OF THE GOVERNING EQUATION

The general governing equation for any cross-section;

$$-EI_W \frac{d^3\theta}{dx^3} + GJ_o \frac{d\theta}{dx} = t_{(x)} \qquad 2.5.1$$

in which $t_{(x)}$ is any continuous function of x, may be

rewritten in non-dimensional form as,

$$\frac{d^3\theta}{d\xi^3} - \alpha^2 H^2 \frac{d\theta}{d\xi} = \frac{-H^3}{EI_W} t_{(\xi)} \qquad 2.5.2$$

where

$$\xi = \frac{x}{H}$$

and

$$\alpha^2 = \frac{GJ_o}{EI_W}$$

The complementary function solution for equation 2.5.2, θ_c, may be obtained from the homogeneous equation and expressed in terms of hyperbolic functions as

$$\theta_c = K_1 + K_2 \cosh \gamma\xi + K_3 \sinh \gamma\xi \qquad 2.5.3$$

where K_1, K_2 and K_3 are constants dependent on the boundary conditions. The particular integral solution θ_p is dependent on the loading function $t_{(x)}$ and may be obtained from the operational equation,

$$D(D^2 - \gamma^2)\theta_p = - \frac{H^3}{EI_W} t_{(\xi)}$$

where D is the operator $\frac{d}{d\xi}$

and $\gamma = \alpha H$

By writing

$$\theta_p = \frac{1}{D\gamma^2} (1 - \frac{D^2}{\gamma^2})^{-1} * \frac{H^3}{EI_W} t_{(\xi)}$$

And expanding the term $(1 - \frac{D^2}{\gamma^2})^{-1}$ as an infinite series the particular solution is given by

$$\theta_p = \frac{H}{GJ_o} (D^{-1} + \frac{D}{\gamma^2} + \frac{D^3}{\gamma^4} + ...) t_{(\xi)} \qquad 2.5.4$$

The complete solution for the governing equation may be obtained as the sum of the complementary function and the particular integral solutions, as,

$$\theta = \theta_c + \theta_p$$

$$= K_1 + K_2 \cosh \gamma\xi + K_3 \sinh \gamma\xi + \frac{H}{GJ_o} (D^{-1} + \frac{D}{\gamma^2} + \frac{D^3}{\gamma^4} + \ldots)$$

$$t_{(\xi)} \qquad 2.5.5$$

2.6 LOAD CASES

The preceding governing equation has been expressed in terms of a general twisting moment distribution which may take the form of any continuous function $t_{(x)}$ over a specific zone of the core height.

In this thesis three standard load cases are considered, a point torque t at the top, a uniformly distributed torque of intensity t per unit height and a triangularly distributed torque varying linearly from zero at the base to a maximum at the top. Uniformly distributed load is usually used to simulate wind actions (27) and point load at the top with triangularly distributed load are used to simulate earthquake actions (28). Due to asymmetry of the wind loading or unsymmetrical arrangement of the structural elements, the above actions will produce torsional loading of similar forms. The applied torque distribution and the resulting twisting moment diagram are shown in Fig. 2.7 for each case of loading.

2.6.1 CONCENTRATED TORQUE AT THE TOP

In the case of a concentrated torque at the top, the twisting moment diagram is shown in Fig. 2.7. The applied torque T on the core at any height is

$$T = t_{(x)} = t$$

In this case the particular solution of equation 2.5.4 becomes

$$\theta_p = \frac{tH\xi}{GJ_o}$$

And the complete solution may be written as

$$\theta = K_1 + K_2 \cosh \gamma\xi + K_3 \sinh \gamma\xi + \frac{tH\xi}{GJ_o} \qquad 2.6.1$$

Assuming that the core is rigidly fixed at the base and free at the top, which is a realistic assumption for most practical cases, the integration constants may be obtained from the following boundary conditions.

At the base $x = 0$ or $\xi = 0$

$$\theta = 0 \text{ and } \frac{d\theta}{dx} = \theta' = 0$$

At the top $x = H$ or $\xi = 1$, the bending moment in each wall is zero and hence

$$\frac{d^2\theta}{d\xi^2} = 0'' = 0$$

the solution constants are then given by

$$K_1 = \frac{-tH}{\gamma GJ_o} \tanh \gamma$$

$$K_2 = \frac{tH}{\gamma GJ_o} \tanh \gamma$$

$$K_3 = \frac{-tH}{\gamma G J_o}$$

The general solution for a core structure fixed at the base and free at the top, subjected to a concentrated torque t at the top, may thus be written as

$$\theta = \frac{tH}{\gamma G J_o} [(\cosh \gamma\xi - 1) \tanh \gamma - \sinh \gamma\xi + \gamma\xi] \qquad 2.6.2$$

2.6.2 UNIFORMLY DISTRIBUTED TORQUE

The twisting moment diagram for a uniformly distributed torque of intensity t is as shown in Fig. 2.7, which can be expressed as a continuous function $t_{(x)}$ by

$$T = t_{(x)} = t(H-x)$$

In non-dimensional form, this becomes,

$$T = t_{(\xi)} = tH(1 - \xi)$$

The particular solution in this case is given by

$$\theta_p = \frac{tH^2}{GJ_o} (\xi - \frac{\xi^2}{2} - \frac{1}{\gamma^2})$$

and the complete solution will become,

$$\theta = K_1 + K_2 \cosh \gamma\xi + K_3 \sinh \gamma\xi + \frac{tH^2}{GJ_o}(\xi - \frac{\xi^2}{2} - \frac{1}{\gamma^2}) \qquad 2.6.3$$

Assuming the same end conditions, that the core is fixed at the base and free at the top, the three integration constants K_1, K_2 and K_3 are obtained as

$$K_1 = \frac{tH^2}{\gamma^2 G J_o} (1 - \frac{(1 + \gamma \sinh \gamma)}{\cosh \gamma})$$

$$K_2 = \frac{tH^2}{\gamma^2 G J_o} \frac{(1 + \gamma \sinh \gamma)}{\cosh \gamma}$$

$$K_3 = \frac{-tH^2}{\gamma^2 GJ_o}\gamma$$

The general solution for a core structure fixed at the base free at the top and subjected to uniformly distributed torque is thus given by

$$\theta = \frac{tH^2}{\gamma^2 GJ_o}[(\cosh \gamma\xi - 1)\ \frac{(1+\gamma \sinh \gamma)}{\cosh \gamma} - \gamma \sinh \gamma\xi + \gamma^2\ (\xi - \frac{\xi^2}{2})] \qquad 2.6.4$$

2.6.3 TRIANGULARLY DISTRIBUTED TORQUE

In the case of a triangularly distributed torque of intensity t, the twisting moment diagram is shown in Fig. 2.7, which may be expressed as a continuous function of the height x as

$$T = t_{(x)} = \frac{t}{2}(H^2 - x^2)$$

which may be recast in non-dimensional form as

$$T = t_{(\xi)} = \frac{tH^2}{2}\ (1 - \xi^2)$$

Using equation 2.5.4, the particular solution becomes

$$\theta_p = \frac{tH^3}{2GJ_o}\ (\xi - \frac{\xi^3}{3} - 2\ \frac{\xi}{\gamma^2})$$

and the complete solution becomes,

$$\theta = K_1 + K_2 \cosh \gamma\xi + K_3 \sinh\gamma\xi + \frac{tH^3}{2GJ_o}(\xi + \frac{\xi^3}{3} - \frac{2\xi}{\gamma^2}) \qquad 2.6.5$$

Assuming again that the core is fixed at the base and free at the top, the integration constants K_1, K_2 and K_3 are

found to be

$$K_1 = -K_2 = \frac{-tH^3}{2\gamma GJ_o}\left(\frac{2}{\gamma \cosh \gamma} + \left(1 - \frac{2}{\gamma}\right) \sinh \gamma\right)$$

$$K_3 = -\frac{th^3}{2\gamma GJ_o}\left(1 - \frac{2}{\gamma^2}\right)$$

Hence the general solution for a core structure fixed at the base, free at the top and subjected to a triangularly distributed torque may be written as

$$\theta = \frac{tH^3}{2\gamma GJ_o}\left[(\cosh \gamma\xi - 1)\left(\frac{2}{\gamma \cosh \gamma} + \left(1 - \frac{2}{\gamma^2}\right)\sinh \gamma\right) - \left(1 - \frac{2}{\gamma^2}\right) \sinh \gamma\xi + \gamma\left(\xi - \frac{\xi^3}{3} - \frac{2\xi}{\gamma^2}\right)\right] \qquad 2.6.6$$

Having obtained the rotation θ, the internal forces follow from the equations derived earlier.

2.7 VALIDITY AND LIMITATIONS OF THE METHOD

Since most core structures in practice can be approximated as a combination of one or more of the configurations considered in Section 2.4 and Appendix A, the above method of analysis can be implemented to analyse any core structure which is open or partially closed by lintel beams and providing no segment is completely closed. It is shown that one general form of equation applies to a wide variety of core cross-sections of multi-cells and multi-bays constructions. A closed form solution may generally be developed for any type of loading in the form of a continuous function as demonstrated in section 2.6. Consequently, the rotation and the corresponding internal forces may be evaluated in the given closed form.

In the above method the core cross section has been considered as an open section disregarding the connecting beams in calculating the St. Venant torsional resistance. But in reality the core is divided into a series of closed zones where connecting beams exist and open zones where wall openings are created for access. Consequently part of the shear flow will circulate around the perimeter of the core and the rest of it will circulate within the wall thickness as shown in Fig. 2.8.II. Therefore the actual St. Venant torsional resistance will be greater than the calculated value. However, because St. Venant torsional resistance is very small compared with the core warping resistance, its effect would not be important.

In the case of unsymmetrical or singly-symmetrical cores, the position of the shear centre of the core cross-section has also been determined assuming an open section. However due to the existence of the connecting beams the position of the shear centre theoretically changes from one zone to another as shown in Fig. 2.8.I. Any overall shear centre will be positioned at a point between the S.C. and C.G. positions, and e will have a value less than that calculated by assuming a complete open section.

In the special case, which is unlikely to arise in practice, where the core is totally open on one side and connecting beams exist on the opposite side, the basic assumption requires that the shear centre coincides with the centroid of the cross-section. By considering the equilibrium of a segment of each panel and the compatibility

conditions for the core shown in Fig. 2.8.III, the vertical shear in the connecting beams will be found to be zero, which would not be true in practice.

The actual core resistance will then be greater than the theoretical one. The discrepancy between the actual and calculated results will depend on the depth of the connecting beams, and will increase with an increase in the depth. However, since the connecting beams in most core structures consist of relatively shallow lintel beams generally less than $\frac{1}{4}$ the storey height acting in conjunction with floor slabs, the discrepancy between the actual and calculated results should be small and should not affect greatly the design calculations. Any design based on the results obtained by the suggested method should thus be conservative.

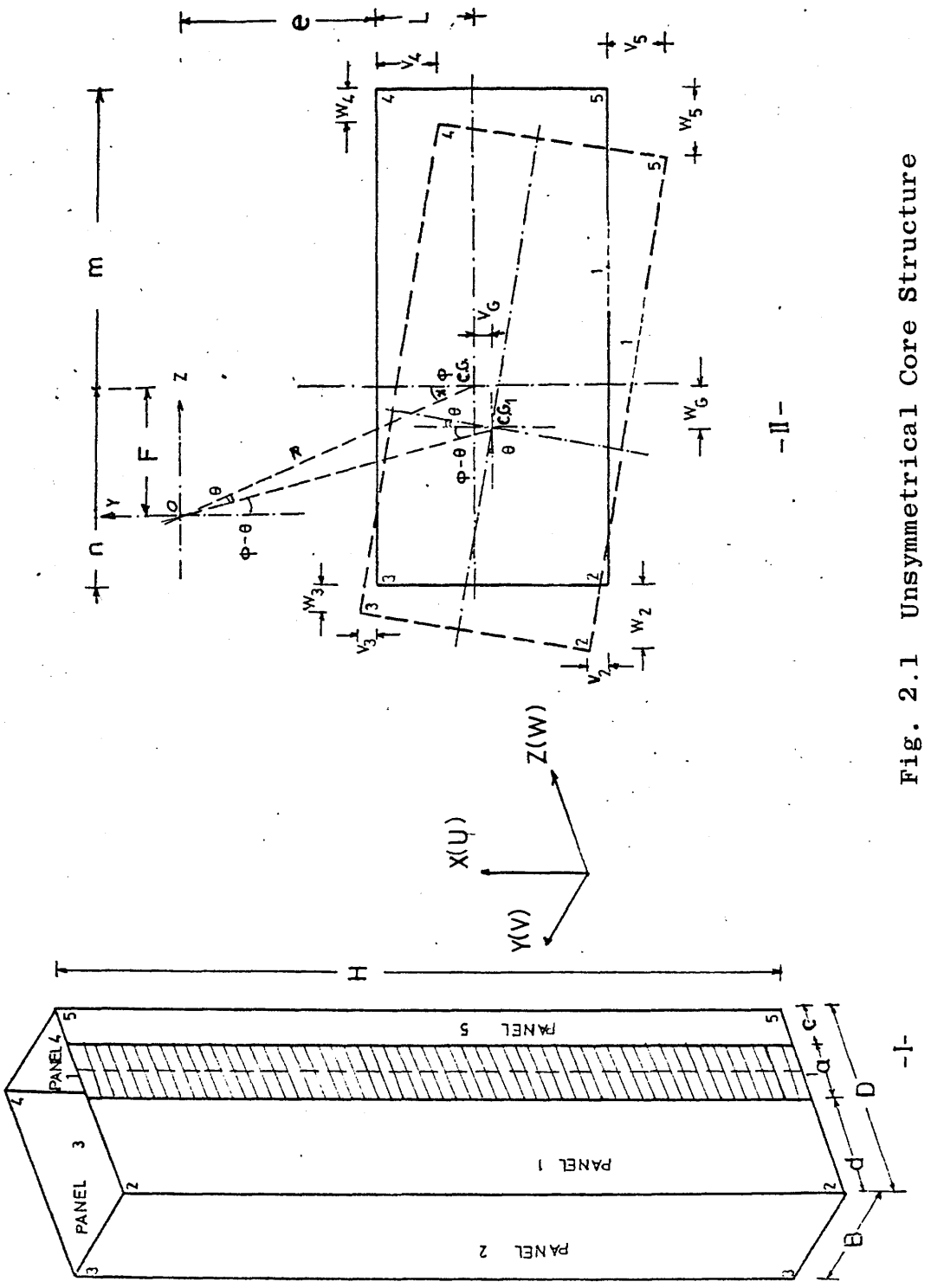

Fig. 2.1 Unsymmetrical Core Structure

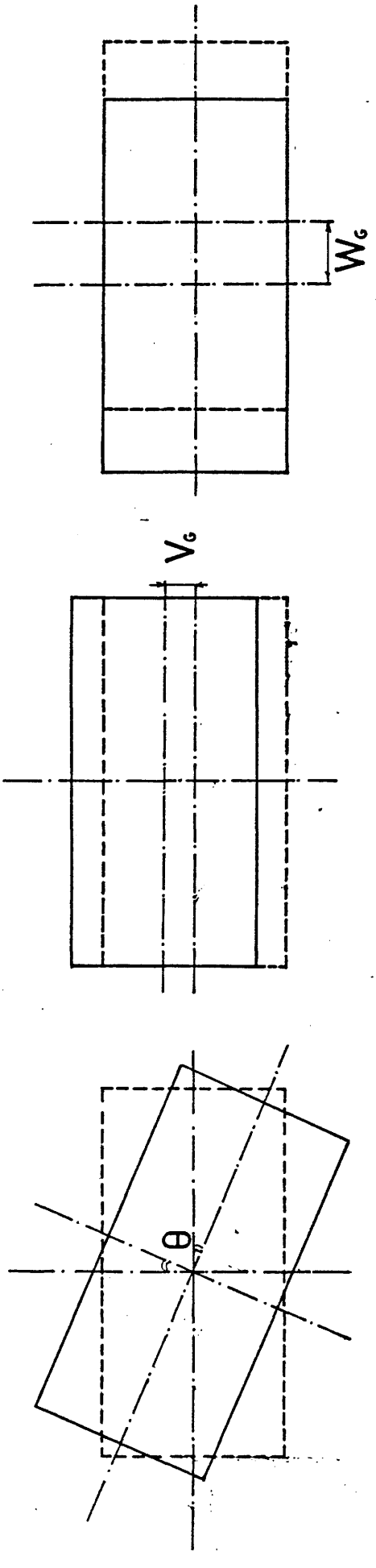

Fig. 2.2 Rigid Body Displacements

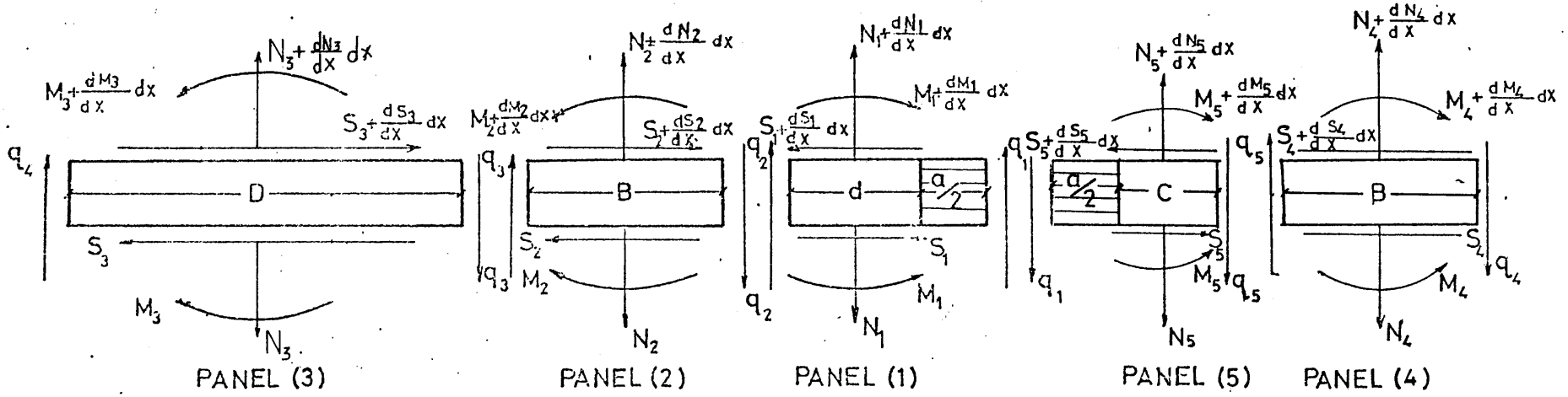

Fig. 2.3 Internal Forces in Core Panels

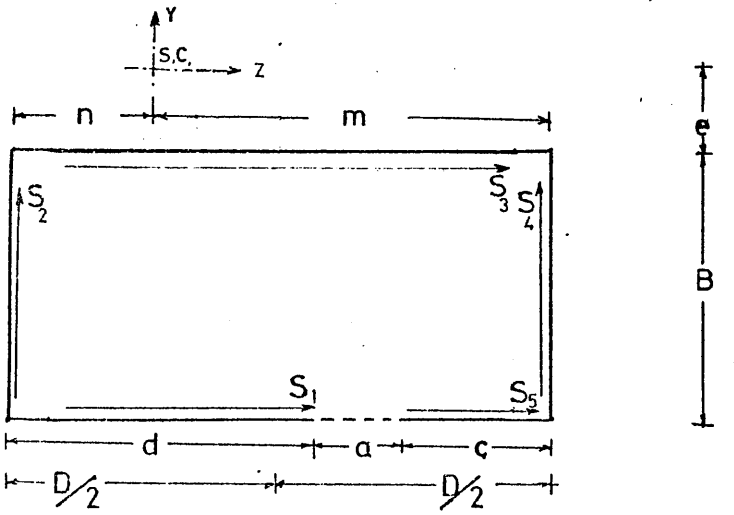

Fig. 2.4 Shear Forces in Core Cross-section

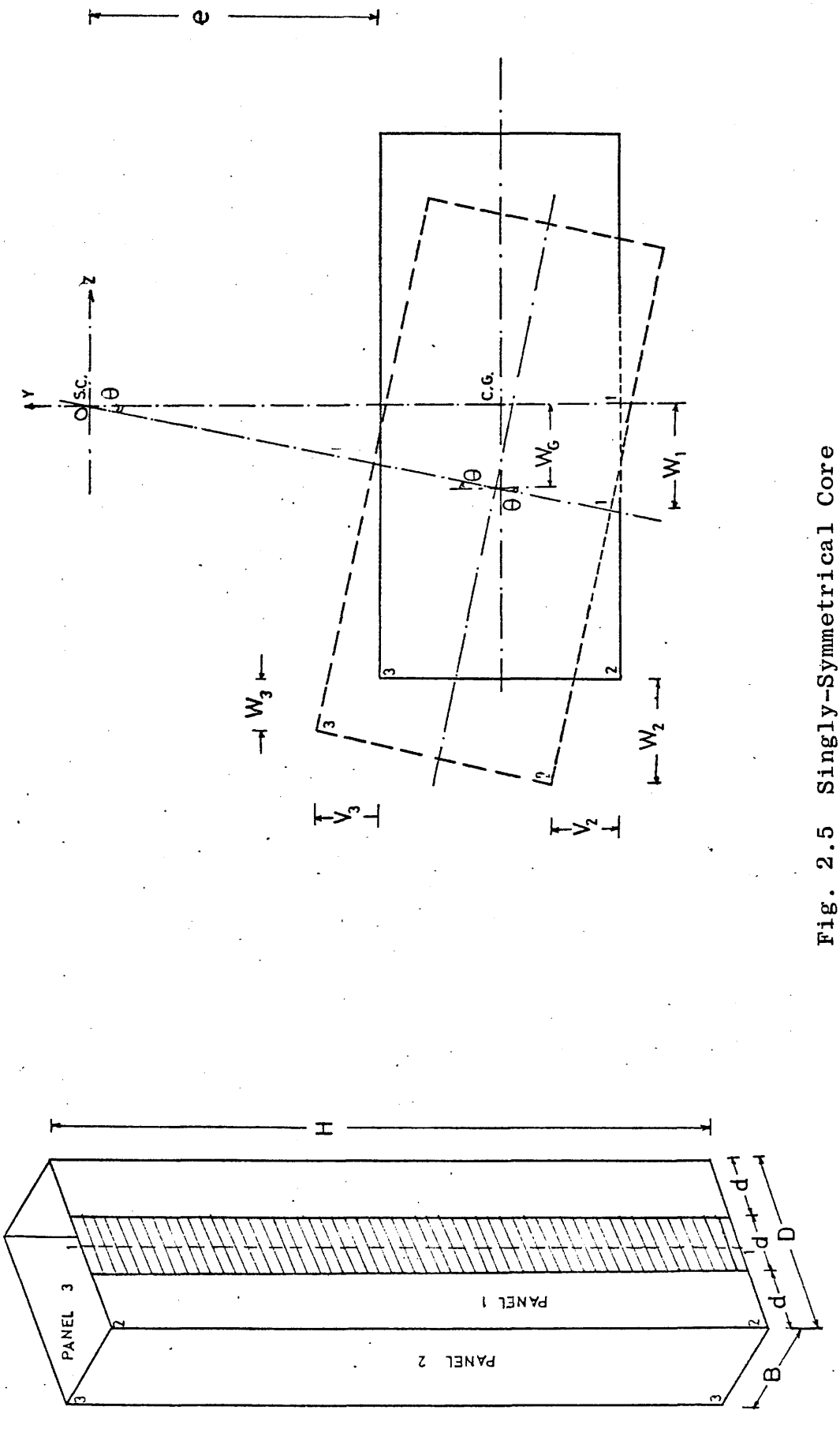

Fig. 2.5 Singly-Symmetrical Core

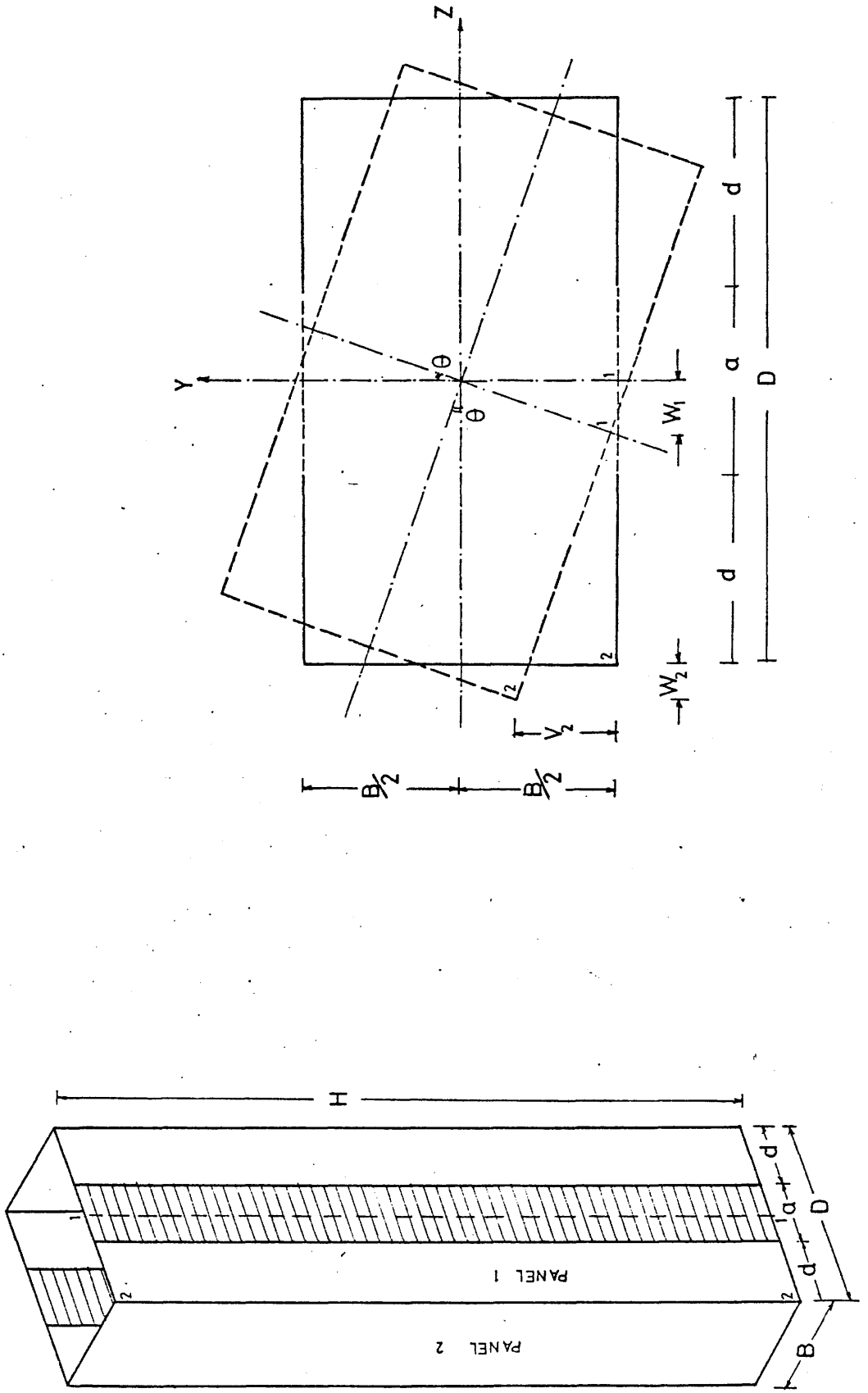

Fig. 2.6 Doubly-Symmetrical Core

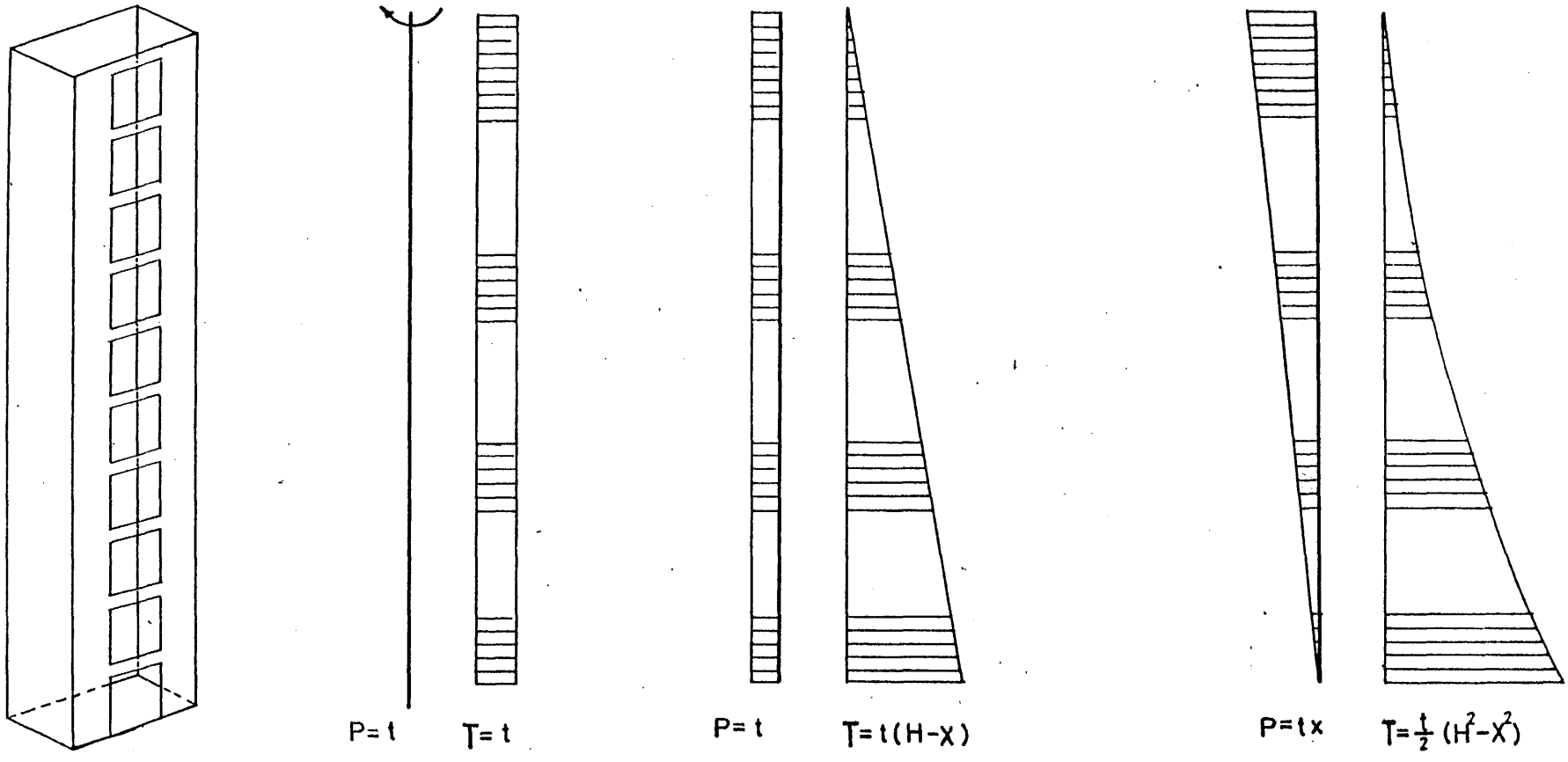

Fig. 2.7 Standard Load Cases, (Point Torque at the Top, Uniformly Distributed Torque and Triangularly Distributed Torque)

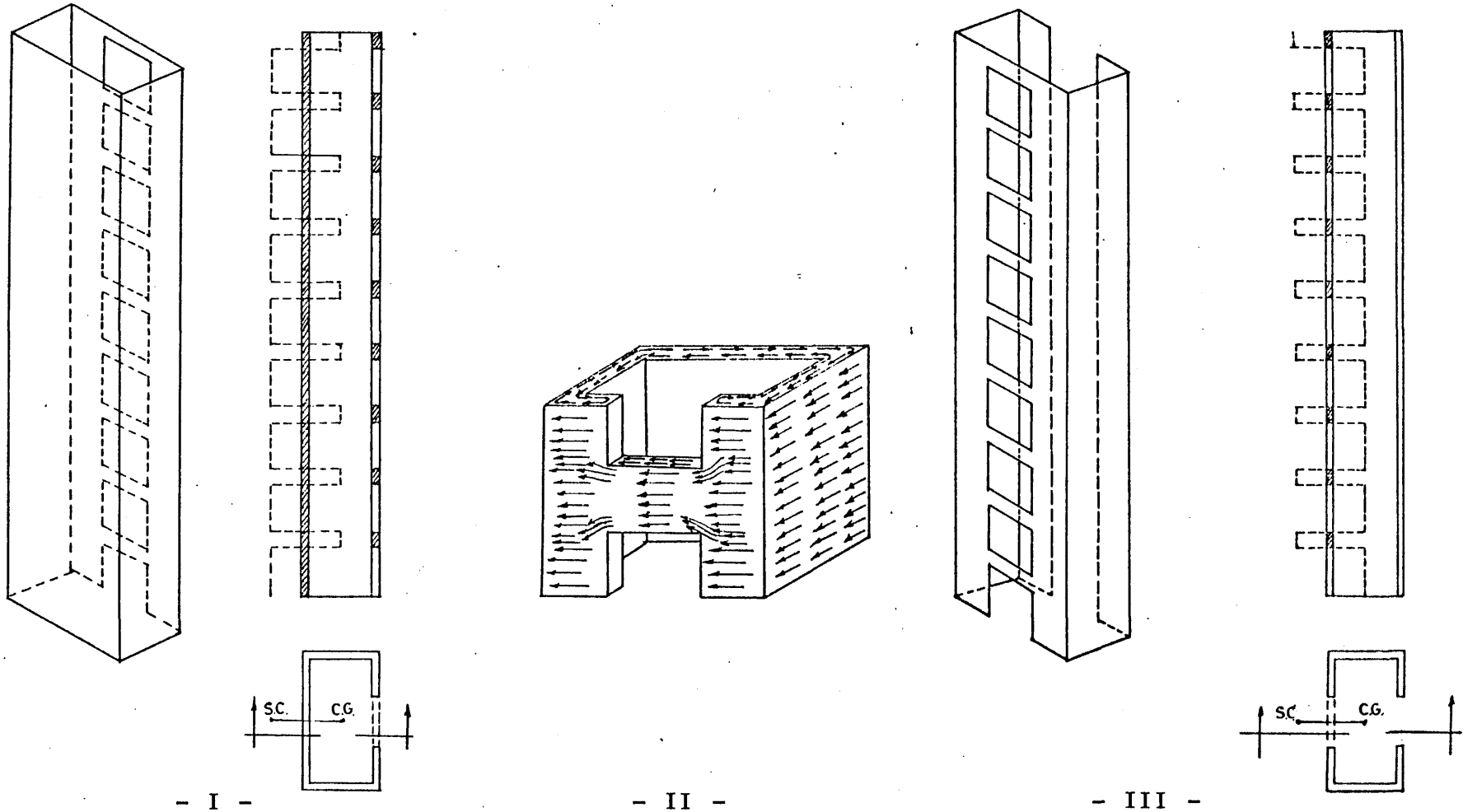

Fig. 2.8 Position of Shear Centre and Effect of Beams on Shear Flow

CHAPTER 3

EFFECT OF END RESTRAINT ON THE ELASTIC BEHAVIOUR OF CORE STRUCTURES

CHAPTER 3

EFFECT OF END RESTRAINT ON THE ELASTIC BEHAVIOUR OF CORE STRUCTURES

3.1 INTRODUCTION

In the preceding analysis, it was assumed that the core is free at the top and fixed to a rigid foundation. However, in many cases a shaft over-run exists to provide space for machinery and other mechanical requirements, which can create a stiffening action across the top of the structure. By including this effect, the core efficiency in resisting loads can increase considerably. A top stiffening beam could also be employed to restrain the warping at the top of the structure. On the other hand the assumption of a rigid base is not strictly true in all cases. The super-structure may be erected on a non-rigid sub-structure or on a certain type of foundation or soil which may allow some relative displacements.

A similar analysis based on the same basic assumptions regarding the structural behaviour is presented in an attempt to examine such influences on the stresses and deformations of the structure. The elastic governing equation remains the same, but the boundary conditions have been modified by introducing two factors R and λ representing respectively the stiffness of the top beam and the flexibility of the foundation.

3.2 INCLUSION OF RESTRAINING ELEMENT AT THE TOP

The stiffened structure shown in Fig. 3.1.I may be simulated as shown in Fig. 3.1.II by replacing the connecting beams by a continuous medium as assumed earlier, and the shaft over-run structure may be represented by a stiffening element of the same stiffness, and included in the analysis as an additional top beam.

3.2.1 THE RESTRAINING FACTOR R

By considering a segment of height dx of each panel within the area of the top stiffening beam and following the same procedure as before, the vertical shear force in the top stiffening beams Q_s in the core shown in Fig. 3.1 is found to be

$$Q_s = - 2\beta_s E_s B D \frac{d\theta}{dx}$$

where

$\beta_s = 12 I_{cs}/a^3$, E_s is the modulus of elasticity of the top beam material and I_{cs} is the moment of inertia of the stiffening element.

The bending moment at the top of the walls adjacent to the connecting beams will be

$$M_1 = - Q_s \frac{(d + a)}{2}$$

And the moment-curvature relationship for the wall is, as before,

$$M_1 = - E I_1 \frac{B}{2} \frac{d^2\theta}{dx}$$

Hence, from the above equations,

$$\frac{d^2\theta}{dx^2} = r \frac{d\theta}{dx} \qquad 3.2.1$$

where

$$r = - 2\beta_s \frac{D(d + a)}{I_1} \quad \frac{E_s}{E}$$

By recasting equation 3.2.1 in non-dimensional form, the top end condition becomes,

$$\frac{d^2\theta}{d\xi^2} = R \frac{d\theta}{d\xi}$$

where

$$R = - rH = - 2\beta_s D \frac{(d + a)}{I_1} H \frac{E_s}{E} \qquad 3.2.2$$

3.2.2 EFFECT OF TOP END RESTRAINT ON BEHAVIOUR OF CORE STRUCTURE

Due to the existence of the top stiffening element, the boundary conditions will be altered to

At the base ($\xi = 0$) , $\theta = 0$ and $\theta' = 0$

At the top ($\xi = 1$) , $\theta'' = R\theta'$

1. CORE STRUCTURES SUBJECTED TO A CONCENTRATED TORQUE AT THE TOP

Solving the general governing equation 2.6.1 for the above boundary conditions, the three integration constants become

$$K_1 = - K_2 = \frac{tH}{\gamma G J_o} \frac{[R(\cosh \gamma - 1) - \gamma \sinh \gamma]}{[\gamma \cosh \gamma - R \sinh \gamma]}$$

$$K_3 = \frac{tH}{\gamma G J_o}$$

The complete solution in this case then becomes

$$\theta = \frac{tH}{GJ_o}\left[\frac{(R(\cosh\gamma-1)-\gamma\sinh\gamma)(1-\cosh\gamma\xi)}{\gamma(\gamma\cosh\gamma-R\sinh\gamma)} - \frac{1}{\gamma}\sinh\gamma\xi+\xi\right] \qquad 3.2.3$$

2. CORE STRUCTURES SUBJECTED TO UNIFORMLY DISTRIBUTED TORQUE

Solving equation 2.6.3 for the same boundary conditions, the integration constants become

$$K_1 = \frac{tH^2}{\gamma GJ_o}\left(\frac{1}{\gamma} - \frac{(R\cosh\gamma - \gamma\sinh\gamma-1)}{(\gamma\,\text{csoh}\,\gamma - R\sinh\gamma)}\right]$$

$$K_2 = -\frac{tH^2}{\gamma GJ_o}\,\frac{(R\cosh\gamma - \gamma\sinh\gamma-1)}{(\gamma\cosh\gamma- R\sinh\gamma)}$$

$$K_3 = \frac{tH^2}{\gamma GJ_o}$$

The complete solution is then,

$$\theta = \frac{tH^2}{GJ_o}\left[\frac{(R\cosh\gamma-\gamma\sinh\gamma-1)(1-\cosh\xi)}{\gamma(\gamma\cosh\gamma - R\sinh\gamma)}\right.$$

$$\left. - \frac{1}{\gamma}\sinh\gamma\,\xi + (\xi - \frac{\xi^2}{2})\right] \qquad 3.2.4$$

3. CORE STRUCTURES SUBJECTED TO TRIANGULARLY DISTRIBUTED TORQUE

For the same boundary conditions, the integration constants of equation 2.6.5 become,

$$K_1 = -K_2 = \frac{tH^3}{2GJ_o}\left[\frac{(R\cosh\gamma-\gamma\sinh\gamma)(1-\frac{2}{\gamma^2})-2(1-\frac{R}{\gamma^2})}{\gamma(\gamma\cosh\gamma-R\sinh\gamma)}\right]$$

$$K_3 = -\frac{tH^3}{2\gamma GJ_o}\,(1-\frac{2}{\gamma^2})$$

The complete solution in this case then becomes

$$\theta = \frac{tH^3}{2GJ_o}\left[\frac{[(R\cosh\gamma-\gamma\sinh\gamma)(1-\frac{2}{\gamma^2})-2(1-\frac{R}{\gamma^2})][1-\cosh\gamma\xi]}{\gamma(\gamma\cosh\gamma-R\sinh\gamma)}\right.$$

$$\left. -(\frac{\gamma^2-2}{\gamma^3})\sinh\gamma\,\xi+(\xi-\frac{\xi^3}{3}-\frac{2\xi}{\gamma^2})\right]$$

3.2.5

3.3 EFFECT OF FLEXIBLE FOUNDATIONS ON THE ELASTIC BEHAVIOUR OF CORE STRUCTURES

3.3.1 ASSUMPTIONS

In the case of a core structure supported on a flexible foundation, the walls undergo settlements due to the base stresses under each wall. In order to simplify the problem and to present the relationship between the structure and the supporting foundation by a single parameter, the following assumptions have been introduced.

1 - The supporting foundation is homogeneous, isotropic and linearly elastic.

2 - The wall/base stiffness ratio n is constant throughout the core walls.

3 - The normal stresses and settlements are distributed uniformly and in proportional to the imposed axial force at the base.

4 - The bending moment stresses and settlements vary linearly and in proportional to the imposed bending moment at the base.

Following the aforementioned assumptions, the compatibility

condition along the line of contraflexure at the middle of the connecting medium as shown in Fig. 3.2.1 may be written as

$$\delta_1 + \delta_2 + \delta_3 + \delta_4 + \delta_5 = 0 \qquad 3.3.1$$

where

$$\delta_1 = 2 \int_0^x \frac{M_1}{EI_1} \frac{(d + a)}{2} dx$$

$$\delta_2 = - 2 \int_0^x \frac{N_1}{EA_1} dx$$

$$\delta_3 = - q_o \frac{a^3 h}{12EI_c}$$

$$\delta_4 = - 2 \frac{N_{10}}{K_v}$$

$$\delta_5 = \frac{2(d + a)}{2} \frac{M_{10}}{K_\varphi}$$

and K_v and K_φ are the axial and rotational flexibility parameters respectively of the foundation.

The first three terms have been used earlier in section 2.4 and represent the vertical displacements due to bending moments, normal forces and flexural deflections of the connecting beams as shown in Fig. 3.2.(2,3 and 4). The last two terms represent the settlements at the base due to the normal forces and bending moments on the two walls as shown in Fig. 3.2(5 and 6).

3.3.2 THE FOUNDATION FLEXIBILITY FACTOR λ

The approach followed allows a simultaneous consideration of the core displacements and settlements and makes it possible to represent the relative foundation flexibility as a single parameter.

For simplicity the derivation of the analytical method is illustrated for singly- and doubly-symmetrical forms of core structures, but it may readily be introduced to the other cores considered earlier in Section 2.4 and Appendix A.

1 - SINGLY-SYMMETRIC CORE ON FLEXIBLE FOUNDATIONS

The singly-symmetric core shown in Fig. 2.5 is considered to be supported on flexible foundations. The equations of the displacements, the equilibrium condition for the internal forces and the moment-curvature relationships are the same as in section 2.4.2.

Because of the foundation flexibility, the core base will undergo five simultaneous settlements which may be illustrated as follows;

(1) Vertical settlement of Panel 1 due to the normal force N_1 which may cause rotation of panel 2 and panel 3 as shown in Fig. 3.3.1 or cause vertical settlement of panel 2 and rotation of panel 3 as in Fig. 3.3.2.

(2) Rotation of panel 1 due to the bending moment M_1 which may cause rotation of panel 2 and 3 as shown in Fig. 3.3.3, or cause vertical settlement of panel 2 and rotation of panel 3 as in Fig. 3.3.4.

(3) Vertical settlement of panel 2 due to the normal force N_2 which may cause panel 1 and panel 3 to rotate as shown in Fig. 3.3.4, or cause a vertical settlement of panel 1 and rotation of panel 3 as in Fig. 3.3.2.

(4) Rotation of panel 2 due to the bending moment M_2, which may cause rotation of panel 1 and 3 as shown in Fig. 3.3.3, or cause vertical settlement of panel 1 and rotation of panel 3 as in Fig. 3.3.1.

(5) Rotation of panel 3 due to the bending moment M_3 which may cause any of the aforementioned deformations which are shown in Fig. 3.3(1, 2, 3, and 4).

The final deformed shape of the base will be a superposition of the aforementioned five cases as in Fig. 3.3.5.

Consequently, the vertical compatibility conditions along lines 1-1, 2-2 and 3-3 may be written respectively as follows

$$\int_o^x \frac{M_1}{EI_1}(d + a)dx - 2\int_o^x \frac{N_1}{EA_1}dx - \frac{q_1}{\beta_1 E} - \delta = 0 \qquad 3.3.2$$

$$\int_o^x \frac{M_1}{EI_1}\frac{d}{2}dx - \int_o^x \frac{M_2}{EI_2}\frac{B}{2}dx + \int_o^x \frac{N_1}{EA_1}dx - \int_o^x \frac{N_2}{EA_2}dx +$$

$$\frac{M_{10}}{K_\psi}\frac{d}{2} + \frac{N_{10}}{K_v} - \frac{M_{20}}{K_\phi}\frac{B}{2} - \frac{N_{20}}{K_v} = 0 \qquad 3.3.3$$

$$- \int_o^x \frac{M_3}{EI_3}\frac{D}{2}dx - \int_o^x \frac{M_2}{EI_2}\frac{B}{2}dx + \int_o^x \frac{N_2}{EA_2}dx -$$

$$\frac{M_{30}}{K_\eta}\frac{D}{2} + \frac{N_{20}}{K_v} - \frac{M_{20}}{K_\phi}\frac{B}{2} = 0 \qquad 3.3.4$$

where

$$\delta = \delta_4 - \delta_5 = \frac{2N_{10}}{K_v} - \frac{M_{10}}{K_\phi}(d + a) \qquad 3.3.5$$

and

$$K_v = C_u n A_1$$

$$K_\psi = C_u n I_1$$

$$K_\phi = C_u n I_2$$

$$K_\eta = C_u n I_3$$

where C_u is the elastic strain constant of the foundation material N/mm^3. Substituting for the bending moment and axial force from equations 2.4.24 and 2.4.32 into equations 3.3.2 and 3.3.5 yields

$$q_1 = -\beta E\left[2\int_0^x BD\frac{d^2\theta}{dx^2}dx + \delta\right] \qquad 3.3.6$$

and

$$\delta = 2\mu BD\left[\frac{d^2\theta}{dx^2}\right]_o \qquad 3.3.7$$

where

$$\mu = \frac{E}{nC_u}$$

From the displacement conditions 2.4.30, and the settlements, Fig. 3.3, the following relationships may be derived at the base:-

$$\psi = -(B + e)\left[\frac{d\theta}{dx}\right]_o \qquad 3.3.8$$

$$\phi = \frac{D}{2}\left[\frac{d\theta}{dx}\right]_o \qquad 3.3.9$$

$$\eta = - e \left[\frac{d\theta}{dx}\right]_o \qquad 3.3.10$$

The force-displacement relationships at the base are given by

$$\psi = \frac{M_{10}}{K_\psi} = - \mu(B + e)\left[\frac{d^2\theta}{dx^2}\right]_o \qquad 3.3.11$$

$$\phi = \frac{M_2}{K_\phi} = \mu \frac{D}{2} \left[\frac{d^2\theta}{dx^2}\right]_o \qquad 3.3.12$$

$$\eta = \frac{M_3}{K_\eta} = - \mu e \left[\frac{d^2\theta}{dx^2}\right]_o \qquad 3.3.13$$

From equation 3.3(8 and 11) or 3.3(9 and 12) or 3.3(10 and 13), the boundary condition at the base may be written as

$$\left[\frac{d\theta}{dx}\right]_o = \mu \left[\frac{d^2\theta}{dx^2}\right]_o \qquad 3.3.14$$

Substituting from equation 3.3(14 and 7) into equation 3.3.6 and integrating yields

$$q_1 = - 2\beta EBD \left[\frac{d\theta}{dx}\right]_x$$

Equation 3.3.14, which represents the boundary condition at the base, may be rewritten in non-dimensional form as follows

$$\frac{d\theta}{d\xi} = \lambda \frac{d^2\theta}{d\xi^2} \qquad 3.3.15$$

where λ is the non-dimensional flexibility parameter of the foundation defined by $\frac{\mu}{H}$.

2 - DOUBLY-SYMMETRIC CORE ON FLEXIBLE FOUNDATIONS

The single-cell doubly-symmetric core shown in Fig. 2.6 is assumed to be based on flexible foundations. The displacement equations and the equilibrium conditions of

the internal forces for each panel are the same as in section 2.4.3. Due to the foundation flexibility the core panels will undergo three simultaneous settlements as follows:-

(1) Vertical settlement of panel 1 due to the normal force N_1, which will cause rotation in panel 2, as in Fig. 3.4.1.

(2) Rotation of panel 1 due to the bending moment M_1, which will cause rotation in panel 2, as in Fig. 3.4.2.

(3) Rotation of panel 2 due to the bending moment M_2, which will cause vertical settlement and rotation of panel 1, as shown in Fig. 3.4(1 and 2).

The compatibility conditions along the lines 1-1 and 2-2, may be written respectively as follows.

$$\int_o^x \frac{M_1}{EI_1} \frac{(d + a)}{2} \, dx - 2 \int_o^x \frac{N_1}{EA_1} \, dx - \frac{q_1}{\beta E} - \delta = 0$$

$$\int_o^x \frac{M_1}{EI_1} \frac{d}{2} \, dx + \int_o^x \frac{N_1}{EA_1} \, dx - \int_o^x \frac{M_2}{EI_2} \frac{B}{2} \, dx + \qquad 3.3.16$$

$$\frac{M_{10}}{K_\psi} \frac{d}{2} + \frac{N_1}{K_v} - \frac{M_2}{K_\phi} \frac{B}{2} = 0$$

Solving the above equations with the internal equilibrium conditions 2.4 (4, 5, 6 and 7) and the moment curvature relationships 2.4.24, yields

$$q_1 = - \beta E \left[\int_o^x BD \frac{d^2\theta}{dx^2} \, dx + \delta \right] \qquad 3.3.17$$

and

$$\delta = \mu . B . D . \left[\frac{d^2\theta}{dx^2}\right]_o \qquad 3.3.18$$

where β and μ are as defined before.

From the displacement conditions 2.4.33, and the settlements Fig. 3.4 the following relationships may be derived at the base

$$\Psi = -\frac{B}{2}\left[\frac{d\theta}{dx}\right]_o \qquad 3.3.19$$

$$\phi = \frac{D}{2}\left[\frac{d\theta}{dx}\right]_o \qquad 3.3.20$$

The last two equations may be rewritten using the force-displacement relationships as

$$\Psi = \frac{M_{1O}}{K_\Psi} = -\mu\,\frac{B}{2}\left[\frac{d^2\theta}{dx^2}\right]_o \qquad 3.3.21$$

$$\phi = \frac{M_{2O}}{K_\phi} = \mu\,\frac{D}{2}\left[\frac{d^2\theta}{dx^2}\right]_o \qquad 3.3.22$$

From equation 3.3.(19 and 21) or equation 3.3.(20 and 22), the base boundary condition may be written as follows.

$$\left[\frac{d\theta}{dx}\right]_o = \mu\left[\frac{d^2\theta}{dx^2}\right]_o \qquad 3.3.23$$

Substituting from equation 3.3 (23 and 18) into equation 3.3.17, the shear flow in the connecting medium becomes

$$q_1 = -\beta EBD\left[\frac{d\theta}{dx}\right]_x$$

The boundary condition at the base 3.3.23, may be rewritten in non-dimensional form as,

$$\left[\frac{d\theta}{d\xi}\right]_o = \lambda\left[\frac{d^2\theta}{d\xi^2}\right]_o \qquad 3.3.24$$

where λ is as defined before.

3.3.4 EFFECT OF FOUNDATION FLEXIBILITY ON THE BEHAVIOUR OF CORE STRUCTURES

For core structures based on flexible foundations and restrained at the top, the boundary conditions will be

At the base ($\xi = 0$) , $\theta = 0$ and $\theta' = \lambda\theta''$

At the top ($\xi = 1$) , $\theta'' = R\theta'$

1 - CORE STRUCTURES SUBJECTED TO CONCENTRATED TORQUE AT THE TOP

The general solution of the governing equation is given in equation 2.6.1. From the above boundary conditions, the constants of integration become

$$K_1 = - K_2 = - \frac{tH}{GJ_o} \frac{[R(1-\cosh \gamma)+ \gamma \sinh \gamma]}{\gamma[(\gamma \cosh \gamma-R \sinh \gamma)-\gamma\lambda(R \cosh \gamma-\gamma \sinh \gamma)]}$$

$$K_3 = \gamma\lambda K_2 - \frac{tH}{\gamma GJ_o}$$

and the complete solution becomes

$$\theta = \frac{tH}{GJ_o}\left[\frac{[\gamma\lambda \sinh \gamma\xi + \cosh \gamma\xi-1][R(1-\cosh \gamma)+\gamma \sinh \gamma]}{[(\gamma \cosh \gamma-R \sinh \gamma)-\gamma\lambda(R \cosh \gamma-\gamma \sinh \gamma)]}\right.$$

$$\left. - \frac{1}{\gamma} \sinh \gamma\xi + \xi\right] \qquad 3.3.25$$

2 - CORE STRUCTURES SUBJECTED TO UNIFORMLY DISTRIBUTED TORQUE

In this case, the general solution of the governing equation is given in equation 2.6.3. The boundary conditions yield

$$K_1 = \frac{tH^2}{\gamma GJ_o}\left[\frac{1}{\gamma} - \frac{[1-(1+\lambda)(R \cosh \gamma-\gamma \sinh \gamma)]}{[(\gamma \cosh \gamma-R \sinh \gamma)-\gamma\lambda(R \cosh \gamma-\gamma \sinh \gamma)]}\right]$$

$$K_3 = \gamma \lambda K_2 - \frac{tH^3}{GJ_o} (1 + \lambda)$$

$$K_2 = \frac{tH^2}{\gamma GJ_o} \frac{[1-(1+\lambda)(R\cosh\gamma-\gamma\sinh\gamma)]}{[(\gamma\cosh\gamma-R\sinh\gamma)-\gamma\lambda(R\cosh\gamma-\gamma\sinh\gamma)]}$$

giving the complete solution as;

$$\theta = \frac{tH^2}{GJ_o}[\frac{[\gamma\lambda\sinh\gamma\xi+\cosh\gamma\xi-1][1-(1+\lambda)(R\cosh\gamma-\gamma\sinh\gamma)]}{\gamma[(\gamma\cosh\gamma-R\sinh\gamma)-\gamma\lambda(R\cosh\gamma-\gamma\sinh\gamma)]} + \xi - \frac{\xi^2}{2} - \frac{(1+\lambda)}{\gamma}\sinh\gamma\xi] \qquad 3.3.26$$

3 - CORE STRUCTURES SUBJECTED TO TRIANGULARLY DISTRIBUTED TORQUE

The general solution of the governing equation for this case is given in equation 2.6.5. The boundary conditions yield

$$K_1 = -K_2 = -\frac{tH^3}{2\gamma GJ_o} \frac{[2(1-\frac{R}{\gamma^2})-(1-\frac{2}{\gamma^2})(R\cosh\gamma-\gamma\sinh\gamma)]}{[(\gamma\cosh\gamma-R\sinh\gamma)-\gamma\lambda(R\cosh\gamma-\gamma\sinh\gamma)]}$$

$$K_3 = \gamma\lambda K_2 - \frac{tH^3}{2\gamma GJ_o}(1-\frac{2}{\gamma^2})$$

and the complete solution becomes

$$\theta = \frac{tH^3}{2GJ_o} [\frac{[2(1-\frac{R}{\gamma^2})-(1-\frac{2}{\gamma^2})(R\cosh\gamma-\gamma\sinh\gamma)][\gamma\lambda\sinh\gamma\xi+\cosh\gamma\xi-1]}{\gamma[(\gamma\cosh\gamma-R\sinh\gamma)-\gamma\lambda(R\cosh\gamma-\gamma\sinh\gamma)]} (\xi - \frac{\xi^3}{3} - \frac{2\xi}{\gamma^2} - \frac{(1-\frac{2}{\gamma^2})}{\gamma}\sinh\gamma\xi)] \qquad 3.3.27$$

3.4 SIGNIFICANCE OF THE PARAMETERS R AND λ

3.4.1 TOP RESTRAINT FACTOR R

The values of the non-dimensional top restraint factor R depend on the core dimensions as well as the stiffness β_s

and the elastic modulus E_s of the top element. In the limit when R is very small, (i.e. $R \longrightarrow 0$) the core will behave as if it is free at the top and equations 3.2 (3, 4 and 5) will be identical to equation 2.6(2, 4 and 6) respectively. As the values of R increase, the freedom of the core to warp and rotate is more restrained. In the other limit when R is very large, ($R \longrightarrow \infty$) the core will tend to behave as fully restrained at the top.

In the case of an unsymmetrical core, or a multi-bay core structure, there will be more than one value for the top end restraint R. It indicates that there is more than one boundary condition at the top and a closed form solution cannot be achieved. To allow for such solution an average value could be taken as the top end restraint R, but the resulting forces and displacements could then only be regarded as approximate and of doubtful accuracy.

3.4.2 THE FOUNDATION FLEXIBILITY FACTOR λ

In the case of a core structure supported on flexible foundations, the flexibility factor λ is independent of the core shape and dimensions, other than the height H. It depends mainly on the elastic properties of the core material and on the supporting foundations.

For a very rigid foundation, the values of λ tend to be very small. At the limiting case when λ approaches zero the core will behave as if it is fixed at the base and equation 3.3 (25, 26 and 27) will be identical to equation 3.3(3, 4, and 5) respectively. In the other

limit when λ is very large, or as λ approaches infinity the core will behave as if it is free at the base which is not possible practically.

The above spectrum of λ values allows for a wide range of foundation conditions to be considered. In reality it will lie within a particular range depending on the nature of the sub-base material and the type and configuration of foundation system.

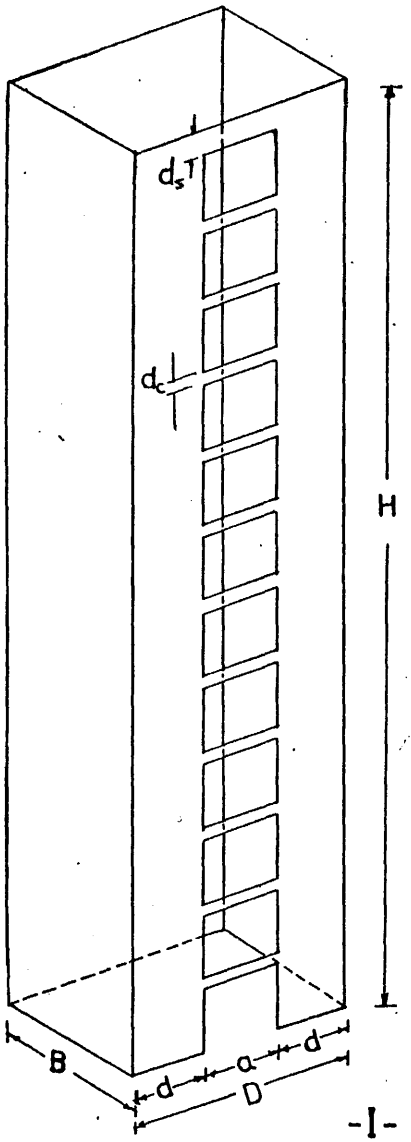

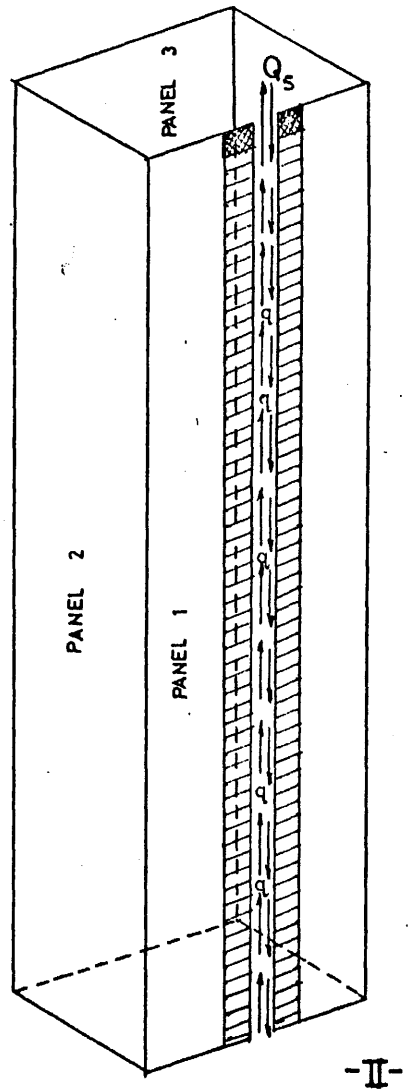

Fig. 3.1 Core structure with stiff top beam and substitute system

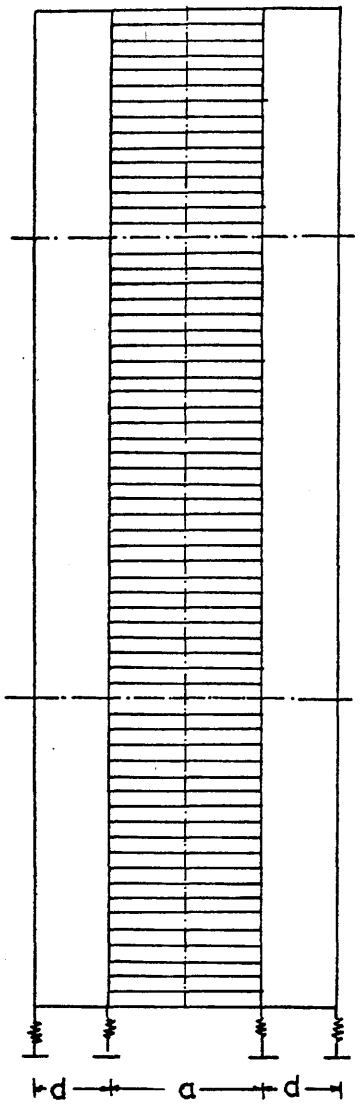

-1-

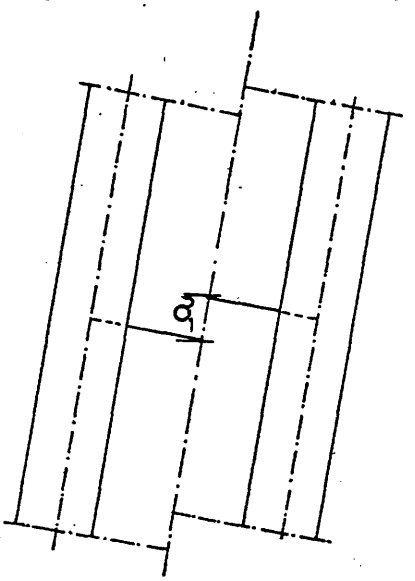

-2-

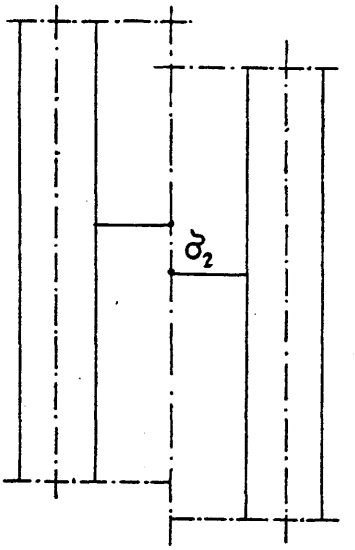

-3-

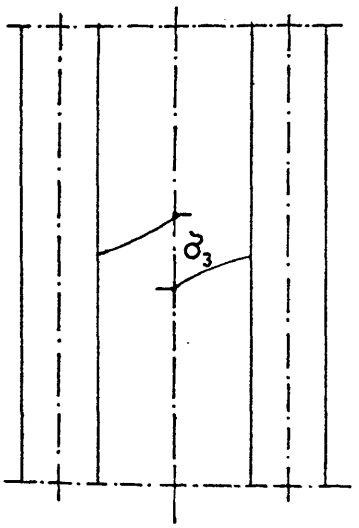

-4-

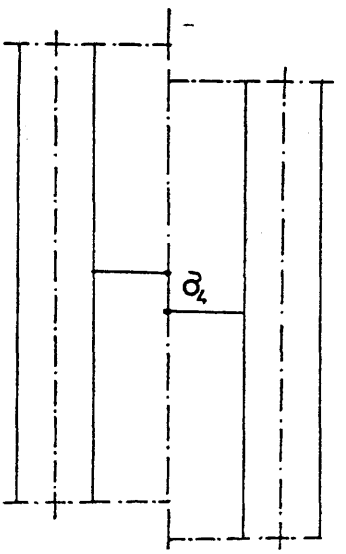

-5-

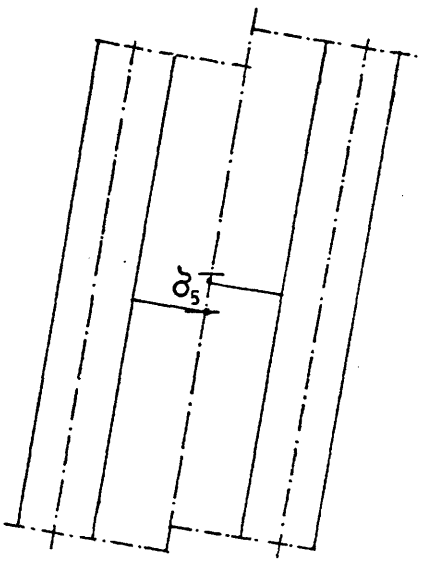

-6-

Fig. 3.2 Deformation of the lamenas

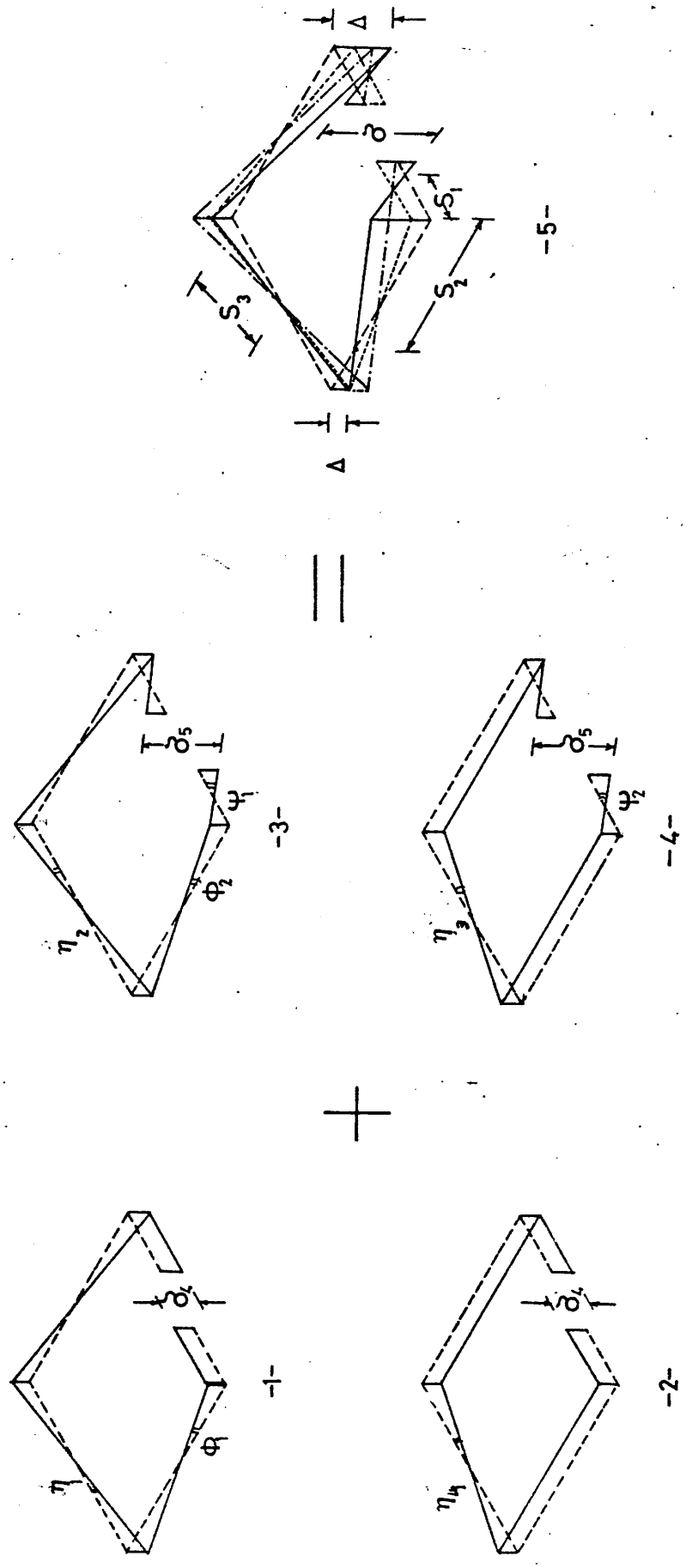

Fig. 3.3 Deformations of a Singly-Symmetric Core Base

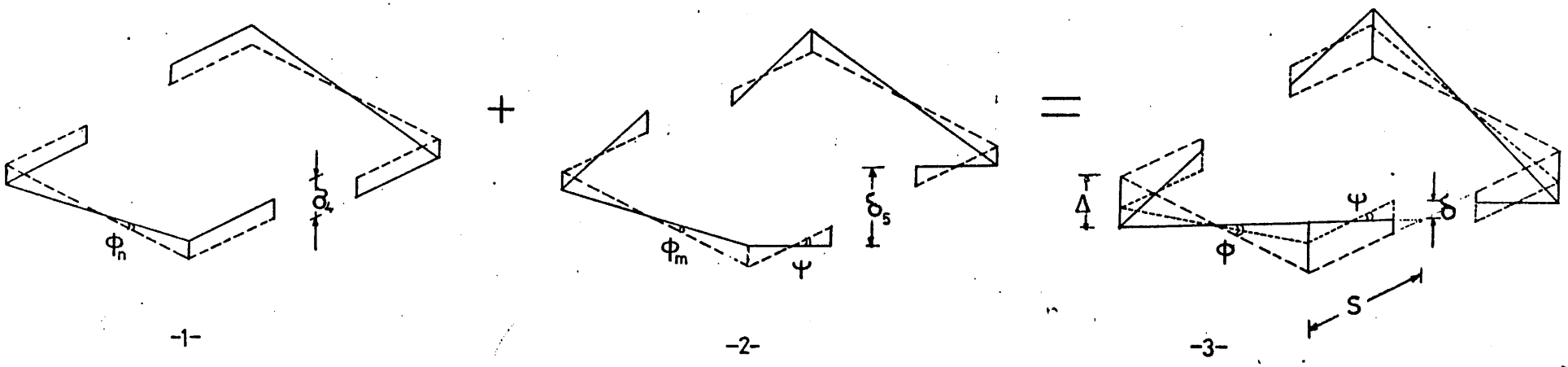

Fig. 3.4 Deformations of a Doubly-Symmetrical Core Base

CHAPTER 4

PARAMETER STUDY AND NUMERICAL EXAMPLES

CHAPTER 4

PARAMETER STUDY AND NUMERICAL EXAMPLES

4.1 INTRODUCTION

In this chapter, a numerical study is presented of the effects of the non-dimensional parameters demonstrated in Chapters 2 and 3, namely, the core relative stiffness constant αH, the top end restraint R and the foundation flexibility λ, on the elastic behaviour of the structure.

Design charts have been introduced to give a quick assessment of the rotation and internal forces in the core, when subjected to the three standard load cases considered in Chapter 2, for various values of αH and end conditions.

Two practical examples have been presented to demonstrate the effect of the aforementioned parameters on a singly-symmetric and doubly-symmetric structure.

4.2 GENERAL FORM OF SOLUTION OF THE GOVERNING EQUATION

The solution of the governing equation illustrated in section 3.3.4 may be recast as a function of non-dimensional parameters U, U1 and U2 for each case of loading as follows:

1 - POINT TORQUE AT THE TOP

The elastic behaviour of core structures based on flexible foundations and provided with a stiffening element at the top, subjected to a point torque at the top, is given in mathematical form in equation 3.3.25, which may be expressed in the form,

$$\theta = \frac{tH}{GJ_o} U \qquad 4.2.1$$

The derivatives are

$$\theta' = \frac{tH}{GJ_o} U1$$

$$\theta'' = \frac{tH}{GJ_o} U2$$

where

$$U = \frac{[\gamma\lambda \sinh \gamma\xi + \cosh \gamma\xi - 1][R(1-\cosh \gamma)+ \gamma \sinh \gamma]}{[(\gamma \cosh \gamma - R \sinh \gamma) - \gamma\lambda (R \cosh \gamma - \gamma \sinh \gamma)]}$$

$$- \frac{1}{\gamma} \sinh \gamma\xi + \xi$$

$$U1 = \frac{d}{d\xi} U \qquad \text{and} \qquad U2 = \frac{d^2}{d\xi^2} U$$

2 - UNIFORMLY DISTRIBUTED TORQUE

Equation 3.3.26 describes the elastic behaviour of core structures subjected to a uniformly distributed torque, and may be expressed as,

$$\theta = \frac{tH^2}{GJ_o} U \qquad 4.2.2$$

The derivatives are

$$\theta' = \frac{tH^2}{GJ_o} U1$$

$$\theta'' = \frac{tH^2}{GJ_o} U2$$

where

$$U = \frac{[\gamma\lambda \sinh \gamma\xi + \cosh \gamma\xi - 1][1 - (1 + \lambda)(R \cosh \gamma-\gamma \sinh \gamma)]}{\gamma[\gamma \cosh \gamma + R \sinh \gamma) - \gamma\lambda(R \cosh \gamma - \gamma \sinh \gamma)]}$$

$$+ \xi - \frac{\xi^2}{2} - \frac{(1 + \lambda)}{\gamma} \sinh \xi$$

and

$$U1 = \frac{d}{d\xi} U \quad , \qquad U2 = \frac{d^2}{d\xi^2} U$$

3 - TRIANGULARLY DISTRIBUTED TORQUE

The elastic behaviour of core structures subjected to a triangularly distributed torque is given by equation 3.3.27, which may be rewritten in the form,

$$\theta = \frac{tH^3}{2GJ_o} U \qquad 4.2.3$$

The derivatives will be

$$\theta' = \frac{tH^3}{2GJ_o} U1$$

$$\theta'' = \frac{tH^3}{2GJ_o} U2$$

where

$$U = \frac{[2(1 - \frac{R}{\gamma^2})-(1 - \frac{2}{\gamma^2})(R \cosh \gamma-\gamma \sinh \gamma)][\gamma\lambda \sinh\gamma\xi + \cosh \gamma\xi-1]}{\gamma[(\gamma \cosh \gamma - R \sinh \gamma)-\gamma\lambda(R \cosh \gamma - \gamma \sinh \gamma)]}$$
$$+ \xi - \frac{\xi^3}{3} - \frac{2\xi}{\gamma^2} - \frac{(1 - \frac{2}{\gamma^2})}{\gamma} \sinh \gamma\xi$$

and

$$U1 = \frac{d}{d\xi} U \quad , \qquad U2 = \frac{d^2}{d\xi^2} U.$$

4.3 EFFECT OF VALUE OF αH ON BEHAVIOUR OF CORE STRUCTURES

It was demonstrated in Chapter 2 that core structures subjected to torsional loading may be described by a single parameter αH, which depends on the core material, configuration and dimensions. The most significant factors are the core height H which varies linearly with αH values and the depth of the connecting beams which varies as a cubic function with α^2 values. The results of a study of the relationship between the maximum angle of rotation at the top represented by the parameter U_{max} and the stiffness parameter αH is shown in Fig. 4.1 (1, 2 and 3) for the three standard loading cases, for a core fixed at the base and free at the top. It shows that as the core stiffness parameter αH increases, its relative effect on the maximum angle of rotation U_{max} decreases.

The variation between the maximum values of the shear flow in the connecting lamina represented by the non-dimensional parameter $U1_{max}$ and αH is shown in Fig. 4.2 (1, 2 and 3). It shows the same form of variation, with the relative change of $U1_{max}$ decreasing as αH increases. The maximum bending moment and normal force in the wall panels represented by the parameter $U2_{max}$, varies linearly with αH as shown in Fig. 4.3 (1, 2 and 3) for the three forms of torsional loading.

4.4 DESIGN CHARTS

It was shown that the core behaviour depends on the core relative stiffness constant αH together with the end

condition parameters R and λ. Design charts drawn up using equations 4.2 (1, 2 and 3), for the variation of the non-dimensional parameters U, U1 and U2 with height ξ, are given in Appendix B.

These sets of graphs allow for a semigraphical evaluation of the angle of rotation and the internal forces of core structures for a range of values of αH between 1 and 6, of R between 0 and 10 and of λ between 0 and 2.5, which cover most of the significant range of practical values of the three variables.

1 - ANGLE OF ROTATION

The angle of rotation Θ_ξ at any level of the core may be evaluated by obtaining the value of U from the relevant chart at the desired level, then substituting into equation 4.2 (1, 2 or 3) according to the form of loading under consideration.

2 - SHEAR FLOW IN THE CONNECTING LAMINAE

The shear flow in the connecting lamina q_1 is a function of the first derivative of the angle of rotation Θ'. It may be calculated at any level by obtaining the corresponding value of U1 for the type of loading in question, then substituting into the appropriate formula from Chapter 2. The shear force in a particular beam can be evaluated by integrating the corresponding area under the curve.

3 - BENDING MOMENTS AND NORMAL FORCES IN THE WALL PANELS

The wall bending moments and normal forces are functions of the second derivative of the angle of rotation θ''. It may be evaluated by obtaining the relevant value of U2 for the type of loading under consideration at the required level and substituting into the appropriate formula from Chapter 2.

4.5 DISTRIBUTION OF THE INTERNAL FORCES THROUGHOUT THE CORE HEIGHT

The vertical distribution of the internal forces, namely, the connecting lamina shear and the bending moments and normal forces in the walls, depend on the form of the applied torque, the core stiffness constant αH and the end restraint parameters R and λ.

4.5.1 VERTICAL DISTRIBUTION OF THE SHEAR FLOW IN THE CONNECTING LAMINAE

The vertical distribution of the shear flow in the connecting laminae is given in Appendix B as a relationship between ξ and U1 for the standard load cases. The values of U1 are always positive throughout the core height. The position of the maximum value varies according to the form of loading and end conditions, and moves downwards as the values of R and λ increase.

4.5.2 VERTICAL DISTRIBUTION OF BENDING MOMENT AND NORMAL FORCE IN THE WALLS

The vertical distribution of the bending moment and normal force in the core walls is given in Appendix B as

a relationship between ξ and U2 for the standard load cases. The maximum values of U2 are always positive for structures fixed at the base and free at the top. As the values of R and λ increase, the negative values of U2 increase near or at the top until the maximum value of U2 will be negative.

4.6 INFLUENCE OF END RESTRAINT PARAMETERS R AND λ ON THE ELASTIC BEHAVIOUR OF CORE STRUCTURES

In order to investigate the effect of the end condition parameters R and λ on the elastic behaviour of core structures subjected to torsional loading, a numerical study was carried out on structures with stiffness values of αH between 1 and 6, top end restraint values of R between 0 and 40, and foundation flexibility factors λ between 0 and 4, subjected to each of the three standard load cases. The interaction effect of the above parameters on the maximum angle of rotation and internal forces are presented in three-dimensional plots.

4.6.1 INFLUENCE OF END RESTRAINTS ON THE MAXIMUM ANGLE OF ROTATION θ_{max}

The influence of the end factors R and λ on the maximum angle of rotation, which is proportional to, and may be represented by the non-dimensional parameter U_{max}, are illustrated in the three-dimensional plots of Figs. 4.4 4.5 and 4.6 for the three standard load cases respectively.

The Figures show that the effects of the end condition parameters R and λ on the maximum angle of

rotation decrease as αH increases, and the maximum rotation of the structure increase with an increase of the foundation flexibility factor λ. The increase in the core rotation may be partially restrained by providing a top end restraint, but the effect of the foundation flexibility parameter λ is more significant than R.

4.6.2 INFLUENCE OF END RESTRAINTS ON THE MAXIMUM VALUES OF LAMINAR SHEAR

The interaction effects of the end conditions parameters R and λ on the maximum values of laminar shear represented by the non-dimensional parameter $U1_{max}$ are shown in Figs. 4.7, 4.8 and 4.9 for the three standard load cases. They show that the maximum laminar shear increases as the foundation flexibility factor λ increases. The increase in U1 values may partially be controlled by increasing the top end restraint R, but the effect of both parameters λ and R is very limited for high values of αH.

4.6.3 INFLUENCE OF END RESTRAINTS ON THE BENDING MOMENTS AND NORMAL FORCES IN WALL PANELS

Figs. 4.10, 4.11 and 4.12 show the combined effect of the end condition parameters λ and R on the absolute maximum values of bending moments and normal forces represented by $U2_{max}$.

They indicate that, for a core structure erected on a fixed foundation, the values of maximum bending moment and normal force in the walls will always be positive and vary linearly with the value of αH. For structures based

on flexible foundations, the negative values of the bending and normal forces will increase and their positive values will decrease as λ increases, until they reach the same value. This is represented by the vertical discontinuity from the positive to the negative sides of the $U2_{max}$ axis. As λ values continue to increase the maximum bending moments and normal forces in the wall panels will be negative.

4.7 NUMERICAL EXAMPLE

In order to illustrate the influence of the significant parameters on the structural behaviour, the particular example of the twenty-storey core shown in Fig. (4.13) is employed. It is termed a Doubly-Symmetric core (D.S.) when provided with two sets of openings on opposite faces, and a Singly-Symmetric core (S.S.) when provided with one set of openings on the front face only. The basic dimensions are shown except for the depth of the connecting beams, the top stiffening beam depth and the foundation flexibility factor. These are given various values to study their numerical influence on the core under the three standard torsional load cases. The modulus of elasticity and Poisson's ratio for the core material are taken to be $E = 30\ kN/mm^2$ and $\gamma = 0.1$ respectively.

The effect of varying the depth d_c of the connecting beams, with the core fixed at the base and free at the top is shown in Table 4.1. The influence of a stiff top beam and the foundation flexibility factor λ are illustrated in Tables 4.2 and 4.3 respectively for a constant connecting

beam depth d_c of 0.5 m.

The results indicate that the core stiffness constant αH is a constant function of the connecting beam depth d_c to the power 1.5. The rotation of the doubly-symmetric core is almost twice as much as the rotation of the singly-symmetric core of the same dimensions and end conditions. The values of the maximum shear in the connecting lamina is slightly higher in the case of the singly-symmetric configuration.

Providing a stiff top beam to the structure reduces the rotation and the shear flow in the connecting beams, but it does not show a significant effect on the bending moments and normal forces in the wall panels.

The increase of the flexibility factor λ slightly increased the maximum angle of rotation and the maximum value of shear flow, but it did reduce the maximum bending moment and normal forces in the wall panels significantly.

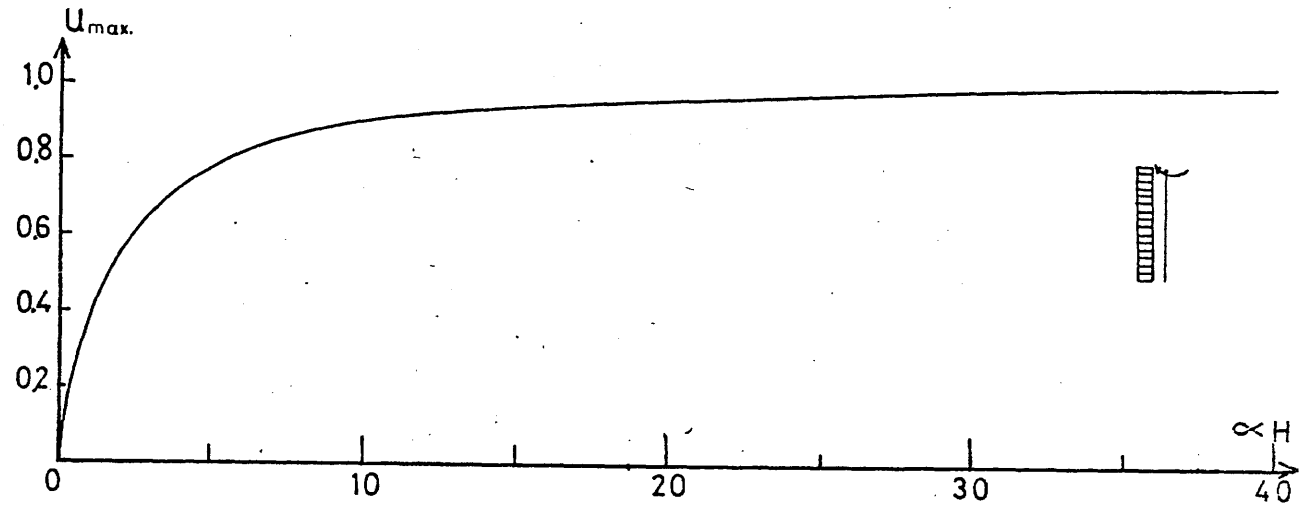

1 - Point torque at the top

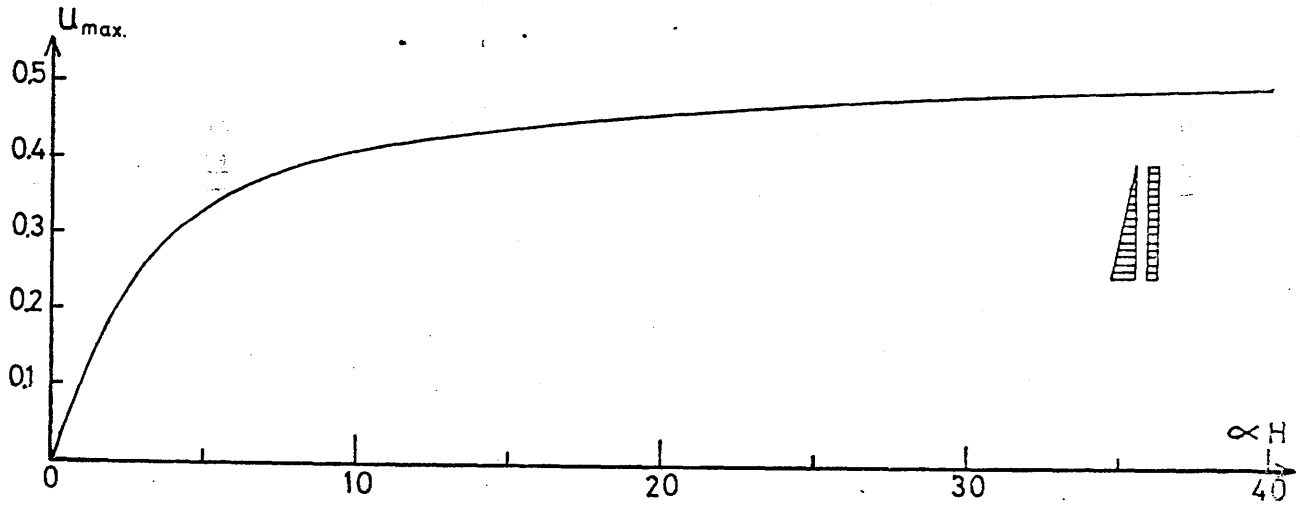

2 - Uniformly distributed torque

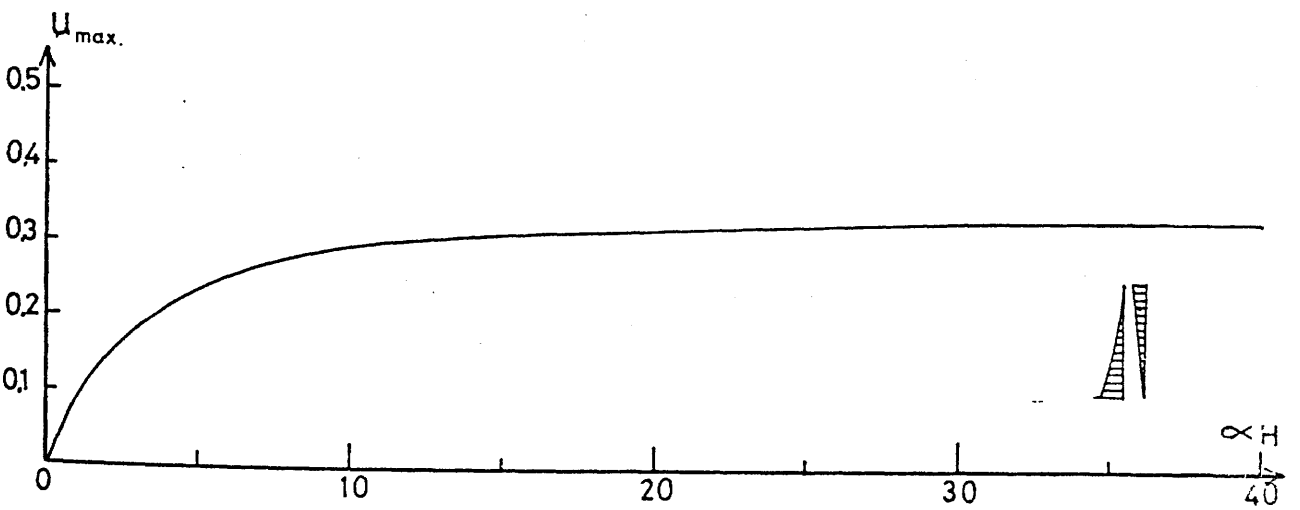

3 - Triangularly distributed torque

Fig. 4.1 Variation of parameter U_{max} with the stiffness factor αH

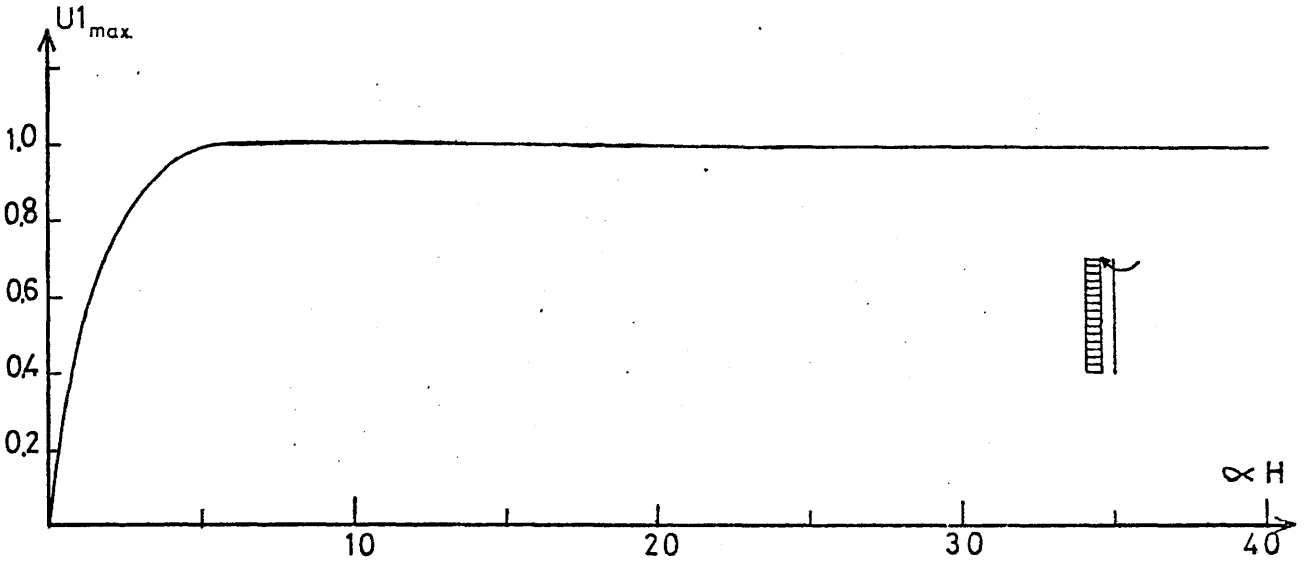

1 - Point torque at the top

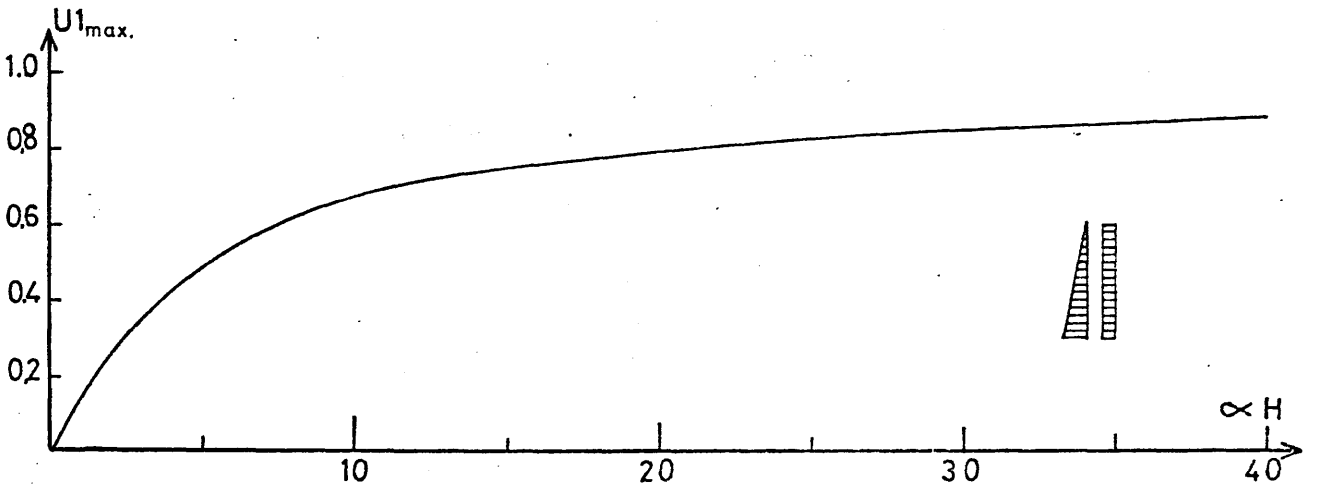

2 - Uniformly distributed torque

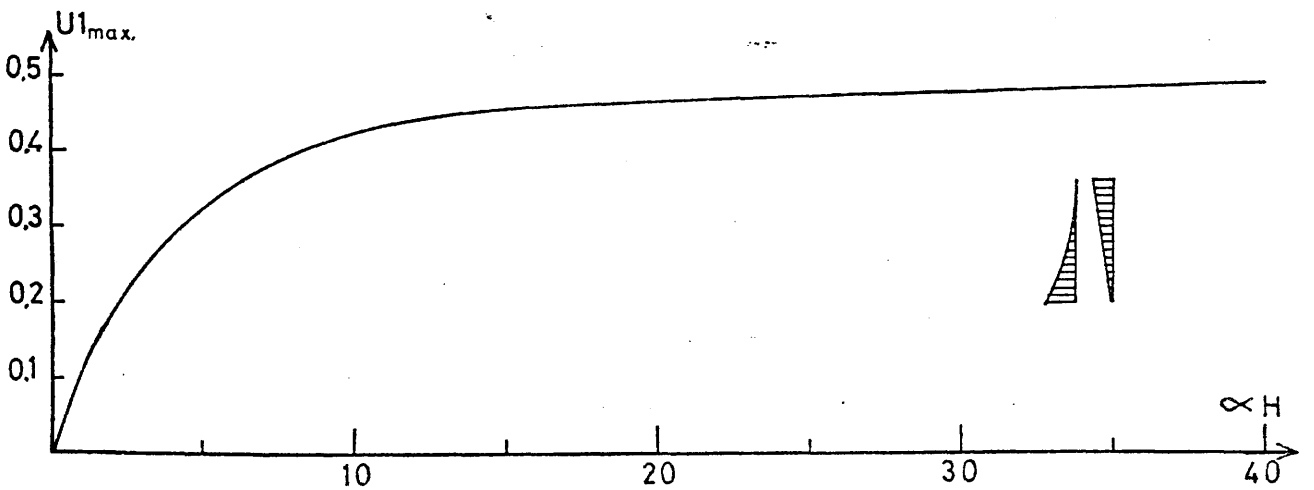

3 - Triangularly distributed torque

Fig. 4.2 Variation of parameter $U1_{max}$ with the stiffness factor αH

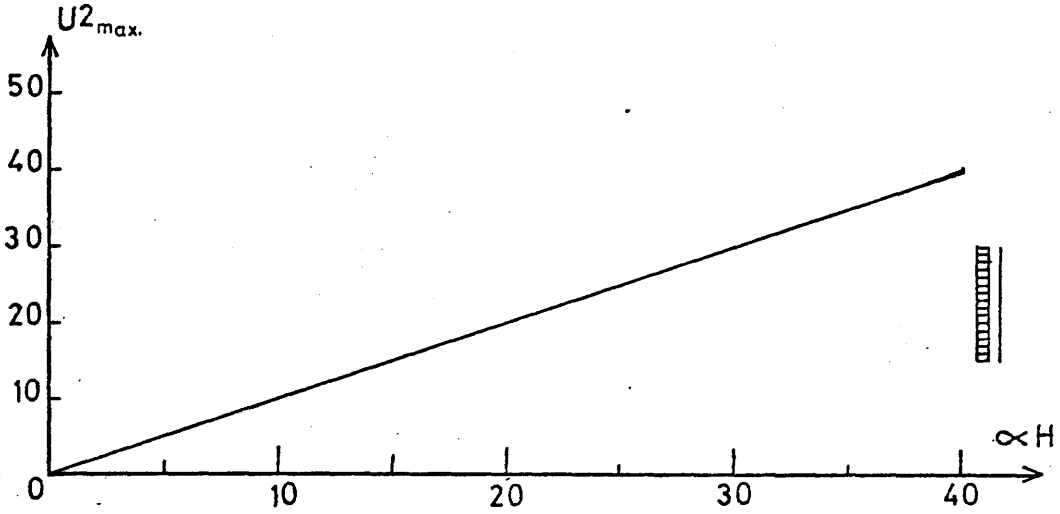

1 - Point torque at the top

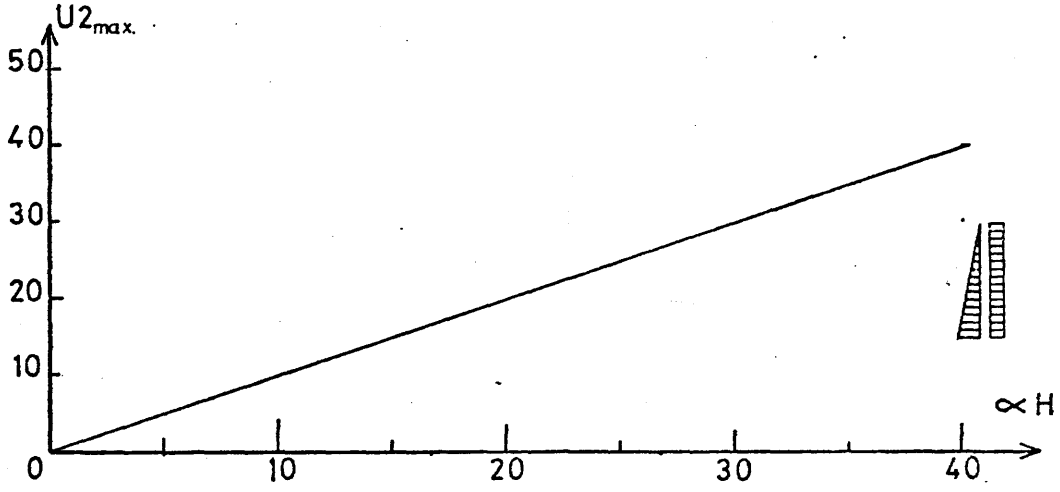

2 - Uniformly distributed torque

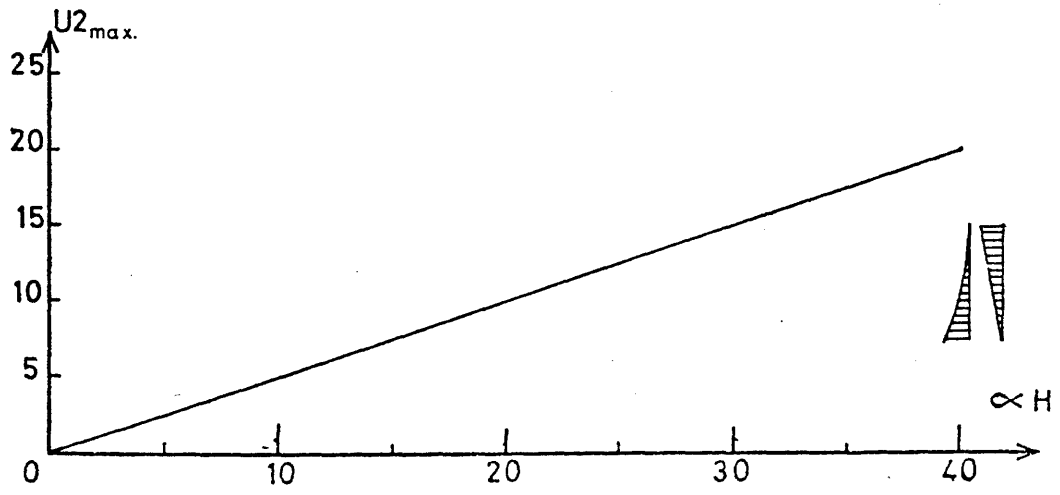

3 - Triangularly distributed torque

Fig. 4.3 Variation of parameter $U2_{max}$ with the stiffness factor αH

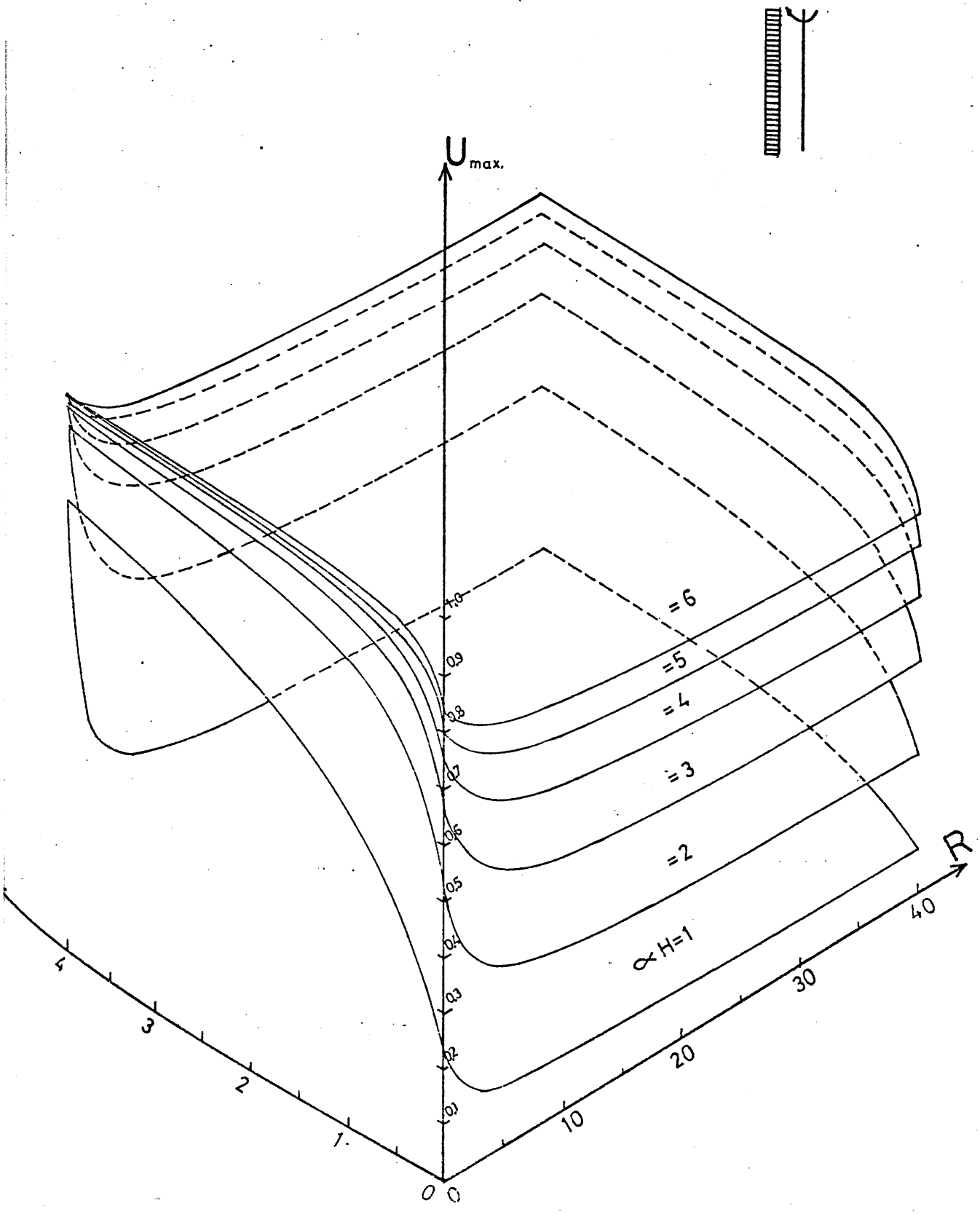

Fig. 4.4 Variation of parameter U_{max}, with top end restraint factor R and base flexibility factor λ for point torque at the top.

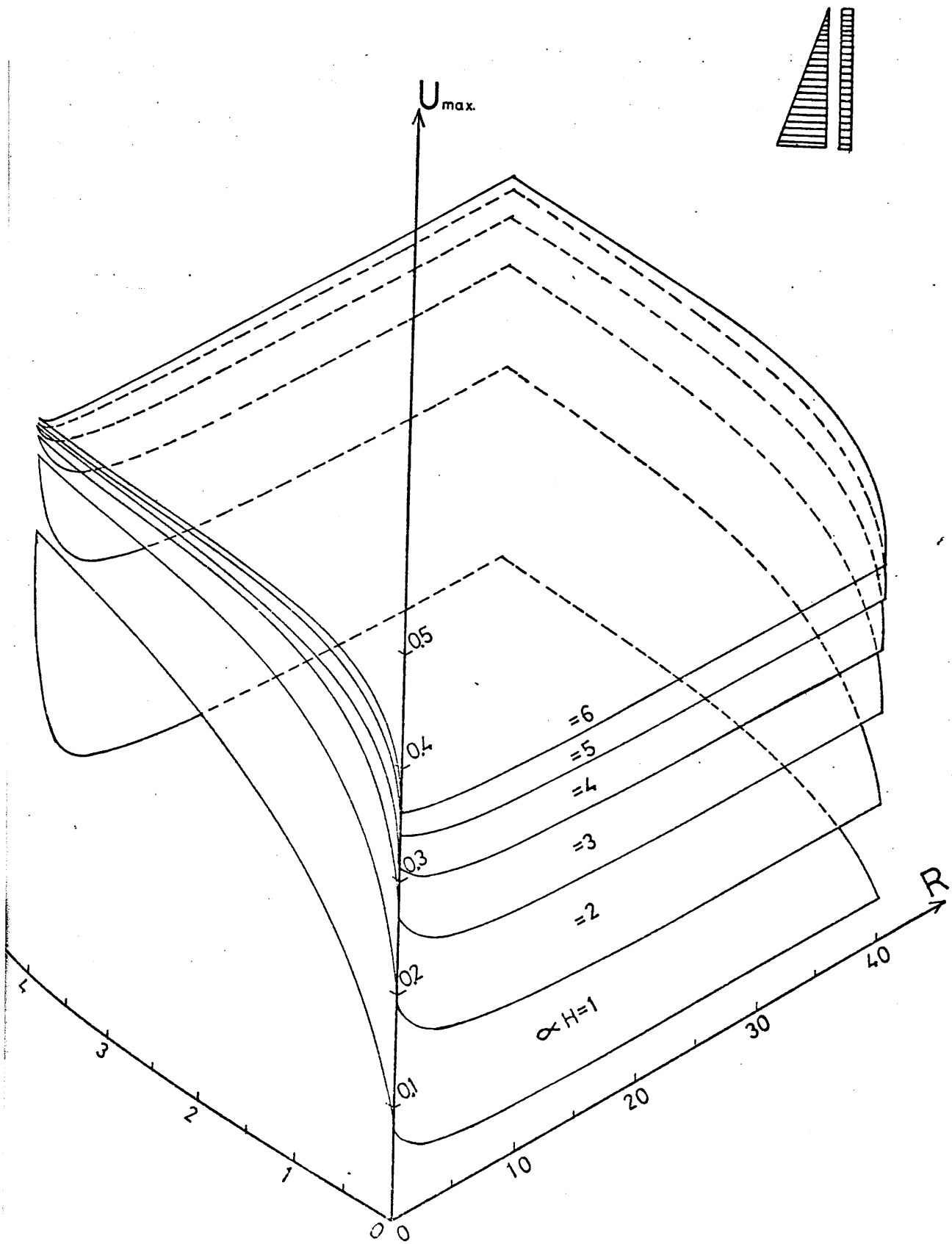

Fig. 4.5 Variation of parameter U_{max} with factors R and λ for uniformly distributed torque

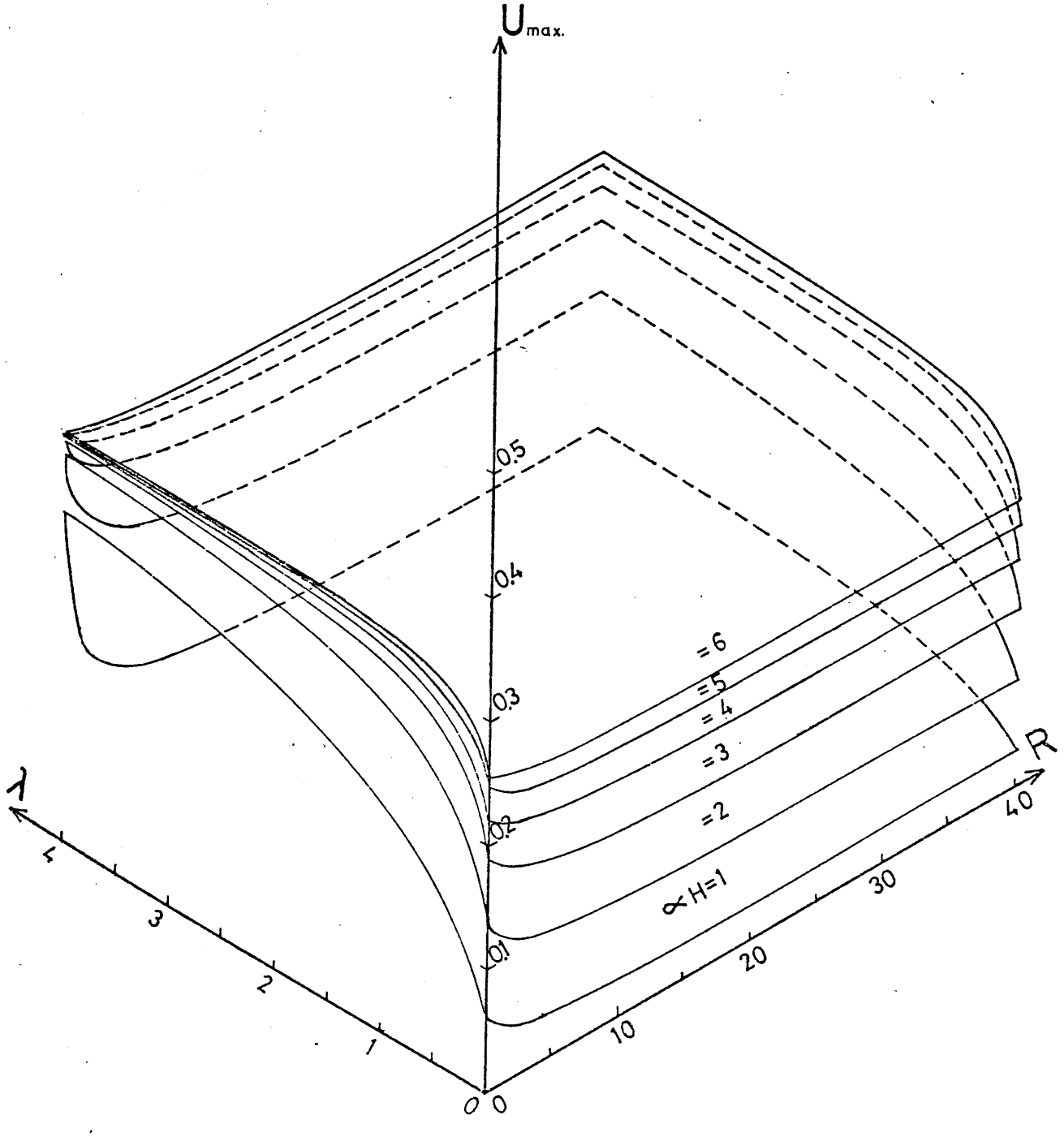

Fig. 4.6 Variation of parameter U_{max} with factors R and λ for triangularly distributed torque

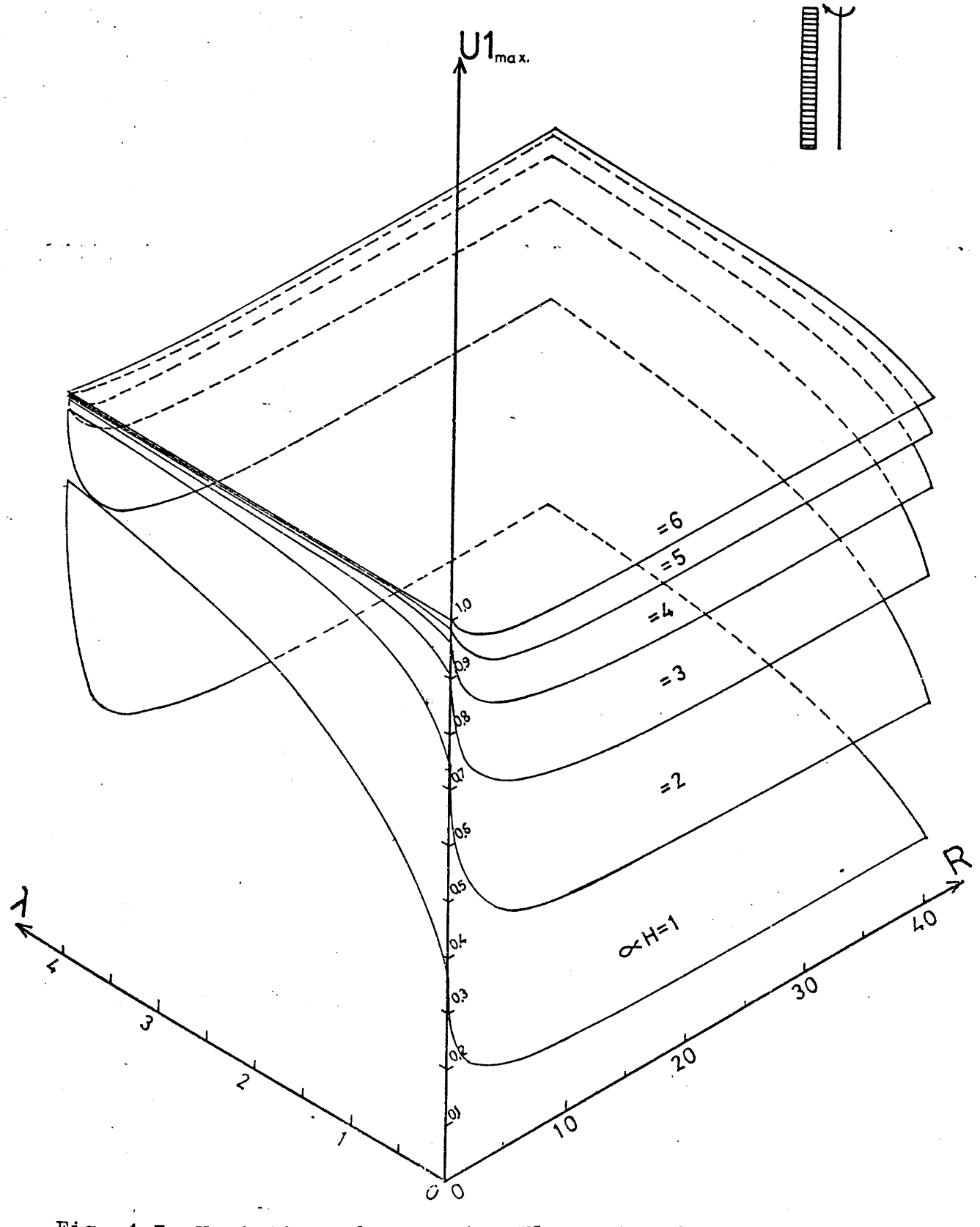

Fig. 4.7 Variation of parameter $U1_{max}$ with factors R and λ for point torque at the top

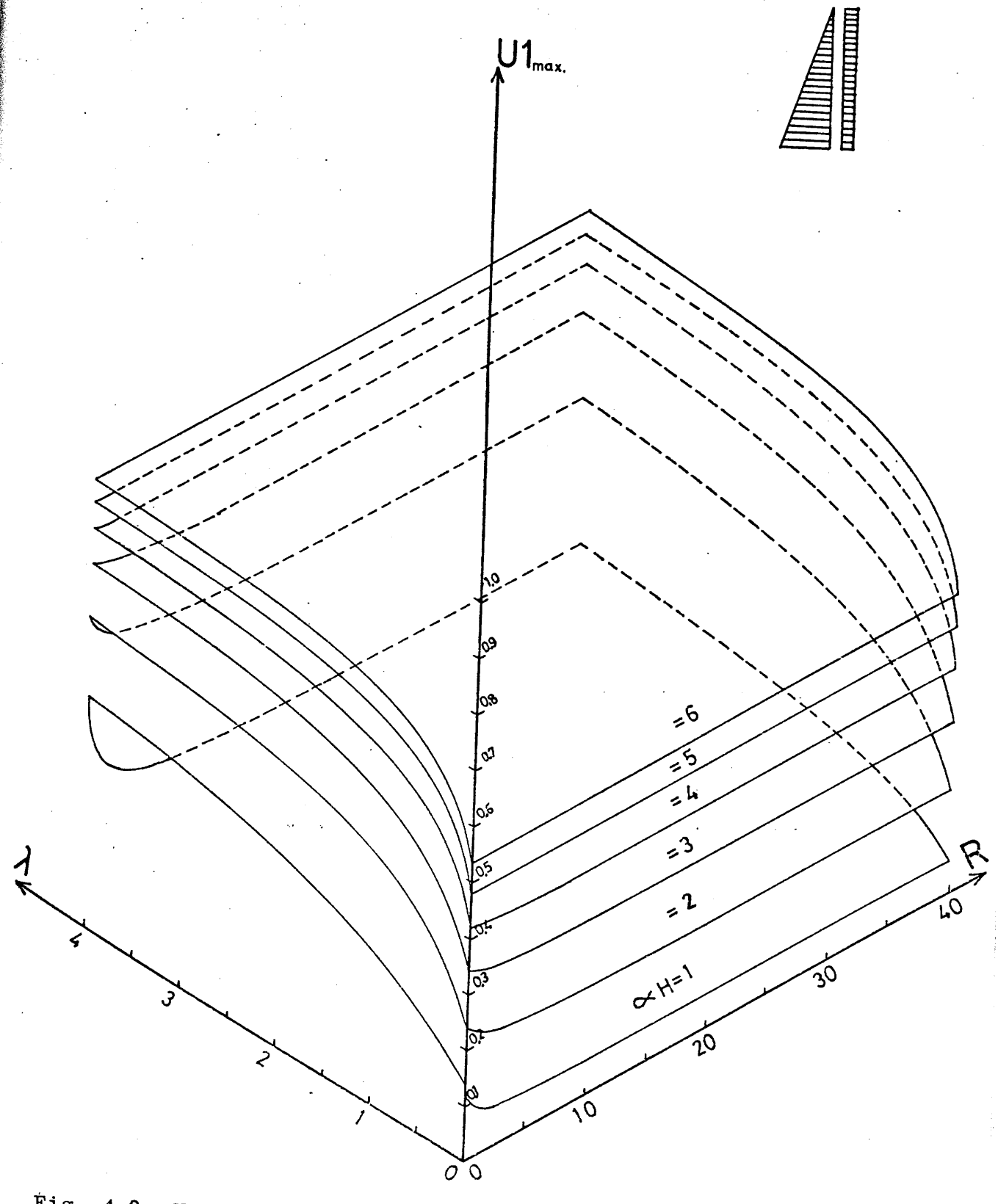

Fig. 4.8 Variation of parameter $U1_{max}$ with factors R and λ for uniformly distributed torque

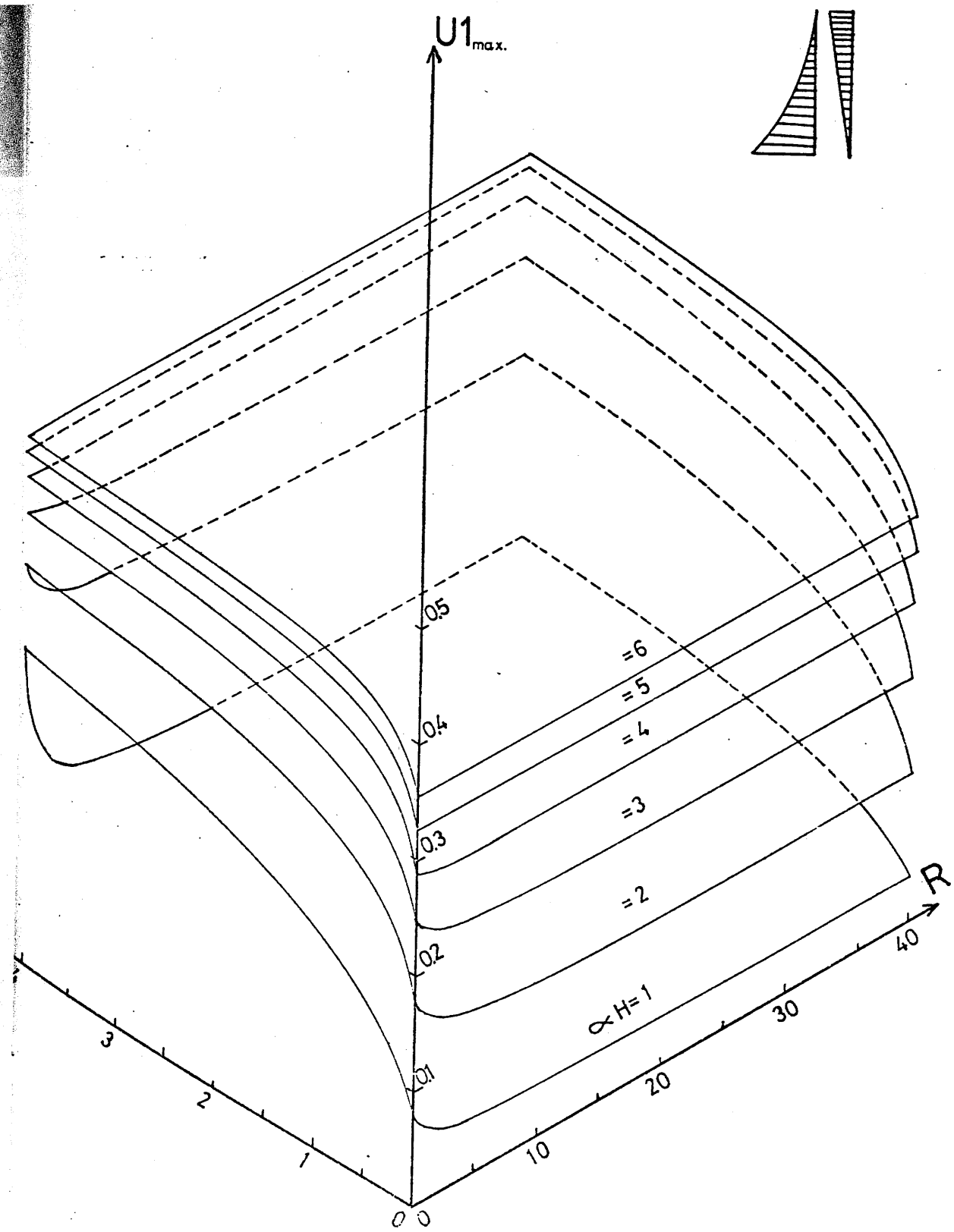

Fig. 4.9 Variation of parameter $U1_{max}$ with factors R and λ for triangularly distributed torque

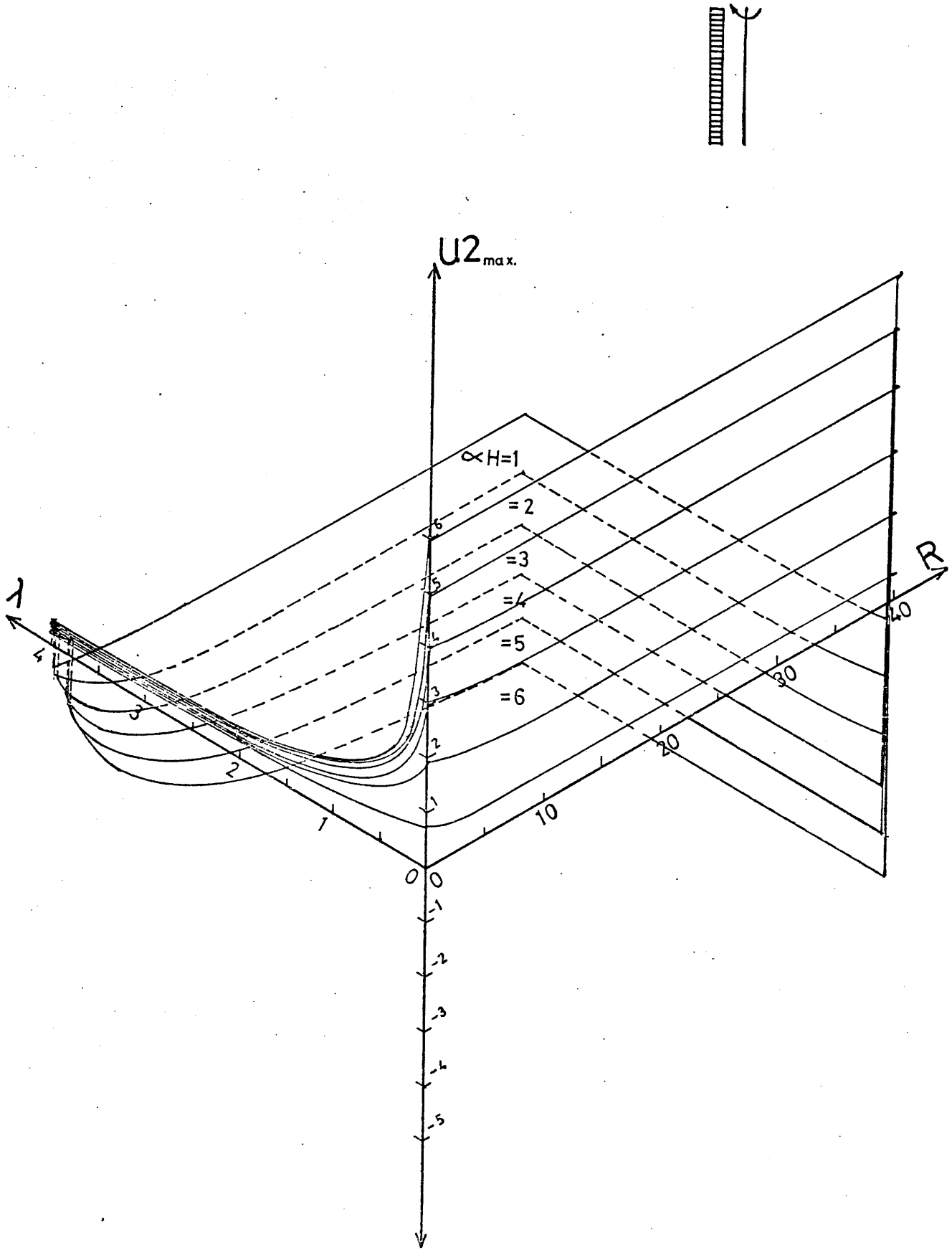

Fig. 4.10 Variation of parameter $U2_{max}$ with factors R and λ for point torque at the top.

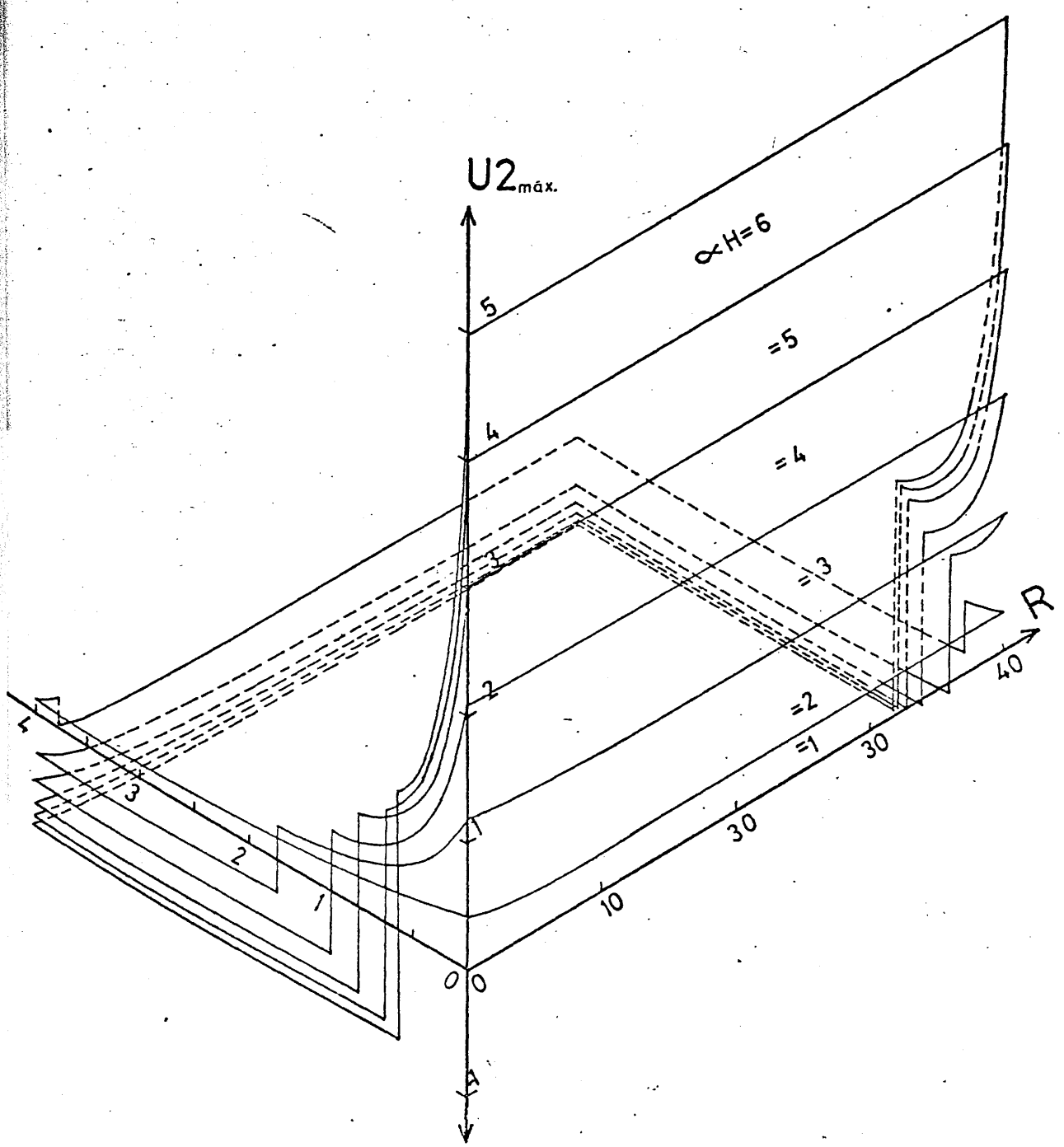

Fig. 4.11 Variation of parameter $U2_{max}$ with factors R and λ for uniformly distributed torque

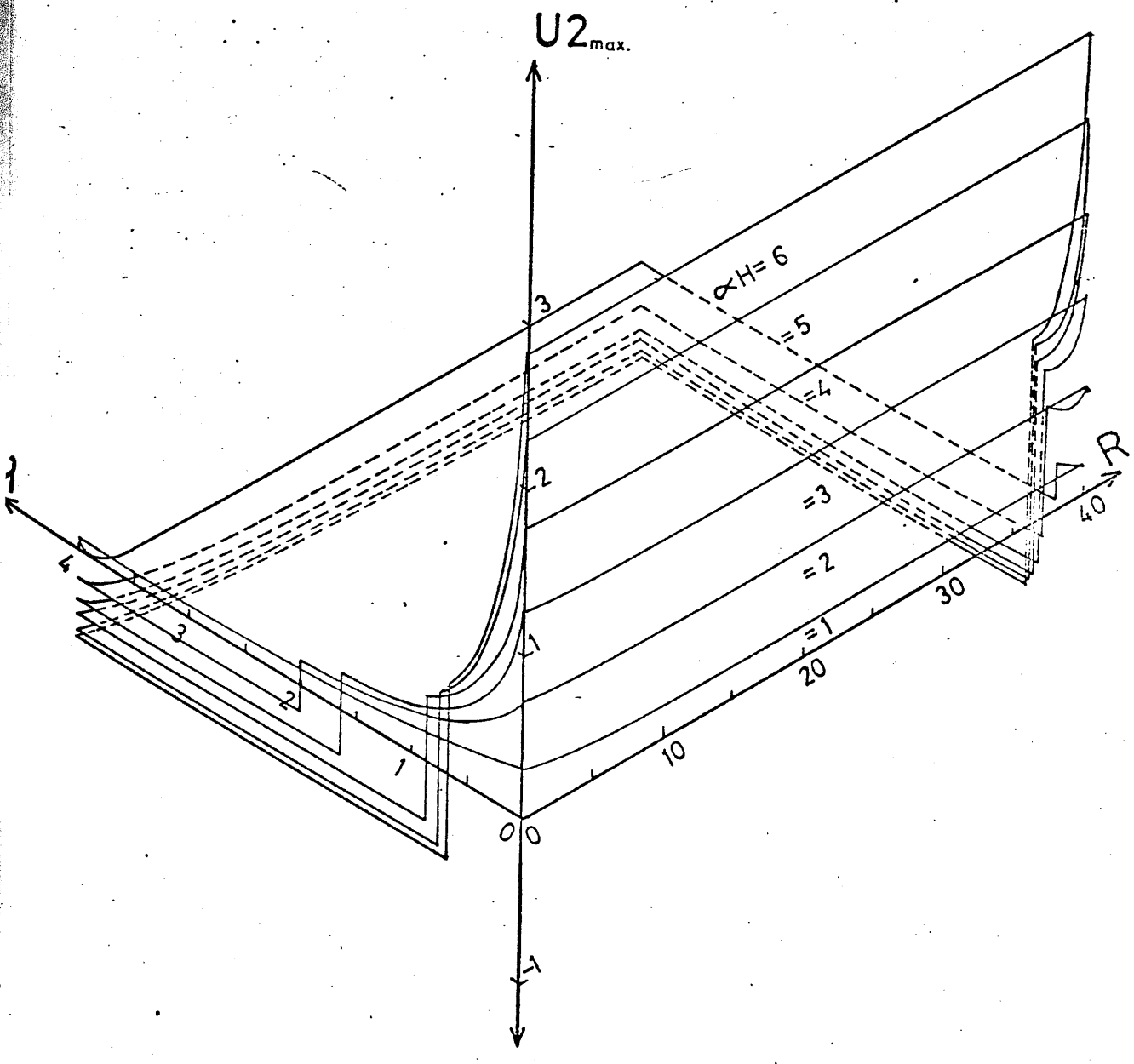

Fig. 4.12 Variation of parameter $U2_{max}$ with factors R and λ for triangularly distributed torque

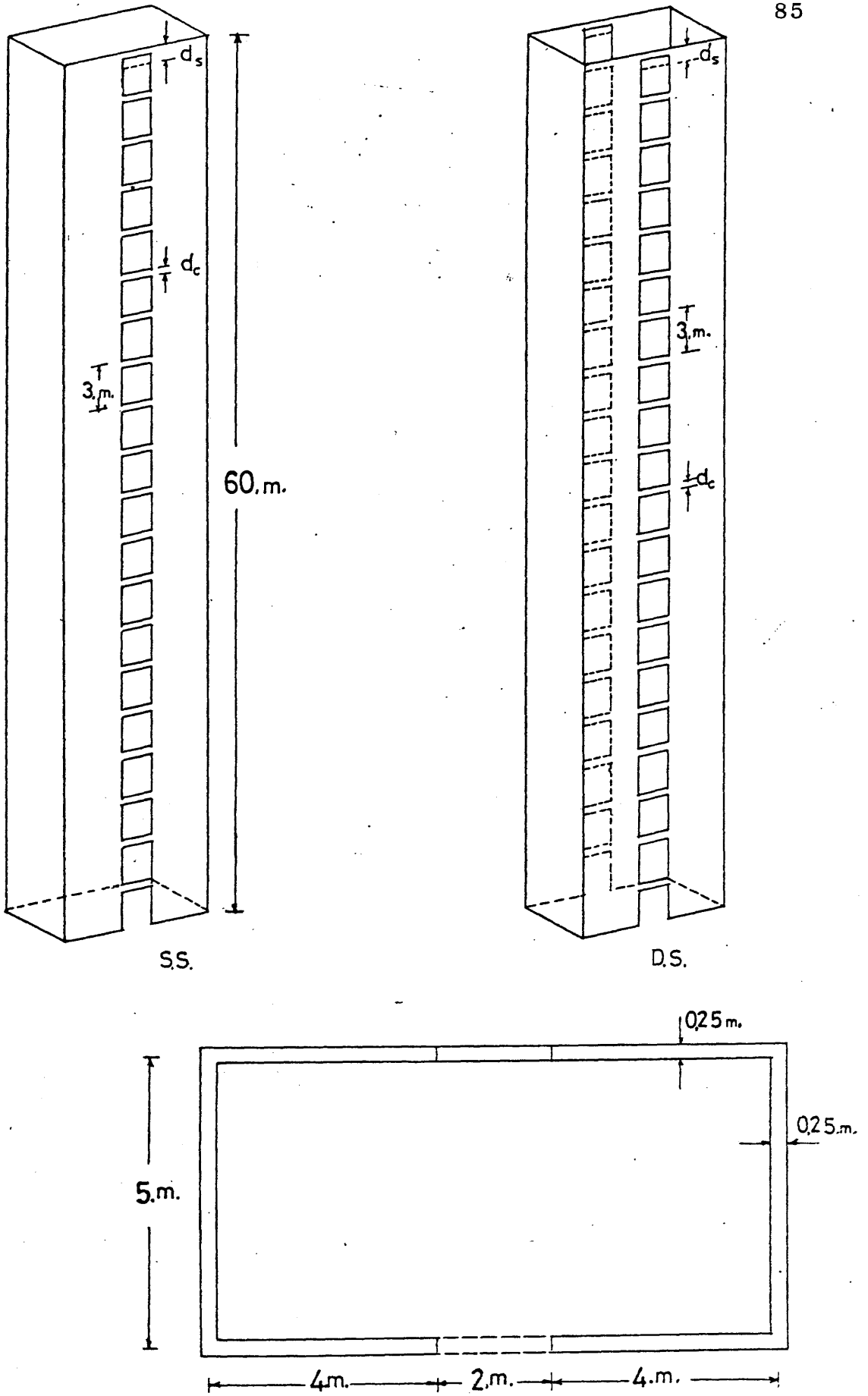

Fig. 4.13 Core structure used in numerical example

d_c mm	αH		θ_{max} 10^{-6} radian		q_{max} N/mm 10^{-3}		M_1 max 10^6 N.mm		M_2 max 10^6 N.mm		M_3 max 10^6 N.mm	N_1 max 10^3 N.m		N_2 max 10^3 N.
	D.S.	S.S.	D.S.	S.S.	D.S.	S.S.	D.S.	S.S.	D.S.	S.S.	S.S.	D.S.	S.S.	S.S.
Point torque at the top t = 10^6 N.mm.														
250	1.506	1.8204	0.9102	0.5653	-5.36	-6.576	-0.08665	-0.1902	0.3385	0.2213	-1.202	0.4549	0.4219	-0.0189
500	4.128	5.0604	0.2306	0.1226	-9.58	-9.823	-0.0348	-0.0721	0.1362	0.0839	-0.4556	0.1831	0.1599	-0.00719
750	7.56	9.282	0.0787	0.0405	-9.96	-9.983	-0.0190	-0.0393	0.0744	0.0457	-0.2484	0.1000	0.0872	-0.00392
1000	11.628	14.28	0.03506	0.01784	-9.98	-9.994	-0.01239	-0.0255	0.04839	0.0297	-0.1614	0.06504	0.0566	-0.00255
Uniformly distributed torque t = 1.0 K.N.mm./mm.														
250	1.506	1.8204	20.95	13.13	-104.9	-130.6	-3.00	-6.891	11.72	8.018	-43.53	15.75	15.28	-0.6877
500	4.128	5.0604	5.74	3.126	-255.0	-291.2	-1.60	-3.483	6.25	4.052	-22.00	8.409	7.724	-0.3475
750	7.56	9.282	2.098	1.101	-359.3	-390.6	-0.99	-2.105	3.87	2.45	-13.30	5.21	4.669	-0.2101
1000	11.628	14.28	0.969	0.5007	-421.2	-446.0	-0.679	-1.426	2.654	1.659	- 9.008	3.567	3.162	-0.142
Triangularly distributed torque t = 1.0 N.mm./mm.														
250	1.506	1.8204	916.3	572.8	-4701.0	-5807.0	-115.1	-260.9	449.5	303.5	-1648.0	604.2	578.6	-26.03
500	4.128	5.0604	246.0	133.0	-10550.0	-11810.0	- 56.39	-120.3	220.3	140.0	- 760.1	296.0	266.8	-12.01
750	7.56	9.282	88.06	45.92	-13970.0	-14860.0	- 33.11	- 69.15	129.3	80.45	- 436.8	173.8	153.4	- 6.90
1000	11.628	14.28	40.18	20.63	-15640.0	-16200.0	- 21.97	- 45.55	85.81	52.99	- 287.7	115.3	101.0	-4.545

Table 4.1 Effect of variation of depth of connecting beams on core actions

d_s mm	R		θ radian 10^{-6}		q_{max} 10^{-3} N/mm		M_1 max 10^6 N.mm		M_2 max 10^6 N.mm		M_3 max 10^6 N.mm	N_1 max 10^3 N		N_3 max 10^3 N
	D.S.	S.S.	D.S.	S.S.	D.S.	S.S.	D.S.	S.S.	D.S.	S.S.	S.S.	D.S.	S.S.	S.S.
Point torque at the top t = 10^6 N.mm.														
250.0	1.318	1.5708	0.2139	0.1157	-8.650	-9.173	-0.0346	-0.0719	0.1352	0.08366	-0.4542	0.1817	0.1595	-0.00717
500.0	10.548	12.564	0.1810	0.1016	-7.787	-8.617	-0.0340	-0.07147	0.1332	0.08315	-0.4515	0.1790	0.1585	-0.007132
750.0	35.598	42.408	0.1687	0.09632	-7.559	-8.459	-0.0339	-0.07131	0.1324	0.08297	-0.4505	0.1780	0.1581	-0.007116
1000.0	84.36	100.50	0.1648	0.09459	-7.487	-8.412	-0.0338	-0.07125	0.1322	0.08290	-0.4501	0.1776	0.1580	-0.007111
Uniformly distributed torque t = 1.0 K.N.mm/mm														
250.0	1.318	1.5708	5.528	3.048	-252.9	-290.4	-1.598	-3.480	6.243	4.049	-21.98	8.391	7.718	-0.3473
500.0	10.548	12.564	5.100	2.890	-249.1	-288.8	-1.592	-3.475	6.217	4.044	-21.95	8.355	7.708	-0.3468
750.0	35.598	42.408	4.940	2.831	-247.6	-288.2	-1.589	-3.474	6.207	4.041	-21.94	8.342	7.704	-0.3466
1000.0	84.36	100.50	4.888	2.811	-247.2	-288.0	-1.588	-3.473	6.204	4.041	-21.94	8.338	7.702	-0.3466
Triangularly distributed torque t = 1.0 N.mm./mm.														
250.0	1.318	1.5708	235.5	129.1	-10430.0	-11750.0	-56.22	-120.2	219.6	139.9	-759.3	295.2	266.6	-11.99
500.0	10.548	12.564	214.8	121.3	-10190.0	-11640.0	-55.90	-120.00	218.3	139.6	-757.8	293.5	266.0	-11.97
750.0	35.598	42.408	207.1	118.4	-10110.0	-11600.0	-55.77	-119.9	217.9	139.5	-757.2	292.8	265.8	-11.96
1000.0	84.36	100.50	204.6	117.4	-10080.0	-11590.0	-55.74	-119.8	217.7	139.4	-757.0	292.6	265.8	-11.96

Table 4.2 Effect of variation of depth of top stiffening beam on core actions

λ	θ 10^{-6} radian		q_{max} 10^{-3} N/mm		M_1 max 10^6 N.mm		M_2 max 10^6 N.mm		M_3 max 10^6 Nmm	N_1 max 10^3 N.		N_2 max 10^3 N.
	D.S.	S.S.	D.S.	S.S.	D.S.	S.S.	D.S.	S.S.	S.S.	D.S.	S.S.	S.S.
Point torque at the top t = 10^6 N.mm												
0.5	0.2803	0.1443	-9.802	-9.914	-0.0113	-0.02043	0.04448	0.02377	-0.1291	0.0597	0.04531	-0.00203
1.00	0.2899	0.1478	-9.844	-9.929	-0.0068	-0.0119	0.0265	0.01385	-00751	0.03572	0.02639	-0.00118
1.50	0.2941	0.1493	-9.862	-9.935	-0.0048	-0.00839	0.0189	0.00976	-0.0530	0.02547	0.01862	-0.00083
2.00	0.2964	0.1501	-9.872	-9.938	-0.0037	-0.00648	0.01473	0.00754	-0.0407	0.01979	0.01438	-0.00064
Uniformly distributed torque t = 1.0 K.N.mm/mm.												
0.5	8.025	4.172	-354.0	-390.4	-0.5229	-0.9866	2.043	1.148	-6.232	2.745	2.188	-0.0984
1.00	8.469	4.344	-386.3	-420.8	-0.3125	+0.6803	1.221	-0.7915	+4.297	1.641	-1.509	0.06788
1.50	8.659	4.415	-402.7	-434.8	+0.3553	0.6908	-1.388	-0.8037	4.364	-1.865	-1.532	0.06894
2.00	8.764	4.454	-412.8	-443.7	+0.3605	0.6970	-1.408	-0.8109	4.403	-1.893	-1.546	0.06955
Triangularly distributed torque t = 1.0 N.mm/mm.												
0.50	326.3	169.1	-13200.0	-14250.0	-18.41	-34.09	71.92	39.66	-215.3	96.66	75.59	-3.401
1.00	341.9	175.1	-14030.0	-14960.0	+11.98	+24.14	-46.80	-28.08	+152.5	-62.90	-53.53	+2.409
1.50	348.6	177.5	-14470.0	-15320.0	12.16	24.31	-47.51	-28.29	153.6	-63.85	-53.92	2.426
2.00	352.3	178.9	-14740.0	-15540.0	12.27	24.41	-47.91	-28.40	154.2	-64.40	-54.13	2.436

Table 4.3 Effect of foundation flexibility factor λ on core actions

CHAPTER 5

ELASTIC BEHAVIOUR OF CORE STRUCTURES WITH STIFFNESS VARIATIONS THROUGHOUT THE HEIGHT

CHAPTER 5

ELASTIC BEHAVIOUR OF CORE STRUCTURES WITH STIFFNESS VARIATIONS THROUGHOUT THE HEIGHT

5.1 INTRODUCTION

In modern multi-storey structures, the dimensions of the core may be changed at certain levels for economic or architectural reasons.

To simulate the problem, the core is assumed to maintain the same cross-sectional shape, but is composed of various zones of different properties. A theoretical analysis for core structures consisting of more than one zone of construction or loading properties, as shown in Fig. 5.1, is considered.

Numerical examples have been examined to demonstrate the effect of changing the wall thickness from one zone to another and the influence of the specific level at which the change occurs, when the core is subjected to any of the standard load cases and end conditions considered previously in Chapters 2 and 3. A comparison with the frame element method of analysis proposed by Macleod and Hosny (17) has been carried out to check the accuracy of the results.

5.2 TYPES OF CHANGE IN STRUCTURAL PROPERTIES

The different properties between one zone and another may take place as dimensional or material changes. The

most common forms of dimensional change are a reduction of the thickness of the walls either on one or both sides of the wall centre line as shown in Fig. 5.2 (II and III), or a reduction in the depth d_c of the connecting beams as in Fig. 5.2.IV; the change in the core material may be in the concrete strength or reinforcement or in the pre-stressing forces for structures built of prestressed concrete.

5.3 ANALYSIS OF CORE STRUCTURES CONSISTING OF VARIOUS ZONES

The general governing equation derived in Chapter 2 is applicable for each zone of a core structure consisting of different zones and subjected to torsional loading, namely

$$-EI_{wi} \frac{d^3\theta}{dx^3} + GJ_i \frac{d\theta}{dx} = t_{(xi)} \qquad 1 \leqslant i \leqslant n \qquad 5.3.1$$

where

i = the zone number

n = total number of zones

$t_{(xi)}$ = the twisting moment distribution in the particular zone.

Solving the above equation for each zone and using the compatibility and equilibrium conditions between each two adjacent zones, which are the angle of rotation θ, the slope θ' and the wall bending moment or normal forces, which must be equal for both zones at the line of discontinuity, a solution may be achieved.

A core structure consisting of 'n' zones, will involve 'n' third order differential governing equations and n-1 lines of discontinuity. An exact solution for such a system will yield 3n constants of integration K_{11} to K_{n3}. These may be evaluated by considering the available three boundary conditions, two at the base, one at the top, and the 3(n-1) compatibility and equilibrium conditions at each line of discontinuity.

The governing equation of zone i may be rewritten as

$$\frac{d^3\theta_i}{dx^3} - \alpha_i^2 \frac{d\theta_i}{dx} = - \frac{t_{(xi)}}{EI_{wi}} \qquad 5.3.2$$

with the solution given by,

$$\theta_i = K_{i1} + K_{i2} \cosh \alpha_i x + K_{i3} \sinh \alpha_i x + P_{(xi)} \qquad 5.3.3$$

the derivatives become

$$\theta_i' = \frac{d\theta_i}{dx} = \alpha_i K_{i2} \sinh \alpha_i x + \alpha_i K_{i3} \cosh \alpha_i x + P'_{(xi)}$$

$$\theta'' = \frac{d^2\theta_i}{dx^2} = \alpha_i^2 K_{i2} \cosh \alpha_i x + \alpha_i K_{i3} \sinh \alpha_i x + P''_{(xi)}$$

where

$\alpha_i^2 = \frac{GJ_i}{EI_{wi}}$, and K_{i1}, K_{i2} and K_{i3} are the general solution constants,

$P_{(xi)}$ is the particular solution and a prime denotes differentiation with respect to x.

A similar set of expressions may be obtained for each zone. The following boundary conditions apply:

At x = 0 $\qquad \theta_1 = 0$ and $\theta_1' = \mu\theta_1''$ $\qquad 5.3.4$

At the top $x = H$ $\quad \theta''_n = r\,\theta'_n$ 5.3.5

At the line of discontinuity between any two zones i and i + 1,

At $x = H_i$ $\quad \theta_i = \theta_{i+1}$, $\theta'_i = \theta'_{i+1}$ and $\theta''_i = v\theta''_{i+1}$ 5.3.6

where v is a discontinuity ratio between the two zones, which may be determined from the moment equilibrium conditions. Particular values are given later for specific situations.

Solving the above equations for the unknown constants of integration and substituting for their values in each zone will yield the angle of rotation and internal forces.

5.4 CORE STRUCTURES COMPOSED OF TWO ZONES OF DIFFERENT WALL THICKNESSES

For economic advantages, a reduction in the thickness of the walls with the height is the most common form of change in core structures. It may take the form of stepped changes with more than one line of discontinuity or only one step at height L as shown in Fig. 5.2.I.

A closed-form solution may be obtained for a core structure consisting of two zones of different wall thicknesses, subjected to any of the three standard load cases under consideration as follows:

5.4.1 POINT TORQUE AT THE TOP

For a core structure consisting of two zones and subjected to a concentrated torque at the top, the governing equation for each zone will be

$$- EI_{w1} \frac{d^3\theta_1}{dx^3} + GJ_1 \frac{d\theta_1}{dx} = t \qquad 0 \leqslant x \leqslant L$$

$$-EI_{w2} \frac{d^3\theta_2}{dx^3} + GJ_2 \frac{d\theta_2}{dx} = t \qquad L \leqslant x \leqslant H$$

And the solutions in terms of θ_1 and θ_2 are

$$\theta_1 = K_1 + K_2 \cosh \alpha_1 x + K_2 \sinh \alpha_1 x + \frac{tx}{GJ_1} \qquad 0 \leqslant x \leqslant L$$

$$\theta_2 = K_4 + K_5 \cosh \alpha_2 x + K_6 \sinh \alpha_2 x + \frac{tx}{GJ_2} \qquad L \leqslant x \leqslant H$$

where

$$\alpha_1^2 = \frac{GJ_1}{EI_{w1}} \quad \text{and} \quad \alpha_2^2 = \frac{GJ_2}{EI_{w2}}$$

From the boundary conditions, the constants of integration become

$$K_1 = - K_2$$

$$K_2 = SK_6 + \frac{t}{WGJ_1} \alpha_1 \sinh \alpha_1 L + \frac{vt}{GJ_2} \frac{\alpha_2 r \cosh \alpha_2 L}{W(\alpha_2 \cosh \alpha_2 H - r \sinh \alpha_2 H)}$$

$$K_3 = \alpha_1 \mu K_2 - \frac{t}{\alpha_1 GJ_1}$$

$$K_4 = K_1 + K_2 \cosh \alpha_1 L + K_3 \sinh \alpha_1 L + \frac{tL}{GJ_1} -$$

$$- [K_5 \cosh \alpha_2 L + K_6 \sinh \alpha_2 L + \frac{tL}{GJ_2}]$$

$$K_5 = K_6 \frac{(r \cosh \alpha_2 H - \alpha_2 \sinh \alpha_2 H)}{(\alpha_2 \cosh \alpha_2 H - r \sinh \alpha_2 H)} + \frac{t}{GJ_2}$$

$$\frac{r}{\alpha_2(\alpha_2 \cosh \alpha_2 H - r \sinh \alpha_2 H)}$$

$$K_6 = t[(\frac{\alpha_1}{W} \sinh \alpha_1 L - \frac{1}{Z}(\cosh \alpha_1 L - 1))/$$

$$GJ_1 + (\frac{V\alpha_2 r \cosh \alpha_2 L}{W(\alpha_2 \cosh \alpha_2 H - r \sinh \alpha_2 H)} -$$

$$\frac{1}{Z} (1 + \frac{r \sinh \alpha_2 L}{(\alpha_2 \cosh \alpha_2 H - r \sinh \alpha_2 H)}))/GJ_2]/(A - S)$$

where

$$v = t_2/t_1$$

$$W = \alpha_1^2(\cosh \alpha_1 L + \alpha_1 \mu \sinh \alpha_1 L)$$

$$S = \frac{v\alpha_2^2}{W} [\sinh \alpha_2 L + \frac{(r \cosh \alpha_2 H - \alpha_2 \sinh \alpha_2 H) \cosh \alpha_2 L}{(\alpha_2 \cosh \alpha_2 H - r \sinh \alpha_2 H)}]$$

$$Z = \alpha_1(\sinh \alpha_1 L + \alpha_1 \mu \cosh \alpha_1 L)$$

$$A = \frac{\alpha_2}{Z} [\cosh \alpha_2 L + \frac{(r \cosh \alpha_2 H - \alpha_2 \sinh \alpha_2 H)\sinh \alpha_2 L}{(\alpha_2 \cosh \alpha_2 H - r \sinh \alpha_2 H)}]$$

5.4.2 UNIFORMLY DISTRIBUTED TORQUE

The governing equations for the two zones of a core when subjected to a uniformly distributed torque of intensity t, may be written as follows

$$- EI_{w1} \frac{d^3\theta_1}{dx^3} + GJ_1 \frac{d\theta_1}{dx} = t(H - x) \qquad 0 \leqslant x \leqslant L$$

$$- EI_{w2} \frac{d^3\theta_2}{dx^3} + GJ_2 \frac{d\theta_2}{dx} = t(H - x) \qquad L \leqslant x \leqslant H$$

The solutions become

$$\theta_1 = K_1 + K_2 \cosh \alpha_1 x + K_3 \sinh \alpha_1 x + \frac{t}{GJ_1} [Hx - \frac{x^2}{2} - \frac{1}{\alpha_1^2}]$$

$$0 \leqslant x \leqslant L$$

$$\theta_2 = K_4 + K_5 \cosh \alpha_2 x + K_6 \sinh \alpha_2 x + \frac{t}{GJ_2} [Hx - \frac{x^2}{2} - \frac{1}{\alpha_2^2}]$$

$$L \leqslant x \leqslant H$$

where

$$K_1 = \frac{t}{\alpha_1^2 GJ_1} - K_2$$

$$K_2 = SK_6 + \frac{t}{WGJ_1}(1 + \alpha_1(\mu + H)\sinh \alpha_1 H) + \frac{tv}{WGJ_2}$$

$$(\frac{\alpha_2 \cosh \alpha_2 L}{\alpha_2 \cosh \alpha_2 H - r \sinh \alpha_2 H} - 1)$$

$$K_3 = \alpha_1 \mu K_2 - \frac{t}{\alpha_1 GJ_1}(\mu + H)$$

$$K_4 = K_1 + K_2 \cosh \alpha_1 L + K_3 \sinh \alpha_1 L + \frac{t}{GJ_1}(HL - \frac{L^2}{2} - \frac{1}{\alpha_1^2})$$

$$- [K_5 \cosh \alpha_2 L + K_6 \sinh \alpha_2 L +$$

$$\frac{t}{GJ_2}(HL - \frac{L^2}{2} - \frac{1}{\alpha_2^2})]$$

$$K_5 = K_6 \frac{(r \cosh \alpha_2 H - \alpha_2 \sinh \alpha_2 H)}{(\alpha_2 \cosh \alpha_2 H - r \sinh \alpha_2 H)} +$$

$$\frac{t}{GJ_2} \frac{1}{\alpha_2(\alpha_2 \cosh \alpha_2 H - r \sinh \alpha_2 H)}$$

$$K_6 = t[[(1 + \alpha_1(\mu + H)\sinh \alpha_1 L)/W + (H - L - (\mu + H)\cosh$$

$$\alpha_1 L)/Z]/GJ_1 +$$

$$[\frac{v}{W}(\frac{\alpha_2 \cosh \alpha_2 L}{\alpha_2 \cosh \alpha_2 H - r \sinh \alpha_2 H} - 1) -$$

$$(H - L + \frac{\sinh \alpha_2 L}{\alpha_2 \cosh \alpha_2 H - r \sinh \alpha_2 H})/Z]/GJ_2]/(A - S)$$

and α_1, α_2, A, S, V, W, and Z are as defined before.

5.4.3 TRIANGULARLY DISTRIBUTED TORQUE

In this case, the governing equations for the two zones are

$$- EI_{w1} \frac{d^3\theta_1}{dx^3} + GJ_1 \frac{d\theta_1}{dx} = \frac{t}{2} (H^2 - x^2) \qquad 0 \leqslant x \leqslant L$$

$$- EI_{w2} \frac{d^3\theta_2}{dx^3} + GJ_2 \frac{d\theta_2}{dx} = \frac{t}{2} (H^2 - x^2) \qquad L \leqslant x \leqslant H$$

And the solution may be expressed as

$$\theta_1 = K_1 + K_2 \cosh \alpha_1 x + K_3 \sinh \alpha_1 x + \frac{t}{2GJ_1} (H^2 x - \frac{x^3}{3} - \frac{2x}{\alpha_1^2}) \qquad 0 \leqslant x \leqslant L$$

$$\theta_2 = K_4 + K_5 \cosh \alpha_2 x + K_6 \sinh \alpha_2 x + \frac{t}{2GJ_2} (H^2 x - \frac{x^3}{3} - \frac{2x}{\alpha_1^2}) \qquad L \leqslant x \leqslant H$$

where

$$K_1 = -K_2$$

$$K_2 = SK_6 + \frac{t}{2GW} [(2L + \alpha_1 (H^2 - \frac{2}{\alpha_1}) \sinh \alpha_1 L) / J_1 + \frac{v}{J_2} (\frac{2\alpha_2 (H - \frac{r}{2}) \cosh \alpha_2 L}{(\alpha_2 \cosh \alpha_2 H - r \sinh \alpha_2 H)} - 2L)]$$

$$K_3 = \alpha_1 \mu K_2 + \frac{t}{2GJ_1 \alpha_1} (\frac{2}{\alpha_1^2} - H^2)$$

$$K_4 = K_1 + K_2 \cosh \alpha_1 L + K_3 \sinh \alpha_1 L + \frac{t}{2GJ_1}(H^3 L - \frac{L^3}{3} - \frac{2L}{\alpha_1^2})$$

$$- [K_5 \cosh \alpha_2 L + K_6 \sinh \alpha_2 L + \frac{t}{2GJ_2}(H^3 L - \frac{L^3}{3} - \frac{2L}{\alpha_2^2})]$$

$$K_5 = K_6 \frac{(r \cosh \alpha_2 H - \alpha_2 \sinh \alpha_2 H)}{(\alpha_2 \cosh \alpha_2 H - r \sinh \alpha_2 H)} + \frac{t}{GJ_2}$$

$$\frac{(H - \frac{r}{\alpha_2^2})}{\alpha_2(\alpha_2 \cosh \alpha_2 H - r \sinh \alpha_2 H)}$$

$$K_6 = \frac{t}{2G(A-S)} [[(2L + \alpha_1(H^2 - \frac{2}{\alpha_1^2}) \sinh \alpha_1 L)/W +$$

$$(H^2 - L^2 - \frac{2}{\alpha_1^2} - (H^2 - \frac{2}{\alpha_1^2}) \cosh \alpha_1 L)/Z]/J_1$$

$$+[\frac{v}{W}(\frac{2\alpha_2(H - \frac{r}{\alpha_2^2}) \cosh \alpha_2 L}{\alpha_2 \cosh \alpha_2 H - r \sinh \alpha_2 H} - 2L) -$$

$$-(H^2 - L^2 - \frac{2}{\alpha_2^2} + \frac{2(H - \frac{r}{\alpha_2^2}) \sinh \alpha_2 L}{\alpha_2 \cosh \alpha_2 H - r \sinh \alpha_2 H})/Z]/J_2$$

and α_1, α_2, A, S, v, W and Z are as defined before.

The corresponding internal forces may be evaluated from the appropriate equations from Chapter 2.

5.5 NUMERICAL EXAMPLE

A numerical study has been carried out on the particular core structure considered in Chapter 4. The core was assumed to consist of two zones of different

wall thicknesses and subjected to the magnitudes of the standard load cases and end condition considered previously. The effect of the type of change, size of change, level of change and the same end restraints on the actions of the doubly-symmetrical case subjected to a uniformly distributed torque are illustrated in this section. The effect of the above changes on the actions of the core structure when subjected to any of the standard load cases are given in Appendix C.

5.5.1 EFFECT OF TYPE OF CHANGE

The change in wall thickness may take any of the two forms described in section 5.2. If the change is assumed to occur on both sides of the centre line, there will be almost no difference between the values of α_1 and α_2 (section 5.3.1), as the corresponding wall thickness will appear in both numerator and denominator in each of them, provided that the St. Venant torsional constant is neglected as being very small.

If the reduction in the thickness of the walls takes place on one side of the centre line only, the core cross-section dimensions will change by $\frac{t_1-t_2}{2}$. In this case the effect on the value of α is very small as may be observed in Table 5.1, which shows the values of α obtained when reducing the wall thickness at one side of the wall centre line.

5.5.2 EFFECT OF SIZE OF CHANGE

The effect of a reduction in the wall thickness at mid-height is illustrated in Fig. 5.3 and Figs. C.1 to C.5, for a core structure free at the top and built in at the base.

It can be observed that the maximum angle of rotation increases as the thickness of the walls decreases. The shear flow in the connecting lamina suffers a sudden change at the line of discontinuity, its value increases rapidly and reaches the maximum just below the line of discontinuity, then drops sharply just above the line and increases gradually according to its original pattern. The ratio between the two values of the shear flow q_1 and q_2 below and above the line of discontinuity is

$$q_2 = v\, q_1$$

where v is the ratio between the thicknesses of the wall above and below the line t_2/t_1.

A redistribution of the internal forces will take place due to the sudden change in the shear in the connecting lamina. It will cause a discontinuity in the distribution of the bending moments and normal forces at the level of change.

5.5.3 EFFECT OF THE LEVEL OF CHANGE

A change in the thickness of the walls may take place at any level L of the height H. Its relative effect will remain the same as may be observed from Figs. 5.4 and

C.6 to C.10, which show the core actions under the same loads and end conditions, while reducing the thickness by 50% at L/H values of 0.25, 0.5, 0.75 and 1.0. The maximum angle of rotation increases as the line of discontinuity moves downward. The shear flow in the connecting lamina will undergo the same type of discontinuous behaviour with a constant ratio between its values below and above the level of change, and the bending moment will vary accordingly.

5.5.4 EFFECT OF END RESTRAINTS

It may be perceived that the core will suffer a similar effect due to a reduction in the thickness of the walls by 50% at mid-height, compared to its original pattern of behaviour, while it is subjected to top end restraint as shown in Figs. 5.5 and C.11 to C.15, or if it is supported on flexible foundations in Figs. 5.6 and C.16 to C.20.

5.6 COMPARISON OF RESULTS WITH FRAME IDEALISATION

In order to check the accuracy of the results obtained using the proposed method, the same examples were reanalysed using the frame element method proposed by Macleod and Hosny (17).

In the frame method of analysis, walls and connecting beams are idealised by a series of line elements with stiffnesses in the plane of the walls and no stiffness out of plane. The elements are connected together by nodes at the corners at each storey level. The same

degrees of freedom are assumed for the same nodes, and a stiff diaphragm joining the nodes at each storey level resists any distortion in cross-sectional shape.

The analysis of the above example when subjected to a uniformly distributed torque was carried out using a standard GENESYS program in Paisley College of Technology. Since in-plane shearing deformations were omitted in the present method, these were also neglected in the formulation for the analysis by the frame analogy.

The results are shown in Figs. 5.8 and 5.7 for singly- and doubly-symmetrical cases respectively. The curves indicate a close agreement between the results obtained from both methods in calculating the angle of rotation Θ and the vertical shear in the connecting beams. However, there were considerable differences in a comparison between the bending moments and normal forces in the wall panels. It was claimed (29) that the accuracy of the results can be improved by increasing the number of nodes for each storey level, because in the frame element method, the walls are connected only at discrete points on each storey level and not connected continuously as in the actual structure. Another run was carried out after doubling the number of nodes, but the results did not improve. It appears possible that the frame analogy does not model accurately the true behaviour of the core.

5.7 DISCUSSION

The above example demonstrates that reducing the thickness of the core walls will significantly increase

the vertical shear force in the connecting beams below the line of discontinuity. This effect is most undesirable as the connecting beams are the weakest element of the core.

The actual reason for the discontinuity is the reduction in the connecting beam stiffness factor β. Another change needs to be carried out to achieve the economical advantage of reducing the amount of material to be used and maintain the original distributions of the internal forces throughout the core. The depth of the connecting beams above the line of discontinuity should be increased so that the connecting beams stiffness factor β will be constant throughout the core height. This will result in increasing the stresses in the walls rather than the beams.

t_2 mm.	250	200	150	100	50
$v = t_2/t_1$	1	0.8	0.6	0.4	0.2
α_2 Doubly-Symmetric	0.6879	0.6897	0.6945	0.7027	0.7145
α_2 Singly-Symmetric	0.8433	0.8468	0.8546	0.8671	0.8848

$t_1 = 250$ mm.

Table 5.1 Variation of the value of α with thickness of the walls.

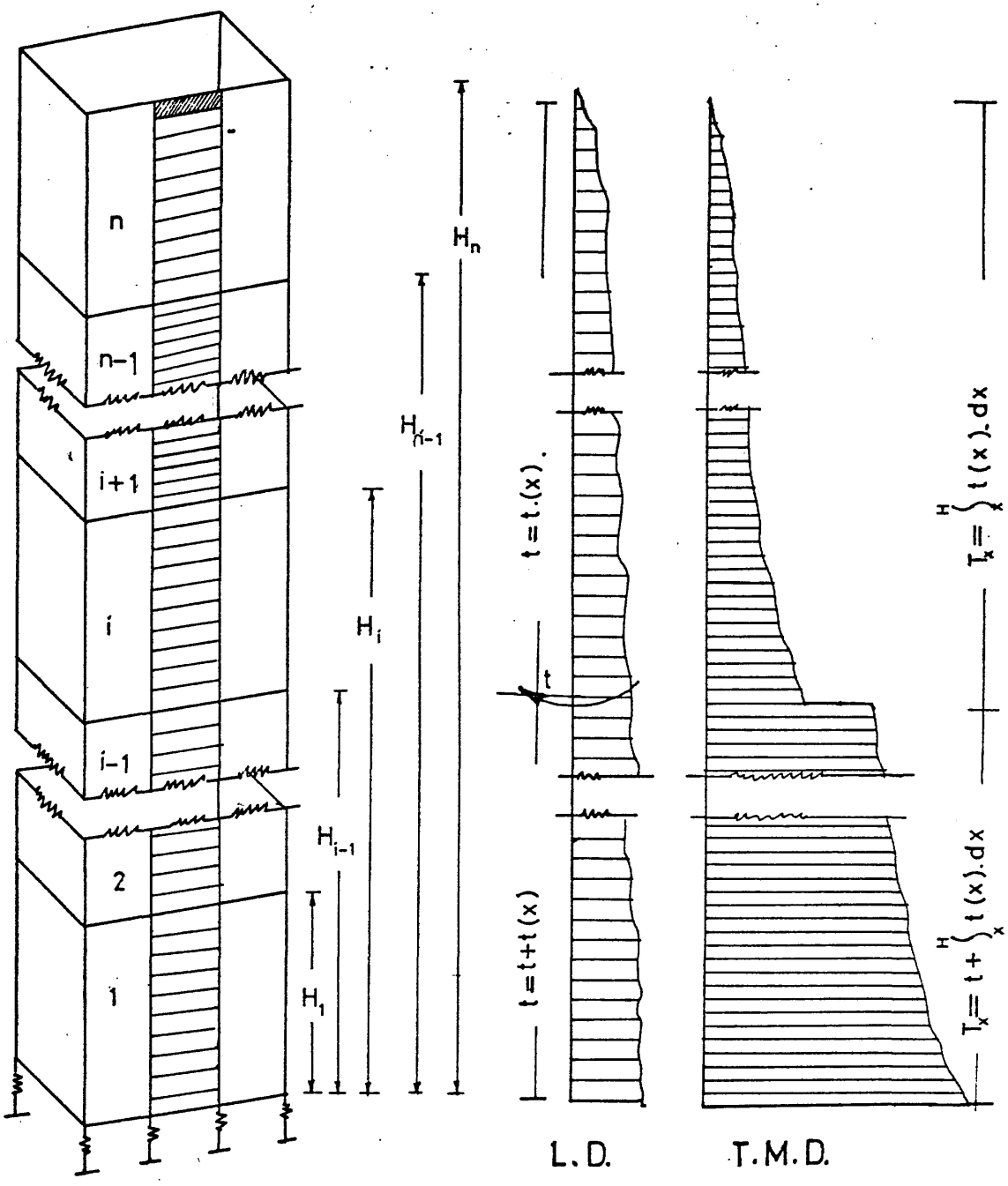

Fig. 5.1 Core structure composed of zones with different properties

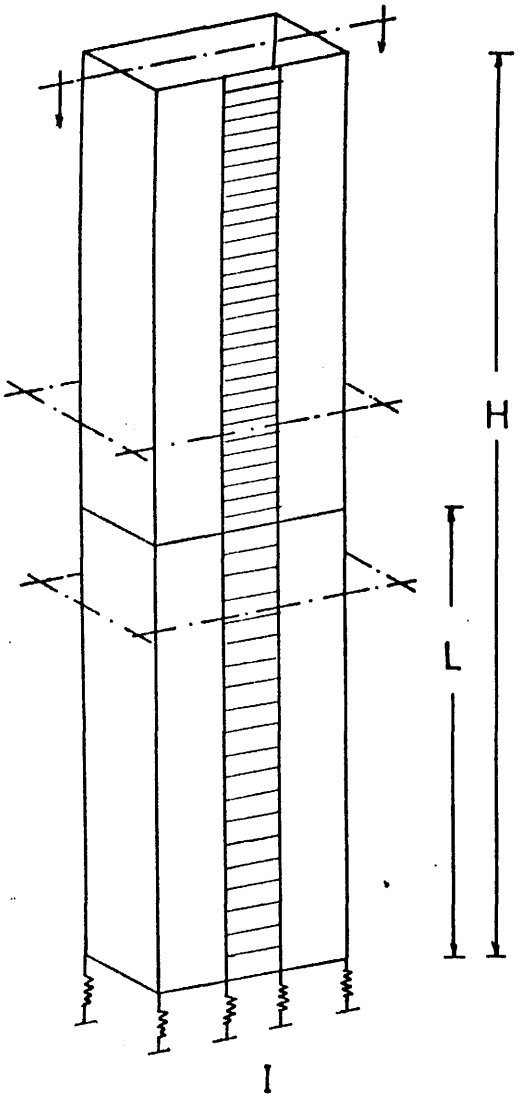

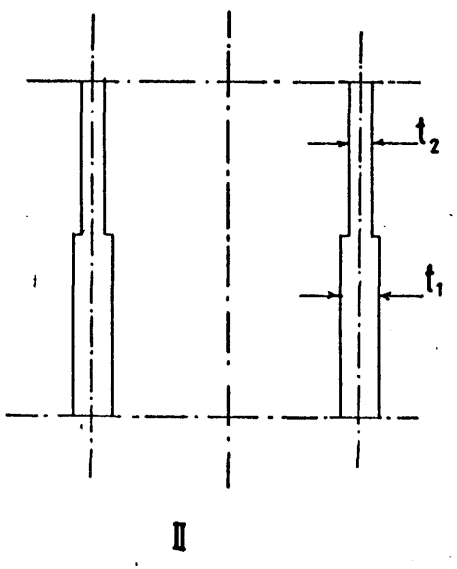

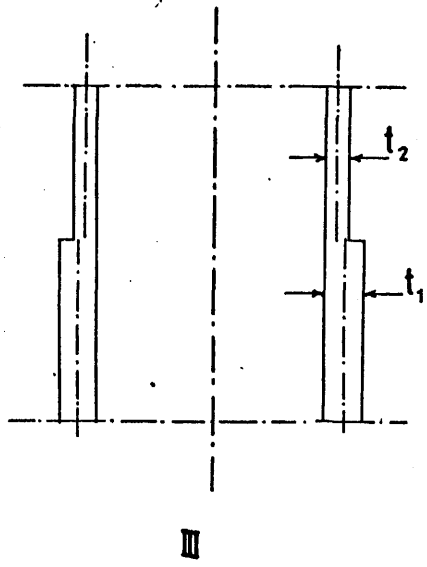

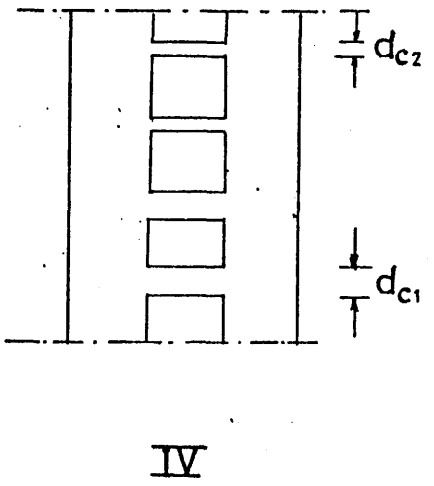

Fig. 5.2 Forms of dimensional changes between two successivw zones.

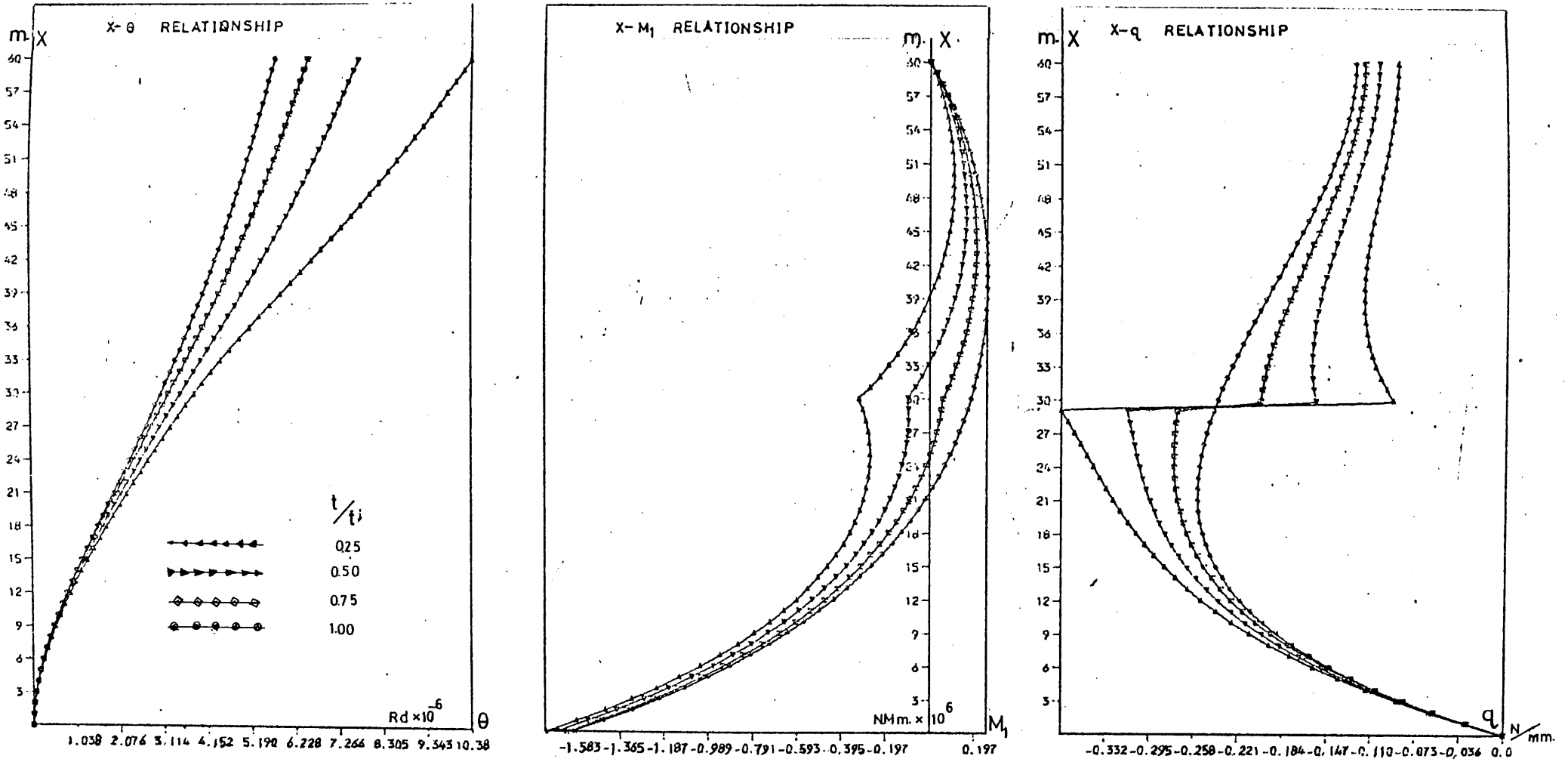

Fig. 5.3 Effect of reduction in wall thickness on primary core actions (Doubly-Symmetric, Uniformly Distributed Torque)

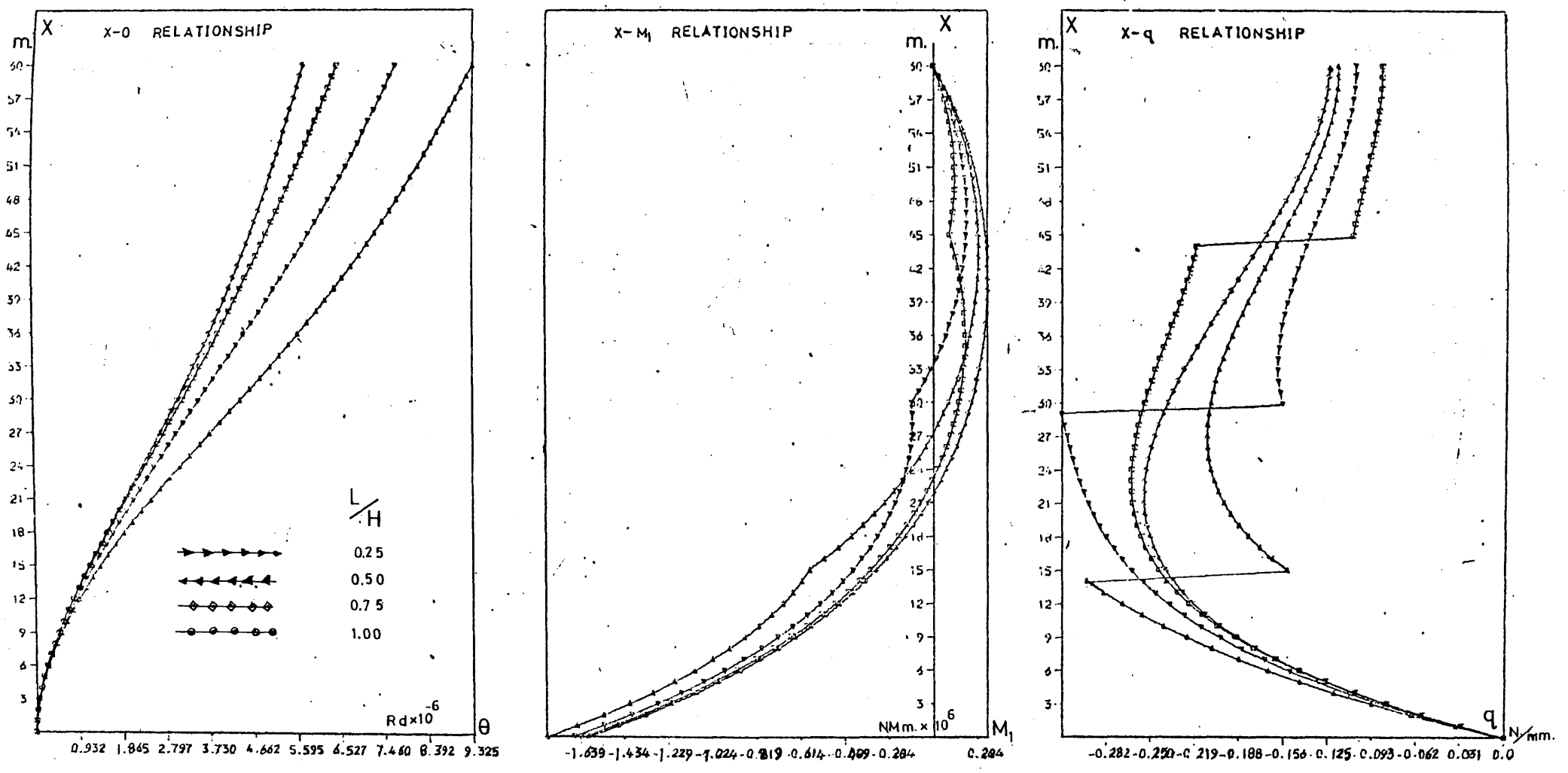

Fig. 5.4 Effect of level at which reduction in wall thickness occurs in primary core actions. (Doubly-Symmetric - Uniformly Distributed Torque)

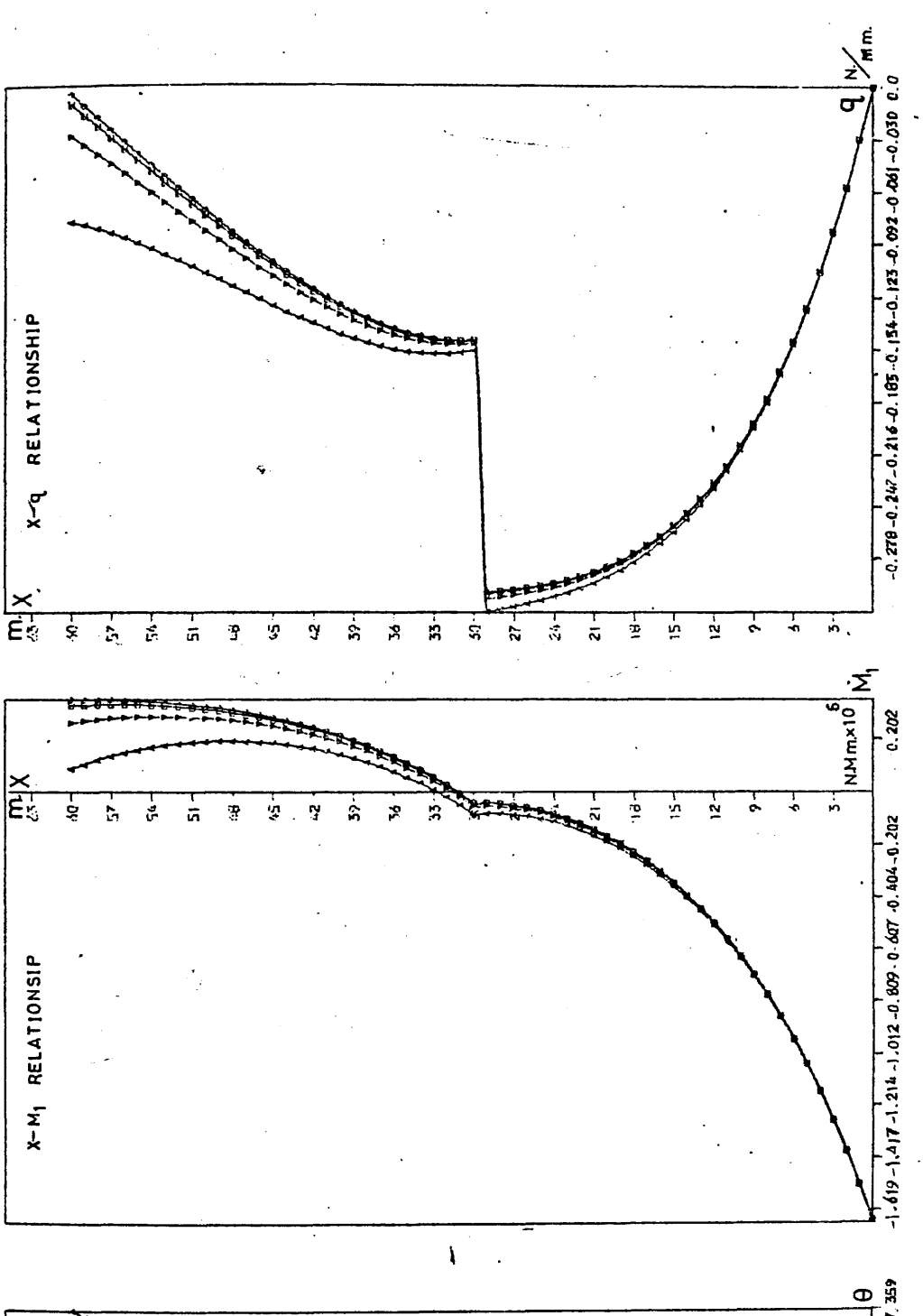

Fig. 5.5 Effect of reduction in wall thickness at mid-height on primary actions of stiffened cores. (Doubly-Symmetric, Uniformly Distributed Torque)

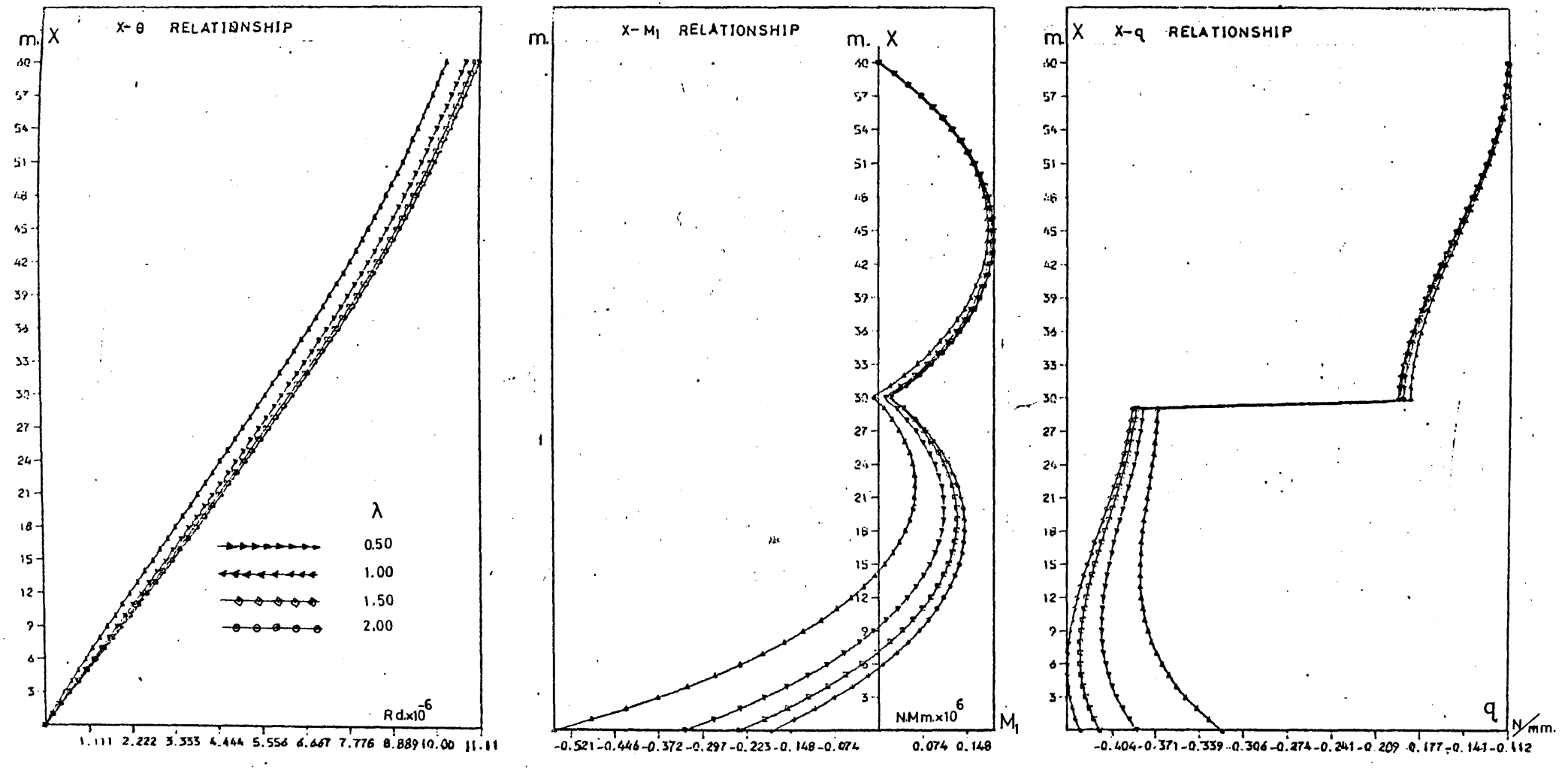

Fig. 5.6 Effect of reduction in wall thickness at mid-height on primary actions in elastically supported core. (Doubly-Symmetric, Uniformly Distributed Torque)

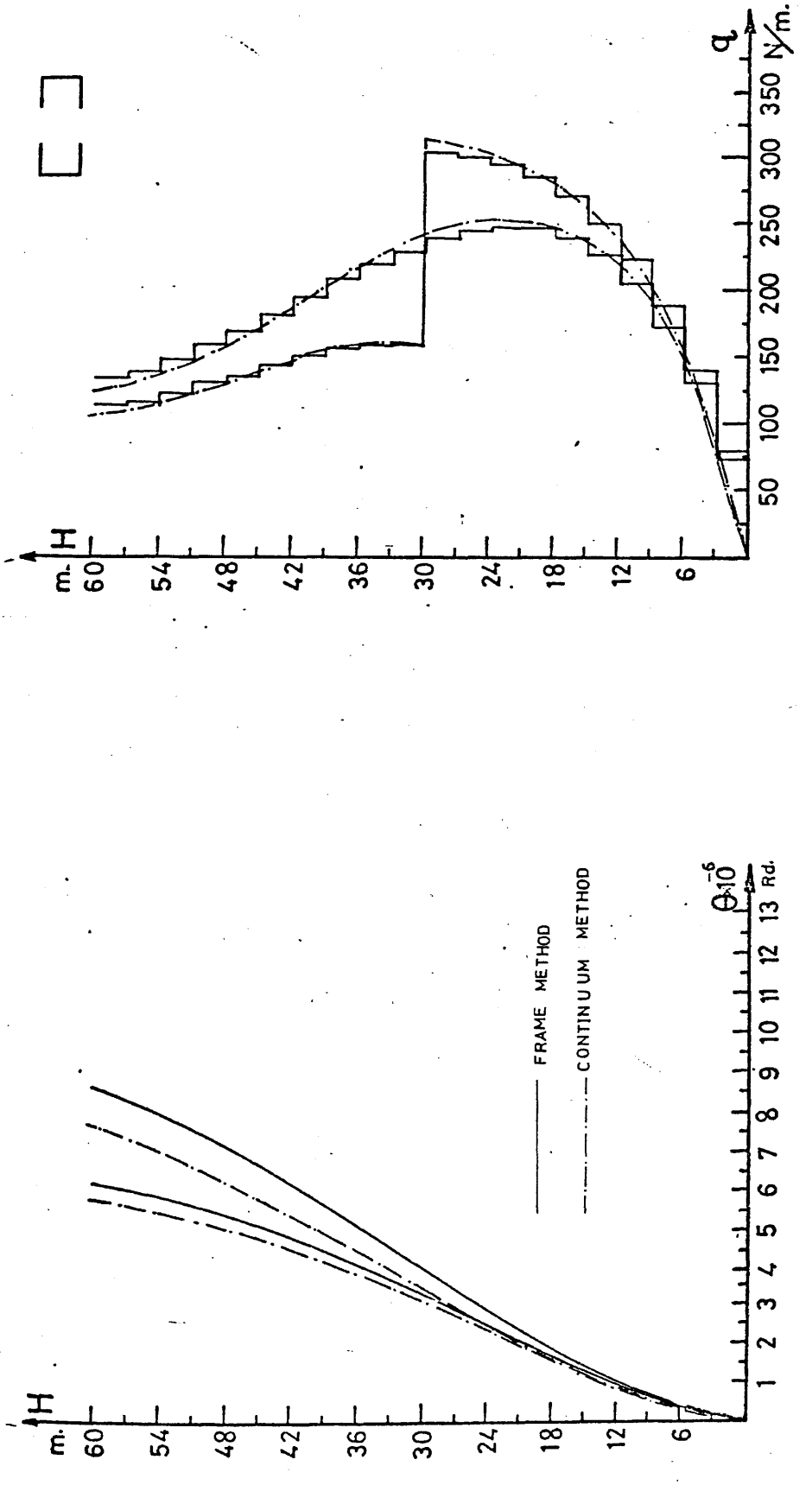

Fig. 5.7 Comparison between present theory and results obtained from frame idealisation model. (Doubly-Symmetric, Uniformly Distributed Torque)

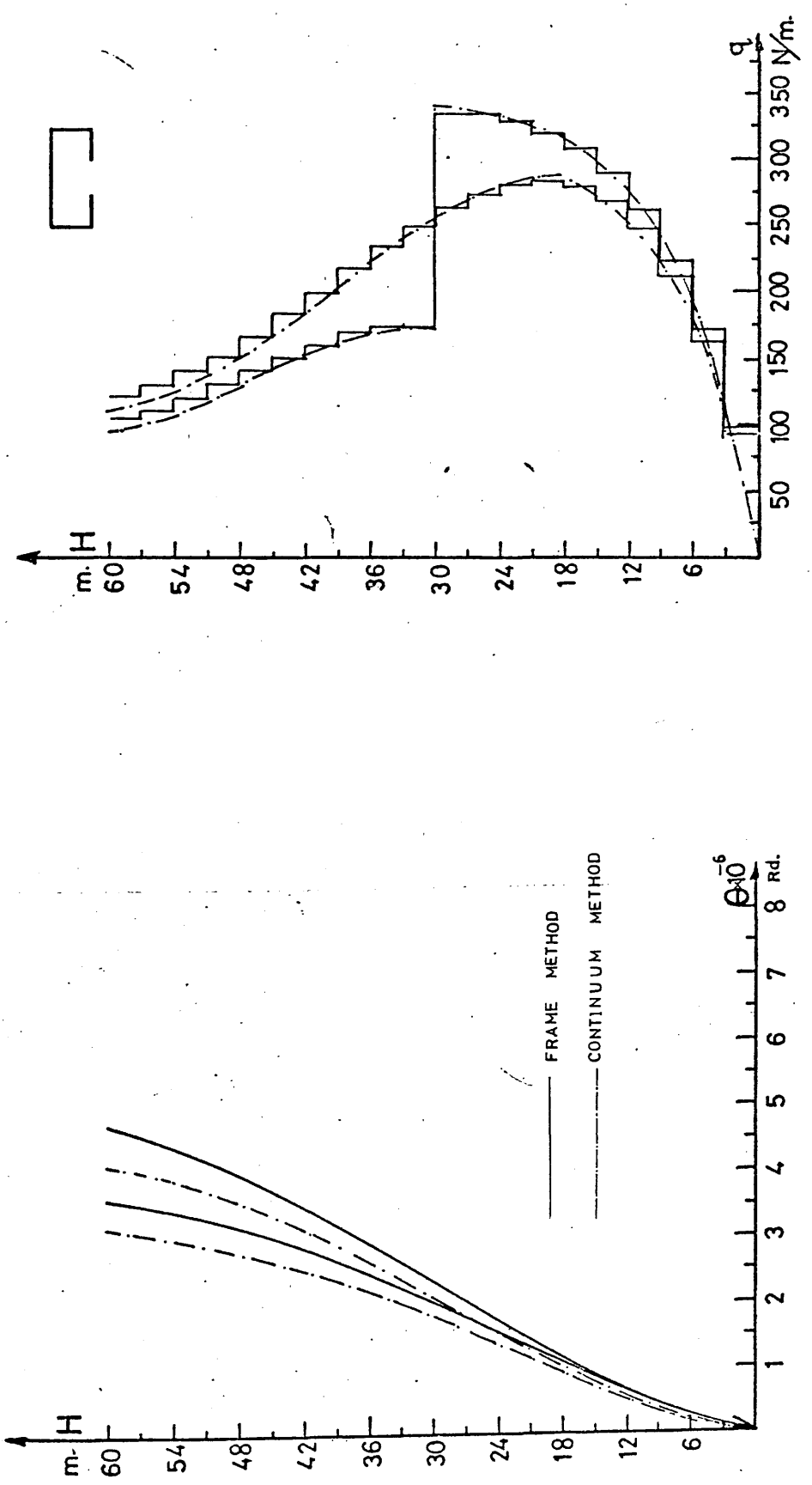

Fig. 5.8 Comparison between present theory and results obtained from frame idealisation model. (Singly-Symmetric, Uniformly Distributed Torque)

CHAPTER 6

ELASTO-PLASTIC ANALYSIS

OF

CORE STRUCTURES

CHAPTER 6

ELASTO-PLASTIC ANALYSIS OF CORE STRUCTURES

6.1 INTRODUCTION

It is now widely recognised that the existence of strong points such as shear cores in tall buildings erected in seismically disrupted areas is essential for the stability and safety of the building (32). In the case of severe wind loading or earthquake actions, the core itself may deform beyond its elastic limit. In this case plastic hinges are assumed to form at the connections between the lintel beams and the adjacent shear walls, if the bending moments in the lintel beams reach their ultimate values. These plastic hinges will develop according to the severity and type of loading, core shape and dimensions, and end conditions.

In this Chapter a theoretical method of analysis, based on the continuous approach, has been proposed to study core structures undergoing post-elastic deformations. In this method the plasticity is assumed to commence at a certain level where the bending moment in the lintel beams reaches its ultimate value. If the load continues to increase, the plastic hinges are assumed to spread throughout the height creating zones where the lintel beams are connected to the adjacent walls through plastic hinges. These zones are termed elasto-plastic zones.

A study of the formation and the sequence in which

the plastic hinges develop throughout the core is presented. A mathematical simulation for core structures consisting of elastic and elasto-plastic zones is proposed and expressions for the various stages of plasticity, under the three standard load cases and end conditions, are given. The ductility requirements and the limits of the proposed method have been discussed.

6.2 ASSUMPTIONS

In addition to the assumptions given in Chapter 2, the following assumptions have been made to achieve a quasi-closed-form solution for core structures undergoing post-elastic deformations.

1 - A plastic hinge will develop at each end of a connecting beam when the end moment reaches the ultimate moment capacity M_{cu} of the beam.

2 - The connecting beams are designed to fail in a flexural mode (21).

3 - The discrete hinges in the beams may be replaced by a continuous equivalent hinge connection for the continuous laminas and the ultimate shear intensity will be $q_u = Q_u/h$.

4 - The plasticity will develop only in the connecting lamina (and the top stiffening beam if it exists).

5 - The rotations of the connecting laminas are assumed to be within the ductility of the plastic hinges.

6 - If the strain in the walls exceeds the ultimate limit (30), the walls are no longer linearly elastic and the analysis will no longer be valid.

6.3 POSITION OF THE FIRST TWO PLASTIC HINGES IN THE CONNECTING LAMINAS

The level of the first two plastic hinges to develop in a connecting lamina may be determined by differentiating the expression given in Chapter 2 for the shear flow q_1 and equating to zero, which will locate the level of the stationary value,

$$\frac{d}{dx} q_1 = A \frac{d^2\theta}{dx^2} = 0 \qquad 6.3.1$$

where A is a constant which depends on the stiffness of the connecting beams and core dimensions, and need not be given explicitly here.

The following condition must also be satisfied,

$$\left[\frac{d^2\theta}{dx^2}\right]_{X-\Delta X} > 0 \qquad 6.3.2$$

which identifies the level of the proper extreme values of the vertical shear flow. It may otherwise be determined approximately from an inspection of plot of the vertical shear distribution in the connecting laminas.

If the core contains more than one set of connecting laminae, the plasticity will commence in the most highly stressed one at the above level.

6.4 SPREAD OF PLASTICITY THROUGHOUT THE CORE

6.4.1 VERTICAL SPREAD

The plasticity may commence at any level in the connecting lamina where the vertical shear flow q equals

the lamina ultimate shear capacity q_u. It will develop throughout the core height according to the type of loading, the core stiffness constant αH, and the end conditions R and λ as follows:

1 - The plasticity may commence at an intermediate height and spread upwards and downwards creating a three zoned structure with a middle elasto-plastic zone and upper and lower elastic zones as shown in Fig. 6.2.I. The limits of the elasto-plastic zone may first reach either the top or the bottom according to the values of the above parameters.

2 - If the plasticity starts at the top (as it will for a core structure free at the top and subjected to a point torque at the top), it will produce a two zoned structure with an upper elasto-plastic zone and a lower elastic zone as shown in Fig. 6.2.II. In this case the zone of plasticity will move downwards only.

3 - It may also commence at the bottom, (in the case of a core supported on very flexible foundations and provided with a very stiff top beam if subjected to a uniformly distributed torque), which will generate a two-zoned core with a lower elasto-plastic zone and an upper elastic zone. The zone of plasticity will only move upward, as shown in Fig. 6.2.IV.

4 - In the case of a core structure with stiffness variations throughout the height, such as a reduction in the thickness of the walls or in the depth of the connecting beams, the plasticity will commence at the

line of discontinuity, Fig. 5.3, and move downwards until the shear in the connecting lamina of the upper part reaches its value of q_u. The zone of plasticity will then move both upwards and downwards. The way in which plasticity may spread throughout the height of a uniform connecting lamina is demonstrated in the chart of Fig. 6.3.

6.4.2 HORIZONTAL SPREAD

The case of a core structure with more than one set of openings or set of connecting laminas (i.e. a multi-bay core), the plasticity will commence at the most stressed lamina when the vertical shear reaches the lamina ultimate shear capacity. It will then spread to any other lamina which reaches the same stage.

In the special case when the stiffness β is constant for all the connecting beams, plasticity will commence at the perimeter nearest to the corners and spread inwards towards the major axes.

6.5 METHOD OF ANALYSIS

For example, the unsymmetrical core structure considered in Chapter 2 is assumed to undergo post-elastic deformations with a central elasto-plastic zone extending from heights L to V, with upper and lower elastic zones as shown in Fig. 6.1.I. The core rigid body rotation is shown in Fig. 2.1.II, and the displacements of the significant points on the perimeter are the same as those given in equation 2.4.3.

ELASTIC ZONES

As the equilibrium conditions for the internal forces and the vertical strain compatibility conditions for the elastic zones 1 and 3 are unaltered, the governing equation will remain the same as that developed in Chapter 2, namely

$$-EI_w \frac{d^3\theta}{dx^3} + GJ_o \frac{d\theta}{dx} = T_{(x)} \qquad \text{where } 0 \leqslant X \leqslant L \quad \text{and} \quad V \leqslant X \leqslant H \qquad 6.5.1$$

ELASTO-PLASTIC ZONE

For the elasto-plastic zone the equilibrium conditions of the internal forces of each panel will be the same as in Chapter 2 except for panel 1 and 5. In this case the vertical shear flow q_1 in the connecting laminas equals the shear capacity q_u of the lamina as shown in Fig. 6.1.II.

The equilibrium conditions for panel 1 and panel 5 will then be as follows:

Panel 1

$$S_1 = \frac{dM_1}{dx} + q_2 \frac{d}{2} - q_u \frac{(d+a)}{2}$$

$$q_u + q_2 + \frac{dN_1}{dx} = 0 \qquad 6.5.2$$

Panel 5

$$S_5 = \frac{dM_5}{dx} + q_5 \frac{c}{2} - q_u \frac{(a+c)}{2}$$

$$\frac{dN_5}{dx} - q_u - q_5 = 0 \qquad 6.5.3$$

In this zone only four compatibility conditions exist as

the line of contraflexure in the laminas does not exist. The compatibility conditions at the four corners are the same as those given in equation 2.4 (20, 21, 22 and 23).

Following the same procedure as in Chapter 2, solving the above equations will yield the axial forces in the panels as given in equation 2.4.25, and the vertical shear at the corners will be

$$q_2 = q_u - EP_2 \frac{d^3\theta}{dx^3}$$

$$q_3 = q_u - EP_3 \frac{d^3\theta}{dx^3} \qquad 6.5.4$$

$$q_4 = q_u - EP_4 \frac{d^3\theta}{dx^3}$$

$$q_5 = q_u - EP_5 \frac{d^3\theta}{dx^3} \qquad 6.5.5$$

where P_1, P_2, P_3, P_4 and P_5 are as given in Chapter 2.

Substituting from the above expressions into equation 2.4(6, 8 and 10) and 6.5.(2 and 3), the horizontal shear forces are found to be,

$$S_1 = -E\left[I_1(e + B) + P_2 \frac{d}{2}\right] \frac{d^3\theta}{dx^3} + q_u \frac{(2d+a)}{2}$$

$$S_2 = -E\left[I_2(n - F) + \frac{B}{2}(P_2 + P_3)\right] \frac{d^3\theta}{dx^3} - q_u B$$

$$S_3 = -E\left[I_3 e - \frac{D}{2}(P_3 + P_4)\right] \frac{d^3\theta}{dx^3} - q_u D \qquad 6.5.6$$

$$S_4 = -E\left[I_4(m + F) - \frac{B}{2}(P_4 + P_5)\right] \frac{d^3\theta}{dx^3} + q_u B$$

$$S_5 = -E\left[I_5(e + B) + \frac{c}{2} P_5\right] \frac{d^3\theta}{dx^3} + q_u \frac{(2c + a)}{2}$$

Substituting from equation 6.5.6 into the overall equilibrium condition for the core cross-section in equation 2.4.28, yields

$$T = -EI_w \frac{d^3\theta}{dx^3} + GJ_p \frac{d\theta}{dx} - C\, q_u \qquad L \leqslant X \leqslant V \qquad 6.5.7$$

where I_w is as defined in Chapter 2 and

$J_p = J$ and $C = 2BD$.

The same method may be followed to analyse any core structure undergoing elasto-plastic deformations, which will yield the same forms of governing equations. In the case of a singly-symmetric core the constant C is the same as given above, but for a doubly-symmetric core as shown in Fig. 2.6, it becomes, $C = B.D$.

6.6 QUASI-CLOSED-FORM SOLUTION FOR ELASTO-PLASTIC BEHAVIOUR OF CORE STRUCTURES

A core structure undergoing elasto-plastic deformations may be considered as a multi-zoned core, the behaviour in each zone being represented by a third order differential equation as described in section 6.5.

The complete solution for the governing equation of the elastic zones is given in equation 2.5.5 in non-dimensional parameters αH and relative height ξ. It may be rewritten for zone 1 and zone 3, Fig. 6.1, in terms of α and X as follows:

For zone 1.

$$\Theta_1 = K_1 + K_2 \cosh \alpha X + K_3 \sinh \alpha X + \left(D^{-1} + \frac{D}{\alpha^2} + \frac{D^3}{\alpha^4} + \ldots\right) \frac{T_{(x)}}{GJ_o} \qquad 0 \leqslant X \leqslant L$$

And for zone 3

$$\theta_3 = K_7 + K_8 \cosh \alpha X + K_9 \sinh \alpha X + \left(D^{-1} + \frac{D}{\alpha^2} + \frac{D^3}{\alpha^4} + \ldots\right) \frac{T_{(x)}}{GJ_o} \qquad V \leqslant X \leqslant H$$

where α is as defined before (section 2.4) and the operator D represents $\frac{d}{dx}$.

Following the same procedure as in Section 2.5 to solve the governing equation 6.5.7, the general solution for an elasto-plastic zone is found to be

$$\theta_2 = K_4 + K_5 \cosh \rho X + K_6 \sinh \rho X + \left(D^{-1} + \frac{D}{\rho^2} + \frac{D^3}{\rho^4} + \ldots\right) \frac{(T_{(x)} + C\, q_u)}{GJ_p} \qquad L \leqslant X \leqslant V$$

where

$$\rho^2 = \frac{GJ_p}{EI_w}$$

For a core structure subjected to a point torque at the top, the complete solution for zones 1, 2 and 3 (Fig. 6.1) will be given respectively as follows.

$$\theta_1 = K_1 + K_2 \cosh \alpha X + K_3 \sinh \alpha X + \frac{tX}{GJ_o} \qquad 0 \leqslant X \leqslant L \qquad 6.6.1$$

$$\theta_2 = K_4 + K_5 \cosh \rho X + K_6 \sinh \rho X + \frac{tX}{GJ_p} + \frac{Cq_u X}{GJ_p} \qquad L \leqslant X \leqslant V \qquad 6.6.2$$

$$\theta_3 = K_7 + K_8 \cosh \alpha X + K_9 \sinh \alpha X + \frac{tX}{GJ_o} \qquad V \leqslant X \leqslant H \qquad 6.6.3$$

If the core is subjected to a uniformly distributed torque, the complete solution for each zone is

$$\theta_1 = K_1 + K_2 \cosh \alpha X + K_3 \sinh \alpha X + \frac{t}{GJ_o}\left(HX - \frac{X^2}{2} - \frac{1}{\alpha^2}\right)$$

$$0 \leqslant X \leqslant L \qquad 6.6.4$$

$$\theta_2 = K_4 + K_5 \cosh \rho X + K_6 \sinh \rho X + \frac{t}{GJ_p}\left(HX - \frac{X^2}{2} - \frac{1}{\rho^2}\right) \frac{C\, q_u\, X}{GJ_p}$$

$$L \leqslant X \leqslant V \qquad 6.6.5$$

$$\theta_3 = K_7 + K_8 \cosh \alpha X + K_9 \sinh \alpha X + \frac{t}{GJ_o}\left(HX - \frac{X^2}{2} - \frac{1}{\alpha^2}\right)$$

$$V \leqslant X \leqslant H \qquad 6.6.6$$

In the case of a triangularly distributed torque the solution is

$$\theta_1 = K_1 + K_2 \cosh \alpha X + K_3 \sinh \alpha X + \frac{t}{2GJ_o}\left(H^2X - \frac{X^3}{3} - \frac{2X}{\alpha^2}\right)$$

$$0 \leqslant X \leqslant L \qquad 6.6.7$$

$$\theta_2 = K_4 + K_5 \cosh \rho X + K_6 \sinh \rho X + \frac{t}{2GJ_p}\left(H^2X - \frac{X^3}{3} - \frac{2X}{\rho^2}\right) + \frac{C\, q_u\, X}{GJ_p}$$

$$L \leqslant X \leqslant V \qquad 6.6.8$$

$$\theta_3 = K_4 + K_5 \cosh \alpha X + K_6 \sinh \alpha X + \frac{t}{2GJ_o}\left(H^2X - \frac{X^3}{3} - \frac{2X}{\alpha^2}\right)$$

$$V \leqslant X \leqslant H \qquad 6.6.9$$

The constants of integration and the limits L and V of the elasto-plastic zone in the above equations may be defined by considering the boundary conditions at the top and at the base as given in equation 5.3 (4 and 5) in addition to the compatibility and equilibrium conditions

between each two adjacent zones. At the boundaries between the elasto-plastic and the elastic zones, the angles of rotation Θ, the slope Θ' and the bending moments and normal forces in the walls are equal for both zones; whilst the laminar shear q_l equals the ultimate shear capacity of the lamina q_u. These conditions may be written as follows for the boundary between zones i and (i + I)

$$\Theta_i = \Theta_{i+1}$$

$$\Theta'_i = \Theta'_{i+1}$$

$$\Theta''_i = \Theta''_{i+1} \qquad 6.6.10$$

$$q_l = q_u$$

Using the above equations, expressions for the elasto-plastic behaviour of core structures have been achieved for the following cases using a step-by-step computation.

6.6.1 CASE I: THREE-ZONED CORE WITH AN ELASTO-PLASTIC ZONE IN THE MIDDLE

In a three-zoned core shown in Fig. 6.2.I, the limits of each zone and the applied torque can be found most conveniently by first locating the level of the first two plastic hinges. Then, by assuming values for either the lower or the upper limit of the middle zone below or above the first value, the other limit and the corresponding value of the applied torque can be calculated from the following expressions for the three standard load cases. This is simpler than increasing the torque above that to cause first yielding and then determining both upper and

lower limits of plasticity.

1 - POINT TORQUE AT THE TOP

For a three-zoned core subjected to a point torque at the top, the condition of overall equilibrium of the core can be obtained by solving equations 6.6.(1,2 and 3) for the boundary conditions given by equations 5.3(4 and 5) and the compatibility and equilibrium conditions in 6.6.10. The limits of each zone may be obtained by satisfying the first equality (i.e. equating the first two terms in equation 6.6.11) and the applied torque value t from the second equality of the condition (i.e. equating any of the above terms to the applied torque t).

$$S_1/(A/J_p + \alpha((\cosh \alpha L-1)(\cosh \alpha L + \alpha\mu \sinh \alpha L)/(\sinh \alpha L + \alpha\mu \cosh \alpha L) - \sinh \alpha L)/J_o) = S_2/(Z/J_p + (r\alpha \cosh \alpha V/(\alpha \cosh \alpha H - r \sinh \alpha H) - W(1 + r \sinh \alpha V/(\alpha \cosh \alpha H - r \sinh \alpha H)))/J_o) = t \quad (6.6.11)$$

where

$$S_1 = Gq_u((\alpha(\cosh \alpha L + \alpha\mu \sinh \alpha L)/(\sinh \alpha L + \alpha\mu \cosh \alpha L)-A)/\beta EBD - CA/GJ_o)$$

$$S_2 = Gq_u(W/\beta EBD - Z(1/\beta EBD + C/GJ_o))$$

$$A = \rho(\sinh \rho L + (\cosh \rho V - \cosh \rho L) \cosh \rho L/(\sinh \rho L - \sinh \rho V))/(\cosh \rho V - \cosh \rho L) \sinh \rho L/(\sinh \rho L-\sinh \rho V))$$

$$W = \alpha(\sinh \alpha V + (r \cosh \alpha H - \alpha \sinh \alpha H) \cosh \alpha V/(\alpha \cosh \alpha H - r \sinh \alpha H))/(\cosh \alpha V + (r \cosh \alpha H - \alpha \sinh \alpha H) \sinh \alpha V/(\alpha \cosh \alpha H - r \sinh \alpha H))$$

The constants for the solutions are then given by

$$K_1 = -K_2$$

$$K_2 = t(\cosh \alpha L-1)/(\alpha GJ_o(\sinh \alpha L + \alpha\mu \cosh \alpha L)) - q_u/(\alpha\beta EBD(\sinh \alpha L + \alpha\mu \cosh \alpha L))$$

$$K_3 = \alpha\mu K_2 - t/\alpha GJ_o$$

$$K_4 = K_1 + K_2 \cosh \alpha L + K_3 \sinh \alpha L + tL/GJ_o - (K_5 \cosh \rho L + K_6 \sinh \rho L + (tL + Cq_uL)/GJ_p)$$

$$K_5 = K_6(\cosh \rho V - \cosh \rho L)/(\sinh \rho L - \sinh \rho V)$$

$$K_6 = -q_u(1/\beta EBD + C/GJ_p)/(\rho(\cosh \rho L +(\cosh \rho V - \cosh \rho L) \sinh \rho L/(\sinh \rho L - \sinh \rho V))) - t/(\rho GJ_p(\cosh \rho L + (\cosh \rho V - \cosh \rho L)\sinh \rho L/(\sinh \rho L - \sinh \rho V)))$$

$$K_7 = K_4 + K_5 \cosh \rho V + K_6 \sinh \rho V + (tV + Cq_uV)/GJ_p - (K_8 \cosh \alpha V + K_9 \sinh \alpha V + tV/GJ_o)$$

$$K_8 = K_9(r \cosh \alpha H - \alpha \sinh \alpha H)/(\alpha\cosh \alpha H - r \sinh \alpha H) + tr/(\alpha GJ_o(\alpha \cosh \alpha H - r \sinh \alpha H))$$

$$K_9 = -(t(1+r \sinh \alpha V/(\alpha\cosh \alpha H - r \sinh \alpha H))/\alpha GJ_o + q_u/\alpha\beta EBD)/(\cosh \alpha V + (r \cosh \alpha H - \alpha \sinh \alpha H)\sinh \alpha V)/(\alpha \cosh \alpha H - r \sinh \alpha H)$$

2 - UNIFORMLY DISTRIBUTED TORQUE

Solving equations 6.6(4,5 and 6) for the above end conditions, the overall equilibrium condition for three-zoned core subjected to a uniformly distributed torque can be expressed as:

$$GS_1/((\alpha(\cosh \alpha L + \alpha\mu \sinh \alpha L)((H+\mu)\cosh \alpha L + L-H)/(\sinh \alpha L + \alpha\mu \cosh \alpha L) - (1 + \alpha(H+\mu)\sinh \alpha L))/$$

$$J_o + (A(H-L+(L-V)\sinh \rho L/(\sinh \rho L - \sinh \rho V)) - \rho(L-V)\cosh \rho L/(\sinh \rho L-\sinh \rho V)+ 1)/J_p) = GS_2/((\rho(L-V)\cosh \rho V/(\sinh \rho L - \sinh \rho V) - Z(H-L+(L-V) \sinh \rho L/(\sinh \rho L - \sinh \rho V))-1)/J_p + (W(H-V)+(W \sinh \alpha V- \alpha \cosh \alpha V)/(\alpha \cosh \alpha H - r \sinh \alpha H)+ 1)/J_o) = t$$

where in this case

$$S_1 = q_u(\alpha(\cosh \alpha L + \alpha\mu \sinh \alpha L)/(\beta EBD(\sinh \alpha L + \alpha\mu \cosh \alpha L)) - A(1/\beta EBD + C/GJ_p)$$

$$S_2 = q_u(Z(1/\beta EBD + C/GJ_p) - W/\beta EBD)$$

$$A = \rho(\sinh \rho L + (\cosh \rho V - \cosh \rho L)\cosh \rho L/(\sinh \rho L - \sinh \rho V))/(\cosh \rho L + (\cosh \rho V - \cosh \rho L)\sinh \rho L/(\sinh \rho L - \sinh \rho V))$$

$$W = \alpha(\sinh \alpha V + (r \cosh \alpha H - \alpha \sinh \alpha H)\cosh \alpha V/(\alpha \cosh \alpha H - r \sinh \alpha H))/(\cosh \alpha V + (r \cosh \alpha H - \alpha \sinh \alpha H) \sinh \alpha V/(\alpha \cosh \alpha H - r \sinh \alpha H))$$

$$Z = \rho(\sinh \rho V + (\cosh \rho V - \cosh \rho L)\cosh \rho V/(\sinh \rho L - \sinh \rho V))/(\cosh \rho L + (\cosh \rho V - \cosh \rho L)\sinh \rho L/(\sinh \rho L - \sinh \rho V))$$

The constants of integration are then given by

$$K_1 = t/\alpha^2 GJ_o - K_2$$

$$K_2 = t((H+\mu) \cosh \alpha L + L-H)/(\alpha GJ_o(\sinh \alpha L + \alpha\mu \cosh \alpha L)) - q_u/(\alpha\beta EBD(\sinh \alpha L + \alpha\mu \cosh \alpha L))$$

$$K_3 = \alpha\mu K_2 - t(H+\mu)/\alpha GJ_o$$

$$K_4 = K_1 + K_2 \cosh \alpha L + K_3 \sinh \alpha L + t(HL-L^2/2 - 1/\alpha^2)/GJ_o - (K_5 \cosh \rho L + K_6 \sinh \rho L + t(HL - L^2/2 - 1/\rho^2)/GJ_p + Cq_uL/GJ_p)$$

$$K_5 = K_6(\cosh \rho V - \cosh \rho L)/(\sinh \rho L - \sinh \rho V) + t(L-V)/(\rho G J_o(\sinh \rho L - \sinh \rho V))$$

$$K_6 = -t(H-L + (L-V)\sinh \rho L/(\sinh \rho L - \sinh \rho V))/(\rho G J_p(\cosh \rho L + \cosh \rho V - \cosh \rho L)\sinh \rho L/(\sinh \rho L - \sinh \rho V))) - q_u(1/\beta EBD + C/GJ_p)/(\rho(\cosh \rho L + (\cosh \rho V - \cosh \rho L)\sinh \rho L/(\sinh \rho L - \sinh \rho V)))$$

$$K_7 = K_4 + K_5 \cosh \rho V + K_6 \sinh \rho V + t(HV - V^2/2 - 1/\rho^2)/GJ_p - (K_8 \cosh \alpha V + K_9 \sinh \alpha V + t(HV - V^2/2 - 1/\alpha^2)/GJ_o) + Cq_u V/GJ_p$$

$$K_8 = K_9(r \cosh \alpha H - \alpha \sinh \alpha H)/(\alpha \cosh \alpha H - r \sinh \alpha H) + t/(\alpha GJ_o(\alpha \cosh \alpha H - r \sinh \alpha H)$$

$$K_9 = -(t(H-V + \sinh \alpha V/(\alpha \cosh \alpha H - r \sinh \alpha H))/GJ_o + q_u/\beta EBD)/(\alpha(\cosh \alpha V + (r \cosh \alpha H - \alpha \sinh \alpha H) \sinh \alpha V/(\alpha \cosh \alpha H - r \sinh \alpha H)))$$

3 - TRIANGULARLY DISTRIBUTED TORQUE

In this case the overall equilibrium condition of the core can be obtained by solving equations 6.6(7,8 and 9) for the above end conditions. It is found to be

$$S_1/((A(H^2 - 2/\alpha^2)(\cosh \alpha L-1)+ L^2) - 2L - \alpha(H^2 - 2/\alpha^2) \sinh \alpha L)/J_o + ((L^2 - V^2)(Z \sinh \rho L - \rho \cosh \rho L)/(\sinh \rho L - \sinh \rho V) + Z(H^2 - L^2 - 2/\rho^2) + 2L)/J_p) = S_2/(((L^2-V^2)(\rho \cosh \rho V - W \sinh \rho L)/(\sinh \rho L - \sinh \rho V) - W(H^2 - L^2 - 2/\rho^2) - 2V)/J_p - (2(H - r/\alpha^2)(\alpha \cosh \alpha V - S \sinh \alpha V)/(\alpha \cosh \alpha H - r \sinh \alpha H) - S(H^2 - V^2 - 2/\alpha^2) - 2V)/J_o) = t$$

where

$$S_1 = 2Gq_u(A/\beta EBD - Z(1/\beta EBD + C/GJ_p))$$

$$S_2 = 2Gq_u(W(1/\beta EBD + C/GJ_p) - S/\beta EBD)$$

$$S = \alpha(\sinh \alpha V + (r \cosh \alpha H - \alpha \sinh \alpha H) \cosh \alpha V / (\alpha \cosh \alpha H - r \sinh \alpha H))/(\cosh \alpha V + (r \cosh \alpha H - \alpha \sinh \alpha H) \sinh \alpha V/(\alpha \cosh \alpha H - r \sinh \alpha H))$$

$$A = \alpha(\cosh \alpha L + \alpha\mu \sinh \alpha L)/(\sinh \alpha L + \alpha\mu \cosh \alpha L)$$

$$Z = \rho(\sinh \rho L + (\cosh \rho V - \cosh \rho L)\cosh \rho L/(\sinh \rho L - \sinh \rho V))/(\cosh \rho L + (\cosh \rho V - \cosh \rho L)\sinh \rho L/(\sinh \rho L - \sinh \rho V))$$

$$W = \rho(\sinh \rho V + (\cosh \rho V - \cosh \rho L)\cosh \rho V/(\sinh \rho L - \sinh \rho V))/(\cosh \rho L + (\cosh \rho V - \cosh \rho L)\sinh \rho L/(\sinh \rho L - \sinh \rho V))$$

The integration constants of equations 6.6(7,8 and 9) are then found to be

$$K_1 = - K_2$$

$$K_2 = t((H^2-2/\alpha^2)(\cosh \alpha L-1) + L^2)/(2GJ_o\alpha(\sinh \alpha L + \alpha\mu \cosh \alpha L)) - q_u/(\alpha\beta EBD(\sinh \alpha L + \alpha\mu \cosh \alpha L))$$

$$K_3 = \alpha\mu K_2 - t(H^2 - 2/\alpha^2)/2\alpha GJ_o$$

$$K_4 = K_1 + K_2 \cosh \alpha L + K_3 \sinh \alpha L + t(H^2L - L^3/3 - 2L/\alpha^2)/2GJ_o - (K_5 \cosh \rho L + K_6 \sinh \rho L + t(H^2L - L^3/3 - 2L/\rho^2)/2GJ_p) + Cq_u L/GJ_p)$$

$$K_5 = K_6(\cosh \rho V - \cosh \rho L)/(\sinh \rho L - \sinh \rho V) + t(L^2-V^2)/(2\rho GJ_o(\sinh \rho L - \sinh \rho V))$$

$$K_6 = (t((L^2 - V^2)\sinh \rho L/(\sinh \rho L - \sinh \rho V) + H^2-L^2-2/\rho^2)/2GJ_p + q_u(C/GJ_p + 1/\beta EBD))/(\rho(\cosh \rho L + (\cosh \rho V -$$

$\cosh \rho L) \sinh \rho L/(\sinh \rho L - \sinh \rho V)))$

$K_7 = K_4 + K_5 \cosh \rho V + K_6 \sinh \rho V + t(H^2V - V^3/3 - 2V/\rho^2)/2GJ_p + Cq_uV/GJ_p - (K_8 \cosh \alpha V + K_9 \sinh \alpha V + t(H^2V - V^3/3 - 2V/\alpha^2)/2GJ_o)$

$K_8 = K_9(r \cosh \alpha H - \alpha \sinh \alpha H)/(\alpha \cosh \alpha H - r \sinh \alpha H) + t(H - r/\alpha^2)/(\alpha GJ_o(\alpha \cosh \alpha H - r \sinh \alpha H))$

$K_9 = -(t(H - r/\alpha^2) \sinh \alpha V/(\alpha \cosh \alpha H - r \sinh \alpha H) + (H^2 - V^2 - 2/\alpha^2)/2)/GJ_o) + q_u/\beta EBD)/(\alpha(\cosh \alpha V + (r \sinh \alpha H - \alpha \sinh \alpha H) \sinh \alpha V/(\alpha \cosh \alpha H - r \sinh \alpha H)))$

6.6.2 CASE II: TWO-ZONED CORE, WITH AN ELASTO-PLASTIC ZONE AT THE TOP

As the plasticity spreads upward and downward, the upper limit of the elasto-plastic zone may reach the top first. It will then create a two-zoned core with an upper elasto-plastic zone and a lower elastic zone as shown in Fig. 6.2.II. Solving the governing equation of the above two zones for the boundary condition in equation 5.3(4 and 5) and the compatibility and equilibrium conditions 6.6.10, the overall equilibrium condition of the core can be obtained for the three standard load cases.

1 - POINT TORQUE AT THE TOP

Solving equations 6.6.(1 and 2) of zone 1 and zone 2 for the above end conditions, the overall equilibrium condition of the core is found to be

$t = S/((Z(\cosh \alpha L-1) - \alpha \sinh \alpha L)/J_o + (W + r(\sinh \rho L - \rho \cosh \rho L)/(\rho \cosh \rho H - r \sinh \rho H))/J_p)$

where

$$S = Gq_u((Z-W)/\beta EBD + Cr(\rho \cosh \rho L - W \sinh \rho L)/(GJ_p (\rho \cosh \rho H - r \sinh \rho H)) - CW/GJ_p)$$

$$W = \rho^2(\sinh \rho L + (r \cosh \rho H - \rho \sinh \rho H) \cosh \rho L/(\rho \cosh \rho H - r \sinh \rho H))/A$$

$$A = \rho(\cosh \rho L + (r \cosh \rho H - \rho \sinh \rho H)\sinh \rho L/(\rho \cosh \rho H - r \sinh \rho H))$$

$$Z = \alpha(\cosh \alpha L + \alpha\mu \sinh \alpha L)/(\sinh \alpha L + \alpha\mu \cosh \alpha L)$$

The integration constants of zone 1 and zone 2, are then found to be

$$K_1 = - K_2$$

$$K_2 = t(\cosh \alpha L - 1)/(\alpha GJ_o(\sinh \alpha L + \alpha\mu \cosh \alpha L)) - q_u/(\alpha\beta EBD(\sinh \alpha L + \alpha\mu \cosh \alpha L))$$

$$K_3 = \alpha\mu K_2 - t/\alpha GJ_o$$

$$K_4 = K_1 + K_2 \cosh \alpha L + K_3 \sinh \alpha L + tL/GJ_o - (K_5 \cosh \rho L + K_6 \sinh \rho L + (t + Cq_u)L/GJ_p)$$

$$K_5 = K_6(r \cosh \rho H - \rho \sinh \rho H)/(\rho \cosh \rho H - r \sinh \rho H) + r(t + Cq_u)/(\rho GJ_p(\rho \cosh \rho H - r \sinh \rho H))$$

$$K_6 = -t(1 + r \sinh \rho L)(\rho \cosh \rho H - r \sinh \rho H))/AGJ_p - q_u(1/\beta EBD + C(1 + r \sinh \rho L/(\rho \cosh \rho H - r \sinh \rho H))/GJ_p)/A$$

2 - UNIFORMLY DISTRIBUTED TORQUE

The equilibrium condition for the core in this case can be obtained by solving equations 6.6.(4 and 5) of zone 1 and zone 2 for the aforementioned end conditions, which will yield

$$t = S_1/((A(H-L) + (A \sinh \rho L - \rho \cosh \rho L)/(\rho \cosh \rho H - r \sinh \rho H) + 1)/J_p - (H + \mu)(\alpha \sinh \alpha L - Z \cosh \alpha L) + Z(H-L) + 1)/J_o)$$

where

$$S_1 = q_u G((Z-A)/\beta EBD + C((\rho r \cosh \rho L - Ar \sinh \rho L)/(\rho \cosh \rho H - r \sinh \rho H) - A)/GJ_p)$$

$$A = \rho(\sinh \rho L + (r \cosh \rho H - \rho \sinh \rho H)\cosh \rho L/(\rho \cosh \rho H - r \sinh \rho H))/(\cosh \rho L + (r \cosh \rho H - \rho \sinh \rho H)\sinh \rho L/(\rho \cosh \rho H - r \sinh \rho H)$$

$$W = \rho(\cosh \rho L + (r \cosh \rho H - \rho \sinh \rho H) \sinh \rho L/(\rho \cosh \rho H - r \sinh \rho H))$$

$$Z = \alpha(\cosh \alpha L + \alpha\mu \sinh \alpha L)/(\sinh \alpha L + \alpha\mu \cosh \alpha L)$$

The integration constants of zones 1 and 2 are then given by

$$K_1 = t/\alpha^2 GJ_o - K_2$$

$$K_2 = t((H+\mu)\cosh \alpha L + L - H)/(\alpha GJ_o(\sinh \alpha L + \alpha\mu \cosh \alpha L)) - q_u/(\alpha\beta EBD(\sinh \alpha L + \alpha\mu \cosh \alpha L))$$

$$K_3 = \alpha\mu K_2 - t(H + \mu)/\alpha GJ_o$$

$$K_4 = K_1 + K_2 \cosh \alpha L + K_3 \sinh \alpha L + t(HL - L^2/2 - 1/\alpha^2)/GJ_o - (K_5 \cosh \rho L + K_6 \sinh \rho L + t(HL - L^2/2 - 1/\rho^2)/GJ_p + Cq_u L/GJ_p)$$

$$K_5 = K_6(r \cosh \rho H - \rho \sinh \rho H)/(\rho \cosh \rho H - r \sinh \rho H) + (rCq_u + t)/(\rho GJ_p(\rho \cosh \rho H - r \sinh \rho H))$$

$$K_6 = -(t(H-L+\sinh \rho L/(\rho \cosh \rho H - r \sinh \rho H))/GJ_p + q_u(1/\beta EBD + C(1 + r \sinh \rho L/(\rho \cosh \rho H - r \sinh \rho H))/GJ_p))/W$$

3 - TRIANGULARLY DISTRIBUTED TORQUE

If the core is subjected to a triangularly distributed torque, the overall equilibrium condition can be obtained by solving equations 6.6.(7 and 8) for the above end condition. It is found to be

$$t = S/(((H^2 - 2/\alpha^2)(Z \cosh \alpha L - \alpha \sinh \alpha L - Z) + ZL^2 - 2L)/2J_o - (H - r/\rho^2)(\rho \cosh \rho L + W \sinh \rho L)/(\rho \cosh \rho H - r \sinh \rho H) + W(H^2 - L^2 - 2/\rho^2)/2-L)/J_p)$$

where

$$S = Gq_u((Z+W)/\beta EBD + C(r(W \sinh \rho L + \rho \cosh \rho L)/(\rho \cosh \rho H - r \sinh \rho H) + W)/GJ_p)$$

$$A = -\rho(\cosh \rho L+(r \cosh \rho H - \rho \sinh \rho H)\sinh \rho L/(\rho \cosh \rho H - r \sinh \rho H))$$

$$W = \rho^2(\sinh \rho L + (r \cosh \rho H - \rho \sinh \rho H)\cosh \rho L/(\rho \cosh \rho H - r \sinh \rho H))/A$$

$$Z = \alpha(\cosh \alpha L + \alpha\mu \sinh \alpha L)/(\sinh \alpha L + \alpha\mu \cosh \alpha L)$$

The integration constants are then given by

$$K_1 = -K_2$$

$$K_2 = t((H^2 - 2/\alpha^2)(\cosh \alpha L-1) + L^2)/(2 GJ_o\alpha(\sinh \alpha L + \alpha\mu \cosh \alpha L)) - q_u)/(\beta EBD\alpha(\sinh \alpha L + \alpha\mu \cosh \alpha L))$$

$$K_3 = \alpha\mu K_2 - t(H^2 - 2/\alpha^2)/2\alpha GJ_o$$

$$K_4 = K_1 + K_2 \cosh \alpha L + K_3 \sinh \alpha L + t(H^2L - L^3/3 - 2L/\alpha^2)/2GJ_o -(K_5 \cosh \rho L + K_6 \sinh \rho L + t(H^2L - L^3/3 - 2L/\rho^2)/2GJ_p)$$

$$K_5 = K_6(r \cosh \rho H - \rho \sinh \rho H)/(\rho \cosh \rho H - r \sinh \rho H) + t(H-r/\rho^2)/(\rho GJ_p(\rho \cosh \rho H - r \sinh \rho H)) + Cq_u r/(GJ_p \rho(\rho \cosh \rho H - r \sinh \rho H))$$

$$K_6 = t((H-r/\rho^2)\sinh \rho L/(\rho \cosh \rho H - r \sinh \rho H) + (H^2 - L^2 - 2/\rho^2)/2)/GJ_p A) + q_u(1/\beta EBD + C(r \sinh \rho L/(\rho \cosh \rho H - r \sinh \rho H) + 1)/GJ_p)/A$$

6.6.3 CASE III: TWO-ZONED CORE, WITH PLASTIC HINGES DEVELOPED IN A TOP STIFFENING BEAM

As the applied torque may continue to increase, the elasto-plastic zone will expand downwards and the shear force in the top stiffening beam Q_s will reach the beam ultimate capacity Q_{su}. Thus two hinges will develop at its ends. They will impose a constant bending moment at the top of the adjacent walls, equal to Q_{su} times the distance between the point of contraflexure and the centroidal axes of the walls, which may be included as a top end condition by equating the expression for the wall bending moment from equation 2.4.24 to the above fixed value at the top, which will yield

$$\theta''_H = \left[\frac{d^2\theta}{dx^2}\right]_H = M_u \qquad 6.6.12$$

where

M_u = a constant which depends on the core dimensions, configuration and the stiffness of the top beam β_s.

In the case of the doubly-symmetric and singly symmetric cores shown in Figs. 2.6 and 2.5, M_u will be given respectively by

$M_u = Q_{su}(d + a)/(E\ I_1\ B)$

and

$M_u = Q_{su}(d + a)/(E\ I_1(B + e))$

For the unsymmetrical core shown in Fig. 2.1, M_u could be taken approximately as an average of its values at the top of the two adjacent walls, namely,

$$M_u = Q_{su}\left[\frac{(a + c)}{I_5} + \frac{(a + d)}{I_1}\right]/2E(B + e)$$

Thus the overall equilibrium condition of the core and the constants of integration of the governing equation for each zone can be obtained for the load cases under consideration as follows.

1 - POINT TORQUE AT THE TOP

The overall equilibrium condition of the core structure shown in Fig. 6.2.III, when subjected to a point torque at the top can be obtained by solving equations 6.6.1 and 6.6.2 for the base end condition given by 5.3.4 and the boundary conditions given in 6.6(10 and 12). It is found to be

$t = S/((Z(\cosh \alpha L-1) - \alpha \sinh \alpha L)/J_o - W/J_p)$

where

$S = G(q_u(CW/GJ_o + (Z + W)/\beta EBD) + M_u(W \sinh \rho L + \rho \cosh \rho L)/\rho \cosh \rho H)$

$A = -\rho(\cosh \rho L - \sinh \rho L \tanh \rho H)$

$W = \rho^2(\sinh \rho L - \cosh \rho L \tanh \rho H)/A$

$Z = \alpha(\cosh \alpha L + \alpha\mu \sinh \alpha L)/(\sinh \alpha L + \alpha\mu \cosh \alpha L)$

and the constants of integration are then given by

$K_1 = -K_2$

$K_2 = t(\cosh \alpha L-1)/(\alpha GJ_o(\sinh \alpha L + \alpha\mu \cosh \alpha L)) - q_u/(\alpha\beta EBD(\sinh \alpha L + \alpha\mu \cosh \alpha L))$

$K_3 = \alpha\mu K_2 - t/\alpha GJ_o$

$K_4 = K_1 + K_2 \cosh \alpha L + K_3 \sinh \alpha L + tL/GJ_o -(K_5 \cosh \rho L + K_6 \sinh \rho L +(t + Cq_u)L/GJ_p)$

$K_5 = M_u/\rho^2 \cosh \rho H - K_6 \tanh \rho H$

$K_6 = t/AGJ_p + q_u(C/GJ_p + 1/\beta EBD)/A + M_u \sinh \rho L/A\rho \cosh \rho H$

2 - UNIFORMLY DISTRIBUTED TORQUE

In this case the overall equilibrium condition of the core can be obtained by solving equations 6.6(4 and 5) for the above end conditions, which will yield,

$t = S/(((H+\mu)(Z \cosh \alpha L - \alpha \sinh \alpha L)+ Z(L-H-1)/J_o - ((W \sinh \rho L + \rho \cosh \rho L)/\rho \cosh \rho H + W(H-L)-1)/J_p)$

where

$S = G(q_u((Z+W)/\beta EBD + CW/GJ_p) + M_u(W \sinh \rho L + \rho \cosh \rho L)/\rho \cosh \rho H)$

$A = -\rho(\cosh \rho L - \sinh \rho L \tanh \rho H)$

$W = \rho^2(\sinh \rho L - \cosh \rho L \tanh \rho H)/A$

$Z = \alpha(\cosh \alpha L + \alpha\mu \sinh \alpha L)/(\sinh \alpha L + \alpha\mu \cosh \alpha L)$

The integration constants of equation 6.6.(4 and 5) for zone 1 and zone 2 respectively are given by

$K_1 = t/\alpha^2 GJ_o - K_2$

$$K_2 = t((H+\mu)\cosh \alpha L + L - H)/(\alpha GJ_o(\sinh \alpha L + \alpha\mu \cosh \alpha L)) - q_u/(\alpha\beta EBD(\sinh \alpha L + \alpha\mu \cosh \alpha L)$$

$$K_3 = \alpha\mu K_2 - t(H+\mu)/\alpha GJ_o$$

$$K_4 = K_1 + K_2 \cosh \alpha L + K_3 \sinh \alpha L + t(HL - L^2/2 - 1/\alpha^2)/GJ_o - (K_5 \cosh \rho L + K_6 \sinh \rho L + t(HL - L^2/2 - 1/\rho^2)/GJ_p + Cq_uL/GJ_p)$$

$$K_5 = t/(\rho^2 GJ_p \cosh \rho H) + M_u/\rho^2 \cosh \rho H - K_6 \tanh \rho H$$

$$K_6 = q_u(1/\beta EBD + C/GJ_o)/A + t(H - L + \sinh \rho L/\rho \cosh \rho H)/AGJ_p + M_u \sinh \rho L/\rho A \cosh \rho H$$

3 - TRIANGULARLY DISTRIBUTED TORQUE

In this case the overall equilibrium condition of the core can be achieved by solving equation 6.6.(7 and 8) for the above end conditions, which will yield

$$t = GS/((ZL^2/2 + (H^2 - 2/\alpha^2)(Z(\cosh \alpha L-1)- \alpha \sinh \alpha L)/2-L)/J_o - (H(\rho \cosh \rho L + W \sinh \rho L)/\rho \cosh \rho H - L + W(H^2 - L^2 - 2/\rho^2)/2)/J_p)$$

where

$$S = M_u(\rho \cosh \rho L + W \sinh \rho L)/\rho \cosh \rho H + q_u((Z + W)/\beta EBD + CW/GJ_p)$$

$$A = -\rho(\cosh \rho L - \sinh \rho L \tanh \rho H)/A$$

$$W = \rho^2(\sinh \rho L - \cosh \rho L \tanh \rho H)/A$$

$$Z = \alpha(\cosh \alpha L + \alpha\mu \sinh \alpha L)/(\sinh \alpha L + \alpha\mu \cosh \alpha L)$$

The constants of integrations are found to be

$$K_1 = - K_2$$

$$K_2 = t((H^2 - 2/\alpha^2)(\cosh \alpha L - 1) + L^2)/(2GJ_o\alpha(\sinh \alpha L + \alpha\mu \cosh \alpha L)) - q_u/\beta EBD\alpha(\sinh \alpha L + \alpha\mu \cosh \alpha L))$$

$$K_3 = \alpha\mu K_2 - t(H^2 - 2/\alpha^2)/2\alpha GJ_o$$

$$K_4 = K_1 + K_2 \cosh \alpha L + K_3 \sinh \alpha L + t(H^2L - L^3/3 - 2L/\alpha^2)/2GJ_o - (K_5 \cosh \rho L + K_6 \sinh \rho L + t(H^2L - L^3/3 - 2L/\rho^2)/2GJ_p + Cq_uL/GJ_p)$$

$$K_5 = tH/GJ_p\, \rho \cosh \rho H + M_u/\rho \cosh \rho H - K_6 \tanh \rho H$$

$$K_6 = q_u(1/\beta EBD + C/GJ_p)/A + M_u \sinh \rho L/A\rho \cosh \rho H + t(H \sinh \rho L/\rho \cosh \rho H + (H^2 - L^2 - 2/\rho^2)/2)/AGJ_p)$$

6.6.4 CASE IV: TWO-ZONED CORE, WITH A LOWER ELASTO-PLASTIC ZONE

If a core is based on a very flexible foundation and provided with a stiff beam at the top, plasticity may theoretically commence at the base or at some intermediate height and spread upwards and downwards, in which case the lower limit may reach the base first. In each case, a two-zoned core is obtained, with a lower elasto-plastic zone as shown in Fig. 6.2.IV. Solving the governing equation of each zone and including the boundary conditions given in 5.3.(4 and 5) and the compatibility and equilibrium conditions in equation 6.6.10, the overall equilibrium condition of the core and the constants of integration can be found for the three particular cases of loading.

1 - POINT TORQUE AT THE TOP

The overall equilibrium condition can be found by

solving equation 6.6.(2 and 3) for the above end conditions, which will yield

$$t = S/(r(\alpha \cosh \alpha V + W \sinh \alpha V)/(\alpha \cosh \alpha H - r \sinh \alpha H) + W)/ J_o - (Z(1 - \cosh \rho V) - \rho \sinh \rho V)/J_p)$$

where

$$S = Gq_u((Z-W)/\beta EBD + C(Z(1 - \cosh \rho V) - \rho \sinh \rho V)/GJ_p)$$

$$A = -\alpha(\cosh \alpha V + (r \cosh \alpha H - \alpha \sinh \alpha H) \sinh \alpha V/(\alpha \cosh \alpha H - r \sinh \alpha H))$$

$$W = \alpha^2(\sinh \alpha V + (r \cosh \alpha H - \alpha \sinh \alpha H) \cosh \alpha V/ (\alpha \cosh \alpha H - r \sinh \alpha H))/A$$

$$Z = -\rho(\cosh \rho V + \rho\mu \sinh \rho V)/(\sinh \rho V + \rho\mu \cosh \rho V)$$

The constants of integration of the elasto-plastic zone and the elastic zone are given respectively as

$$K_4 = - K_5$$

$$K_5 = -(q_u(1/\beta EBD + C(1 - \cosh \rho V)/GJ_p) + t(1 - \cosh \rho V)/GJ_o)/ (\rho(\sinh \rho V + \rho\mu \cosh \rho V))$$

$$K_6 = \rho\mu K_5 - (t + Cq_u)/\rho GJ_p$$

$$K_7 = K_4 + K_5 \cosh \rho V + K_6 \sinh \rho V + (t + Cq_u)V/GJ_p - (K_8 \cosh \alpha V + K_9 \sinh \alpha V + tV/GJ_o)$$

$$K_8 = K_9(r \cosh \alpha H - \alpha \sinh \alpha H)/(\alpha \cosh \alpha H - r \sinh \alpha H) + tr/(\alpha GJ_o(\alpha \cosh \alpha H - r \sinh \alpha H))$$

$$K_9 = t(H - V + \sinh \alpha V/(\alpha \cosh \alpha H - r \sinh \alpha H))/AGJ_o + q_u/\beta EBD$$

2 - UNIFORMLY DISTRIBUTED TORQUE

In this case the overall equilibrium condition of the core can be found by solving equations 6.6(5 and 6) for the above end conditions, which will yield.

$$t = SG/((W(H-V) + (W \sinh \alpha V + \alpha \cosh \alpha V)/(\alpha \cosh \alpha H - r \sinh \alpha H)-1)/J_o + (1-Z(H-V)+(H+\mu)(\rho \sinh \rho V + Z \cosh \rho V))/J_p)$$

where

$$S = q_u((Z-W)/\beta EBD-C(\rho \sinh \rho V + Z(\cosh \rho V-1))/GJ_p)$$

The functions A, W and Z are as given above.

The constants of integration of the solution for each zone are found to be

$$K_4 = t/\rho^2 GJ_o - K_5$$

$$K_5 = -t(H-V-(H+\mu)\cosh \rho V)/(\rho GJ_p(\sinh \rho V + \rho\mu \cosh \rho V)) - q_u(1/\beta EBD + C(1 - \cosh \rho V)/GJ_p)/(\rho \sinh \rho V - \rho^2\mu \cosh \rho V)$$

$$K_6 = \rho\mu K_5 - t(H+\mu)/\rho GJ_p - Cq_u/\rho GJ_p$$

$$K_7 = K_4 + K_5 \cosh \rho V + K_6 \sinh \rho V + t(HV - V^2/2 - 1/\rho^2)/GJ_p + Cq_u V/GJ_p - (K_8 \cosh \alpha V + K_9 \sinh \alpha V + t(HV - V^2/2 - 1/\alpha^2)/GJ_o)$$

$$K_8 = K_9(r \cosh \alpha H - \alpha \sinh \alpha H)/(\alpha \cosh \alpha H - r \sinh \alpha H) + t/(\alpha GJ_o(\alpha \cosh \alpha H - r \sinh \alpha H))$$

$$K_9 = t(H-V + \sinh \alpha V/(\alpha \cosh \alpha H - r \sinh \alpha H))/AGJ_o + q_u/A\beta EBD$$

3 - TRIANGULARLY DISTRIBUTED TORQUE

In this case the overall equilibrium condition for the core is obtained by solving equations 6.6.(8 and 9) for the above end conditions, and yields.

$$t = GS/(((H - r/\alpha^2)(W \sinh \alpha V + \alpha \cosh \alpha V)/(\alpha \cosh \alpha H - r \sinh \alpha H) + W(H^2 - V^2 - 2/\alpha^2)/2)/J_o) - ((H^2 - 2/\rho^2)(Z(1 - \cosh \rho V) - \rho \sinh \rho V) - V(ZV + 2))/2J_p)$$

where

$$S = q_u((Z-W)/\beta EBD + C(Z(1 - \cosh \rho V) - \rho \sinh \rho V)/GJ_p)$$

The functions A, W and Z are as given above.

The constants of integration are given by

$$K_4 = -K_5$$

$$K_5 = -t((H^2 - 2/\rho^2)(1 - \cosh \rho V) - V^2)/(2\rho GJ_p(\sinh \rho V + \rho\mu \cosh \rho V)) - q_u(1/\beta EBD + C(1 - \cosh \rho V)/GJ_p)/(\rho \sinh \rho V + \rho^2 \mu \cosh \rho V)$$

$$K_6 = \rho \mu K_5 - t(H^2 - 2/\rho^2)/2\rho GJ_p - Cq_u/\rho GJ_p$$

$$K_7 = K_4 + K_5 \cosh \rho V + K_6 \sinh \rho V + t(H^2V - V^3/3 - 2V/\rho^2) + Cq_uV/GJ_p - (K_8 \cosh \alpha V + K_9 \sinh \alpha V + t(H^2V - V^3/3 - 2V/\alpha^2)/2GJ_o)$$

$$K_8 = K_9(r \cosh \alpha H - \alpha \sinh \alpha H)/(\alpha \cosh \alpha H - r \sinh \alpha H) + t(H-r/\alpha^2)/(\alpha GJ_o(\alpha \cosh \alpha H - r \sinh \alpha H))$$

$$K_9 = t((H^2 - V^2 - 2/\alpha^2) + 2(H-r/\alpha^2) \sinh \alpha V/(\alpha \cosh \alpha H - r \sinh \alpha H))/2AGJ_o + q_u/A\beta EBD$$

6.6.5 CASE V: CORE STRUCTURE WITH THE PLASTICITY SPREAD OVER ALL CONNECTING BEAMS EXCEPT THE TOP STIFFENING BEAM

In this case, the core is considered to consist of one elasto-plastic zone as shown in Fig. 6.2.V. The core behaviour is governed by equation 6.5.7, when extending the limits so that L = 0 and V = H. The general solutions of the above equation is given in equations 6.6.(2,5 and 8) for the standard load cases. The constants of integration may be obtained by including the boundary conditions given in 5.3(4 and 5) for each loading case as follows.

1 - POINT TORQUE AT THE TOP

If the core is subjected to a point torque at the top, the integration constants of equation 6.6.2 are given by

$$K_4 = -K_5$$

$$K_5 = (t + Cq_u)(r - (r \cosh \rho H - \rho \sinh \rho H))/AGJ_p$$

$$K_6 = \rho \mu K_5 - (t + Cq_u)/\rho GJ_p$$

where

$$A = \rho((\rho \cosh \rho H - r \sinh \rho H) - \rho \mu(r \cosh \rho H - \rho \sinh \rho H))$$

2 - UNIFORMLY DISTRIBUTED TORQUE

In this case, the integration constants of equation 6.6.5 are found to be

$$K_4 = t/\rho^2 GJ_p - K_5$$

$$K_5 = t(1-(H+\mu)(r \cosh \rho H - \rho \sinh \rho H))/AGJ_p + Cq_u$$
$$(r-(r \cosh \rho H - \rho \sinh \rho H))/AGJ_p$$

$$K_6 = \rho\ \mu\ K_5 - (t(H+\mu) + Cq_u)/\rho GJ_p$$

3 - TRIANGULARLY DISTRIBUTED TORQUE

In this case, the integration constants of equation 6.6.8 may be expressed as follows

$$K_4 = -K_5$$

$$K_5 = t(H-r/\rho^2 - (H^2 - 2/\rho^2)(r \cosh \rho H - \rho \sinh \rho H)/2)/AGJ_p + Cq_u(r-(r \cosh \rho H - \rho \sinh \rho H)/AGJ_p$$

$$K_6 = \rho\ \mu\ K_5 - t(H^2 - 2/\rho^2)/2\rho GJ_p - Cq_u/\rho GJ_p$$

6.6.6 CASE VI: CORE STRUCTURE WITH THE PLASTICITY SPREAD OVER ALL CONNECTING BEAMS AND THE TOP STIFFENING BEAM

If the shear force in the top stiffening beam Q_s reaches the beam ultimate capacity Q_{su}, the beam will yield, developing a plastic hinge at each end as shown in Fig. 6.2.VI. In this case, the core behaviour is governed by equation 6.5.7 and its general solutions for the three standard load cases are given in equations 6.6(2,5 and 8). The constants of integration may be obtained by including the top boundary condition given in equation 6.6.12 and the boundary condition of a core structure based on flexible foundation given in 5.3.4 as follows:

1 - POINT TORQUE AT THE TOP

If the core is subjected to a point torque at the top, the integration constants of equation 6.6.2 become

$$K_4 = -K_5$$

$$K_5 = (\rho(t + Cq_u) \sinh \rho H/GJ_p + M_u)/A$$

$$K_6 = \rho \mu K_5 - (t + Cq_u)/\rho GJ_p$$

where

$$A = \rho^2(\cosh \rho H - \rho \mu \sinh \rho H)$$

2 - UNIFORMLY DISTRIBUTED TORQUE

In this case, the constants of integration of equation 6.6.5 become

$$K_4 = t/\rho GJ_p - K_5$$

$$K_5 = (t(1 + \rho(H + \mu)/GJ_p) + Cq_u \rho \sinh \rho H/GJ_p + M_u)/A$$

$$K_6 = \rho \mu K_5 - t(H + \mu)/\rho GJ_p - Cq_u/\rho GJ_p$$

3 - TRIANGULARLY DISTRIBUTED TORQUE

In this case, the integration constants of equation 6.6.8 are found to be

$$K_4 = -K_5$$

$$K_5 = (t(H + \rho(H^2 - 2/\rho^2)\sinh \rho H/2)/GJ_p + Cq_u \rho \sinh \rho H/ GJ_p + M_u)/A$$

$$K_6 = \rho \mu K_5 - t(H^2 - 2/\rho^2)/2GJ_p - Cq_u)\rho GJ_p$$

By evaluating the constants of integration for each zone for any of the above cases, the behaviour being traced in a step-by-step manner from the development of the first plastic hinge, subsequently, the angle of rotation Θ and the internal forces in the core walls and connecting beams can be found.

6.7 DUCTILITY REQUIREMENT AND LIMITATION OF THE METHOD

6.7.1 ROTATIONAL DUCTILITY OF THE PLASTIC HINGES

In the above cases it was tacitly assumed that the hinges contain sufficient ductility to allow the plasticity to spread throughout all the connecting beams and the top stiffening beam. In practice the rotational ductility of the hinges depends on the beam depth, type and arrangement of the reinforcement in the beams. Thus it is necessary to check the rotation of the plastic hinge ϕ_p against its maximum allowable rotation ϕ_{p_u}, so that the calculation will be stopped if this maximum value were reached. By evaluating the wall rotations and axial deformation, it can be shown from Fig. 6.4 that the plastic lamina rotation ϕ_p at any height in the elasto-plastic zone is given by

$$\phi_p = \phi + \psi - \phi_y \qquad 6.7.1$$

where

ϕ_p is the plastic laminar rotation

ϕ_y is the maximum elastic rotation of the lamina

ϕ is the angle of slope of the lamina at mid-span

ψ is the elastic rotation of the wall

Substituting for the above deformations in terms of the forces will yield,

$$\phi_p = \frac{d+a}{a} \int_o^x \frac{M_1}{EI_1}\,dx - \frac{2}{a} \int_o^x \frac{N_1}{EA_1}\,dx - \frac{q_u}{a\beta E} \qquad 6.7.2$$

On substituting for M_1 and N_1 in the above equation, it can be proved that for both doubly and singly symmetric cores,

$$\phi_p = \frac{B.D}{a} \frac{d\theta}{dx} - \frac{q_u}{a\beta E}$$

For the unsymmetrical core, ϕ_p values could be taken approximately as the average of the following two values as a rough guide

$$\phi_p = \frac{1}{a}[(c+a)(e+B) - 2(c_5 + c_2 - c_4 - c_3 + P)] \frac{d\theta}{dx} + \frac{q_u}{a\beta E}$$

$$\phi_p = \frac{1}{a}[(d+a)(e+B) - 2P] \frac{d\theta}{dx} + \frac{q_u}{a\beta E}$$

The level of the maximum plastic laminar rotation is the same as the level of the first plastic hinge given by equation 6.3 (1 and 2).

6.7.2 LIMITS OF THE EXISTING METHOD

1 - FAILURE OF THE CONNECTING BEAMS

If the rotations of a plastic hinge reach its ultimate allowable rotation, a failure will occur and the beam will no longer play any part in resisting the applied torque. In this stage the above analysis is no longer valid. However the same method of analysis can be used considering an additional zone where q_u equal zero as represented by zone 4 in Fig. 6.2.VII.

2 - NON-LINEAR BEHAVIOUR OF THE CORE WALLS

In the above analysis it was assumed that the walls will remain linearly elastic throughout all the stages of loading and plasticity. However, as the applied torque increases from one stage to another, the stresses in the walls increase, which will have certain effects on the performance of the walls. This effect will take the form

of tensile cracks on some parts of the walls and will eventually reduce the strength of the walls. In this case the analysis may continue assuming a new zone with walls having less strength than the others, as shown in zone 5 Fig. 6.2.VII.

With the continuous increase of the applied torque, either hinges may develop in the tension side of the walls, if they are under-reinforced or a compression crush will occur in the compression sides in the case of over-reinforced walls. In these two cases, the above analysis will no longer be valid.

Any of the above limits may be set to terminate the analysis according to the accuracy required and type of walls involved.

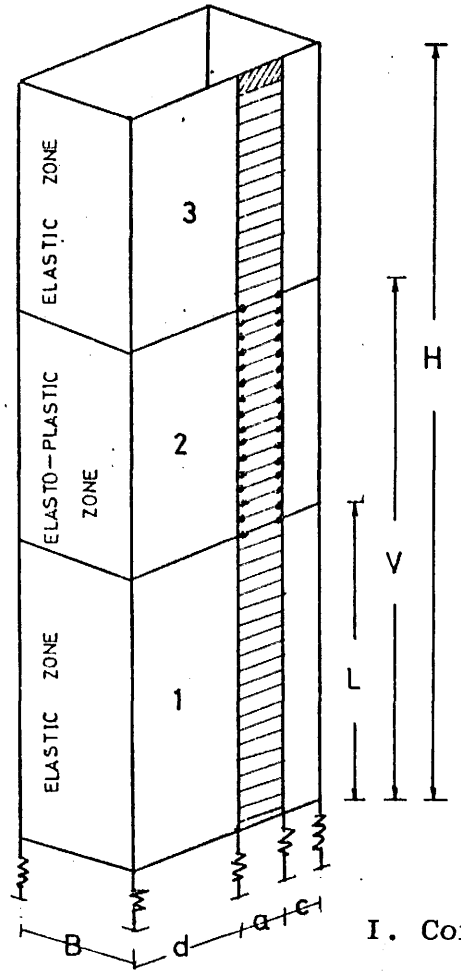

I. Core with elasto-plastic zone in middle

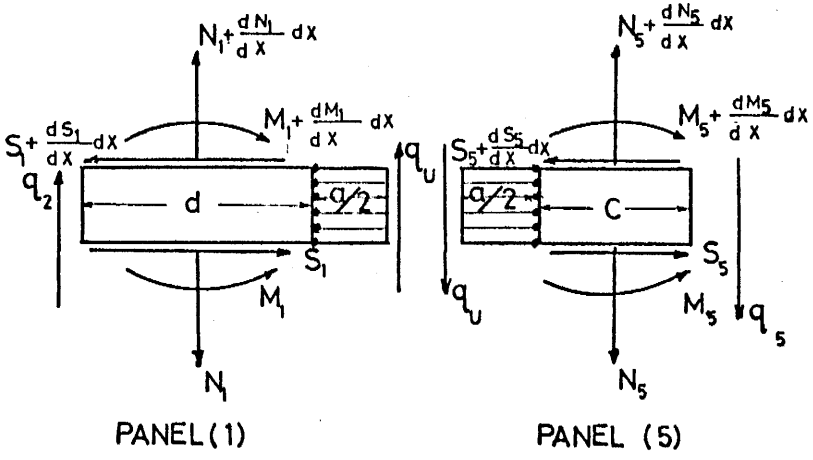

II. Internal forces in the two front panels in the elasto-plastic zone

Fig. 6.1 Core structure undergoing elasto-plastic deformations

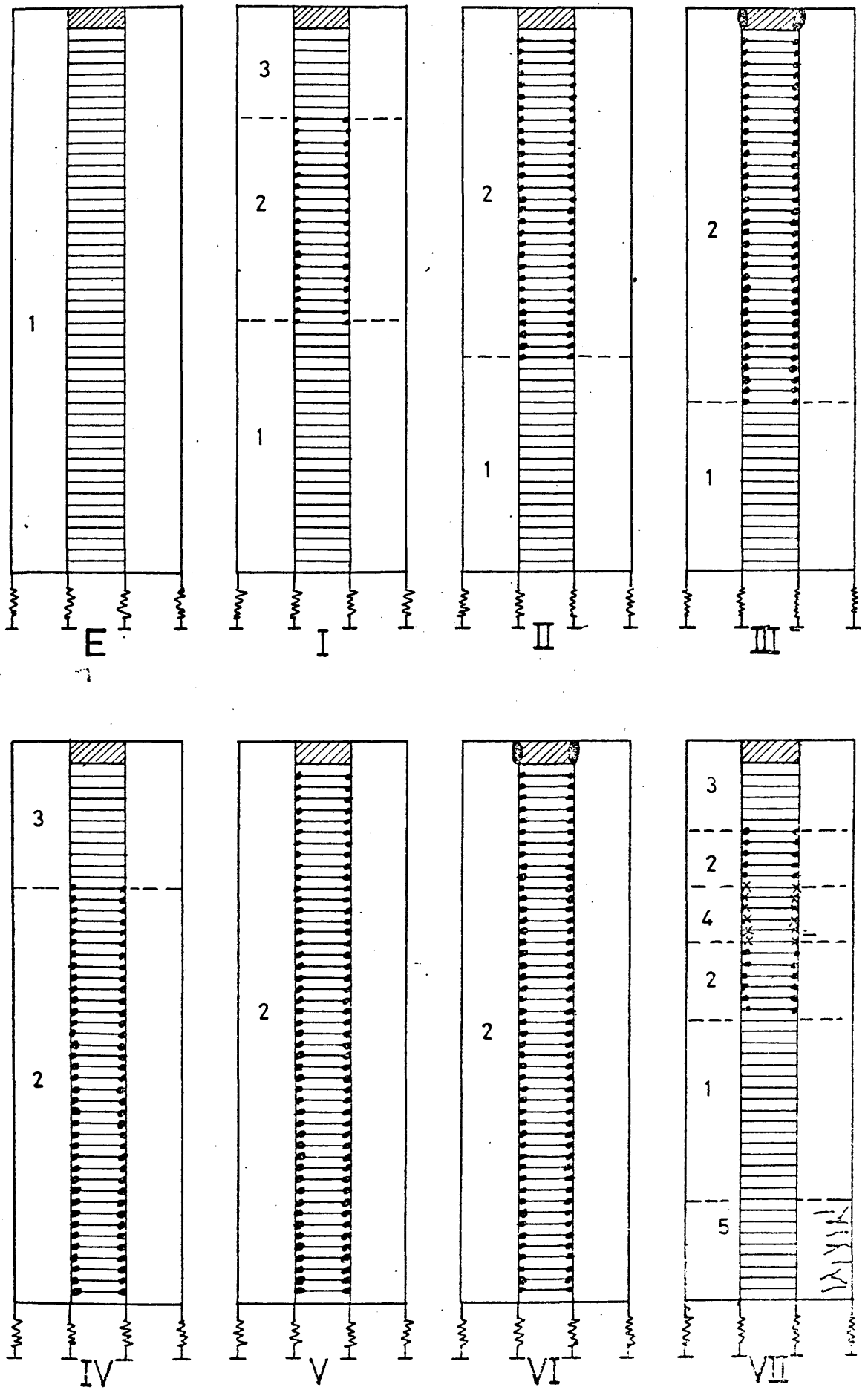

Fig. 6.2 Possible stages of plasticity development in core structures with stiffening top beam and elastic foundations

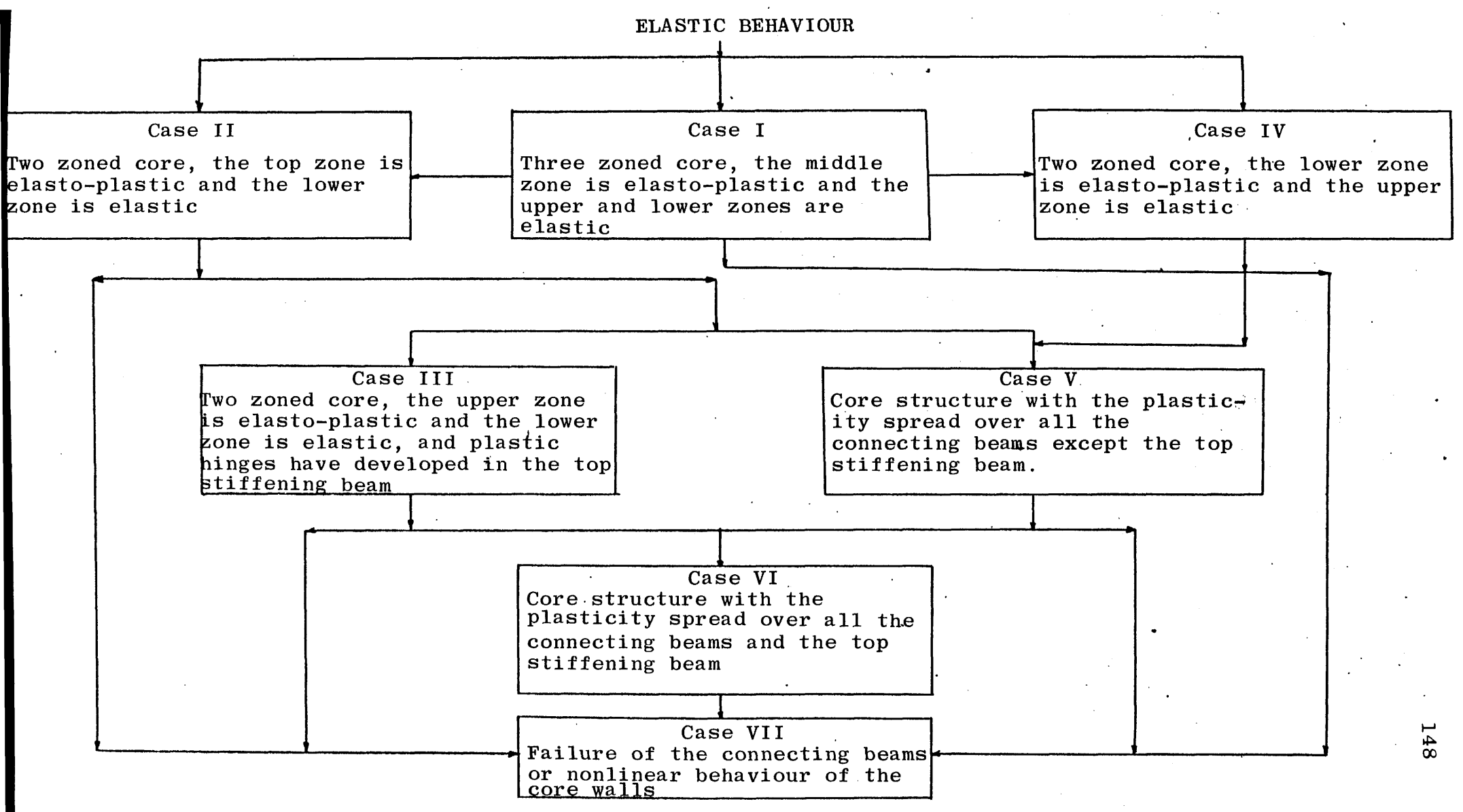

Fig. 6.3 Possible sequence of plasticity development throughout the core height

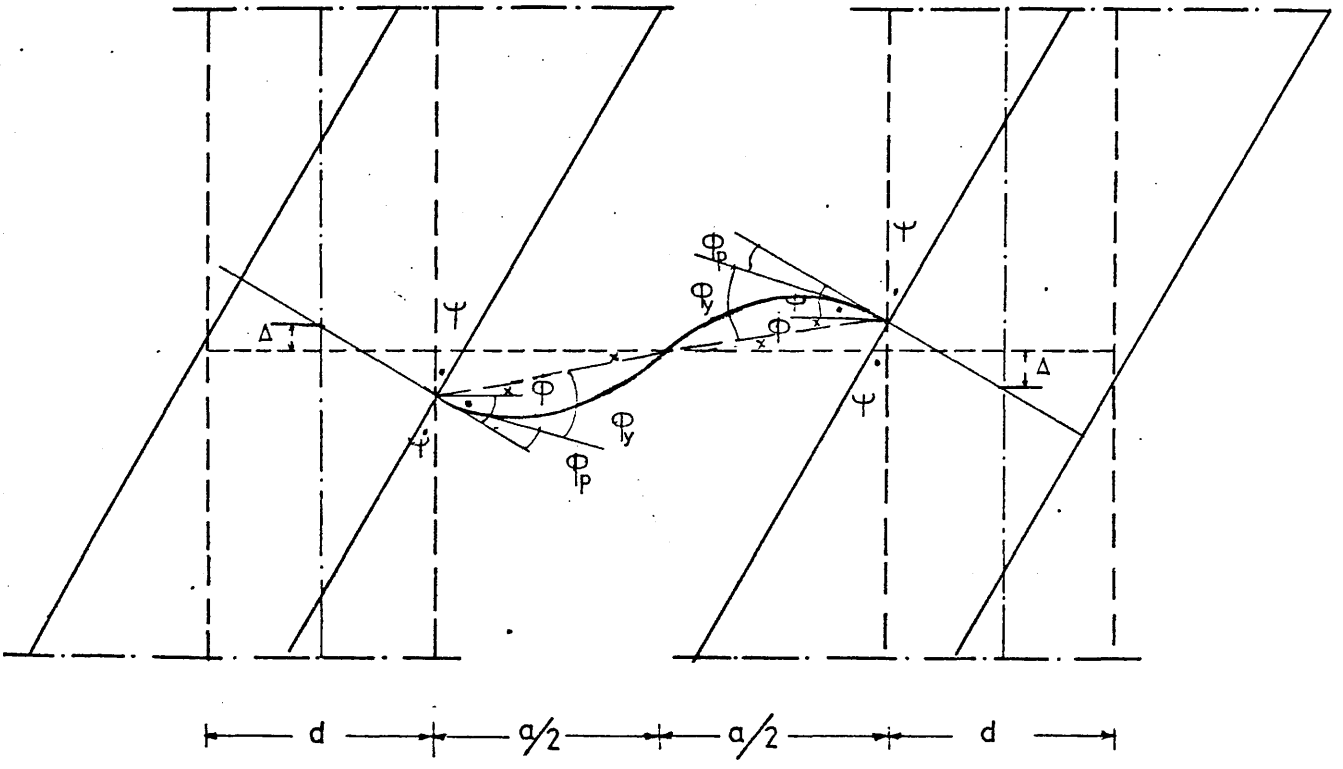

Fig. 6.4 Deformations of connecting lamina and adjacent walls in the elasto-plastic zone

CHAPTER 7

NUMERICAL COMPUTATION

CHAPTER 7

NUMERICAL COMPUTATION

7.1 INTRODUCTION

The present chapter is concerned with the application of the methods of analysis presented in the previous chapters in order to achieve numerical values for the displacements and internal forces of core structures undergoing elastic and elasto-plastic deformations.

Although the mathematical modelling of the behaviour of core structures have been achieved, a full utilisation requires the use of a computer. This is due to the fact that the core behaviour passes through different stages where the core equilibrium condition may only be satisfied by making some assumptions and testing them through a trial and error procedure. Thus, the author resorted to computer programming to achieve numerical values for the mathematical expressions of the elastic and elasto-plastic behaviour of core structures.

The core structures employed in Chapter 4 have again been used as an illustrative example for singly and doubly symmetrical cases with different relative stiffness and end conditions, whilst subjected to the standard cases of loading under consideration. The stages of computation have been explained, the logic sequential order of the computer program used is demonstrated, and illustrations and discussions of the results obtained are presented.

7.2 COMPUTER PROGRAMMING

Some programs were developed according to the requirement of specific tasks such as calculating and plotting the non-dimensional design curves or solving core structures with stiffness variations throughout the height, or to study the effect of the core relative stiffness parameter αH and the boundary conditions parameters R and λ on the elastic and elasto-plastic behaviour of core structures.

The above programs were written in FORTRAN for implementation on the I.C.L. 1904S computer of the University of Strathclyde. The main functions of each program are discussed in the following sections and the source programs are available in the Department of Civil Engineering, University of Glasgow.

7.2.1 PROGRAMS FOR DEVELOPING DESIGN CHARTS (PREC 1, 2 and 3)

The main function of these programs is to calculate the values of U, U1, U2 for given values of αH, R and λ, according to the expressions given in Chapter 4 for the three standard load cases. The calculated results are stored and plotted against the relative height ξ as shown in Appendix B.

7.2.2 PROGRAMS TO STUDY THE ELASTIC BEHAVIOUR OF CORE STRUCTURES WITH STIFFNESS VARIATIONS (PRTH 11, 12 and 13)

These programs were developed to study the elastic

behaviour of core structures with stiffness variations throughout the height according to the method given in Chapter 5. They were designed to calculate the constants GJ_o, I_w and α for each zone and the end condition parameters R and λ from the given core dimensions, material properties and end conditions. Substituting from the above values into the mathematical solutions given in Chapter 5, the core rotations and internal forces are calculated, stored and plotted in the required form.

7.2.3. STUDY OF THE ELASTIC AND ELASTO-PLASTIC BEHAVIOUR OF CORE STRUCTURES (PREPS)

The program PREPS was developed to study the elastic and elasto-plastic behaviour of core structure. It was built up of a series of subroutines each performing a distinct function, which are run by a master driving program. The program was used to study the example structure considered in Chapter 4, but it can be used to study any core configuration by modifying the subroutine STR.

The computation of the displacements and internal forces for a core structure undergoing elastic and elasto-plastic deformations may be divided into four main stages carried out within the program PREPS as follows.

i - CORE PROPERTIES AND APPLIED LOADING

The following parameters are provided as input data; the core height H, the storey height h, core type and configuration, the dimensions of the walls and connecting

beams a, B, D, d, dc, the thickness of the walls th, the material properties given by Young's modulus E and Poisson's ratio ν, the end conditions given by the depth of the top stiffening beam d_s and the foundation flexibility factor λ, type of loading and the density of the applied torque t.

The following core parameters are then calculated; the shear modulus G, St. Venant torsional rigidity GJ, the stiffness of the connecting laminas β, torsional rigidity of the core GJ_o, the warping moment of inertia I_w, the core relative stiffness constant αH, the ultimate shear capacity of the connecting lamina and the top stiffening beam q_u and Q_{su}, the ultimate allowable strain of the walls STN, the top end restraint r and the foundation flexibility parameter μ. The above parameters are then stored and recalled in further stages of computation.

ii - ELASTIC BEHAVIOUR OF THE STRUCTURE

The above parameters are used to calculate the integration constants, the rotations and the internal forces from the expressions given in chapters 2 and 3 for the required loading. The results obtained are printed and stored to be plotted if needed. The calculated shear flows in the connecting laminas are checked against the laminas ultimate capacity q_u, and if it exceeds the assigned value, the calculations will proceed to the elasto-plastic behaviour stage.

iii - PLASTICITY PROPAGATION THROUGHOUT THE CORE HEIGHT

In these stages of computation the behaviour of the core is followed from the purely elastic state through the appropriate elasto-plastic cases according to the core properties, type of loading and end conditions as illustrated in chapter 6. The density of the applied torque t, the limits of the elasto-plastic zone L and V and the constants of integration for each zone K_i are evaluated, printed and stored for each case accordingly.

iv - CALCULATION OF THE CORE ANGLE OF ROTATION AND INTERNAL FORCES

At any stage of loading, it is possible to calculate the core angle of rotation Θ and the internal forces in the core elements q, q_s, M_i, N_i, S_i at any level for design requirements and to check for the safety of the structure according to the British Code CP 110. From the calculated results, the maximum angle of rotation Θ_{max}, the density of the applied torque t and the limits of the elasto-plastic zones, L anv V, are stored and plotted by using an automatic graph-plotter instructed by "GHOST" plotting routines from the I.C.L. computer software library. The logic sequential order of the above program is given in Appendix D.

7.2.4 COMMAND SYSTEM FOR RUNNING THE PROGRAMS

All the above programs and separate data files were stored in the 1904S I.C.L. computer. A general system of

instructions was stored in the computer which is known as "MACRO". Only the desired program and the corresponding data file are called and compiled by stating their names in calling the MACRO. The compiled program is executed and the results printed and stored in another file. If the results are correct and reasonably arranged, it is ordered to be plotted using the graph plotter.

7.3 NUMERICAL RESULTS

The particular core structure shown in Fig. 4.13 have been used as illustrative examples to study the effect of the structural parameters αH, R and λ on the elasto-plastic behaviour of core structures.

As the pattern of behaviour is independent of the core configuration, only the doubly symmetrical case was considered. The above parameters were given the same values as in Chapter 4, while the core was considered to be subjected to the three standard load cases. The development of the plasticity throughout the core height and the corresponding maximum angle of rotation are drawn against the applied torque in Fig. 7.1 to 7.9 for the above cases. At any stage of loading the limits of the elasto-plastic zone and the corresponding maximum angle of rotation could be found by drawing a vertical line passing through the value of the applied torque.

7.3.1 EFFECT OF THE PARAMETER αH ON THE ELASTO-PLASTIC BEHAVIOUR OF CORE STRUCTURES

Changes in the values of the parameters αH were achieved by assigning different values to the depth of the connecting beams as shown in Table 4.1. Consequently the ultimate shear, and corresponding bending moment, capacities of the connecting laminas have increased linearly with the depth. The values of the required applied torque to cause formation of the first plastic hinge with the corresponding level and maximum angle of rotation are given in Table 7.1. The variation in values of the required applied torque is due to the difference in the increase between the ultimate capacity and the vertical shear of the connecting laminas.

The patterns in which the plasticity have developed throughout the core height and the corresponding maximum angles of rotation are shown in Figs. 7.(1, 2 and 3) for the three standard load cases. The above patterns have followed the modes which were predicted from the distribution of the vertical shear in the connecting lamina, given in Appendix B, for the core end conditions and type of loading.

It can be concluded that the core maximum angles of rotation will decrease as the values of αH increase, but the rate of the plasticity development throughout the core height will increase.

7.3.2 EFFECT OF THE TOP END RESTRAINT PARAMETER R IN THE ELASTO-PLASTIC BEHAVIOUR OF CORE STRUCTURES

To study the effect of the top end restraint parameter R, the same core structure was provided with a top stiffening beam with variable depth and stiffening factor as shown in Table 4.2. The depth of the connecting beams was fixed at 0.5m. The load at which the first plastic hinges have developed, the level concerned, and the corresponding maximum angle of rotation for the various values of R, are given in Table 7.2. The propagation of plasticity throughout the core height and the corresponding maximum angle of rotation are shown in Figs. 7. (4, 5 and 6) for the three load cases.

It is seen that the existence of a top stiffening beam increases the torque required to form the first plastic hinge, moves its level downwards and decreases the corresponding maximum angle of rotation. The rate of the above effects decreases with the increase in value of R. The rate of the development of plasticity throughout the core height and the core maximum rotation decrease with the increase of the top restraining parameter R.

7.3.3 EFFECT OF FOUNDATION FLEXIBILITY PARAMETER λ ON ELASTO-PLASTIC BEHAVIOUR OF CORE STRUCTURES

The same core structure was assumed to be erected on flexible foundations with different flexibility parameters λ having the range of values given in Table 4.3. In this case the required torque to form the first plastic hinge

decreases and its level will move downwards as the flexibility parameter λ increases, but in the meantime the corresponding core rotation will increase as is shown in Table 4.3. The rate of propagation of plasticity throughout the core height and the corresponding maximum angle of rotation increases as the flexibility parameter λ increases, as shown in Figs. 7.(7, 8 and 9) for the three standard load cases. This is because the connecting beams will be more active in resisting the warping of the core to compensate for the weakness of the foundation.

αH		1.506	4.128	7.560	11.628
Point Torque	t x 10^6 N.m.	13.58	15.21	21.96	29.20
	X. m.	60.00	60.00	60.00	60.00
	θ x 10^{-3} Rd.	0.01236	0.003508	0.001729	0.001024
Uni. Dist. Torque	t x 10^6 N.m./m.	0.6950	0.5719	0.6087	0.6923
	X. m.	37.98	21.67	16.09	12.66
	θ x 10^{-3} Rd.	0.01456	0.003286	0.001279	0.0006715
Triang. Dist. Torque	t x 10^6 N.m./m.	0.01551	0.01382	0.01566	0.01865
	X. m.	41.52	24.99	19.39	15.87
	θ x 10^{-3} Rd.	0.01421	0.0034	0.00138	0.000749

Table 7.1 Effect of value of αH on the formation of the first plastic hinge

R		0.0	1.318	10.548	35.598	84.36
Point Torque	$t \times 10^{6}$ N.m.	15.21	16.86	18.71	19.29	19.48
	X. m.	60.0	40.03	32.38	30.79	30.34
	$\theta_m \times 10^{-3}$ Rd.	0.003508	0.003669	0.003498	0.003385	0.003339
Uni. Dist. Torque	$t \times 10^{6}$ N.m./m.	0.5719	0.5765	0.5855	0.5888	0.5899
	X. m.	21.67	21.41	20.94	20.77	20.72
	$\theta_m \times 10^{-3}$ Rd.	0.003286	0.003188	0.002986	0.002909	0.002884
Triang. Dist. Torque	$t \times 10^{6}$ N.m./m.	0.01382	0.01398	0.01431	0.01442	0.01446
	X. m.	24.99	24.54	23.75	23.48	23.39
	$\theta_m \times 10^{-3}$ Rd.	0.0034	0.003294	0.003073	0.002988	0.00296

Table 7.2 Effect of value of R on the formation of the first plastic hinge.

	λ	0.0	0.5	1.0	1.5	2.0
Point Torque	$t \times 10^{6}$ N.m.	15.28	14.88	14.81	14.79	14.77
	X. m.	60.00	60.00	60.00	60.00	60.00
	$\theta_m \times 10^{-3}$ Rd.	0.003508	0.00417	0.004295	0.004349	0.004378
Unif. Dist. Torque	$t \times 10^{6}$ N.m./m.	0.5719	0.4119	0.3775	0.3620	0.3532
	X. m.	21.69	10.67	7.215	5.471	4.411
	$\theta_m \times 10^{-3}$ Rd.	0.003286	0.00306	0.003199	0.003136	0.003097
Triang. Dist. Torque	$t \times 10^{6}$ N.m./m.	0.01382	0.01105	0.01039	0.01008	0.00989
	X. m.	24.99	15.17	11.51	9.425	8.035
	$\theta_m \times 10^{-3}$ Rd.	0.0034	0.003607	0.003353	0.003514	0.003486

Table 7.3 Effect of value of λ on the formation of the first plastic hinge

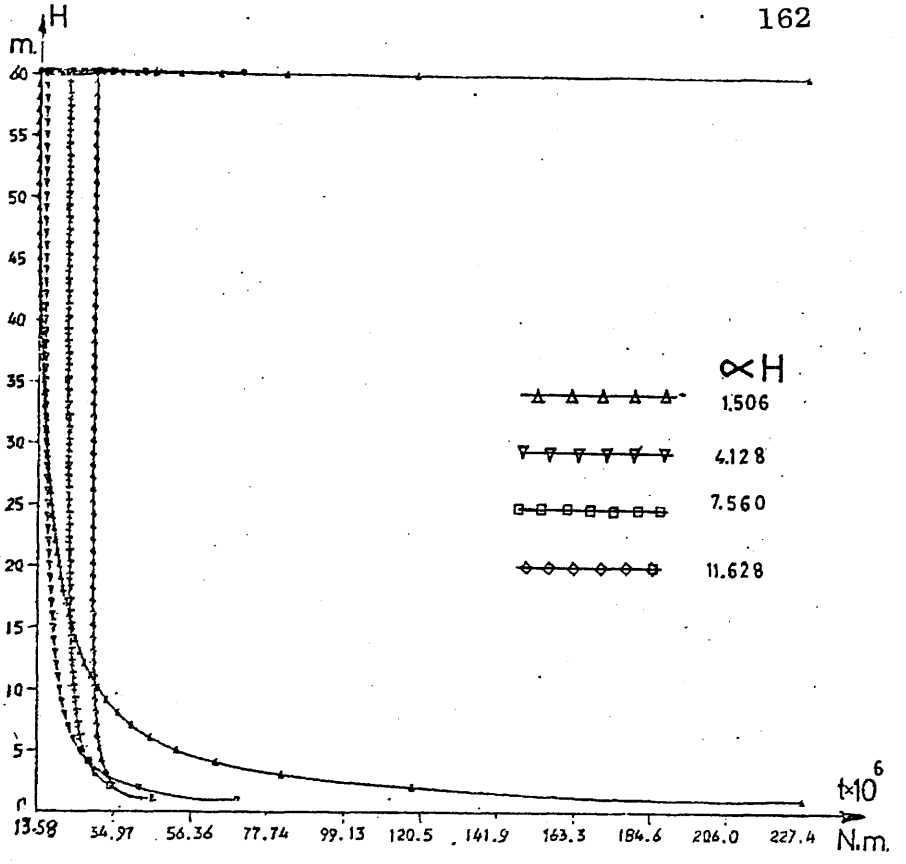

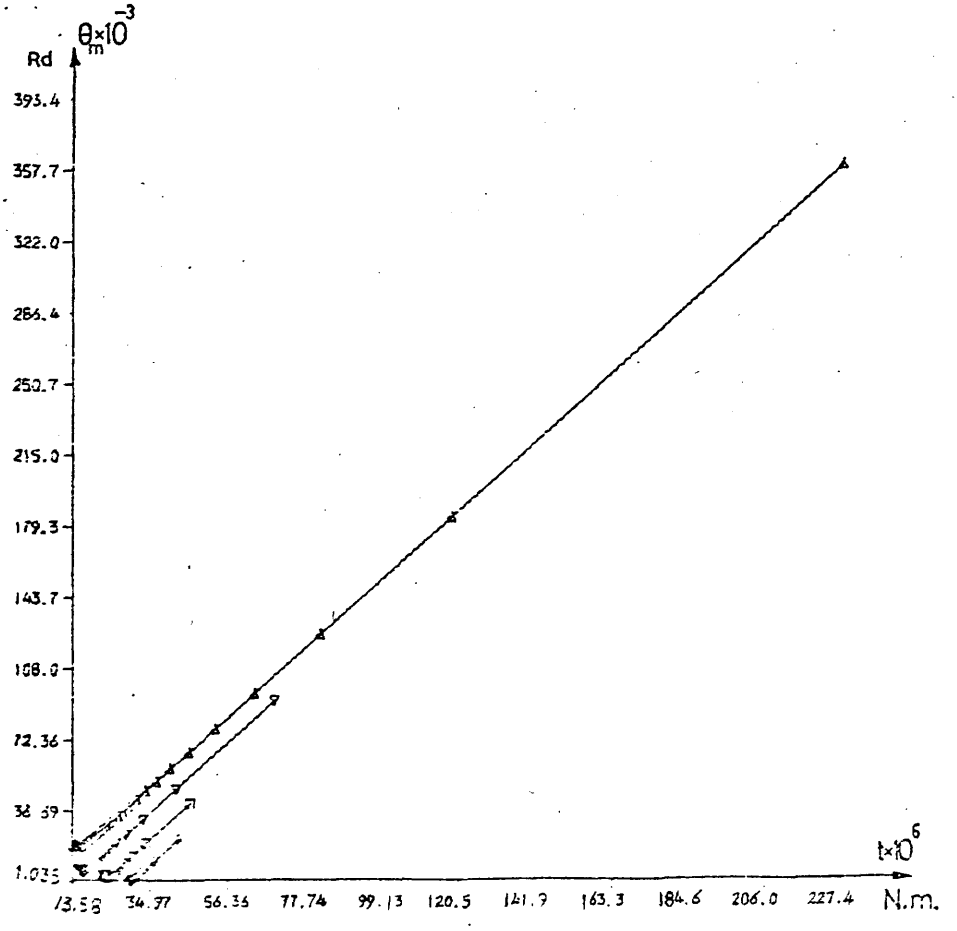

Fig. 7.1 Effect of value of αH on the development of plasticity throughout the core and the corresponding maximum angles of rotation (Doubly Symmetric - Point Torque at the top)

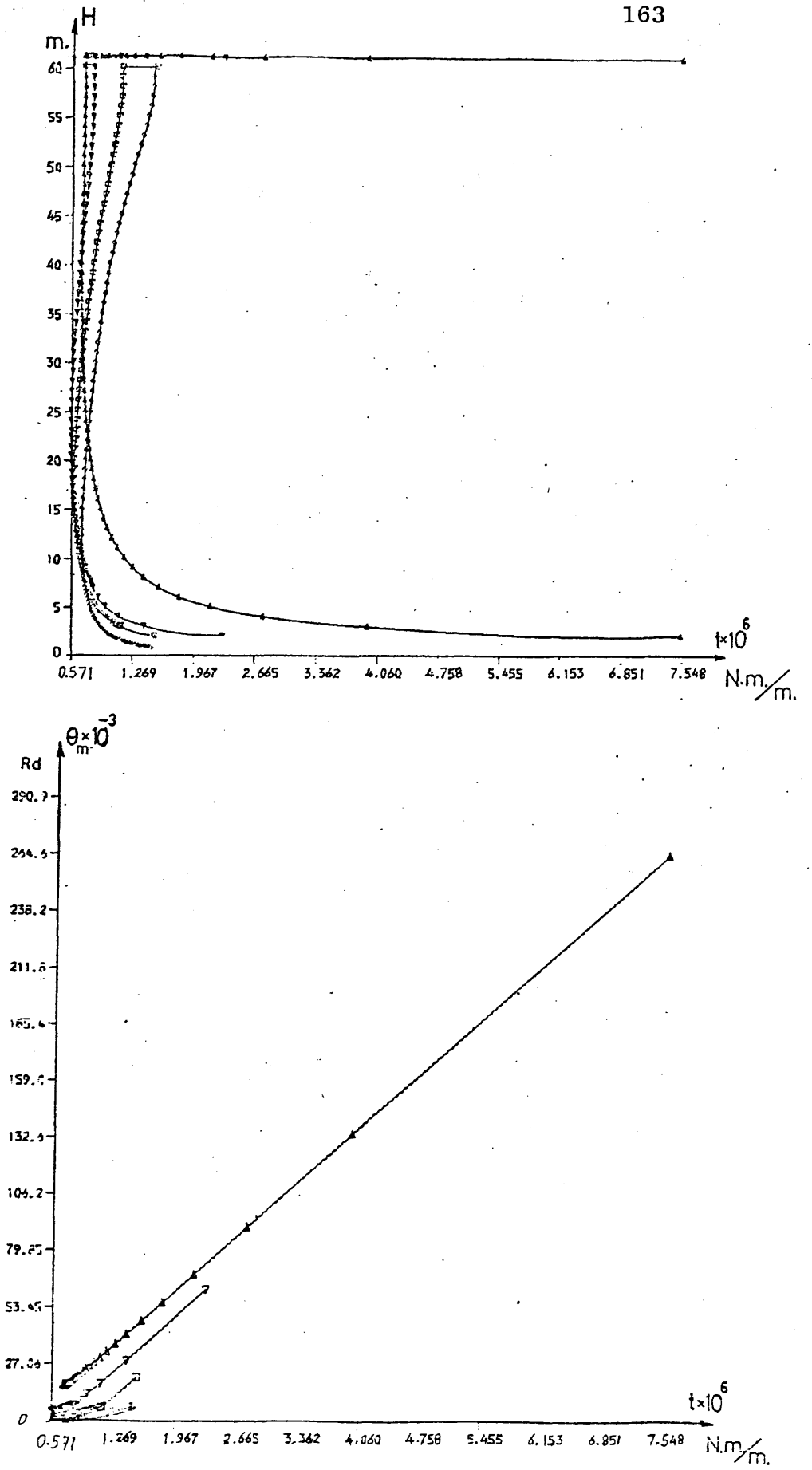

Fig. 7.2 Effect of value of αH on the development of plasticity throughout the core and the corresponding maximum angles of rotation (Doubly Symmetric - Uniformly Distributed Torque):

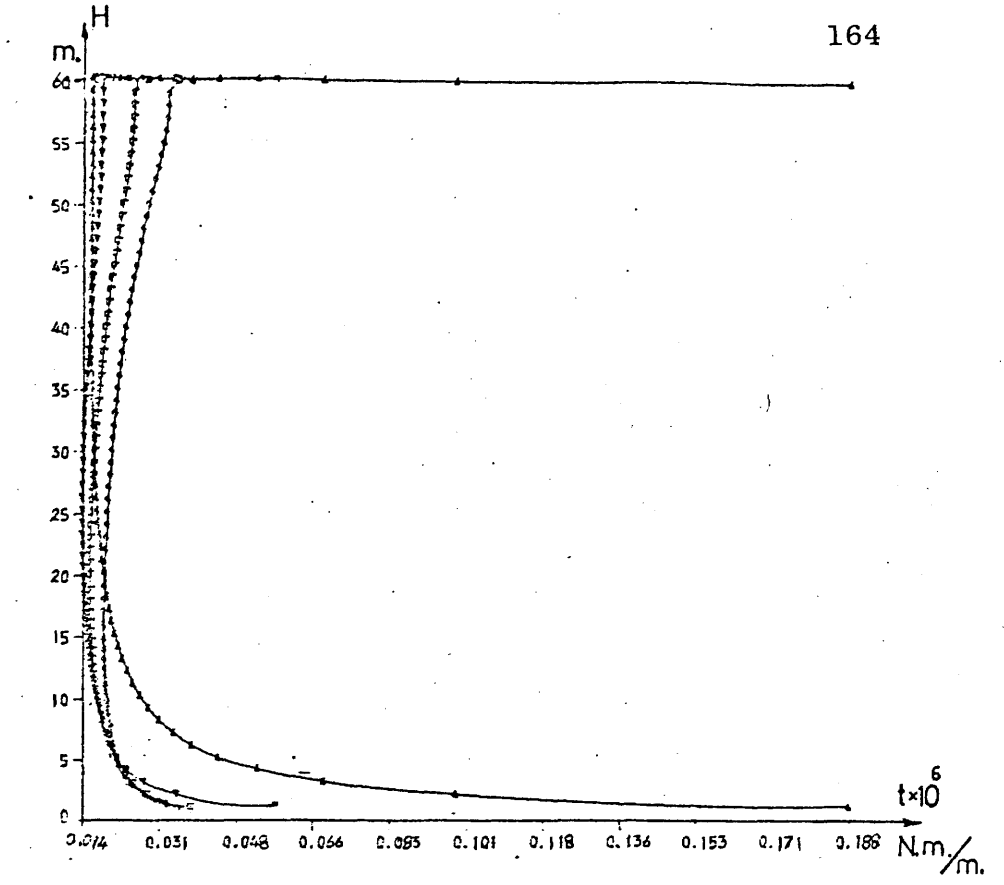

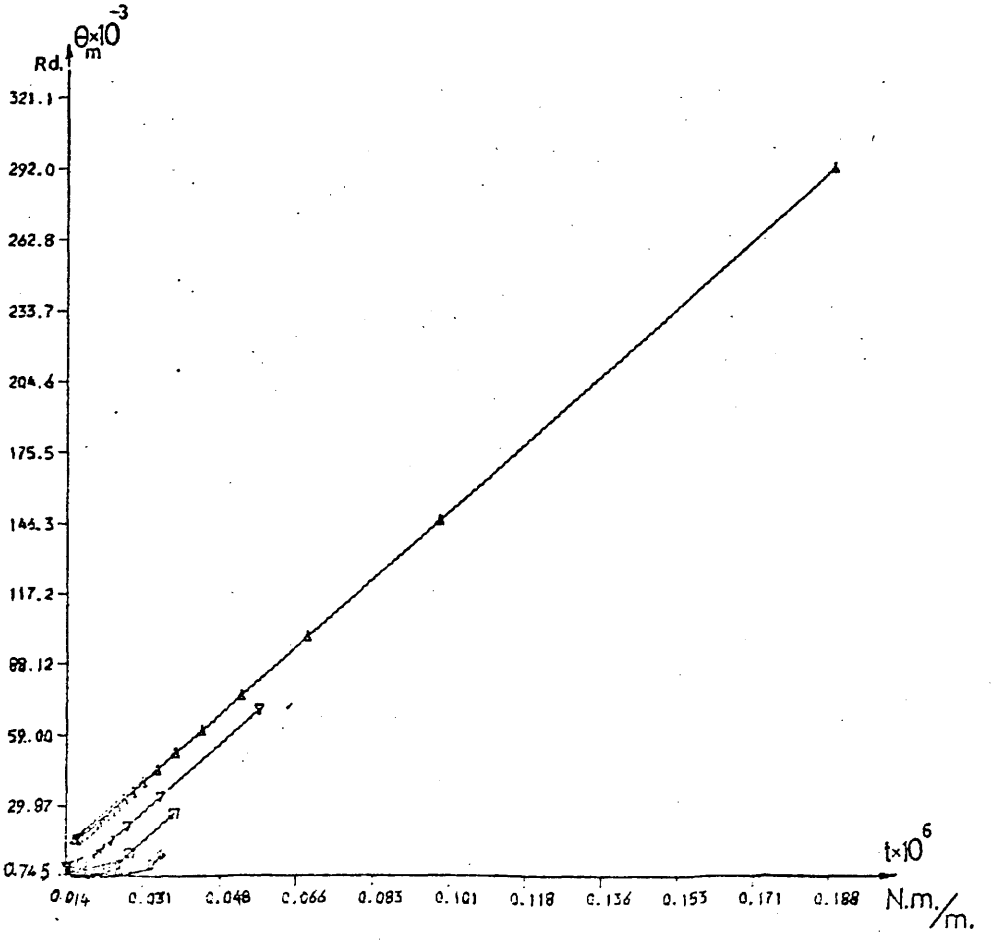

Fig. 7.3 Effect of value of αH on the development of plasticity throughout the core and the corresponding maximum angles of rotation (Doubly Symmetric - Triangularly Distributed Torque)

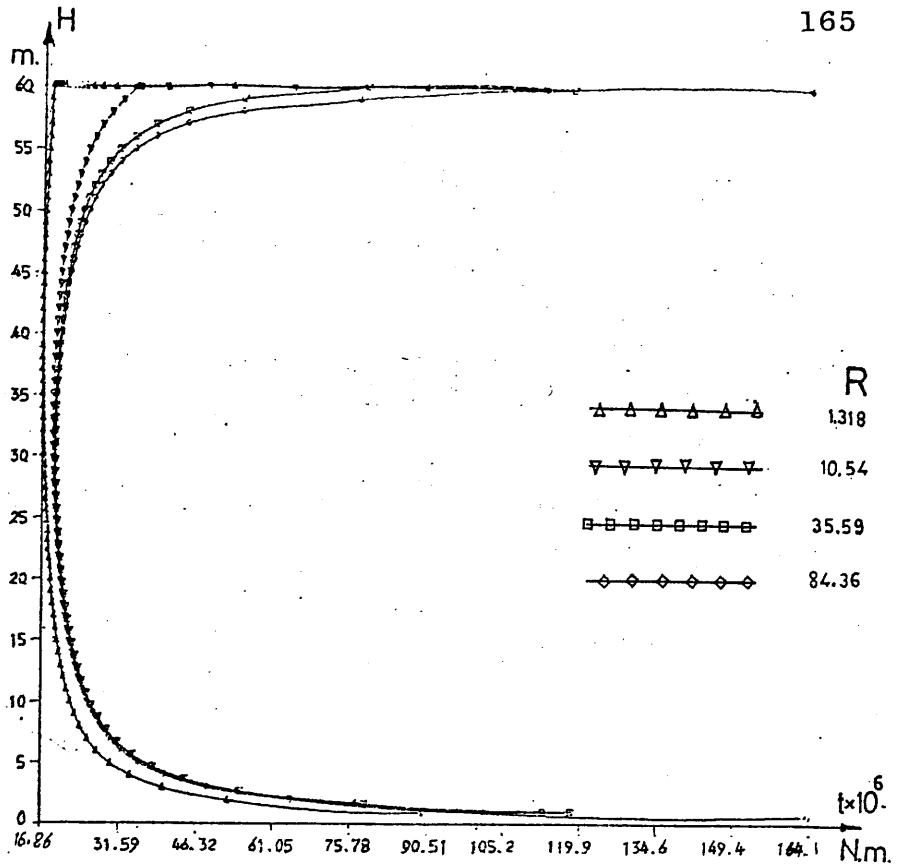

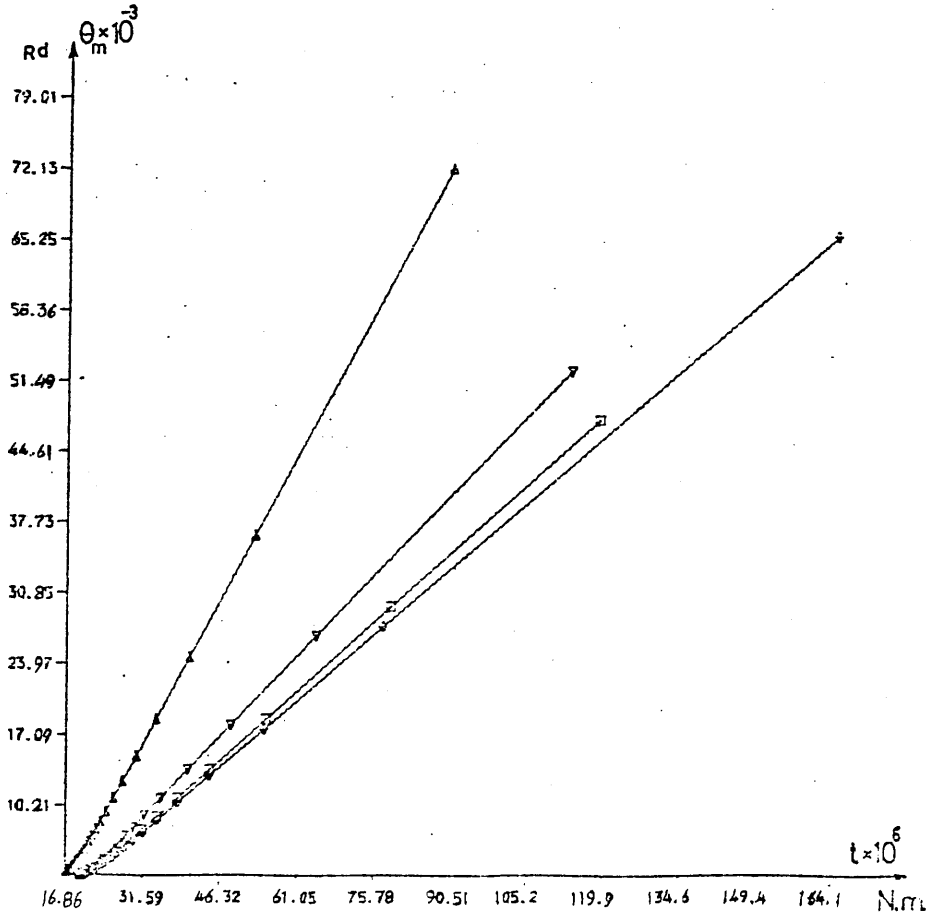

Fig. 7.4 Effect of value of R on the development of plasticity throughout the core and the corresponding maximum angles of rotation (Doubly Symmetric - Point Torque at the top)

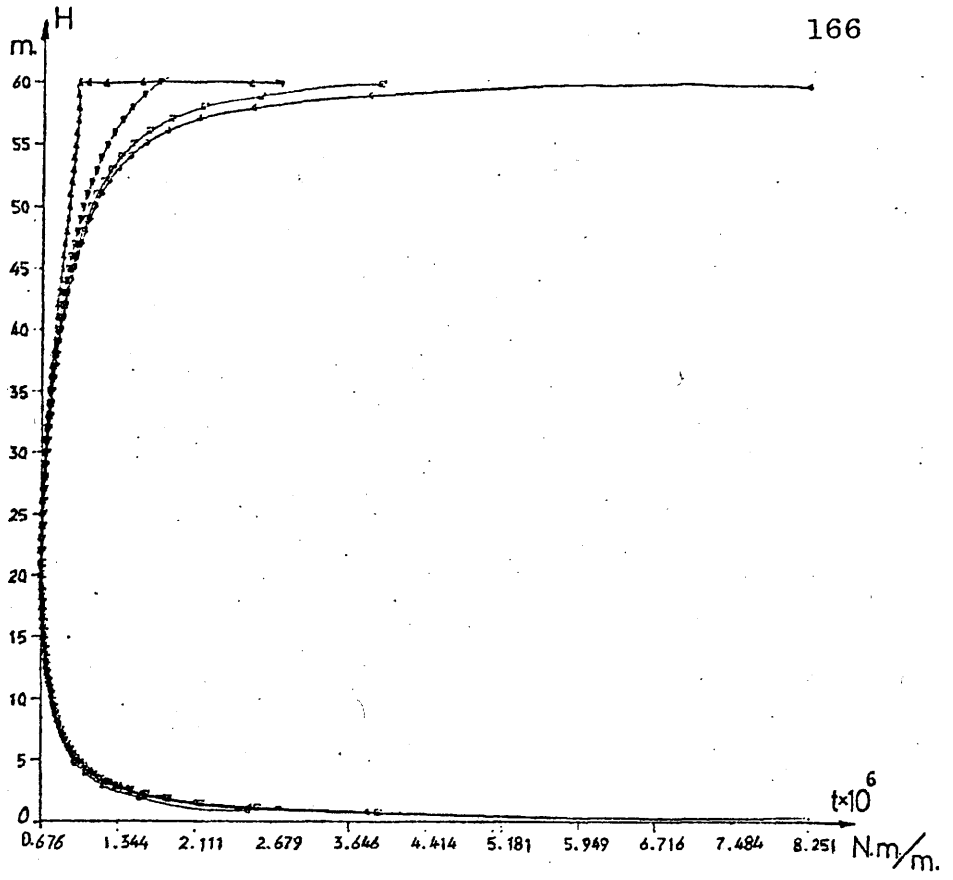

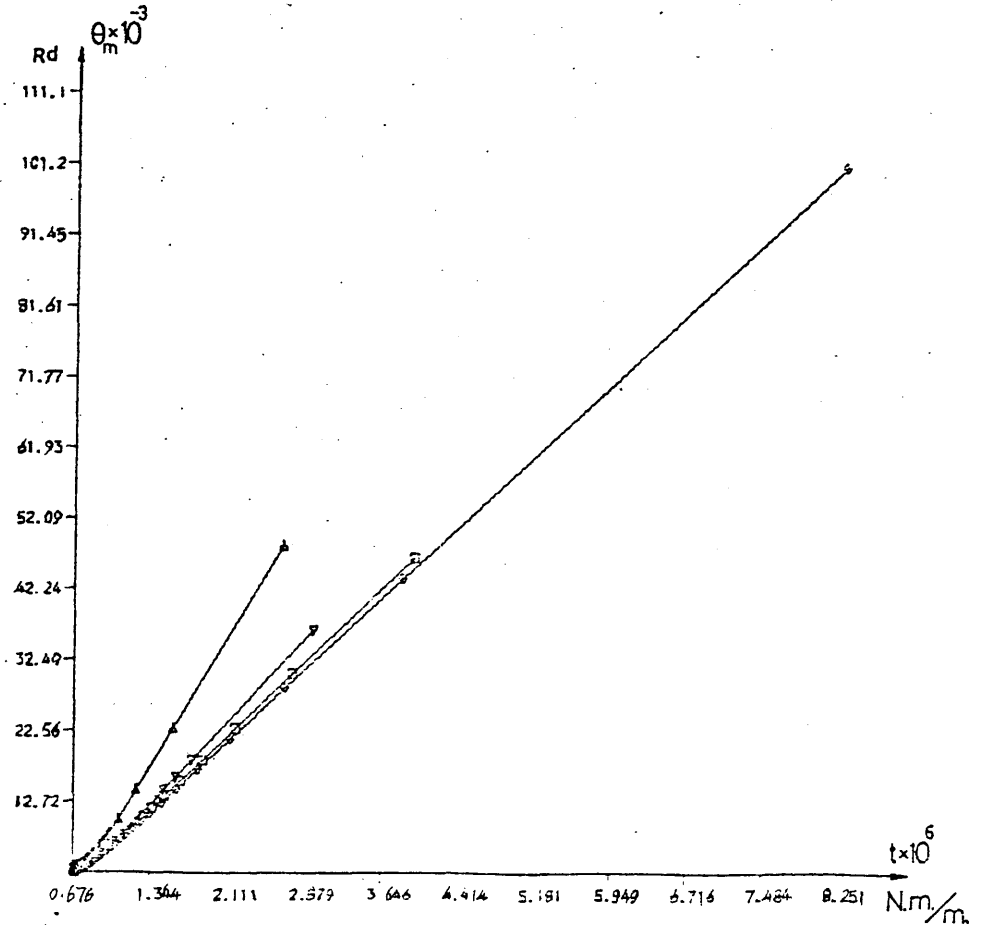

Fig. 7.5 Effect of value of R on the development of plasticity throughout the core and the corresponding maximum angles of rotation (Doubly Symmetric - Uniformly Distributed Torque)

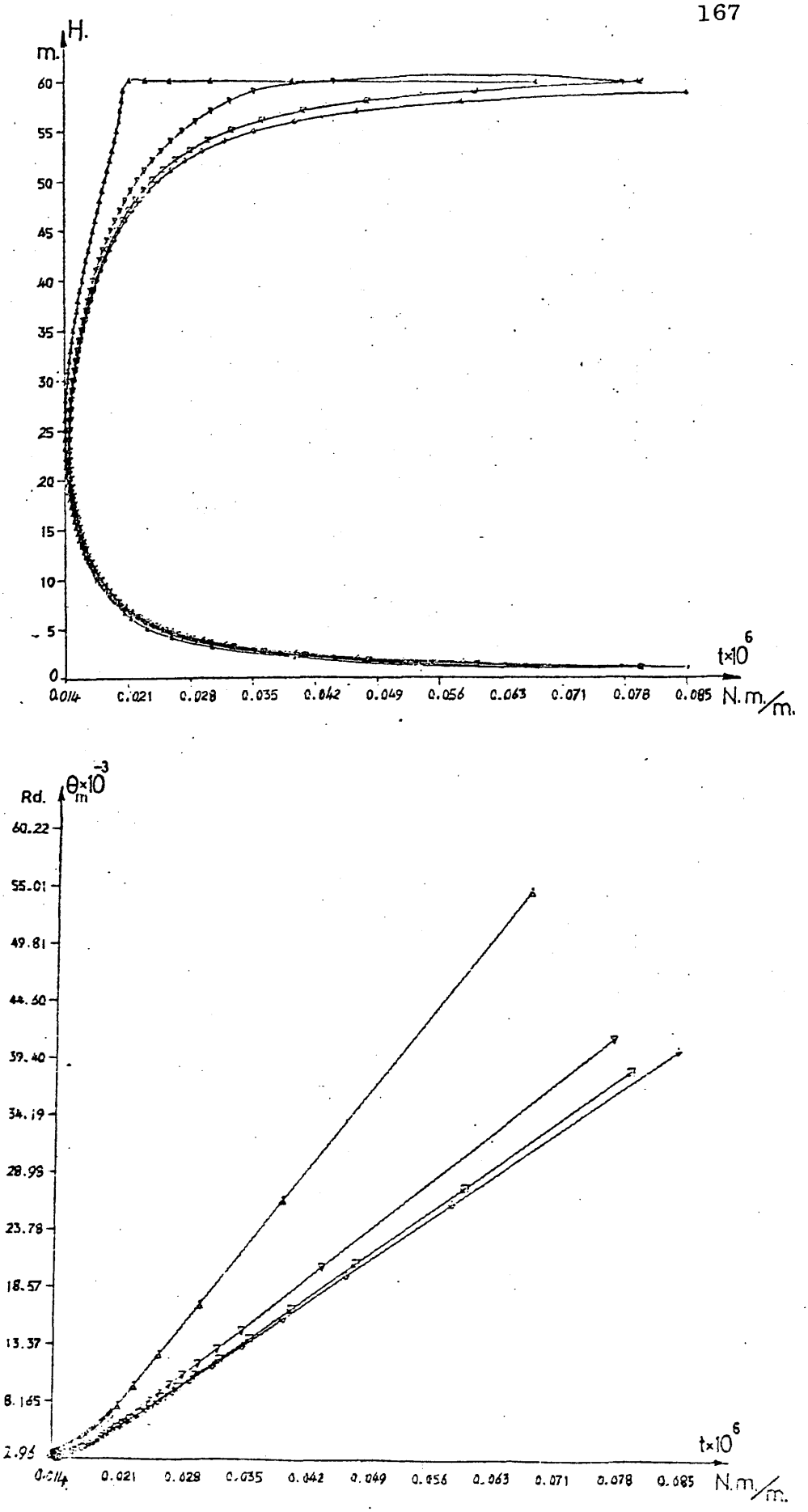

Fig. 7.6 Effect of value of R on the development of plasticity throughout the core and the corresponding maximum angles of rotation (Doubly Symmetric - Triangularly Distributed Torque).

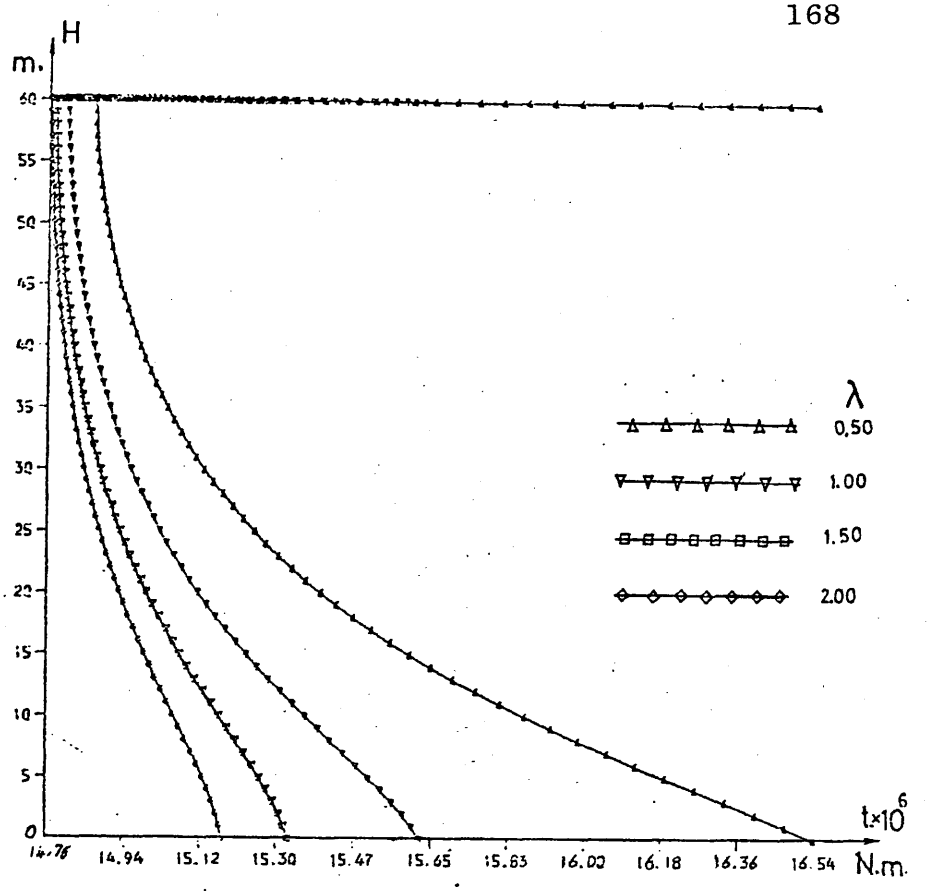

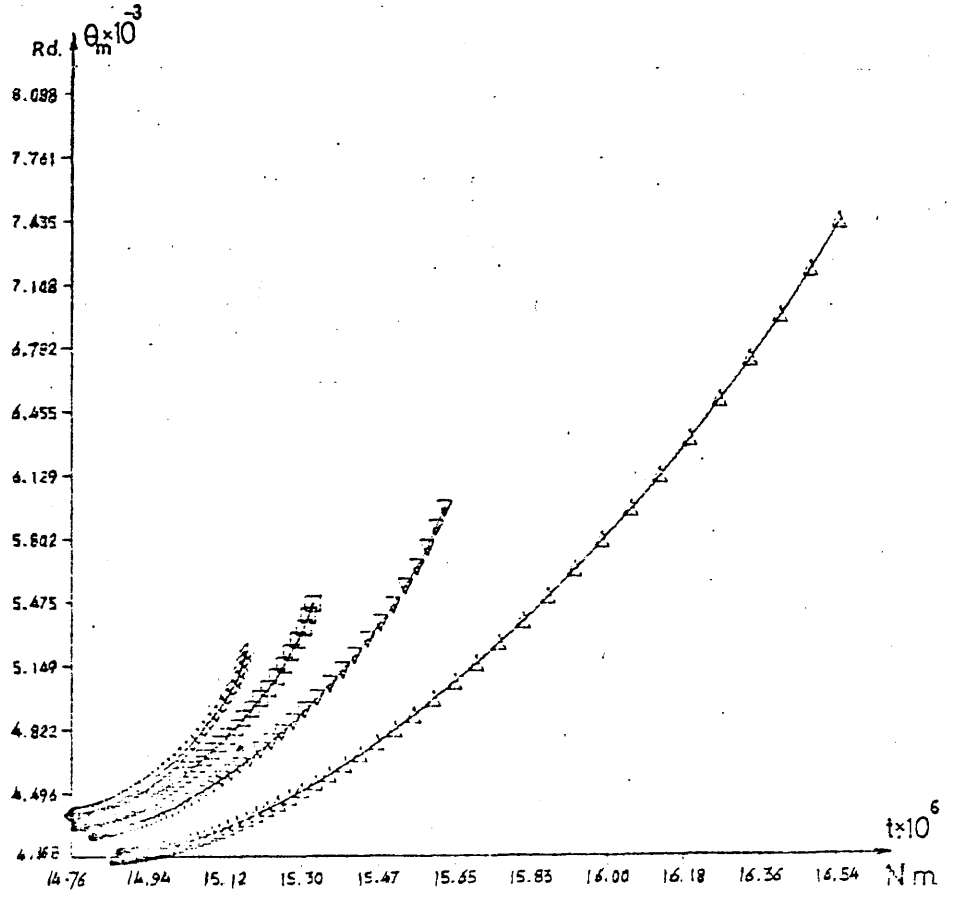

Fig. 7.7 Effect of value of λ on the development of plasticity throughout the core and the corresponding maximum angles of rotation (Doubly Symmetric - Point Torque at the top)

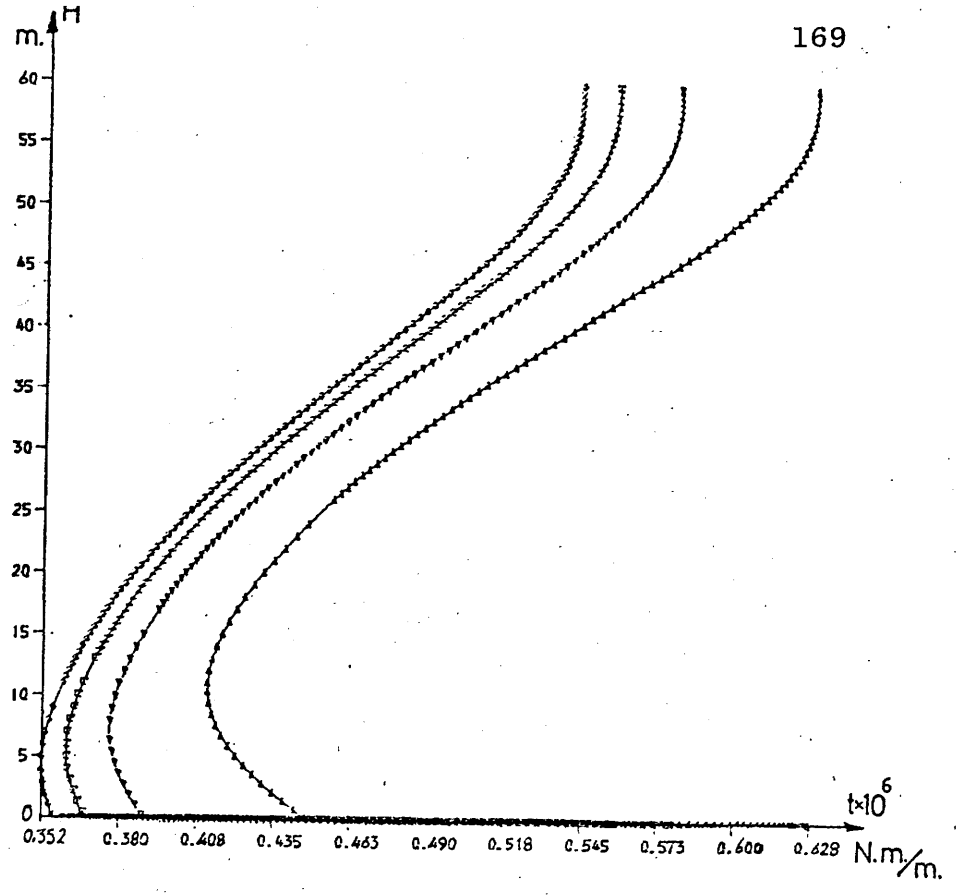

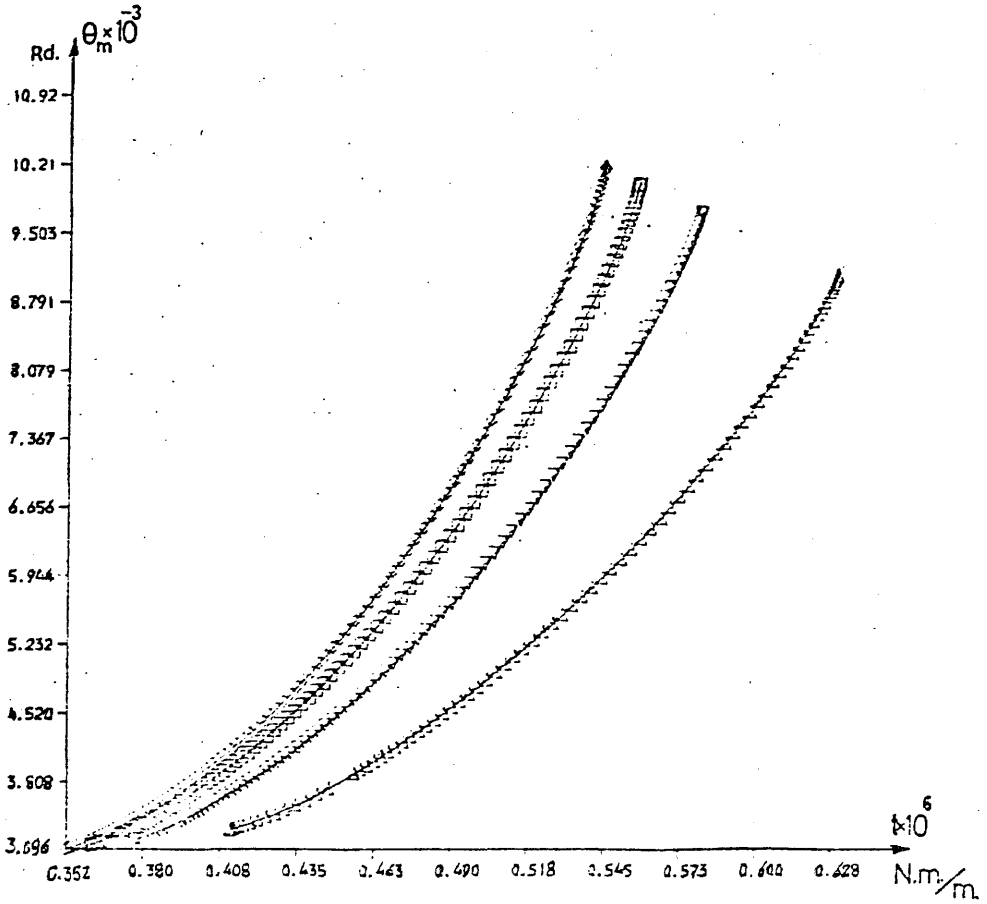

Fig. 7.8 Effect of value of λ on the development of plasticity throughout the core and the corresponding maximum angles of rotation (Doubly Symmetric - Uniformly Distributed Torque)

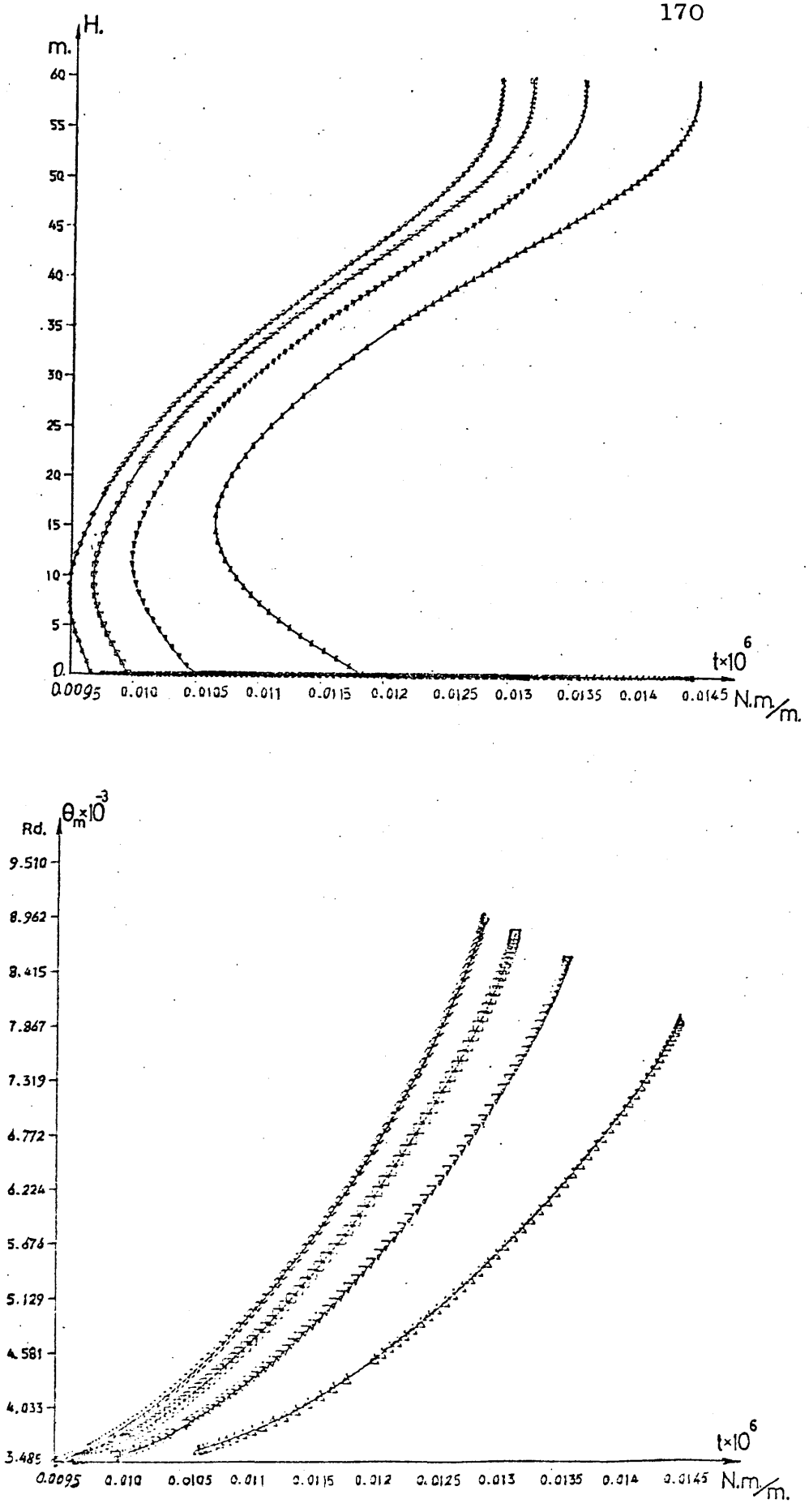

Fig. 7.9 Effect of value of λ on the development of plasticity throughout the core and the corresponding maximum angles of rotation (Doubly Symmetric - Triangularly Distributed Torque)

CHAPTER 8

EXPERIMENTAL INVESTIGATION

CHAPTER 8

EXPERIMENTAL INVESTIGATION

8.1 INTRODUCTION

In order to substantiate the methods of analysis demonstrated in chapter 2 and chapter 6 for the elastic and elasto-plastic behaviour of core structures subjected to torsional loading, two sets of experimental investigations were carried out. The first set of experiments was conducted on perspex acrylic models to study the elastic behaviour of core structures in the following situations.

1 - Singly-symmetric core, fixed at the base, free at the top and subjected to a point torque at the top.
2 - Singly-symmetric core, fixed at the base, restrained at the top and subjected to a point torque at the top.
3 - Doubly-symmetric core, fixed at the base, free at the top and subjected to a point torque at the top.
4 - Doubly-symmetric core, fixed at the base, restrained at the top and subjected to a point torque at the top.

The second set of experiments was carried out on microconcrete models, which were built and tested to study the elastic and elasto-plastic behaviour of core structures for the first and third cases of the above set.

The various aspects of the experimental investigation, comparison between the experimental and theoretical results and discussion of results are given in this chapter.

8.2 EXPERIMENTAL STUDY OF THE ELASTIC BEHAVIOUR OF CORE STRUCTURES

8.2.1 CHOICE OF MATERIAL

The selection of a suitable material for models designed to simulate the elastic response of core structures depends upon several requirements. The chosen material must show a linear stress-strain relationship, the strains induced by a reasonable test load should be of sufficient magnitude to be measured accurately and the material should be isotropic and homogeneous.

In addition to the above requirements, the material must be available, relatively inexpensive and not difficult to be machined and fabricated.

Therefore, it was decided to construct the models from perspex acrylic sheets, as it satisfies the aforementioned requirements.

The perspex has some disadvantages as a modelling material. Its properties are affected by changes in room temperature and humidity, and it creeps under loads. However, if the necessary precautions are taken during testing, results of reasonable accuracy may be obtained using perspex models.

8.2.2 MODEL CONFIGURATIONS AND DIMENSIONS

Two perspex models were constructed to simulate twelve-storey singly and doubly symmetrical cores. The configurations and dimensions of the models are shown in Fig. 8.1, and their geometrical properties are given in

Table 8.1.

Each model was cemented into a relatively rigid base of 25 mm thick perspex plate. The cross-sectional shape of each core was held undistorted by using circular plates fitted at each second level, the top plate was used to transmit the torsional loading to the core as shown in Plates 8.1 and 8.2. After the initial series of tests were completed, two aluminium plates were cemented and bolted through four holes to the top connecting beams to simulate a top end restraining beam.

8.2.3 TEST FRAME FOR PERSPEX MODELS

The test frame in which the perspex models were mounted during the test is shown in Plates 8.1 and 8.2. It consists of a heavy horizontal I beam at the floor level, two vertical columns welded to it at each end and a rectangular base fixed at mid span of the horizontal beam. Two 50 mm diameter pulleys, fixed at the tops of two opposite columns, one on each side were employed to transmit horizontal loads to the models. The horizontal I beam was 310 x 205 mm and 1150 mm length; the first two columns were made of two equal angles 150 x 150 mm and the second two columns were made of two equal channels 102 x 51 mm. The rectangular steel base was made of four square hollow sections 60 x 60 mm welded together and fixed to another two square hollow sections 100 x 100 mm. which in turn were welded to the I beam. The perspex base of the model was further strengthened by placing another steel diaphragm above it. The steel diaphragm, the perspex base

and the fixed base were firmly clamped together by $\frac{1}{2}$ inch diameter screwed rods to form a fixed end condition at the base.

A secondary frame was built around the model of light aluminium bars to attach the dial gauges for the measurements of the displacements.

8.2.4 MEASUREMENTS OF STRAINS AND ROTATIONS

i - STRAIN MEASUREMENTS

Electrical resistance strain gauges type "EA-41-600BH-120" were used to measure the strains induced on the models by the applied torque. Four sets of strain gauges were fixed to each model. The first set was placed at the top tension side of each connecting beam to assess the shear forces in the beams. The second set was fixed at mid-height of the first storey at 5 mm. from the corners. The third set was fixed near the top of the walls to measure the effect of the top end restraint. The last set of strain gauges was placed on the inner face of the walls at the same level and position as the second set to provide a check on any out-of-plane bending. The positions and numbers of the strain gauges of the first three sets are shown in Fig. 8.2 for the two models.

All the strain gauges were glued to the model by "M-BOND-200" adhesive and covered by a coat of "M-COAT-D" for insulation and protection. The resistance of each gauge was checked by "AVO-METER" to ensure that there were no faults in the gauges or the connections. Then the

strain gauges were wired to a switch and balance unit model "SB-1"; each unit provides a means of monitoring the output of ten strain gauges, which in turn were connected in parallel to a portable strain indicator model "P-350A". Both of them were made by "Vishay Instruments".

For each switch and balance unit, a dummy gauge was provided by a perspex model not under test, which has the same properties as the perspex of the test model, fitted with identical strain gauge to those on the test model.

ii - ROTATION MEASUREMENTS

During the tests the displacements of the models were measured by "MERCER" dial gauges with a maximum travel of 26 mm. and a sensitivity of 0.01 mm per division, which were attached to the light aluminium frame surrounding the model. The dial gauges were positioned at the ends of the circular diaphragm arms a distance L apart, (where L was nominally 600 mm.), at each second floor level as shown in Plate 8.1 and 8.2.

The angle of rotation θ and the position of the shear centre at the levels given in Fig. 8.2 have been calculated by taking the readings g_1 and g_2 as shown in Fig. 8.3 and substituting in the following cases.

The angle of rotation θ for the singly symmetrical model was evaluated from the expression

$$\theta = \frac{g_1}{S} = \frac{g_2}{L-S}$$

where

L = the distance between the dial gauges at the same level

g_1 and g_2 = the dial gauge displacements measured simultaneously.

$$S = \frac{g_1 L}{g_1 + g_2}$$

The distance e of the shear centre from the back wall will be given by

$$e = L\left(\frac{1}{2} - \frac{g_2}{g_1 + g_2}\right) - \frac{B}{2}$$

In the case of the doubly symmetrical model, θ was evaluated from the expression

$$\theta = \frac{g_1 + g_2}{L}$$

8.2.5 DETERMINATION OF THE ELASTIC PROPERTIES OF PERSPEX

In order to evaluate the stresses induced in the models from the strain gauge readings and to compare the experimental results with the calculated results using the proposed theoretical analysis, the elastic properties of the perspex, namely Young's modulus E and Poisson's ratio γ were evaluated. Two test specimens, 5 x 37.5 x 305 mm., were cut from the same sheets of perspex as were the walls of the models. Three electrical resistance strain gauges were fixed on each specimen, two longitudinally on the centre line at mid-span on opposite faces and the third in the perpendicular direction at a distance of 12.5 mm. from the mid-span position. The specimens were tested in bending between two level supports, 240 mm. apart, two equal loads being applied at the third points of the span

to produce a constant bending moment and no shear in the region of the strain gauges. Specimens were loaded gradually by small increments and the readings of a dial guage positioned at mid-span of the specimen and the strain gauges were recorded. The same number of readings were recorded during the gradual unloading, each specimen being tested four times, twice on each face.

Young's modulus was evaluated from the results of the deflection readings and strain readings separately by using a desk calculator to perform a least squares linear regression, which is designed to minimise the sum of the squares of the deviations of the actual points from the straight line of best fit. Poisson's ratio was evaluated by dividing the strain of the lateral gauge by the corresponding strain of the longitudinal gauge.

The average values of Young's modulus and Poisson's ratio, which were used in the theoretical analysis of the perspex models and for the evaluation of stresses are given in Table 8.1.

8.2.6 TEST PROCEDURES

The model was fixed to the test frame by screwed rods passing through its base. The surrounding light frame was fixed in position and the dial gauges were positioned at the right levels and touching the arms of the horizontal plates at the required length L. Two extra dial gauges were positioned on two opposite corners at the top of the model in an attempt to measure the warping displacements. Two screw nails were fixed to the top

horizontal plate with two cords attached to them and running over the two side pulleys; a hanger was attached to the end of each cord on which weights could be placed.

Prior to each test, the model was loaded to half the intended maximum load and unloaded. The actual test usually started 30 minutes after the unloading to ensure that all the components were fully settled.

Before starting to load the model for the test, the reading of each strain gauge was recorded and the dial gauges were set to zero. The weights were placed on the hangers almost at the same time with care to avoid any impact effects, in increments of 5 lb. A time interval of 10 minutes was allowed after each load increment before the readings were taken to permit the gauges to settle to reasonably stable values. Six increments of loadings were applied in each test, and the rotations and strains were recorded in the same order throughout.

In order to minimise the errors due to creep in the perspex, after recording the readings of the last load increment, the model was unloaded by equal decrements and a separate set of readings were recorded. The mean of the two results obtained from loading and unloading was used in comparing the experimental with the theoretical results.

8.2.7 THEORETICAL ANALYSIS

The models were analysed theoretically to provide a comparison between the experimental and the theoretical

results. In the theoretical analysis, the models were considered to be fixed at the base, free at the top in the first case and restrained at the top in the second case.

The values given in Table 8.1 were incorporated into the solutions given in Chapter 2 and 3 to evaluate the internal forces and rotations of the models when subjected to the corresponding values of point torque at the top.

8.2.8 COMPARISON BETWEEN EXPERIMENTAL AND THEORETICAL RESULTS

The results of the experimental investigation carried out on the perspex models as described before are presented graphically and compared with the analytical solutions corresponding to each particular test as follows:

i - ROTATIONS

The core maximum rotation when the models are restrained and unrestrained at the top are calculated from the measured displacements and plotted against the applied torque in Figs. 8.5 and 8.9 for the singly and doubly symmetrical models respectively. The angles of rotation at the maximum applied torque are calculated in the same way at different levels throughout the height of the models and compared with the corresponding theoretical values for both models in Fig. 8.6 and Fig. 8.10.

The results show good agreement for both models where there is no end restraint at the top. When a stiff top beam has been provided to the models, a small

reduction in the rotation of the singly symmetrical model has been recorded, but the theoretical results have been reduced significantly due to the effect of the top end restraint. However in the doubly symmetrical model the good agreement has been maintained although the experimental results are slightly greater than the theoretical results.

ii - VERTICAL SHEAR IN THE CONNECTING BEAMS

The vertical shear in each connecting beam is deduced from the bending moment calculated from the readings of the strain gauges for the maximum applied torque and plotted with the theoretical shear force distribution for both models in Fig. 8.7 and 8.11.

The plots of the experimental values follow the same characteristic form of curve obtained from the theoretical calculations. The existence of a top end restraint did reduce the theoretical values of the shear force significantly. However the same effects have not been verified to the same degree experimentally, and may have been due to the difficulty of determining these relatively small forces.

iii - STRESSES IN THE WALLS

The stresses in the walls were evaluated from the readings of the strain gauges and plotted together with the theoretical stress distribution at the levels of the strain gauges in Figs. 8.8 and 8.12 for the two models.

The correspondence between the experimental and

theoretical results appears to be good in all the cases at the lower levels. In the cases when a top stiff beam is present the stresses at the top of the walls are greater than the theoretical values near the beams and in the opposite sense at the adjacent corners.

8.2.9 DISCUSSION OF RESULTS

To draw any sound conclusions from a comparison between the experimental and the theoretical results, the various possible sources of error should be identified, eliminated if possible or accounted for, in both sides.

In the experiments, the errors in the experimental results may be attributed to three main sources, the modelling material, the accuracy in constructing and testing the models, and the deficiencies in obtaining and analysing the results.

The properties of perspex are affected by changes in room temperature and humidity. To compensate for these effects dummy strain gauges were attached to a perspex model not under test and connected to the switch and balance unit. However, these errors are not expected to be significant as the entire test used to take an average of two hours inside a reasonably controlled laboratory under atmospheric conditions.

Although the loads were increased and decreased by a fixed increment and readings were taken at fixed time intervals after each increment or decrement and the two values averaged, the readings taken at the last stages of loading are greater than the actual values. Because of

the tendency of perspex to creep under loads, the models continued to creep under the existing loads, so that the rotations did not decrease after the first two decrements of loading. In some tests it continued to increase after the first decrement. The models were cut and constructed accurately but a complete symmetry may not be achieved because of possible variations in the thickness of the walls and the local restraining effect of the external diaphragms. The applied torque was created by hanging two equal weights at the ends of two cords passing over two pulleys which may have different frictional resistances and will result in two unequal applied loads at the model. However, in all the tests fairly symmetrical conditions were achieved as indicated by displacement and strain measurements.

The perspex base of the model may suffer local strains due to the actions of the walls. This will increase the measured rotations and decrease the stresses in the walls.

The top added stiffening beams were bolted to the model through four bolts, two at the third points of the top connecting beam and one at the centre line of each wall. It may have resulted in four axial forces at the top rather than the usual connecting beam actions.

The strain gauges and the strain indicator were carefully checked before performing each test to detect any errors due to defects in them. The accuracy of the readings measured from strain gauges may be affected by the local stiffening effect of the strain gauge and the adhesive on the perspex especially in such small sections

as the connecting beams. The errors involved in these cases are expected to be very small.

The dial gauges located at the ends of the two arms of the circular diaphragms showed higher values of rotation θ in the earlier tests, due to the flexibility of the arms. The tests were repeated after reducing the distance between the dial gauges at each level and adding another two dial gauges around the model itself near the top as a further check.

Two dial gauges were located above the model on two opposite corners to measure the warping strains on the walls, but they did not give any meaningful readings. This was not unexpected due to the very small deflections concerned.

Each test was carried out twice with 24 hours difference in time and the results of the tests were averaged and compared against the theoretical values.

Any inaccuracy associated with the theoretical analysis can be attributed to the following sources:

In the theoretical analysis the transverse stiffness of the walls was neglected by idealising the walls as thin plates. This will result in an underestimation of the torsional resistance of the models. However, in the models tested the thicknesses of the walls were relatively small compared to the other dimensions of the models and the errors due to that source should be small.

The second source of errors comes from neglecting St. Venant torsional resistance of the closed cross-section

parts of the models at each connecting beam, which would result in an underestimation of the stiffness of models.

Another source of error which arises from replacing the discrete connecting beams by a continuous medium. The accuracy of the above approach increases with an increase of the number of connecting beams. Considering the number of the connecting beams to the overall dimensions of the models, the errors in this case should be quite small.

8.3 EXPERIMENTAL STUDY OF THE ELASTO-PLASTIC BEHAVIOUR OF CORE STRUCTURES

The aim of this investigation was to check the validity of the proposed method of analysis of the elasto-plastic behaviour of core structures, as well as to study the crack pattern of such partially closed box structures.

Testing models constructed from materials having a linear elastic behaviour is unsatisfactory as concrete is known to have a nonlinear stress-strain characteristics even in the range of the working loads. Therefore, to conduct investigations into the behaviour of real concrete structures up to the state of failure, tests must be carried out on small concrete models to provide a pattern of behaviour as close as possible to that of real structures.

It was not required to simulate a specific prototype structure. The basic requirements were to construct a core which would have substantially the same material properties as any reinforced concrete structure, and which would have a shape and dimensional ratios which could be scaled up to give a real core structure. It was also required to allow a realistic study of the core overall behaviour, cracking propagation and mode of failure. Two models were built of singly and doubly symmetrical forms, to study the complete behaviour to failure in each case.

8.3.1 DESIGN OF THE MODELS

It was considered desirable to make the models as

large as possible in order to minimise the size and shrinkage effects and to reduce the percentages of tolerances connected with the construction processes, but this was limited by the loading equipment and the space available in the laboratory. A controlling factor was the thickness of the walls which would allow two cages of reinforcement and the aggregate particles to pass through. The core dimensions were chosen in reasonable proportions with the chosen thickness as shown in Fig. 8.13. The design of the models was based on the assumptions that:-

1 - The concrete does not resist tension.

2 - The distribution of the concrete strain is linear across each wall.

3 - A rectangular stress block is appropriate for the concrete in compression.

4 - The strain in the steel is the same as that in the concrete surrounding it.

The beams and walls were designed to be under-reinforced to allow the steel to yield first, prevent sudden failure, allow for large deflection and crack propagation, and for the full strength of the structure to be realised.

8.3.2 MATERIALS FOR CONSTRUCTION OF THE MODELS

1 - CONCRETE MIX DESIGN

A local HYNDFORD sand with grading as shown in Fig. 8.14 was chosen along with ordinary Portland Cement to construct the models. Three trial mixes were made and tested for compression and indirect tension by using cubes

of 37.5 mm for compression tests and 37.5 x 75 mm cylinders for indirect tension tests. The mix proportions and the averages of the results of the tests are given in Table 8.2.

The first mix was chosen as the most suitable one, considering its workability, f_{cu}/f_t (ratio of compression strength to tensile strength) and its setting time to allow for the casting of the whole model before the initial setting time is reached.

2 - REINFORCEMENT OF THE MODELS

The model reinforcement was required to have a stress-strain relationship as close as possible to the short term design stress-strain curve for reinforcement given in The British Standard Code of Practice CP 110. Four different types of reinforcements were considered so that a suitable one or a combination of more than one of them could be incorporated in constructing the models. These were,

1 - Plain rods
2 - Threaded rods
3 - Deformed bars similar in appearance to the hot rolled ribbed high yield reinforcing bars used in practice.
4 - Small diameter wire ropes consisting of seven wires twisted around one of them.

The second and third types of reinforcement proved suitable to provide sufficient bond and crack patterns which were reasonably close to the prototype which they were meant to simulate as found in other experiments (31).

However they were omitted because of the high cost involved in buying the threaded rods, which were not available in the required lengths, or manufacturing a deforming machine to produce deformed bars. Therefore the choice was limited to the first and last types, both of them being cold rolled mild steel having a stress-strain behaviour reasonably close to the required pattern, but which do not have a definite yield point.

The discriminating factor was their bond characteristics, since it was required to provide sufficient bond to cause complete yield failure without any slip between the reinforcement and the concrete, as well as an overall cracking pattern similar to what would occur in a real structure. Thus, three sets of experiments were carried out to provide information about their bond characteristics.

I - CONCENTRIC PULLOUT TEST

This test was carried out on four groups of reinforcements, 3 mm diameter plain rods and 7 x 0.7 mm, 7 x 1.0 mm and 7 x 1.25 mm diameter twisted wire ropes embedded in 37.5 x 75 mm cylindrical specimens as shown in Plate 8.3. The average of the best four results of each group are given in Table 8.3, expressed as a pull-out force per millimetre of the embedded length.

II - ECCENTRIC PULLOUT TEST (Bending Bond Strength)

A - STRAIGHT BEAMS

A set of five beams of dimensions 30 x 50 x 300 mm were symmetrically reinforced with two plain rods of 3 mm

diameter on each side and provided with vertical double links of 1.2 mm diameter every 25 mm. They were simply supported on a 200 mm clear span and tested with a point load at the centre.

All the beams failed due to slipping of the rods with one major crack under the loading point because of lack of bond between the concrete and the plain rods.

B - U-SHAPED BEAMS

Another set of three beams were designed to simulate the actual conditions of reinforcement length and detailing in the models. The beams were constructed in a U-shape with a cross-section of 30 x 50 mm, 400 mm main span and 200 mm in each leg as shown in Plate 8.3. The first beam was reinforced by plain rods and vertical links as before, the second beam was reinforced similarly, but was provided with extra aluminium angles fixed to the rods at the corners, and the last beam was reinforced with 7 x 1.0 mm twisted wires, two in each side and the same number of links. The beams were tested under a central point load on the span of 200 mm. The first two beams failed due to lack of bond with a major crack under the loading point, concrete failure at the inner corners due to the pulling out of the reinforcement and yield failure of the steel in the outer corners due to the concentration of tensile stresses at the corners. In the third beam the failure was clearly due to yield of the reinforcement with one major crack under the loading point and some minor cracks

in the surrounding zone; no cracks were observed near the corners. In the meantime no diagonal tension cracks were observed in any of the above tests due to the existence of the vertical stirrups.

As a result, it was decided to use wire ropes for reinforcing the models according to the design requirements.

8.3.3 CONSTRUCTION OF THE MODELS

Each of the models was constructed in four stages as follows.

i - PREPARING THE FORMWORK

The shuttering was made of two main parts, a fixed part composed of a horizontal board with Polystyrene blocks arranged in distances equal to the depth of the connecting beams to create the openings in the front wall, and two vertical wooden shutters to determine the outer faces of the side walls, as shown in Plate 8.4. The second part was in the shape of a closed box as shown in Plates 8.5 and 8.6 (for the singly and doubly symmetrical sections respectively) to be placed inside the outer part as shown in Plate 8.7 to create the core hole and the side and back walls.

ii - ARRANGING THE REINFORCEMENT

Two different sizes of wire ropes were used in reinforcing the models. The connecting beams were symmetrically reinforced with three wire ropes 7 x 0.7 mm on each surface and provided with vertical stirrups of

1.2 mm plain rods every 25 mm. The walls were reinforced with 7 x 1.25 mm diameter wire ropes and provided with horizontal links made of 7 x 0.7 mm diameter wire ropes spaced at every 50 mm.

The reinforcements for the connecting beams were placed to a high degree of accuracy to ensure sufficient cover through its full length. The same accuracy could not be achieved in locating the reinforcement for the walls due to the flexibility of the wires and their long lengths, as well as the larger spacing between the stirrups.

The reinforcement for the walls was extended outside the formwork to create hangers at the top and to allow for a sufficient anchorage length for embedment in the base. The detailing of the model reinforcement is shown in Fig. 8.16. The base was reinforced with 10 mm diameter deformed bars as shown in Fig. 8.17.

iii - CASTING THE MODEL

The outer shuttering was fixed to a vibrating table to ensure good compaction all through the model during casting. The front wall was concreted first up to its full thickness and partially vibrated. The inner shuttering was then placed inside the outer part and fixed by nailing its top and bottom to the side walls of the outer shuttering as shown in Plate 8.7. The concrete was then poured in to create the two side walls and the back wall. The whole model was vibrated until air bubbles failed to appear.

iv - CASTING THE BASE OF THE MODEL

After 24 hours the outside shuttering was struck and the model was kept under wet conditions for one week. The inner shuttering was then removed and the model lifted using the top hangers and placed on a steel chair to support the model during casting the base. The extra lengths of the reinforcement of the walls were embedded in the base.

The base was provided with four rods of one inch diameter each near the corners to fix the model to the laboratory strong floor. Plate 8.8 shows the adjustment of the doubly symmetrical model during casting the base. Control specimens were taken from the same batch during the casting of each model, and kept and cured under the same conditions as the models.

8.3.4 LOADING AND SUPPORTING SYSTEMS

The models were tested under a concentrated torque at the top by using two hydraulic jacks to impose two equal and opposite forced on the model. The jacks were supported against two steel columns with a load cell behind each one as shown in Plate 8.9. The loads were produced by a hydraulic pump forming part of a system capable of providing four independently controlled pressure points although only two points were used.

A steel diaphragm consisting of two separate parts built of 75 x 75 mm square hollow sections and joined together by two $\frac{3}{4}$ inch threaded tie rods, to fit exactly around the model, was fixed around the core at the top.

The two rounded ends of the hydraulic jacks were arranged to meet the top diaphragm at two opposite sides and at equal distances from the centre line of the core.

A reinforced concrete roof slab was fitted at the top of the model to ensure that the top end will rotate as one unit and create only torsional loading. Another four steel diaphragms made of 25 x 25 mm square hollow sections were firmly tied around the core at four different levels to prevent any out of shape distortions during the test. The diaphragms consisted of three sections welded together to form a U-shape, and the fourth was bolted across to form the closed section, through threaded rods welded to the ends of the arms of the U-section.

The model base was fixed to the laboratory strong floor slab by four threaded tie rods, each of one inch diameter, through the holes created in the base during casting.

8.3.5 INSTRUMENTATION, MEASUREMENTS, AND DATA PROCESSING

Three different types of measurements were required to be recorded during the test, namely, the load applied at each jack unit, the displacements of the model in the two major (Y and Z) coordinate directions at four different levels, and the strains at chosen points on the beams and walls of the model.

For load measurements, two N.C.B./M.R.E. load cells (type 403 manufactured by W.H. MAYES & SON (WINDSOR) LTD) were positioned behind the hydraulic jacks. They were connected to a digital computer (type PDP-8/L) which in

turn was connected to a remote data display to give instantaneous readings of the actual loads applied to the model. The model displacements were measured by NOVATECH (type RR-102S) electrical transducers with two inch strokes. They were fixed at chosen points at four different levels to a metallic frame erected around the model to measure the displacements in the Y and Z directions as shown in Fig. 8.4.

Strain gauges (type EA-06-500BH-120 with 120 $\pm$ 0.15% Ohms resistance and 2.04 $\pm$ 0.5% gauge factor at 75°F) were used to measure the strains in the model at chosen points. The positions of the strain gauges and the levels of the transducers are shown in Fig. 8.18 for both models.

All the instruments and their readings were controlled and recorded by the PDP-8/L digital computer through a remote controller which allowed the readings to be taken at any stage during testing of the models.

Data processing comprises three stages, firstly, taking the initial readings for the above measurements, subtracting them and setting zero initial readings for the following stages. The second stage was carried out with the aid of the remote data display, when the applied loads were equal to the required values at both jacks, a new scanning for the measurements was ordered to be carried out and recorded by the remote controller. In the third stage, the recorded data were converted and printed out in the form of KN, for loads, mm,for displacements, and microstrains, for strains.

8.3.6 TEST PROCEDURES

Prior to each test, the loading equipment, the measuring instruments, and the connections were checked to be in working order and an initial reading was taken. The loads were applied through the two hydraulic jacks and increased by increment of 100 lb on each jack until the core ultimate strength was attained. There was a time lag between the two jacks in reaching the required load in every increment due to the fact that they were independently controlled.

After each increment the computer recorded and printed the required measurements which take an average of 58 seconds to complete. The surface of the model was examined and all the observed cracks were marked and numbered in correspondence to the applied load.

In the first (singly symmetrical)model, the first six increments appeared to be within the elastic limit, as cracks were only observed after the seventh increment and continued to develop thereafter with the load increases. For the second (doubly symmetrical) model, the first crack appeared without being able to record any readings due to fault in the channel connected to the load cells, but the loads were released immediately. The model was reloaded again after ensuring that the system was working normally.

8.3.7 THEORETICAL RESULTS

The two models were analysed theoretically by incorporating the properties of the models given in Table

8.5 in the computer program described in Chapter 7. The calculated results were compared with the experimental results obtained from the model tests and discussed in the following sections.

8.3.8 EXPERIMENTAL RESULTS AND COMPARISON BETWEEN THE EXPERIMENTAL AND THEORETICAL RESULTS

1 - CONTROL SPECIMENS

The control specimens taken during the casting of the models were tested 24 hours before testing the corresponding core model.

The compressive strengths of the concrete, f_{cu} and f_{cc}, were obtained from the average of the results of testing 8 cubes of 37.5 mm and 4 cylinders of 37.5 x 75 mm respectively. The indirect tensile strength f_t was obtained from the average of the results of testing 4 cylinders of the above sizes. The modulli of elasticity were obtained from testing 150 x 300 mm cylinders according to B.S. 188-1952. The above results are given in Table 8.4 for each model.

The stress-strain characteristic of the concrete used for the models and its corresponding modulus of elasticity-strain relationship are given in Figs. 8.19 and 8.20. These curves were drawn from tests on cubes of 37.5 mm. A similar attempt to draw the same relationships by testing cylinders of 37.5 x 75 mm failed due to the difficulty of achieving two smooth and parallel faces. A typical stress-strain characteristic relationship for 7 x 0.7 mm wire

rope used in reinforcing the connecting beams is given in Fig. 8.15. The value of the modulus of elasticity E_s was taken as an average of the best 8 results of tests carried out on 7 x 0.7 mm and 7 x 1.25 mm wire ropes.

ii - ROTATIONS

The measured rotations are compared with the corresponding theoretically calculated values in Figs. 8.21 and 8.22 for the singly-symmetric model and in Figs. 8.27 and 8.28 for the doubly-symmetrical core. In the first case, good agreement has been achieved within the elastic and elasto-plastic limits, but as the cracks in the walls increased the discrepancy between the two values increased. In the second case the measured rotations were greater than the theoretically calculated ones, because of the initial cracks developed in the model before unloading and reloading it and the distortion of the cross-section of the model. The intermediate diaphragms proved to be too flexible to prevent as distortions.

iii - VERTICAL SHEAR AND DEVELOPMENT OF PLASTICITY IN THE CONNECTING BEAMS

The vertical shear in the connecting beams was assessed by measuring strains on the compression faces of each beam. The measured shear distributions are compared with the theoretically calculated values in Fig. 8.23 and Fig. 8.(29 and 30) for the singly and doubly symmetrical models respectively. In the first case the measured shear was less than the theoretically calculated

values. In the second case a meaningful shear pattern could not be achieved in the two sets of connecting beams because of lack of symmetry due to unsymmetrical cracks in the walls and distortion of the core cross-section. A comparison between the theoretical and actual sequence of plasticity development in the connecting beams are given in Figs. 8.24 and 8.31 for the two models. In both cases, the plasticity commenced at an intermediate height and not at the top as expected theoretically, probably because of the restraining effect of the top diaphragm. In the doubly-symmetrical model the plasticity did not follow the same sequence in both sides because of the aforementioned reasons.

iv - STRESSES IN THE WALLS

Stresses calculated from the measured strains at the outside faces of the walls at different stages of loading are compared with the corresponding theoretical stress distributions in Figs. 8.25 and 8.32 for the two models. For the singly-symmetric model, good agreement was obtained at the shown three stages of loading, shown for the completely uncracked model, at the first crack observed in the connecting beams and after the plasticity had developed in all the connecting beams.

In the doubly-symmetrical model most of the measured strains were less than the theoretically calculated values because of the release of stresses due to the wall cracks.

v - CRACK PATTERN AND MODE OF FAILURE

The crack patterns in the outside faces of the model walls are shown in Plate 8.(11 and 12) and Plate 8.(13 and 14) for the singly and doubly symmetrical models respectively.

In the first model, cracks were observed in beam numbers 3, 4, 5 and 6 at a torque of 1.411×10^6 N.mm, at a torque equal to 1.82×10^6 N.mm cracks appeared in beams 1 and 2. The first horizontal tension cracks were observed in wall panel 1 at a torque equal to 2.85×10^6 N.mm. At a torque equal to 3.439×10^6 N.mm, torsion cracks were observed in the two side walls and at a torque equal to 3.978×10^6 N.mm cracks appeared in the back wall. In the later stages of loading, cracks were observed in the opposite directions in the interior faces of the back wall and two side walls to those on the exterior faces. The crack patterns in the exterior and interior sides of the unfolded model are shown in Fig. 8.26.

In the second model, the initial cracks which occurred before the actual test were marked in red as may be seen in Plates 8.(13 and 14). In the actual test cracks continued to develop throughout the model. Tension cracks formed the dominating pattern at the front and back walls under the loading points, however torsional cracks covered all the walls. In the interior sides the cracks were mainly in the opposite directions to those on exterior sides as shown in Fig. 8.33.

8.3.9 DISCUSSION OF RESULTS

The results obtained from the above tests were influenced by various factors which should be accounted for if the results are to be correctly interpreted. These factors may be summarised as, the accuracy in constructing the models, the properties of the models materials, the end conditions, the applied loads and the reactions of the models.

Although great care was taken during constructing the models, there were some differences in the thickness of the walls. In the first (Singly-Symmetrical) model the thickness of the front wall was 32 mm., in the back wall it varied from 30 mm. near the corners to 33 mm. at the middle and the two side walls were 30 mm. In the second (Doubly-Symmetric) model, the front wall was 33 mm, the back wall was 30 mm. and the two side walls were 29 mm in thickness. The above differences in the dimensions of the models were not expected to affect their overall behaviour significantly.

In the above comparisons, the theoretical values were calculated for a constant elastic modulus for the concrete. The discrepancy between the stresses calculated from the measured strains and the corresponding theoretically calculated values increased with the applied load because of the non-linear variation of the stress-strain relationship of the model material as shown in Fig. 8.19. An accurate assessment of the stresses at any stage of loading must take into account the actual value of the modulus of

elasticity at each particular stage as it varies considerably within the limits of allowable strain as shown in Fig. 8.20.

Each model was built into a very heavy concrete base which was considered to provide to a good degree of accuracy a fixed end condition. No relative movements between the concrete base and the laboratory floor were recorded. However the top steel diaphragm did impose vertical warping restraints on the models which probably affected the rotations and the internal force distributions.

Since the two hydraulic jacks were independently controlled, they gained the required load increment at different times in each torque increment. These resulted in the models being subjected to both torsion and bending actions for short periods between the stages of loading. These intervals were short and the actual readings were only recorded after the two jacks had settled at the required load in each stage, so that these effects were ignored.

During testing of the models, a certain amount of cross-section distortion was observed from the measured displacements and the directions of cracks. These distortions were more pronounced in the doubly-symmetrical model, for which its two channels displaced in two opposite directions as shown in Fig. 8.35. Therefore the rotations calculated from the measured displacements will be greater than the predicted values.

The cracks observed in the models during the tests

were due to three different actions. Spiral cracks occurred around the models on the outside perimeter due to the torsional shear flow around the walls and connecting beams. In the interior sides of the walls, the cracks were developed in two opposite directions, the first cracks developed in the same directions as in the outer sides because of the same action; the second cracks developed after the beams had cracked and only a St. Venant torsional shear was circulating within the thickness of the walls. This action created shear forces in the opposite direction to the former in the interior sides as shown in Fig. 8.34. Horizontal cracks were observed near the base on the walls subjected to the thrust of the jacks, because of the out of plane bending effects produced by the applied loads on normal panels.

MODEL PROPERTIES	Notation	Singly Symmetric	Doubly Symmetric
Total height	H	730 mm	730 mm
Core width	D	150 mm	200 mm
Core depth	B	150 mm	120 mm
Clear span of the connecting beams	a	80 mm	80 mm
Width of the adjacent walls	d	35 mm	60 mm
Storey height	h	60 mm	60 mm
Wall thickness	th	5 mm	5 mm
Depth of connecting beams	dc	10 mm	10 mm
Depth of the top stiffening elements	ds	20 mm	20 mm
Thickness of the top stiffening element	ths	9.4 mm	9.4 mm
Modulus of elasticity of the perspex	E_p	3260 N/mm^2	3260 N/mm^2
Poisson's ratio of the perspex	γ	0.395	0.395
Modulus of elasticity of the stiffening element	E_s	70150 N/mm^2	70150 N/mm^2
Connecting beam stiffness factor	β	0.1627 10^{-3}	0.1627 10^{-3}
Top end restraint constant	r	-2.0977 mm^{-1}	-1.046 mm^{-1}
St. Venant's torsional rigidity	GJ	2.531 10^7	7.008 10^7
Core constant of rigidity	GJ_o	10.993 10^8	6.81 10^8
Core warping moment of inertia	I_w	5.6979 10^{10} mm^6	8.8704 10^{10} mm^6
Core constant	α	0.002433 mm^{-1}	0.001535 mm^{-1}

Table 8.1 Geometrical and material properties of perspex models

Mix No.	W/C	A/C	f_{cu} N/mm^{-2}	f_t N/mm^{-2}
1	0.6	3	43.6	3.8
2	0.75	4	40.2	4.1
3	0.6	4	31.3	3.1

Table (8.2) Results of trial concrete mixes

Type of reinforcement	3 mm rods	7 x 0.7 mm wires	7 x 1.0 mm wires	7 x 1.25 mm wires
Ultimate bond	18.32 N/mm	y*	y*	44.85 N/mm

* Steel yield before bond failure

Table (8.3) Bond strength of the trial reinforcement

Property / Model	f_{cu} N/mm^2	f_{cc} N/mm^2	f_t N/mm^2	E kN/mm^2	γ
Singly Symmetrical	35.41	24.06	2.85	19.75	0.0566
Doubly Symmetrical	29.08	20.94	2.72	17.5	0.0623

Table (8.4) Properties of the concrete used to construct models

MODEL PROPERTIES	Notation	Singly Symmetric	Doubly Symmetric
Total height	H	1400 mm	1400 mm
Core width	D	400 mm	400 mm
Core depth	B	200 mm	200 mm
Span of the connecting beams	a	200 mm	200 mm
Width of the adjacent walls	d	100 mm	100 mm
Storey height	h	200 mm	200 mm
Wall thickness	th	30 mm	30 mm
Depth of the connecting beams	d_c	50 mm	50 mm
Modulus of elasticity of concrete	E	19.75 KN/mm^2	17.5 KN/mm^2
Poisson's ratio	γ	0.056	0.056
Connecting beam stiffness factor	β	4.687×10^{-3}	4.687×10^{-3}
Top end restraint	r	0.0	0.0
St. Venant's torsional rigidity	GJ	8.416×10^{10}	5.965×10^{10}
Torsional rigidity of core	GJ_o	131.85×10^{10}	60.65×10^{10}
Warping moment of inertia of core	I_w	10.75×10^{12}	9.20×10^{12}
Core constant	α	2.442×10^{-3}	1.902×10^{-3}

Table 8.5 Geometrical and material properties of micro-concrete models

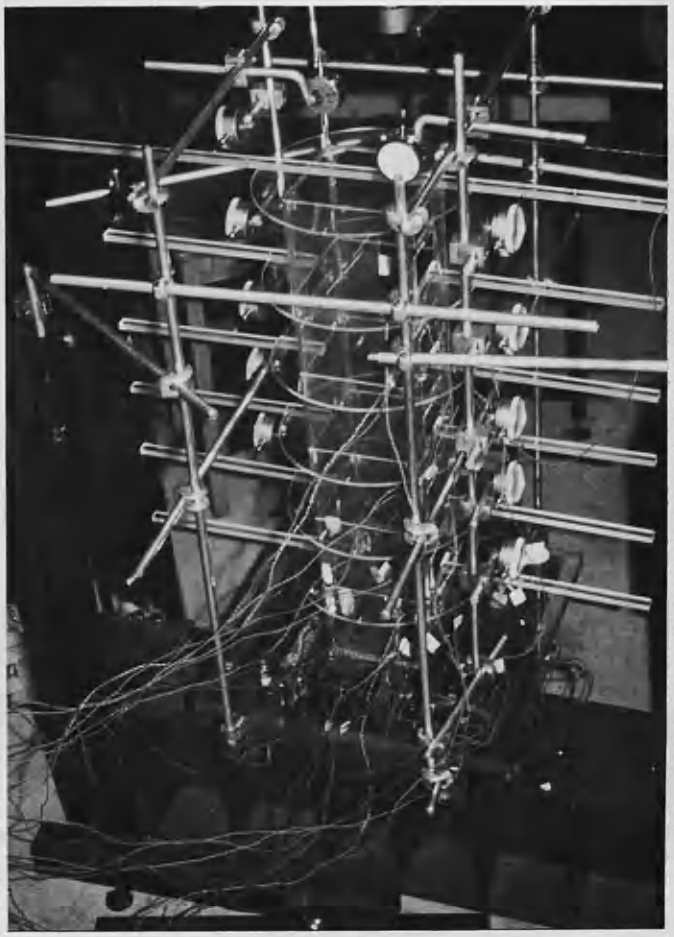

Plate 8.1 Perspex model in test frame

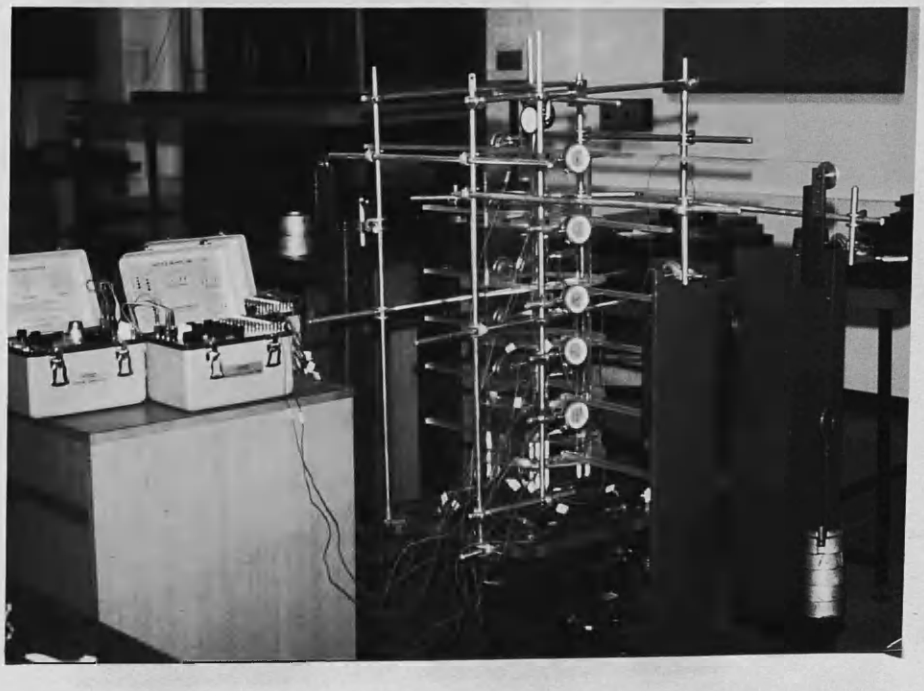

Plate 8.2 Model under test

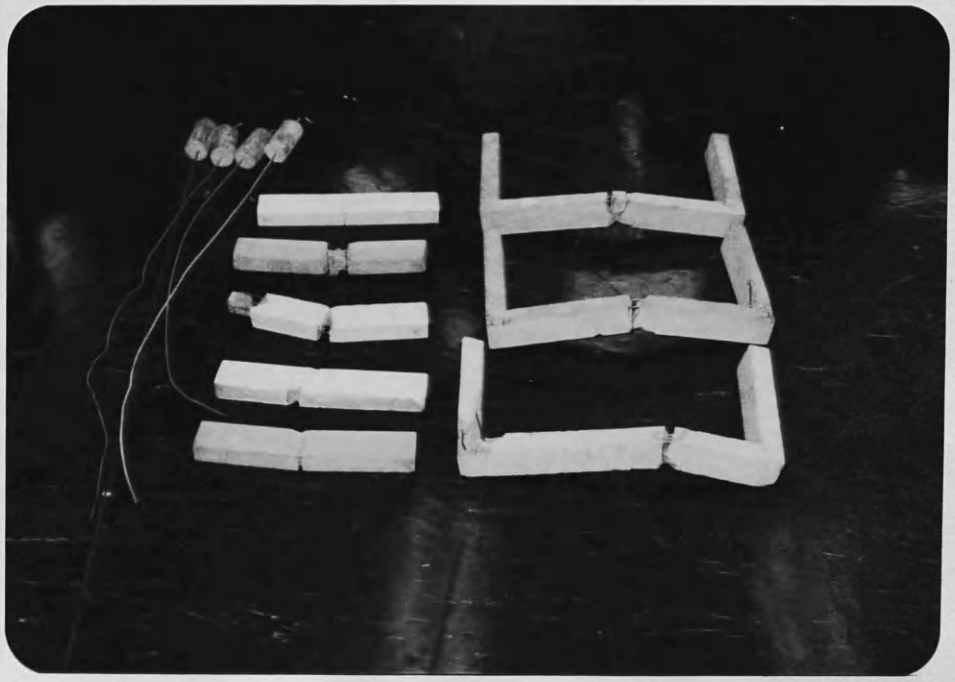

Plate 8.3 Control specimens and beams for primary tests

Plate 8.4 Outer shuttering and reinforcement of the front wall

Plate 8.5 Inner shuttering and reinforcement of the back wall (singly symmetrical model)

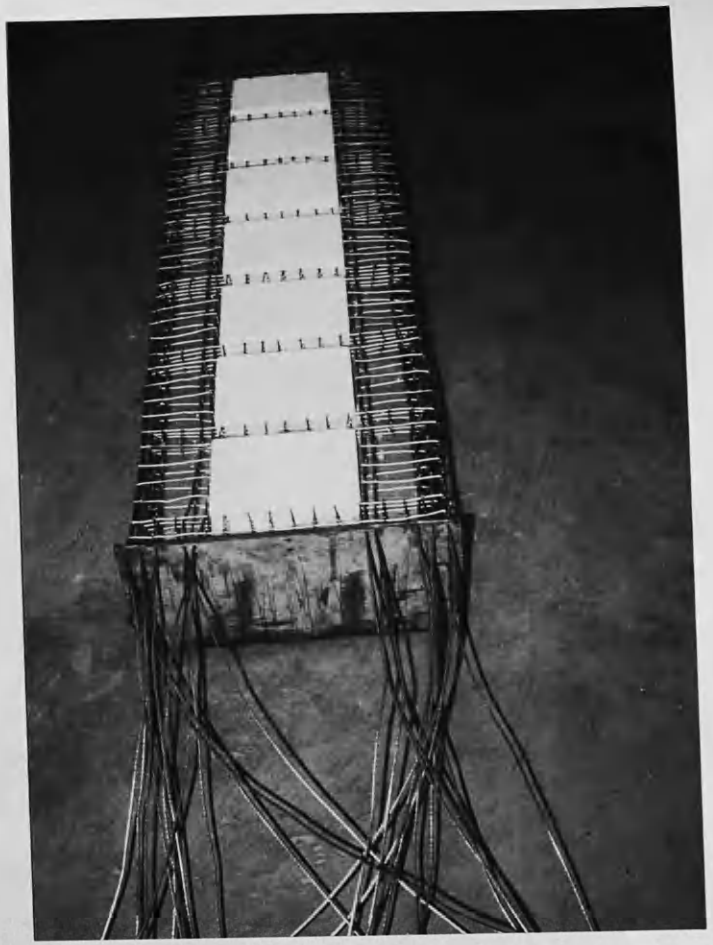

Plate 8.6 Inner shuttering and reinforcement of the back wall (doubly symmetrical model)

Plate 8.7 Shuttering of doubly symmetrical model

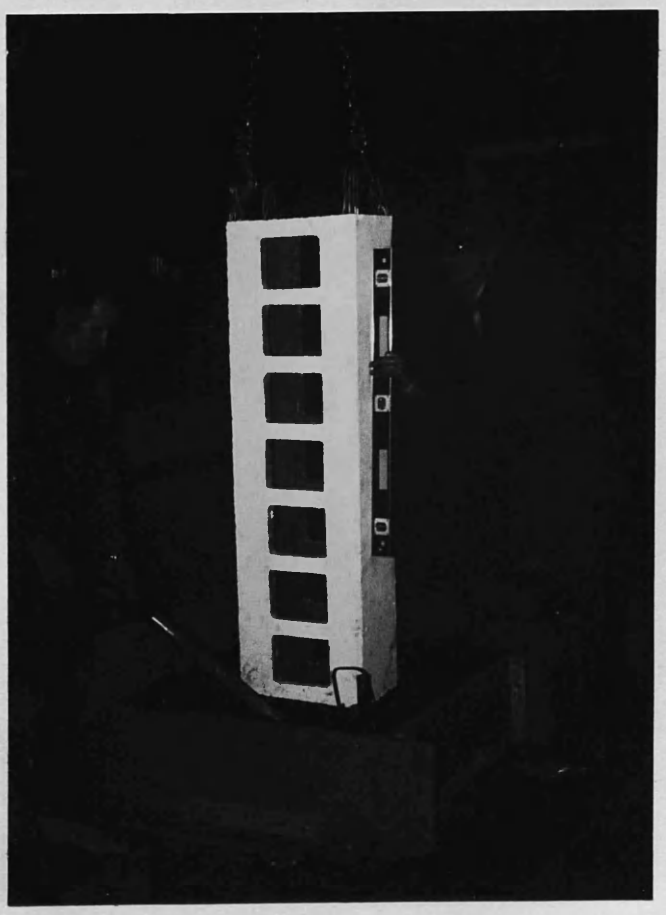

Plate 8.8 Casting of base of model

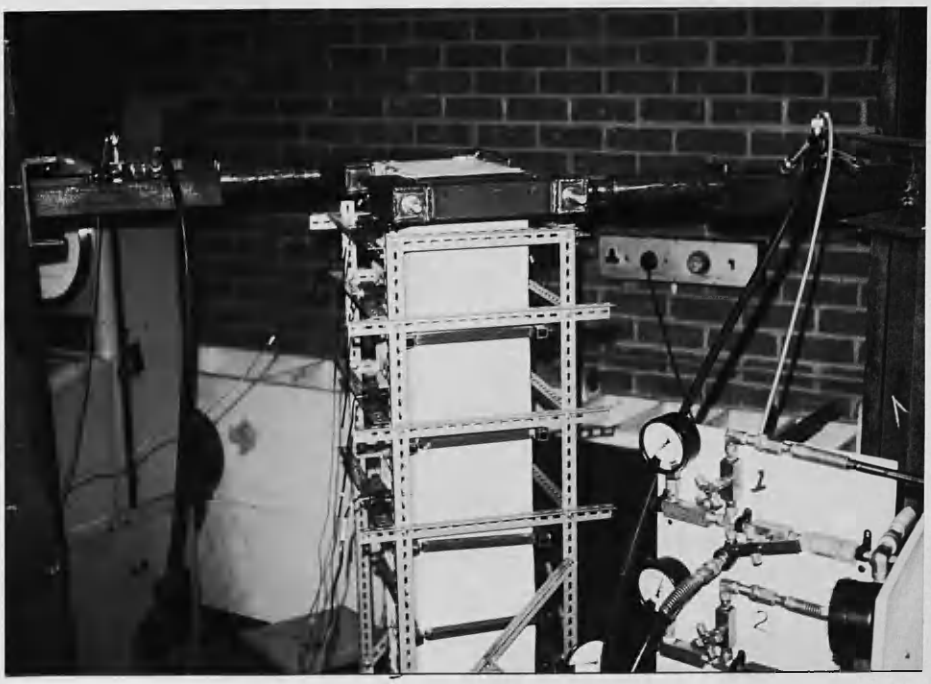

Plate 8.9 Loading system to create point torque at top

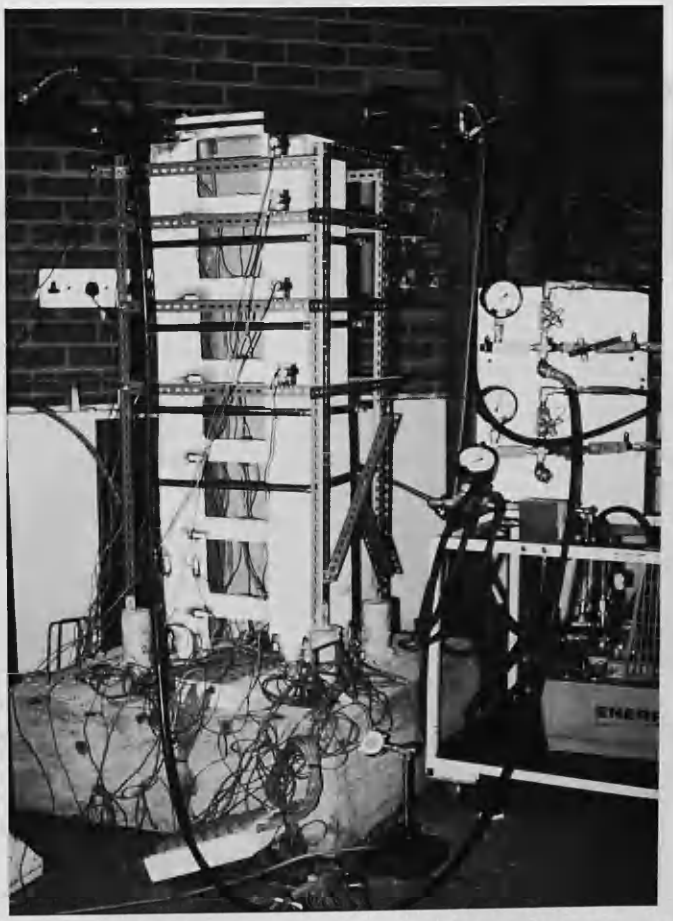

Plate 8.10 Model under test

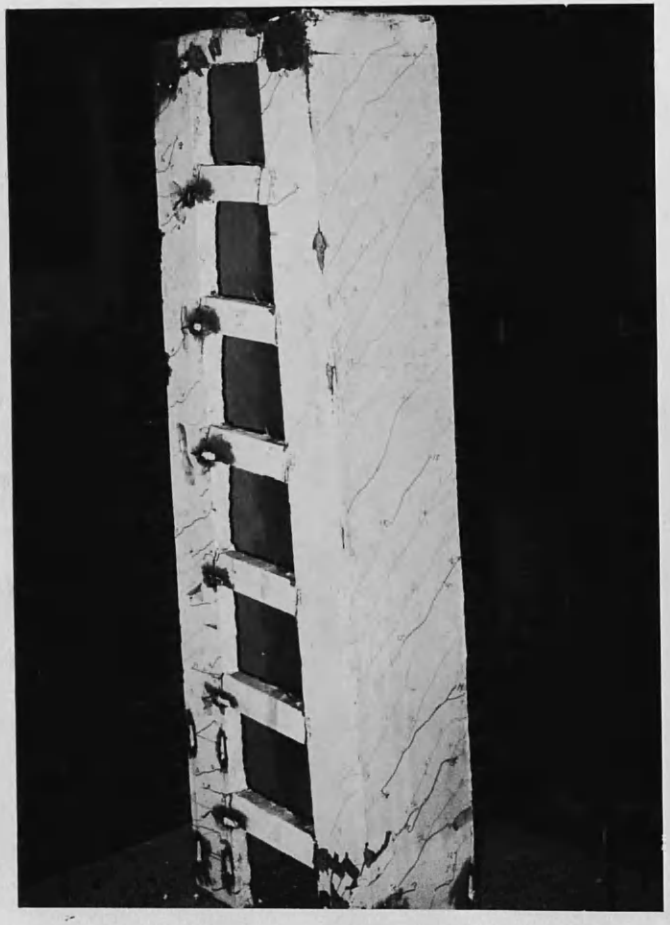

Plate 8.11 Crack pattern in the front wall and side wall 4 (Model 1)

Plate 8.12 Crack pattern in the back wall and side wall 2

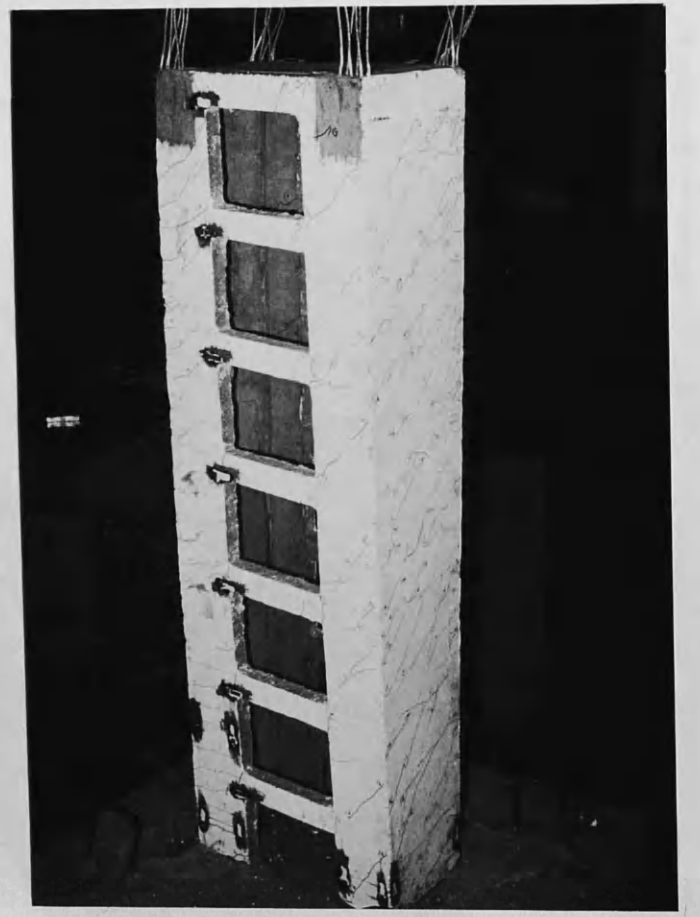

Plate 8.13 Crack pattern in front wall and side wall 4 (Model 2)

Plate 8.14 Crack pattern in back wall and side wall 2 (Model 2)

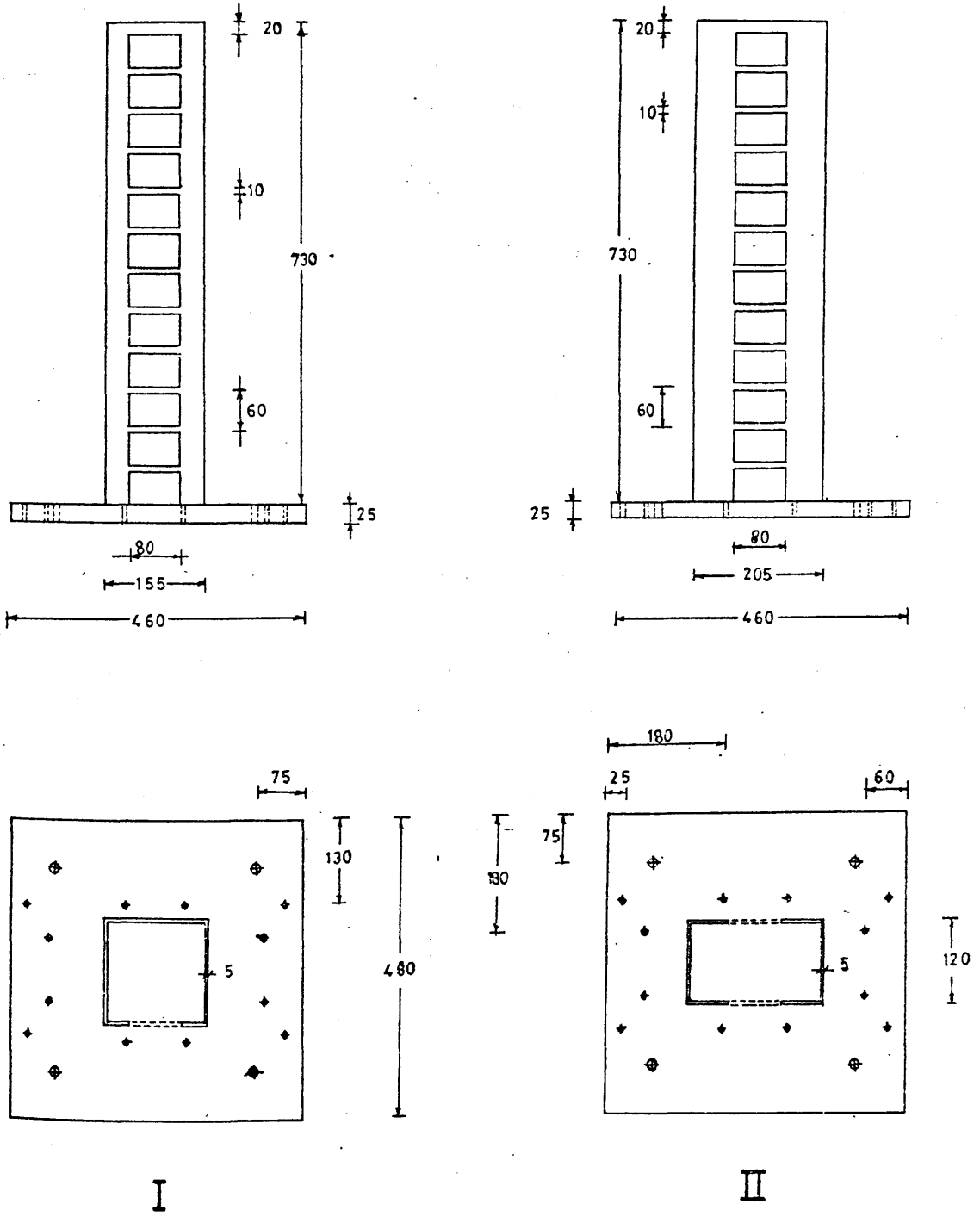

Fig. 8.1 Configurations and dimensions of the two perspex models

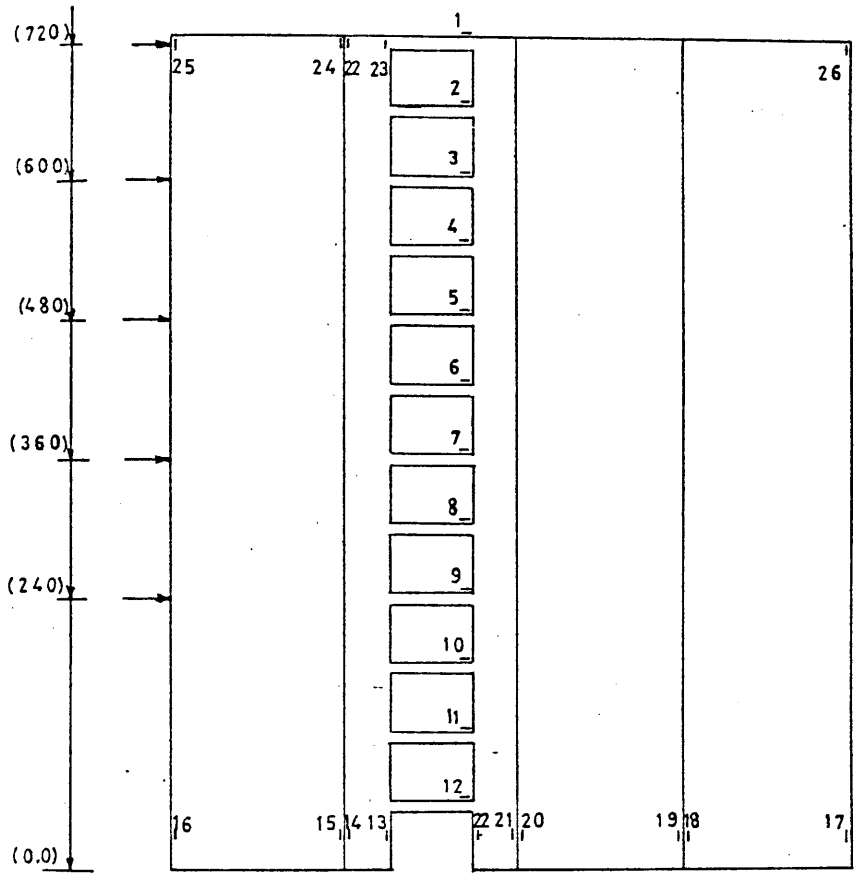

I. Singly-symmetric model

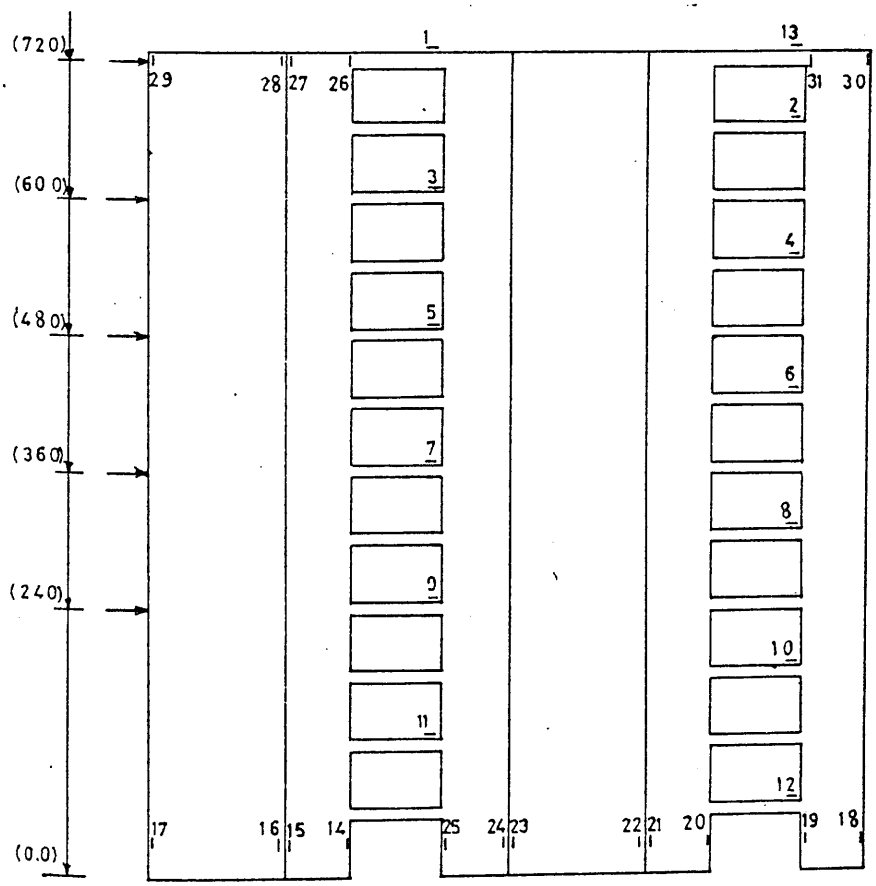

II. Doubly Symmetric model

Fig. 8.2 Positions of strain gauges and levels of dial gauges

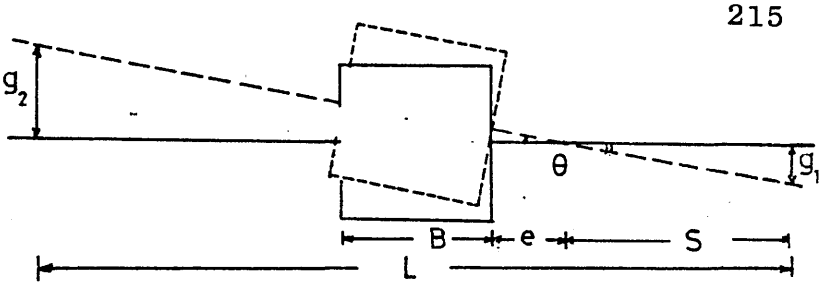

Singly Symmetrical model

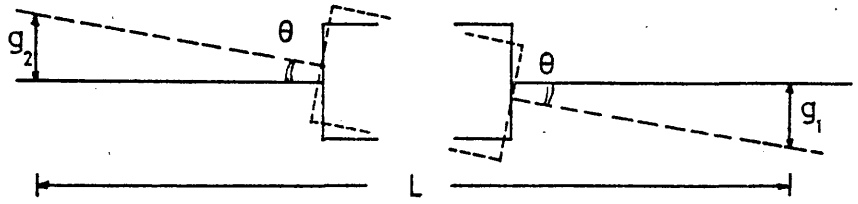

Doubly Symmetrical model

Fig. 8.3 Displacement measurements of perspex modes

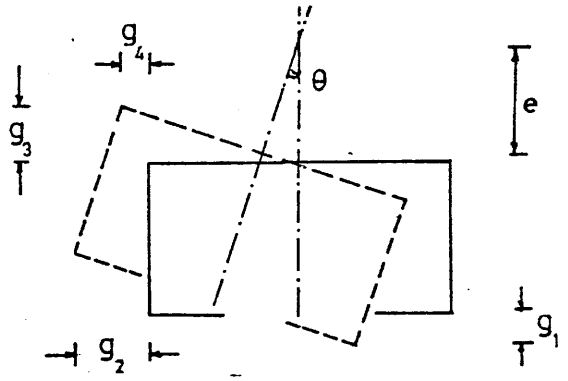

I. Singly symmetrical model

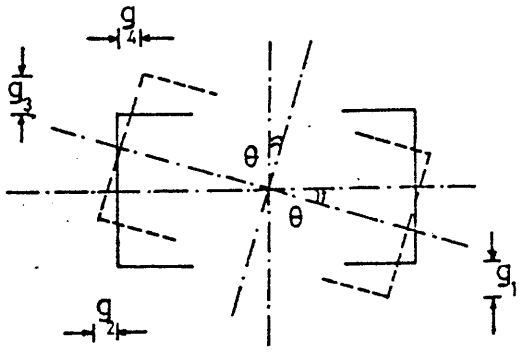

II. Doubly symmetrical model

Fig. 8.4 Displacement measurements of concrete models

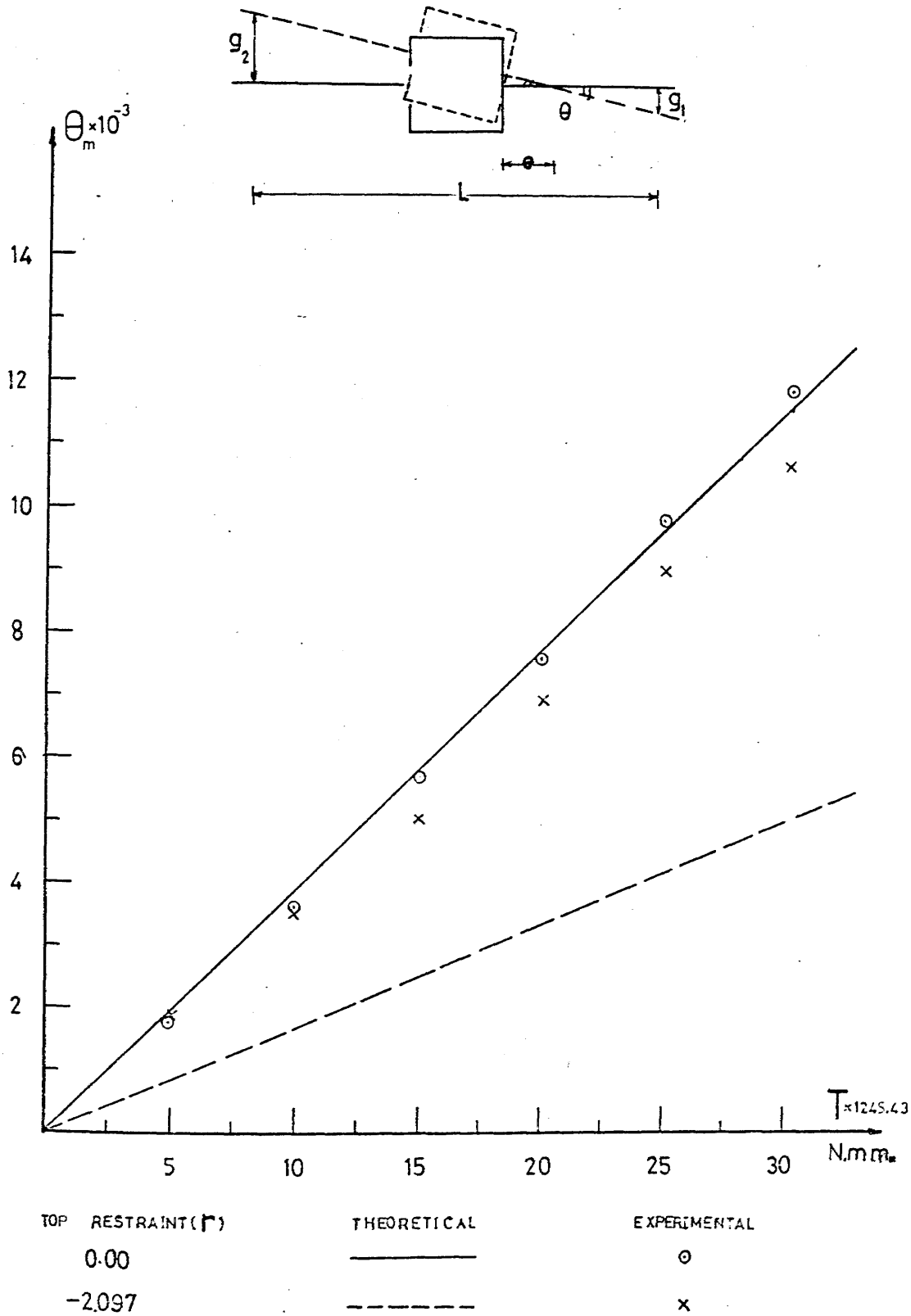

Fig. 8.5 Torque-rotation relationship for singly symmetrical perspex model

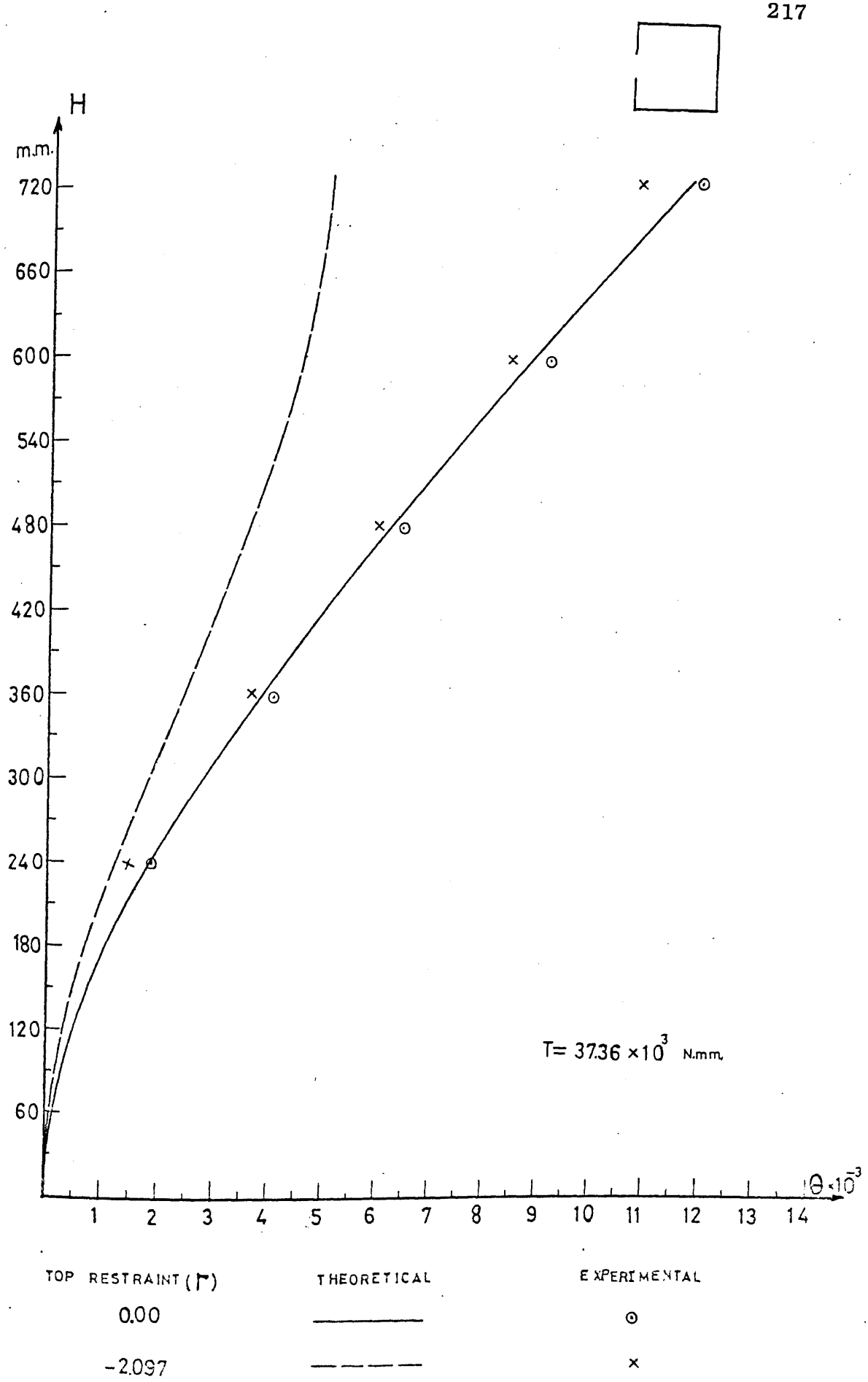

Fig. 8.6 Variation of core rotation throughout height

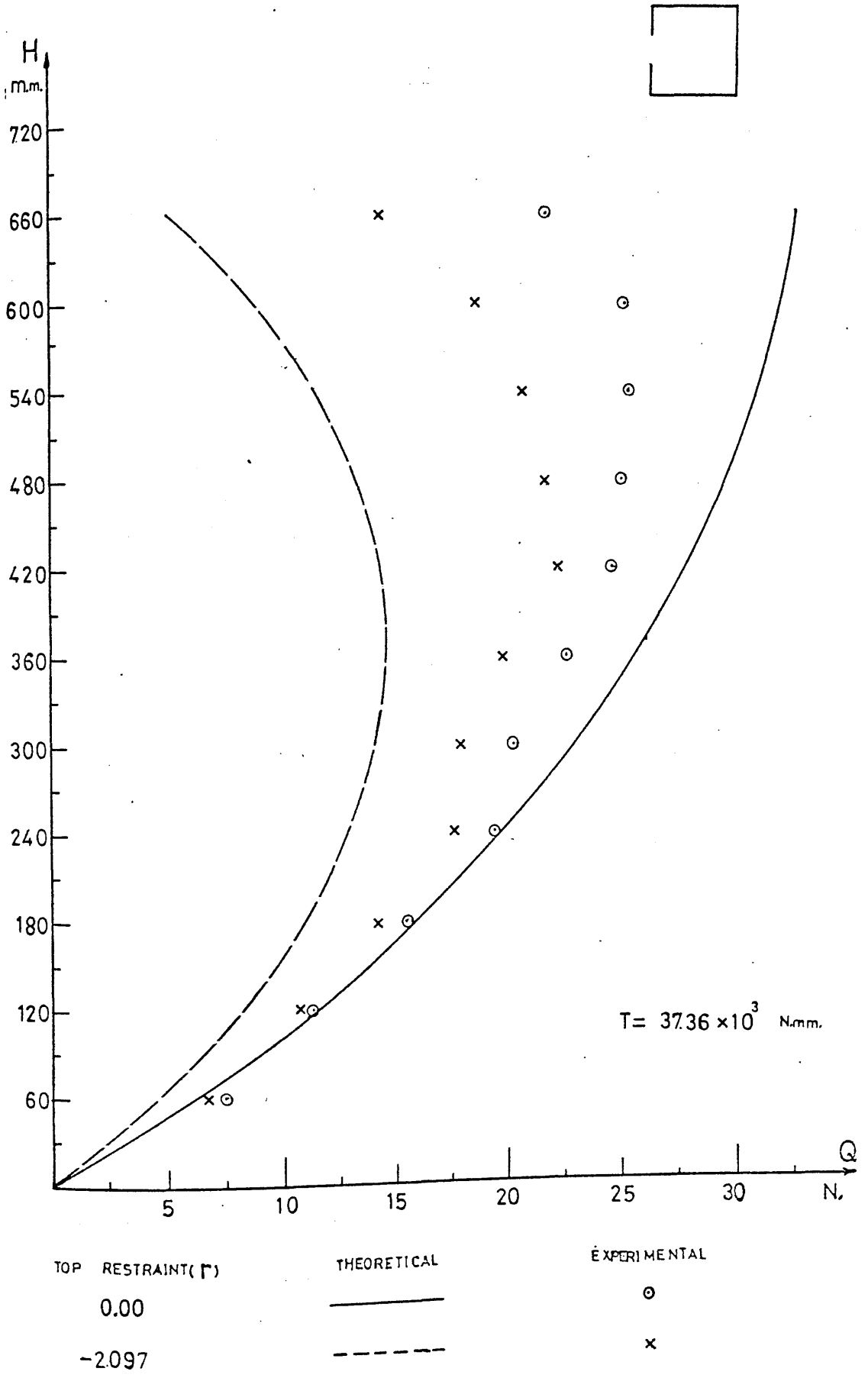

Fig. 8.7 Vertical shear forces in connecting beams

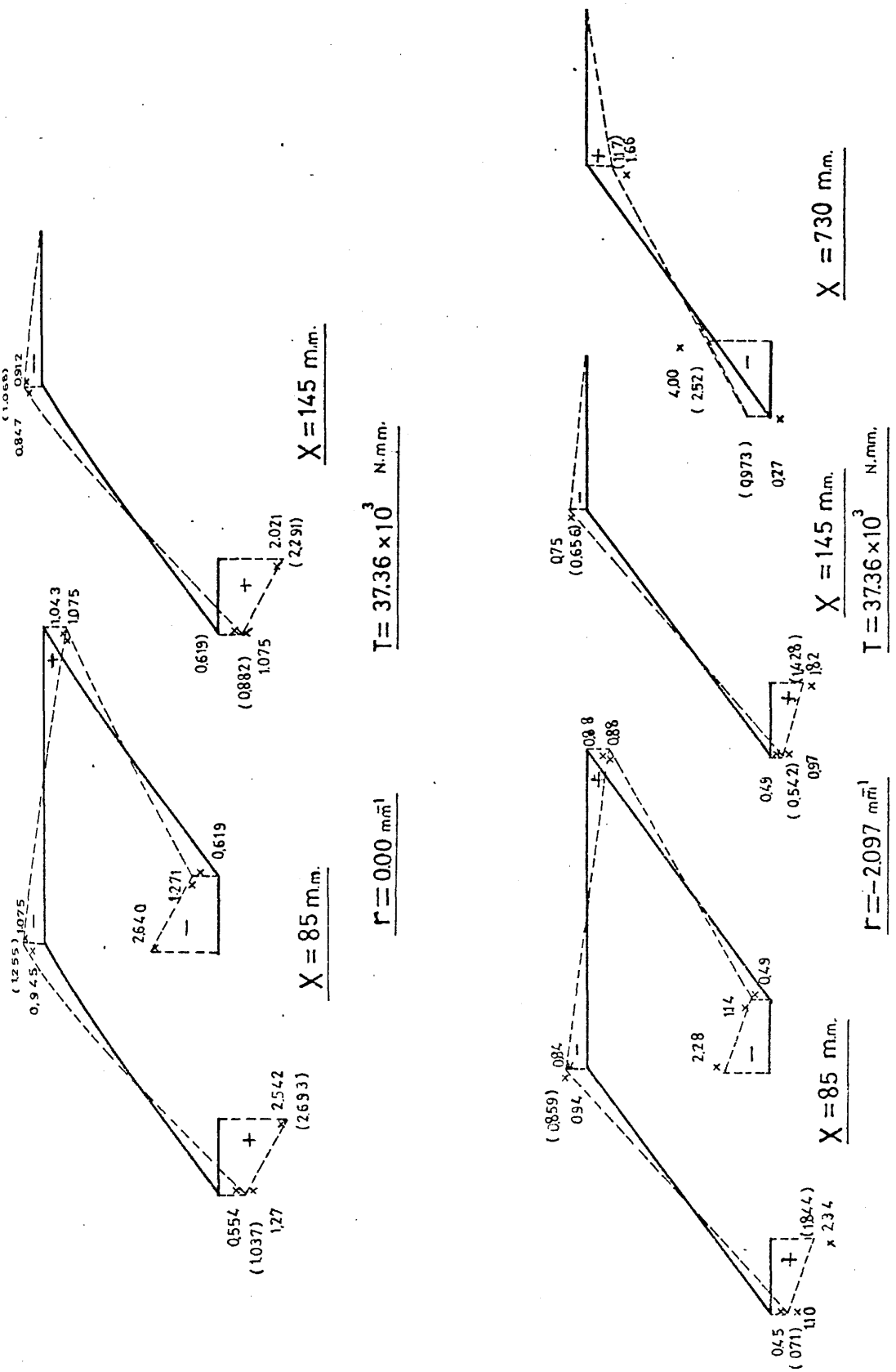

Fig. 8.8 Comparison of stresses in walls of Singly Symmetrical perspex model

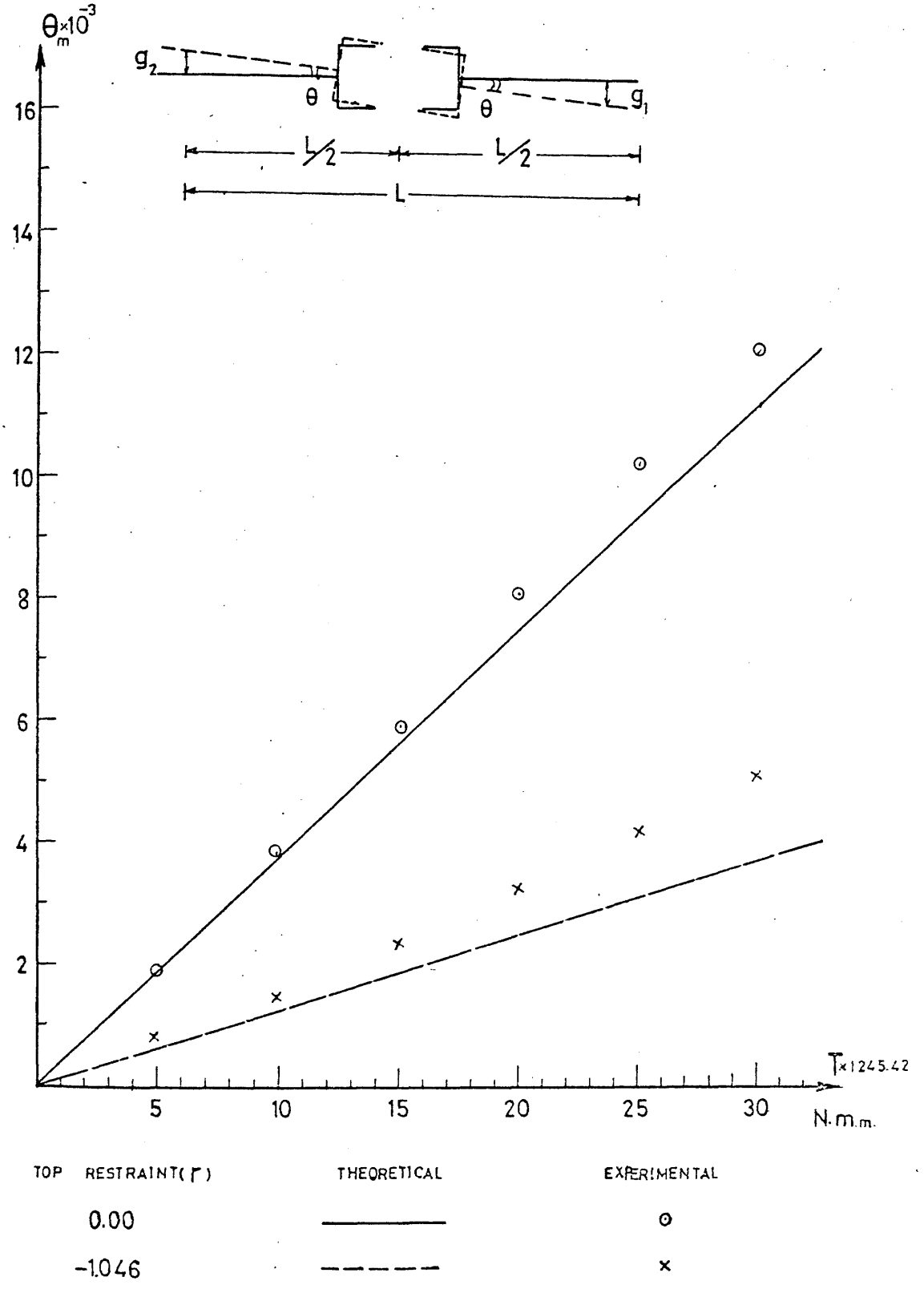

Fig. 8.9 Torque rotation relationship for doubly symmetrical perspex model

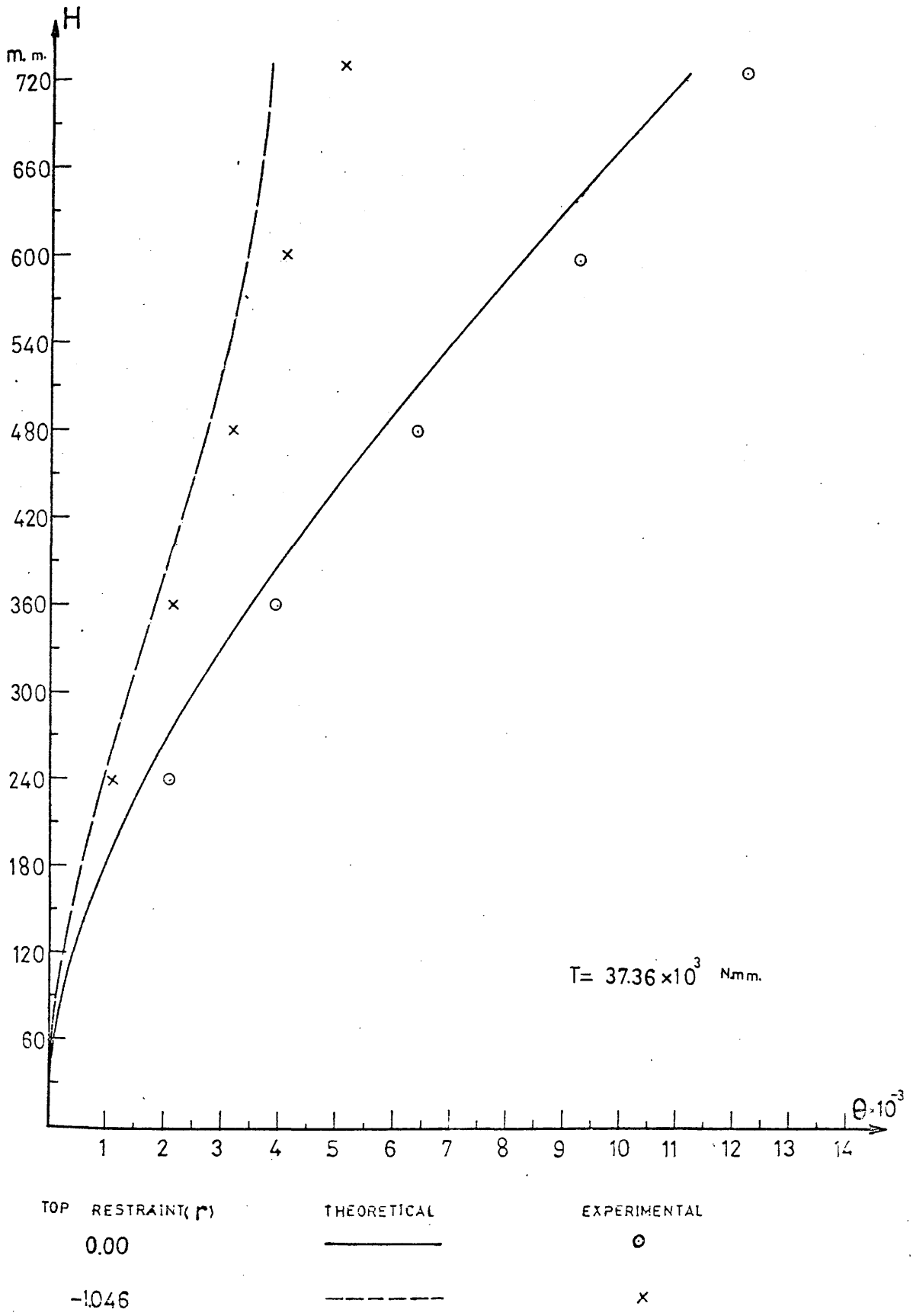

Fig. 8.10 Variation of core rotation throughout height

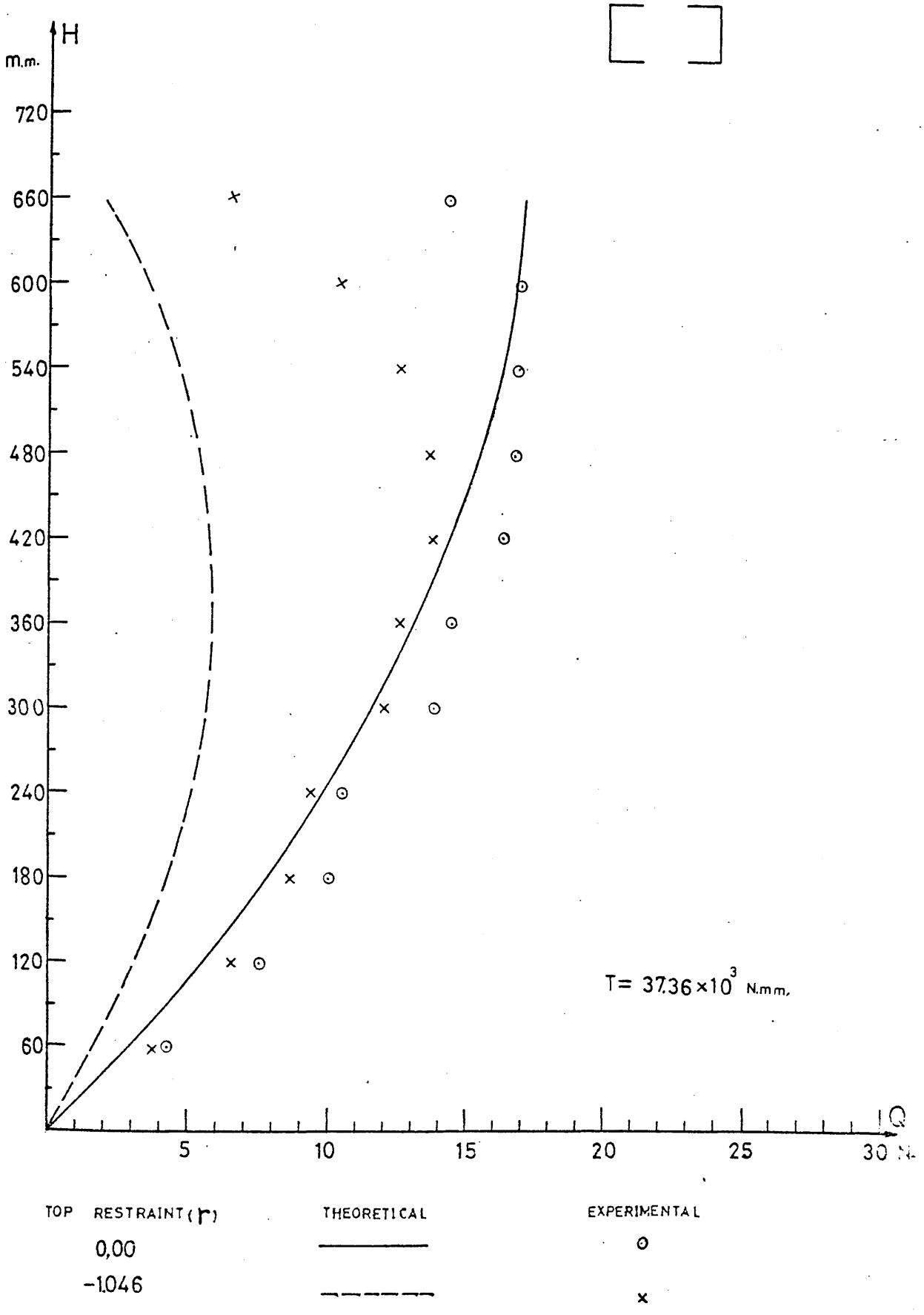

Fig. 8.11 Vertical shear forces in connecting beams

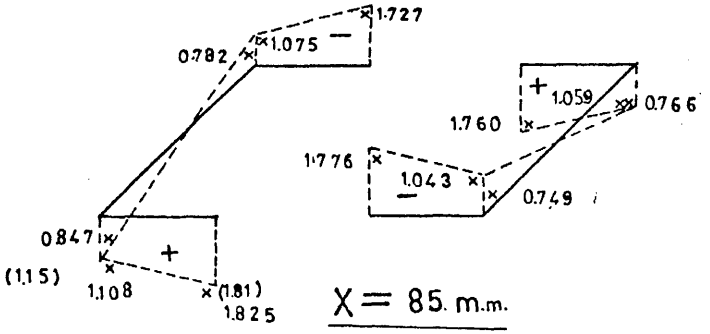

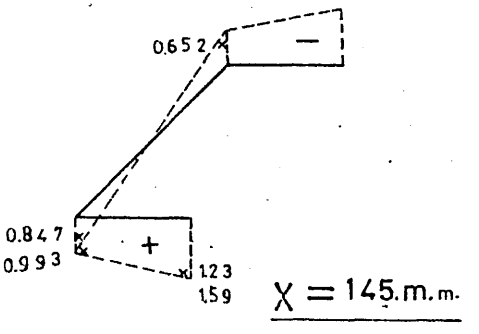

r = 0.00 mm^{-1} T = 37.36×10^3 N.mm.

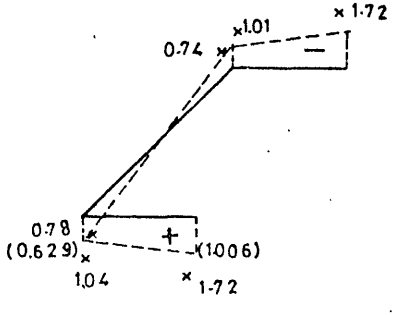

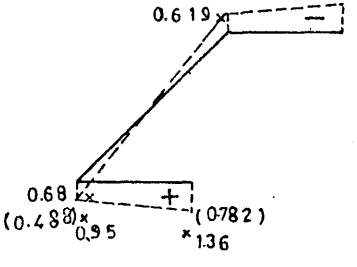

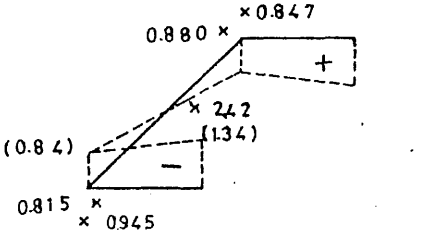

r = −1.046 mm^{-1} T = 37.36×10^3 N.mm.

Fig. 8.12 Comparison of stresses in walls of doubly symmetrical perspex model

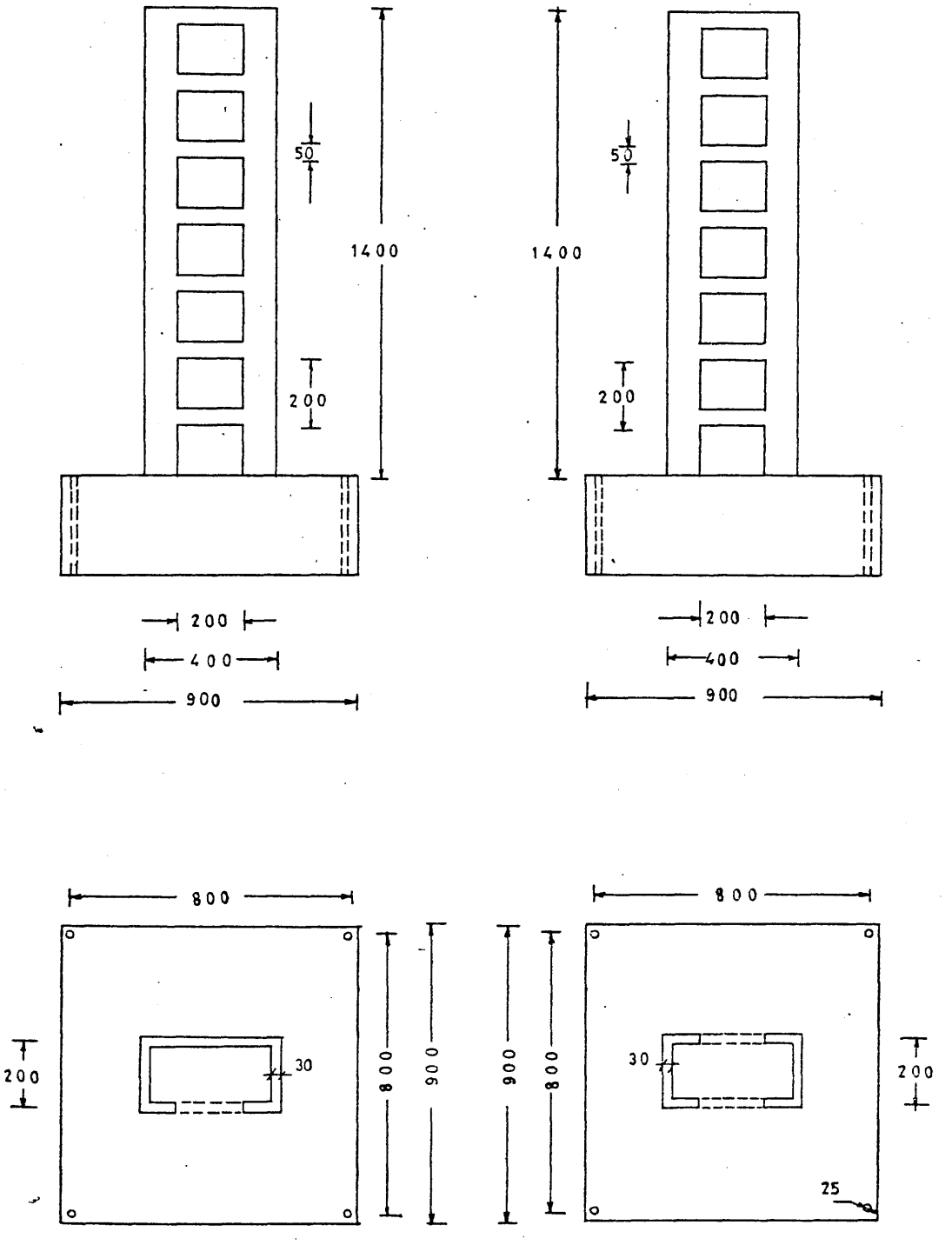

Fig. 8.13 Configuration and nominal dimensions of microconcrete models

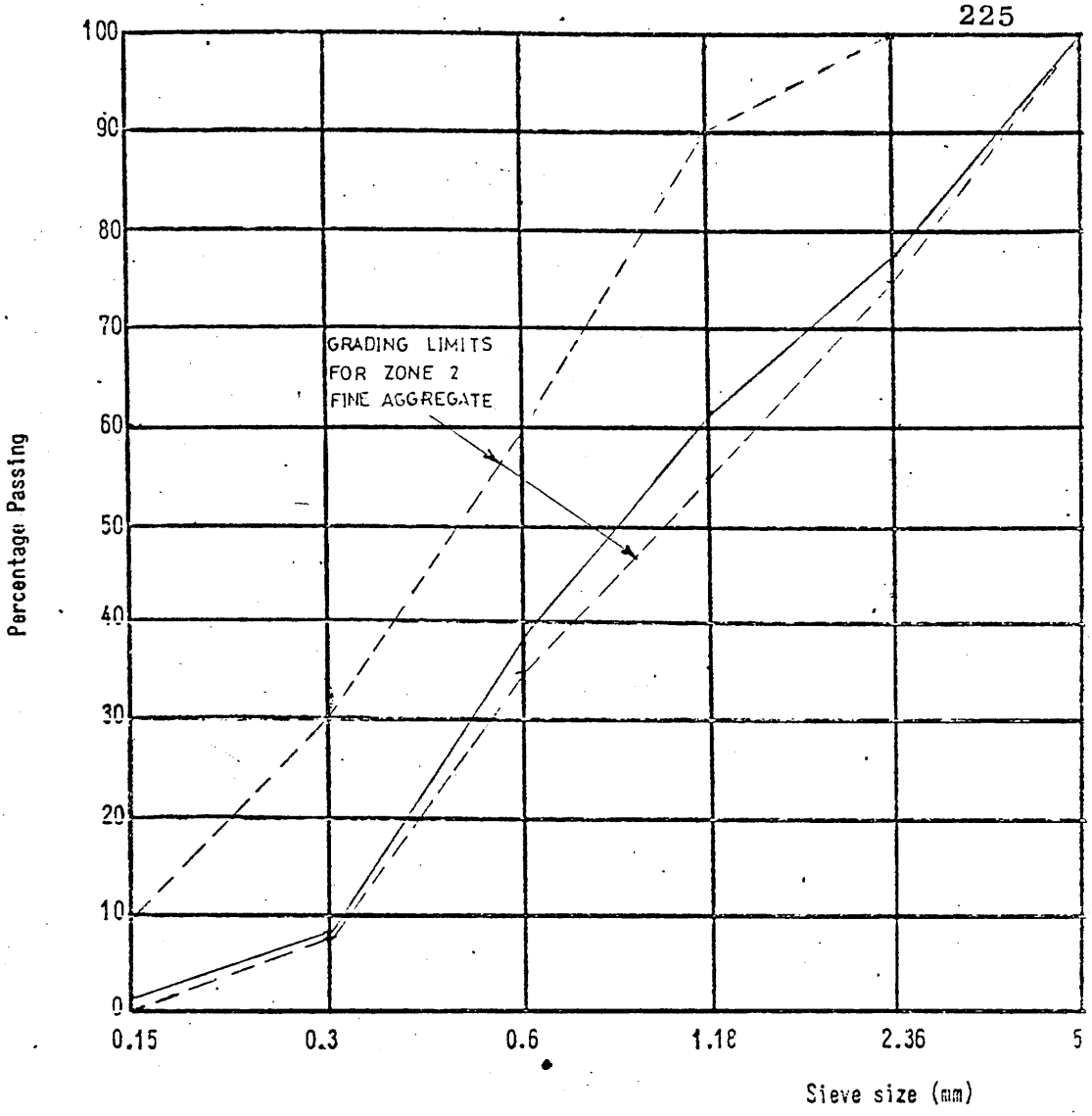

Fig. 8.14 Grading of sand used in concrete

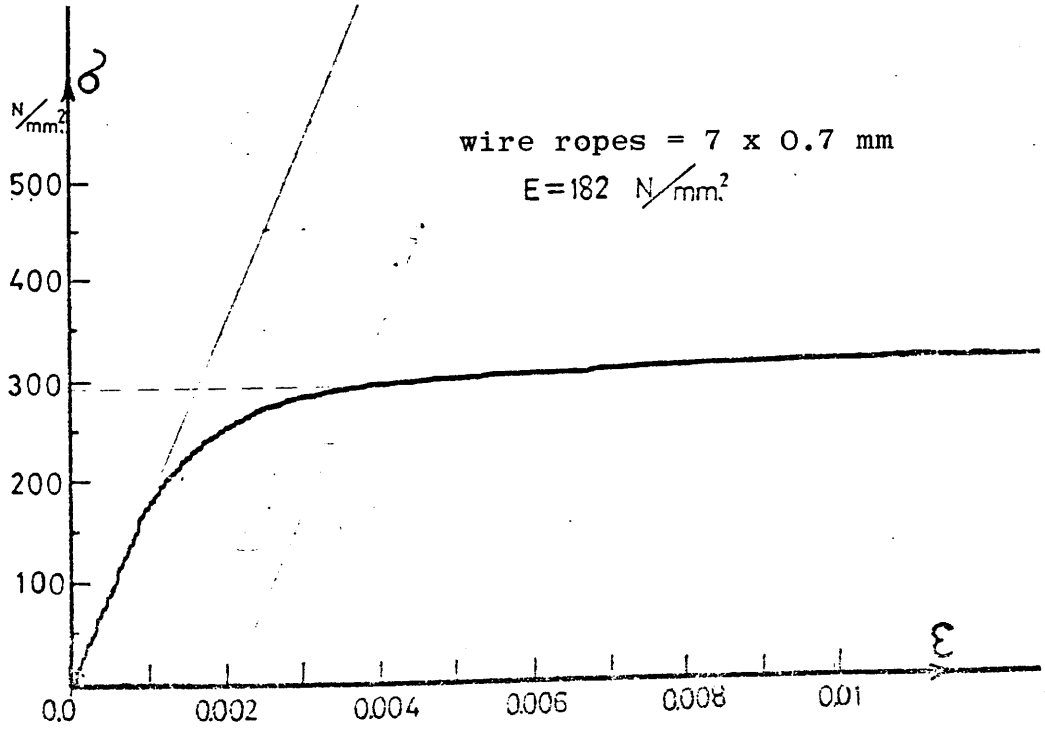

Fig. 8.15 Typical stress-strain relations for core reinforcement

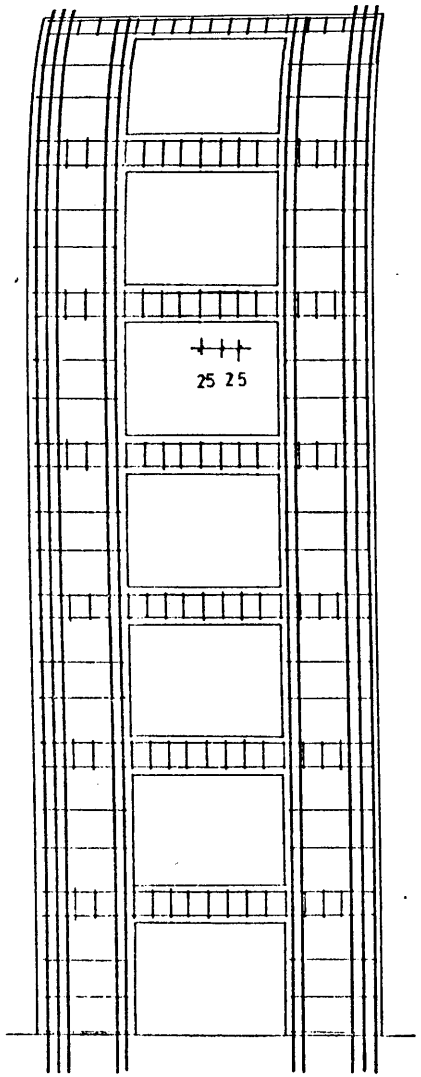

Front wall (model 1 and 2)

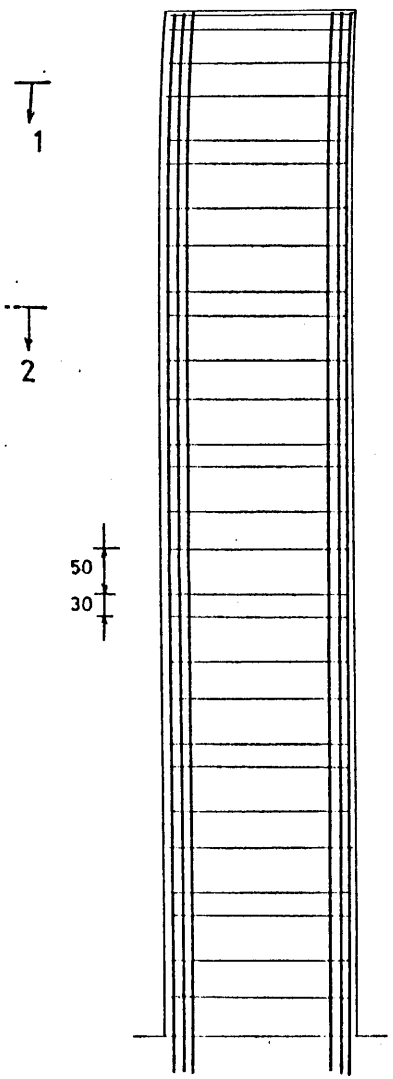

Side wall (model 1 and 2)

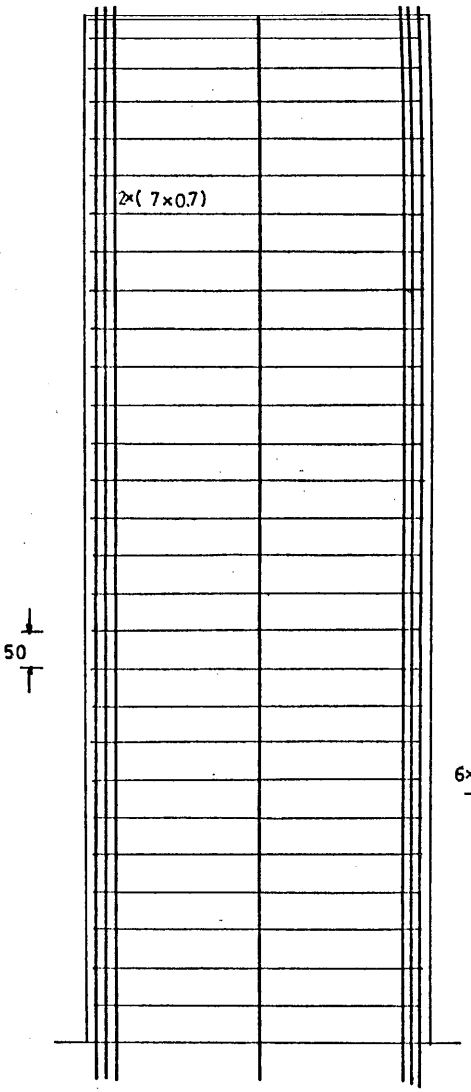

Back wall (model 1)

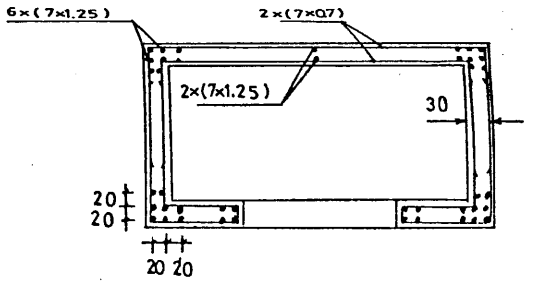

Model (1)

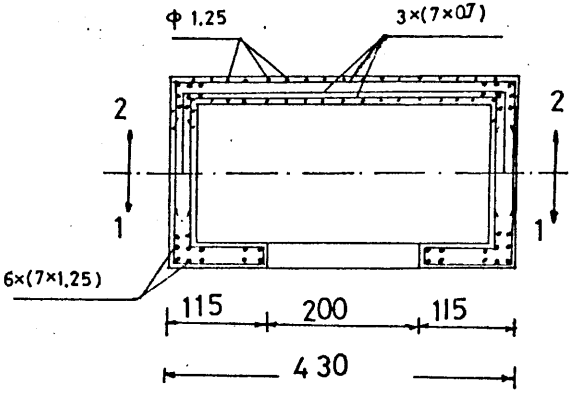

Model (2)

Fig. 8.16 Detailing of the reinforcement of the micro-concrete models

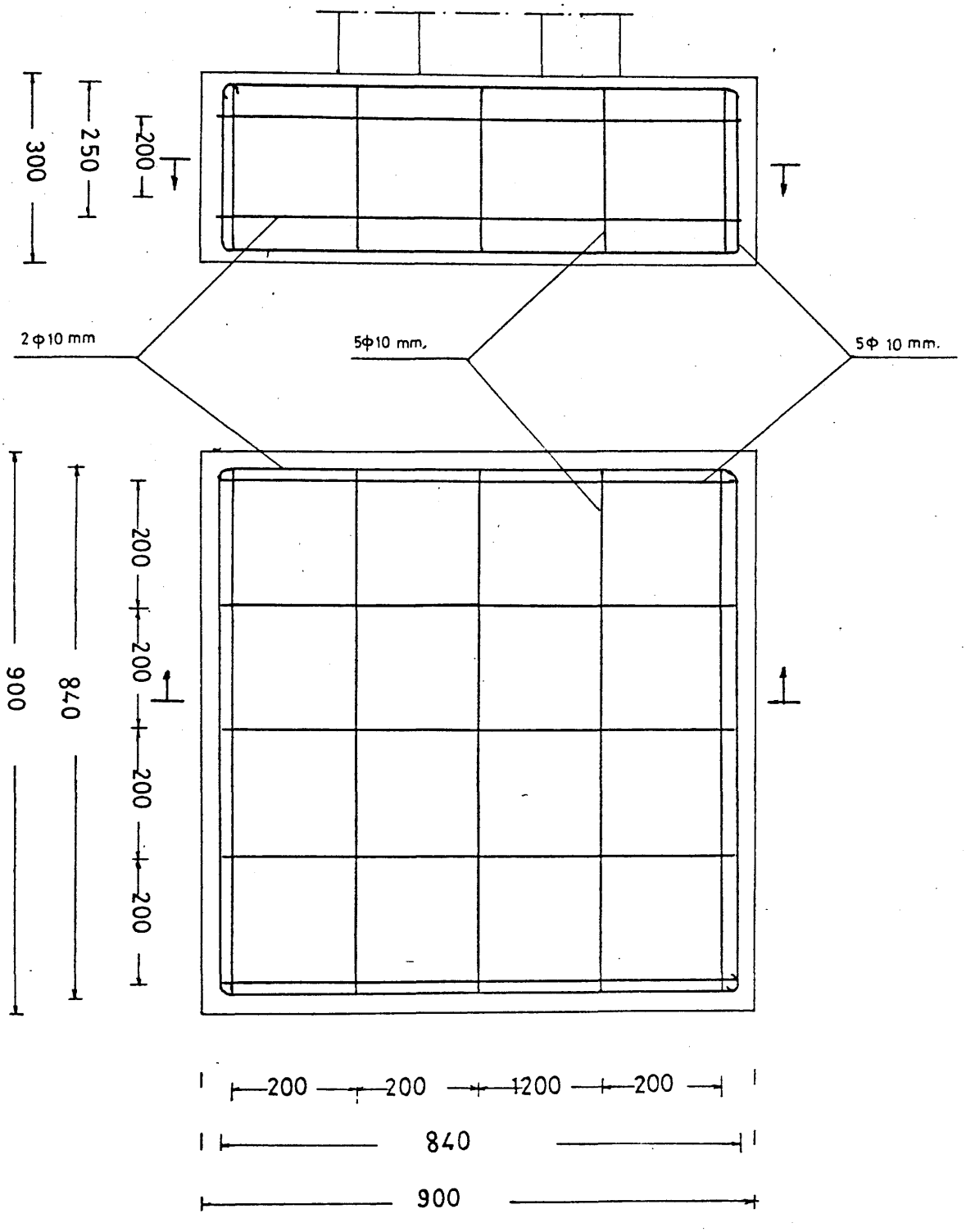

Fig. 8.17 Detailing of the reinforcement of the models base

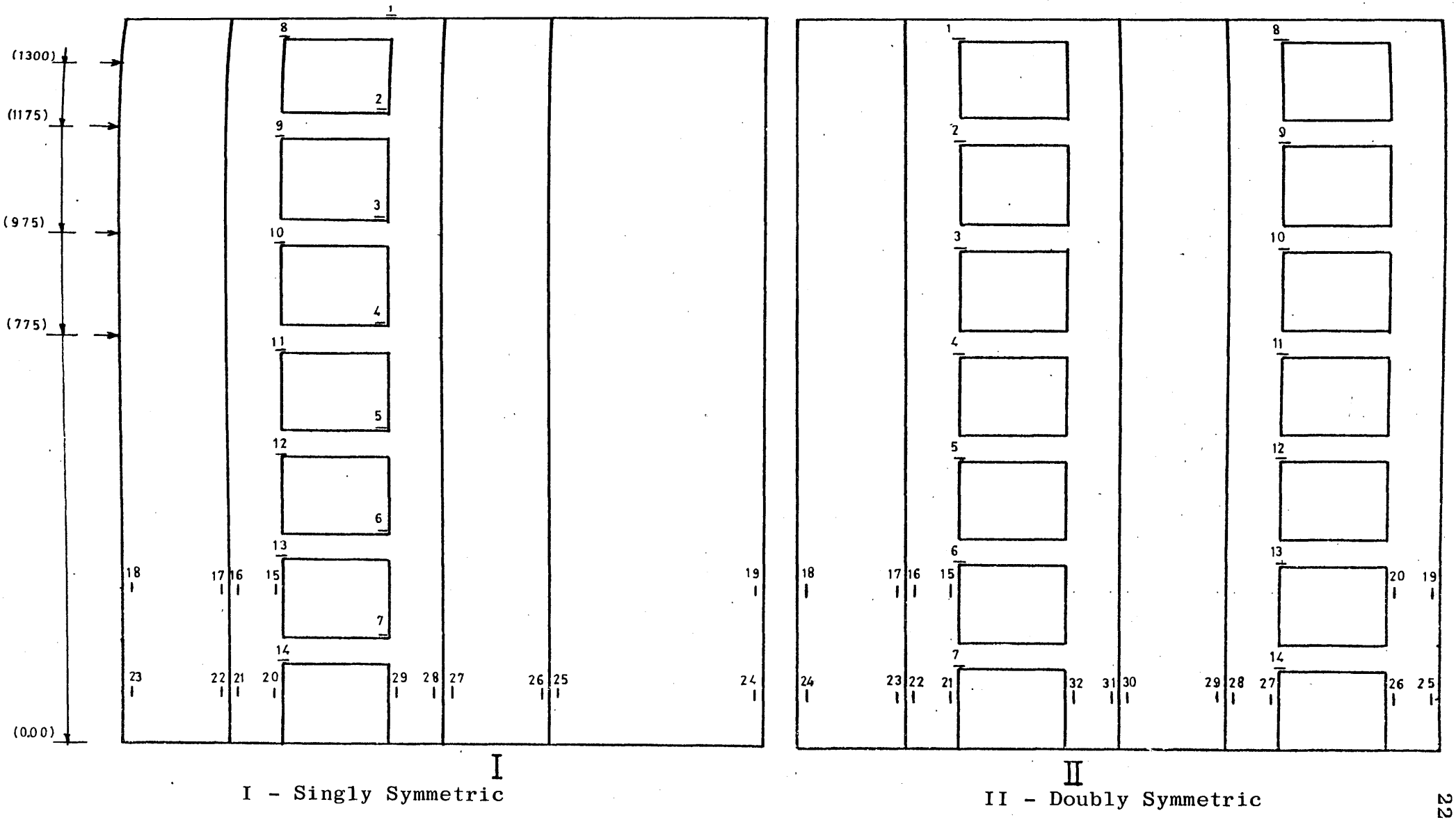

I - Singly Symmetric

II - Doubly Symmetric

Fig. 8.18 Positions of strain gauges and levels of transducers

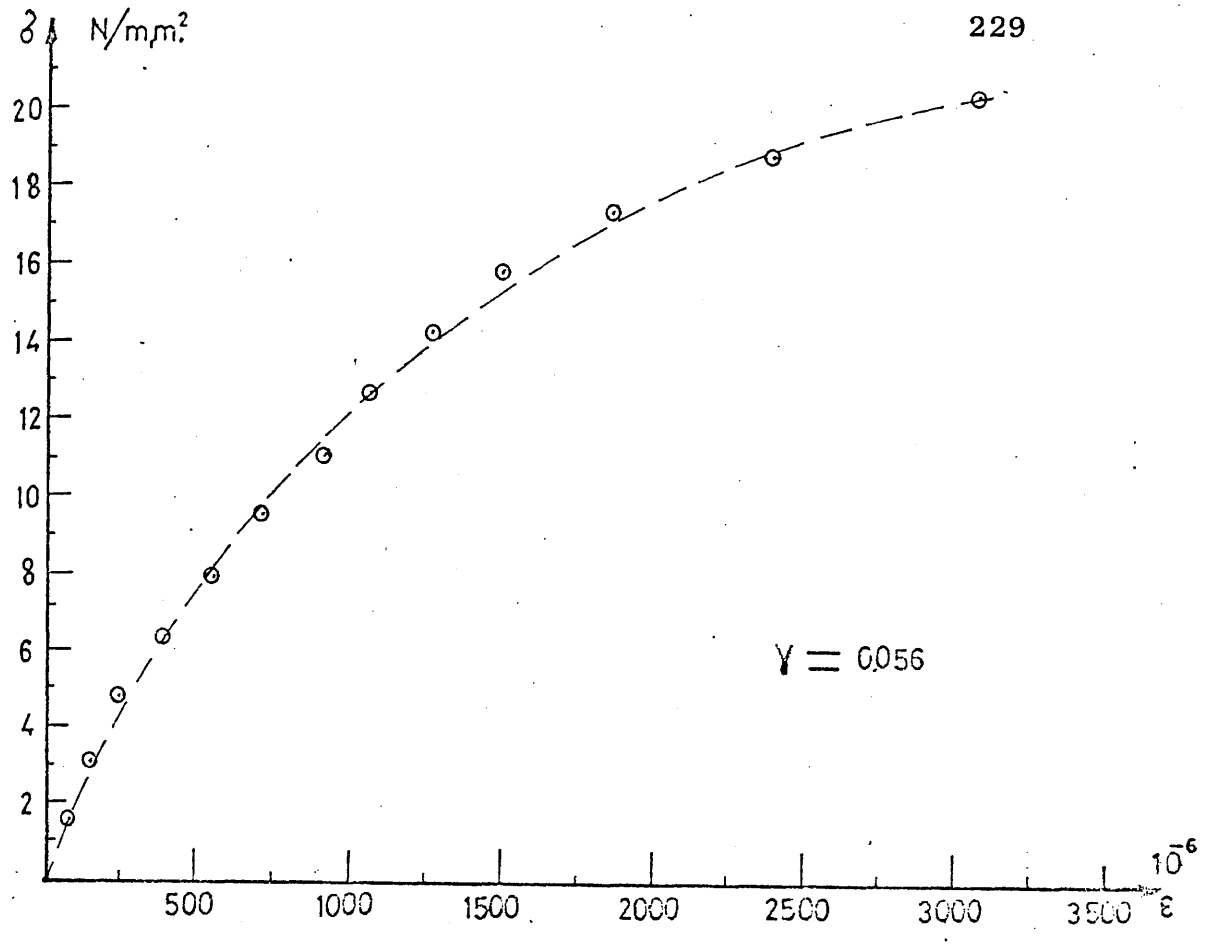

Fig. 8.19 Typical stress-strain relationships of concrete specimen

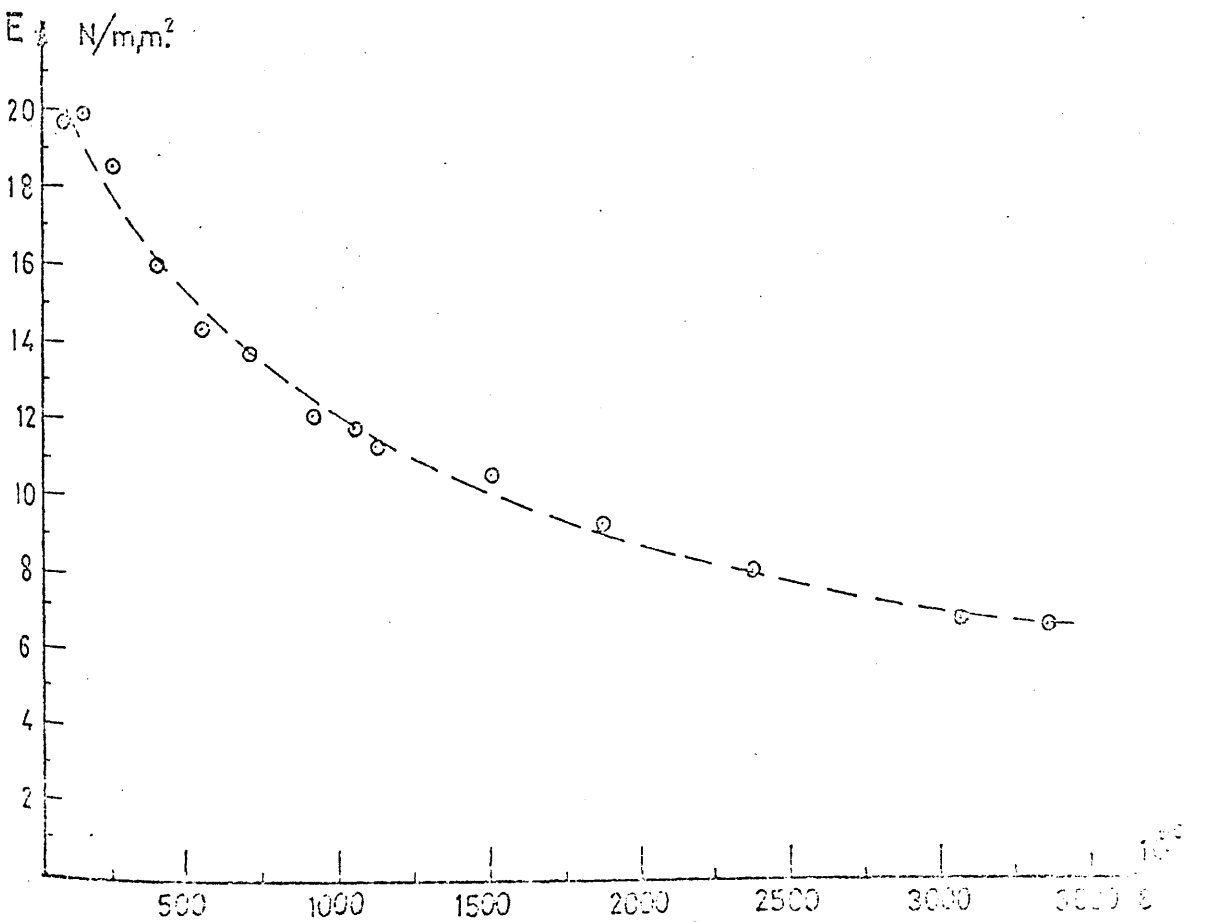

Fig. 8.20 Modulus of elasticity-strain relationship of a concrete specimen

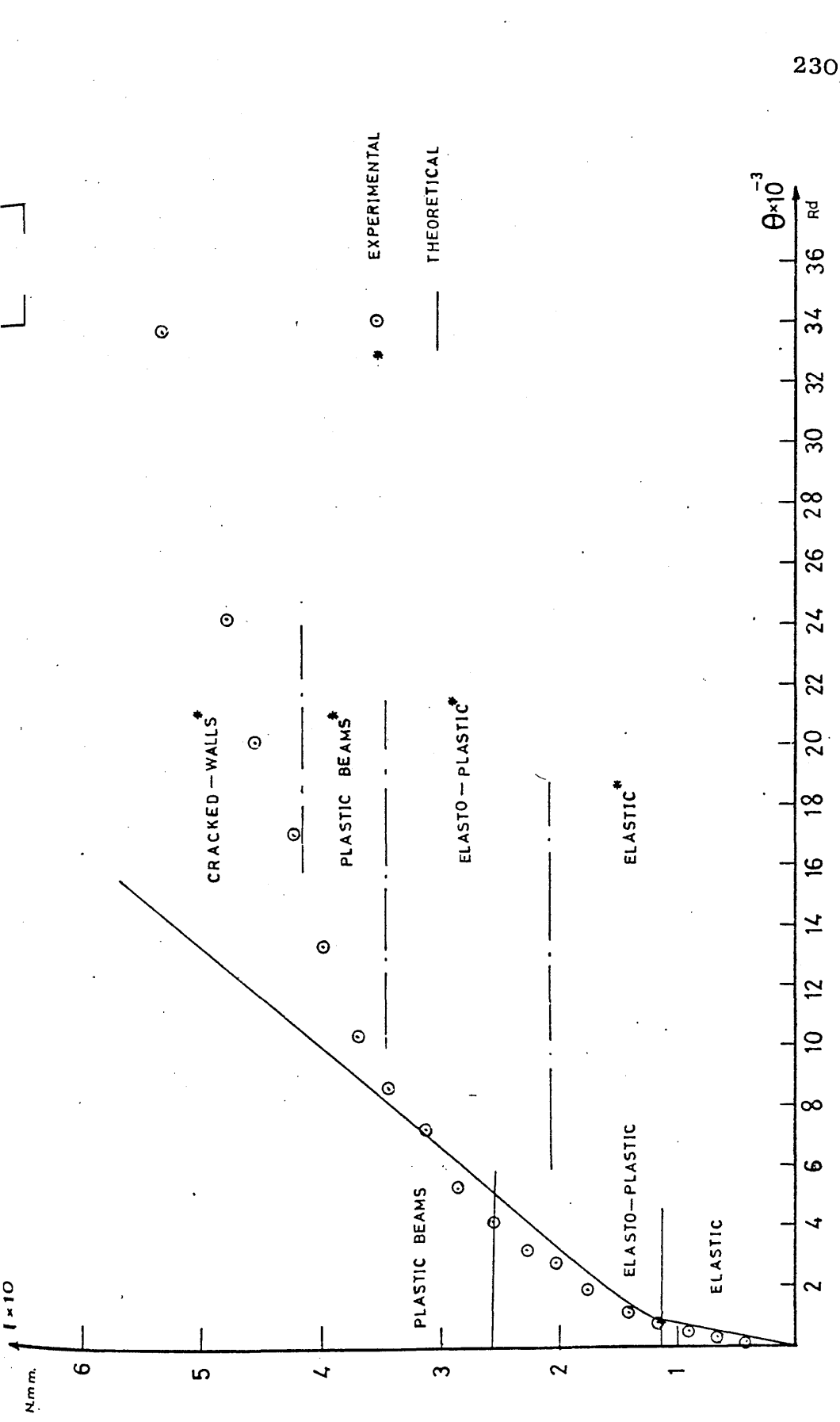

Fig. 8.21 Torque-rotation relationship of singly-symmetrical model

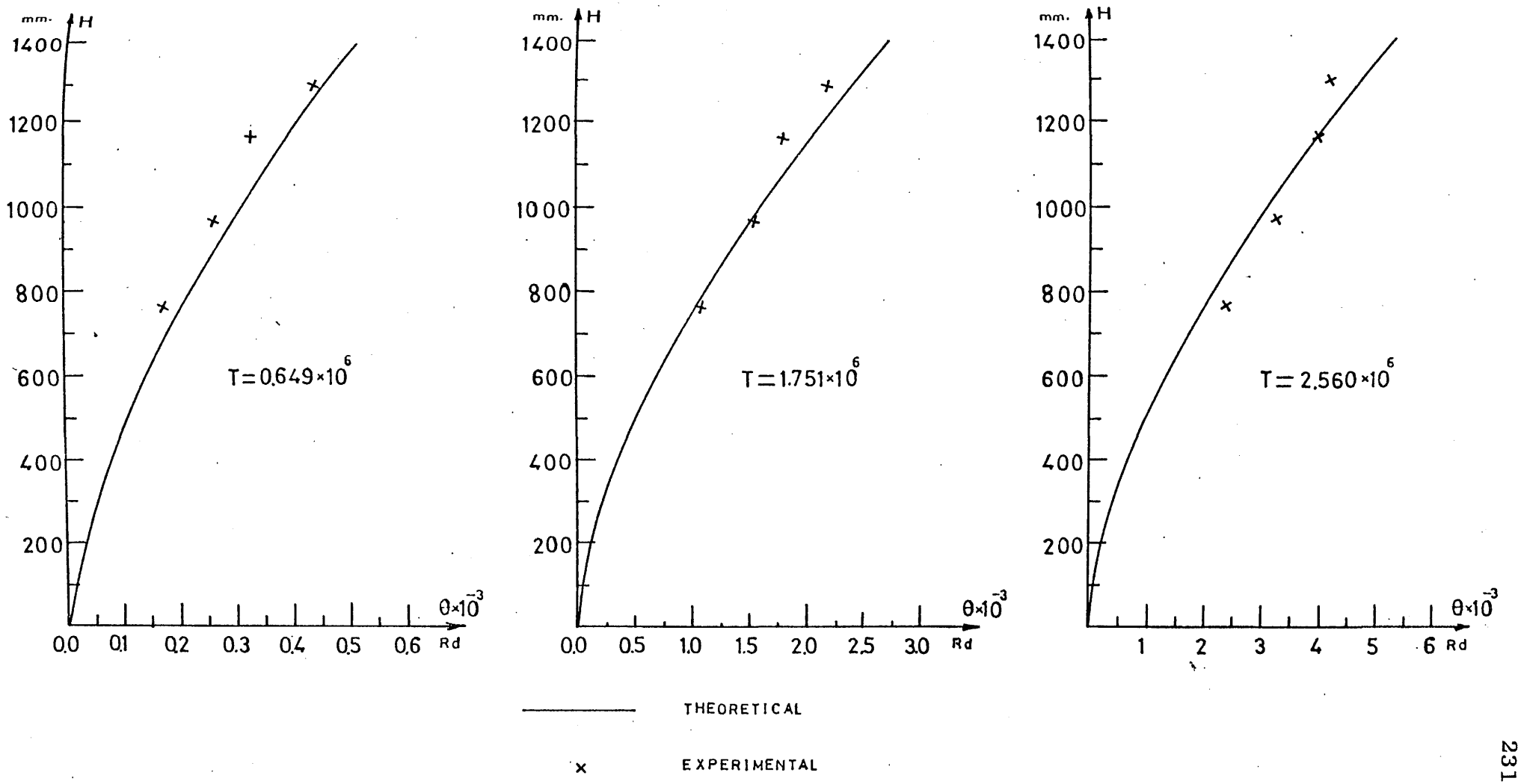

Fig. 8.22 Model rotation profiles at different stages of loading (singly-symmetric model)

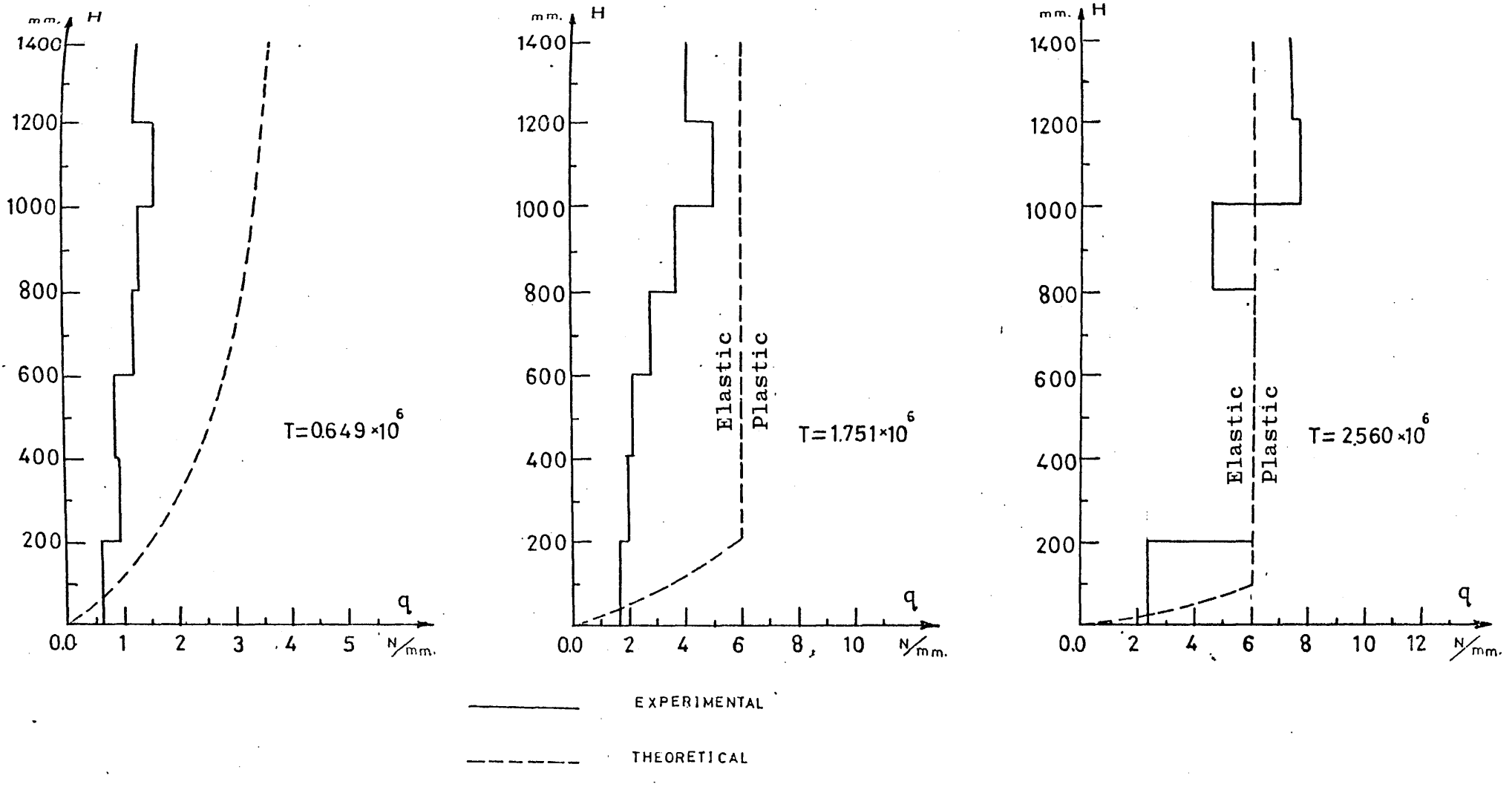

Fig. 8.23 Vertical shear distribution in connecting beams (Singly-symmetric model)

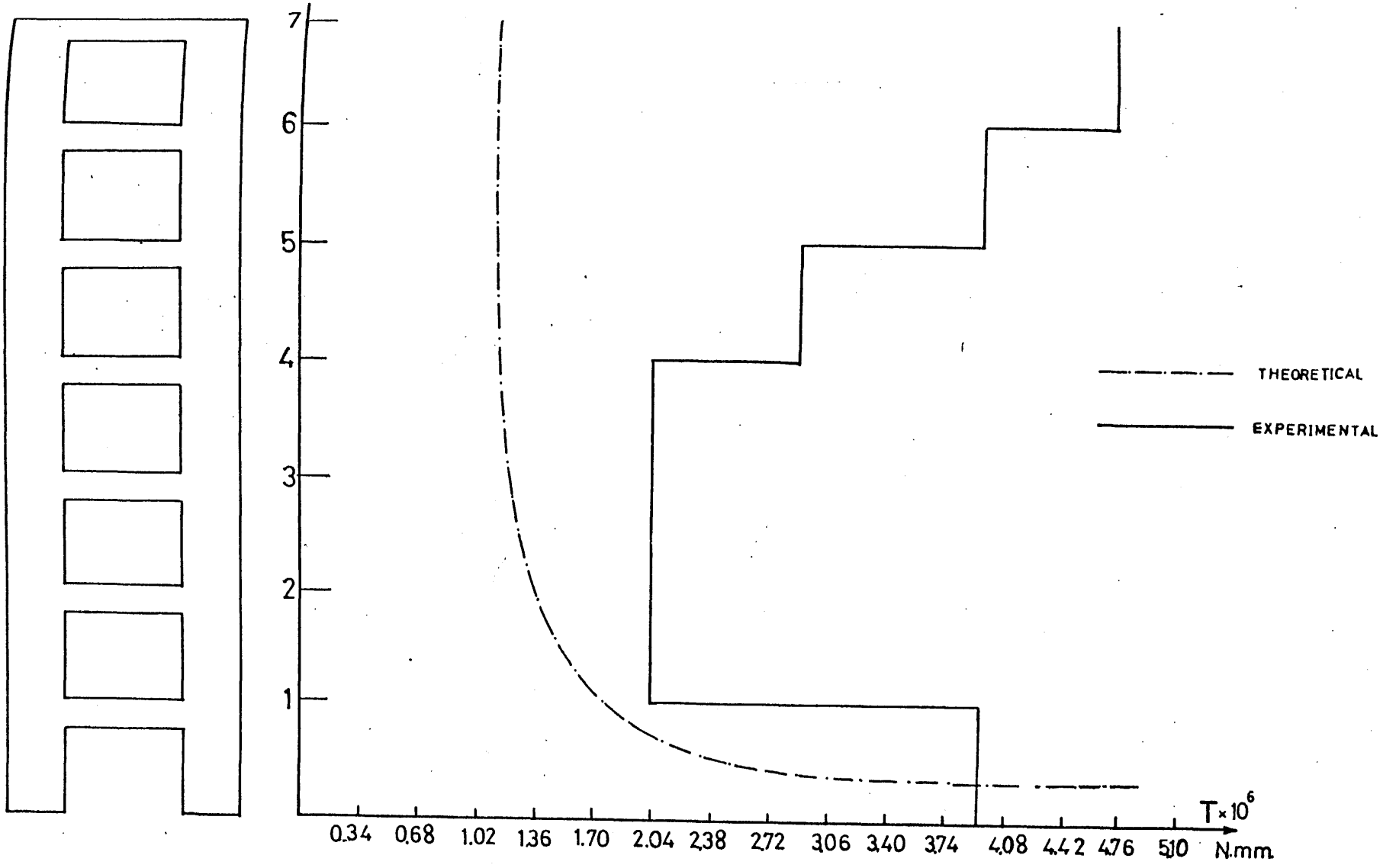

Fig. 8.24 Development of plasticity in the connecting beams (Singly-symmetric model)

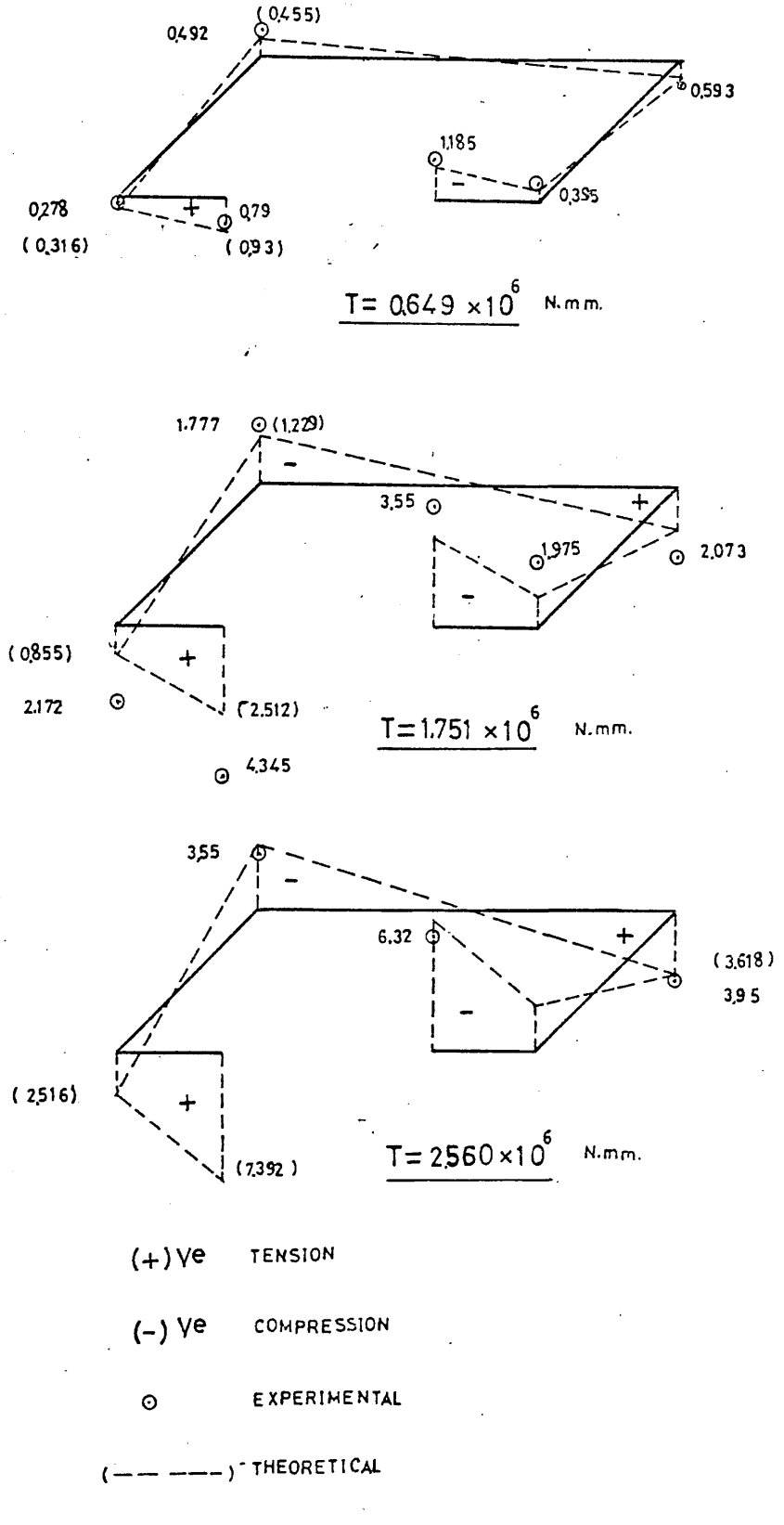

Fig. 8.25 Stresses at level of strain gauges (Singly-symmetric model)

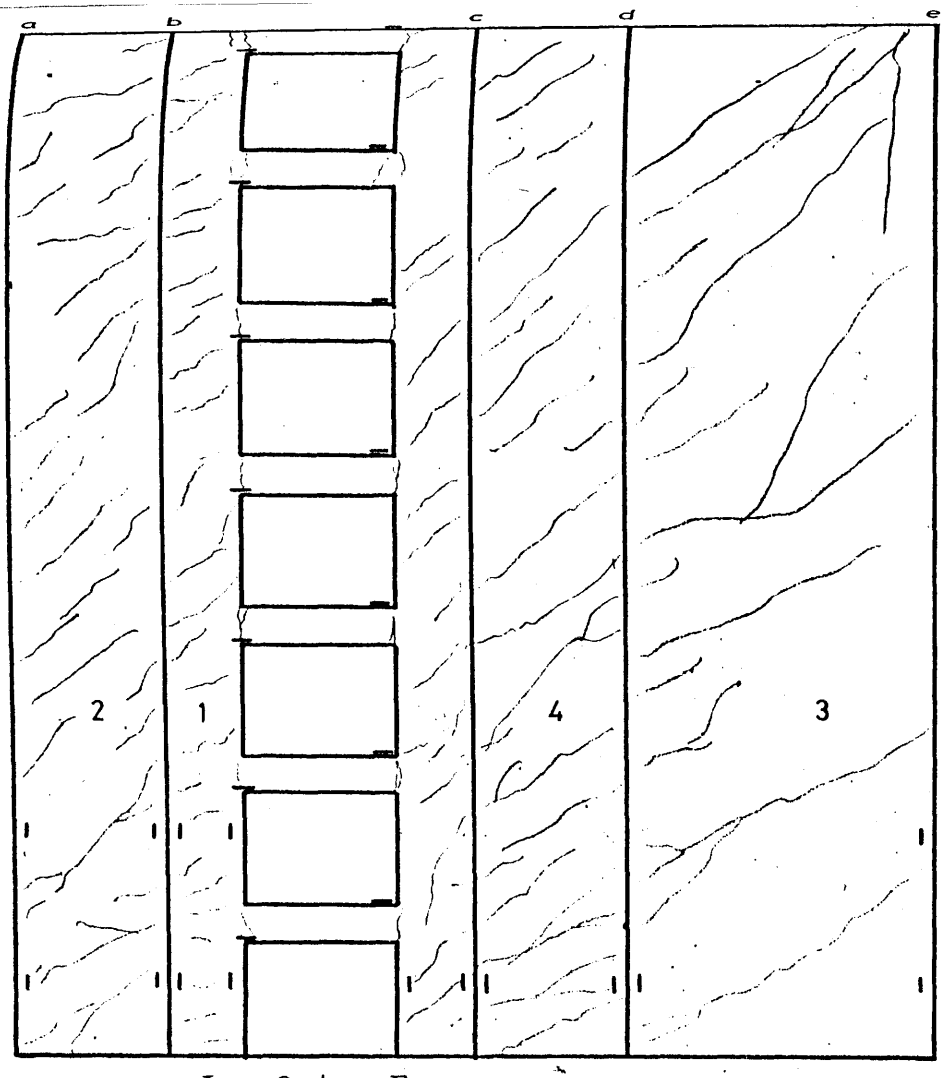

I - Outer Faces

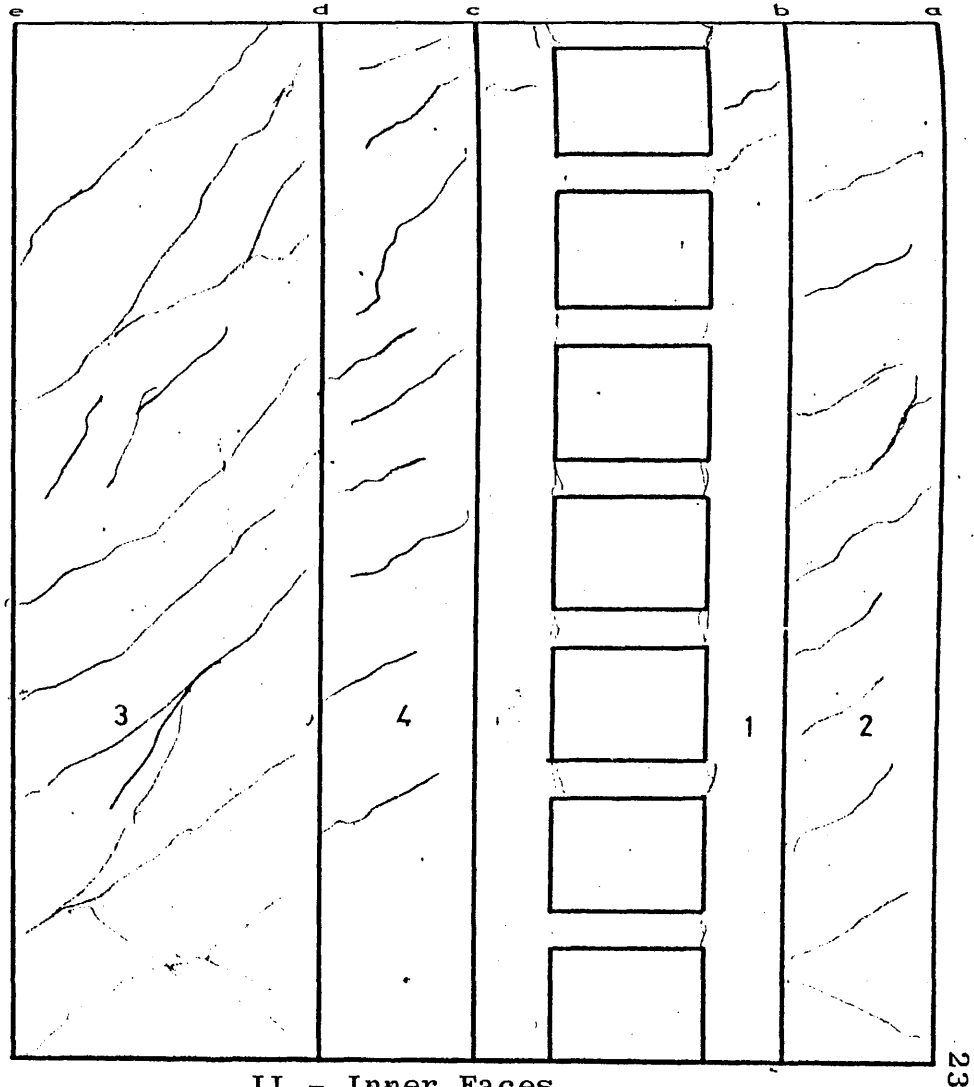

II - Inner Faces

Fig. 8.26 Crack patterns of model walls (Singly-symmetric)

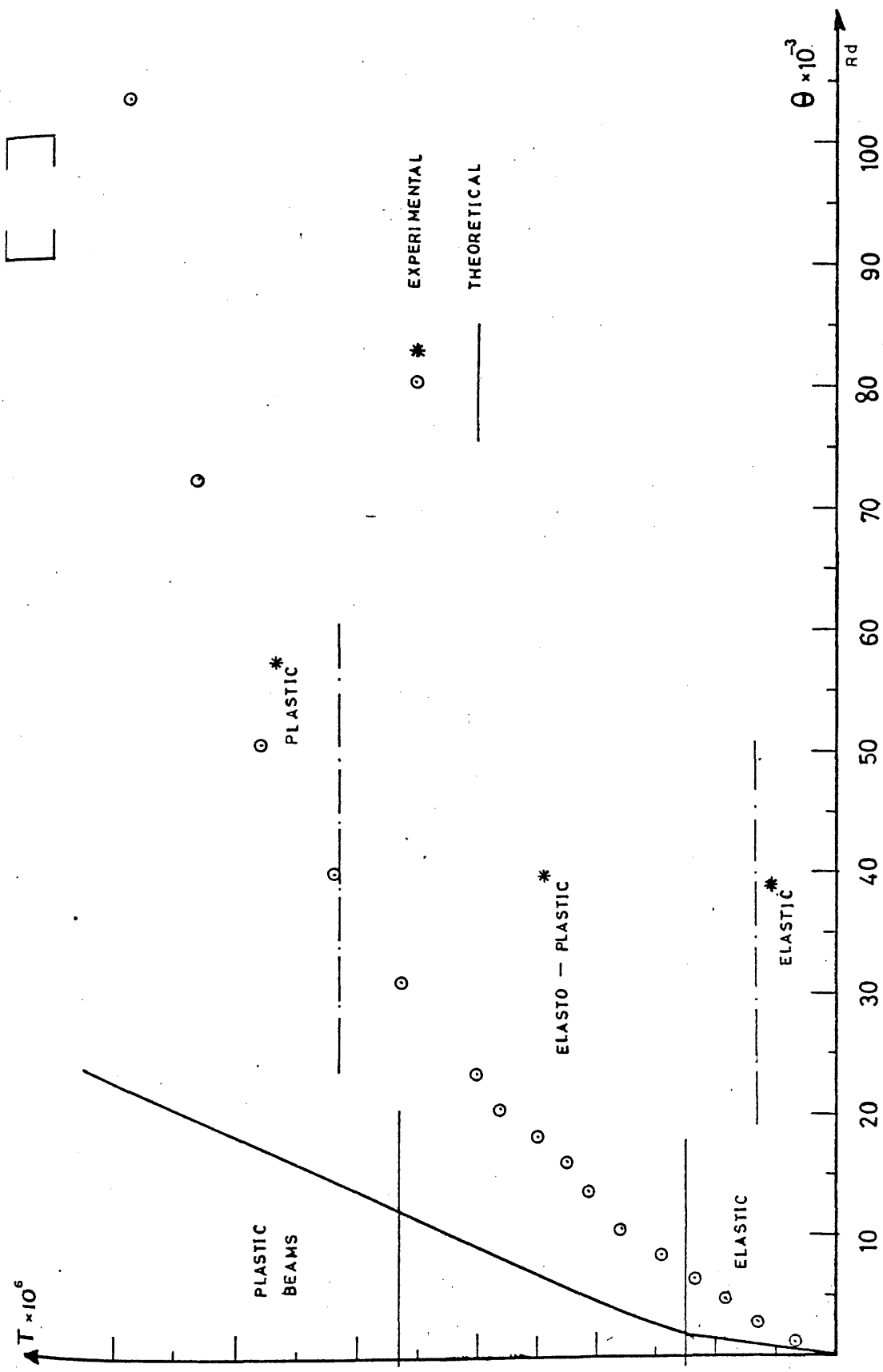

Fig. 8.27 Torque rotation relationship for doubly-symmetrical model

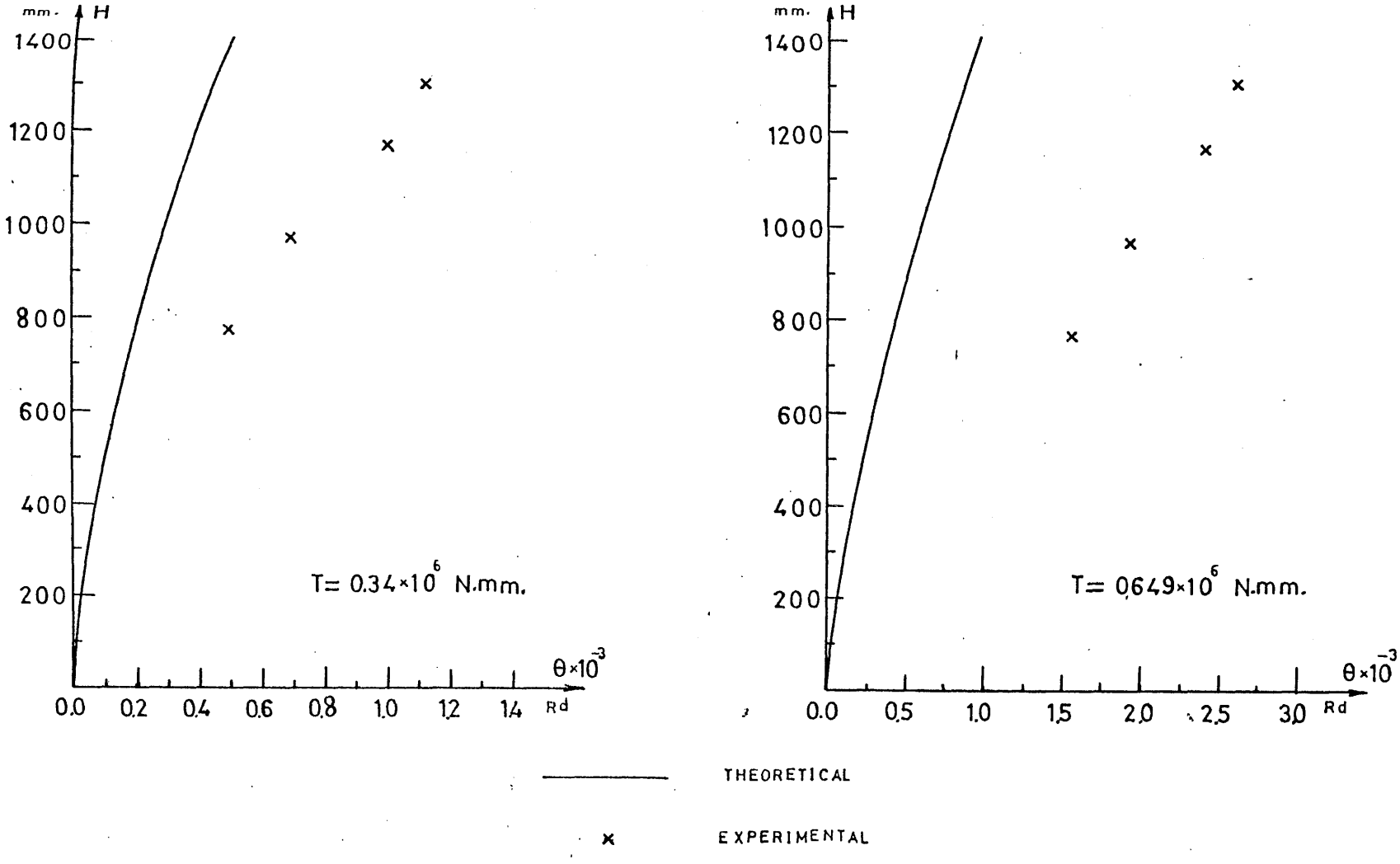

Fig. 8.28 Model rotation proviles at different stages of loading (Doubly-symmetrical model)

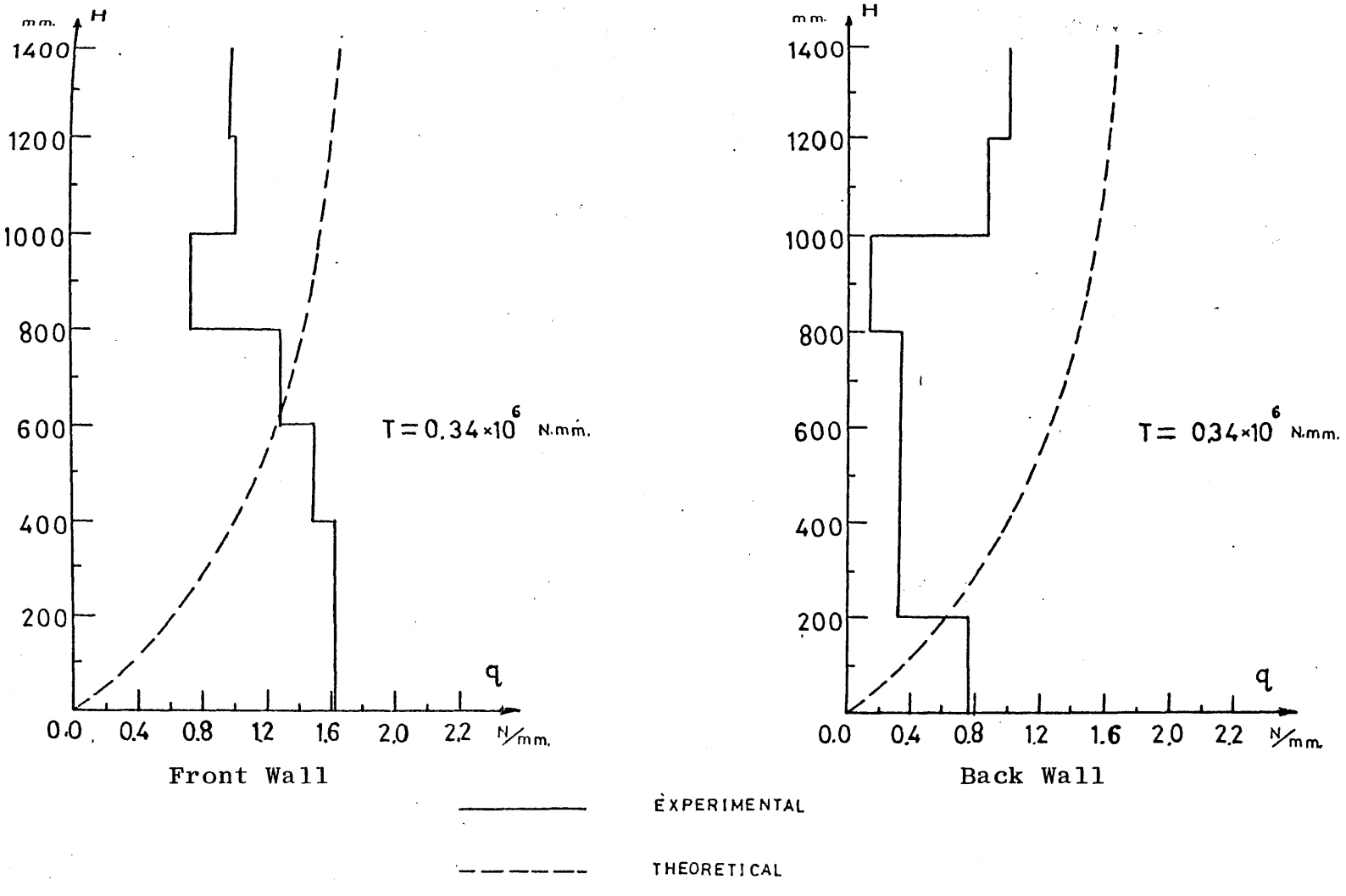

Fig. 8.29 Vertical shear distribution in connecting beams (Doubly-symmetrical model)

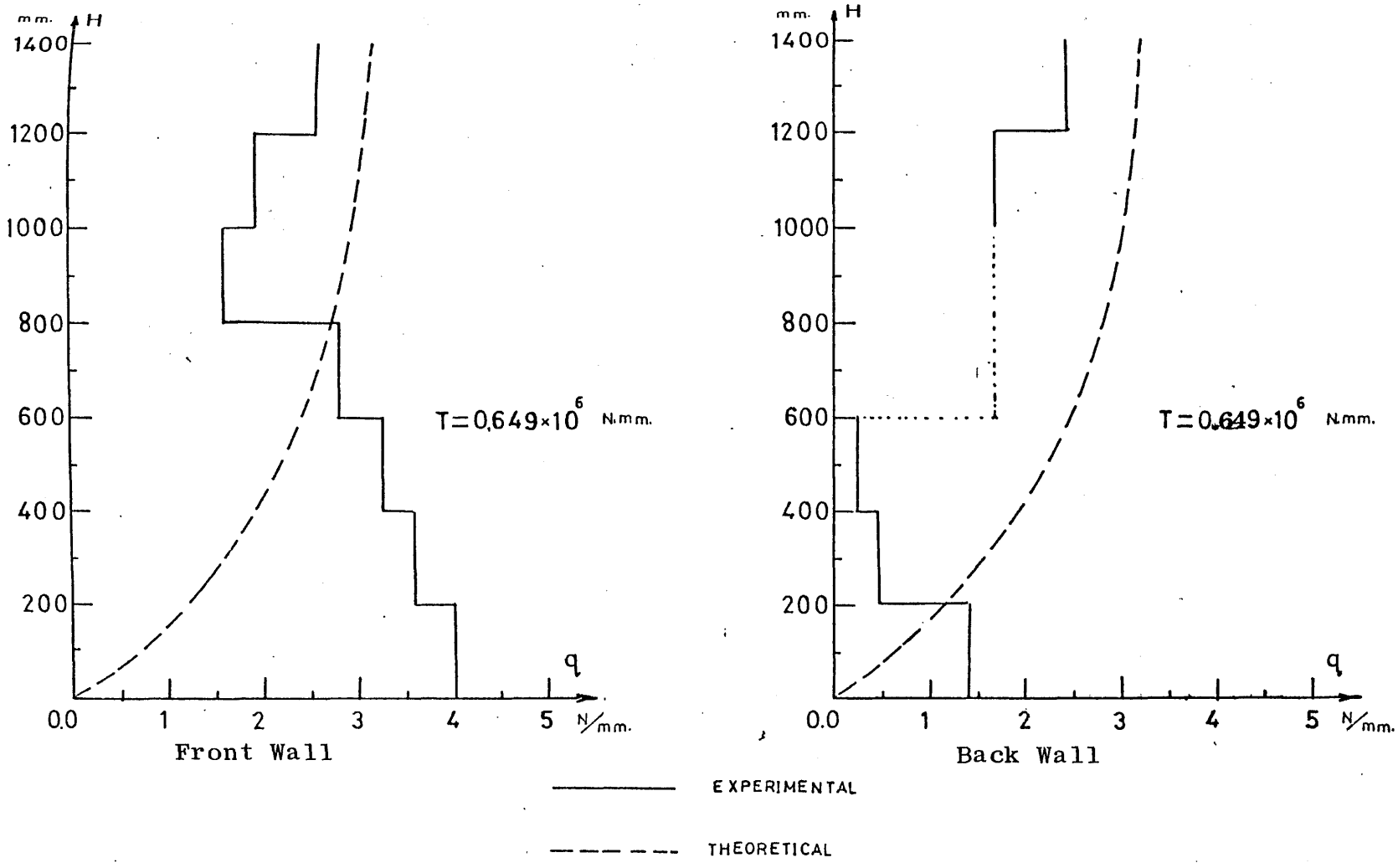

Fig. 8.30 Vertical shear distribution in connecting beams (Doubly-symmetrical model)

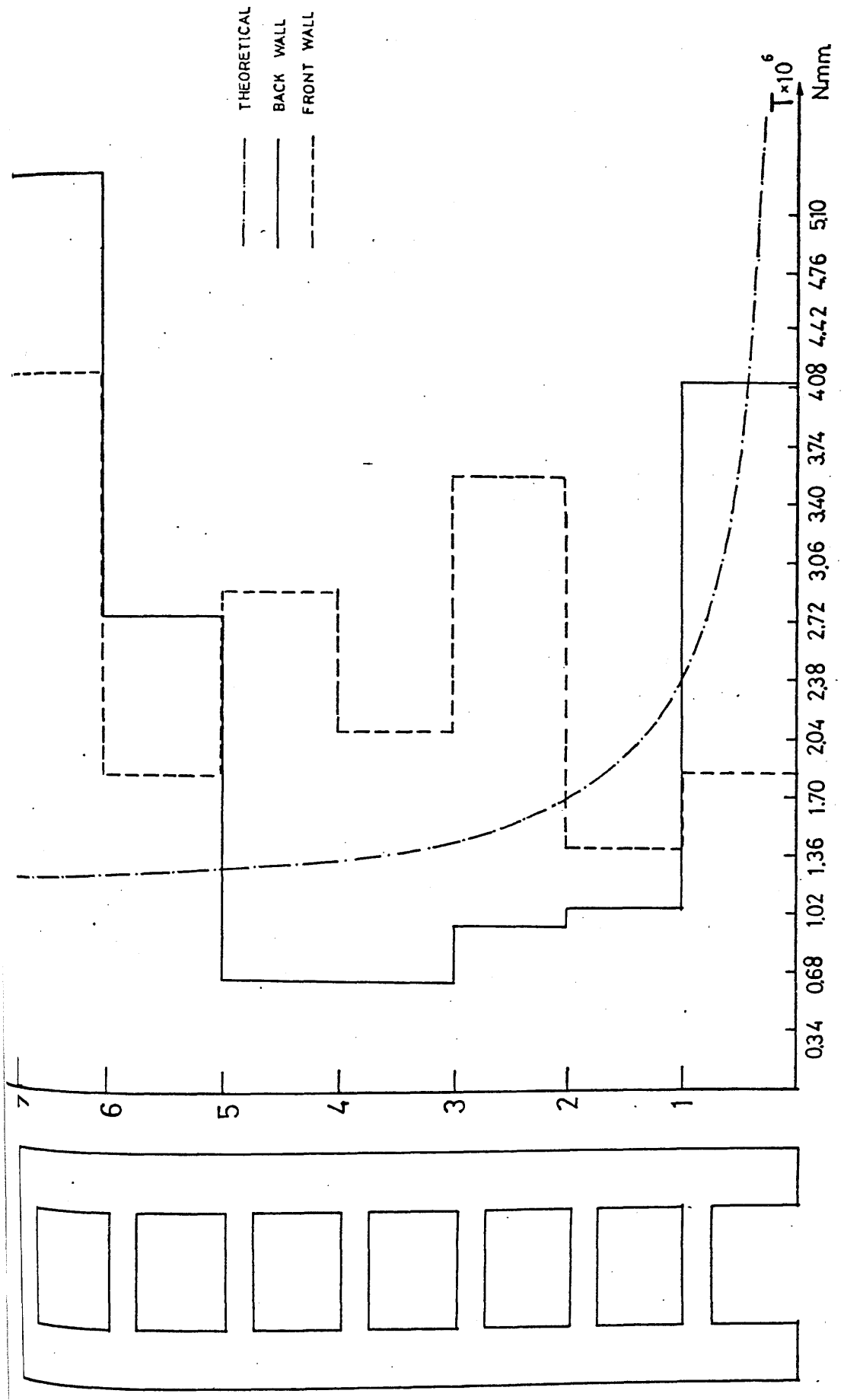

Fig. 8.31 Development of plasticity in the connecting beams (Doubly-symmetrical model)

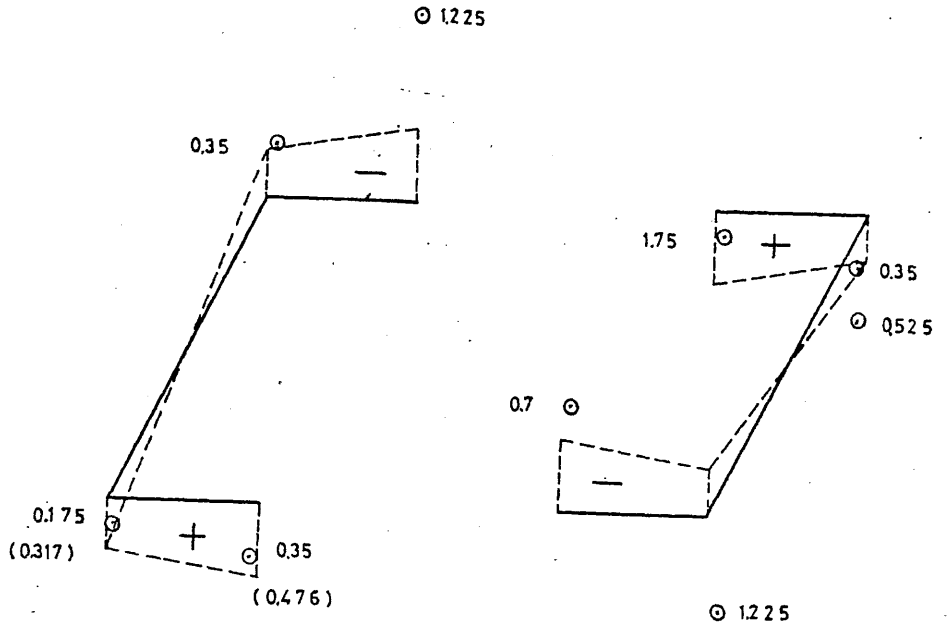

$T = 0.34 \times 10^{6}$ N.mm.

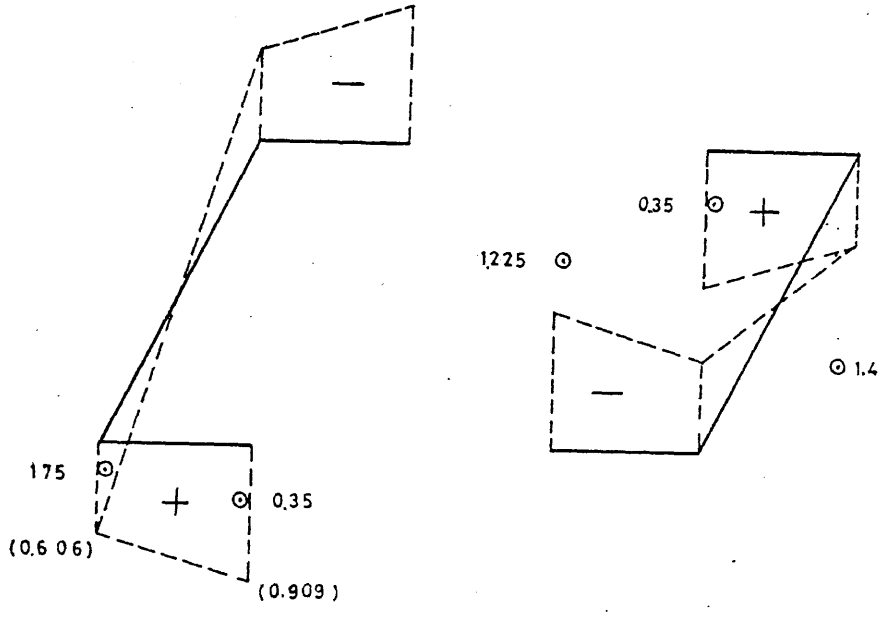

$T = 0.649 \times 10^{6}$ N.mm.

⊙ EXPERIMENTAL (+) TENSION

(– – – – – –) THEORETICAL (—) COMPRESSION

Fig. 8.32 Stresses at level of strain gauges (Doubly-symmetric model)

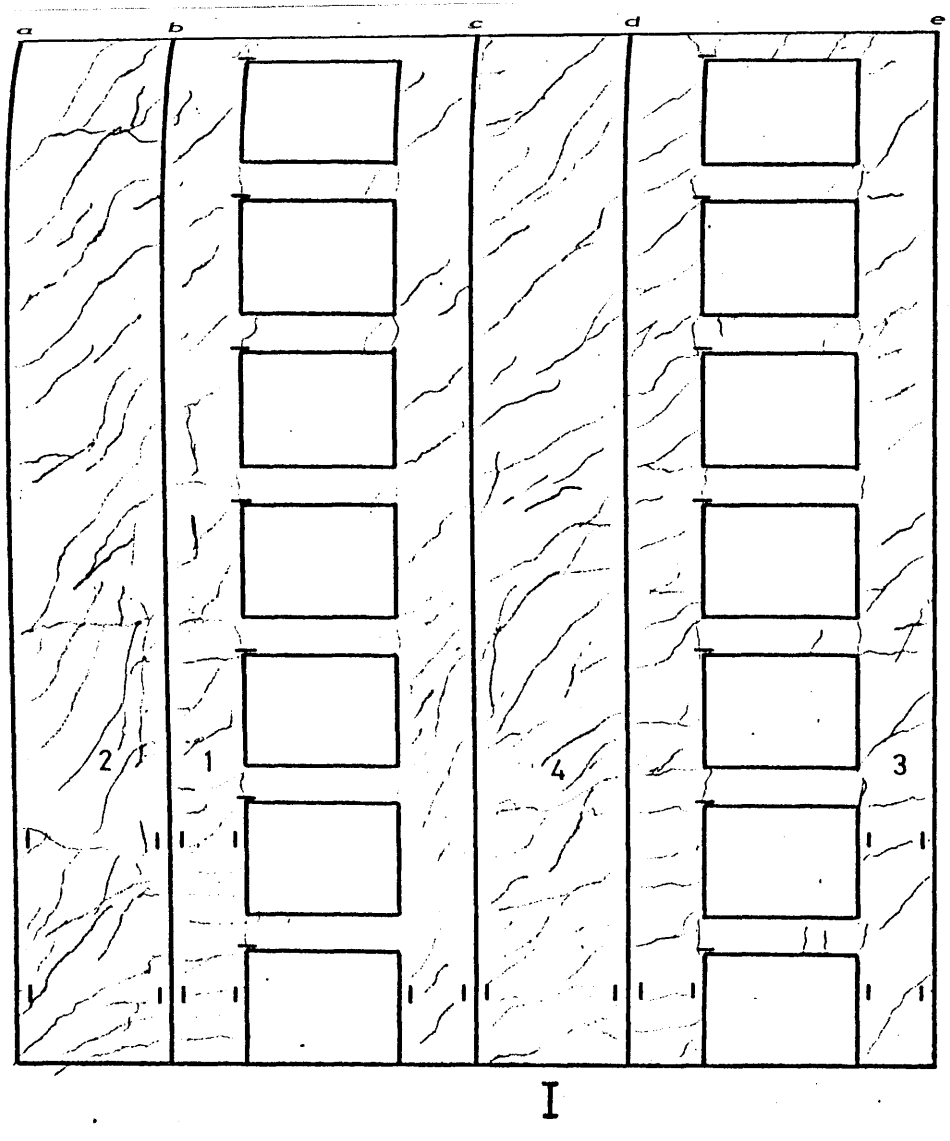

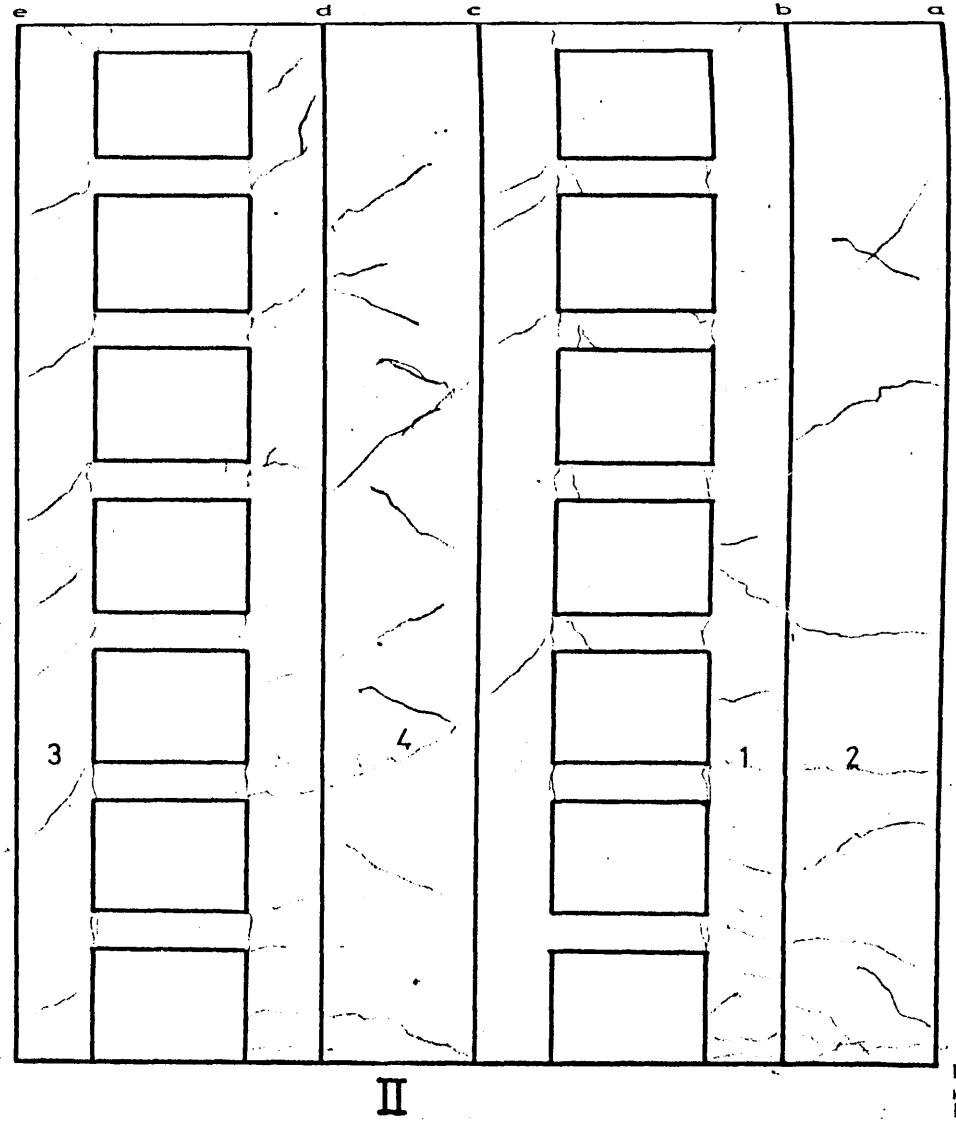

Fig. 8.33 Crack patterns for the model walls
(Doubly-symmetrical model)

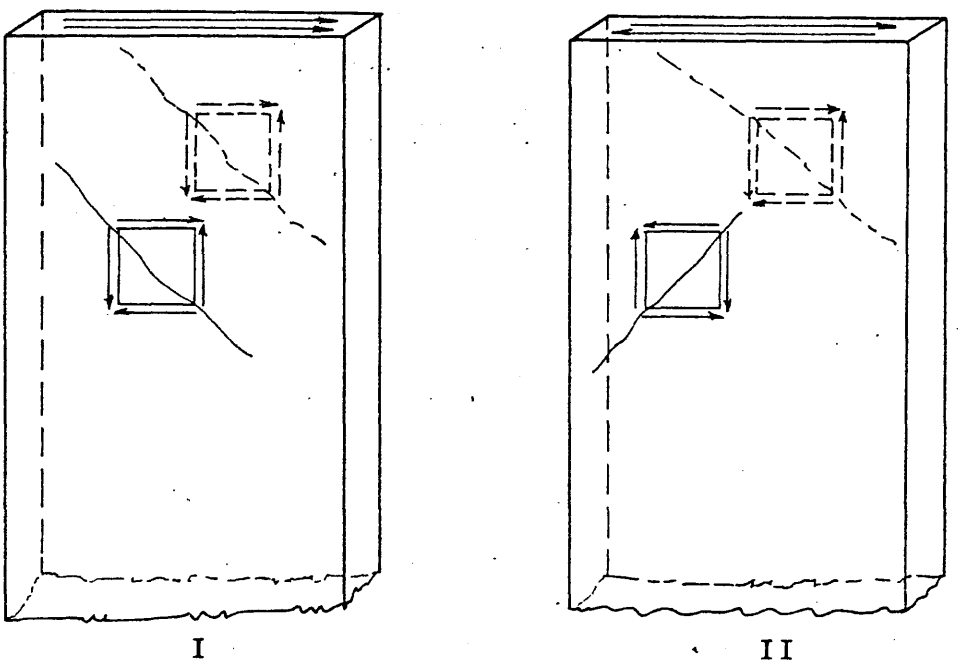

Fig. 8.34 Types of shear cracks in the walls

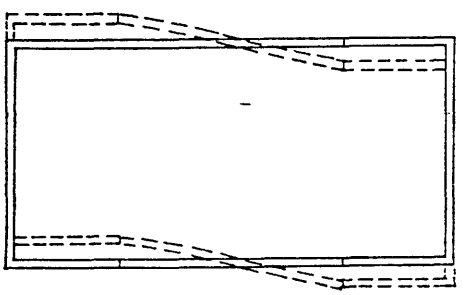

Fig. 8.35 Distorted shape of the doubly symmetric model

CHAPTER 9

CONCLUSIONS
AND
SUGGESTIONS FOR FUTURE WORK

CHAPTER 9

CONCLUSIONS AND SUGGESTIONS FOR FUTURE WORK

9.1 CONCLUSIONS

A theoretical method has been presented for the analysis of core structures subjected to torsional loading. In the method, the core is considered to consist of vertical plates rigidly connected together along their edges, and, by using the engineering theory of bending in conjunction with the continuous connection technique the core behaviour is represented by a third order governing differential equation. The governing equation is expressed in terms of a single variable Θ, the angle of rotation and a single non-dimensional parameter αH, the core relative stiffness. The method can be implemented to analyse any core structure which is open or partially closed by lintel beams providing no segment is completely closed. The accuracy of the method must be expected to decrease with an increase of the depth of the connecting beams. Closed-form solutions of the governing equation are given for three standard load cases, a point torque at the top, a uniformly distributed torque and a triangularly distributed torque. Solutions in similar forms can be obtained for any other form of loading expressed as an integrable function of the height.

The restraining effect of a stiff element at the top has been included in the analysis by introducing a non-dimensional parameter R as a restraining end condition at

the top, whose value can vary theoretically from zero for a core free at the top to infinity for a totally restrained end. The method used tends to over estimate R values since it treats the restraint as acting on a line at the top. In the case of unsymmetrical or multi-bayed cores the R value cannot be defined.

The effect of the flexibility of an elastic foundation on the core behaviour have been considered and expressed in terms of a single non-dimensional parameter λ, which can vary theoretically from zero for a core structure totally fixed at the base to infinity for the unrealistic case of a core free at the base. The above spectrum of λ values allows a wide range of foundation conditions to be considered. However, in reality, this value will be within a particular range depending on the nature of the sub-base material and the type and configuration of the foundations. Solutions are given for the governing equation for the above end conditions when the core is subjected to any of the three standard load cases considered. A numerical study of the interactive effect of the parameters αH, R and λ has been carried out, which showed that their relative effects on the primary actions of core structures decreases as their values increase.

The above solutions have been used to draw design charts for core structures subjected to any of three standard load cases within the practical limits of the above parameters. They can be used to calculate the angle of rotation, the vertical shear in the connecting laminas

and the normal forces and bending moments in the walls at any level of the core height. They are presented in general terms and are applicable to any core configuration providing that the core relative stiffness αH has been evaluated using the method proposed in Chapter 2 and the parameters of the end conditions have been estimated as shown in Chapter 3. Numerical examples have been presented to illustrate the various effects of the above parameters on the maximum angle of rotation and the internal force distributions in the cases of singly and doubly symmetrical cores. Although in both cases the parameter αH increases as an exponential function to the power 1.5 of the connecting beam depth, the internal force distributions have different forms. The parameter R is a cubic function of the depth of the stiff top beam. The flexibility of the foundation has a very significant effect on the values of bending moments and normal forces in the walls, the reduction in these values exceeding 90% of the original values of a fixed base when λ has a value of 2, and the internal forces are redistributed in a way which a greater resistance against loading is assigned to the connecting beams.

A solution for core structures with stiffness variations throughout the height was achieved by considering the core to consist of various zones and satisfying the conditions of equilibrium and compatibility between each two successive zones. Expressions are given for the elastic behaviour of core structures consisting of two

zones and subjected to the standard load cases. The same numerical example was used to illustrate the influence of a stiffness change, with particular emphasis on reducing the thickness of the walls. The method is limited to certain types of changes and cannot be applied directly to other variations such as changing the width of openings or the configuration of the core.

A comparison between the proposed method and frame analysis method was carried out using the example structure used in Chapter 4. Good agreement was achieved when comparing the results obtained from both methods for the rotations and the vertical shear in the connecting beams. However, the same agreement could not be achieved when comparing the bending moments and normal forces in the walls.

The method was extended to study core structures undergoing post-elastic deformations by assuming that plastic hinges will develop in the connections between the lintel beams and the adjacent walls when the moment in the beams reaches an ultimate value. In this case the core is considered to consist simultaneously of elastic and elasto-plastic zones. An investigation of the sequence in which the plasticity will commence and develop in core structures is presented. Mathematical expressions for the overall equilibrium condition in each stage of plasticity are given for a single bay core subjected to the standard load cases.

The above expressions were employed in a computer

program and the same numerical example was used to study the effect of the parameters αH, R and λ on the development of plasticity throughout the core height. The results obtained followed the mode predicted from the shear distribution in the connecting lamina. However, the method is not very accurate as it does not account for the effects of cracks in the walls and beams on the stiffness of the core, and considers the beams either fully elastic or fully plastic. Although the method is applicable for any core configuration considered, it is very lengthy and impractical to be used in more complicated cases considering the number of equations involved. In such cases some other numerical technique may be attempted.

The results of the experimental investigation on perspex models followed the same pattern as predicted in the analytical solutions. Good agreement was achieved in comparing the values obtained from the experimental and theoretical investigations, although the effect of a stiff top beam was over estimated theoretically being more pronounced in the singly symmetric case. The effects of the cracks on the behaviour of the reinforced concrete models were very significant. In general, the behaviour and the internal force distribution showed a reasonable agreement with the analytical solutions within the elastic and elasto-plastic limits. The method presents a reasonably accurate tool to designers to analyse the elastic behaviour of most core structures subjected to torsional loading which only requires the use of the widely

known engineering theory of bending and the solution of a third order differential equation. All the calculations for the elastic and elasto-plastic behaviour of a core can be carried out with a desk calculator or a small computer.

9.2 SUGGESTIONS FOR FUTURE WORK

In addition to the factors considered to affect the core behaviour, a number of related factors need to be examined. In a tall building the core is seldom subjected to pure torsion, but is generally subjected to bending, shear and torsion actions. The combined effect of the above loadings on the core behaviour needs to be examined. The load applied to the core results from the redistribution of the external applied loads on structural elements of the building, which needs to be determined as part of an overall analysis of the entire building.

The existence of floor slabs outside and inside the core shaft which are in many cases connected to the beams and walls of the core, impose a warping restraint against torsional deformations of the core. It would be desirable to assess this effect on the core behaviour.

The method will be more accurate if the effect of the connecting beams is considered when locating the position of the shear centre.

A study of the detailing of the joints between the connecting beams and the walls is needed to give a more practical assessment of the plastic moment and ductility of the hinges.

The prospects of a complete failure of the core and the mechanisms associated with it need to be examined.

REFERENCES

1. Khan, F.R.,
"Current Trends in Concrete High-rise Buildings".
'Tall Buildings', A. Coull and B. Stafford Smith, ed.,
Pergamon Press, 1967, pp.571-590.

2. Khan, F.R., and Amin, N.R.
"Analysis and Design of Framed Tube Structures for
Tall Concrete Buildings",
The Structural Engineer, Vol. 48, Aug. 1970, pp.
301-306.

3. Jenkins, W.M. and Harrison, T.
"Analysis of Tall Buildings with Shear Walls under
Bending and Torsion",
'Tall Buildings', A. Coull and B. Stafford Smith, ed.,
Pergamon Press, 1967, pp.413-449.

4. Vlasov, V.Z.,
"Thin-Walled Elastic Beams",
Translated from Russian by the Israel Program for
Scientific Translation, Jerusalem, 1961.

5. Taranath, B.S. and Stafford Smith, B.
"Torsion Analysis of Shear Core Structures"
A.C.I. Publication, SP 35, 1971, pp.239-263.

6. Stafford Smith, B. and Taranath, B.S.
"The Analysis of Tall Core-Supported Structures
Subjected to Torsion"
Proc. Inst. of Civ. Eng., Vol. 53, Part 2, September
1972, pp.173-187.

7. Heidebrecht, A.C. and Stafford Smith, B.
"Approximate Analysis of Open-section Shear Walls
Subjected to Torsional Loading"
Journal of Structural Division, A.S.C.E., Vol. 99,
ST. 12, December 1973, pp.2355-2373.

8. Khan, M.A. and Stafford Smith, B.
"Restraining Action of Bracing in Thin-Walled Open-Section Beams"
Proc. Inst. of Civ. Eng., Vol. 59, Part 2, March 1975, pp.67-78.

9. Rosman, R.
"Torsion of Perforated Concrete Shafts"
Journal of Structural Division, A.S.C.E., Vol. 95, ST. 5, May 1969, pp.991-1010.

10. Michael, D.
"Torsional Coupling of Core Walls in Tall Buildings"
The Structural Engineer, Vol. 47, February 1969, pp.67-71.

11. Tso, W.K. and Biswas, J.K.
"Analysis of Core Wall Structure Subjected to Applied Torque"
Building Science, Vol. 8, 1973, pp.251-257.

12. Rutenberg, A.V. and Tso, W.K.
"Torsional Analysis of Perforated Core Structure"
Journal of the Structural Division, A.S.C.E., Vol. 101, ST. 3, March 1975, pp.539-550.

13. Coull, A.
"Torsion of Structural Cores on Deformable Foundations"
Building Science, Vol. 10, 1975, pp.57-64.

14. Liauw, T.C. and Leung, K.W.
"Torsion Analysis of Core Wall Structures by Transfer Matrix Method"
The Structural Engineer, Vol. 53, April 1975, pp.187-194.

15. Liauw, T.C.
"Torsion of Multi-Storey Spatial Core Walls"
Proc. Inst. of Civ. Eng., Vol. 65, Part 2, September 1978, pp.601-609.

16. Goodno, B.J. and Gere, M.J.
"Analysis of Shear Cores Using Superelements"
Journal of the Structural Division, A.S.C.E., Vol. 102, ST. 1, January 1976, pp.267-283.

17. Macleod, I.A. and Hosny, H.M.
"Frame Analysis of Shear Wall Cores"
Journal of the Structural Division, A.S.C.E., Vol. 103, ST. 10, October 1977, pp.2037-2047.

18. Nayar, K.K. and Coull, A.
"Elasto-Plastic Analysis of Coupled Shear Walls"
Journal of the Structural Division, A.S.C.E., Vol. 102, ST. 9, September 1976, pp.1845-1860.

19. Glück, J.
"Elasto-Plastic Analysis of Coupled Shear Walls"
Journal of the Structural Division, A.S.C.E., Vol. 99, ST. 8, August 1973, pp. 1743-1760.

20. Paulay, T.
"Coupling Beams of Reinforced Concrete Shear Walls"
Journal of the Structural Division, A.S.C.E., Vol. 97, ST. 3, March 1971, pp.843-862.

21. Paulay, T.
"Ductile Behaviour of Coupled Shear Walls"
Journal of the Structural Division, A.S.C.E., Vol. 102, ST. 1, January 1976, pp. 93-108.

22. Irwin, A.W. and Ord, A.E.
"Cyclic Load Tests on Shear Wall Coupling Beams"
Proc. Inst. of Civ. Eng., Vol. 61, Part 2, June 1976, pp.331-341.

23. Irwin, A.W. and Andrew, N.
"Torsional Performance of Coupled Channels in Tall Buildings"
Proc. Inst. of Civ. Eng., Vol. 61, Part 2, December 1976, pp.773-783.

24. Megson, T.H.
"Linear Analysis of Thin-Walled Elastic Structures"
Surrey University Press, 1974.

25. Paz, M., Patrick, C., and Schrader, P.
"Computer Determination of the Shear Centre of Open and Closed Sections"
Computers and Structures, Vol. 6, 1976, pp.117-125.

26. Housner, G.W. and Vreeland, T. Jr.
"The Analysis of Stress and Deformation"
The Macmillan Company, New York, 1966.

27. Coull, A. and Choudhury, J.R.
"Stresses and Deflections in Coupled Shear Wall"
A.C.I., Proceedings, Vol. 64, No. 2, February 1967, pp.65-72.

28. Coull, A. and Choudhury, J.R.
"Analysis of Coupled Shear Walls"
A.C.I. Proceedings, Vol. 64, No. 9, September 1967, pp.587-593.

29. Hosny, H.M.
"Load Distribution in Shear-Wall Structures"
Ph.D. Thesis, 1976, Paisley College of Technology, Paisley.

30. British Standards Institute CP 110: Part 1, "The Structural Use of Concrete", 1972.

31. Harry G. Harris, Gajanan M. Sabnis and Richard N. White
"Reinforcement for Small Scale Direct Models of Concrete Structures"
A.C.I. Publication, SP 24, 1968, pp.141-149.

32. Mark Fintel
"Ductile Shear Walls in Earthquake Resistant Multi-storey Buildings"
A.C.I., Proceedings, Vol. 71, June 1974, pp.296-305.

APPENDIX A

CORE STRUCTURES WITH PARTICULAR CONFIGURATIONS

APPENDIX A

The method illustrated in Chapter 2 has been utilised to study other more complex core configurations which do not fit directly into the simple general cases considered there. Expressions are given to evaluate the relevant stiffness parameter αH for each particular case.

I - MULTI-CELL, MULTI-BAY, SINGLY-SYMMETRIC CORE

A multi-cell, multi-bay, singly-symmetric core as shown in Fig. A.1.I will rotate about its shear centre at distance e from the centre line of the back wall as shown in Fig. A.1.II, from which the displacements of various points may be obtained. The equilibrium conditions for the internal forces of a segment of height dx from each panel may be derived from Fig. A.2.

In this case, six vertical strain compatibility conditions must be considered, at the mid-span positions of the connecting mediums along lines 0-0 and 1-1, at the end corners along lines 2-2 and 3-3, and at the interaction of the cross panel 6 with the front and back walls along lines 4-4 and 5-5. These give respectively

$$\int_0^x \frac{M_4}{EI_4}\frac{(c+L)}{2}dx + \int_0^x \frac{M_5}{EI_5}\frac{(F+L)}{2}dx - \int_0^x \frac{N_4}{EA_4}dx - \frac{q_o}{\beta_o E} = 0 \qquad \text{I-1}$$

$$\int_0^x \frac{M_1}{EI_1}\frac{(d+a)}{2}dx + \int_0^x \frac{M_4}{EI_4}\frac{(c+a)}{2}dx - \int_0^x \frac{N_1}{EA_1}dx + \int_0^x \frac{N_4}{EA_4}dx - \frac{q_1}{\beta_1 E} = 0 \qquad \text{I-2}$$

$$\int_o^x \frac{M_1}{EI_1}\frac{d}{2}\,dx - \int_o^x \frac{M_2}{EI_2}\frac{B}{2}\,dx + \int_o^x \frac{N_1}{EA_1}\,dx - \int_o^x \frac{N_2}{EA_2}\,dx = 0 \qquad \text{I-3}$$

$$\int_o^x \frac{M_2}{EI_2}\frac{B}{2}\,dx + \int_o^x \frac{M_3}{EI_3}\frac{D}{2}\,dx - \int_o^x \frac{N_2}{EA_2}\,dx = 0 \qquad \text{I-4}$$

$$\int_o^x \frac{M_6}{EI_6}\frac{B}{2}\,dx + \int_o^x \frac{N_6}{EA_6}\,dx - \int_o^x \frac{N_4}{EA_4}\,dx = 0 \qquad \text{I-5}$$

$$\int_o^x \frac{M_3}{EI_3}\left(L + \frac{c+F}{2}\right)dx + \int_o^x \frac{M_6}{EI_6}\frac{B}{2}\,dx - \int_o^x \frac{N_6}{EA_6}\,dx = 0 \qquad \text{I-6}$$

On solving the above equations, in conjunction with the moment-curvature relationships for the core panels, expressions for the internal forces can be obtained. Considering the overall equilibrium condition of the core cross-section as shown in Fig. A.3, it can be proved that the core behaviour will follow the general governing equation

$$-EI_w\frac{d^3\theta}{dx^3} + GJ_o\frac{d\theta}{dx} = T$$

where

$$I_w = (B+e)^2(2I_1 + 2I_4 + I_5) + I_3 e^3 + \frac{I_6}{2}(c+F+2L)^2 + I_2\frac{D^2}{2} + A_1\left(\frac{d}{2}(B+e) + \frac{D}{2}(B-e)\right)^2 + A_2\frac{D^2}{2}\left(\frac{B}{2}-e\right)^2 + A_6(c+F+2L)^2\left(\frac{B}{2}-e\right)^2 + \frac{A_4}{2}(c+F+2L)^2(B-e)^2$$

and

$$J_o = \frac{2EB^2}{G} [\beta_1(2a + 2d + c)^2 + \beta_o(c + F + 2L)^2] + J$$

where

$$\beta_o = \frac{12 I_{cL}}{L^3 h} \quad \text{and} \quad \beta_1 = \frac{12 I_{ca}}{a^3 h}$$

In these expressions I_{cL} and I_{ca} are the moments of inertia of the connecting beams of lengths L and a respectively as in Fig. A.1.

II - MULTI-BAY, SINGLY-SYMMETRIC CORE

By omitting the inner cross-walls from the core shown in Fig. A.1, a single cell, multi-bay core is obtained as shown in Fig. A.7. This core will have the same displacements as the multi-cell one. The equilibrium conditions for a segment of height dx of the existing panels could be obtained from Fig. A.2.

In this case, only the first four vertical strain compatibility conditions need to be considered, which are given in equations I.(1,2,3 and 4). Following the same procedure as before, the parameters in the same general governing equation are found to be

$$I_w = (B + e)^2(2I_1 + 2I_4 + I_5) + I_2 \frac{D^2}{2} + I_3 e^2 + A_2 \frac{D^2}{2}$$
$$(\frac{B}{2} - e)^2 + A_1 D(B - e)(\frac{d}{2}(B + e) + \frac{D}{2}(B - e))$$

and

$$J_o = \beta_1 \frac{E}{G}[((2a + 2d + c) \frac{(B+e)}{2} + \frac{D}{2} (B-e) - K)$$
$$(D(B-e) + (B+e)(c + 2a + 2d))] + \beta_o \frac{E}{G}$$
$$[((c + F + 2L)\frac{(B+e)}{2} + K)(B+e)(2L + c + F)] + J$$

where

$$K = (c_1c_3 + c_4c_2)/(c_3 - c_2)$$

and

$$c_1 = (2a + 2d + c)\frac{(B + e)}{2} + \frac{D}{2}(B - e) - \frac{BD\,\beta_o}{\beta_1 + B_o}$$

$$c_2 = (1 - \frac{\beta_o}{\beta_1 + \beta_o})/\beta_1 E$$

$$c_3 = 1/E(\beta_1 + \beta_o)$$

$$c_4 = (c + F + 2L)\frac{(B + e)}{2} - \frac{\beta_1 B D}{\beta_1 + \beta_o}$$

III - MULTI-CELL, MULTI-BAY, DOUBLY-SYMMETRIC CORE

In these cases the core will rotate about the centroid of the cross-section C.G. as shown in Fig. A.4.II, from which the displacements of various points may be obtained. The equilibrium conditions for the internal forces of a segment of height dx from each panel could be derived from Fig. A.5.

The conditions of vertical strain compatibility along the lines of contraflexure O-O and 1-1 at the mid-span positions of the connecting mediums, and along the lines of interaction between the cross panels with the side walls, 2-2 and 4-4, may be written respectively as follows,

$$\int_o^x \frac{M_3}{EI_3}\frac{(c+L)}{2}\,dx + \int_o^x \frac{M_4}{EI_4}\frac{(L+F)}{2}dx - \int_o^x \frac{N_3}{EA_3}\,dx - \frac{q_o}{\beta_o E} = 0$$

III-1

$$\int_o^x \frac{M_1}{EI_1}\frac{(d+a)}{2}dx + \int_o^x \frac{M_3}{EI_3}\frac{(c+a)}{2}dx - \int_o^x \frac{N_1}{EA_1}dx +$$

$$\int_o^x \frac{N_3}{EA_3}dx - \frac{q_1}{\beta_1 E} = 0 \qquad \text{III-2}$$

$$\int_o^x \frac{M_1}{EI_1}\frac{d}{2}dx - \int_o^x \frac{M_2}{EI_2}\frac{B}{2}dx + \int_o^x \frac{N_1}{EA_1}dx = 0 \qquad \text{III-3}$$

$$\int_o^x \frac{M_5}{EI_5}\frac{B}{2}dx - \int_o^x \frac{N_3}{EI_3}dx = 0 \qquad \text{III-4}$$

On solving the above equations in conjunction with the moment-curvature relationships for the core panels, expressions for the internal forces can be obtained. Considering the overall equilibrium condition of the core cross-section as shown in Fig. A.6 will yield the same general governing equation with the parameters I_w and J_o expressed as follows.

$$I_w = B^2\left[I_1 + I_3 + \frac{I_4}{2}\right) + I_5\frac{(c + F + 2L)^2}{2} + I_2\frac{D^2}{2}$$

$$+ A_1\frac{B^2}{4}(d + D)^2 + A_4\frac{B^2}{4}(c + F + 2L)^2$$

and

$$J_o = \frac{E}{G}B^2[\beta_1(2d + 2a + c)^2 + \beta_o(c + F + 2L)^2] + J$$

where β_o and β_1 are as defined before.

IV - MULTI-BAY, DOUBLY-SYMMETRIC CORE

If the inner cross walls in the above core structure are removed, the core cross-section will be as shown in Fig. A.8. The core displacements, the equilibrium conditions for the internal forces and the vertical strain compatibility between the existing panels are the same as before. Following the same procedure as before, the parameters of the general governing equation are found to be

$$I_w = B^2(I_1 + I_3 + \frac{I_4}{2}) + I_2 \frac{D^2}{2} + A_1 \frac{B^2 D}{4} (d + D) + A_3 \frac{B^2 d}{4}(d+D)$$

and

$$J_o = \beta_o \frac{E}{G} B(2L + F + c)(\frac{B}{4}(2L + c + F) + K) + \beta_1 \frac{E}{G} B$$

$$(2d + 2a + c + D)(\frac{B}{4}(2d + 2a + c + D) - K) + J$$

where

$$K = -(c_1 c_4 + c_2 c_3)/(c_2 - c_4)$$

$$c_1 = \frac{B}{4}(2d + 2a + c + D - 2\beta_o D/\beta_1 + \beta_o)$$

$$c_2 = \frac{1}{\beta_1 E} (1 - \frac{\beta_o}{\beta_1 + \beta_o})$$

$$c_3 = (2L + c + F - \frac{2\beta_1 D}{\beta_1 + \beta_o})$$

$$c_4 = \frac{1}{E(\beta_1 + \beta_o)}$$

V - MULTI-CELL, SINGLY-SYMMETRIC CORE

In this case a singly-symmetric core structure with an intermediate wall having a set of openings at a distance

c from the back solid wall is assumed to rotate around its shear centre S.C. as shown in Fig. A.9. Following the same procedure as before, the core displacements, the equilibrium conditions of the internal forces and the moment curvature relationships of the core panels may be derived from Fig. A.9. . The vertical strain compatibility conditions along the lines of interaction between the core panels O-O, 1-1, 2-2, 3-3 and 4-4 will be given respectively by

$$\int_o^x \frac{M_4}{EI_4}(L + M)dx = 2\int_o^x \frac{N_4}{EA_4}dx - \frac{q_o}{\beta_o E} = 0$$

$$\int_o^x \frac{M_1}{EI_1}(d+a)dx - 2\int_o^x \frac{N_1}{EA_1}dx - \frac{q_1}{\beta_1 E} = 0$$

$$\int_o^x \frac{M_2}{EI_2}\frac{B}{2}dx - \int_o^x \frac{M_1}{EI_1}\frac{d}{2}dx + \int_o^x \frac{N_2}{EA_2}dx - \int_o^x \frac{N_1}{EA_1}dx = 0$$

$$\int_o^x \frac{M_2}{EI_2}\frac{B}{2}dx + \int_o^x \frac{M_3}{EI_3}\frac{D}{2}dx - \int_o^x \frac{N_2}{EA_2}dx = 0$$

$$\int_o^x \frac{M_4}{EI_4}\frac{L}{2}dx + \int_o^x \frac{N_4}{EA_4}dx - \int_o^x \frac{M_2}{EI_2}(\frac{B}{2} - c)dx - \int_o^x \frac{N_2}{EA_2}dx = 0$$

From the above conditions, expressions for the internal forces can be obtained. Considering the overall equilibrium of the core cross-section, the parameters in the same general governing equation are found to be

$$I_w = 2I_1(B+e)^2 + 2I_4(c+e)^2 + I_2D^2 + A_1(d(B+e) + D(B-e))^2$$
$$+ A_2 \frac{D^2}{2}(\frac{B}{2} - e)^2 + \frac{A_4}{2} (L(c+e) + D(c-e))^2$$

and

$$J_o = 4 \frac{E}{G} D^2(\beta_1 B^2 + \beta_o c^2) + J$$

VI - MULTI-CELL, DOUBLY-SYMMETRIC CORE

In the case of a multi-cell, doubly-symmetric core consisting of two solid side walls and four cross-walls with openings arranged as shown in Fig. A.10, rotation will occur about its centroid. The core displacements, the equilibrium conditions for the internal forces and the moment-curvature relationships for the core panels can be derived from Fig. A.10. The vertical strain compatibility conditions between the core panels along line 0-0, 1-1, 2-2 and 3-3 are found to be

$$\int_o^x \frac{M_3}{EI_3} (L+m)dx - 2 \int_o^x \frac{N_3}{EA_3} dx - \frac{q_o}{\beta_o E} = 0$$

$$\int_o^x \frac{M_1}{EI_1} (a+d)dx - 2 \int_o^x \frac{N_1}{EA_1} dx - \frac{q_1}{\beta_1 E} = 0$$

$$\int_o^x \frac{M_2}{EI_2} \frac{B}{2} dx - \int_o^x \frac{M_1}{EI_1} \frac{d}{2} dx - \int_o^x \frac{N_1}{EA_1} dx = 0$$

$$\int_o^x \frac{M_2}{EI_2} cdx - \int_o^x \frac{M_3}{EI_3} \frac{L}{2} dx - \int_o^x \frac{N_3}{EA_3} dx = 0$$

Substituting from the solution of the above equations into

the overall equilibrium condition of the core cross-section, the parameters I_w and J_o in the same general governing equation are found to be

$$I_w = I_1 B^2 + I_2 \frac{D^2}{2} + 4I_3 c^2 + A_2 \frac{B^2}{4}(d + D)^2 + A_3 \frac{C^2}{4}(L + D)$$

and

$$J_o = \frac{2E}{G} D^2 [\beta_1 B^2 + \beta_o C^2] + J$$

VII - SINGLY-SYMMETRIC CORE WITH UNEQUAL SIDE CHANNELS

Under torsional loading, a core structure composed of two unequal channels will rotate about its shear centre at point O as shown in Fig. A.11. Considering the displacements of the core, the moment-curvature relationships of the core panels and the internal forces equilibrium conditions of the panels of the core, the vertical strain compatibility conditions along the line 0-0, 1-1 and 2-2 can be written respectively as follows

$$\int_o^x \frac{M_1}{EI_1} \frac{(d+a)}{2} dx - \int_o^x \frac{N_1}{EA_1} dx + \int_o^x \frac{M_3}{EI_3} \frac{(c+a)}{2} dx - \int_o^x \frac{N_3}{EA_3} dx - \frac{q_1}{\beta_1 E} = 0$$

$$\int_o^x \frac{M_1}{EI_1} \frac{d}{2} dx + \int_o^x \frac{N_1}{EA_1} dx - \int_o^x \frac{M_2}{EI_2} \frac{B}{2} dx = 0$$

$$\int_o^x \frac{M_4}{EI_4} \frac{B}{2} dx + \int_o^x \frac{M_3}{EI_3} \frac{C}{2} dx + \int_o^x \frac{N_3}{EA_3} dx = 0$$

Solving the above equations for the internal forces and substituting in the overall equilibrium condition of the core cross-section will yield the same general governing equation with the parameters I_w and J_o expressed as follows

$$I_w = \frac{B^2}{2}(I_1 + I_3) + I_4(D-e)^2 + I_2 e^2 + A_1 \frac{B^2}{2}(\frac{d}{2} + e)^2 + A_3 \frac{B^2}{2}(D + \frac{c}{2} - e)^2$$

and

$$J_o = 2\beta_1 \frac{E}{G} B^2 D^2 + J$$

VIII - CORE STRUCTURE WITH CONNECTING BEAMS AT THE CORNERS

If a core structure with four sets of openings at the corners and four solid walls at its sides, is subjected to torsional loading, it will rotate about the core centre of gravity at point O as shown in Fig. A.12. Following the same procedure in deriving the core displacements, the moment-curvature relationships of the core panels and the equilibrium conditions of the internal forces, the vertical strain compatibility condition along the line 1-1 can be written as follows

$$\int_o^x \frac{M_2}{EI_2} \frac{B}{2} dx - \int_o^x \frac{M_1}{EI_1} \frac{D}{2} dx - \frac{q_1}{E}[\frac{1}{\beta_1} + \frac{1}{\beta_o}] = 0$$

Considering the overall equilibrium condition of the cross-section of the core, and substituting from the above equations for the horizontal shear forces, it is found that the core behaviour will follow the same general governing equation, with the relevant parameters defined as,

$$I_w = I_1 \frac{B^2}{2} + I_2 \frac{D^2}{2}$$

and

$$J_o = \beta \frac{E}{G} B^2 D^2 + J$$

where

$$\frac{1}{\beta} = \frac{1}{\beta_1} + \frac{1}{\beta_o}$$

IX - CORE STRUCTURES WITH INCLINED WALLS

The above method can be utilised to study core structures with walls inclined on plan by considering the in-plane components of the displacements of the inclined wall in evaluating the moment-curvature relationship. Following the same procedure to study the core structure shown in Fig. A.13, the displacements of the core, moment-curvature relationships of the core panels and the equilibrium condition of the internal forces can be derived from the above Figure. The vertical strain compatibility conditions along the lines 0-0, 1-1 and 2-2 in this case are given by

$$\int_o^x \frac{M_1}{EI_1} (d+a)dx - 2 \int_o^x \frac{N_1}{EA_1} dx - \frac{q_1}{\beta_1 E} = 0$$

$$\int_o^x \frac{M_1}{EI_1} \frac{d}{2} dx - \int_o^x \frac{M_2}{EI_2} \frac{n}{2} dx - \int_o^x \frac{N_2}{EA_2} dx + \int_o^x \frac{N_1}{EA_1} dx = 0$$

$$\int_o^x \frac{M_2}{EI_2} \frac{n}{2} dx + \int_o^x \frac{M_3}{EI_3} \frac{m}{2} dx - \int_o^x \frac{N_2}{EA_2} dx = 0$$

Solving the above equations and substituting for the horizontal shear forces in the overall equilibrium condition of the core cross-section, the parameters I_w and J_o of the same general governing equation are found to be

$$I_w = I_1 B^2 + I_2 \frac{R^2}{2} \cos \phi + I_3 \frac{D^2}{2} + c_1 Bd + 2nR(c_1 + c_2) + mD(c_1 + c_2)$$

and

$$J_o = K_1 \frac{E}{G}[B(2d + a) + 4nR + Dm] + J$$

where

$$c_1 = A_1[\frac{Bd}{2} + nR \cos \phi + \frac{Dm}{4}]$$

$$c_2 = A_2[nR \cos \phi + \frac{Dm}{4}]$$

$$K_1 = \beta_1[\frac{B}{2}(d+a) + 2(\frac{Bd}{4} + nR \cos \phi + \frac{Dm}{4})]$$

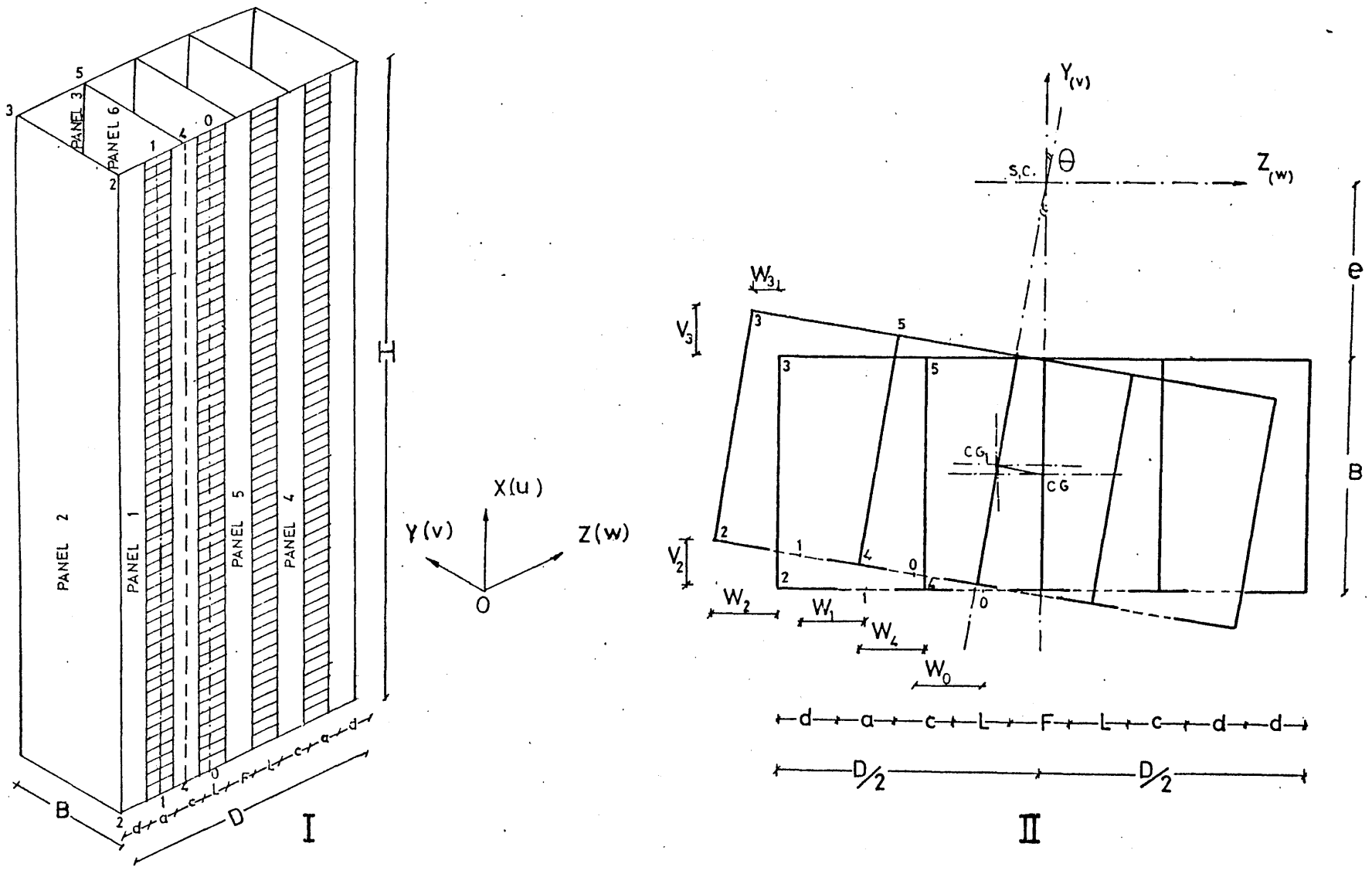

Fig. (A.1) Multi-Cell, Multi-Bay, Singly-Symmetric Core

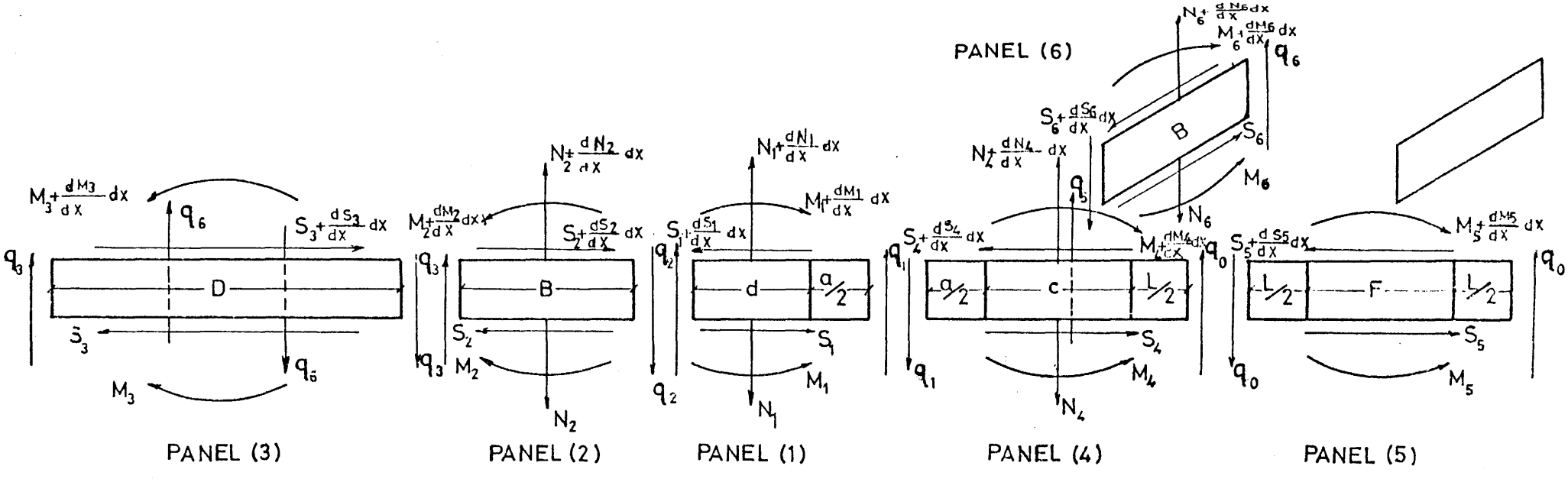

Fig. A.2

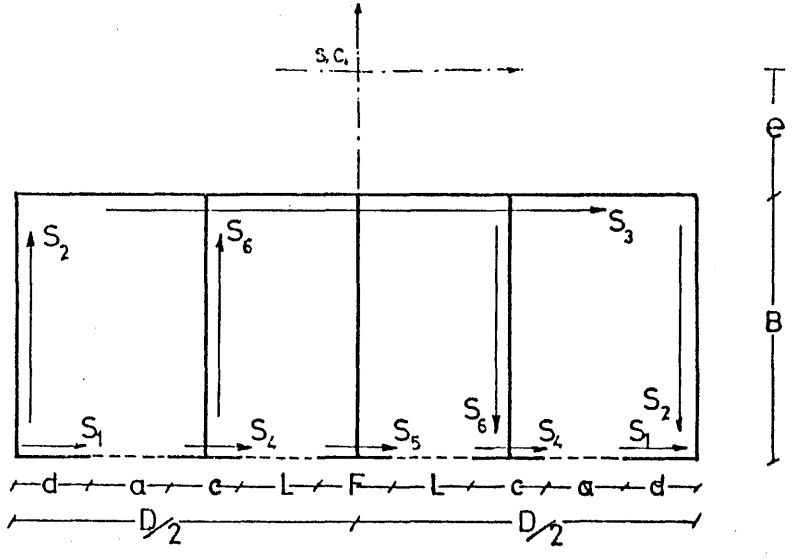

Fig. A.3

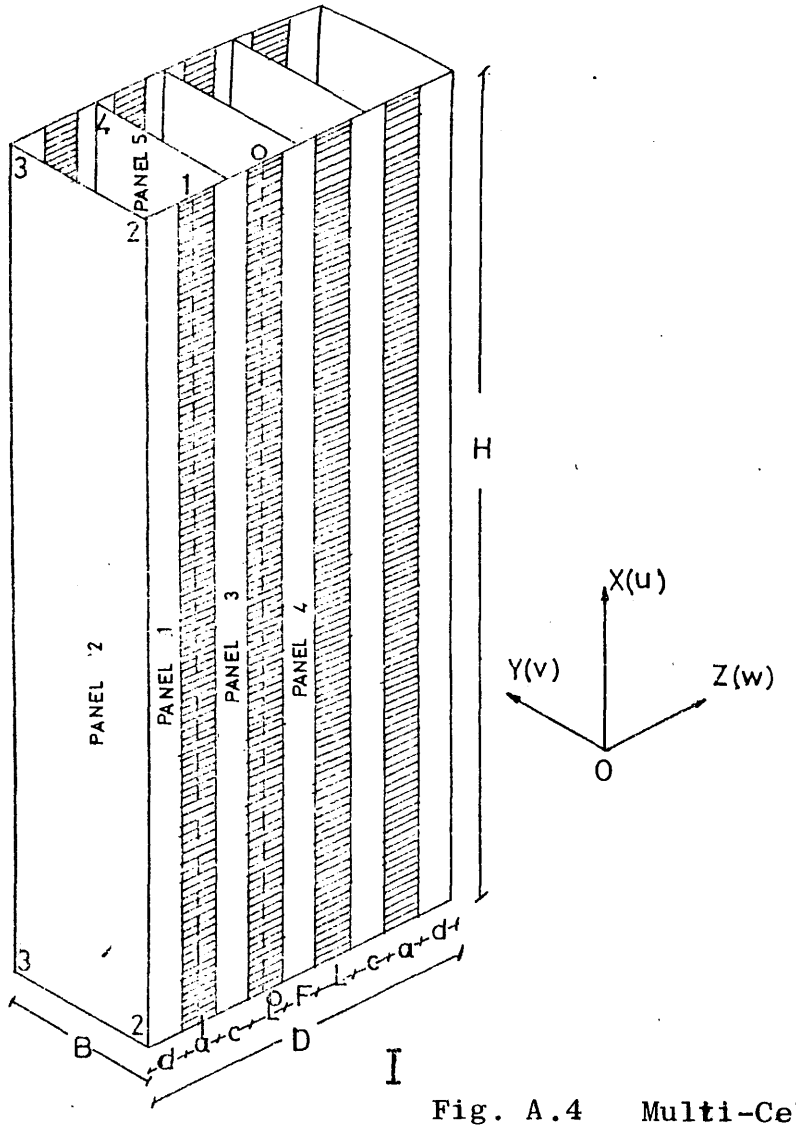

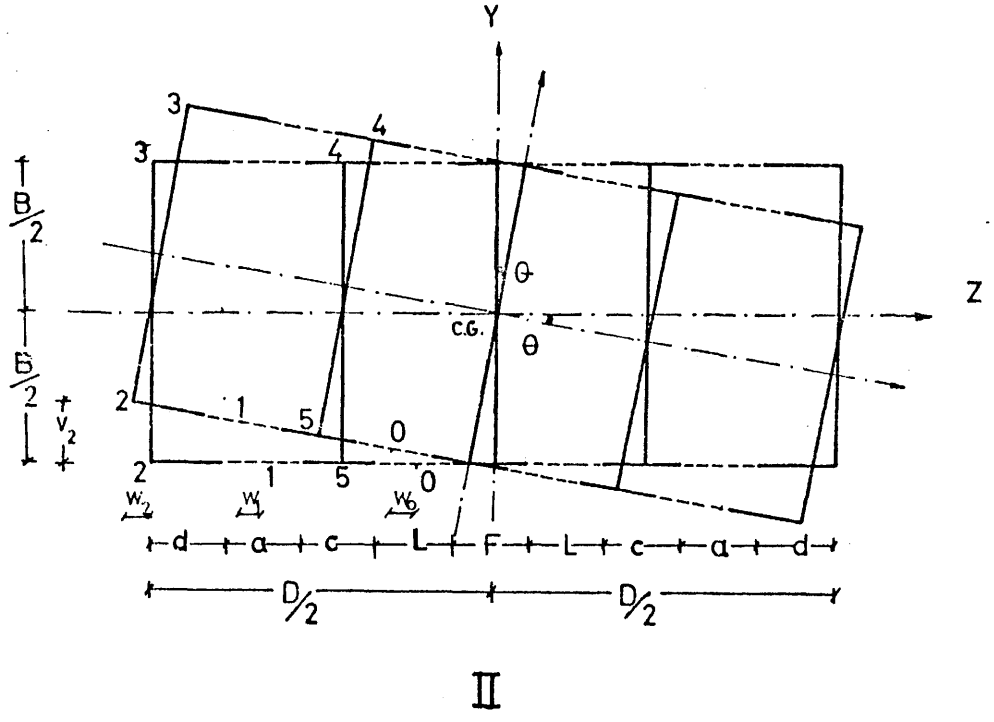

Fig. A.4 Multi-Cell, Multi-Bay, Doubly-Symmetric Core

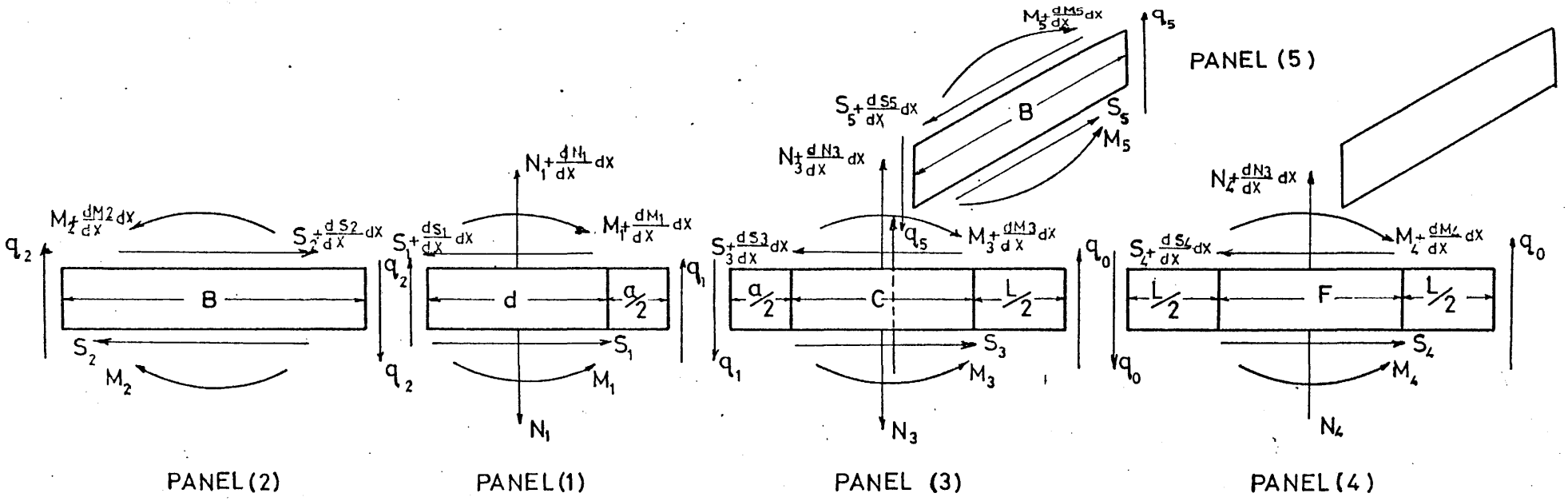

Fig. A.5

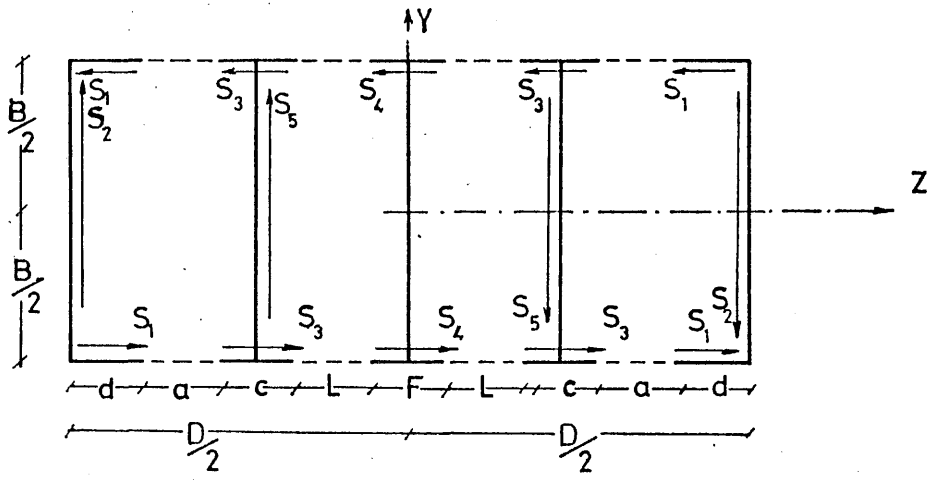

Fig. A.6

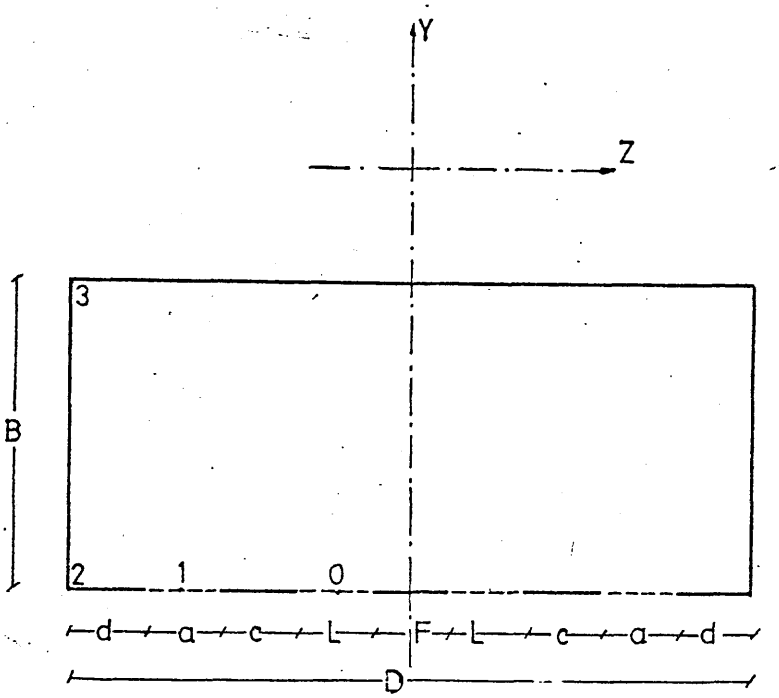

Fig. A.7 Multi-Bay, Singly-Symmetric Core

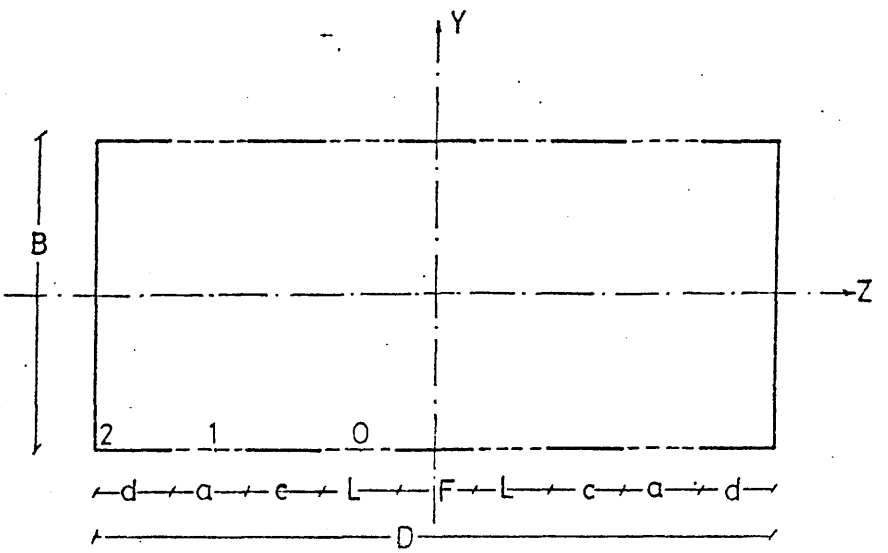

Fig. A.8 Multi-Bay, Doubly-Symmetric Core

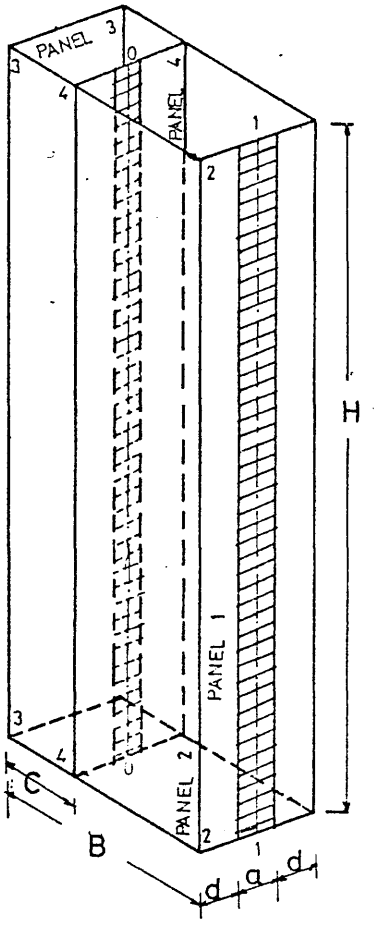

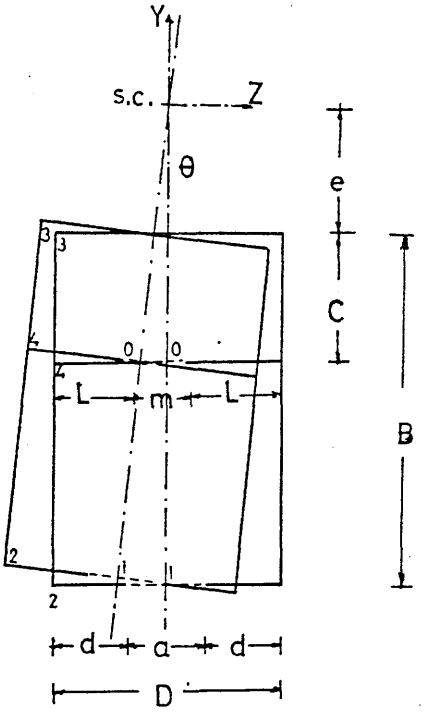

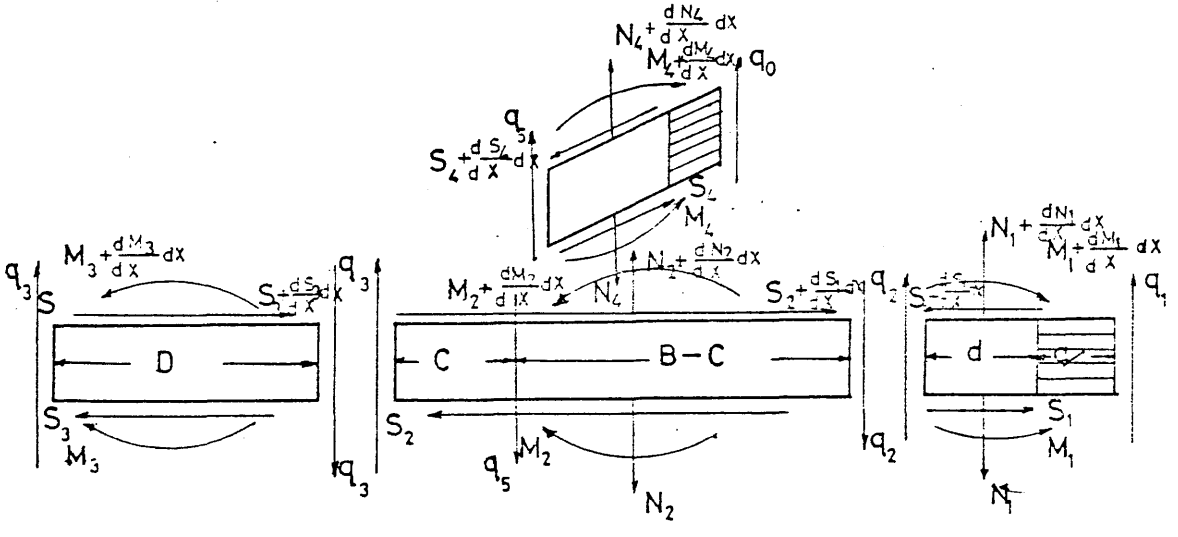

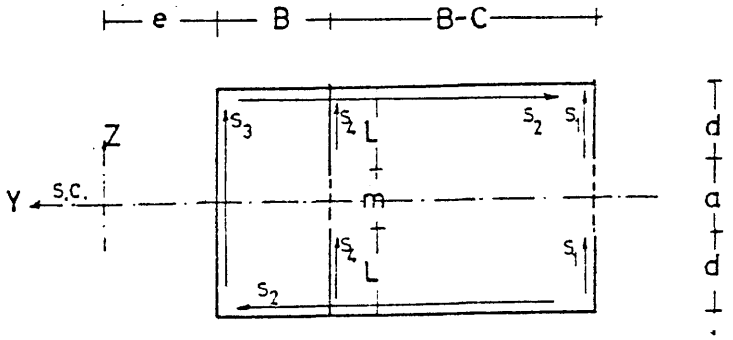

Fig. A.9 Multi-Cell, Singly-Symmetric Core

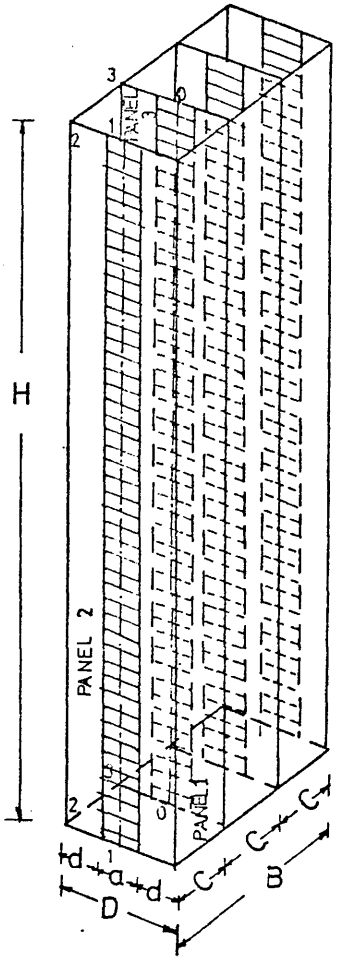

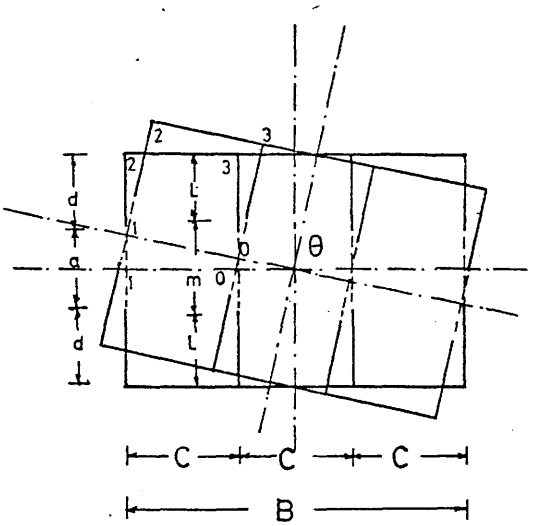

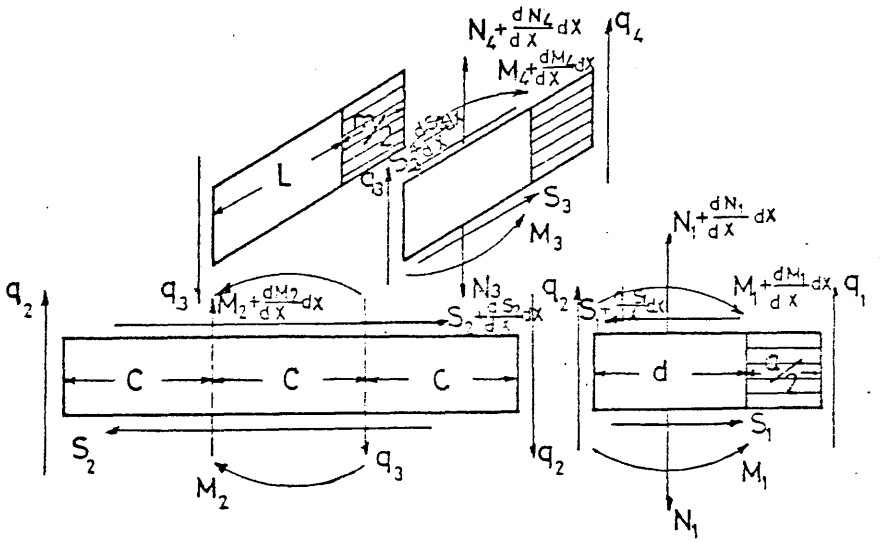

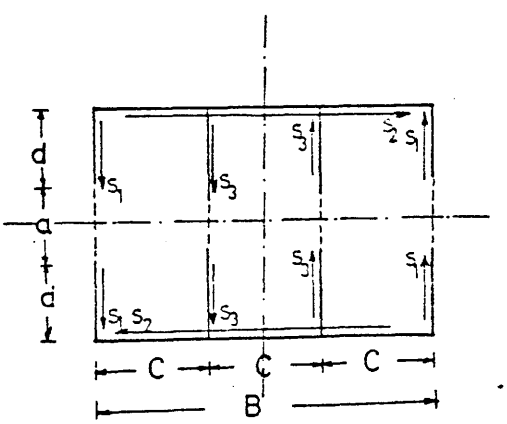

Fig. A.10 Multi-Cell, Doubly-Symmetric Core

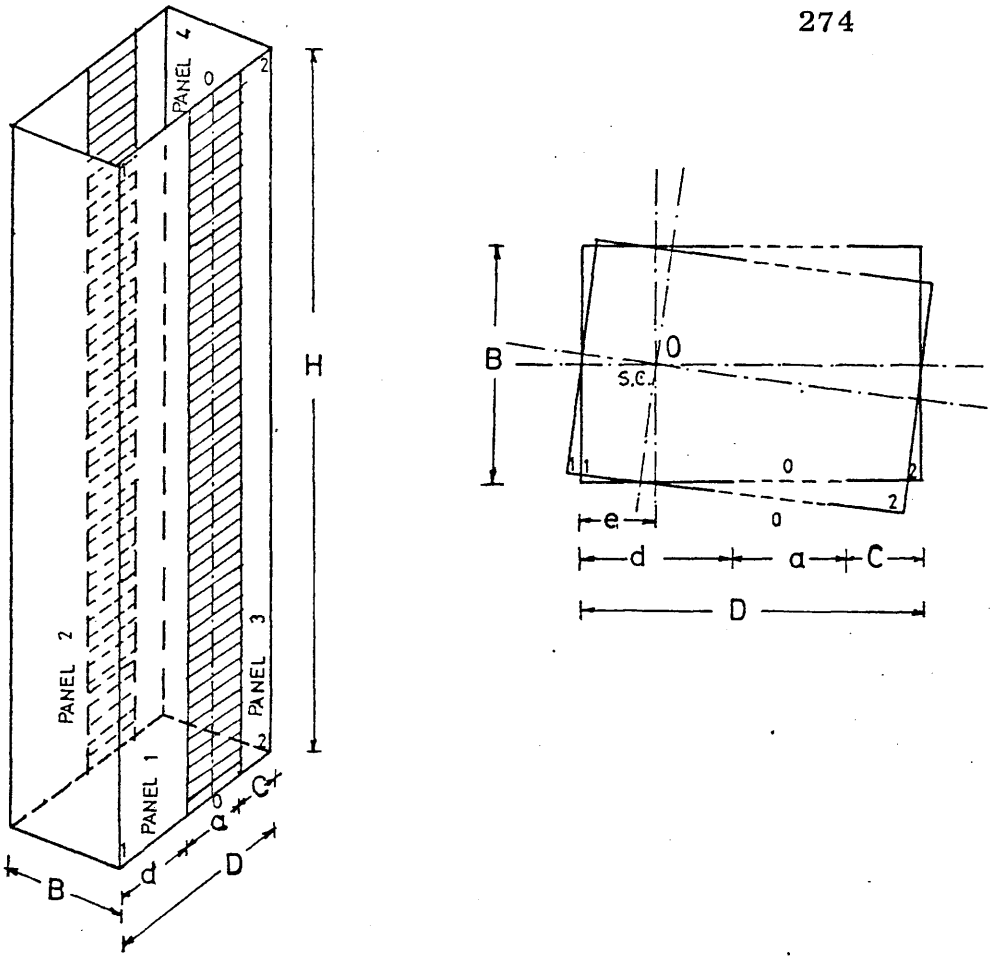

Fig. A.11 Singly-Symmetric Core with Unequal Side Channels

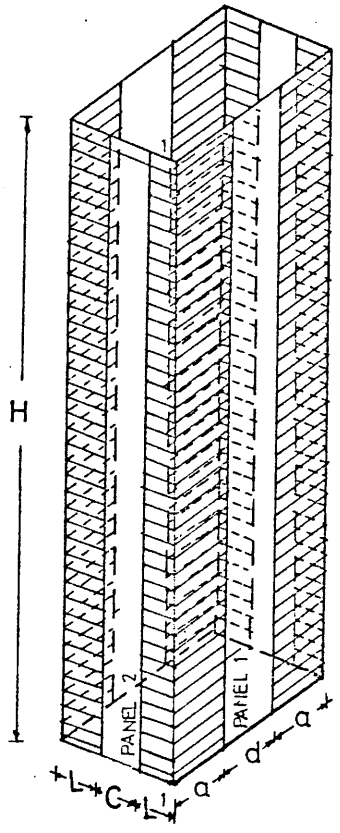

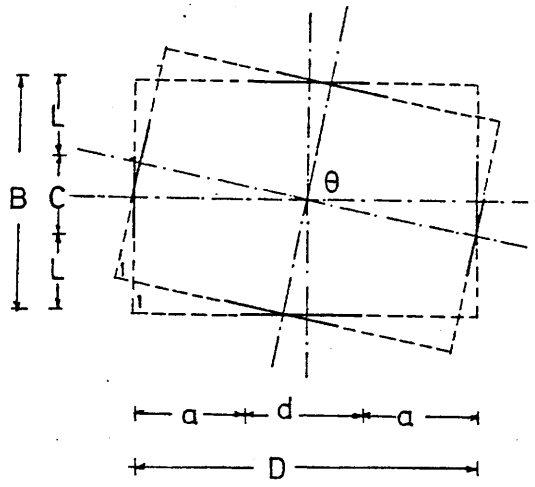

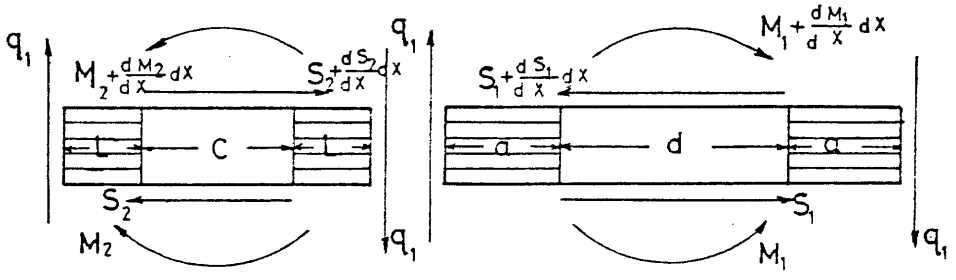

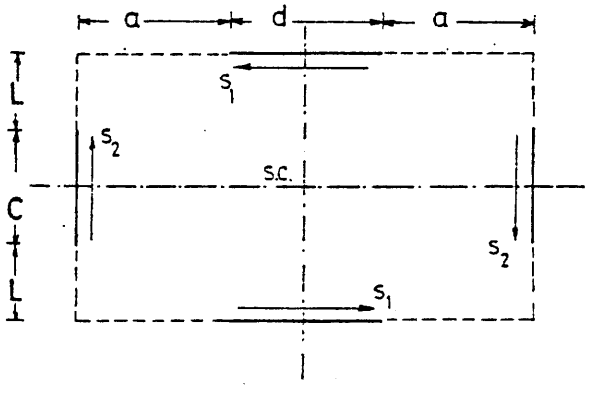

Fig. A.12 Core Structure with Connecting Beams at the Corners

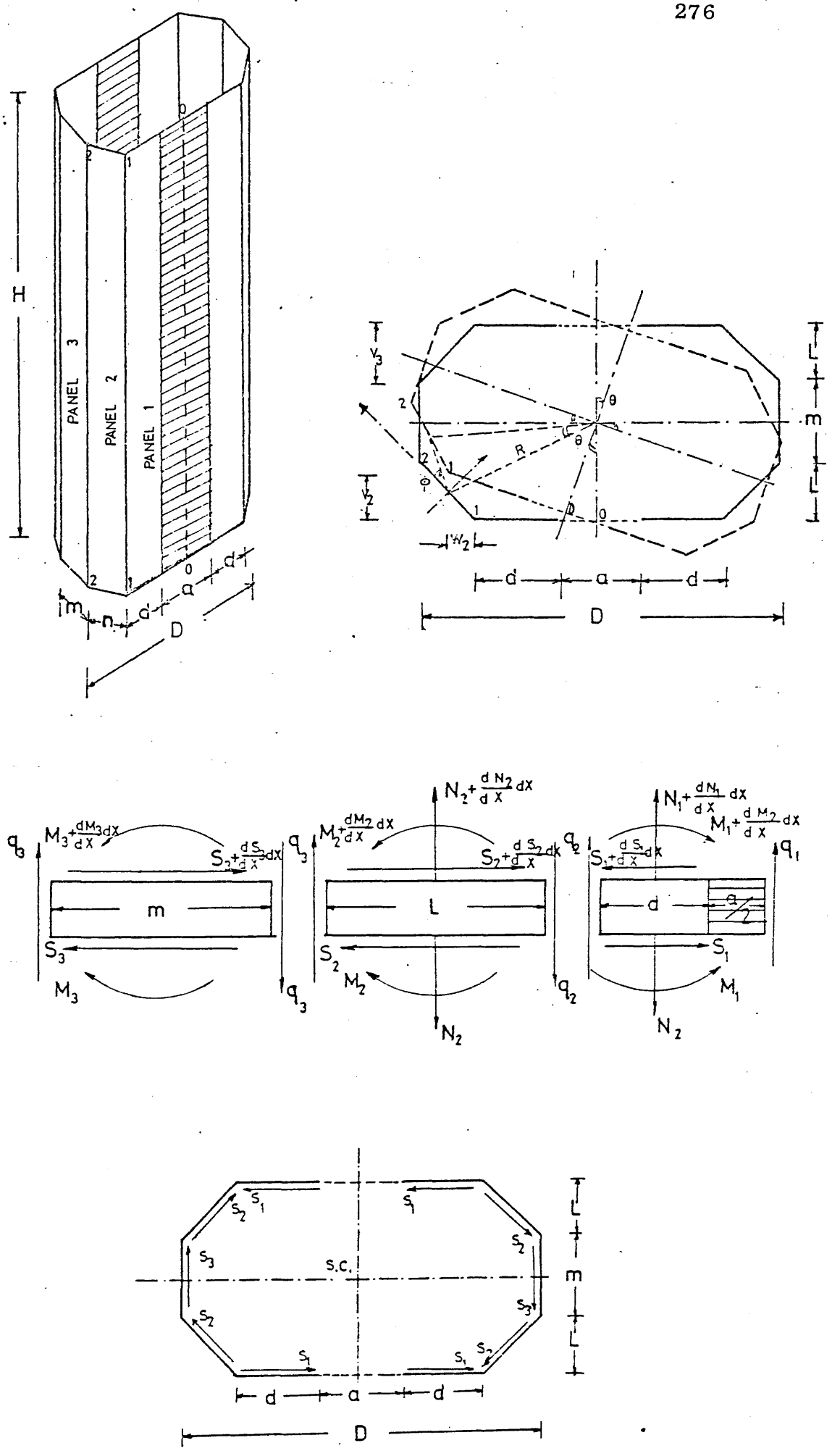

Fig. A.13 Core Structure with Inclined Walls

APPENDIX B

DESIGN CHARTS

APPENDIX B

DESIGN CHARTS

The expressions presented in Chapter 4 for the parameters U, U1 and U2 for the three standard load cases have been used to produce design charts. These allow a semigraphical evaluation of the angle of rotation, the vertical shear forces in the connecting beams and the bending moments and normal forces in the walls over the height ξ. The curves are presented for a range of values of α_H between 0 and 6, and end conditions R between 1 and 10 and λ between 0 and 2.5.

The charts are presented in three main sets in the following figures:-

B.I.1 to B.I.16 : Variations of the parameters U, U1 and U2 with height ξ for a core subjected to a point torque at the top.

B.II.1 to B.II.16: Variations of U, U1 and U2 with ξ for a uniformly distributed torque.

B.III.1 to B.III.16: Variations of U, U1 and U2 with ξ for a triangularly distributed torque.

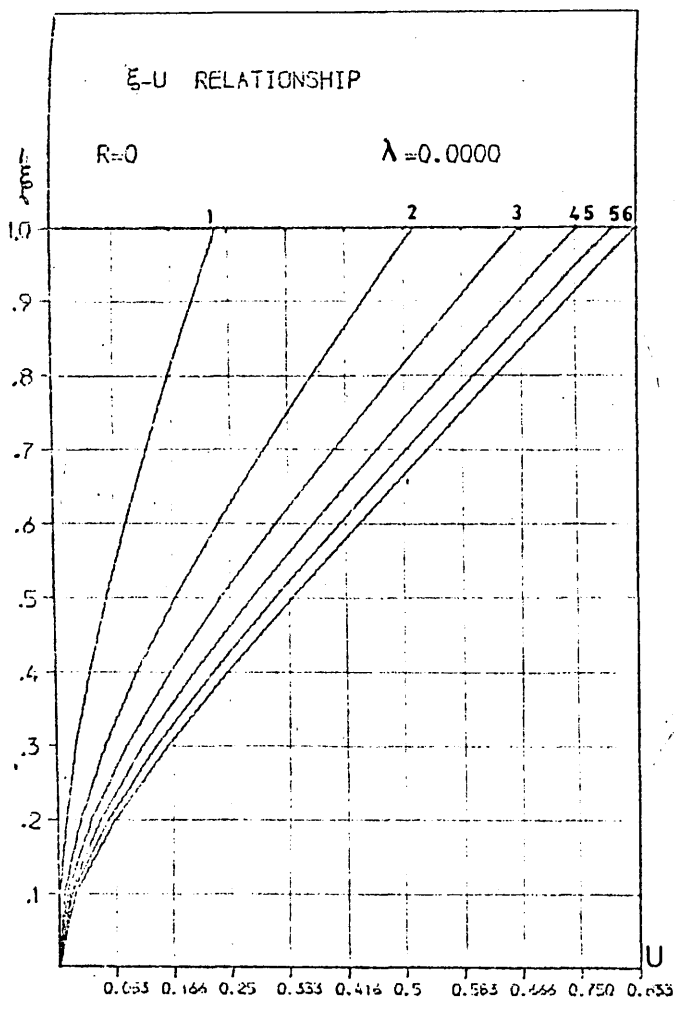
ξ-U RELATIONSHIP
R=0
λ =0.0000
ξ
1.0
.9
.8
.7
.6
.5
.4
.3
.2
.1
1
2
3
4
5
6
U
0.083 0.166 0.25 0.333 0.416 0.5 0.583 0.666 0.750 0.833

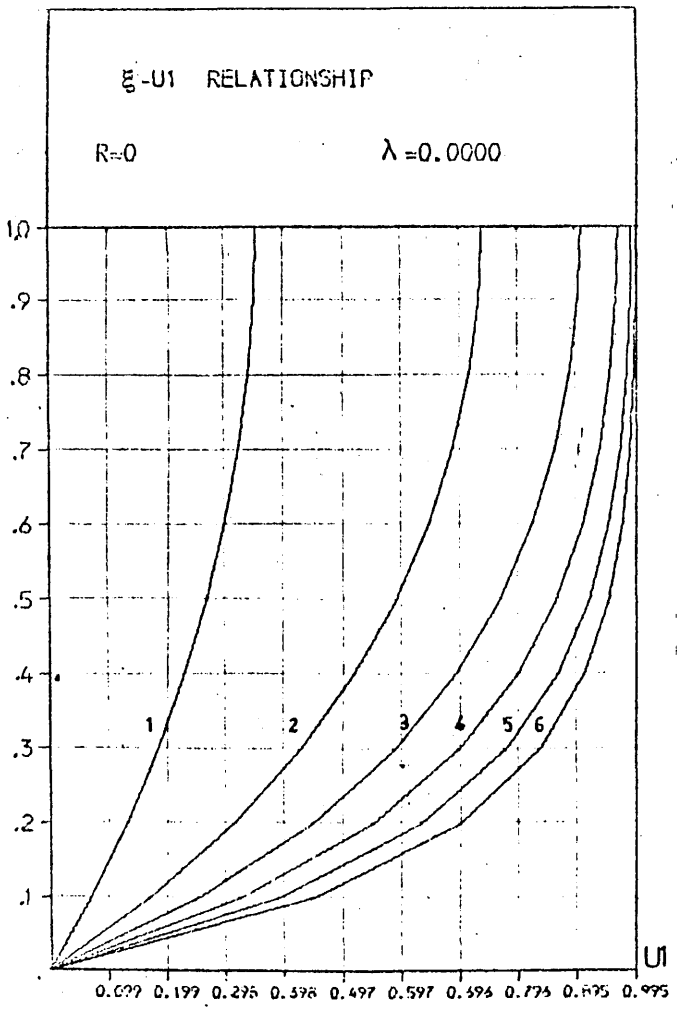
ξ-U1 RELATIONSHIP
R=0
λ =0.0000
1.0
.9
.8
.7
.6
.5
.4
.3
.2
.1
1
2
3
4
5
6
U1
0.099 0.199 0.298 0.398 0.497 0.597 0.696 0.796 0.895 0.995

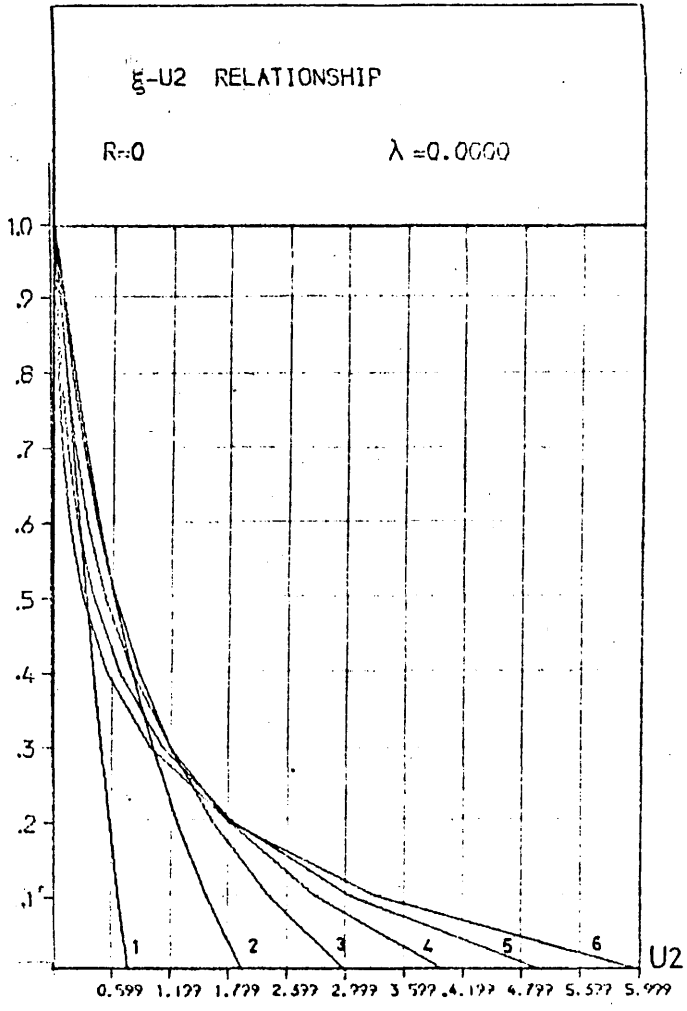
ξ-U2 RELATIONSHIP
R=0
λ =0.0000
1.0
.9
.8
.7
.6
.5
.4
.3
.2
.1
1
2
3
4
5
6
U2
0.599 1.199 1.799 2.399 2.999 3.599 4.199 4.799 5.399 5.999

Fig. B.I.1

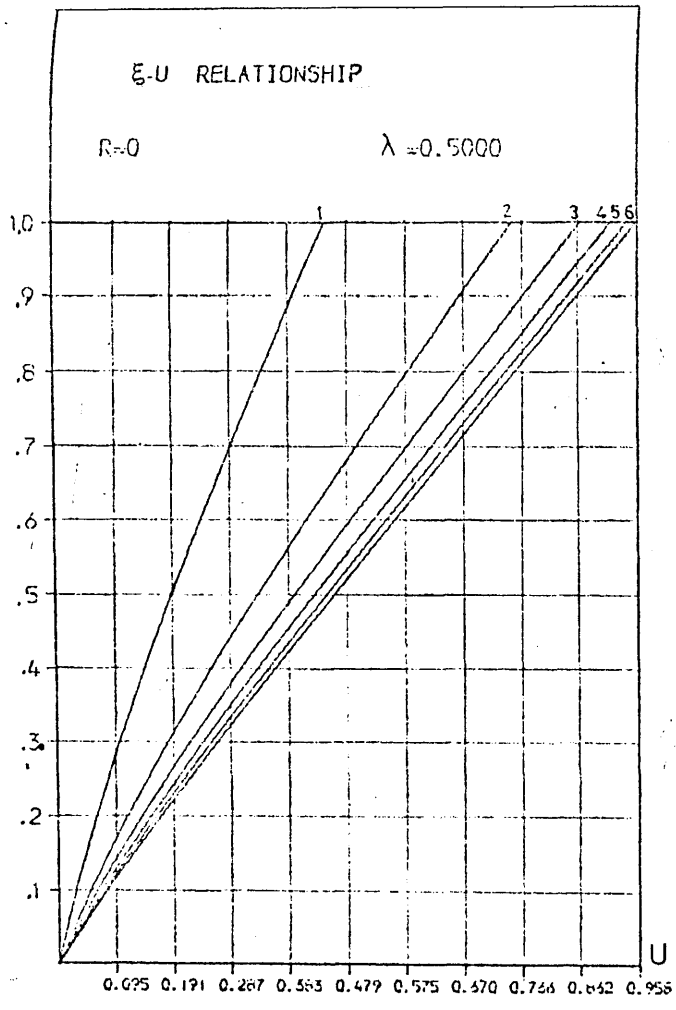
ξ-U RELATIONSHIP
R=0
λ =0.5000
1.0
.9
.8
.7
.6
.5
.4
.3
.2
.1
1
2
3
4
5
6
U
0.095 0.191 0.287 0.383 0.479 0.575 0.670 0.766 0.862 0.958

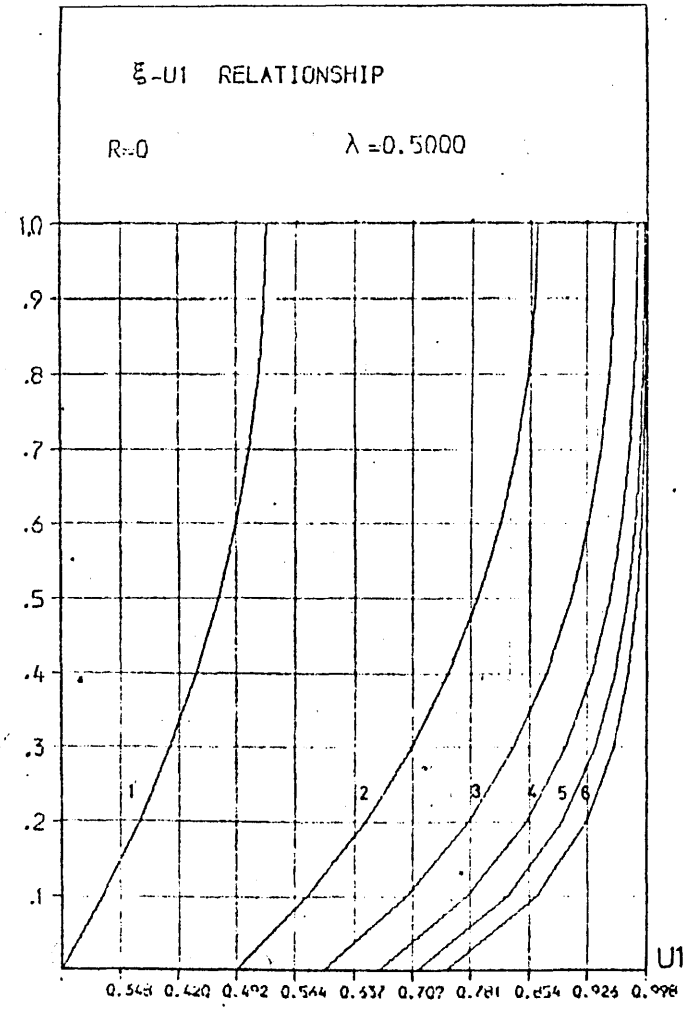
ξ-U1 RELATIONSHIP
R=0
λ =0.5000
1.0
.9
.8
.7
.6
.5
.4
.3
.2
.1
1
2
3
4
5
6
U1
0.348 0.420 0.492 0.564 0.637 0.709 0.781 0.854 0.926 0.998

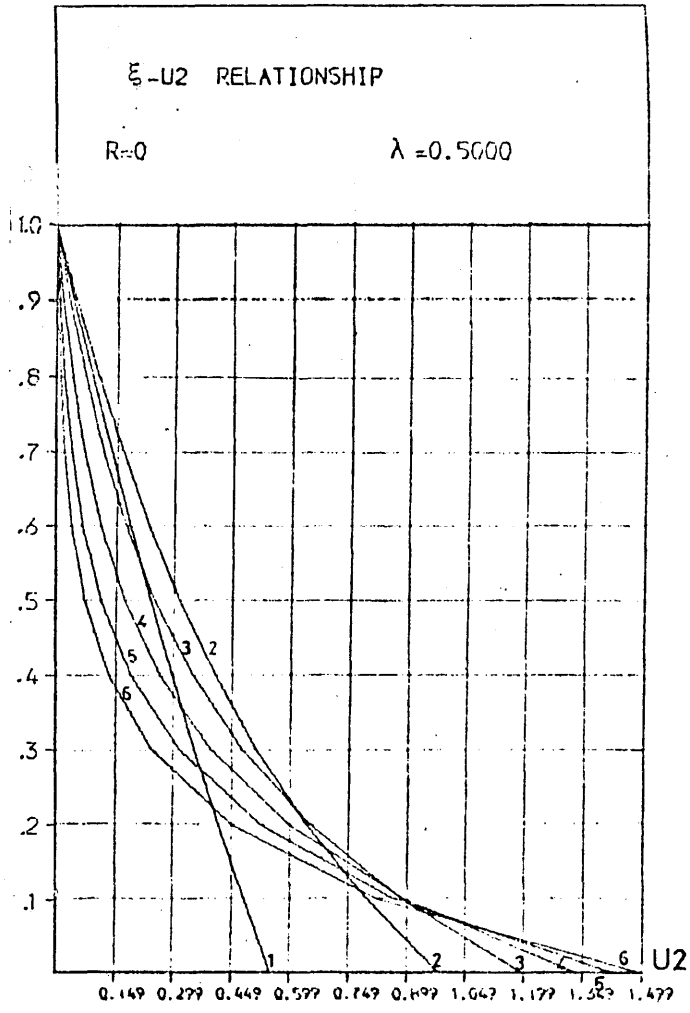
ξ-U2 RELATIONSHIP
R=0
λ =0.5000
1.0
.9
.8
.7
.6
.5
.4
.3
.2
.1
1
2
3
4
5
6
U2
0.149 0.299 0.449 0.599 0.749 0.899 1.047 1.199 1.349 1.499

Fig. B.I.2

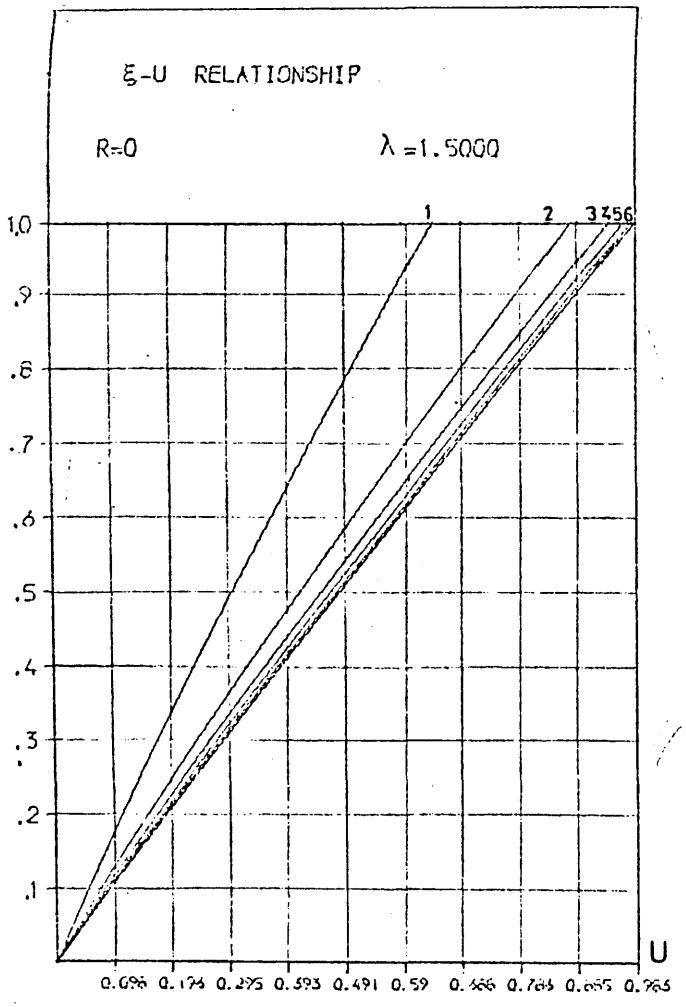
ξ-U RELATIONSHIP
R=0
λ =1.5000
1
2
3456
1.0
.9
.8
.7
.6
.5
.4
.3
.2
.1
U
0.096 0.194 0.295 0.393 0.491 0.59 0.666 0.765 0.865 0.965

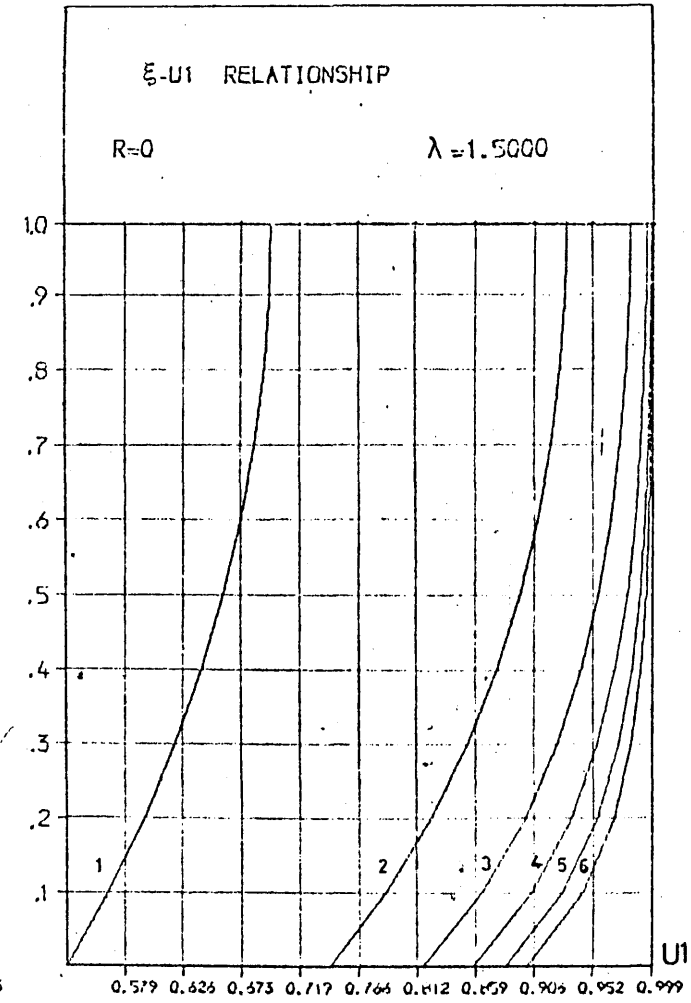
ξ-U1 RELATIONSHIP
R=0
λ =1.5000
1.0
.9
.8
.7
.6
.5
.4
.3
.2
.1
1
2
3
4
5
6
U1
0.579 0.626 0.673 0.719 0.766 0.812 0.859 0.906 0.952 0.999

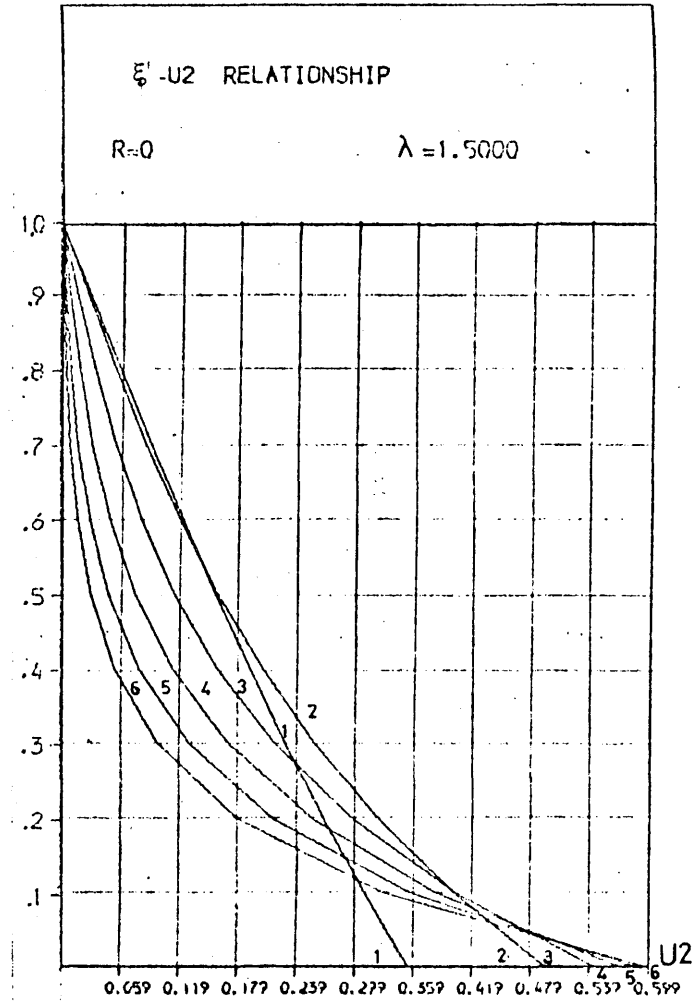
ξ'-U2 RELATIONSHIP
R=0
λ =1.5000
1.0
.9
.8
.7
.6
.5
.4
.3
.2
.1
6
5
4
3
2
1
1
2
3
4
5
6
U2
0.059 0.119 0.179 0.239 0.299 0.359 0.419 0.479 0.539 0.599

Fig. B.I.3

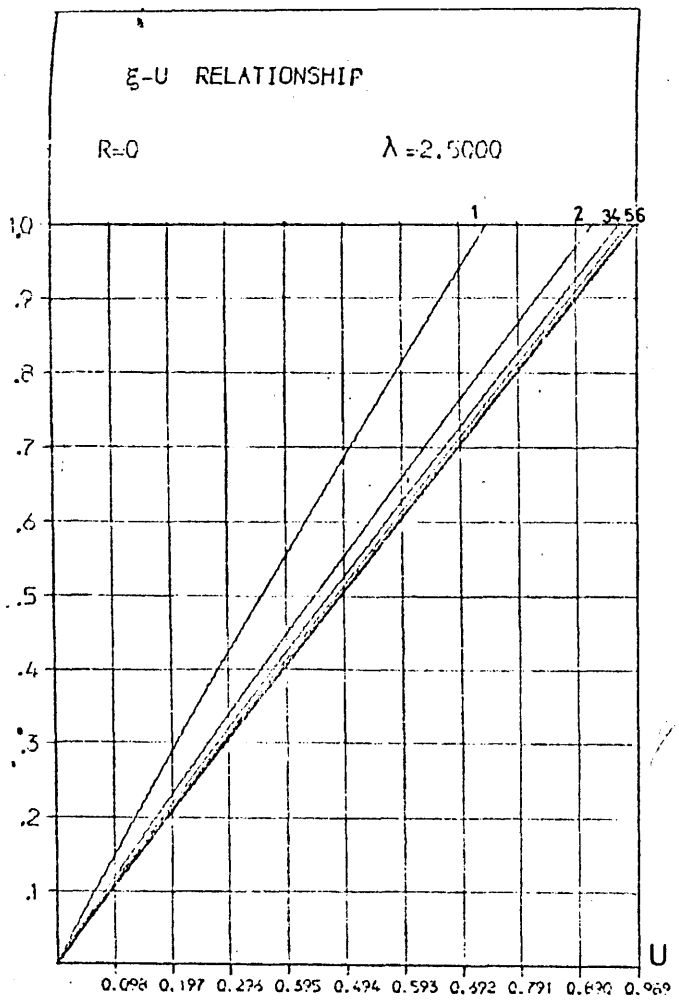
ξ-U RELATIONSHIP
R=0
λ =2.5000
1.0
.9
.8
.7
.6
.5
.4
.3
.2
.1
1
2
3
4
5
6
0.098 0.197 0.296 0.395 0.494 0.593 0.692 0.791 0.890 0.989
U

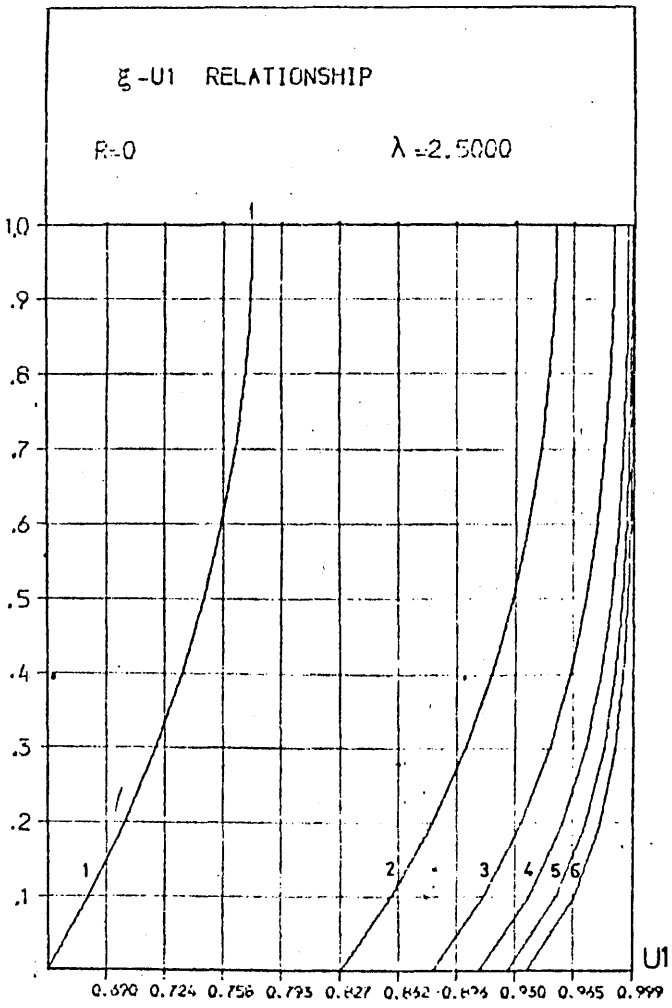
ξ-U1 RELATIONSHIP
R=0
λ =2.5000
1.0
.9
.8
.7
.6
.5
.4
.3
.2
.1
1
2
3
4
5
6
0.690 0.724 0.758 0.793 0.827 0.862 0.896 0.930 0.965 0.999
U1

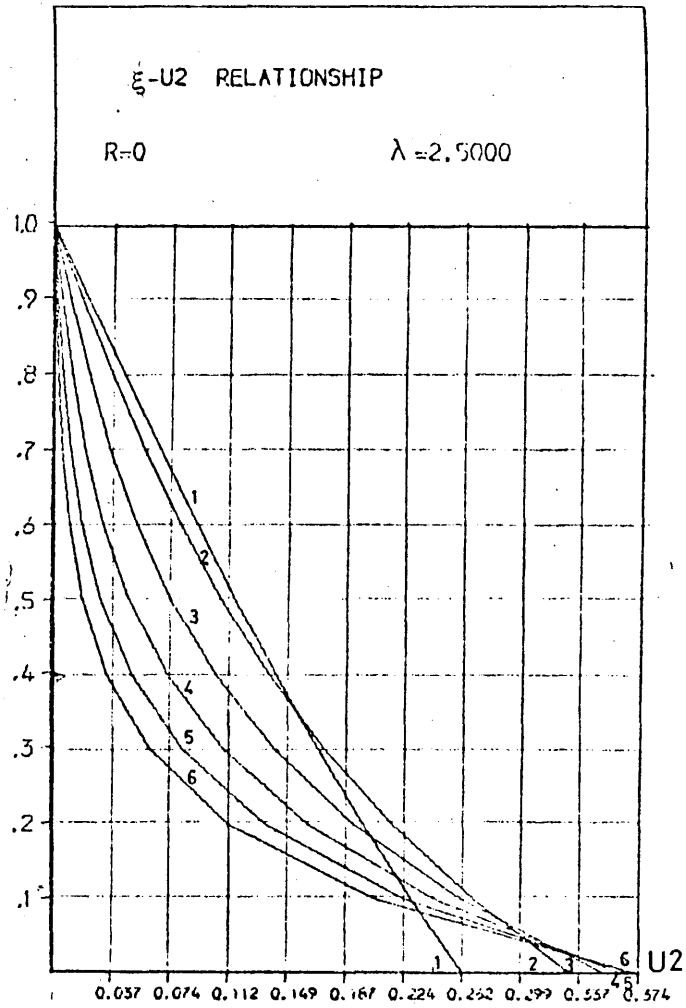
ξ-U2 RELATIONSHIP
R=0
λ =2.5000
1.0
.9
.8
.7
.6
.5
.4
.3
.2
.1
1
2
3
4
5
6
0.037 0.074 0.112 0.149 0.187 0.224 0.262 0.299 0.557 0.574
U2

Fig. B.I.4

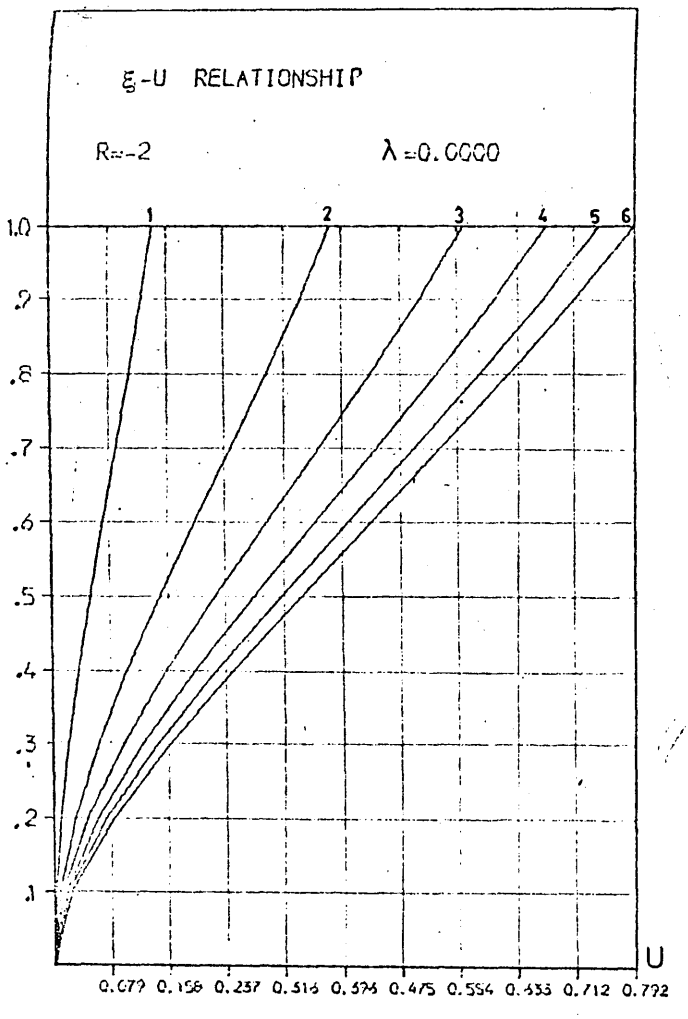
ξ-U RELATIONSHIP
R=-2
λ =0.0000
1
2
3
4
5
6
1.0
.9
.8
.7
.6
.5
.4
.3
.2
.1
U
0.079 0.158 0.237 0.316 0.395 0.475 0.554 0.633 0.712 0.792

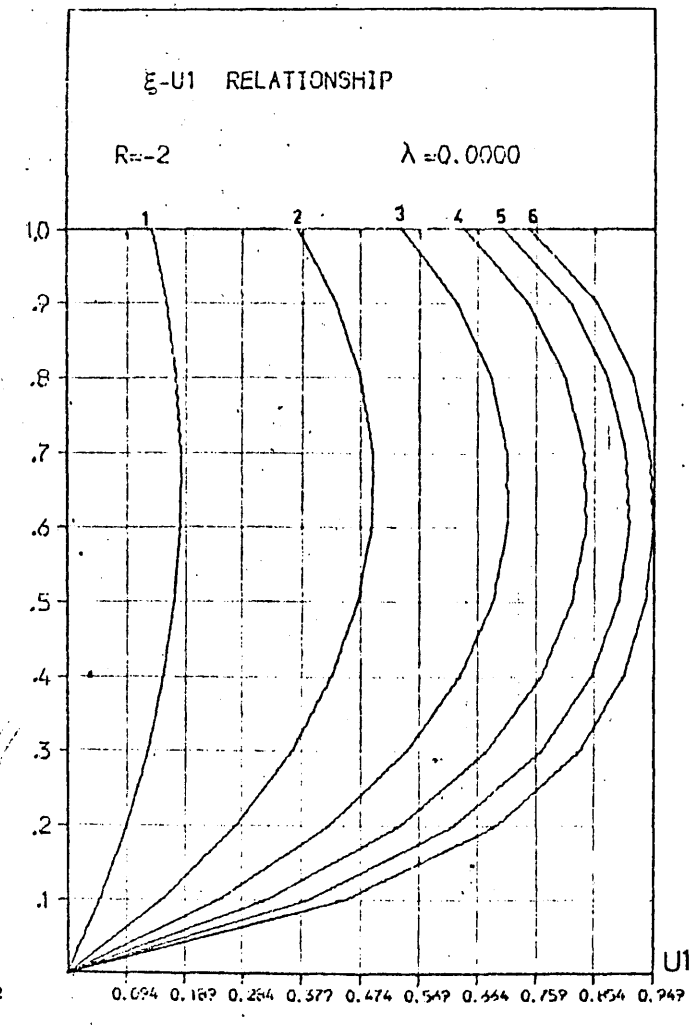
ξ-U1 RELATIONSHIP
R=-2
λ =0.0000
1
2
3
4
5
6
1.0
.9
.8
.7
.6
.5
.4
.3
.2
.1
U1
0.094 0.189 0.284 0.377 0.474 0.569 0.664 0.759 0.854 0.949

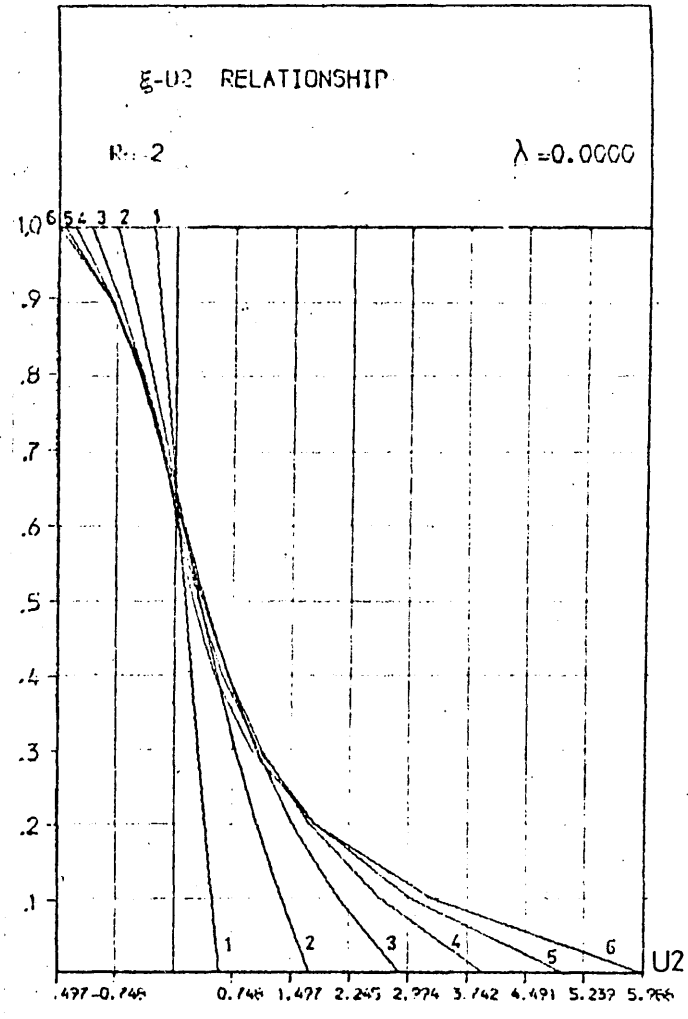
ξ-U2 RELATIONSHIP
λ =0.0000
6
5
4
3
2
1
1.0
.9
.8
.7
.6
.5
.4
.3
.2
.1
U2
.497-0.748
0.748 1.497 2.245 2.994 3.742 4.491 5.239 5.988

Fig. B.I.5

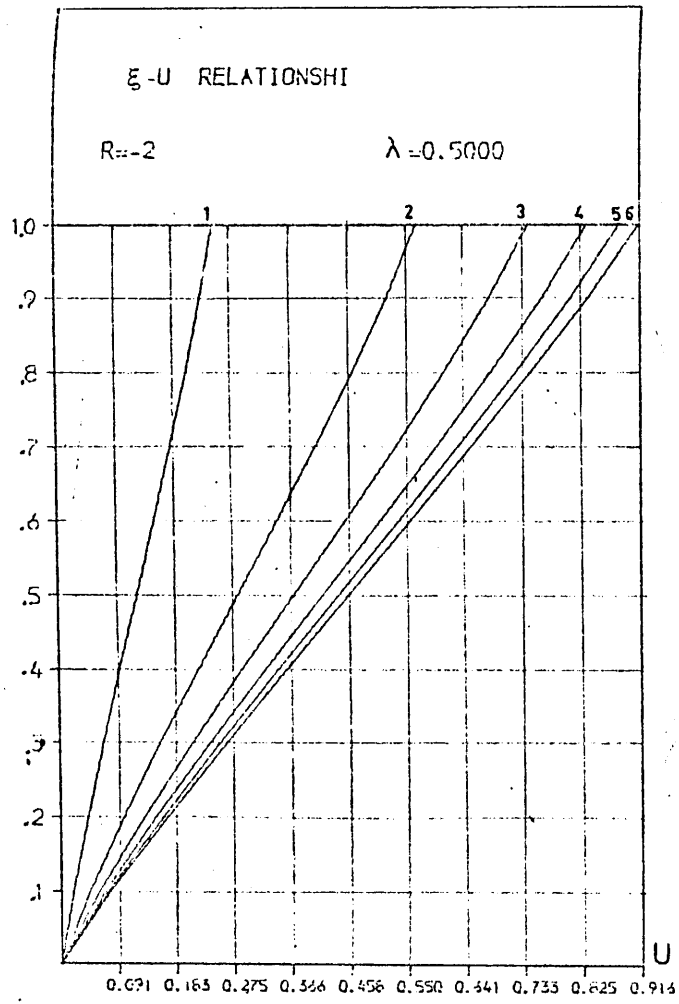
ξ-U RELATIONSHI
R=-2
λ =0.5000
1
2
3
4
5
6
1.0
.9
.8
.7
.6
.5
.4
.3
.2
.1
U
0.091 0.183 0.275 0.366 0.458 0.550 0.641 0.733 0.825 0.916

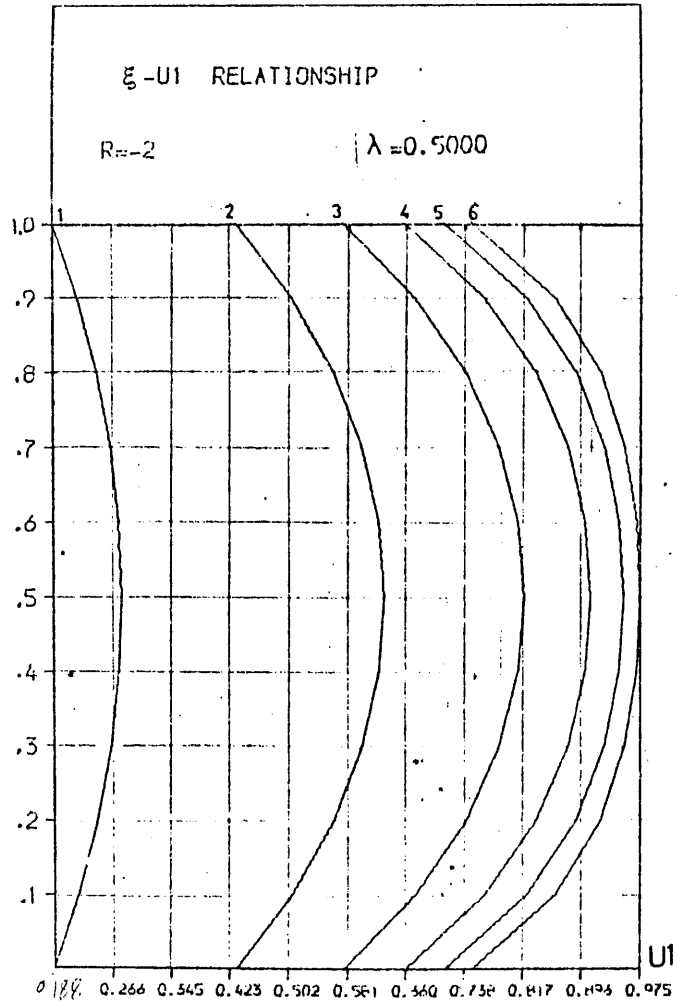
ξ-U1 RELATIONSHIP
R=-2
λ =0.5000
1
2
3
4
5
6
1.0
.9
.8
.7
.6
.5
.4
.3
.2
.1
U1
0.188 0.266 0.345 0.423 0.502 0.581 0.660 0.738 0.817 0.896 0.975

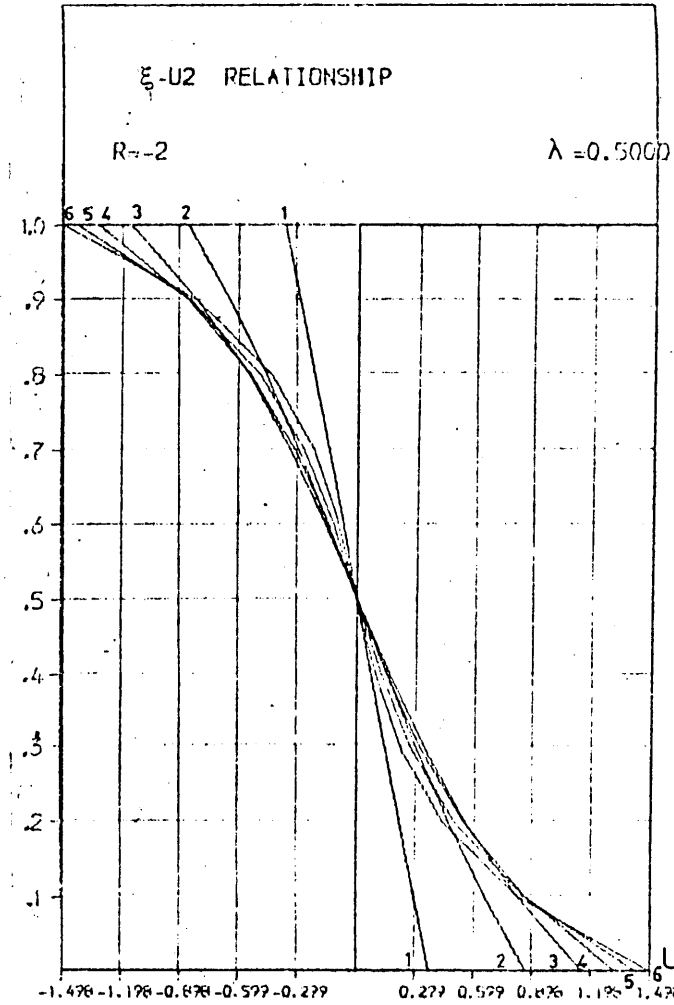
ξ-U2 RELATIONSHIP
R=-2
λ =0.5000
6
5
4
3
2
1
1.0
.9
.8
.7
.6
.5
.4
.3
.2
.1
U2
-1.426 -1.198 -0.970 -0.742 -0.514
0.514 0.742 0.970 1.198 1.426

Fig. B.I.6

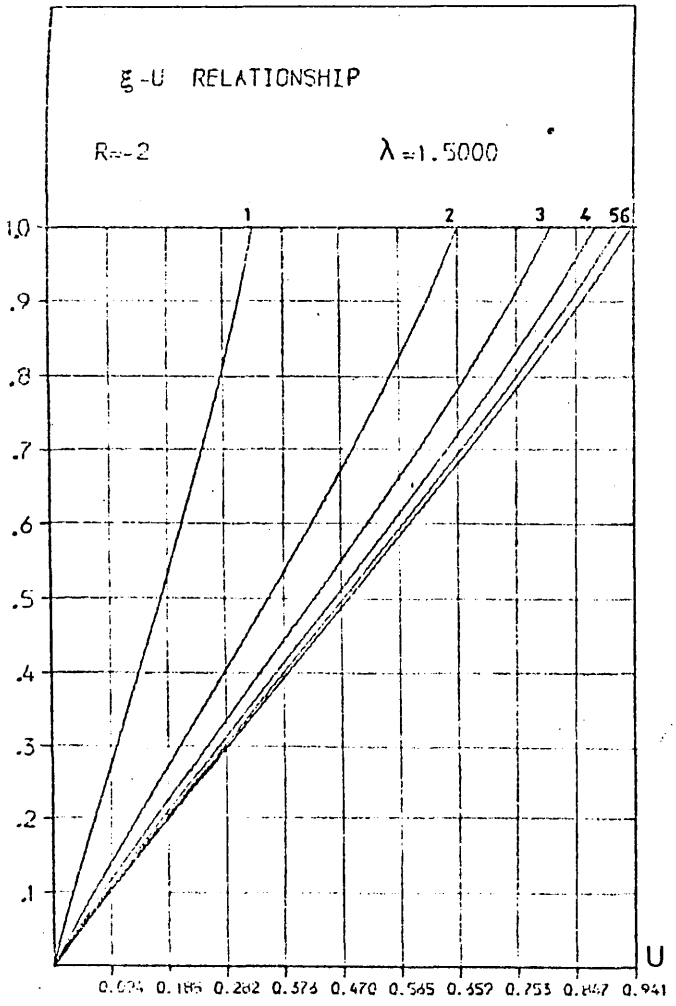
ξ-U RELATIONSHIP
R=-2
λ=1.5000
1
2
3
4
5
6
1.0
.9
.8
.7
.6
.5
.4
.3
.2
.1
U
0.094 0.188 0.282 0.376 0.470 0.565 0.659 0.753 0.847 0.941

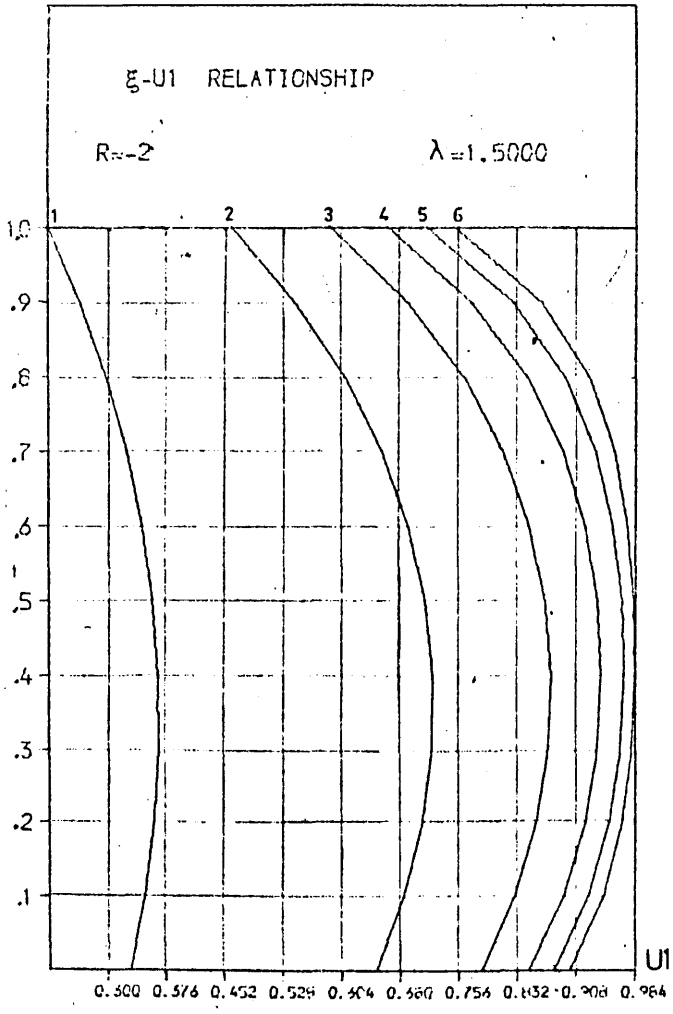
ξ-U1 RELATIONSHIP
R=-2
λ=1.5000
1
2
3
4
5
6
1.0
.9
.8
.7
.6
.5
.4
.3
.2
.1
U1
0.500 0.576 0.452 0.529 0.604 0.680 0.756 0.832 0.908 0.984

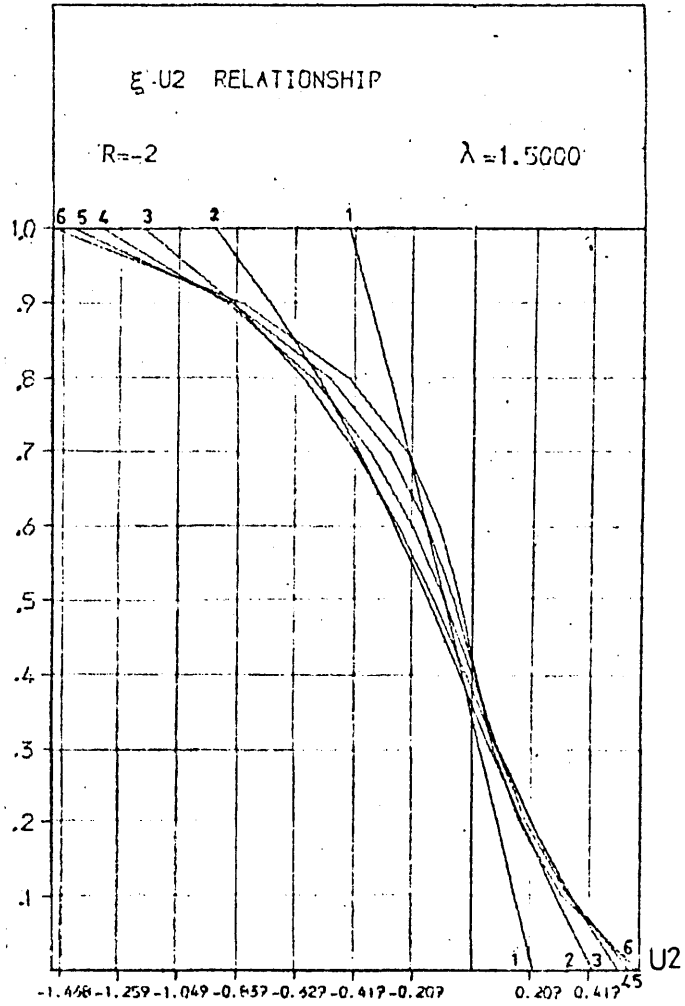
ξ-U2 RELATIONSHIP
R=-2
λ=1.5000
6
5
4
3
2
1
1.0
.9
.8
.7
.6
.5
.4
.3
.2
.1
U2
-1.468 -1.259 -1.049 -0.839 -0.629 -0.419 -0.209 0.209 0.419 0.629

Fig. B.I.7

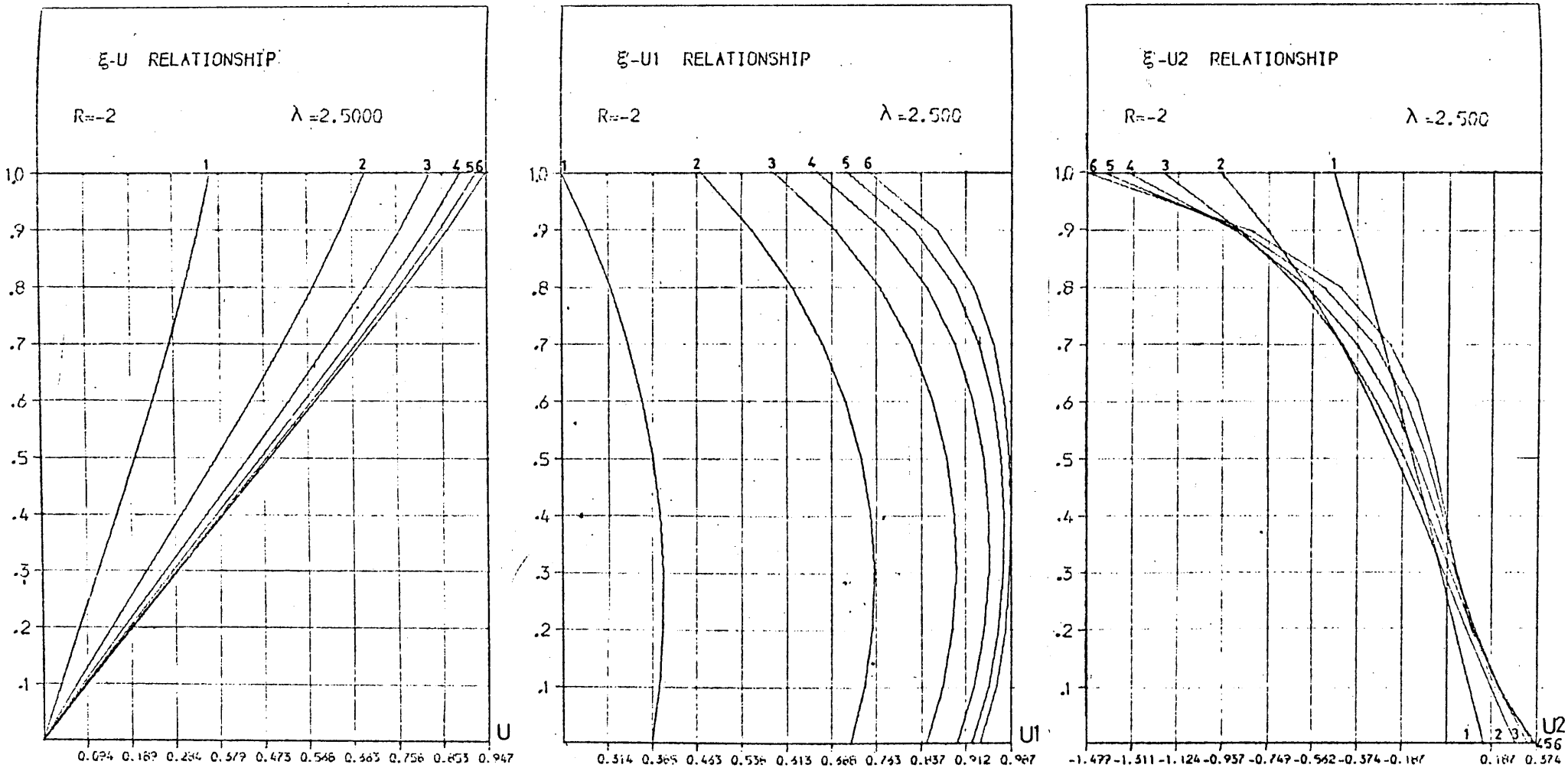
ξ-U RELATIONSHIP
R=-2
λ =2.5000
1.0
.9
.8
.7
.6
.5
.4
.3
.2
.1
U
0.094 0.189 0.284 0.379 0.473 0.568 0.663 0.756 0.853 0.947
ξ-U1 RELATIONSHIP
R=-2
λ =2.500
U1
0.314 0.365 0.463 0.536 0.613 0.688 0.763 0.837 0.912 0.987
ξ-U2 RELATIONSHIP
R=-2
λ =2.500
U2
-1.477 -1.311 -1.124 -0.937 -0.749 -0.562 -0.374 -0.187 0.187 0.374

Fig. B.I.8

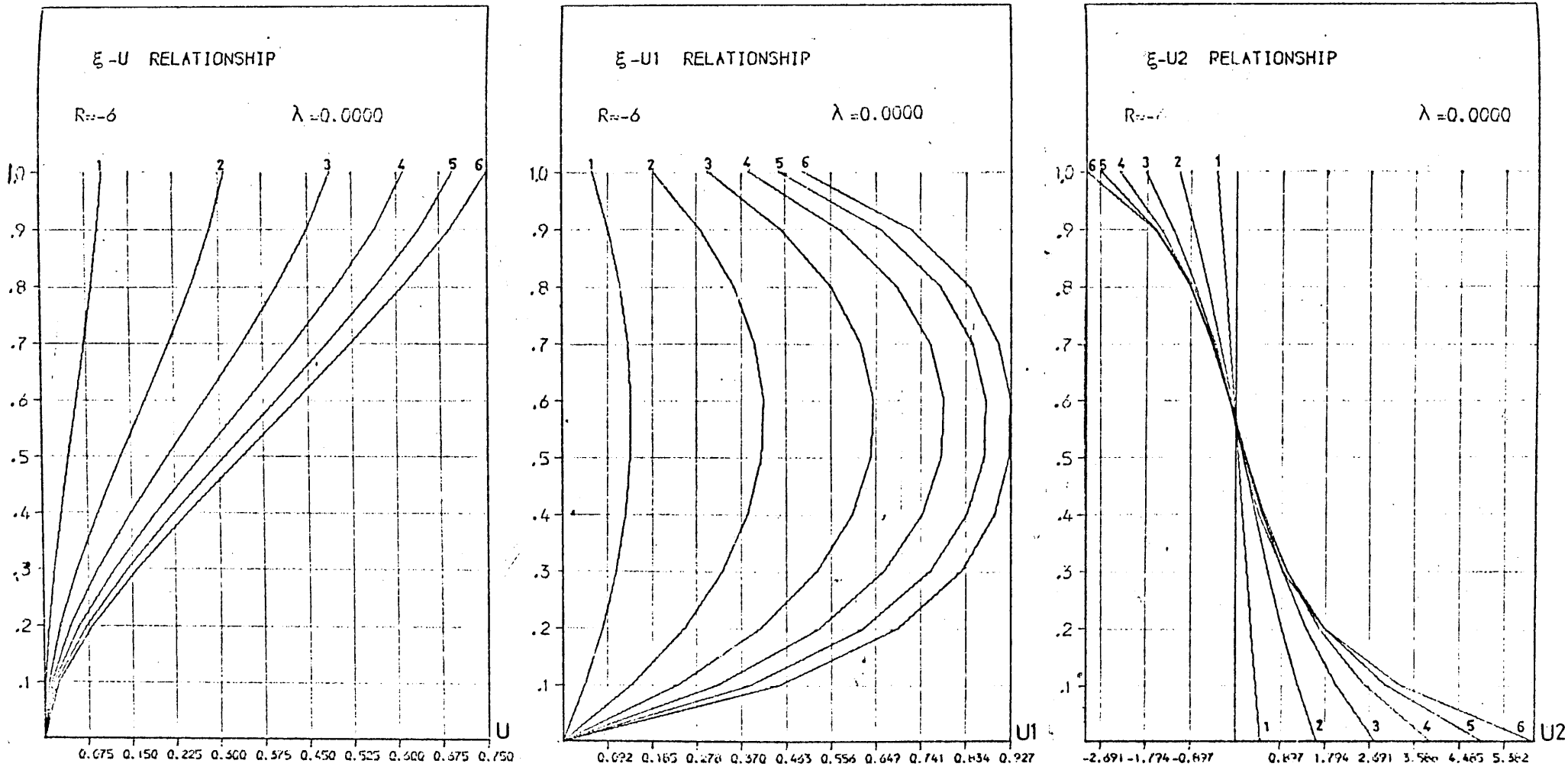
ξ-U RELATIONSHIP
R=-6
λ =0.0000
1.0
.9
.8
.7
.6
.5
.4
.3
.2
.1
1
2
3
4
5
6
U
0.075 0.150 0.225 0.300 0.375 0.450 0.525 0.600 0.675 0.750
ξ-U1 RELATIONSHIP
R=-6
λ =0.0000
U1
0.092 0.185 0.278 0.370 0.463 0.556 0.647 0.741 0.834 0.927
ξ-U2 RELATIONSHIP
λ =0.0000
U2
-2.691 -1.794 -0.897
0.897 1.794 2.691 3.588 4.485 5.382

Fig. B.I.9

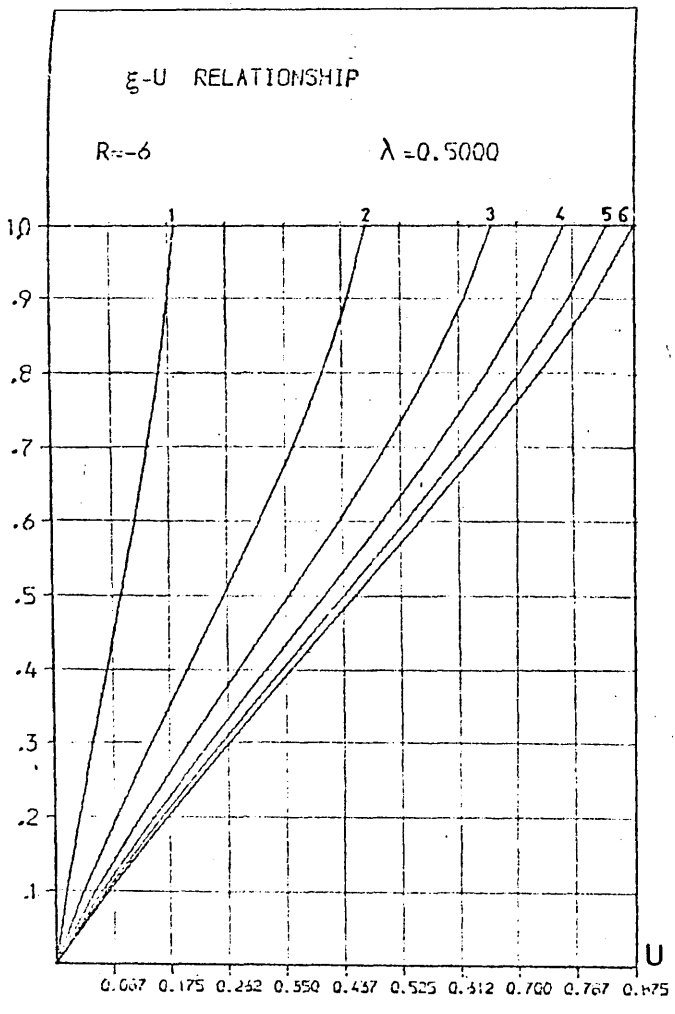
ξ-U RELATIONSHIP
R=-6
λ =0.5000
1.0
.9
.8
.7
.6
.5
.4
.3
.2
.1
1
2
3
4
5
6
U
0.087 0.175 0.262 0.350 0.437 0.525 0.612 0.700 0.787 0.875

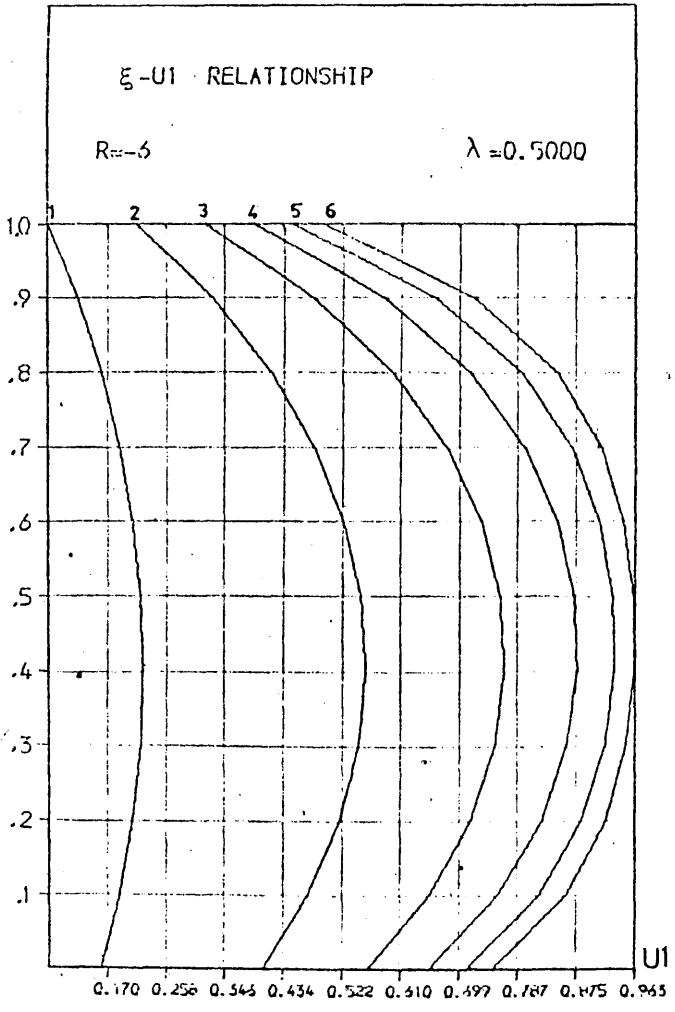
ξ-U1 RELATIONSHIP
R=-6
λ =0.5000
1.0
.9
.8
.7
.6
.5
.4
.3
.2
.1
1
2
3
4
5
6
U1
0.170 0.256 0.346 0.434 0.522 0.610 0.699 0.787 0.875 0.963

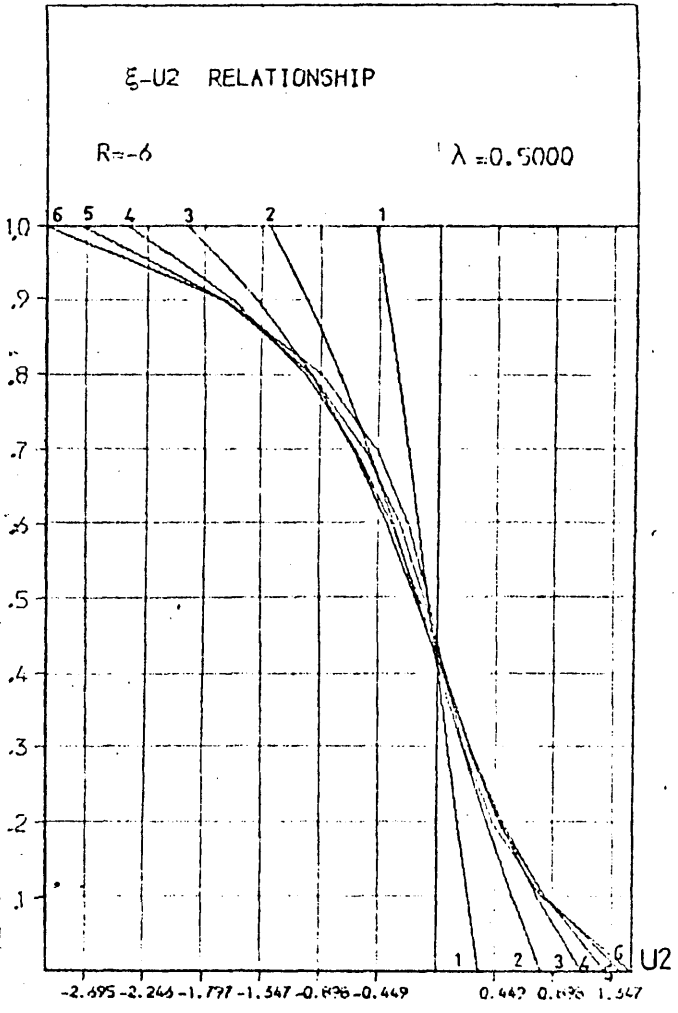
ξ-U2 RELATIONSHIP
R=-6
λ =0.5000
1.0
.9
.8
.7
.6
.5
.4
.3
.2
.1
6
5
4
3
2
1
U2
-2.695 -2.246 -1.797 -1.347 -0.898 -0.449
0.449 0.898 1.347

Fig. B.I.10

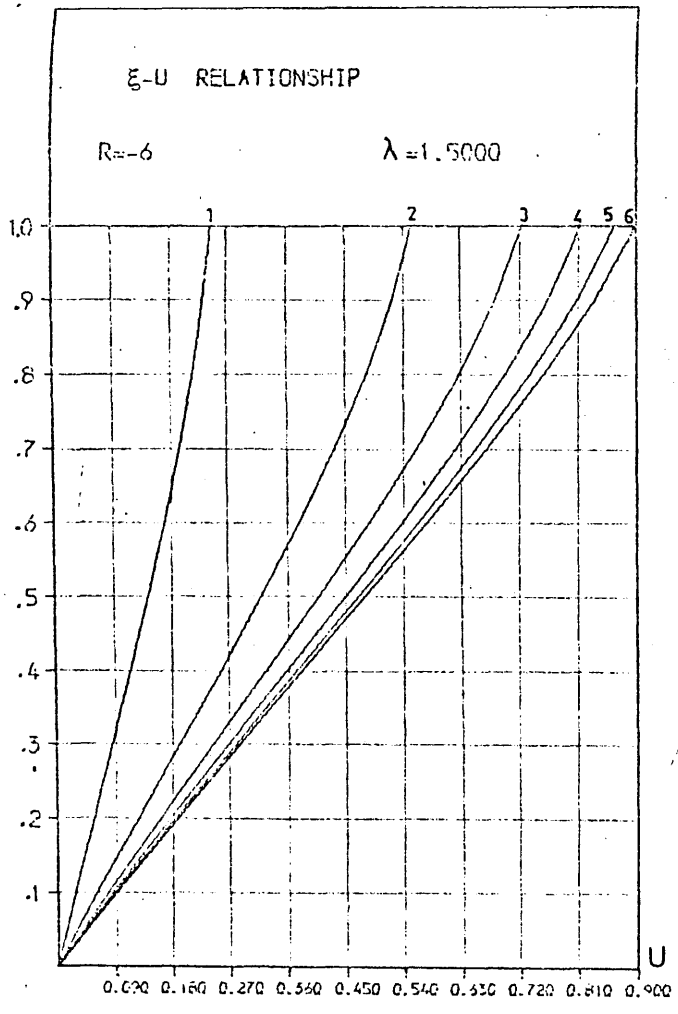
ξ-U RELATIONSHIP
R=-6
λ =1.5000
1.0
.9
.8
.7
.6
.5
.4
.3
.2
.1
1
2
3
4
5
6
U
0.090 0.180 0.270 0.360 0.450 0.540 0.630 0.720 0.810 0.900

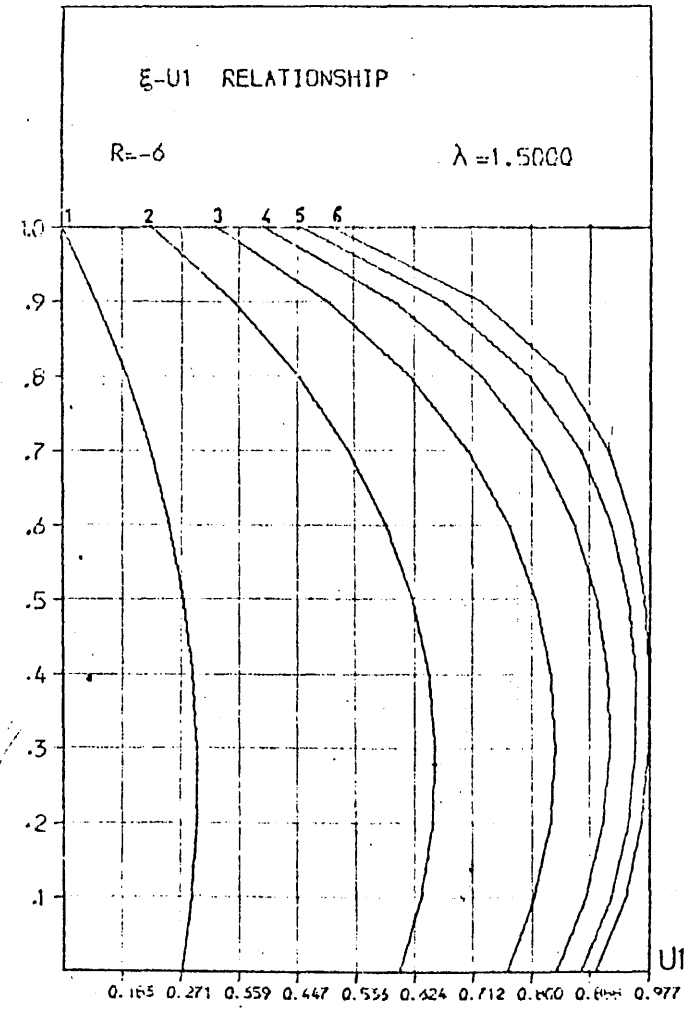
ξ-U1 RELATIONSHIP
R=-6
λ =1.5000
1.0
.9
.8
.7
.6
.5
.4
.3
.2
.1
1
2
3
4
5
6
U1
0.165 0.271 0.559 0.447 0.555 0.624 0.712 0.977

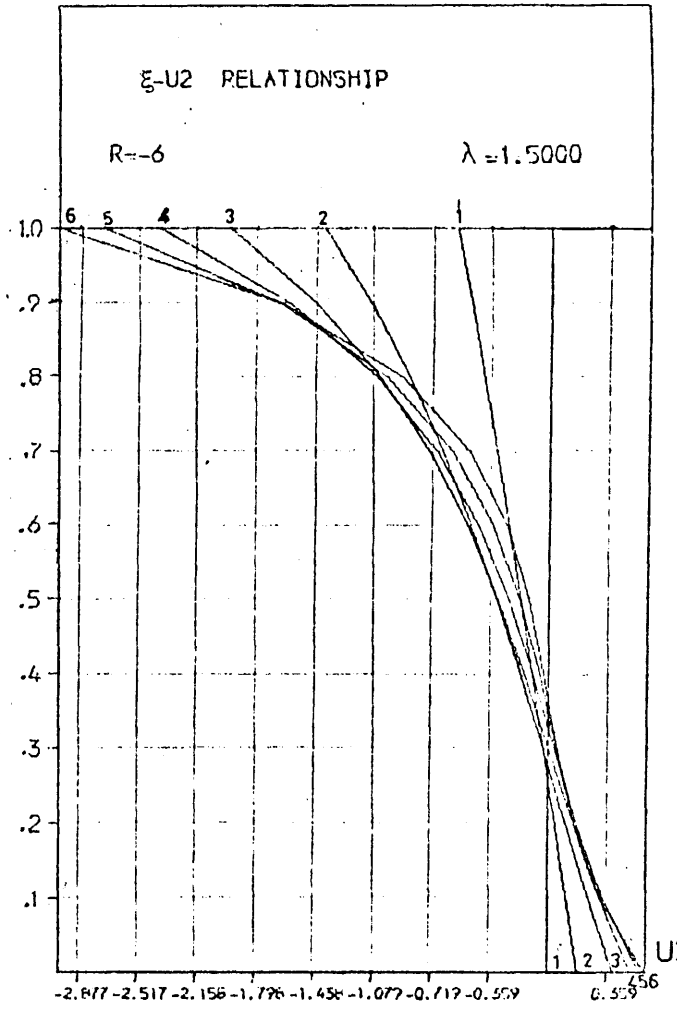
ξ-U2 RELATIONSHIP
R=-6
λ =1.5000
1.0
.2
.8
.7
.6
.5
.4
.3
.2
.1
6
5
4
3
2
1
1
2
3
4
5
6
U2
-2.877 -2.517 -2.156 -1.796 -1.436 -1.077 -0.717 -0.359
0.359

Fig. B.I.11

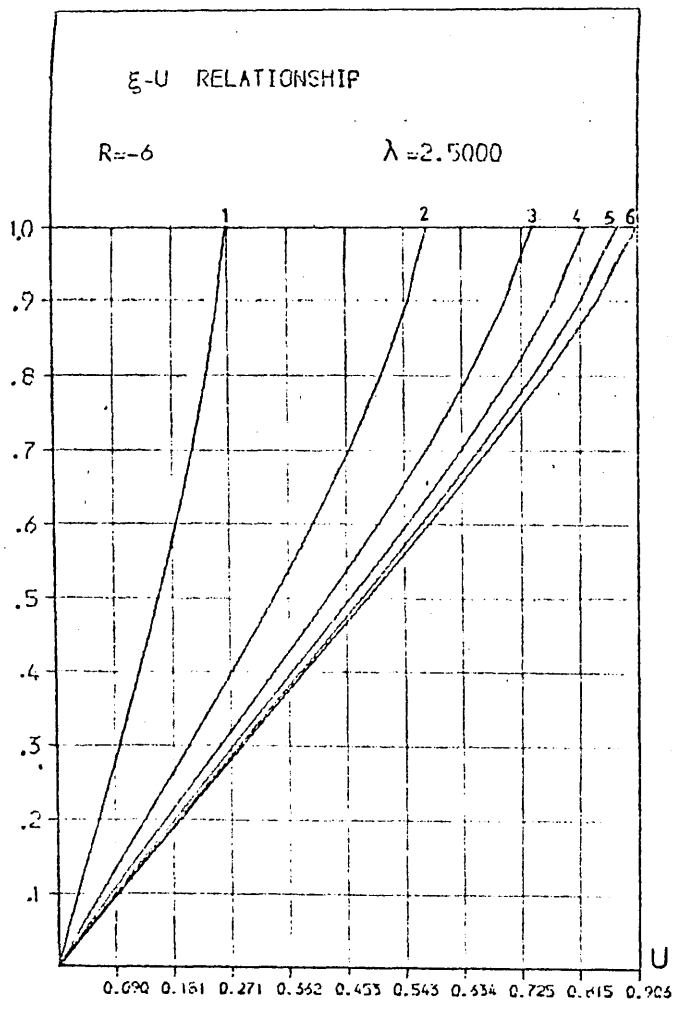
ξ-U RELATIONSHIP
R=-6
λ =2.5000
1.0
.9
.8
.7
.6
.5
.4
.3
.2
.1
1
2
3
4
5
6
U
0.090 0.181 0.271 0.362 0.453 0.543 0.634 0.725 0.815 0.906

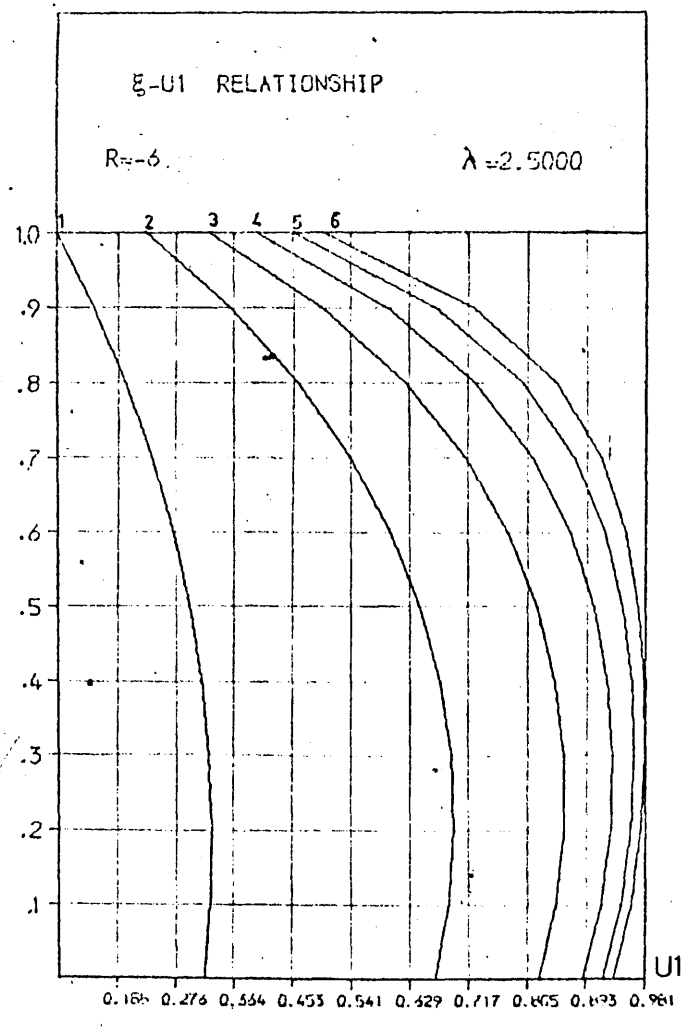
ξ-U1 RELATIONSHIP
R=-6
λ =2.5000
1.0
.9
.8
.7
.6
.5
.4
.3
.2
.1
1
2
3
4
5
6
U1
0.168 0.276 0.364 0.453 0.541 0.629 0.717 0.805 0.893 0.981

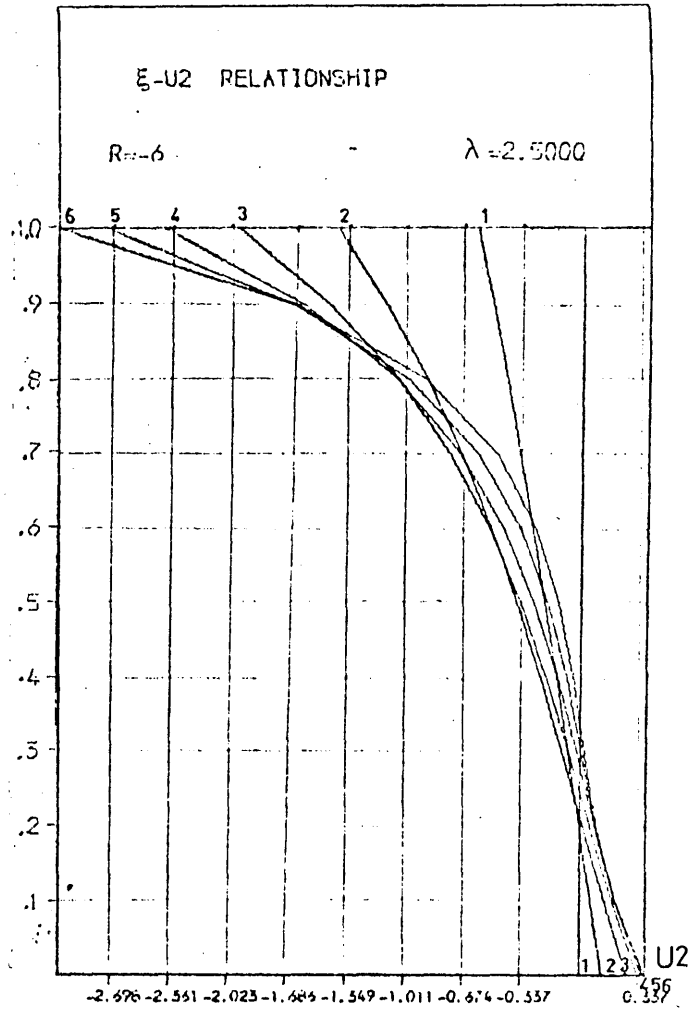
ξ-U2 RELATIONSHIP
R=-6
λ =2.5000
1.0
.9
.8
.7
.6
.5
.4
.3
.2
.1
6
5
4
3
2
1
1 2 3
4 5 6
U2
-2.696 -2.561 -2.023 -1.685 -1.549 -1.011 -0.674 -0.537
0.337

Fig. B.I.12

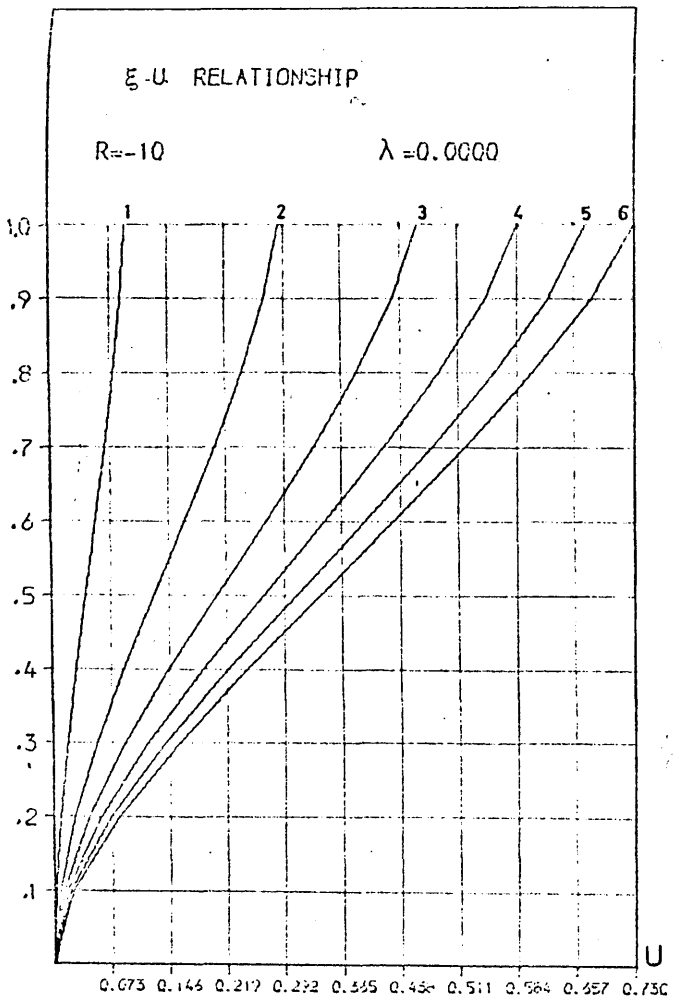
ξ-U RELATIONSHIP
R=-10
λ =0.0000
1.0
.9
.8
.7
.6
.5
.4
.3
.2
.1
1
2
3
4
5
6
U
0.073 0.146 0.219 0.292 0.365 0.438 0.511 0.584 0.657 0.730

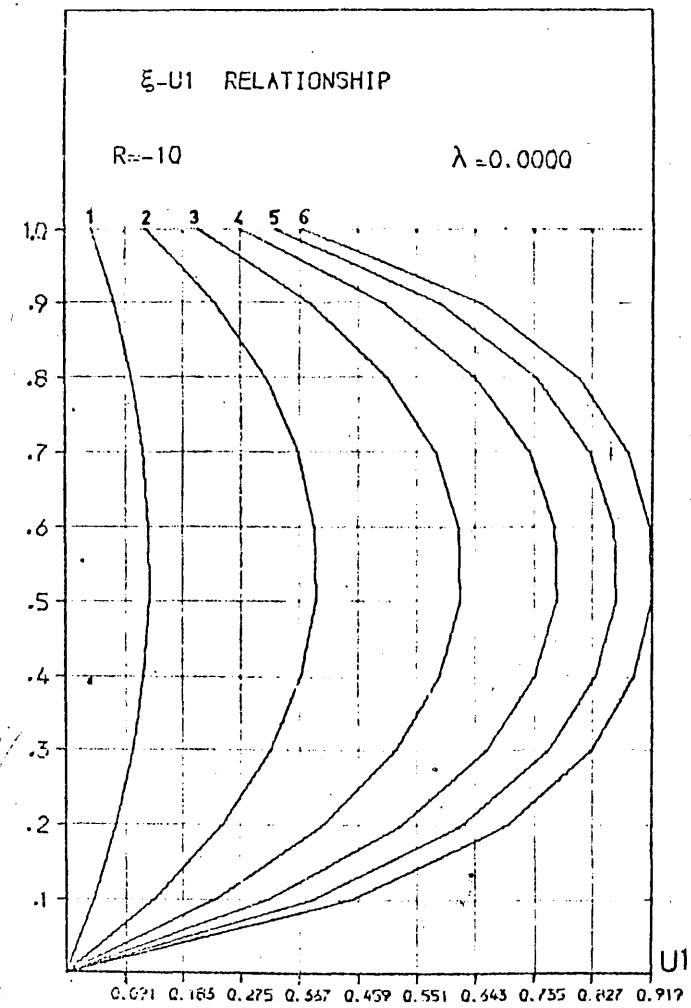
ξ-U1 RELATIONSHIP
R=-10
λ =0.0000
1.0
.9
.8
.7
.6
.5
.4
.3
.2
.1
1
2
3
4
5
6
U1
0.091 0.183 0.275 0.367 0.459 0.551 0.643 0.735 0.827 0.919

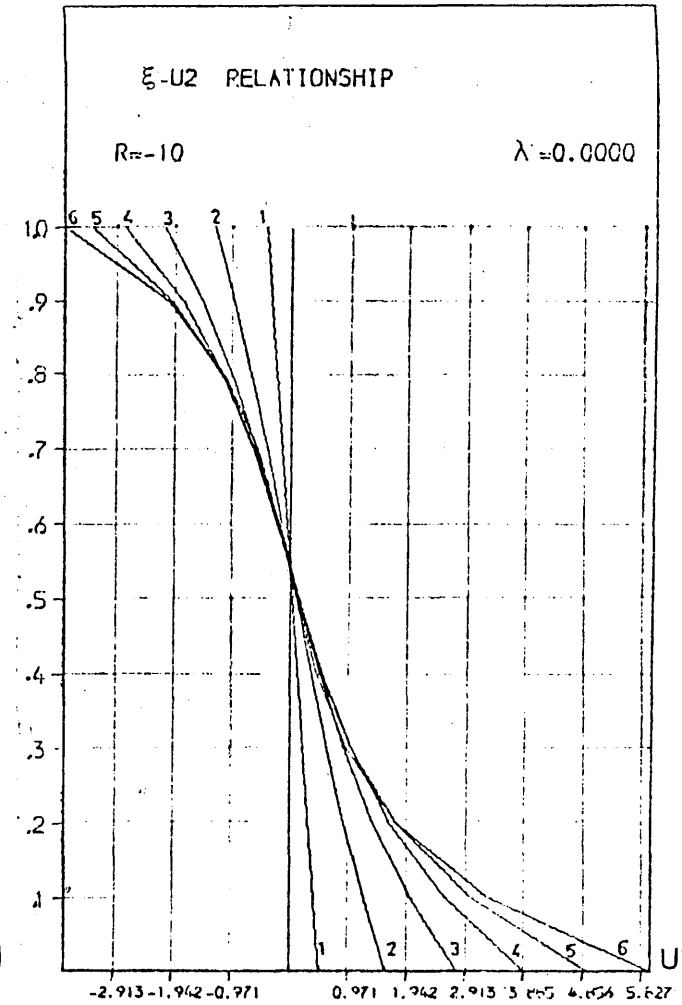
ξ-U2 RELATIONSHIP
R=-10
λ =0.0000
1.0
.9
.8
.7
.6
.5
.4
.3
.2
.1
6
5
4
3
2
1
1
2
3
4
5
6
U2
-2.913 -1.942 -0.971
0.971 1.942 2.913 5.627

Fig. B.I.13

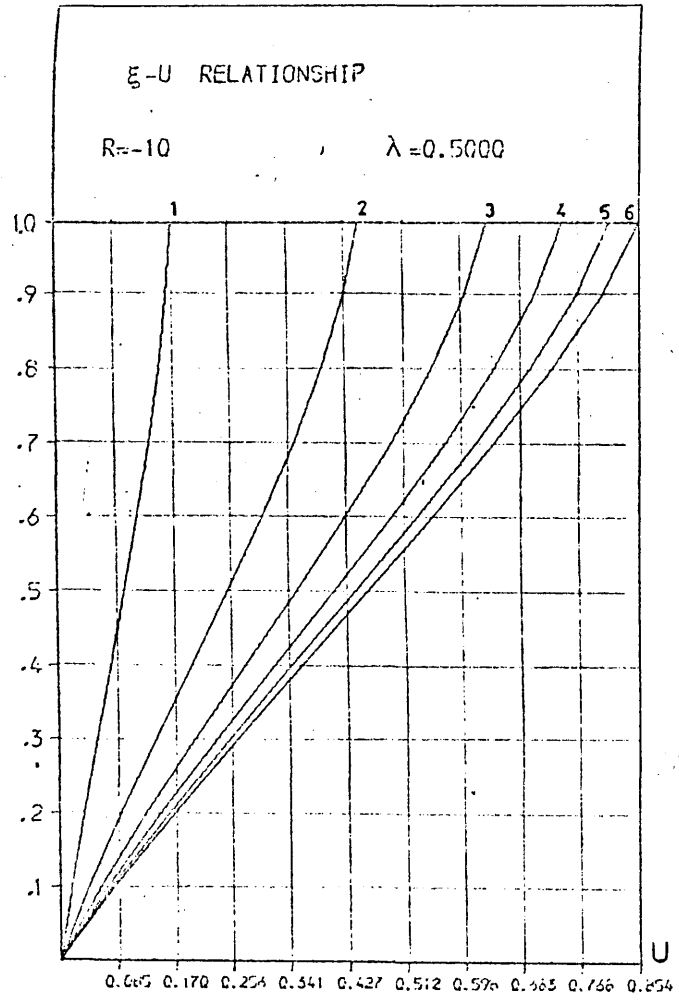
ξ-U RELATIONSHIP
R=-10
λ =0.5000
1
2
3
4
5
6
1.0
.9
.8
.7
.6
.5
.4
.3
.2
.1
U

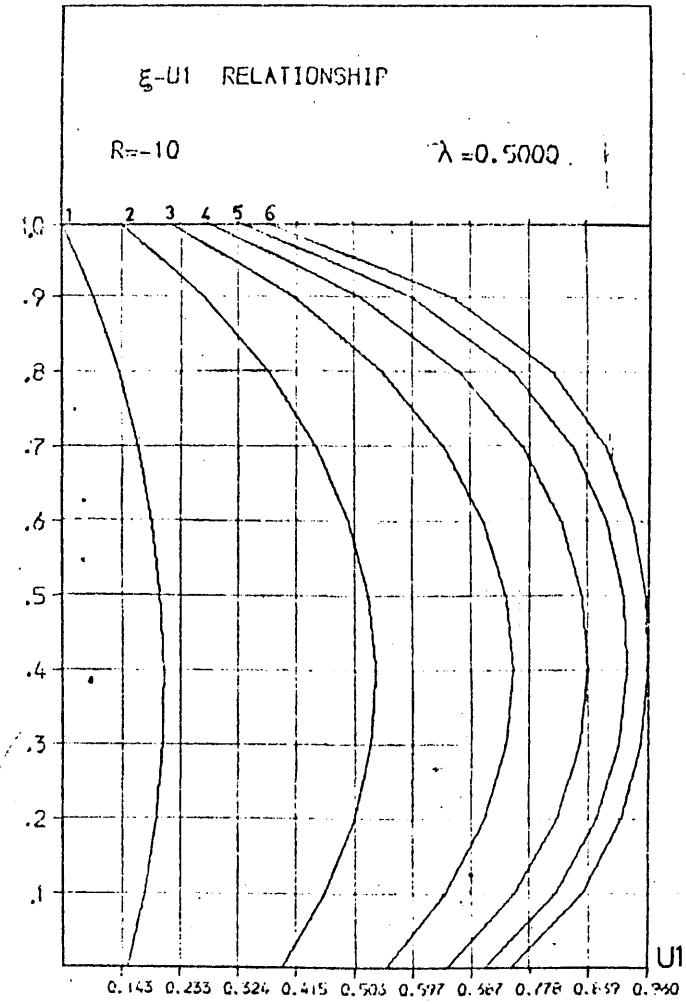
ξ-U1 RELATIONSHIP
R=-10
λ =0.5000
1
2
3
4
5
6
1.0
.9
.8
.7
.6
.5
.4
.3
.2
.1
U1

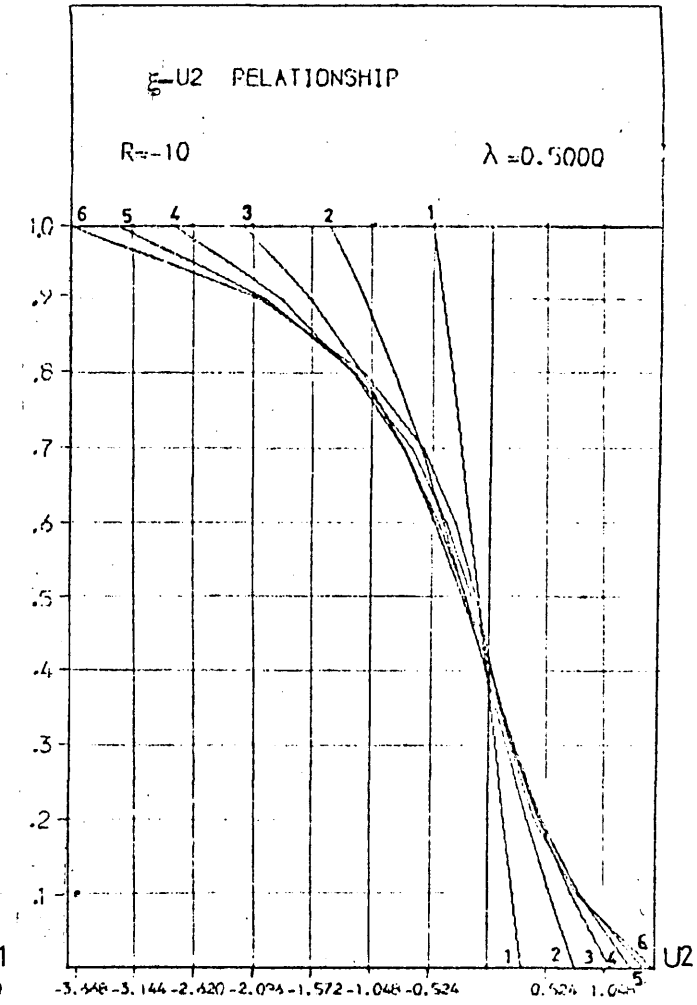
ξ-U2 RELATIONSHIP
R=-10
λ =0.5000
6
5
4
3
2
1
1.0
.9
.8
.7
.6
.5
.4
.3
.2
.1
U2

Fig. B.I.14

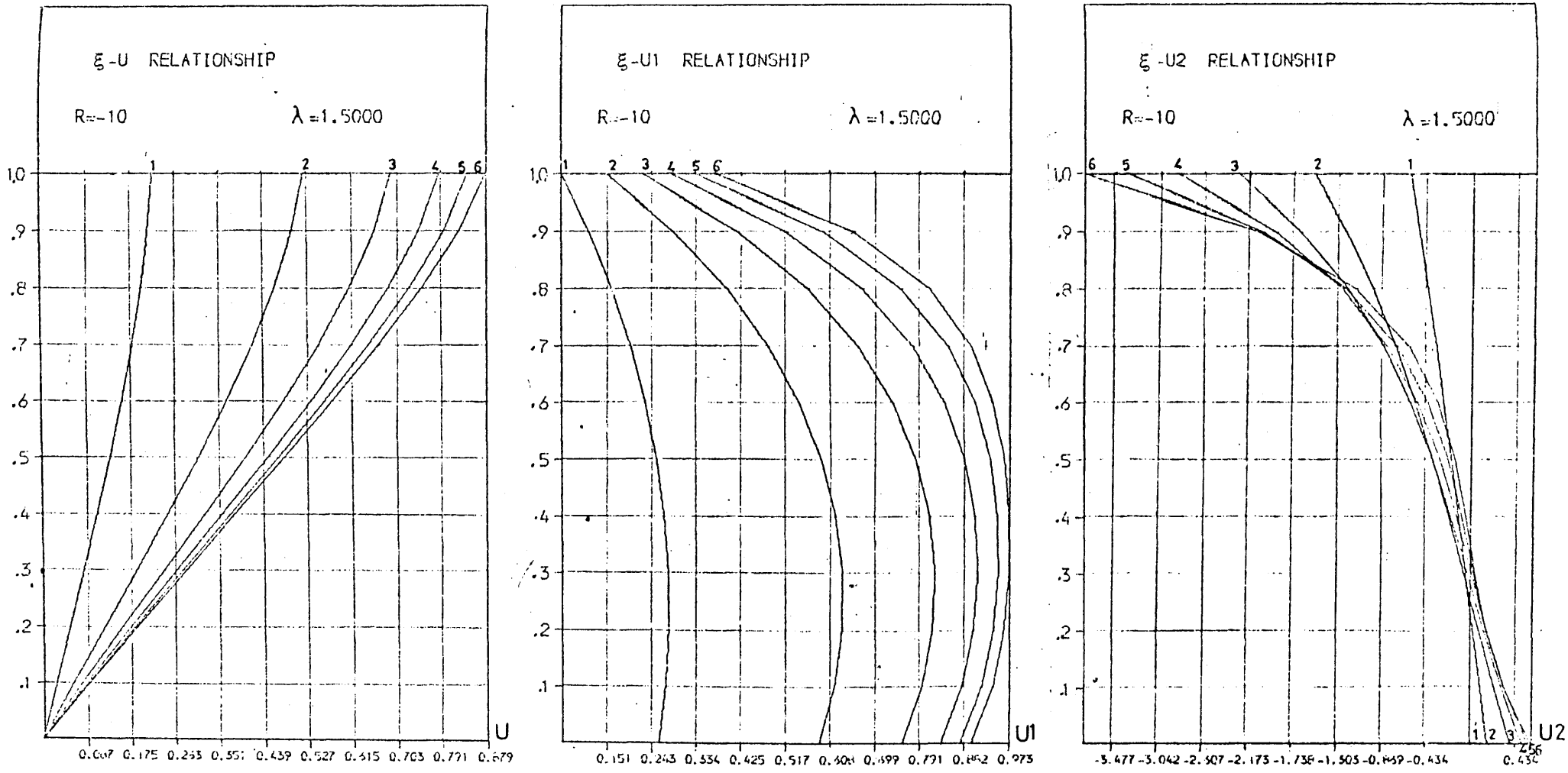
ξ-U RELATIONSHIP
R=-10
λ=1.5000
1.0
.9
.8
.7
.6
.5
.4
.3
.2
.1
1
2
3
4
5
6
U
0.007 0.175 0.243 0.551 0.439 0.527 0.615 0.703 0.791 0.879
ξ-U1 RELATIONSHIP
R=-10
λ=1.5000
U1
0.151 0.243 0.334 0.425 0.517 0.608 0.699 0.791 0.882 0.973
ξ-U2 RELATIONSHIP
R=-10
λ=1.5000
U2
-3.477 -3.042 -2.607 -2.173 -1.738 -1.303 -0.869 -0.434
0.430

Fig. B.I.15

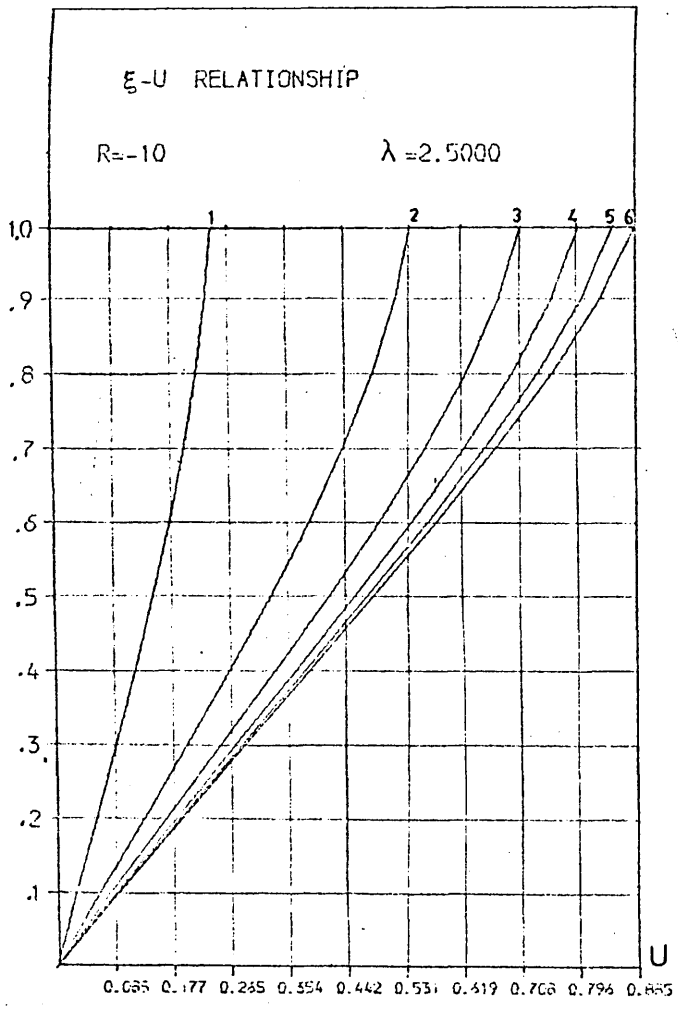
ξ-U RELATIONSHIP
R=-10
λ =2.5000
1.0
.9
.8
.7
.6
.5
.4
.3
.2
.1
1
2
3
4
5
6
U
0.088 0.177 0.265 0.354 0.442 0.531 0.619 0.708 0.796 0.885

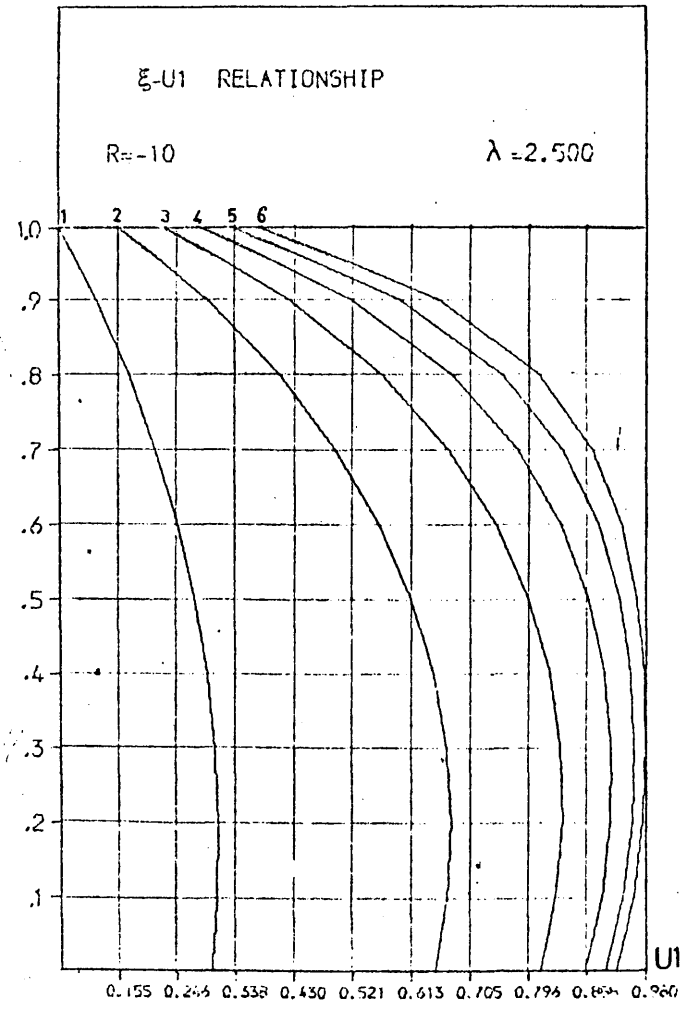
ξ-U1 RELATIONSHIP
R=-10
λ =2.500
1.0
.9
.8
.7
.6
.5
.4
.3
.2
.1
1
2
3
4
5
6
U1
0.155 0.244 0.338 0.430 0.521 0.613 0.705 0.796 0.888 0.980

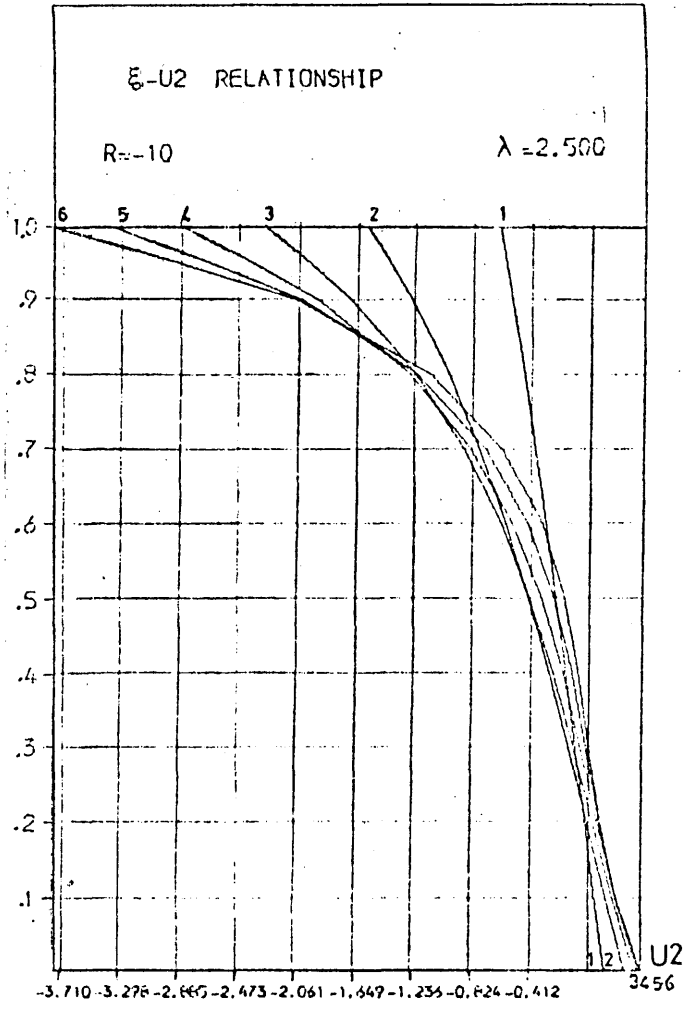
ξ-U2 RELATIONSHIP
R=-10
λ =2.500
1.0
.9
.8
.7
.6
.5
.4
.3
.2
.1
6
5
4
3
2
1
1
2
3
4
5
6
U2
-3.710 -3.276 -2.865 -2.473 -2.061 -1.649 -1.235 -0.824 -0.412

Fig. B.I.16

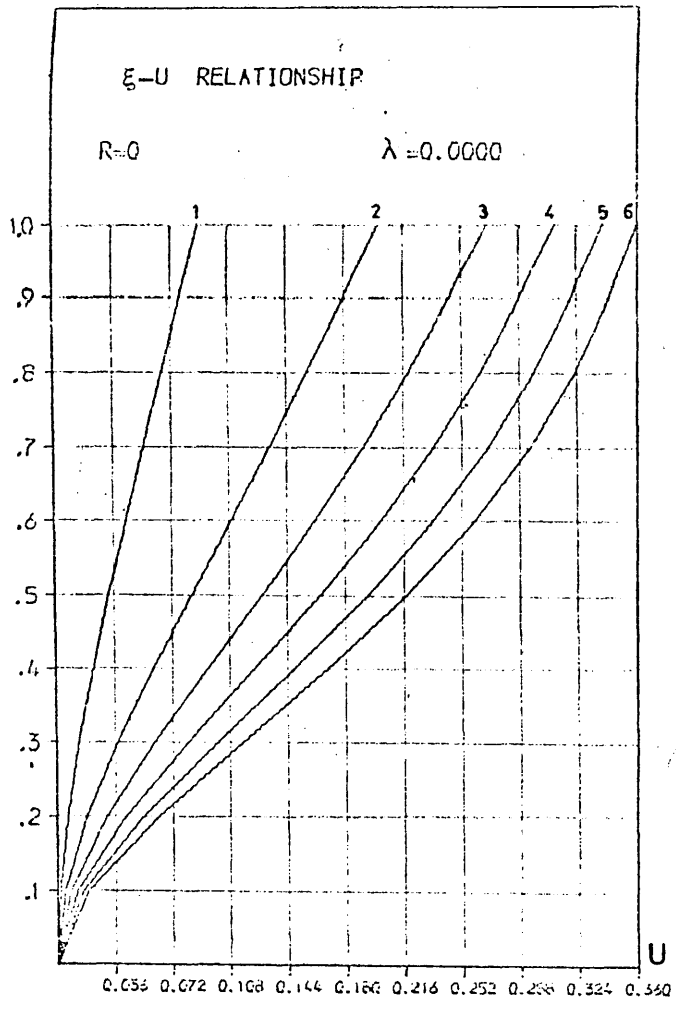
ξ-U RELATIONSHIP
R=0
λ =0.0000
1
2
3
4
5
6
1.0
.9
.8
.7
.6
.5
.4
.3
.2
.1
U
0.036 0.072 0.108 0.144 0.180 0.216 0.252 0.288 0.324 0.360

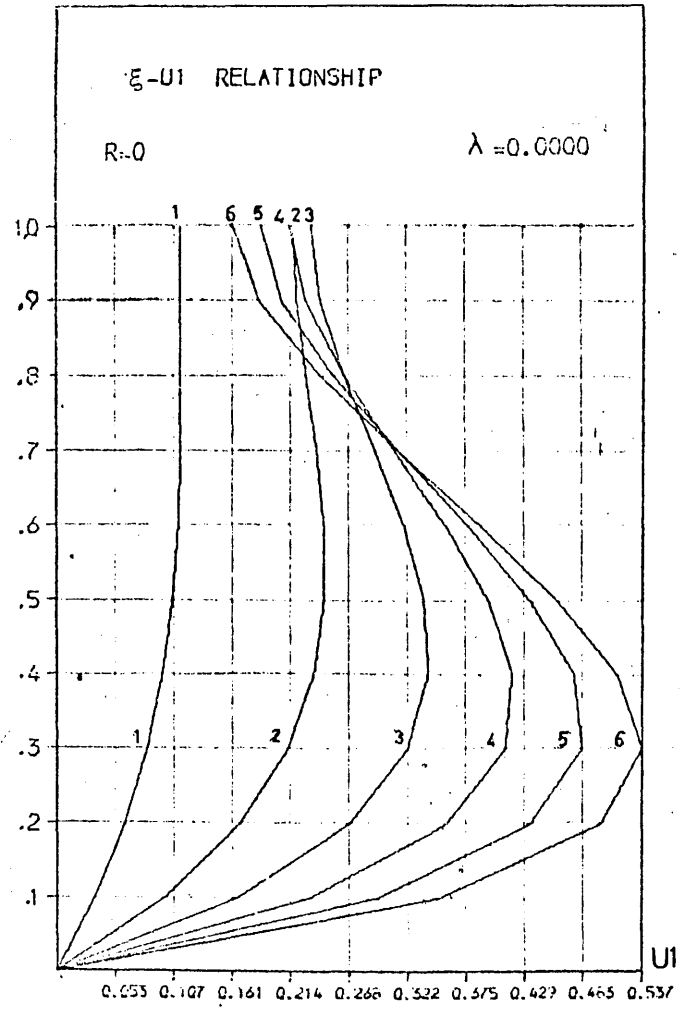
ξ-U1 RELATIONSHIP
R=0
λ =0.0000
1
6 5 4 2 3
1.0
.9
.8
.7
.6
.5
.4
.3
.2
.1
U1
0.053 0.107 0.161 0.214 0.268 0.322 0.375 0.429 0.483 0.537

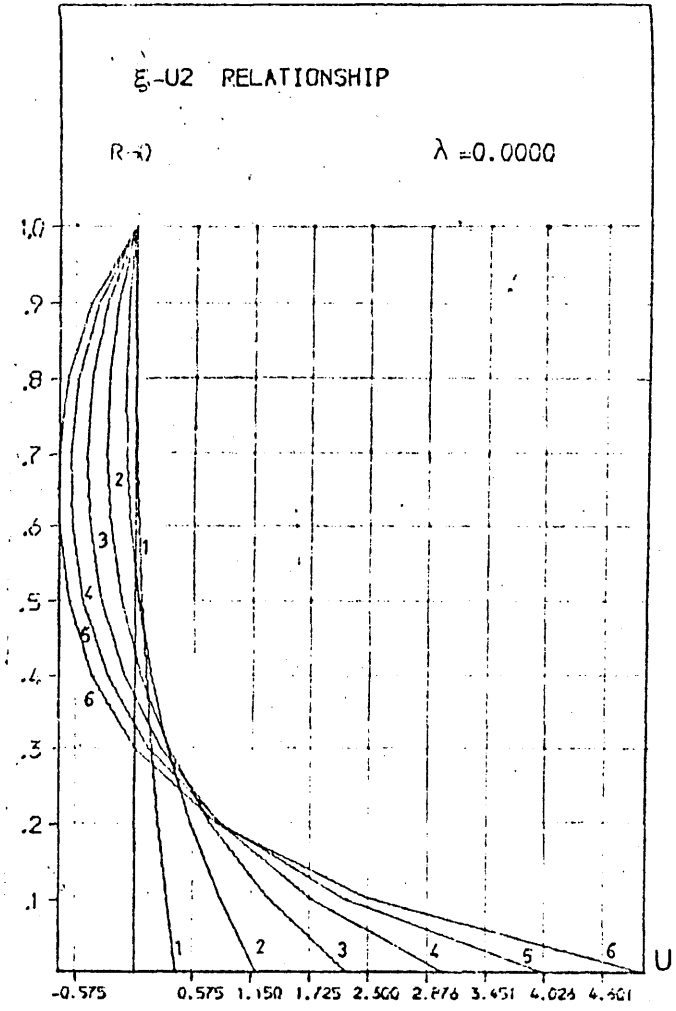
ξ-U2 RELATIONSHIP
R=0
λ =0.0000
1.0
.9
.8
.7
.6
.5
.4
.3
.2
.1
U2
-0.575
0.575 1.150 1.725 2.300 2.876 3.451 4.026 4.601

Fig. B.II.1

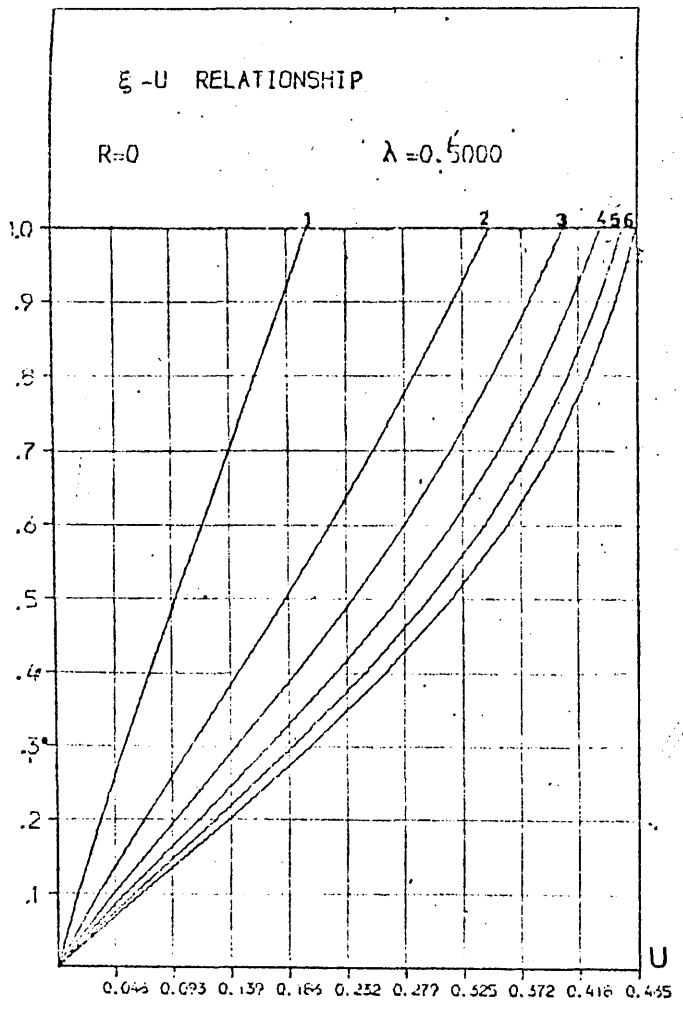
ξ -U RELATIONSHIP
R=0
λ =0.5000
1.0
.9
.8
.7
.6
.5
.4
.3
.2
.1
1
2
3
4
5
6
U
0.046 0.093 0.139 0.186 0.232 0.279 0.325 0.372 0.418 0.465

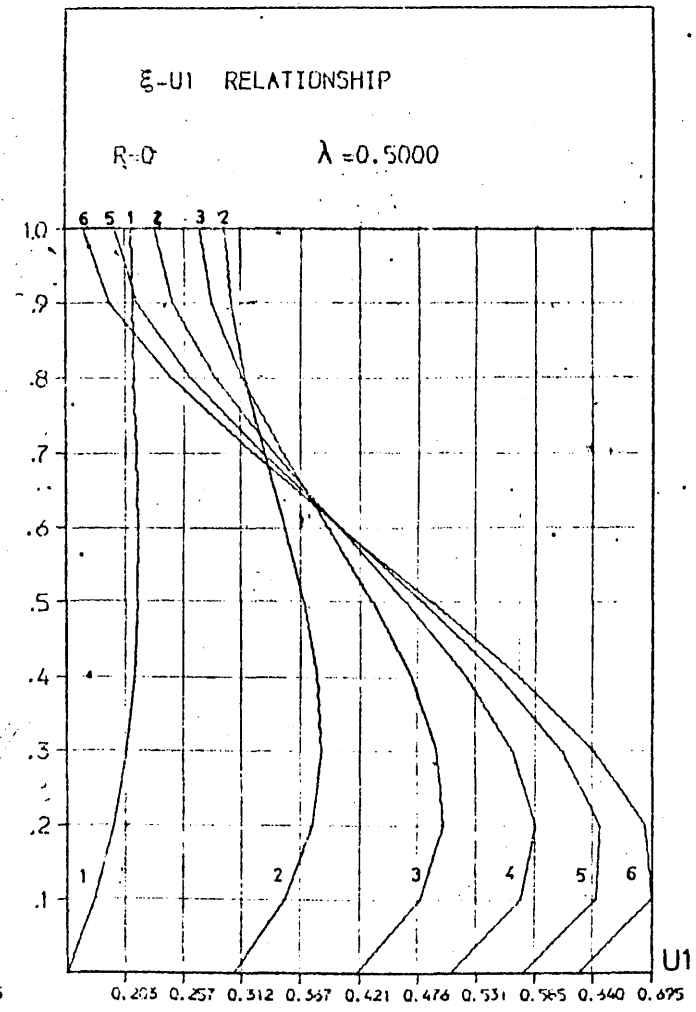
ξ-U1 RELATIONSHIP
R=0
λ =0.5000
1.0
.9
.8
.7
.6
.5
.4
.3
.2
.1
6 5 1 2 3 2
1
2
3
4
5
6
U1
0.203 0.257 0.312 0.367 0.421 0.476 0.531 0.585 0.640 0.695

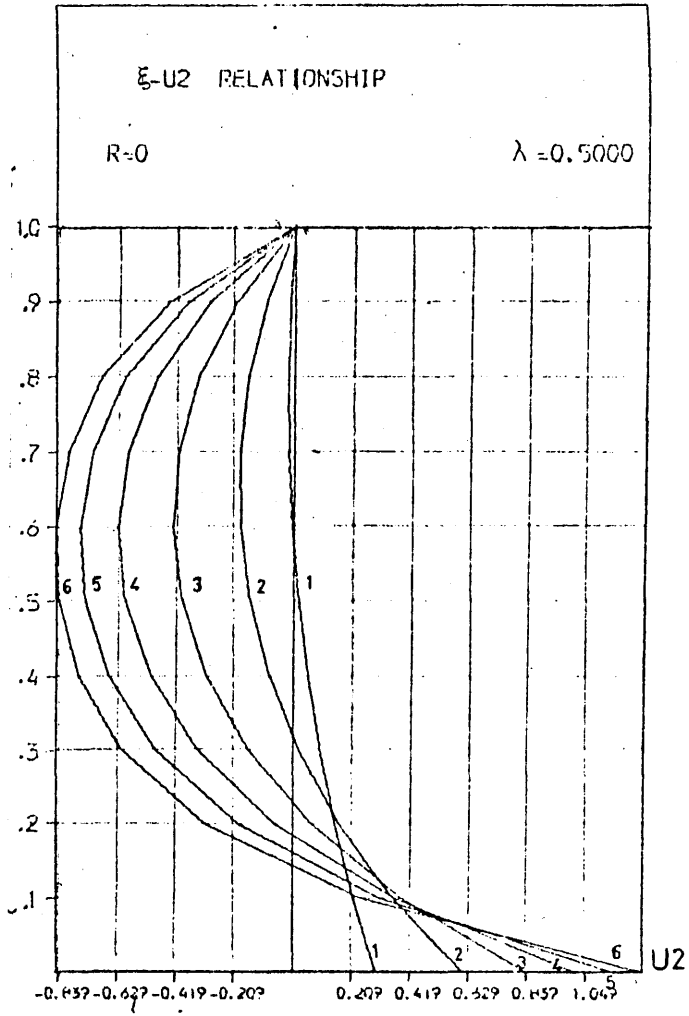
ξ-U2 RELATIONSHIP
R=0
λ =0.5000
1.0
.9
.8
.7
.6
.5
.4
.3
.2
.1
6 5 4 3 2 1
1
2
3
4
6
5
U2
-0.832 -0.627 -0.419 -0.209
0.209 0.419 0.629 0.837 1.049

Fig. B.II.2

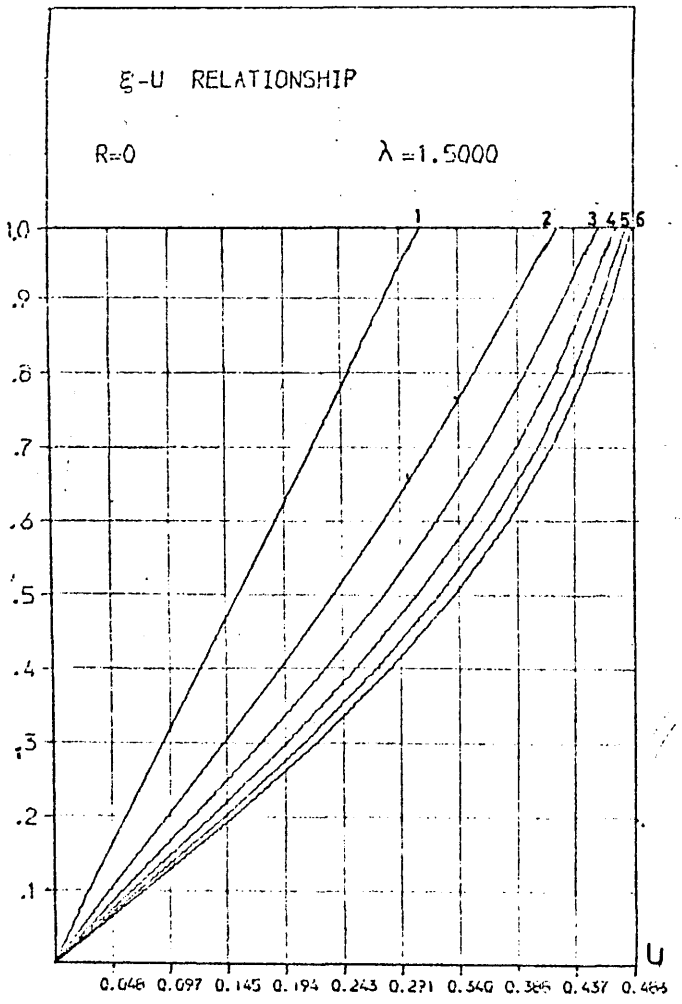
ξ-U RELATIONSHIP
R=0
λ =1.5000
1.0
.9
.8
.7
.6
.5
.4
.3
.2
.1
1
2
3
4
5
6
U
0.048 0.097 0.145 0.194 0.243 0.291 0.340 0.389 0.437 0.486

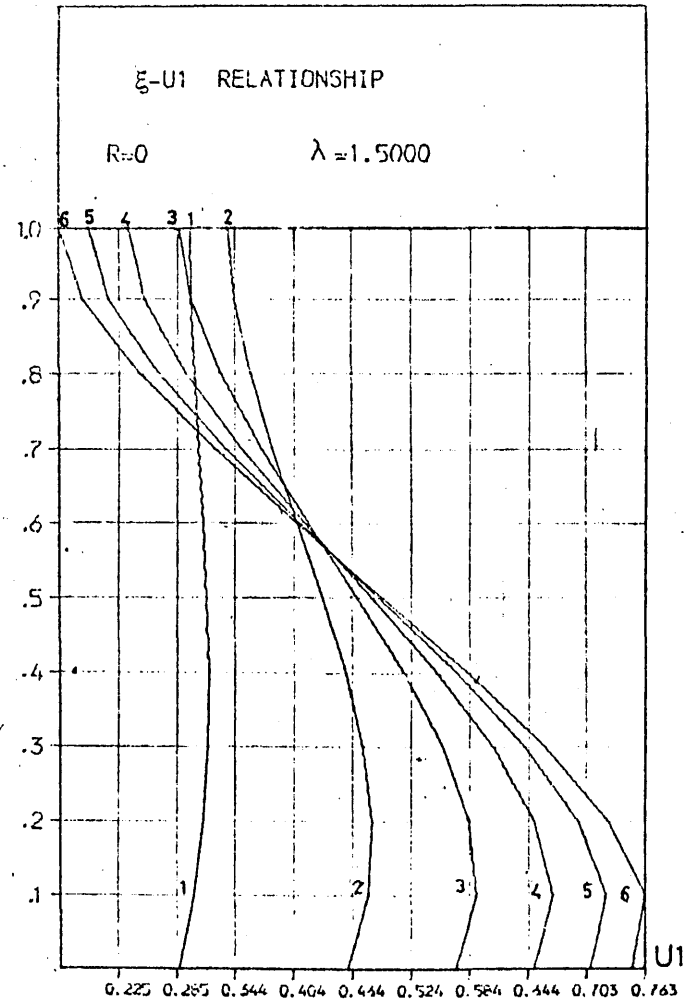
ξ-U1 RELATIONSHIP
R=0
λ =1.5000
1.0
.9
.8
.7
.6
.5
.4
.3
.2
.1
6 5 4 3 1 2
1
2
3
4
5
6
U1
0.225 0.285 0.344 0.404 0.444 0.524 0.584 0.644 0.703 0.763

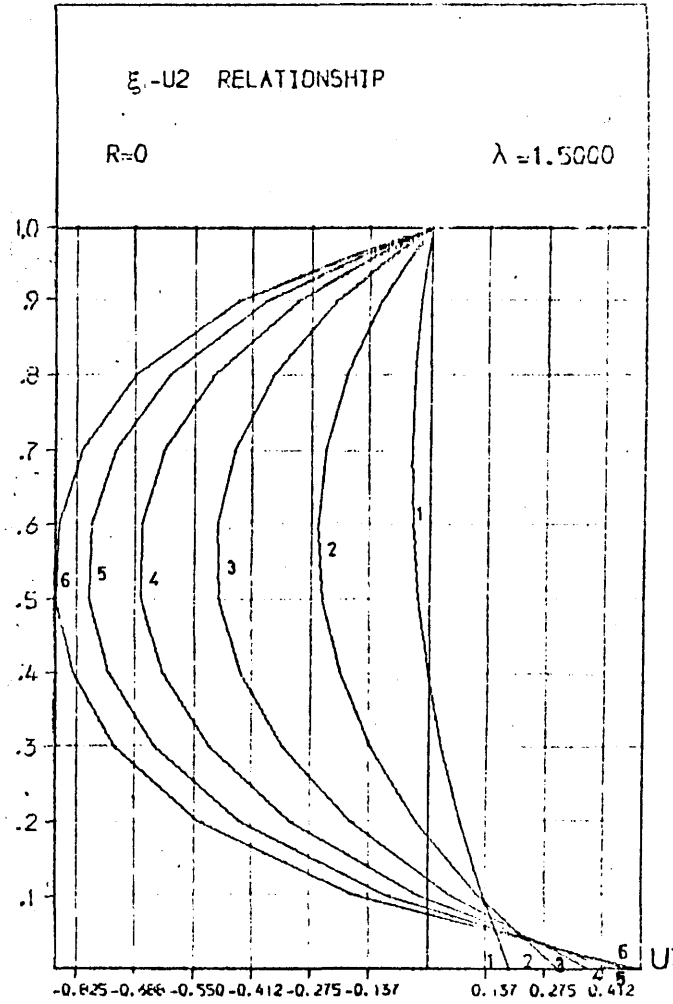
ξ-U2 RELATIONSHIP
R=0
λ =1.5000
1.0
.9
.8
.7
.6
.5
.4
.3
.2
.1
1
2
3
4
5
6
U2
-0.825 -0.688 -0.550 -0.412 -0.275 -0.137
0.137 0.275 0.412

Fig. B.II.3

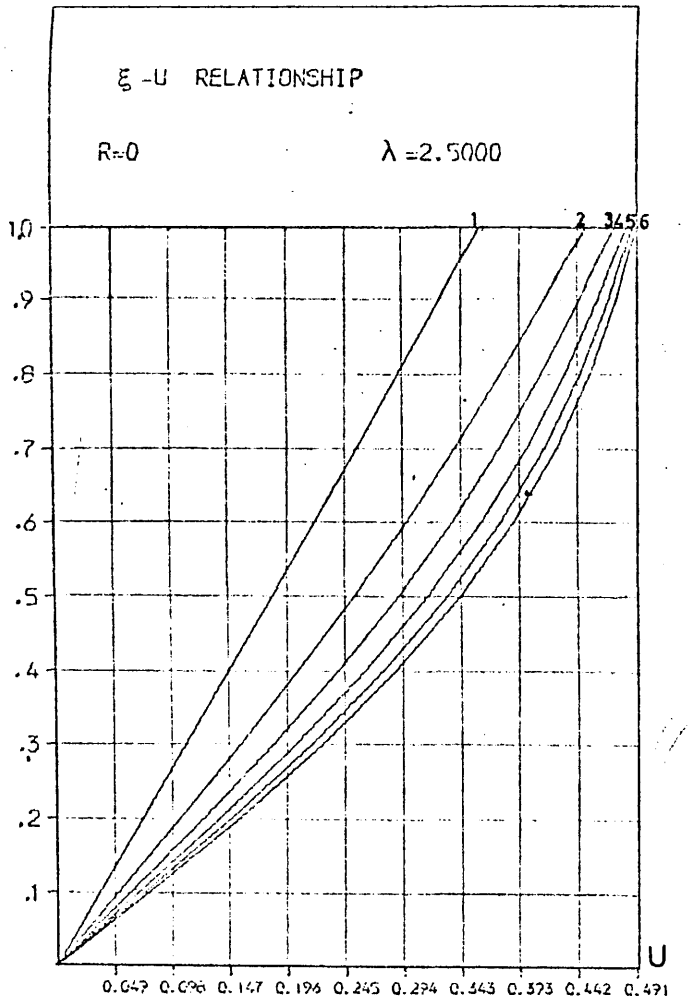
ξ -U RELATIONSHIP
R=0
λ =2.5000
1.0
.9
.8
.7
.6
.5
.4
.3
.2
.1
1
2 3 4 5 6
0.049 0.098 0.147 0.196 0.245 0.294 0.343 0.393 0.442 0.491
U

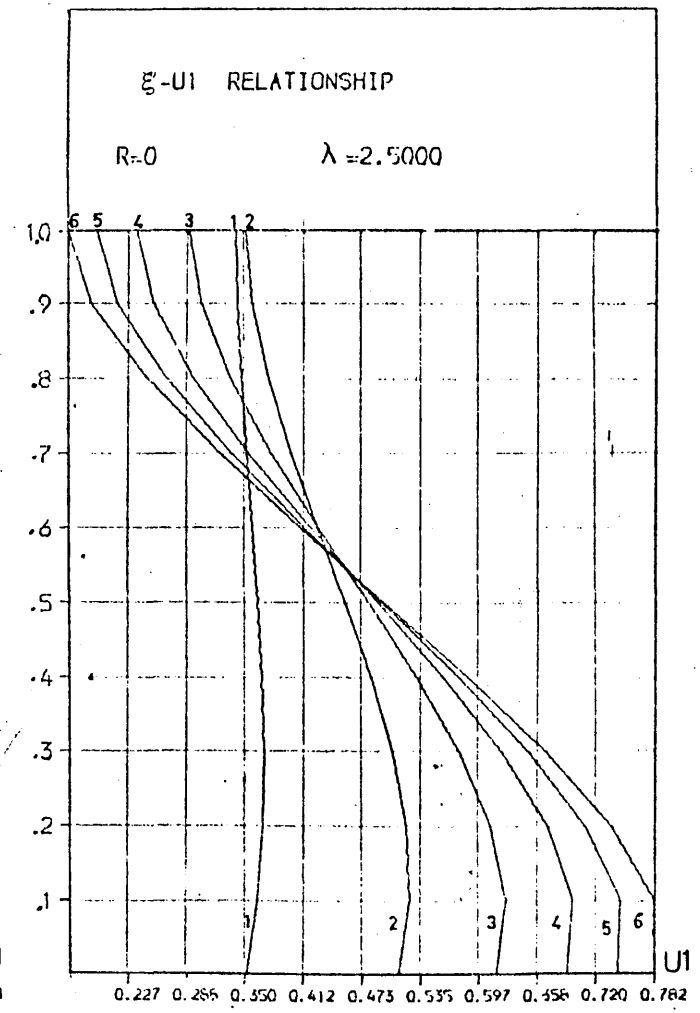
ξ-U1 RELATIONSHIP
R=0
λ =2.5000
1.0
.9
.8
.7
.6
.5
.4
.3
.2
.1
6 5 4 3 1 2
1
2 3 4 5 6
0.227 0.266 0.350 0.412 0.473 0.535 0.597 0.658 0.720 0.782
U1

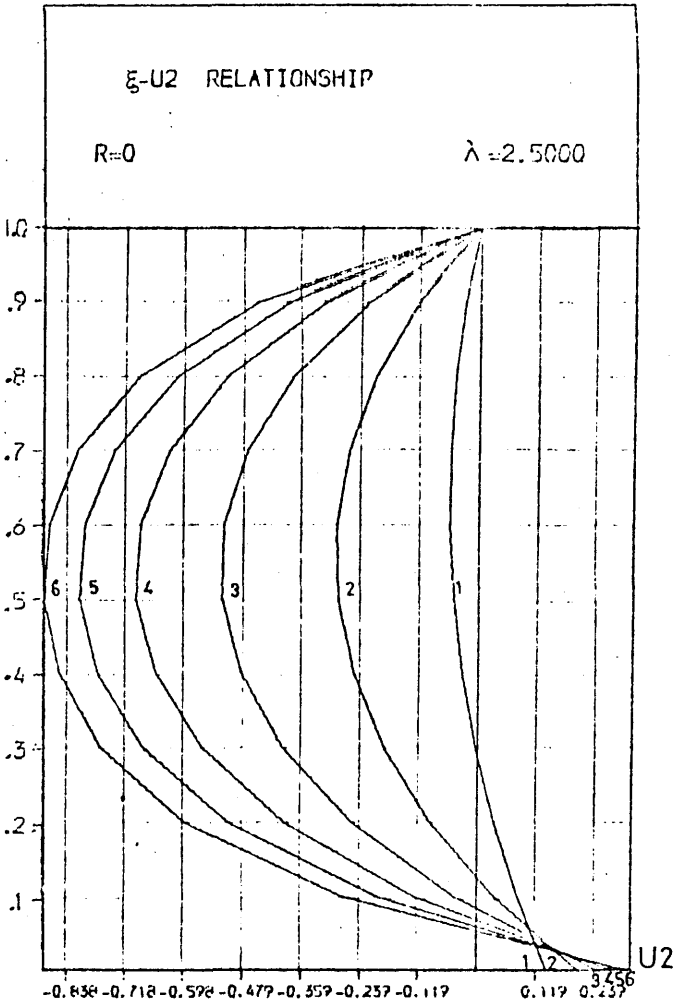
ξ-U2 RELATIONSHIP
R=0
λ =2.5000
1.0
.9
.8
.7
.6
.5
.4
.3
.2
.1
6 5 4 3 2 1
1 2 3 4 5 6
-0.838 -0.718 -0.598 -0.479 -0.359 -0.237 -0.119 0.119 0.237
U2

Fig. B.II.4

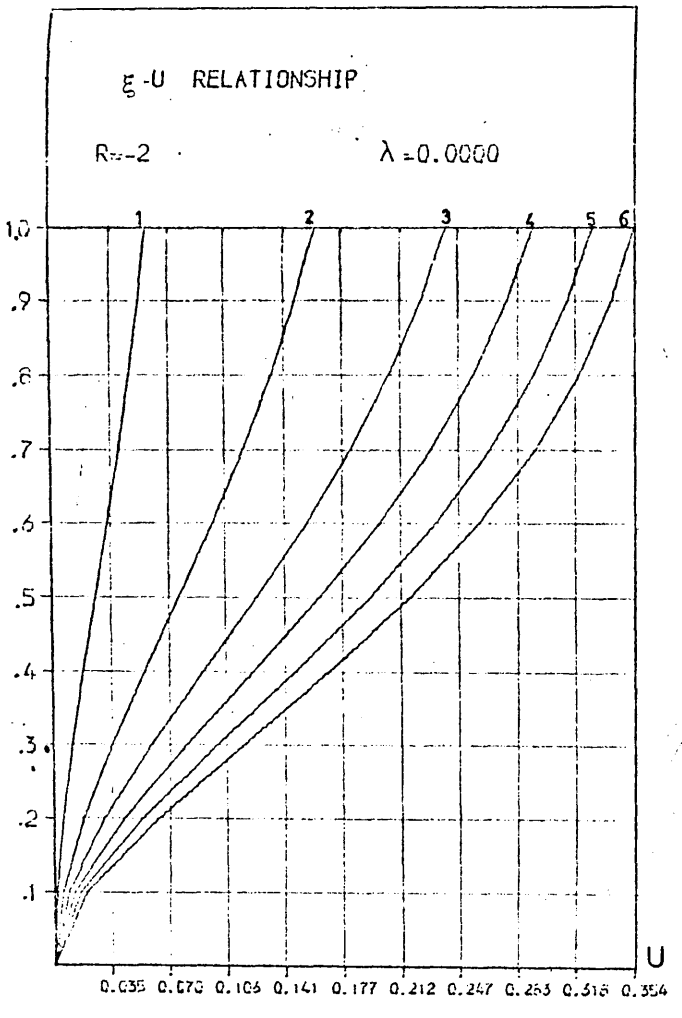
ξ -U RELATIONSHIP
R=-2
λ =0.0000
1.0
.9
.8
.7
.6
.5
.4
.3
.2
.1
1
2
3
4
5
6
U
0.035 0.070 0.106 0.141 0.177 0.212 0.247 0.283 0.318 0.354

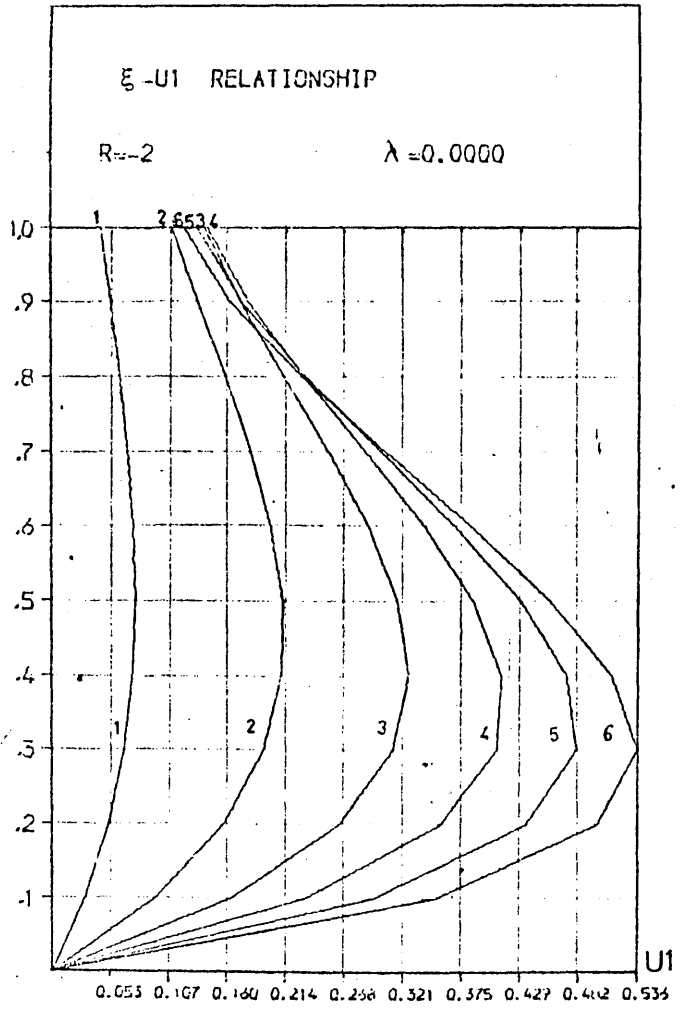
ξ -U1 RELATIONSHIP
R=-2
λ =0.0000
1.0
.9
.8
.7
.6
.5
.4
.3
.2
.1
1
2
3
4
5
6
U1
0.053 0.107 0.160 0.214 0.268 0.321 0.375 0.427 0.482 0.536

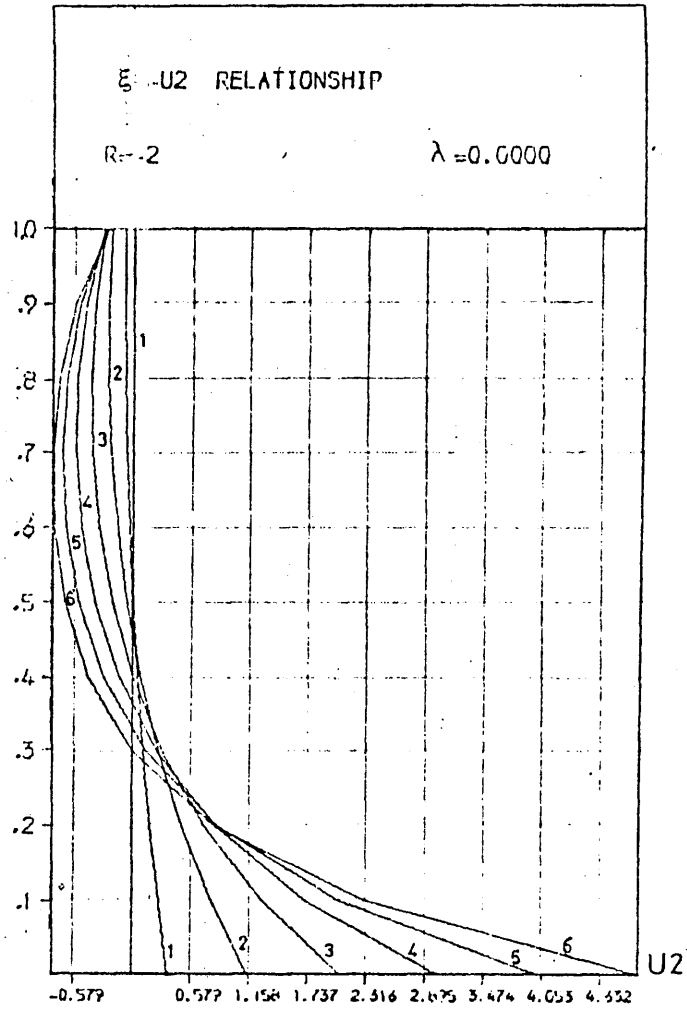
ξ -U2 RELATIONSHIP
R=-2
λ =0.0000
1.0
.9
.8
.7
.6
.5
.4
.3
.2
.1
1
2
3
4
5
6
U2
-0.579
0.577 1.158 1.737 2.316 2.895 3.474 4.053 4.632

Fig. B.II.5

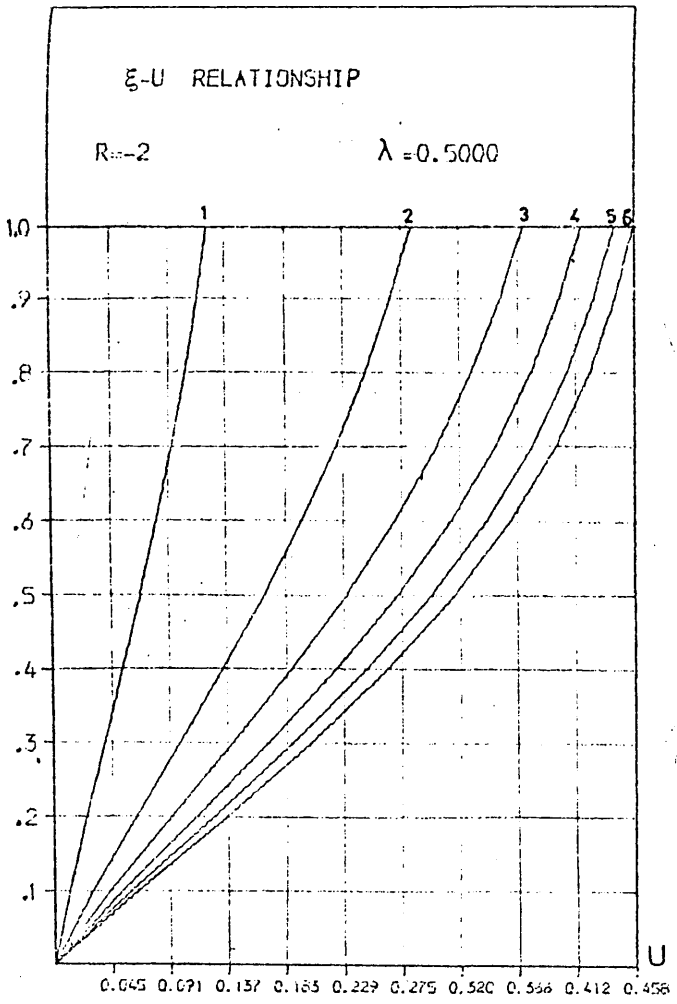
ξ-U RELATIONSHIP
R=-2
λ =0.5000
1.0
.9
.8
.7
.6
.5
.4
.3
.2
.1
1
2
3
4
5
6
U
0.045 0.091 0.137 0.183 0.229 0.275 0.320 0.366 0.412 0.458

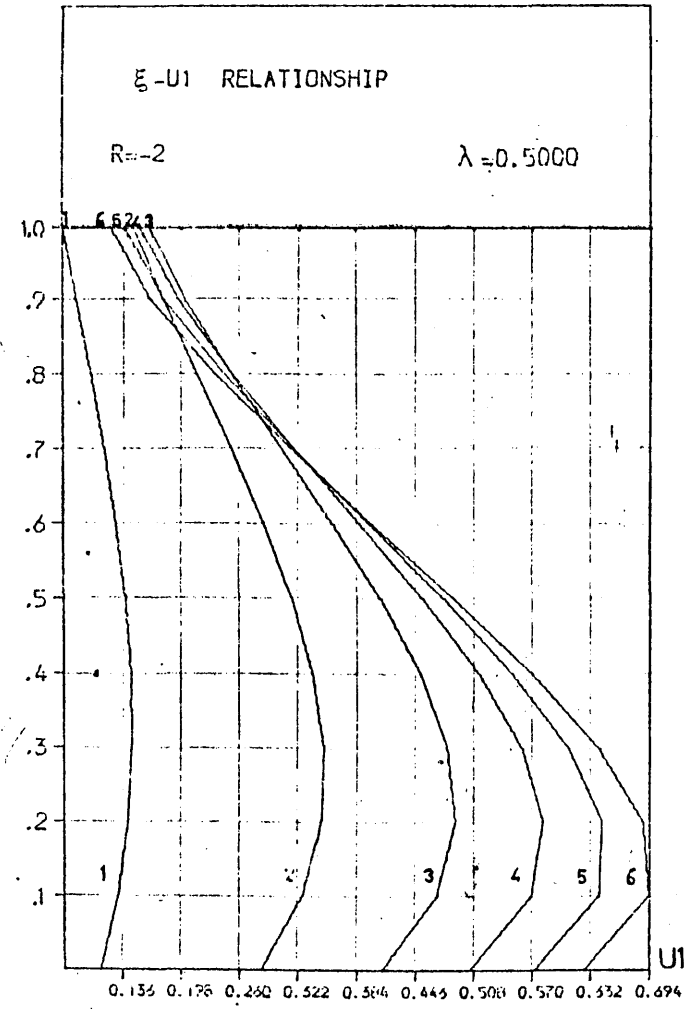
ξ-U1 RELATIONSHIP
R=-2
λ =0.5000
1.0
.9
.8
.7
.6
.5
.4
.3
.2
.1
1
3
4
5
6
U1
0.136 0.176 0.260 0.322 0.384 0.446 0.508 0.570 0.632 0.694

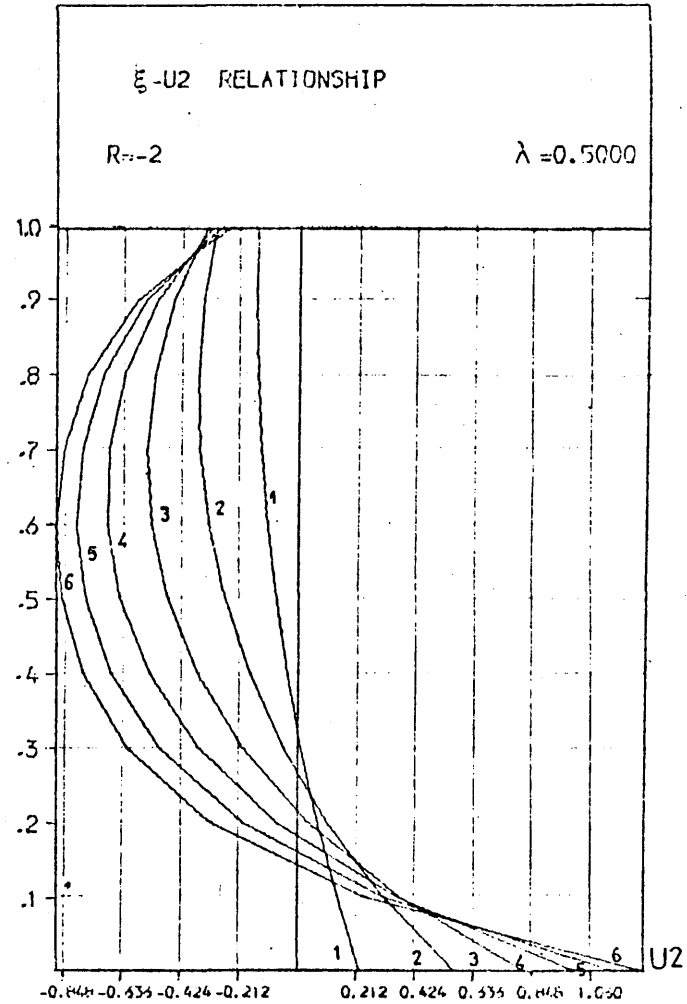
ξ-U2 RELATIONSHIP
R=-2
λ =0.5000
1.0
.9
.8
.7
.6
.5
.4
.3
.2
.1
1
2
3
4
5
6
U2
-0.848 -0.636 -0.424 -0.212
0.212 0.424 0.636 0.848 1.060

Fig. B.II.6

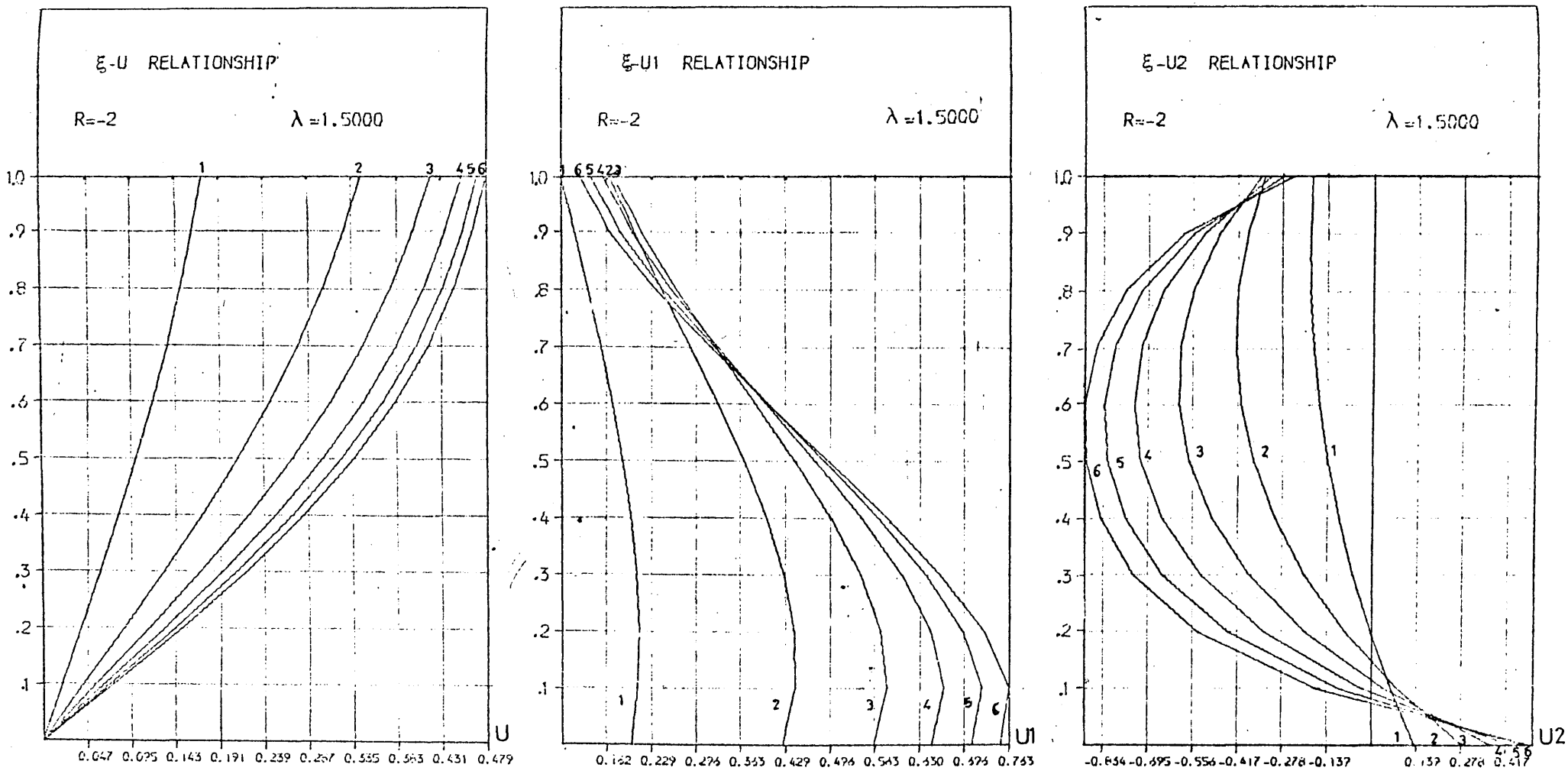
ξ-U RELATIONSHIP
R=-2
λ =1.5000
1
2
3
4
5
6
1.0
.9
.8
.7
.6
.5
.4
.3
.2
.1
U
0.047 0.095 0.143 0.191 0.239 0.287 0.335 0.383 0.431 0.479
ξ-U1 RELATIONSHIP
R=-2
λ =1.5000
U1
0.162 0.229 0.296 0.363 0.429 0.496 0.563 0.630 0.696 0.763
ξ-U2 RELATIONSHIP
R=-2
λ =1.5000
U2
-0.834 -0.695 -0.556 -0.417 -0.278 -0.137
0.137 0.278 0.417

Fig. B.II.7

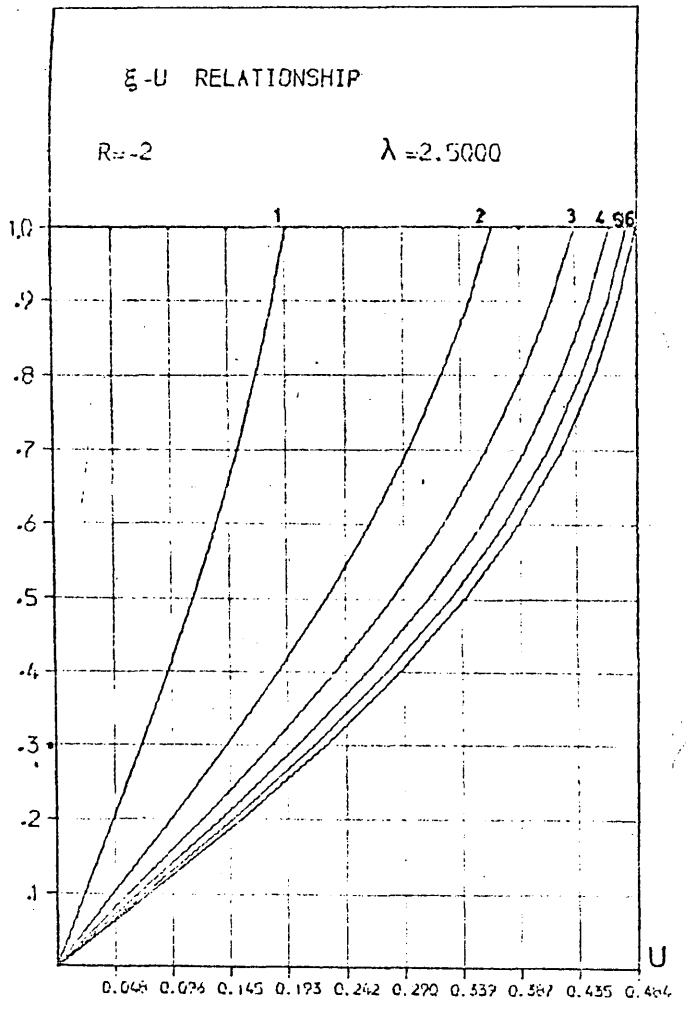
ξ-U RELATIONSHIP
R=-2
λ =2.5000
1.0
.9
.8
.7
.6
.5
.4
.3
.2
.1
1
2
3
4
5
6
U
0.048 0.096 0.145 0.193 0.242 0.290 0.339 0.387 0.435 0.484

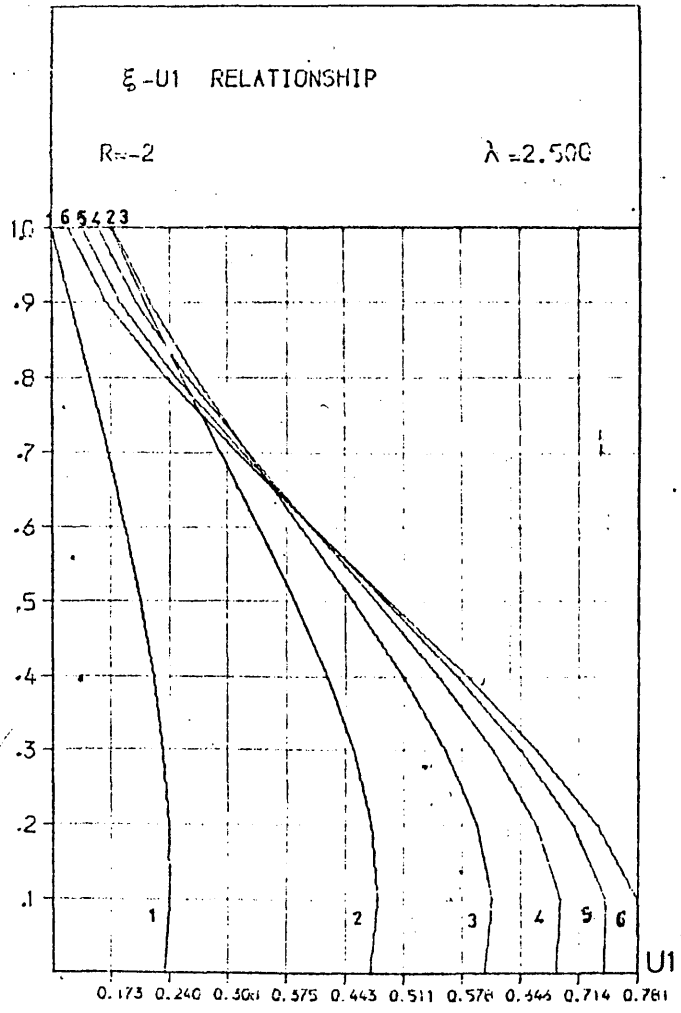
ξ-U1 RELATIONSHIP
R=-2
λ =2.500
1.0
.9
.8
.7
.6
.5
.4
.3
.2
.1
6 5 4 2 3
1
2
3
4
5
6
U1
0.173 0.240 0.308 0.375 0.443 0.511 0.578 0.646 0.714 0.781

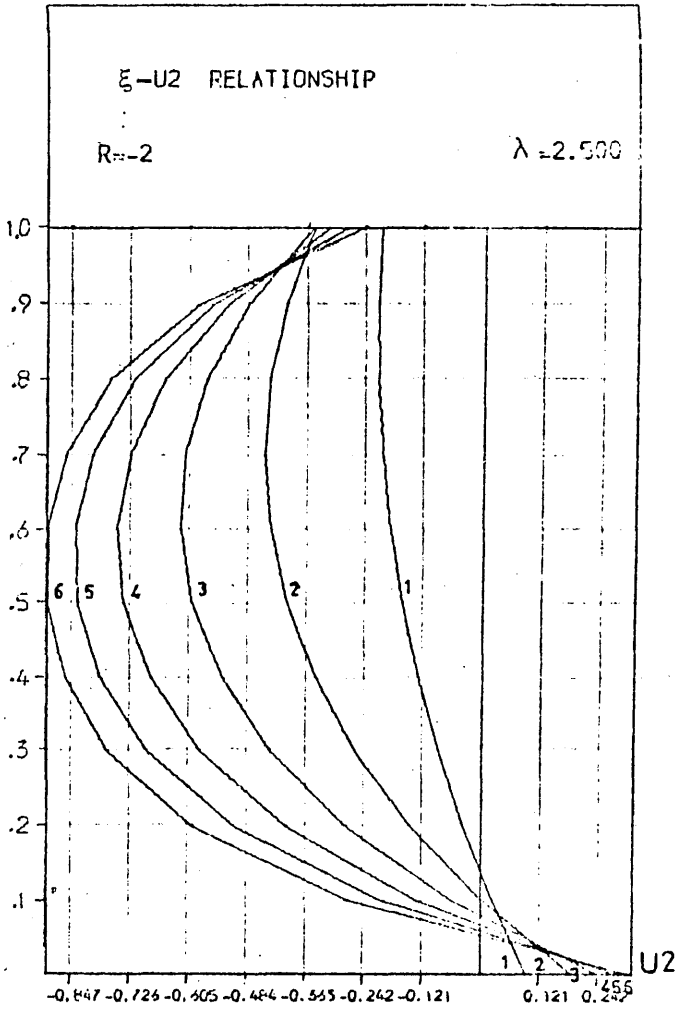
ξ-U2 RELATIONSHIP
R=-2
λ =2.500
1.0
.9
.8
.7
.6
.5
.4
.3
.2
.1
6
5
4
3
2
1
1
2
3
4
5
6
U2
-0.847 -0.726 -0.605 -0.484 -0.363 -0.242 -0.121
0.121 0.242

Fig. B.II.8

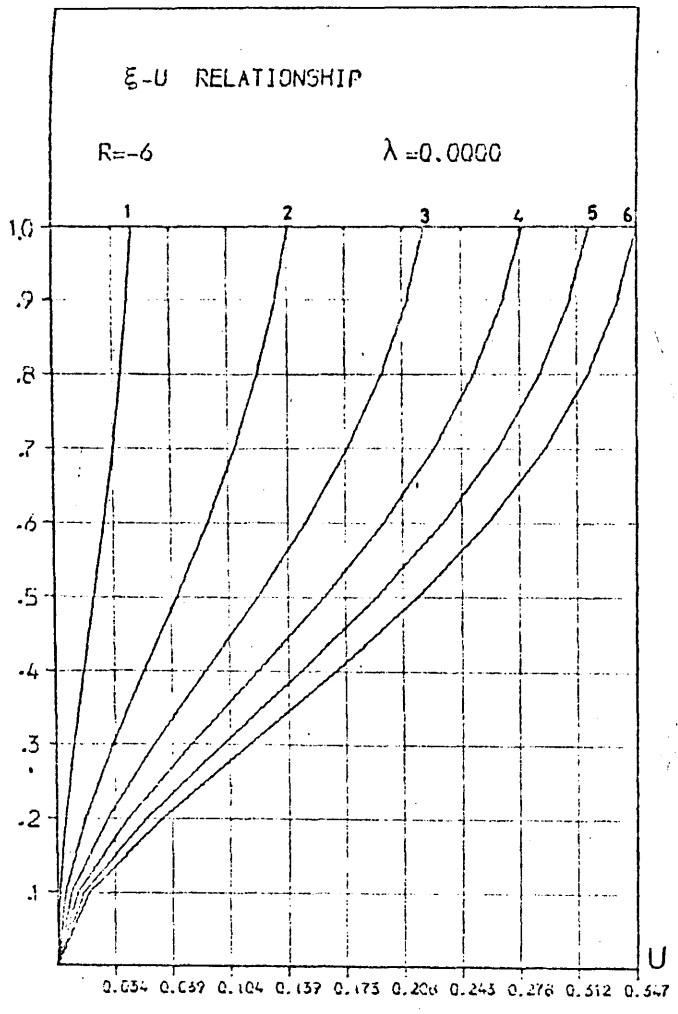
ξ-U RELATIONSHIP
R=-6
λ =0.0000
1
2
3
4
5
6
1.0
.9
.8
.7
.6
.5
.4
.3
.2
.1
U
0.054 0.079 0.104 0.129 0.153 0.178 0.203 0.228 0.252 0.277

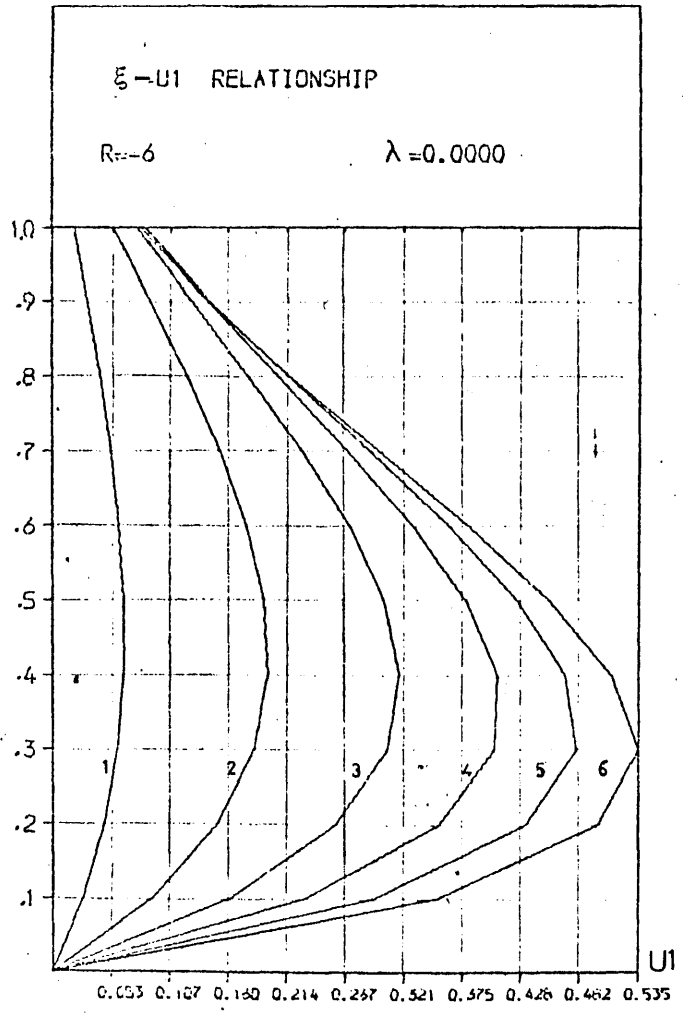
ξ-U1 RELATIONSHIP
R=-6
λ =0.0000
1.0
.9
.8
.7
.6
.5
.4
.3
.2
.1
1
2
3
4
5
6
U1
0.053 0.107 0.160 0.214 0.267 0.321 0.375 0.428 0.482 0.535

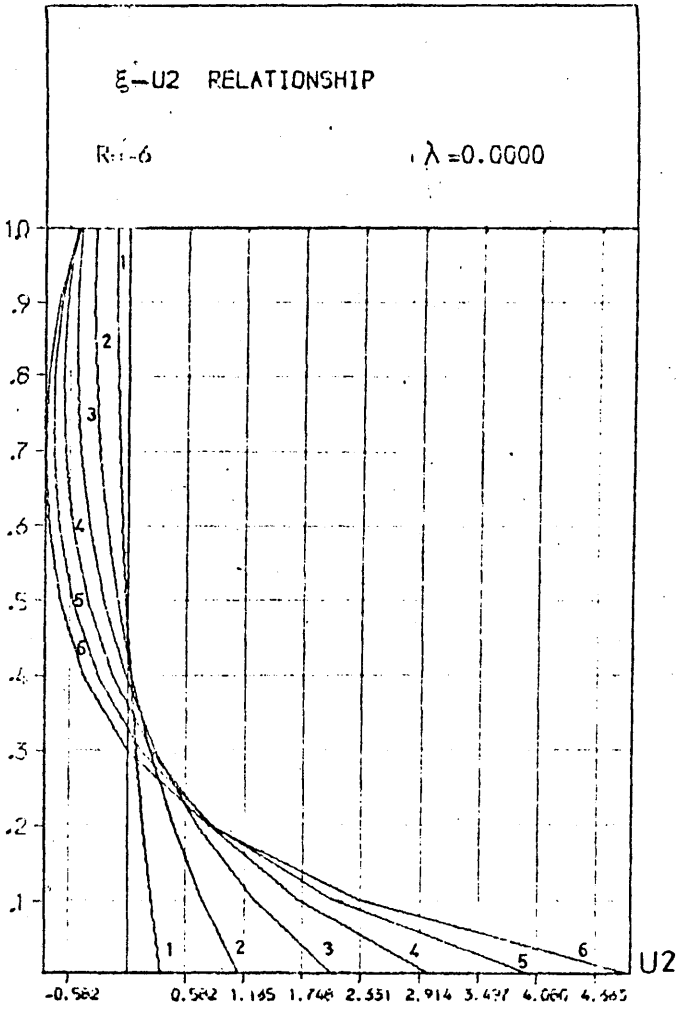
ξ-U2 RELATIONSHIP
R=-6
λ =0.0000
1.0
.9
.8
.7
.6
.5
.4
.3
.2
.1
1
2
3
4
5
6
U2
-0.582
0.582 1.165 1.748 2.331 2.914 3.497 4.080 4.663

Fig. B.II.9

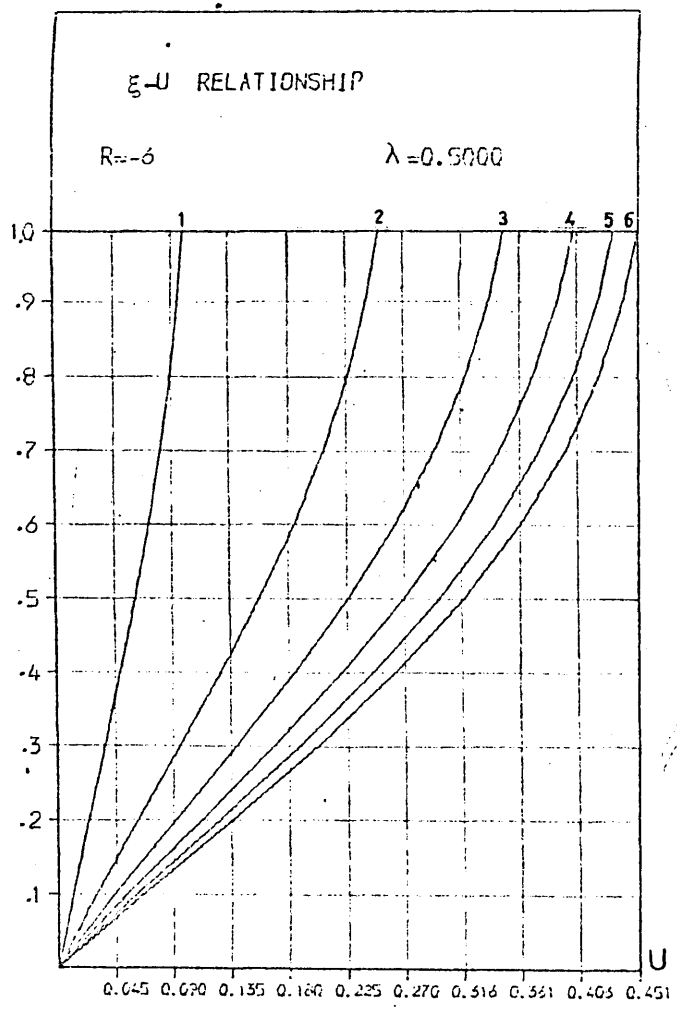
ξ-U RELATIONSHIP
R=-6
λ =0.5000
1
2
3
4
5
6
1.0
.9
.8
.7
.6
.5
.4
.3
.2
.1
U
0.045 0.090 0.135 0.180 0.225 0.270 0.316 0.361 0.406 0.451

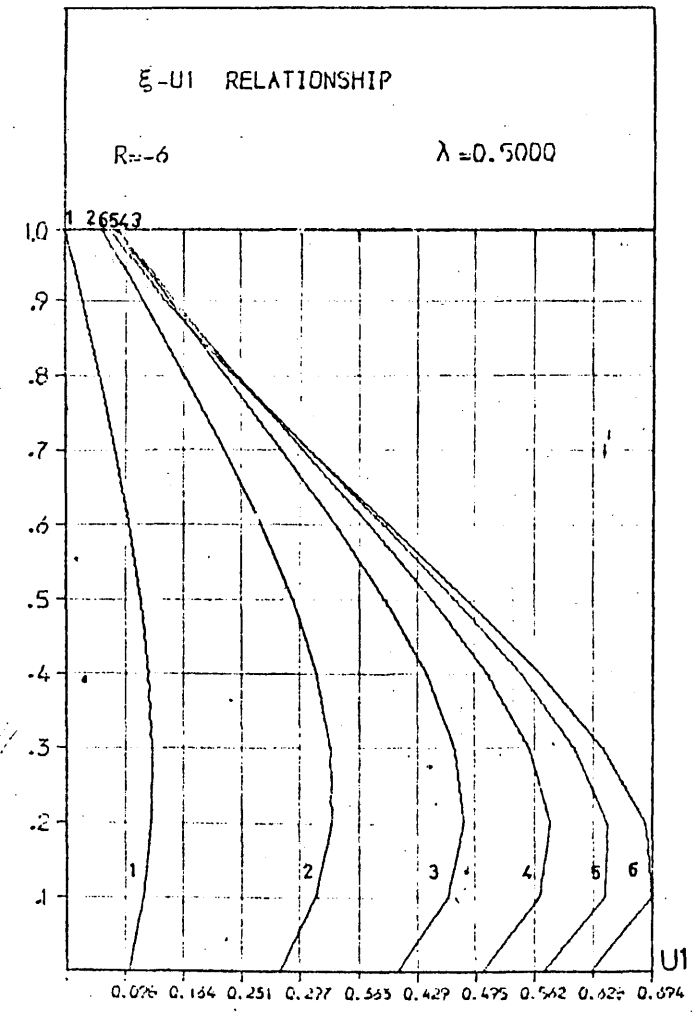
ξ-U1 RELATIONSHIP
R=-6
λ =0.5000
1 2 6 5 4 3
1.0
.9
.8
.7
.6
.5
.4
.3
.2
.1
U1
0.026 0.164 0.251 0.277 0.365 0.429 0.495 0.562 0.629 0.674

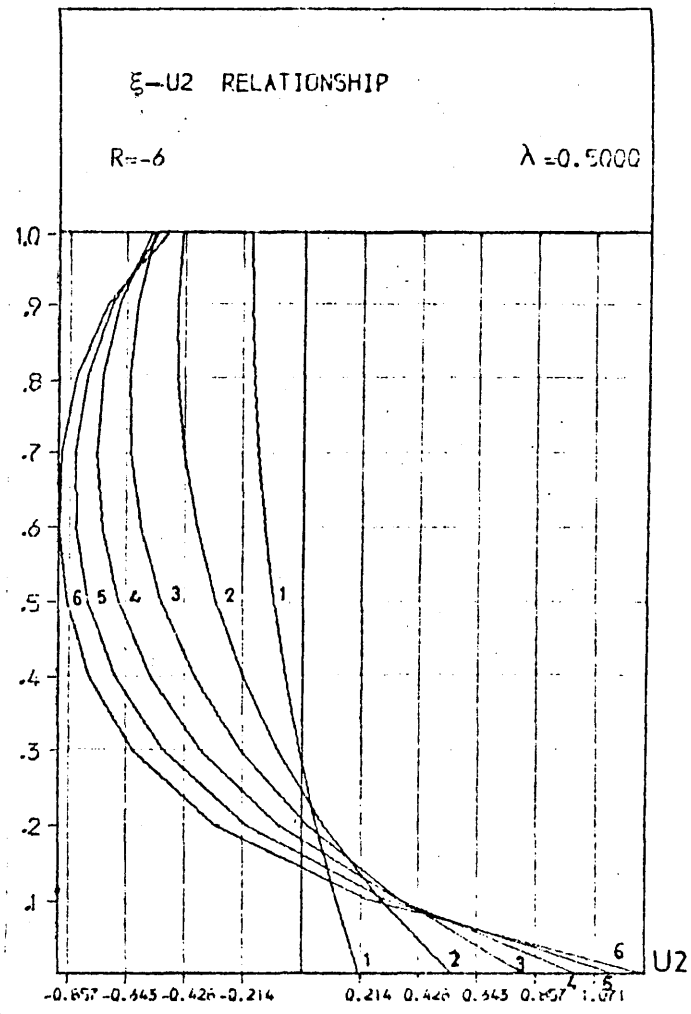
ξ-U2 RELATIONSHIP
R=-6
λ =0.5000
6 5 4 3 2 1
1.0
.9
.8
.7
.6
.5
.4
.3
.2
.1
U2
-0.857 -0.645 -0.426 -0.214
0.214 0.426 0.643 0.857 1.071

Fig. B.II.10

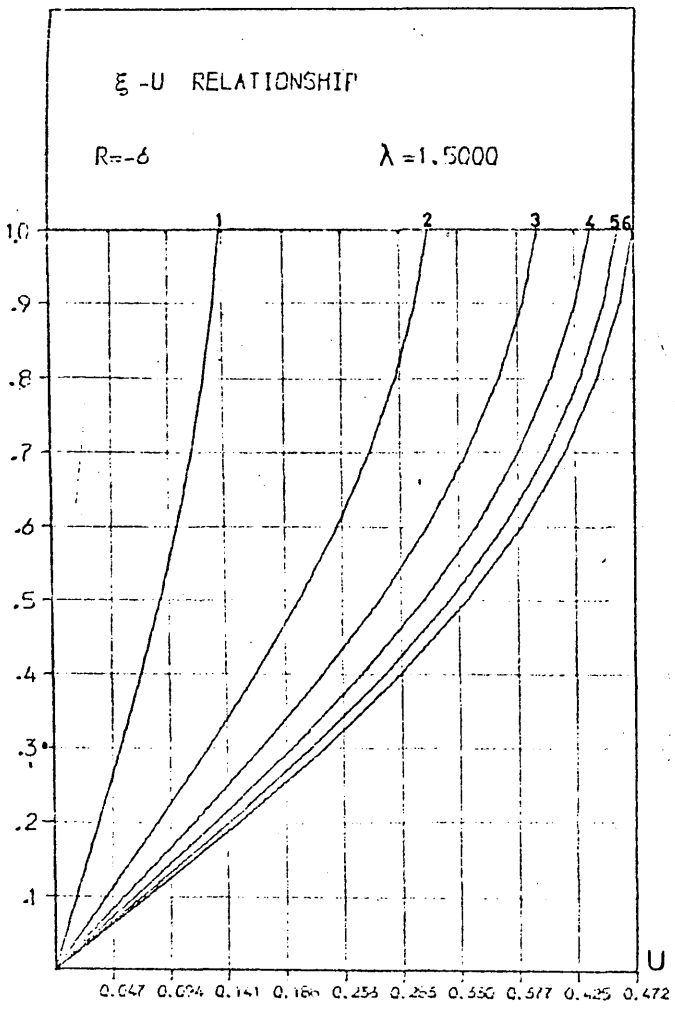
ξ -U RELATIONSHIP
R=-6
λ =1.5000
1.0
.9
.8
.7
.6
.5
.4
.3
.2
.1
1
2
3
4
5
6
U
0.047 0.094 0.141 0.188 0.236 0.283 0.330 0.377 0.425 0.472

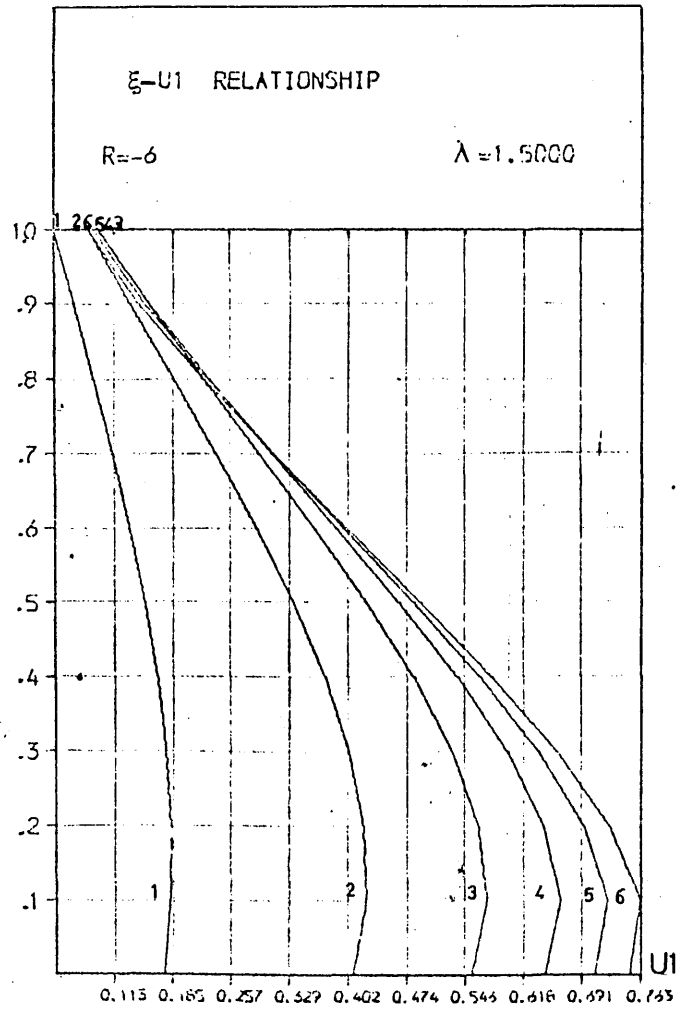
ξ-U1 RELATIONSHIP
R=-6
λ =1.5000
1.0
.9
.8
.7
.6
.5
.4
.3
.2
.1
1 2 6 5 4 3
1
2
3
4
5
6
U1
0.115 0.185 0.257 0.329 0.402 0.474 0.546 0.618 0.691 0.763

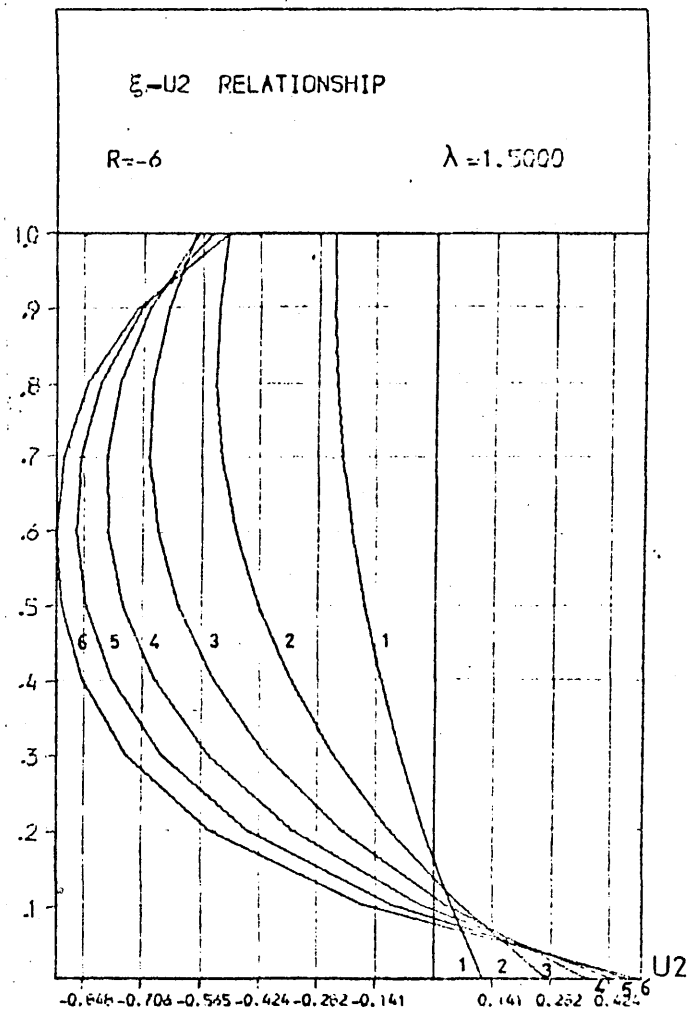
ξ-U2 RELATIONSHIP
R=-6
λ =1.5000
1.0
.9
.8
.7
.6
.5
.4
.3
.2
.1
6
5
4
3
2
1
U2
-0.848 -0.706 -0.565 -0.424 -0.282 -0.141
0.141 0.282 0.424

Fig. B.II.11

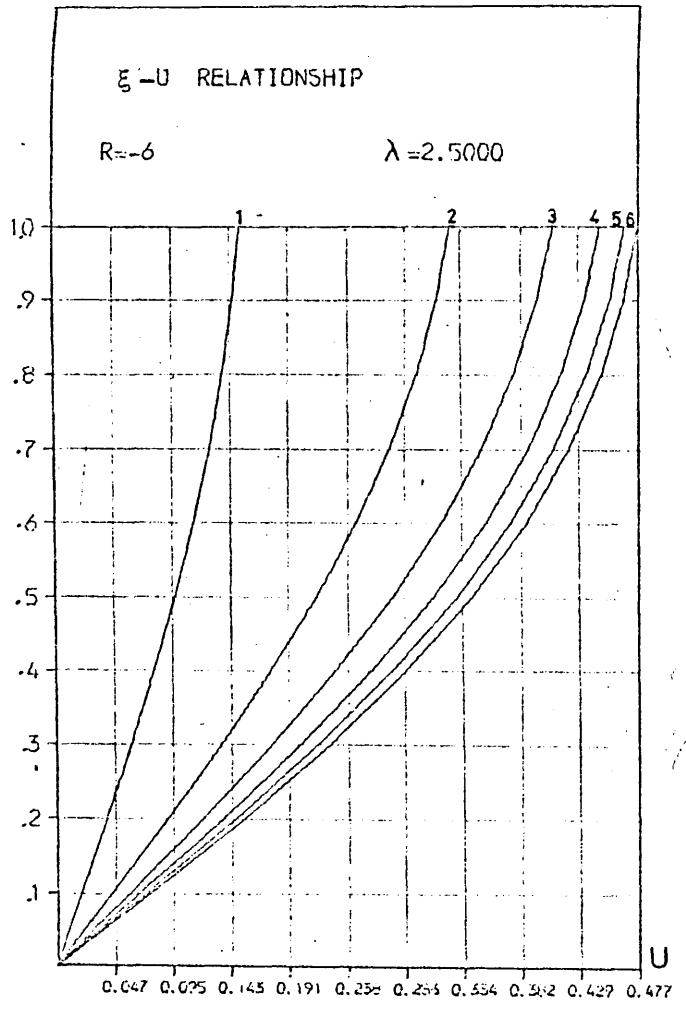
ξ –U RELATIONSHIP
R=-6
λ =2.5000
1
2
3
4
5
6
1.0
.9
.8
.7
.6
.5
.4
.3
.2
.1
U
0.047 0.095 0.145 0.191 0.25

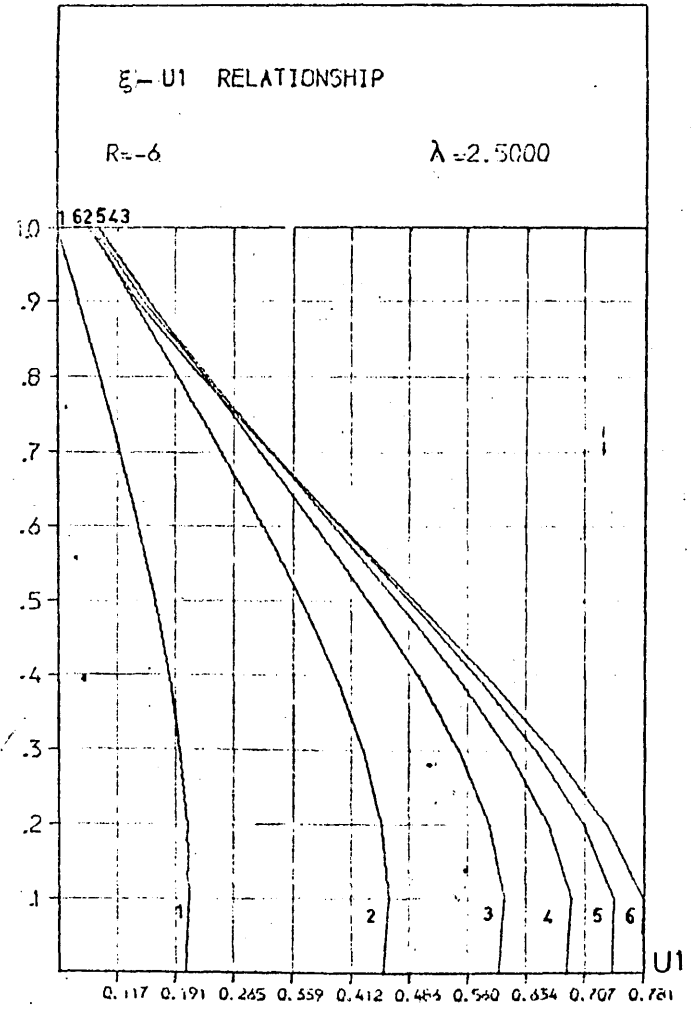
ξ– U1 RELATIONSHIP
R=-6
λ =2.5000
1 6 2 5 4 3
1.0
.9
.8
.7
.6
.5
.4
.3
.2
.1
1
2
3
4
5
6
U1
0.117 0.191 0.265 0.559 0.412 0.486 0.560 0.634 0.707 0.781

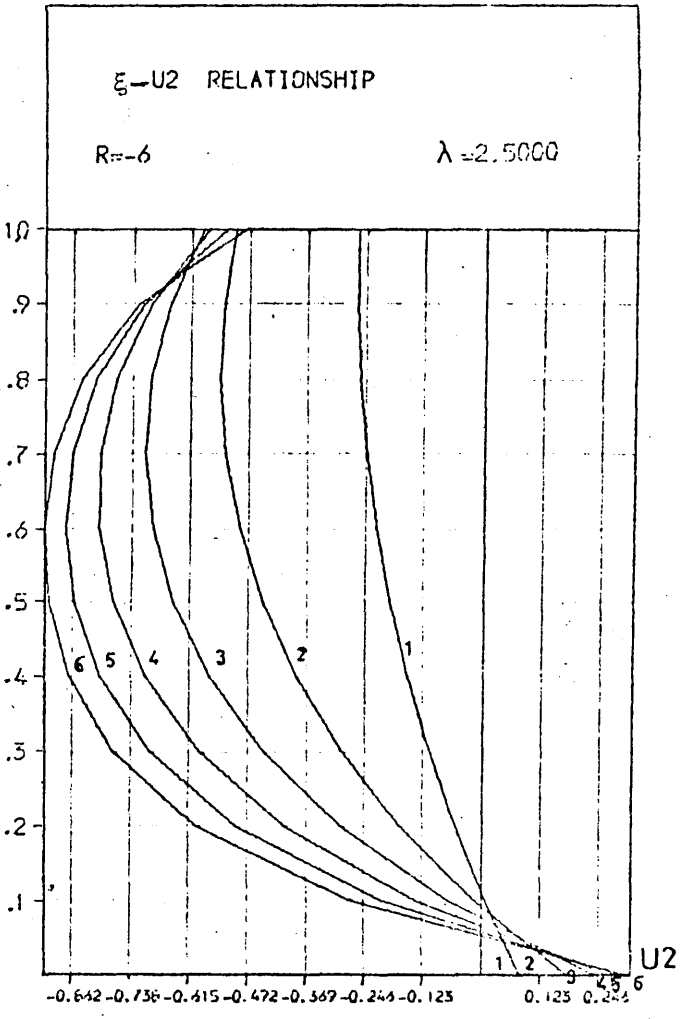
ξ–U2 RELATIONSHIP
R=-6
λ =2.5000
1.0
.9
.8
.7
.6
.5
.4
.3
.2
.1
6
5
4
3
2
1
1
2
3
4
5
6
U2
-0.642 -0.736 -0.615 -0.472 -0.367 -0.244 -0.123
0.125

Fig. B.II.12

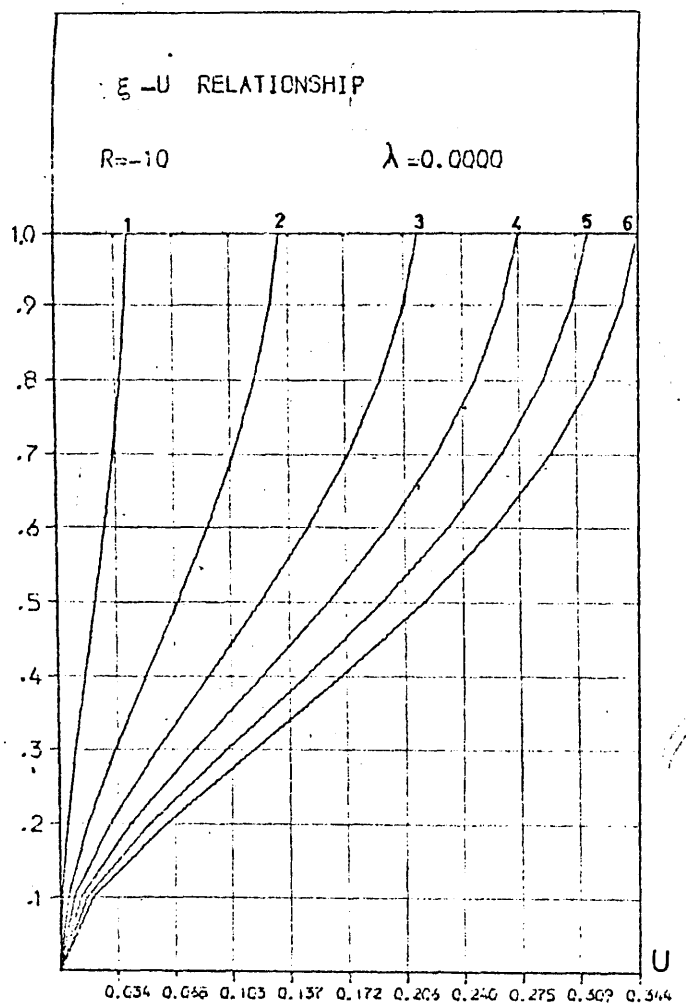
ξ –U RELATIONSHIP
R=-10
λ =0.0000
1
2
3
4
5
6
1.0
.9
.8
.7
.6
.5
.4
.3
.2
.1
U
0.034 0.068 0.103 0.137 0.172 0.206 0.240 0.275 0.309 0.344

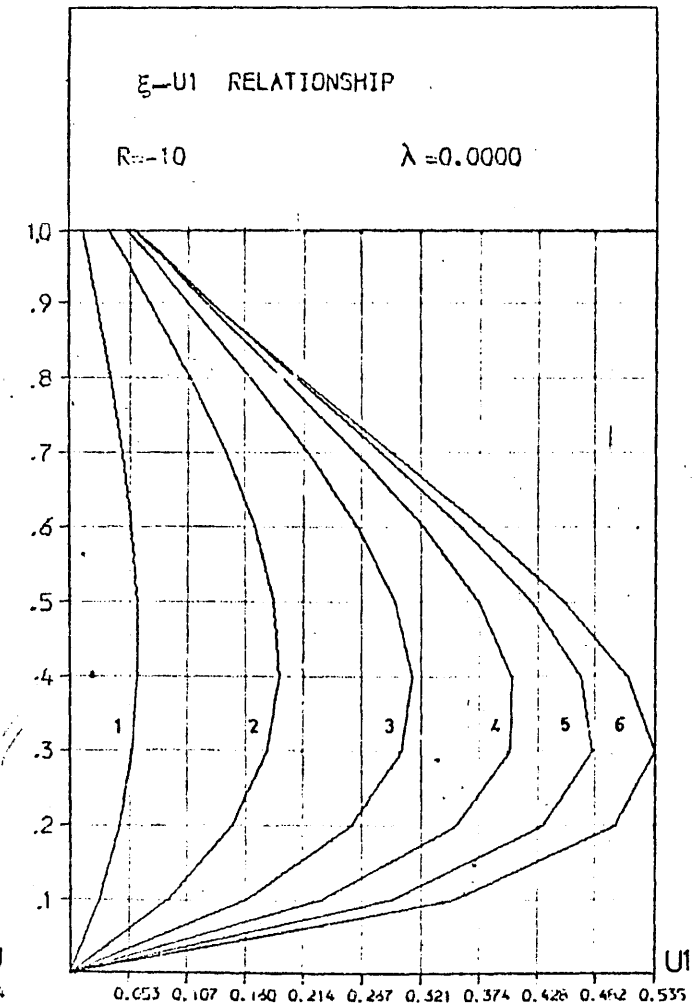
ξ–U1 RELATIONSHIP
R=-10
λ =0.0000
1
2
3
4
5
6
1.0
.9
.8
.7
.6
.5
.4
.3
.2
.1
U1
0.053 0.107 0.160 0.214 0.267 0.321 0.374 0.428 0.482 0.535

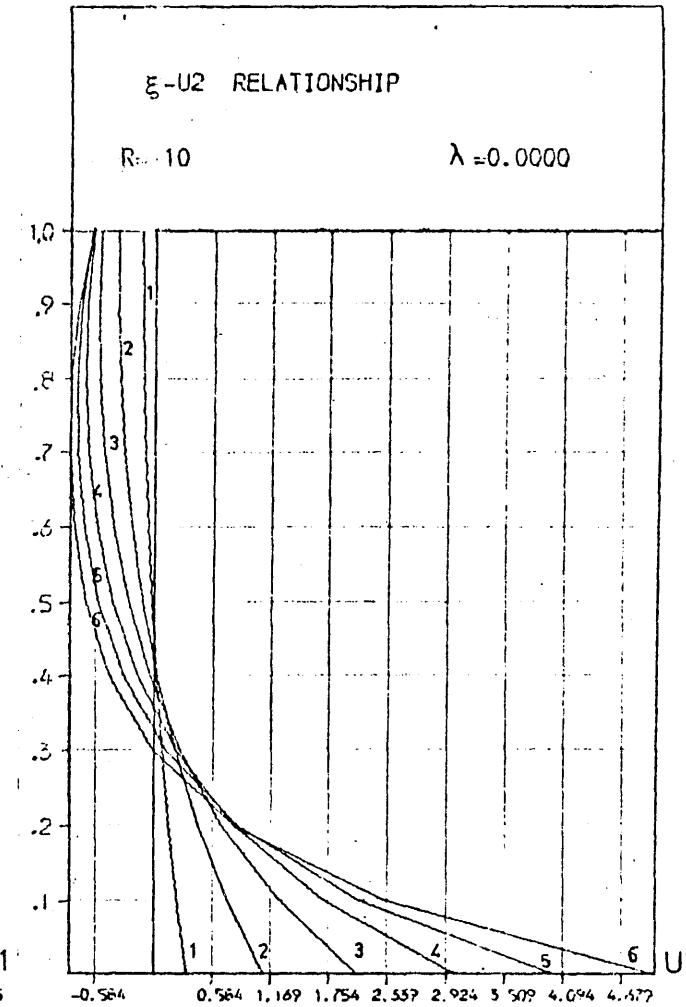
ξ-U2 RELATIONSHIP
R=-10
λ =0.0000
1
2
3
4
5
6
1.0
.9
.8
.7
.6
.5
.4
.3
.2
.1
U2
-0.564
0.564 1.169 1.754 2.339 2.924 3.509 4.094 4.679

Fig. B.II.13

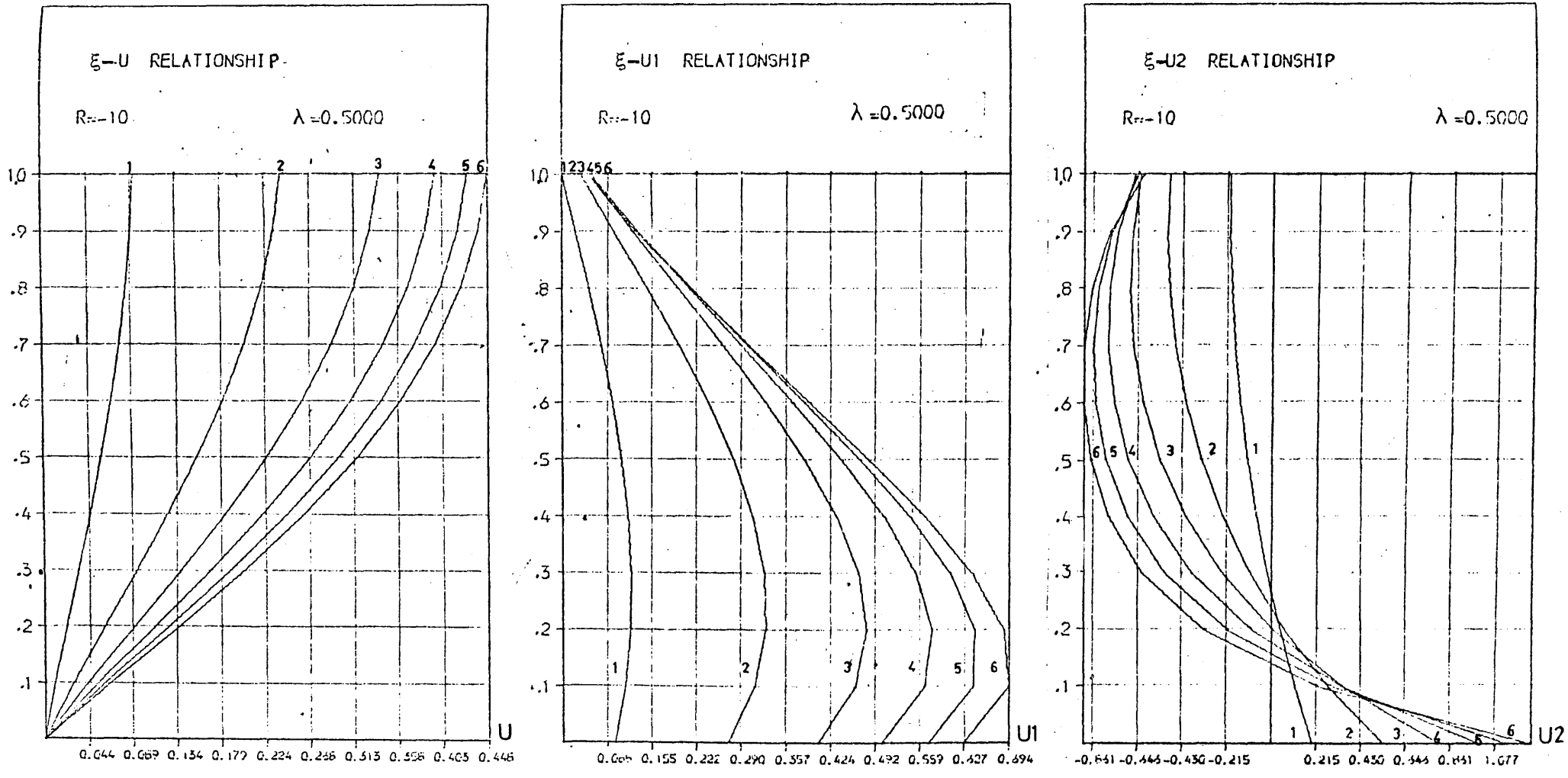
ξ–U RELATIONSHIP
R=–10
λ =0.5000
1
2
3
4
5 6
1.0
.9
.8
.7
.6
.5
.4
.3
.2
.1
U
0.044 0.089 0.134 0.179 0.224 0.268 0.313 0.358 0.403 0.448
ξ–U1 RELATIONSHIP
R=–10
λ =0.5000
123456
1
2
3
4
5
6
U1
0.0eb 0.155 0.222 0.290 0.357 0.424 0.492 0.559 0.627 0.694
ξ–U2 RELATIONSHIP
R=–10
λ =0.5000
6 5 4 3 2 1
1
2
3
6
5
6
U2
-0.641 -0.646 -0.430 -0.215
0.215 0.430 0.646 0.861 1.077

Fig. B.II.14

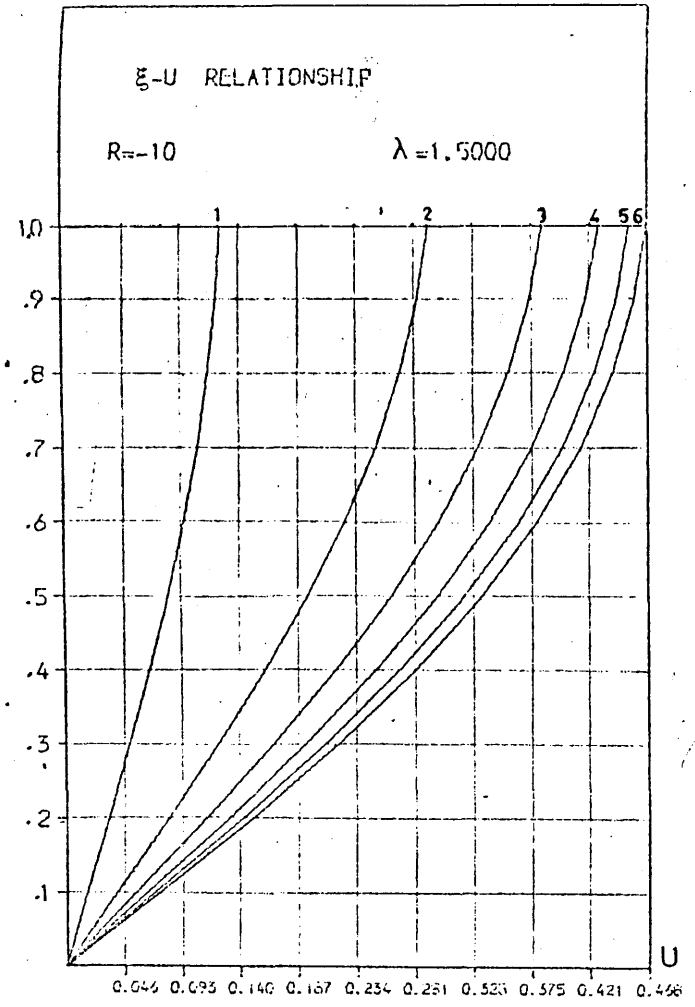
ξ-U RELATIONSHIP
R=-10
λ =1.5000
1
2
3
4
5
6
1.0
.9
.8
.7
.6
.5
.4
.3
.2
.1
U
0.044 0.093 0.140 0.187 0.234 0.281 0.328 0.375 0.421 0.468

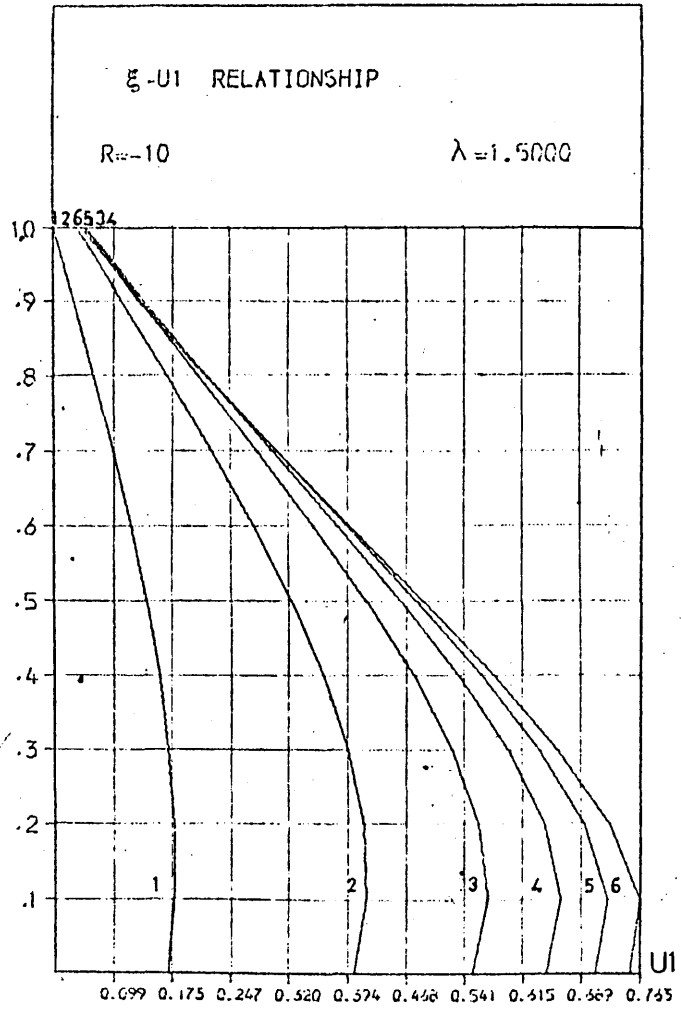
ξ-U1 RELATIONSHIP
R=-10
λ =1.5000
1
2
3
4
5
6
1.0
.9
.8
.7
.6
.5
.4
.3
.2
.1
U1
0.099 0.175 0.247 0.320 0.394 0.468 0.541 0.615 0.689 0.763

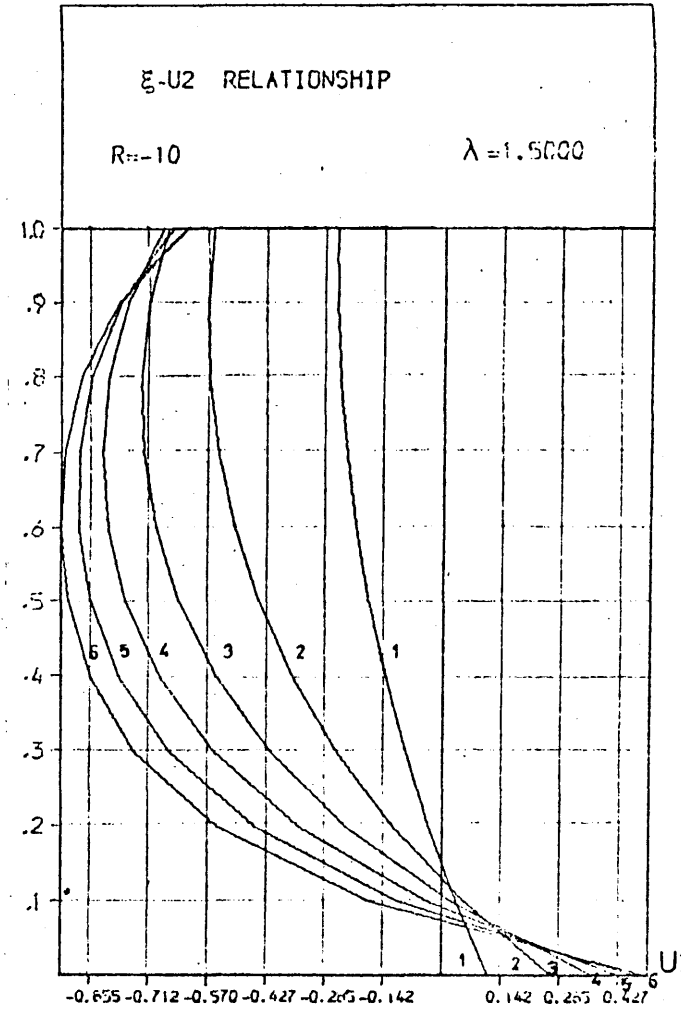
ξ-U2 RELATIONSHIP
R=-10
λ =1.5000
6
5
4
3
2
1
1.0
.9
.8
.7
.6
.5
.4
.3
.2
.1
U2
-0.655 -0.712 -0.570 -0.427 -0.285 -0.142 0.142 0.285 0.427

Fig. B.II.15

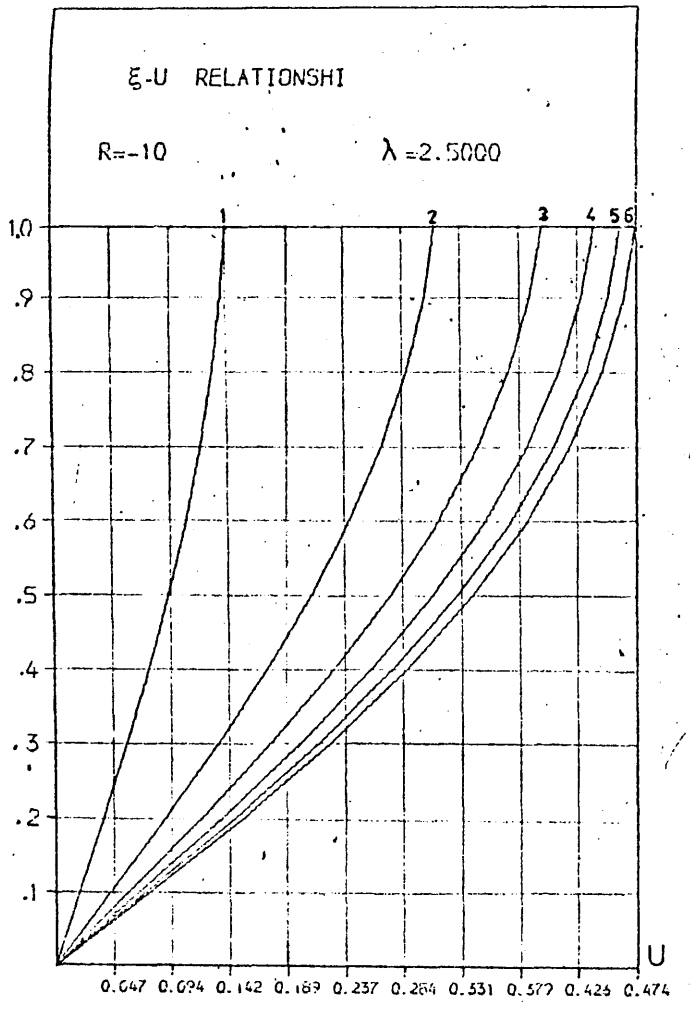
ξ-U RELATIONSHI
R=-10
λ =2.5000
1.0
.9
.8
.7
.6
.5
.4
.3
.2
.1
1
2
3
4
5
6
U
0.047 0.094 0.142 0.189 0.237 0.284 0.331 0.379 0.426 0.474

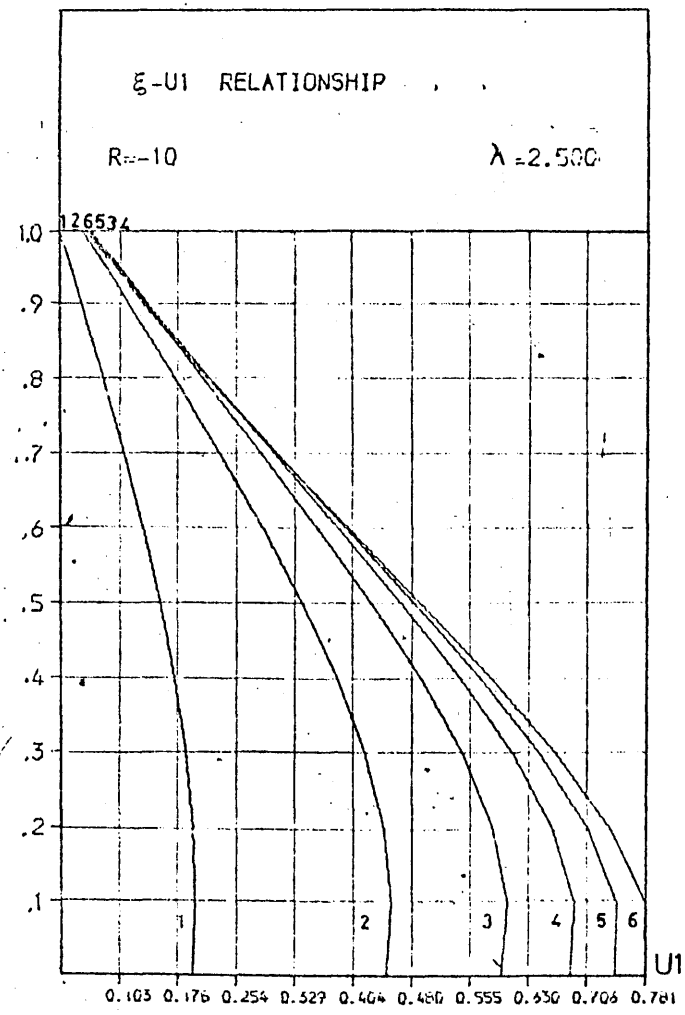
ξ-U1 RELATIONSHIP
R=-10
λ =2.500
1.0
.9
.8
.7
.6
.5
.4
.3
.2
.1
1
2
3
4
5
6
U1
0.103 0.176 0.254 0.329 0.404 0.480 0.555 0.630 0.706 0.781

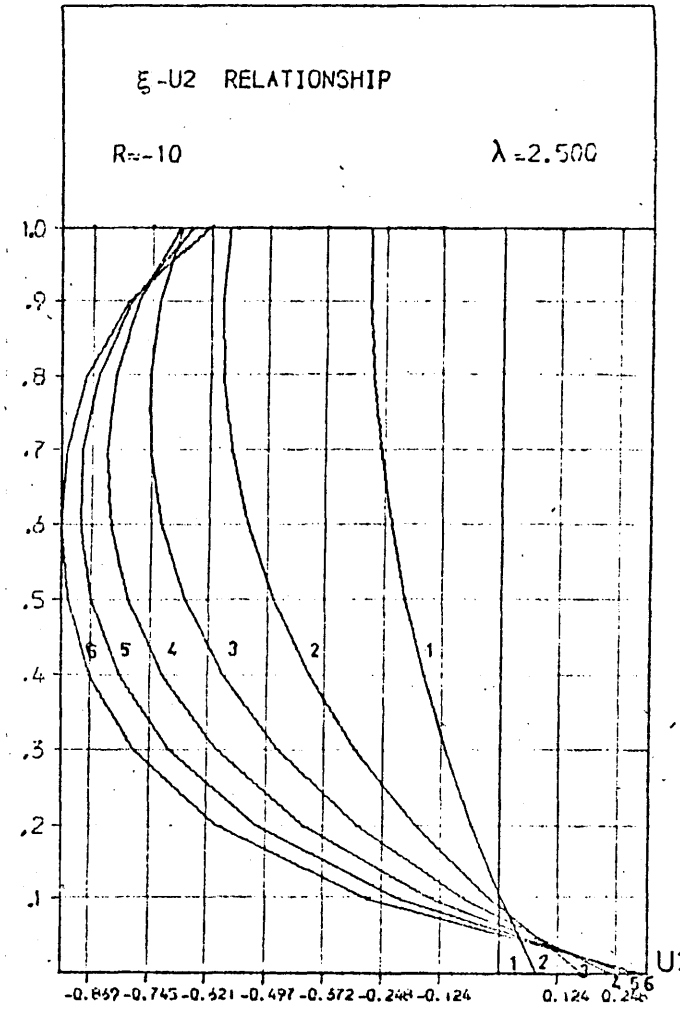
ξ-U2 RELATIONSHIP
R=-10
λ =2.500
1.0
.9
.8
.7
.6
.5
.4
.3
.2
.1
6
5
4
3
2
1
U2
-0.869 -0.745 -0.621 -0.497 -0.372 -0.248 -0.124
0.124

Fig. B.II.16

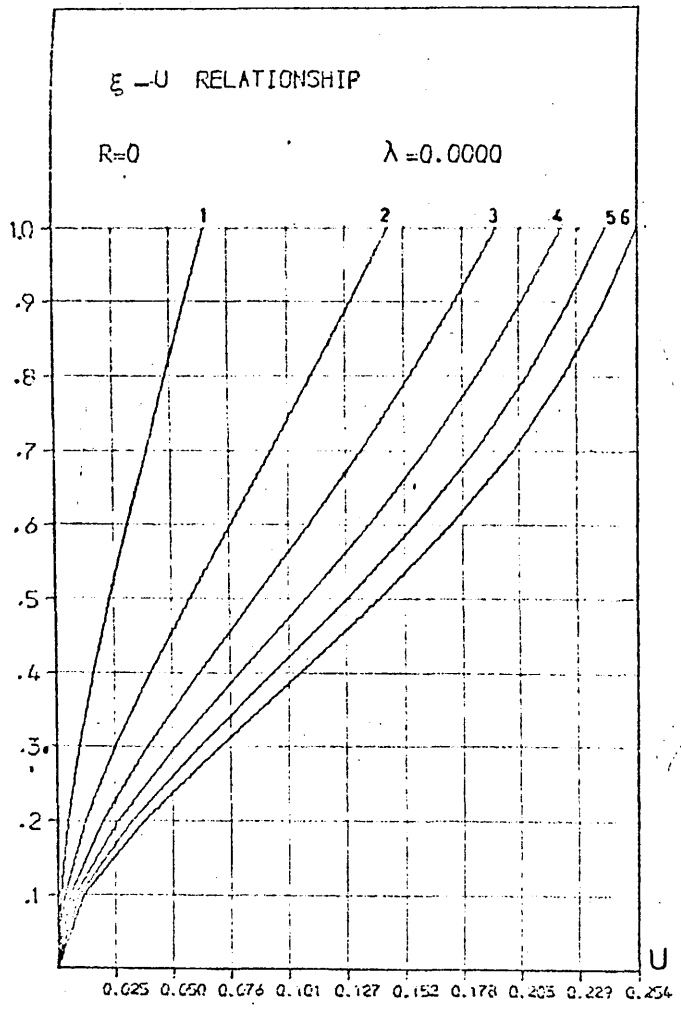
ξ –U RELATIONSHIP
R=0
λ =0.0000
1.0
.9
.8
.7
.6
.5
.4
.3
.2
.1
1
2
3
4
5 6
U
0.025 0.050 0.076 0.101 0.127 0.152 0.178 0.203 0.229 0.254

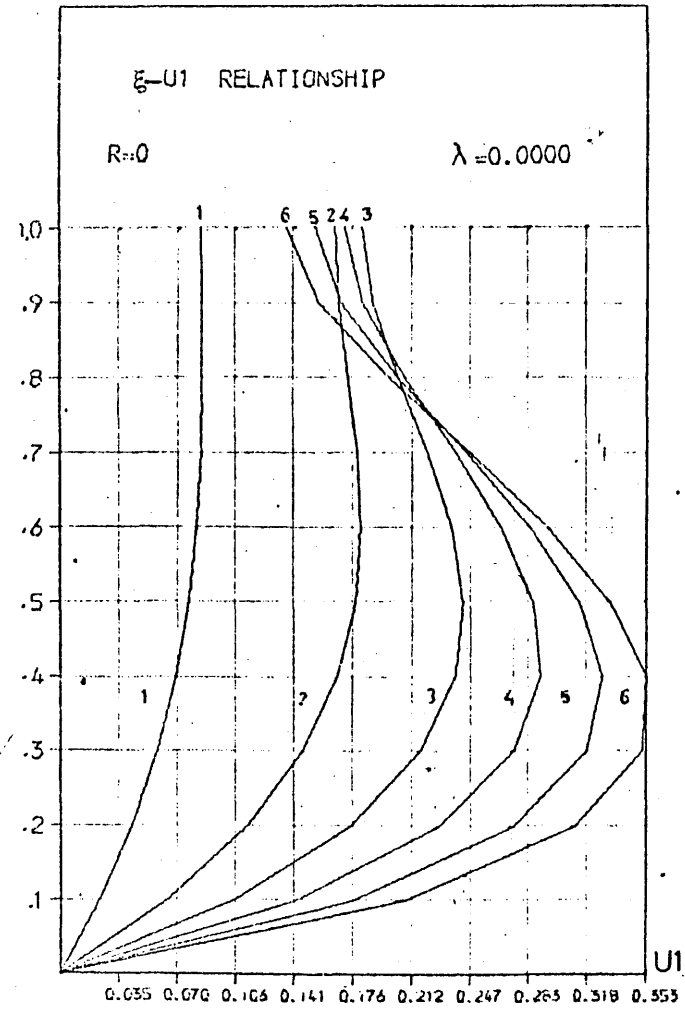
ξ–U1 RELATIONSHIP
R=0
λ =0.0000
1.0
.9
.8
.7
.6
.5
.4
.3
.2
.1
1
6 5 2 4 3
1
2
3
4
5
6
U1
0.035 0.070 0.106 0.141 0.176 0.212 0.247 0.283 0.318 0.353

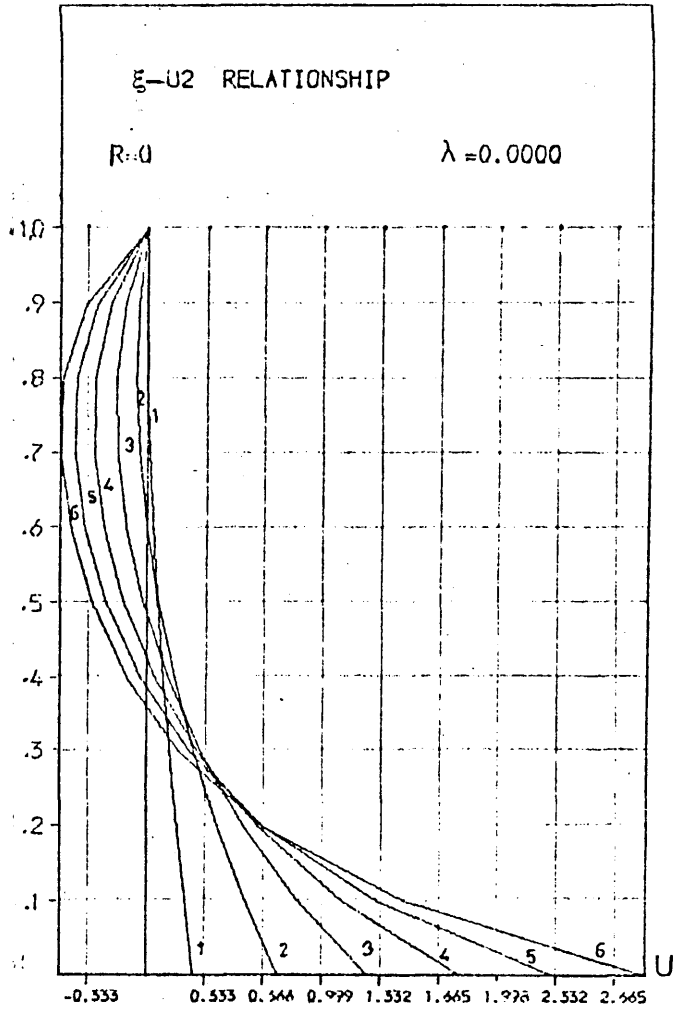
ξ–U2 RELATIONSHIP
R=0
λ =0.0000
1.0
.9
.8
.7
.6
.5
.4
.3
.2
.1
2
1
3
5
4
6
1
2
3
4
5
6
U2
-0.333
0.533 0.666 0.999 1.332 1.665 1.998 2.332 2.665

Fig. B.III.1

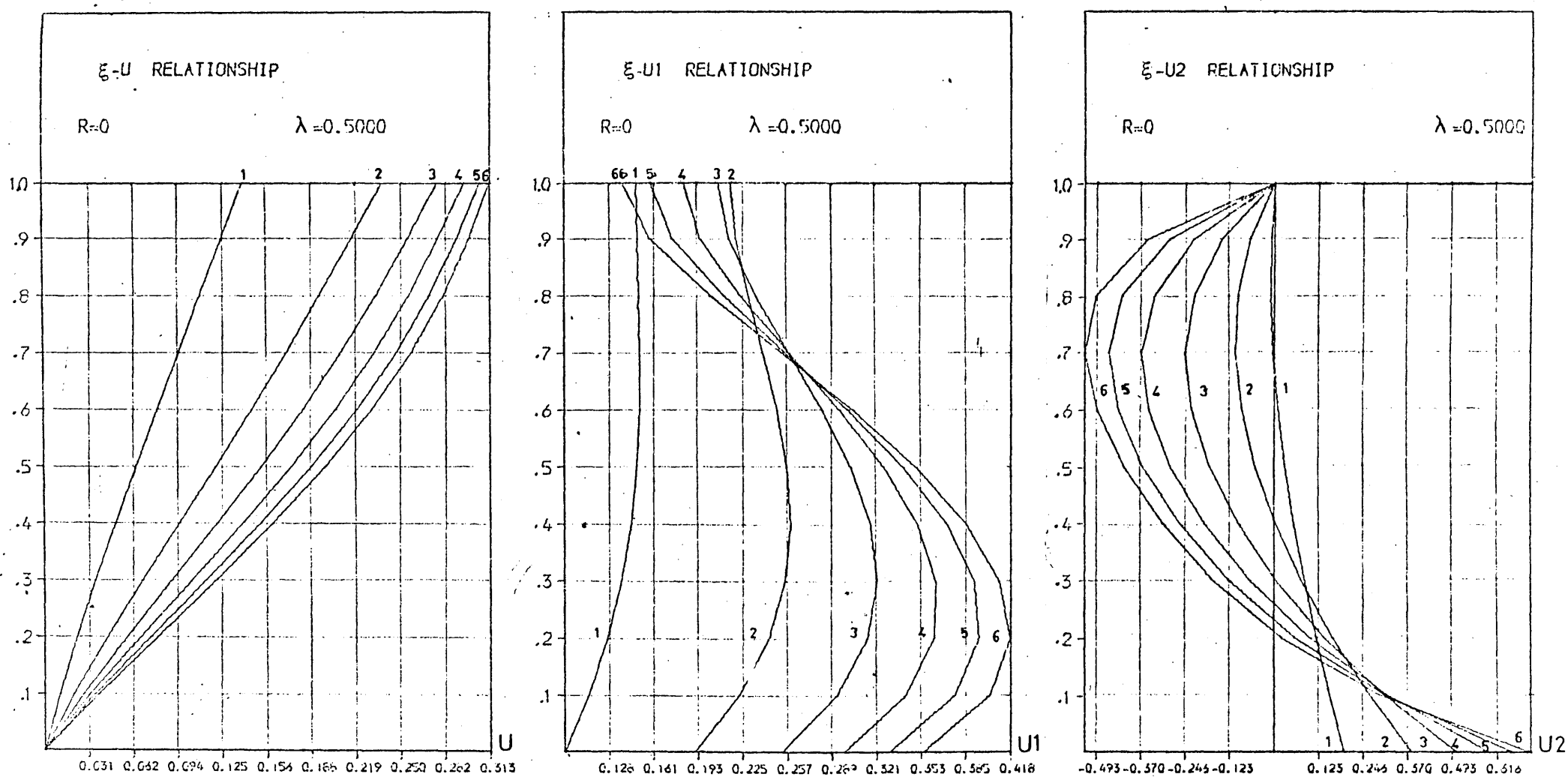
ξ-U RELATIONSHIP
R=0
λ =0.5000
1.0
.9
.8
.7
.6
.5
.4
.3
.2
.1
1 2 3 4 5 6
U
0.031 0.062 0.094 0.125 0.156 0.188 0.219 0.250 0.282 0.313
ξ-U1 RELATIONSHIP
R=0
λ =0.5000
6 6 1 5 4 3 2
1 2 3 4 5 6
U1
0.126 0.161 0.193 0.225 0.257 0.289 0.321 0.353 0.385 0.418
ξ-U2 RELATIONSHIP
R=0
λ =0.5000
6 5 4 3 2 1
1 2 3 4 5 6
U2
-0.493 -0.370 -0.246 -0.123
0.123 0.246 0.370 0.493 0.616

Fig. B.III.2

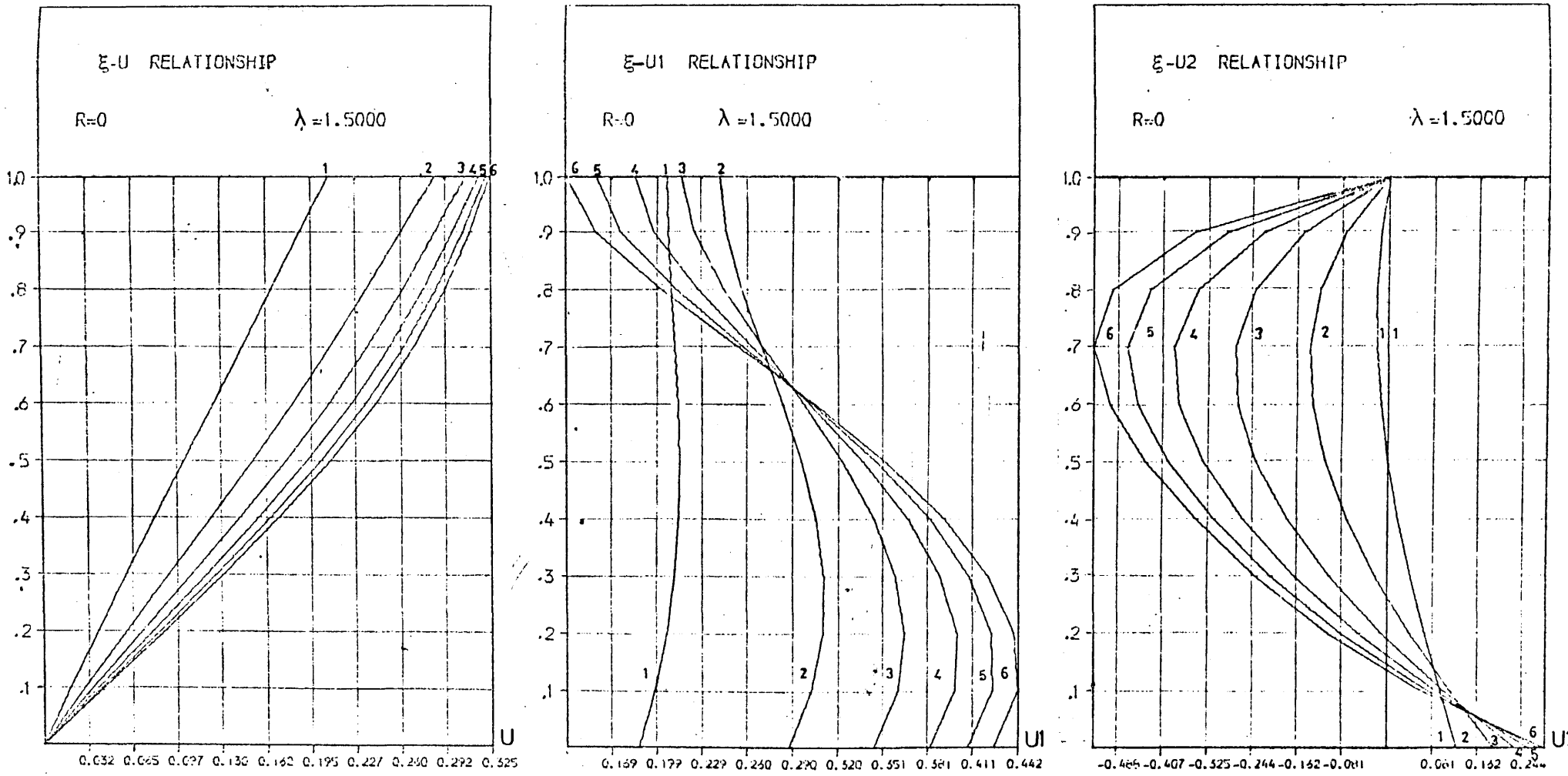
ξ-U RELATIONSHIP
R=0
λ =1.5000
1.0
.9
.8
.7
.6
.5
.4
.3
.2
.1
1 2 3 4 5 6
U
0.032 0.065 0.097 0.130 0.162 0.195 0.227 0.260 0.292 0.325
ξ-U1 RELATIONSHIP
R=0
λ =1.5000
6 5 4 1 3 2
1 2 3 4 5 6
U1
0.169 0.199 0.229 0.260 0.290 0.320 0.351 0.381 0.411 0.442
ξ-U2 RELATIONSHIP
R=0
λ =1.5000
6 5 4 3 2 1 1
1 2 3 6 4 5
U2
-0.466 -0.407 -0.525 -0.244 -0.162 -0.081
0.081 0.162 0.244

Fig. B.III.3

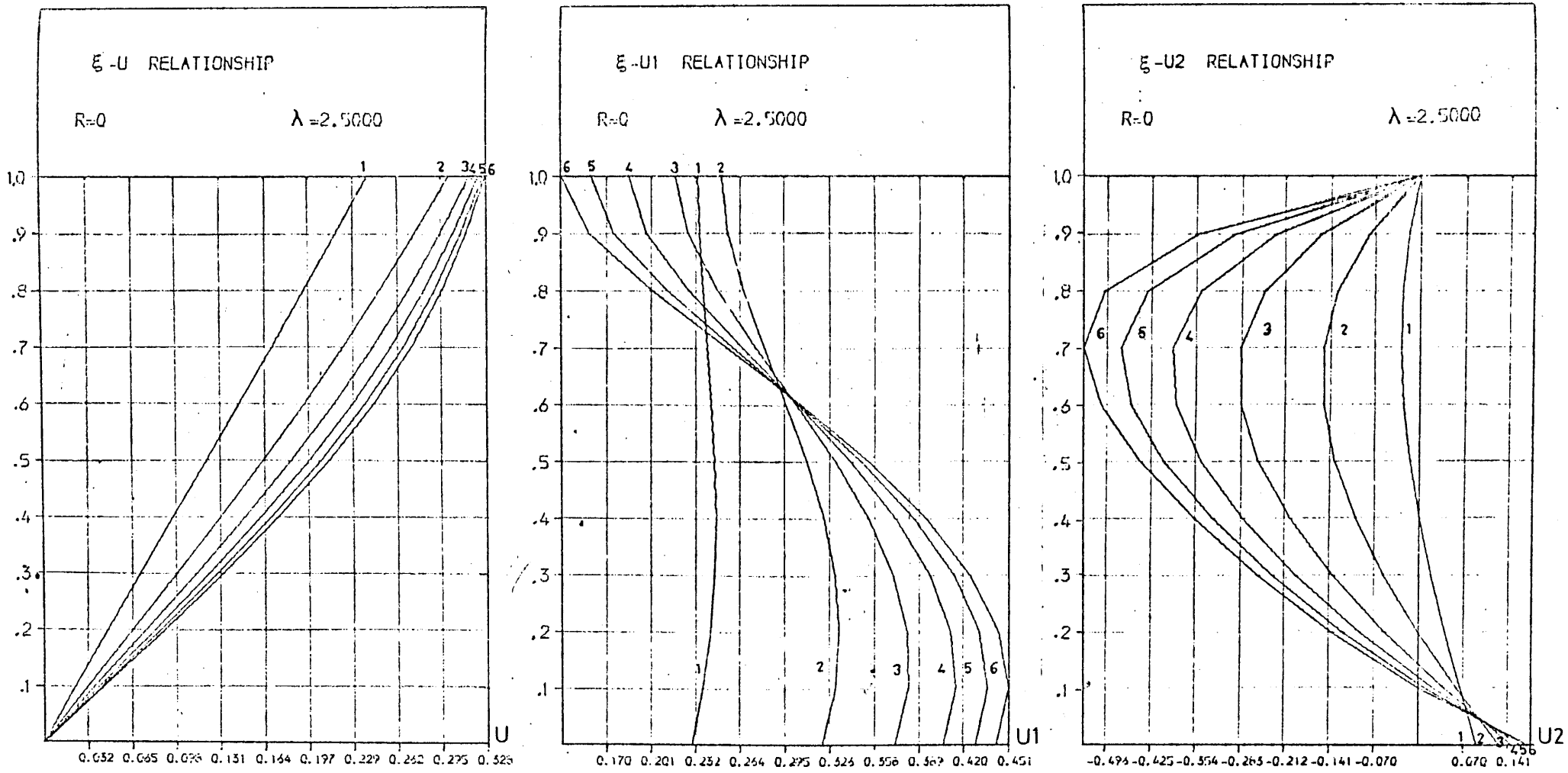
ξ -U RELATIONSHIP
R=0
λ =2.5000
U
ξ -U1 RELATIONSHIP
R=0
λ =2.5000
U1
ξ -U2 RELATIONSHIP
R=0
λ =2.5000
U2

Fig. B.III.4

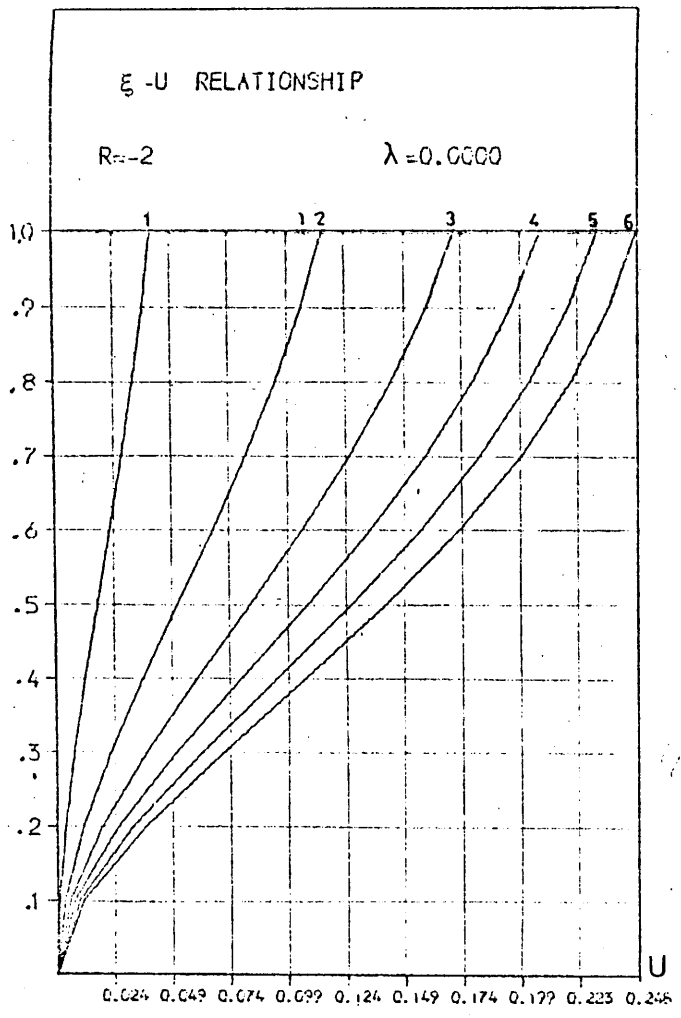
ξ -U RELATIONSHIP
R=-2
λ =0.0000
1
1 2
3
4
5
6
1.0
.9
.8
.7
.6
.5
.4
.3
.2
.1
U
0.024 0.049 0.074 0.099 0.124 0.149 0.174 0.199 0.223 0.248

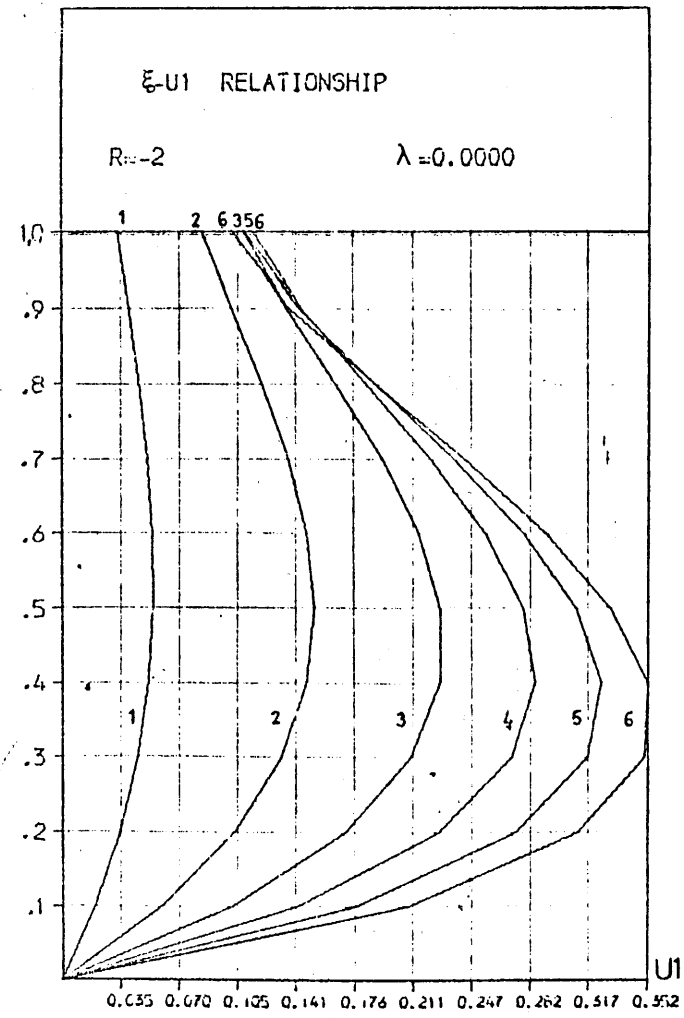
ξ-U1 RELATIONSHIP
R=-2
λ =0.0000
1
2 6 3 5 6
1.0
.9
.8
.7
.6
.5
.4
.3
.2
.1
1
2
3
4
5
6
U1
0.035 0.070 0.105 0.141 0.176 0.211 0.247 0.282 0.317 0.352

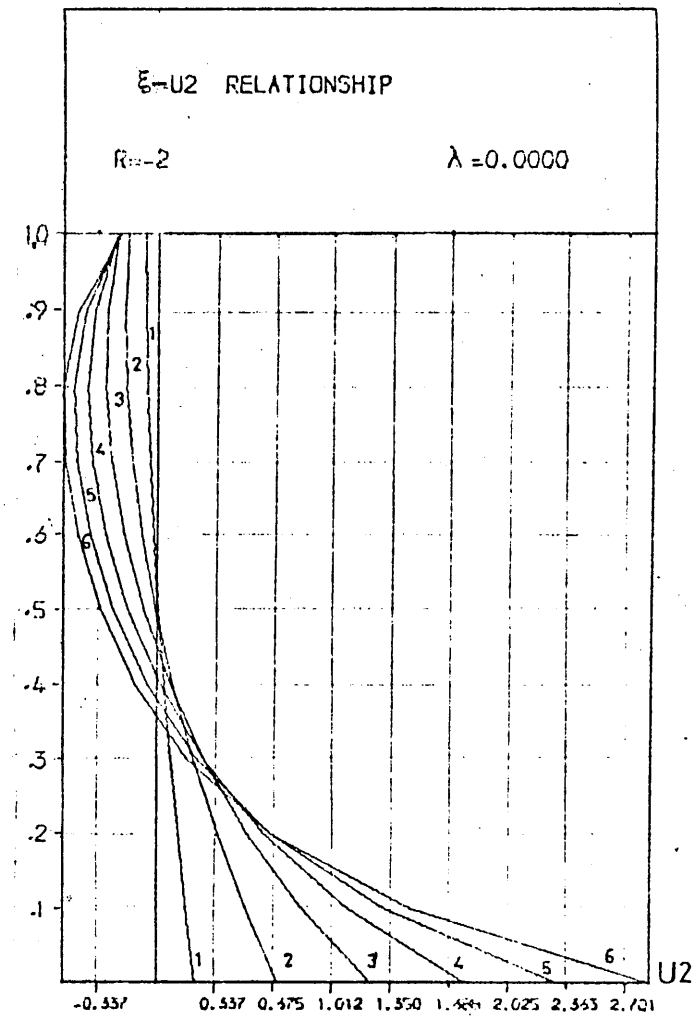
ξ-U2 RELATIONSHIP
R=-2
λ =0.0000
1.0
.9
.8
.7
.6
.5
.4
.3
.2
.1
1
2
3
4
5
6
1
2
3
4
5
6
U2
-0.337
0.337 0.675 1.012 1.350 1.688 2.025 2.363 2.701

Fig. B.III.5

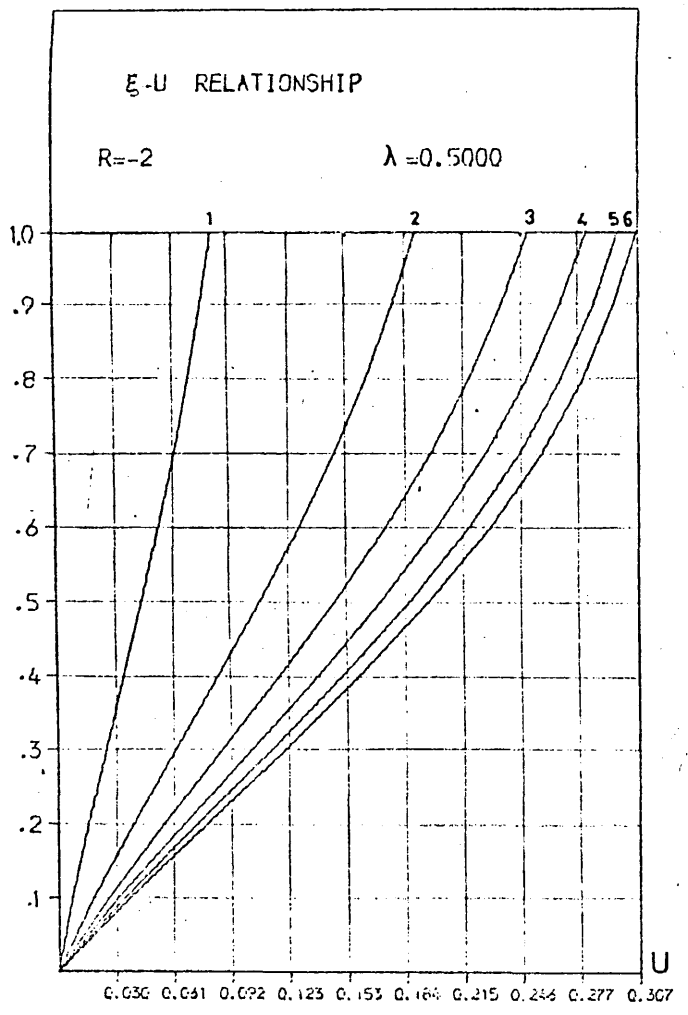
ξ-U RELATIONSHIP
R=-2
λ =0.5000
1
2
3
4
5
6
1.0
.9
.8
.7
.6
.5
.4
.3
.2
.1
U
0.030 0.061 0.092 0.123 0.153 0.184 0.215 0.246 0.277 0.307

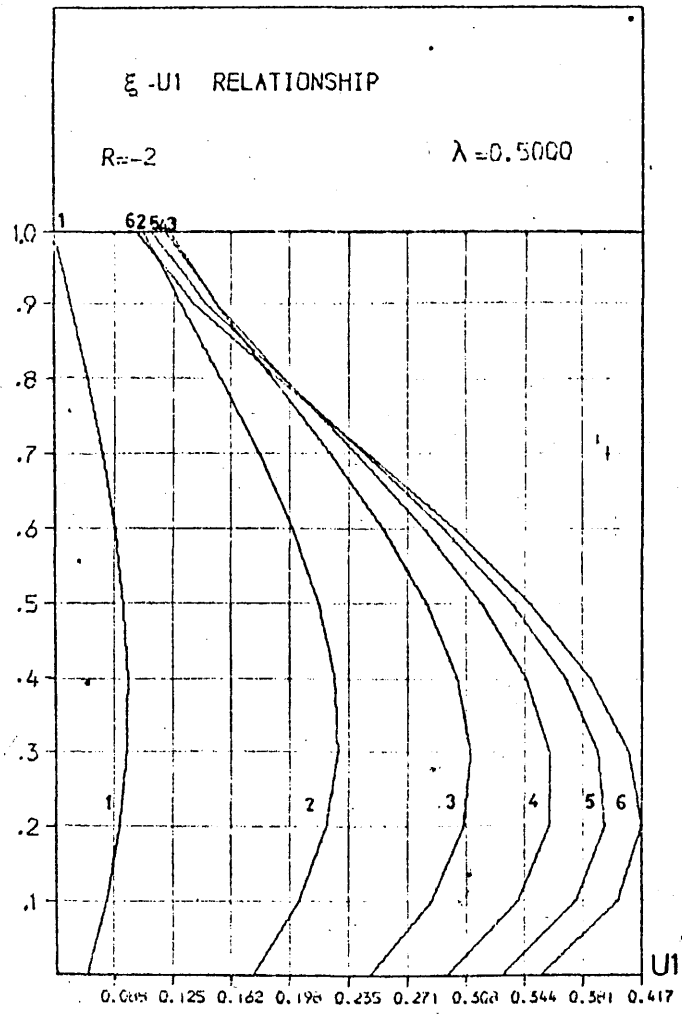
ξ-U1 RELATIONSHIP
R=-2
λ =0.5000
1
6
5
4
3
2
1.0
.9
.8
.7
.6
.5
.4
.3
.2
.1
U1
0.125 0.162 0.198 0.235 0.271 0.508 0.544 0.581 0.417

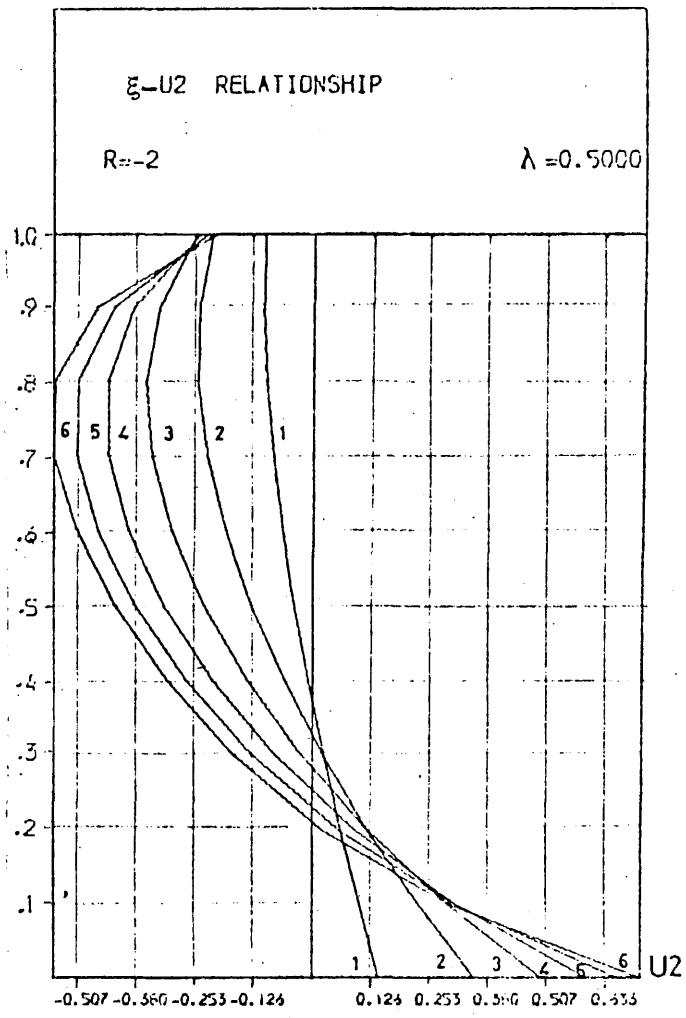
ξ-U2 RELATIONSHIP
R=-2
λ =0.5000
6
5
4
3
2
1
1.0
.9
.8
.7
.6
.5
.4
.3
.2
.1
U2
-0.507 -0.380 -0.253 -0.126
0.126 0.253 0.380 0.507 0.633

Fig. B.III.6

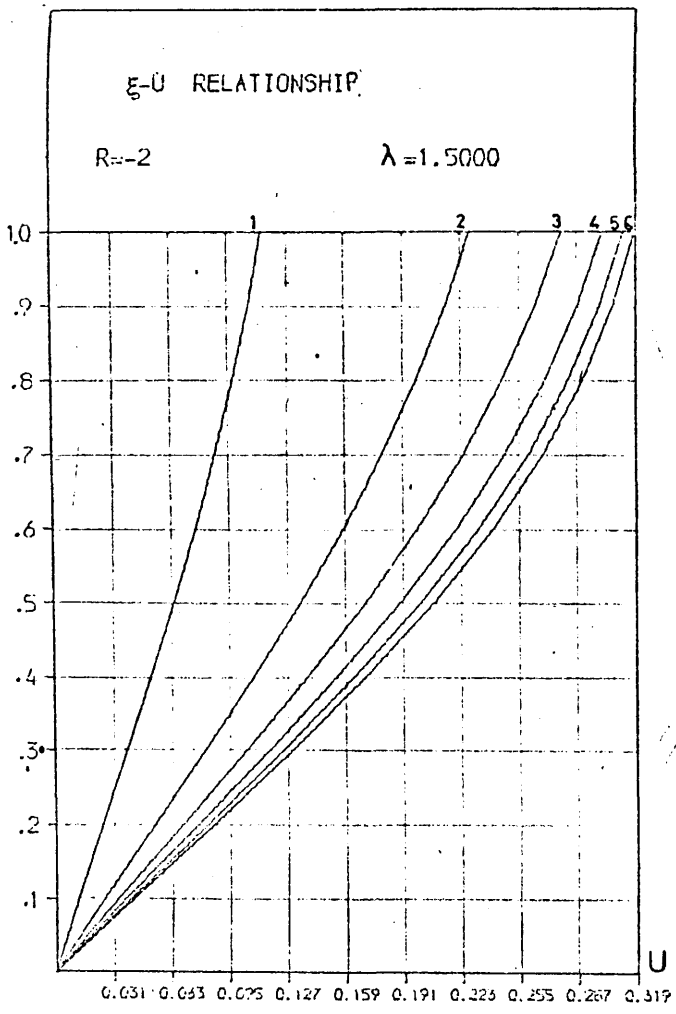
ξ-U RELATIONSHIP
R=-2
λ =1.5000
1.0
.9
.8
.7
.6
.5
.4
.3
.2
.1
1
2
3
4
5
6
U
0.031 0.063 0.095 0.127 0.159 0.191 0.223 0.255 0.287 0.319

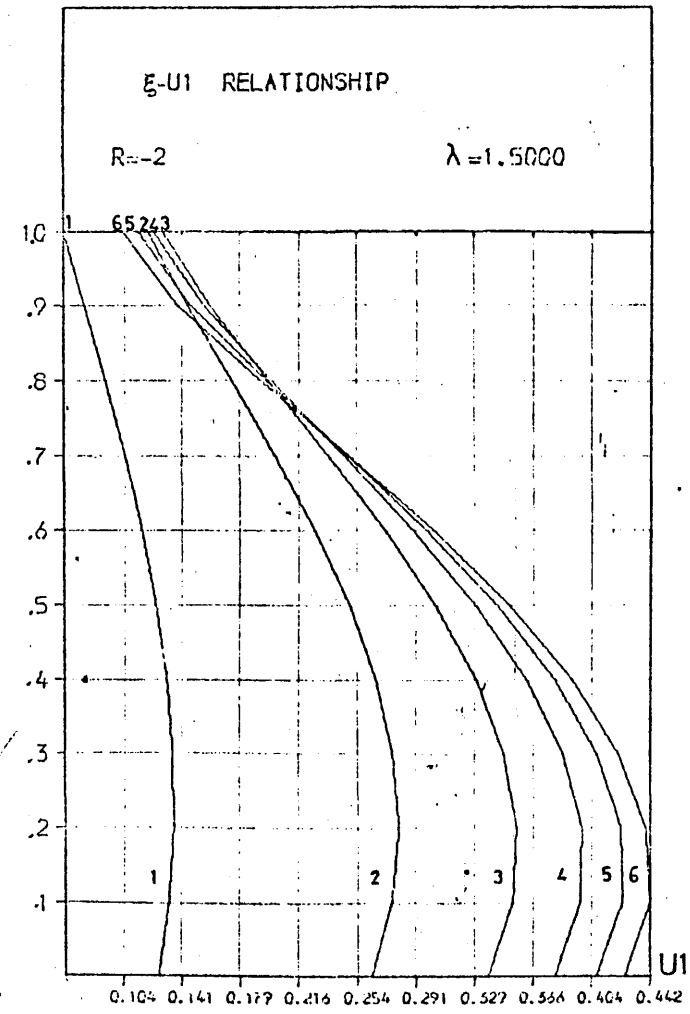
ξ-U1 RELATIONSHIP
R=-2
λ =1.5000
1.0
.9
.8
.7
.6
.5
.4
.3
.2
.1
1 6 5 2 4 3
1
2
3
4
5
6
U1
0.104 0.141 0.179 0.216 0.254 0.291 0.327 0.366 0.404 0.442

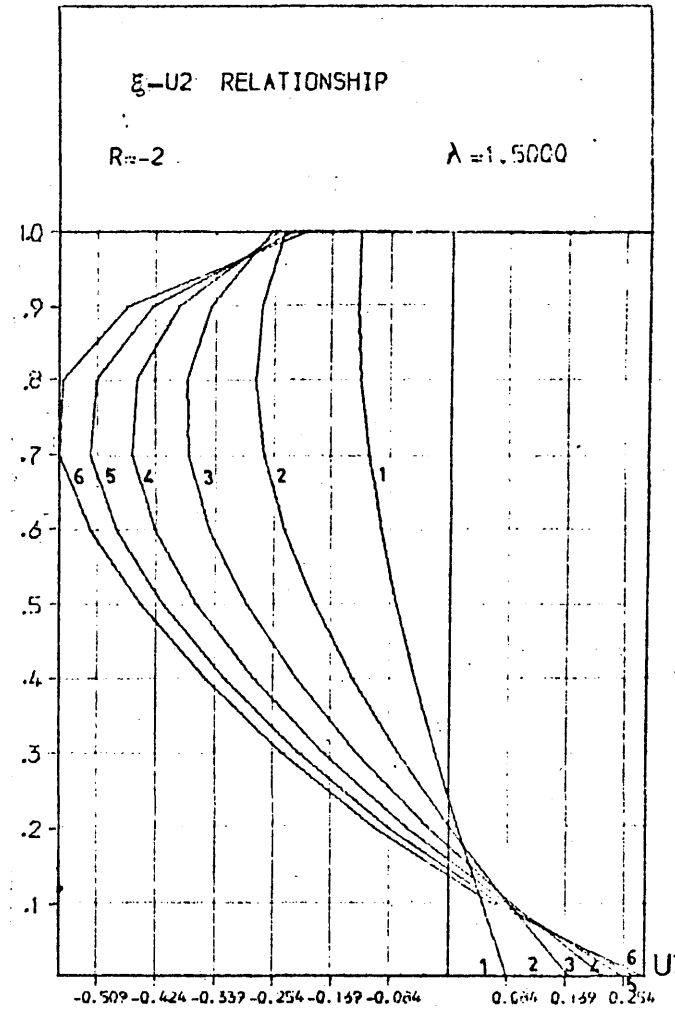
ξ-U2 RELATIONSHIP
R=-2
λ =1.5000
1.0
.9
.8
.7
.6
.5
.4
.3
.2
.1
6
5
4
3
2
1
1
2
3
4
6
U2
-0.509 -0.424 -0.337 -0.254 -0.169 -0.084
0.084 0.169 0.254

Fig. B.III.7

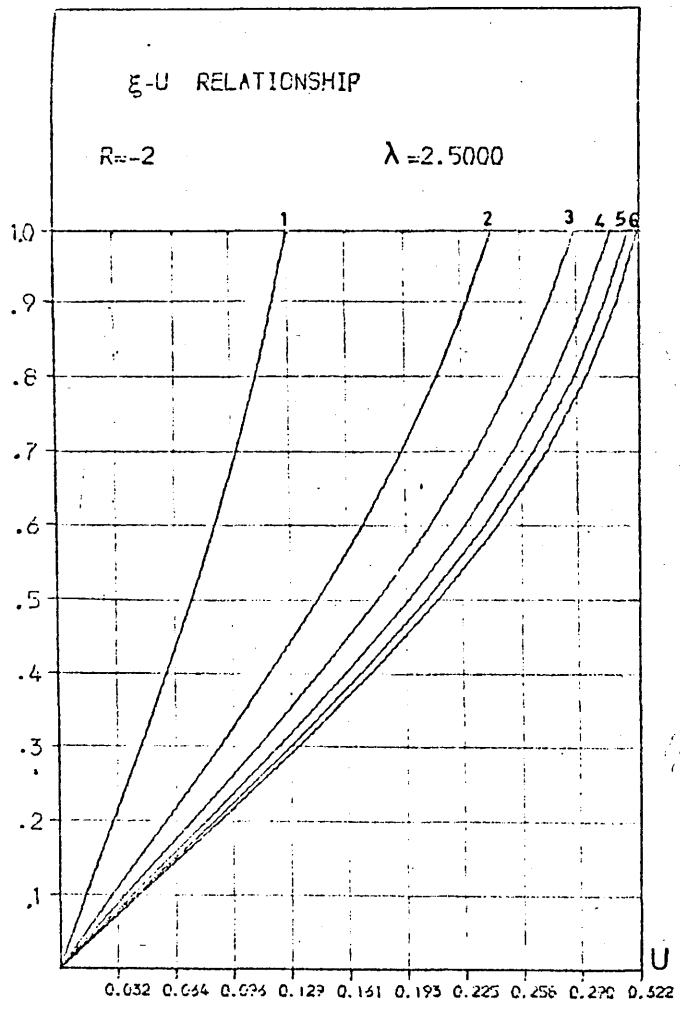
ξ-U RELATIONSHIP
R=-2
λ =2.5000
1.0
.9
.8
.7
.6
.5
.4
.3
.2
.1
1
2
3
4
5
6
U
0.032 0.064 0.096 0.129 0.161 0.193 0.225 0.256 0.290 0.322

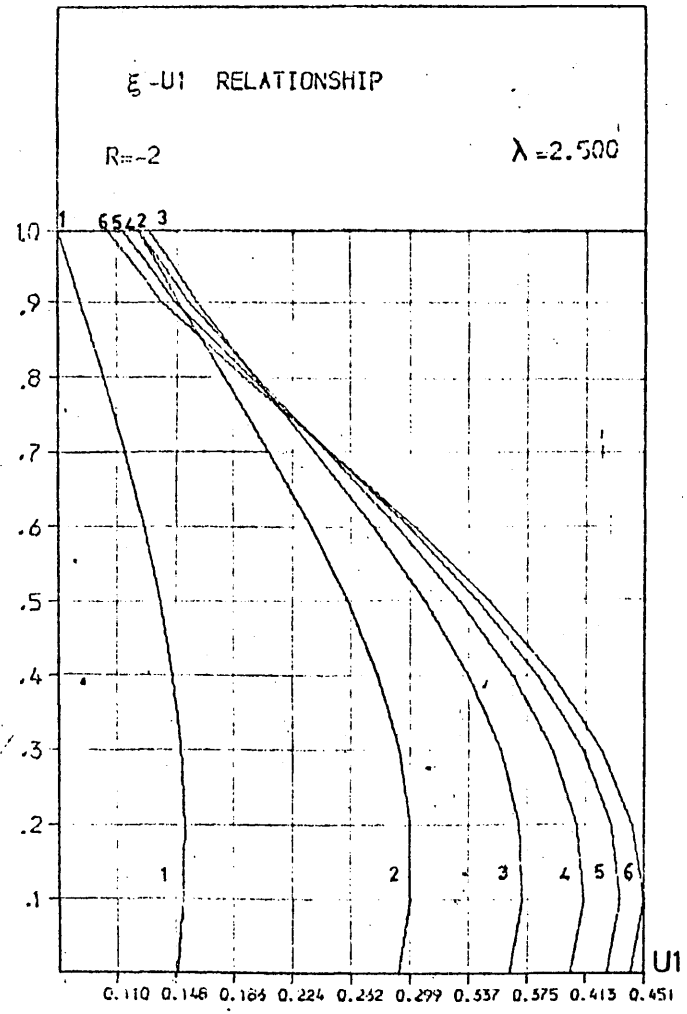
ξ-U1 RELATIONSHIP
R=-2
λ =2.500
1.0
.9
.8
.7
.6
.5
.4
.3
.2
.1
1 6 5 4 2 3
1
2
3
4
5
6
U1
0.110 0.146 0.184 0.224 0.262 0.299 0.537 0.575 0.413 0.451

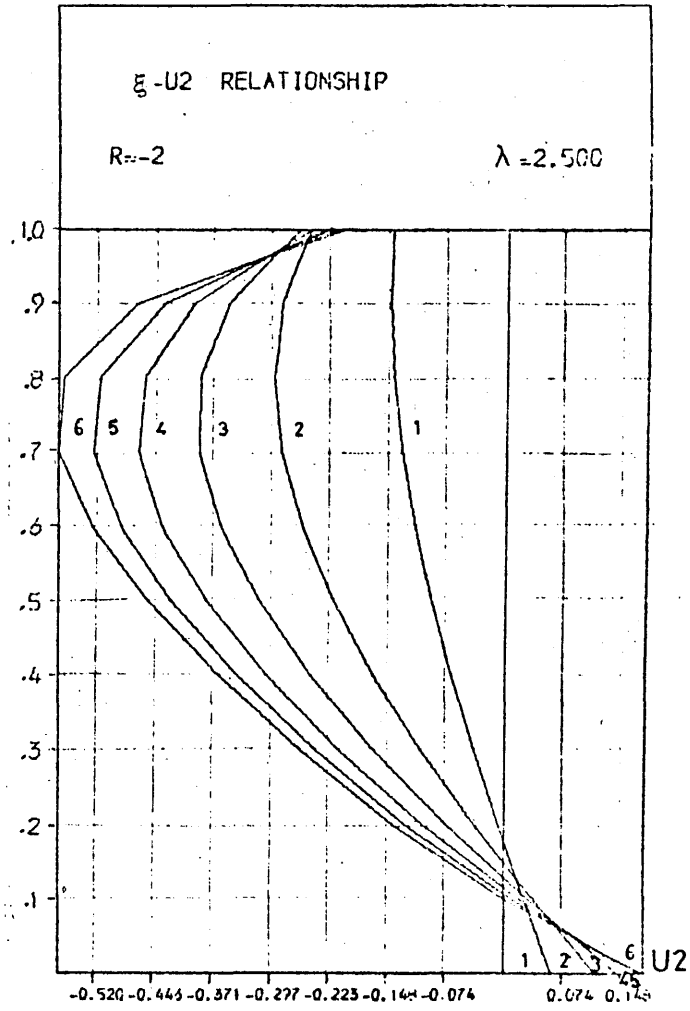
ξ-U2 RELATIONSHIP
R=-2
λ =2.500
1.0
.9
.8
.7
.6
.5
.4
.3
.2
.1
6
5
4
3
2
1
1
2
3
6
U2
-0.520 -0.446 -0.371 -0.297 -0.223 -0.148 -0.074
0.074

Fig. B.III.8

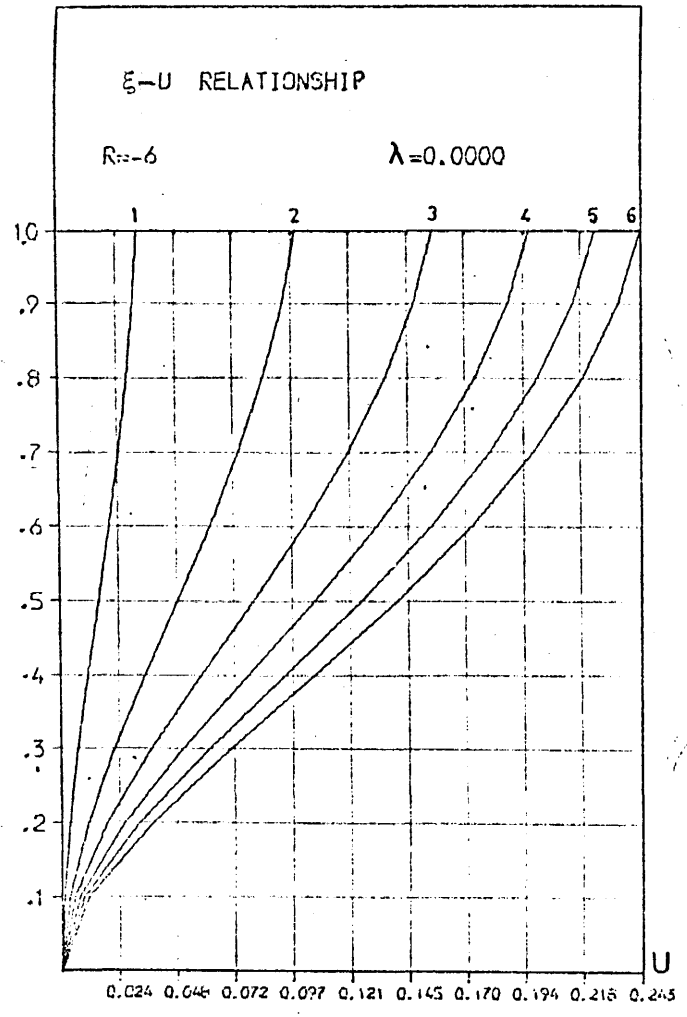
ξ–U RELATIONSHIP
R=-6
λ=0.0000
1
2
3
4
5
6
1.0
.9
.8
.7
.6
.5
.4
.3
.2
.1
U
0.024 0.048 0.072 0.097 0.121 0.145 0.170 0.194 0.218 0.245

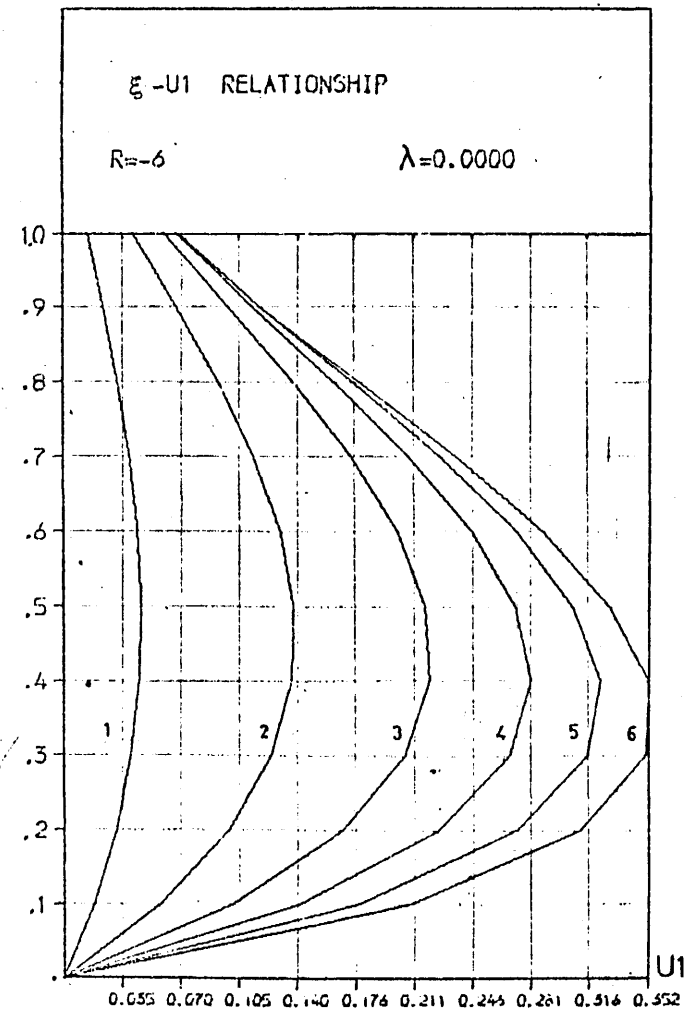
ξ –U1 RELATIONSHIP
R=-6
λ=0.0000
1.0
.9
.8
.7
.6
.5
.4
.3
.2
.1
1
2
3
4
5
6
U1
0.035 0.070 0.105 0.140 0.176 0.211 0.246 0.281 0.516 0.552

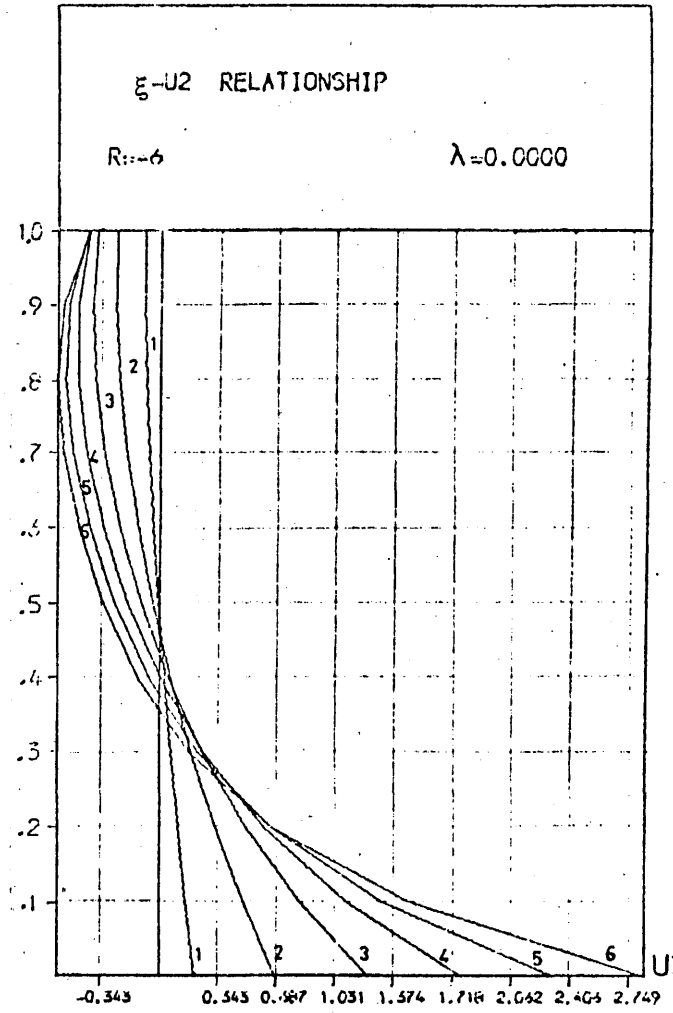
ξ–U2 RELATIONSHIP
R=-6
λ=0.0000
1.0
.9
.8
.7
.6
.5
.4
.3
.2
.1
1
2
3
4
5
6
U2
-0.343
0.343 0.687 1.031 1.374 1.718 2.062 2.406 2.749

Fig. B.III.9

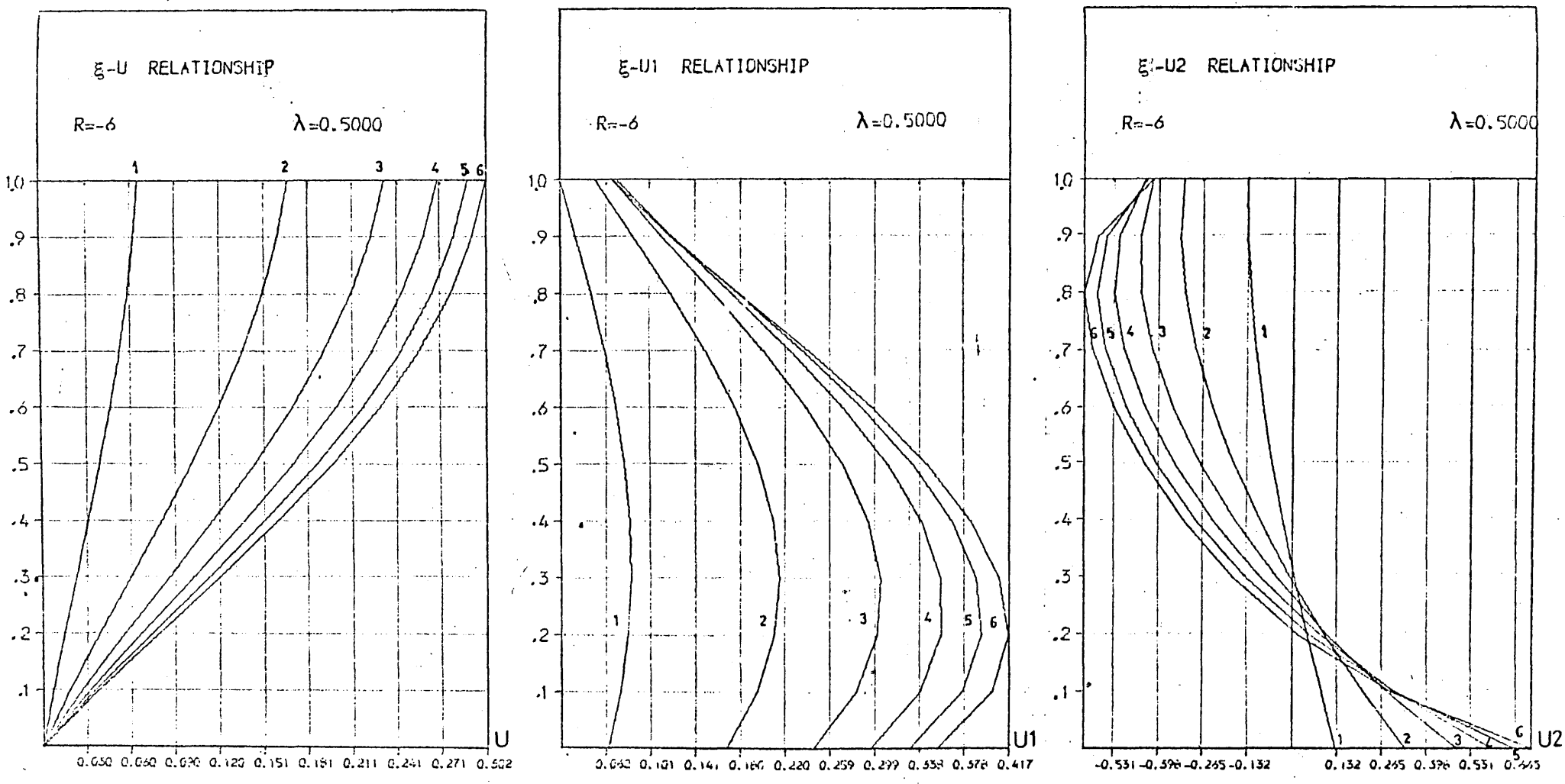
ξ-U RELATIONSHIP
R=-6
λ=0.5000
1
2
3
4
5
6
1.0
.9
.8
.7
.6
.5
.4
.3
.2
.1
U
0.030 0.060 0.090 0.120 0.151 0.181 0.211 0.241 0.271 0.302
ξ-U1 RELATIONSHIP
R=-6
λ=0.5000
U1
0.062 0.101 0.141 0.180 0.220 0.259 0.299 0.338 0.378 0.417
ξ-U2 RELATIONSHIP
R=-6
λ=0.5000
U2
-0.531 -0.398 -0.265 -0.132
0.132 0.265 0.398 0.531

Fig. B.III.10

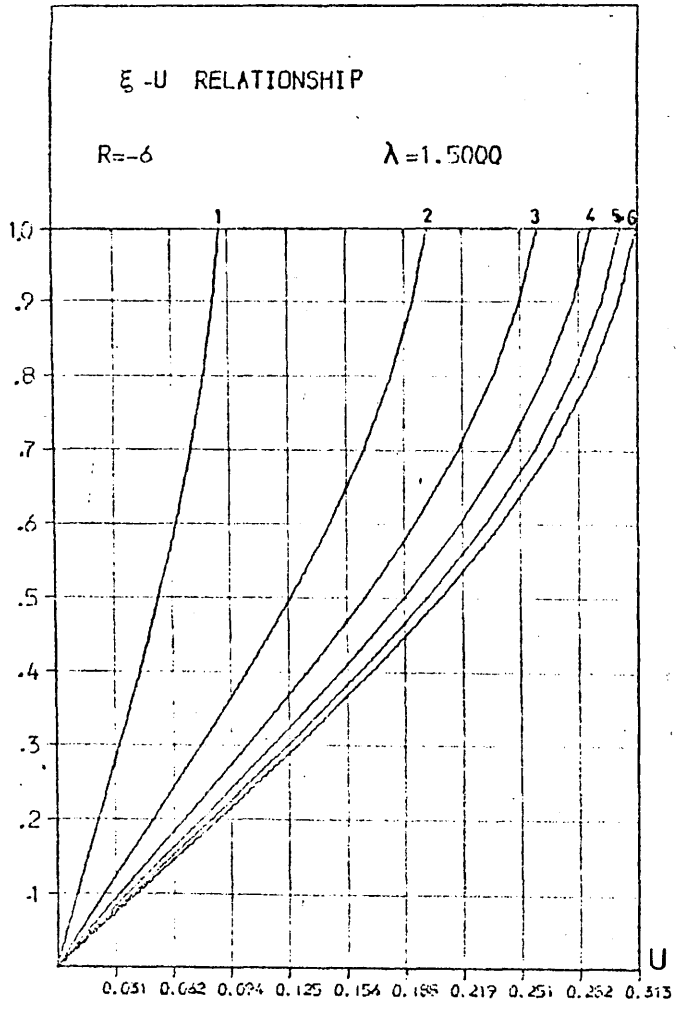
ξ -U RELATIONSHIP
R=-6
λ=1.5000
1
2
3
4
5
6
1.0
.9
.8
.7
.6
.5
.4
.3
.2
.1
U
0.051 0.082 0.094 0.125 0.156 0.188 0.219 0.251 0.282 0.313

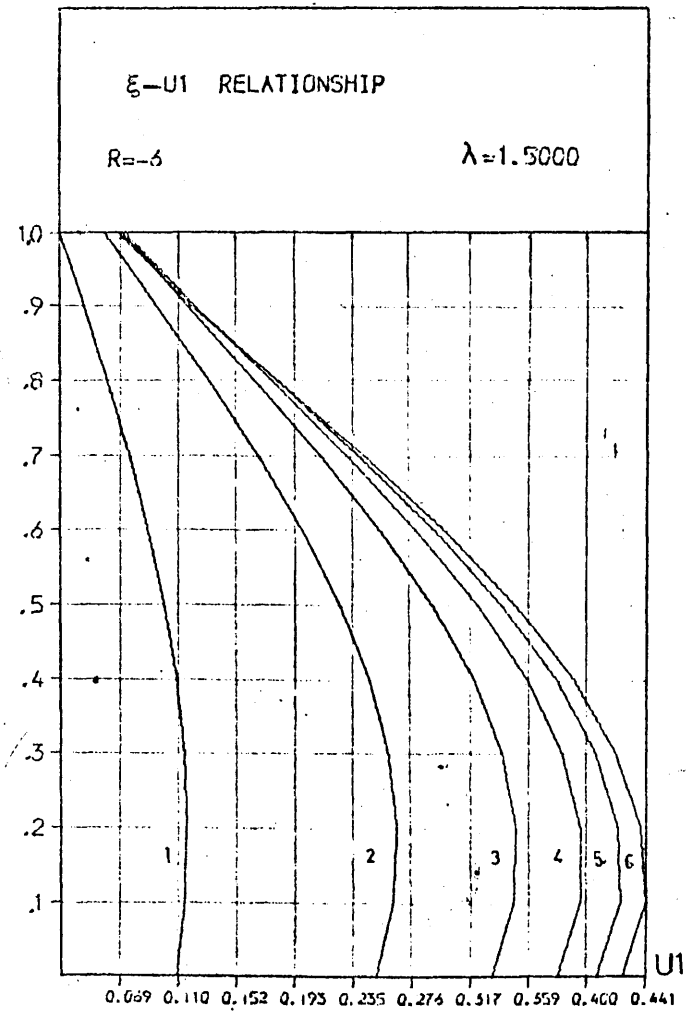
ξ-U1 RELATIONSHIP
R=-6
λ=1.5000
1.0
.9
.8
.7
.6
.5
.4
.3
.2
.1
1
2
3
4
5
6
U1
0.069 0.110 0.152 0.193 0.235 0.276 0.317 0.359 0.400 0.441

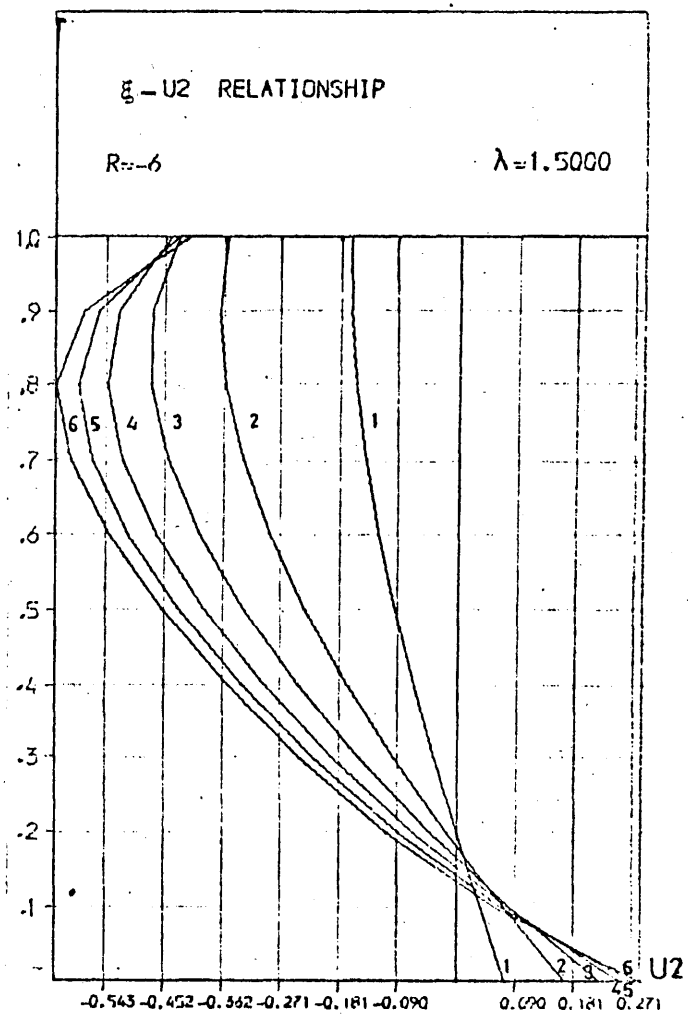
ξ-U2 RELATIONSHIP
R=-6
λ=1.5000
1.0
.9
.8
.7
.6
.5
.4
.3
.2
.1
6
5
4
3
2
1
U2
-0.543 -0.452 -0.362 -0.271 -0.181 -0.090
0.090 0.181 0.271

Fig. B.III.11

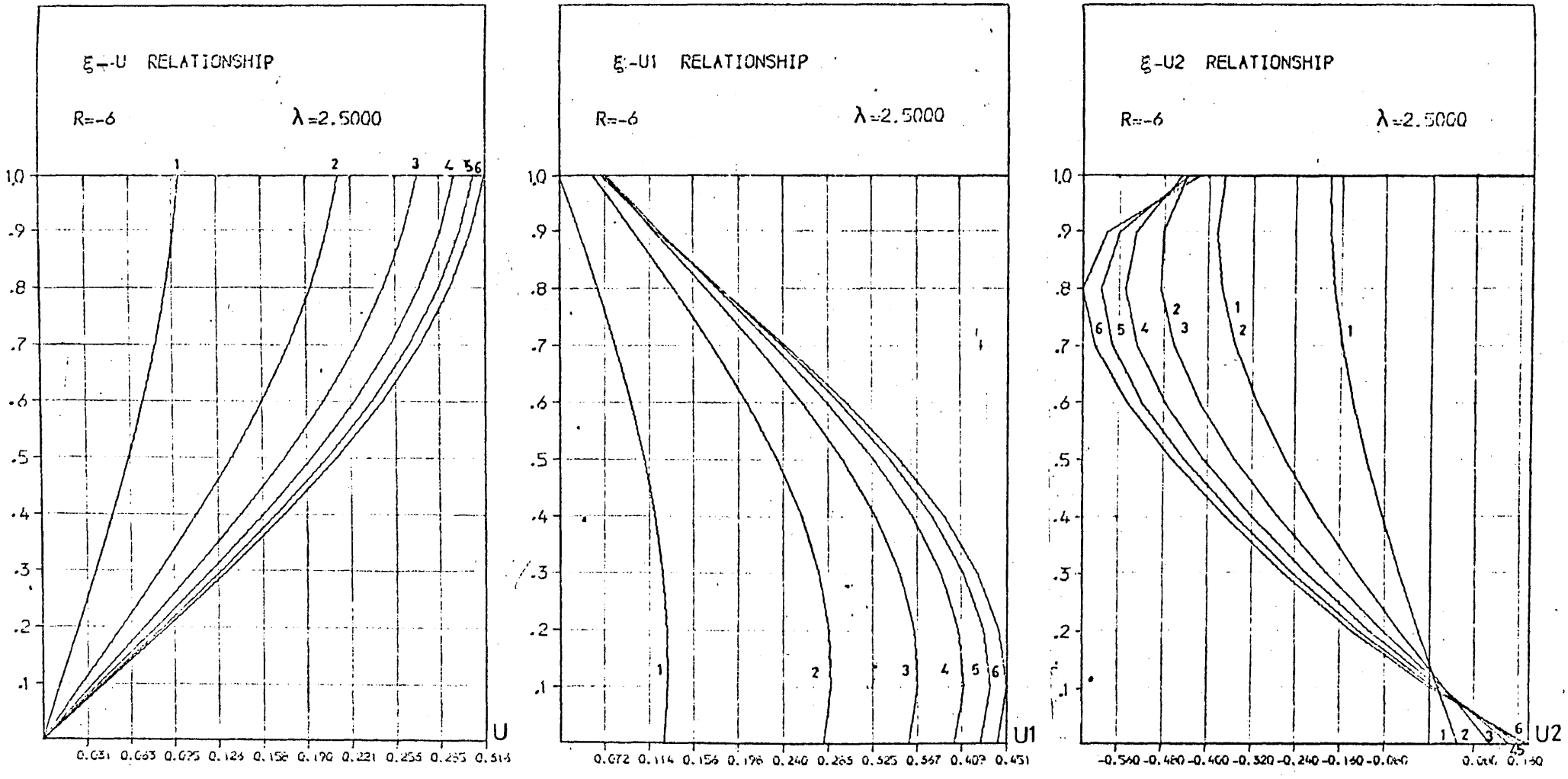
ξ-U RELATIONSHIP
R=-6
λ=2.5000
1.0
.9
.8
.7
.6
.5
.4
.3
.2
.1
1
2
3
4
5
6
U
0.031 0.063 0.095 0.126 0.158 0.190 0.221 0.253 0.285 0.316
ξ-U1 RELATIONSHIP
R=-6
λ=2.5000
U1
0.072 0.114 0.156 0.198 0.240 0.285 0.525 0.567 0.409 0.451
ξ-U2 RELATIONSHIP
R=-6
λ=2.5000
U2
-0.560 -0.480 -0.400 -0.320 -0.240 -0.160 -0.080

Fig. B.III.12

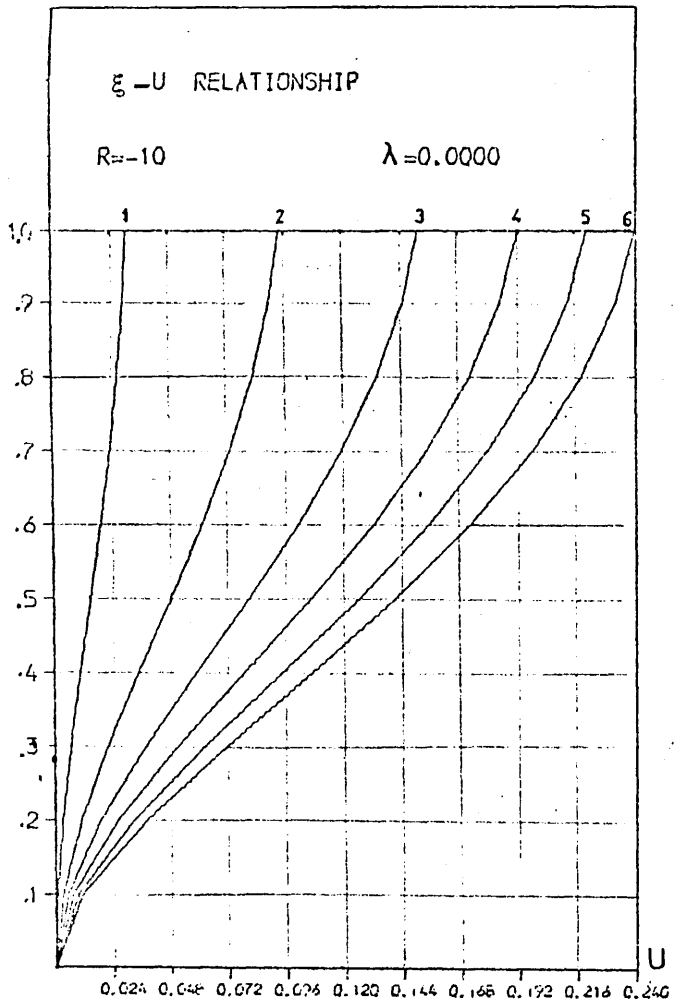
ξ –U RELATIONSHIP
R=-10
λ=0.0000
1
2
3
4
5
6
1.0
.9
.8
.7
.6
.5
.4
.3
.2
.1
U
0.024 0.048 0.072 0.096 0.120 0.144 0.168 0.192 0.216 0.240

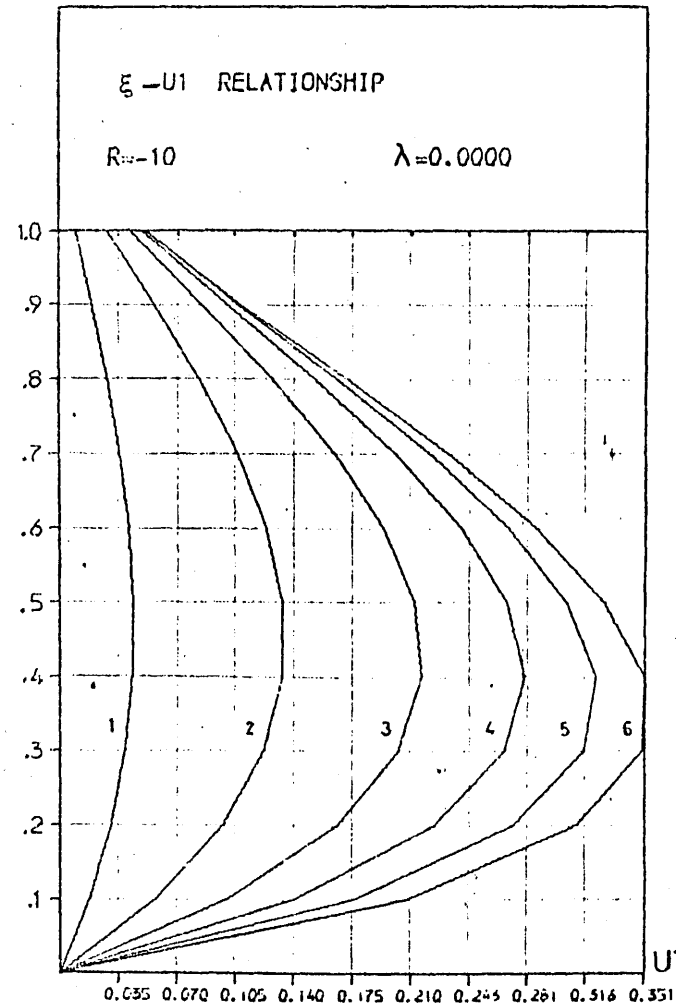
ξ –U1 RELATIONSHIP
R=-10
λ=0.0000
1.0
.9
.8
.7
.6
.5
.4
.3
.2
.1
1
2
3
4
5
6
U1
0.035 0.070 0.105 0.140 0.175 0.210 0.245 0.281 0.316 0.351

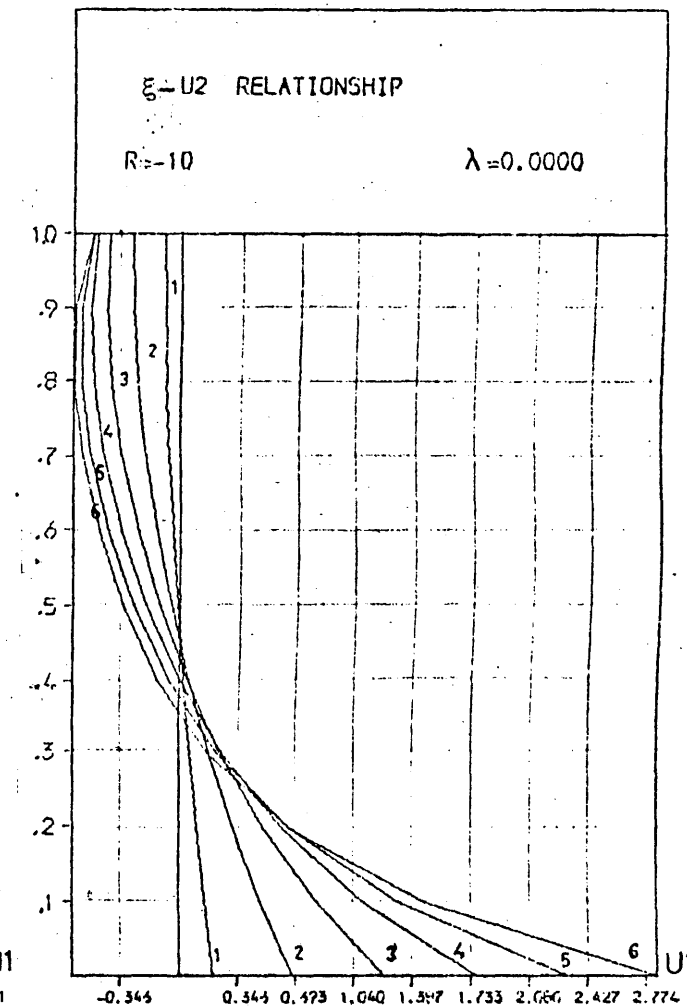
ξ –U2 RELATIONSHIP
R=-10
λ=0.0000
1.0
.9
.8
.7
.6
.5
.4
.3
.2
.1
1
2
3
4
5
6
U2
-0.344
0.344 0.693 1.040 1.387 1.733 2.080 2.427 2.774

Fig. B.III.13

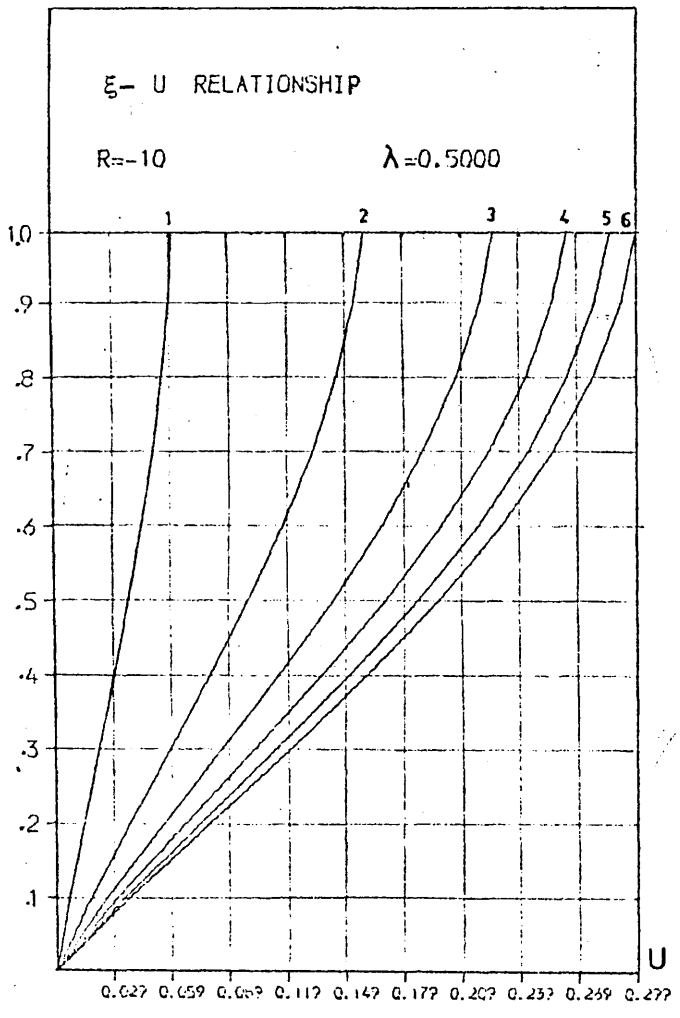
ξ- U RELATIONSHIP
R=-10
λ=0.5000
1
2
3
4
5
6
1.0
.9
.8
.7
.6
.5
.4
.3
.2
.1
U
0.027 0.059 0.069 0.112 0.142 0.179 0.209 0.233 0.269 0.272

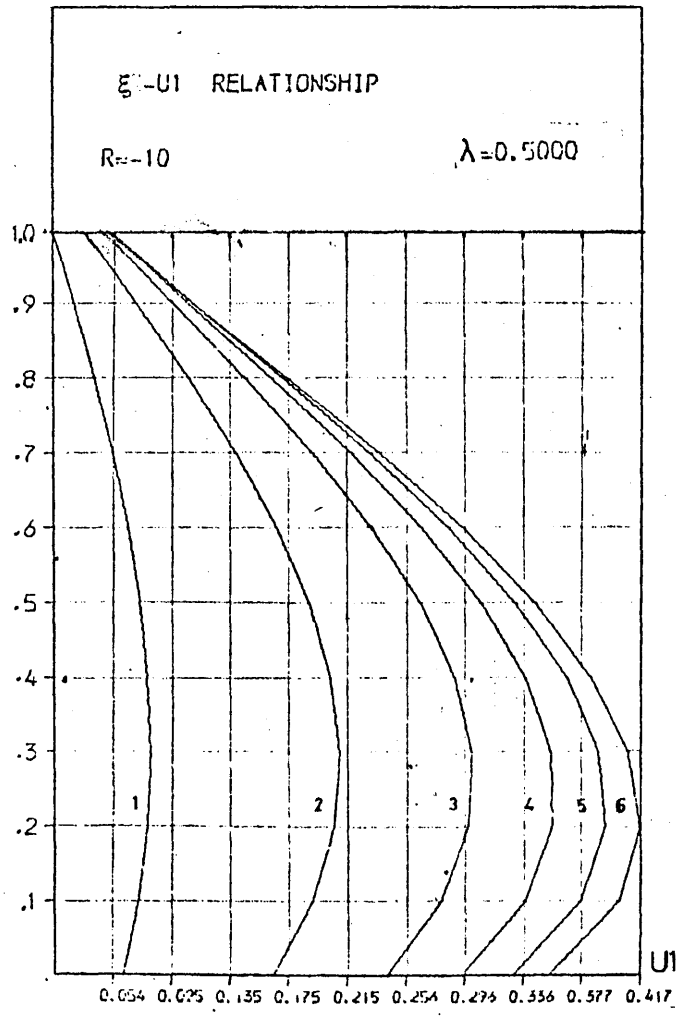
ξ-U1 RELATIONSHIP
R=-10
λ=0.5000
1
2
3
4
5
6
1.0
.9
.8
.7
.6
.5
.4
.3
.2
.1
U1
0.054 0.095 0.135 0.175 0.215 0.254 0.296 0.336 0.377 0.417

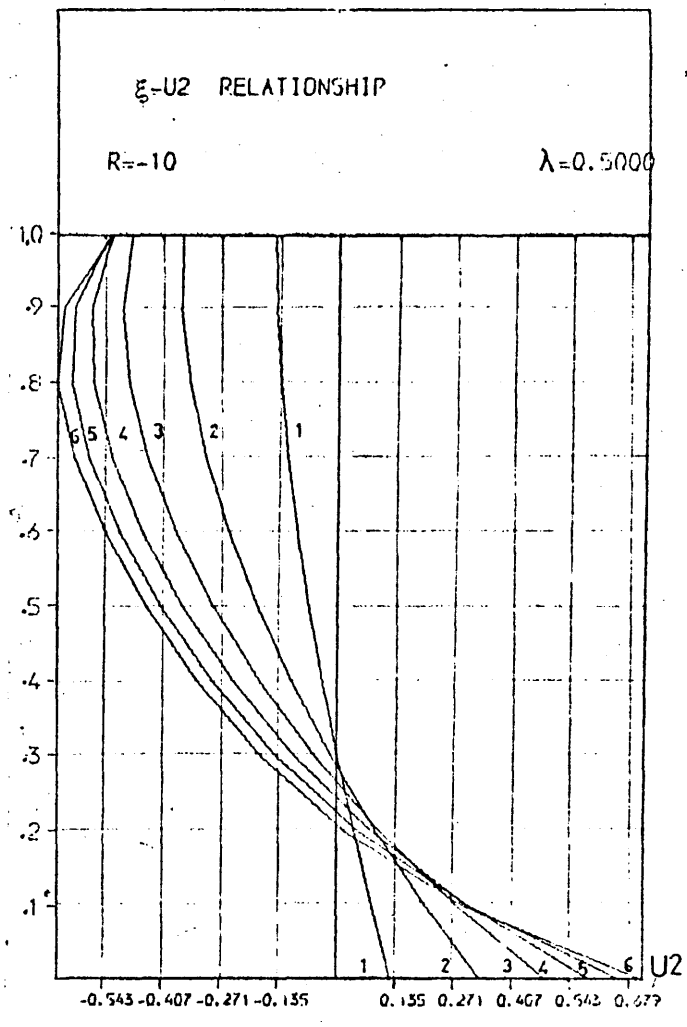
ξ-U2 RELATIONSHIP
R=-10
λ=0.5000
6
5
4
3
2
1
1.0
.9
.8
.7
.6
.5
.4
.3
.2
.1
U2
-0.543 -0.407 -0.271 -0.135
0.135 0.271 0.407 0.543 0.679

Fig. B.III.14

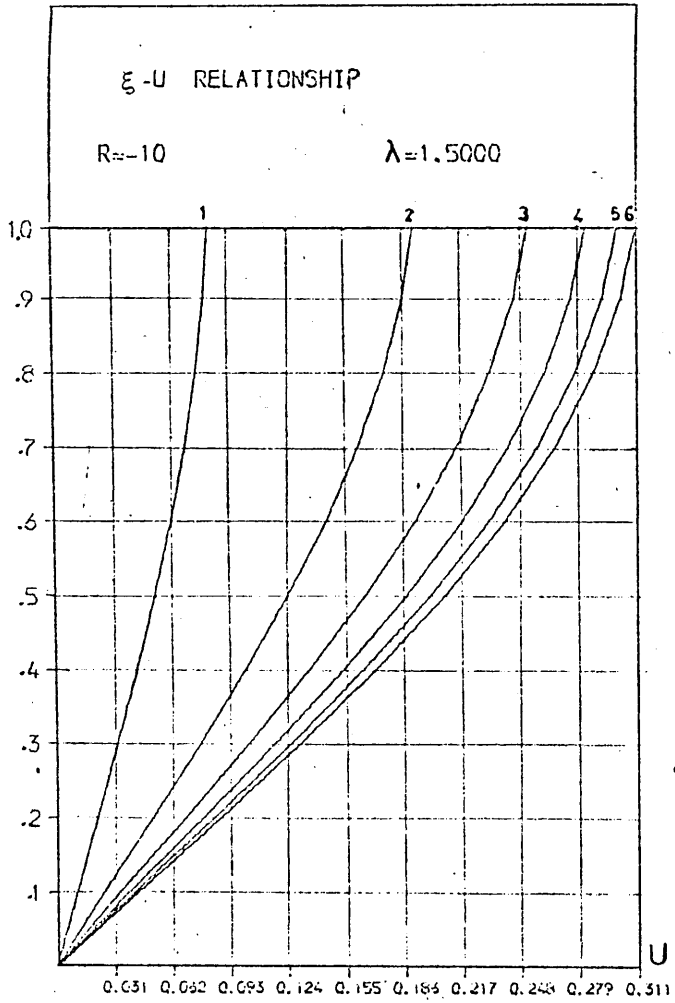
ξ -U RELATIONSHIP
R=-10
λ=1.5000
1
2
3
4
5
6
1.0
.9
.8
.7
.6
.5
.4
.3
.2
.1
U
0.031 0.062 0.093 0.124 0.155 0.186 0.217 0.248 0.279 0.311

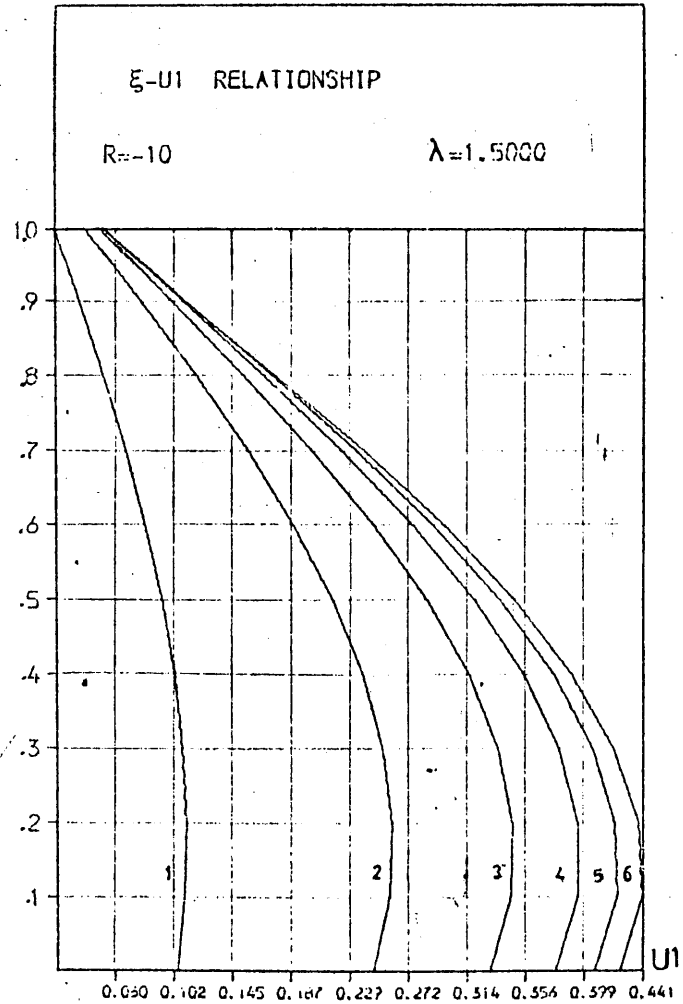
ξ-U1 RELATIONSHIP
R=-10
λ=1.5000
1.0
.9
.8
.7
.6
.5
.4
.3
.2
.1
1
2
3
4
5
6
U1
0.060 0.102 0.145 0.187 0.227 0.272 0.314 0.356 0.399 0.441

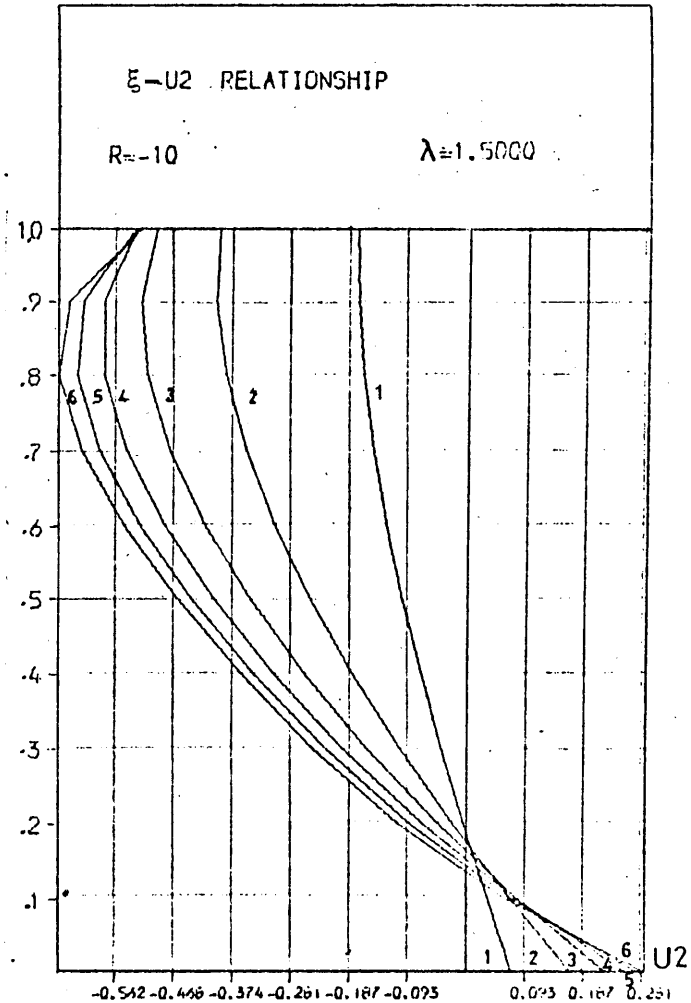
ξ-U2 RELATIONSHIP
R=-10
λ=1.5000
1.0
.9
.8
.7
.6
.5
.4
.3
.2
.1
6
5
4
3
2
1
U2
-0.542 -0.468 -0.374 -0.281 -0.187 -0.095
0.093 0.187 0.281

Fig. B.III.15

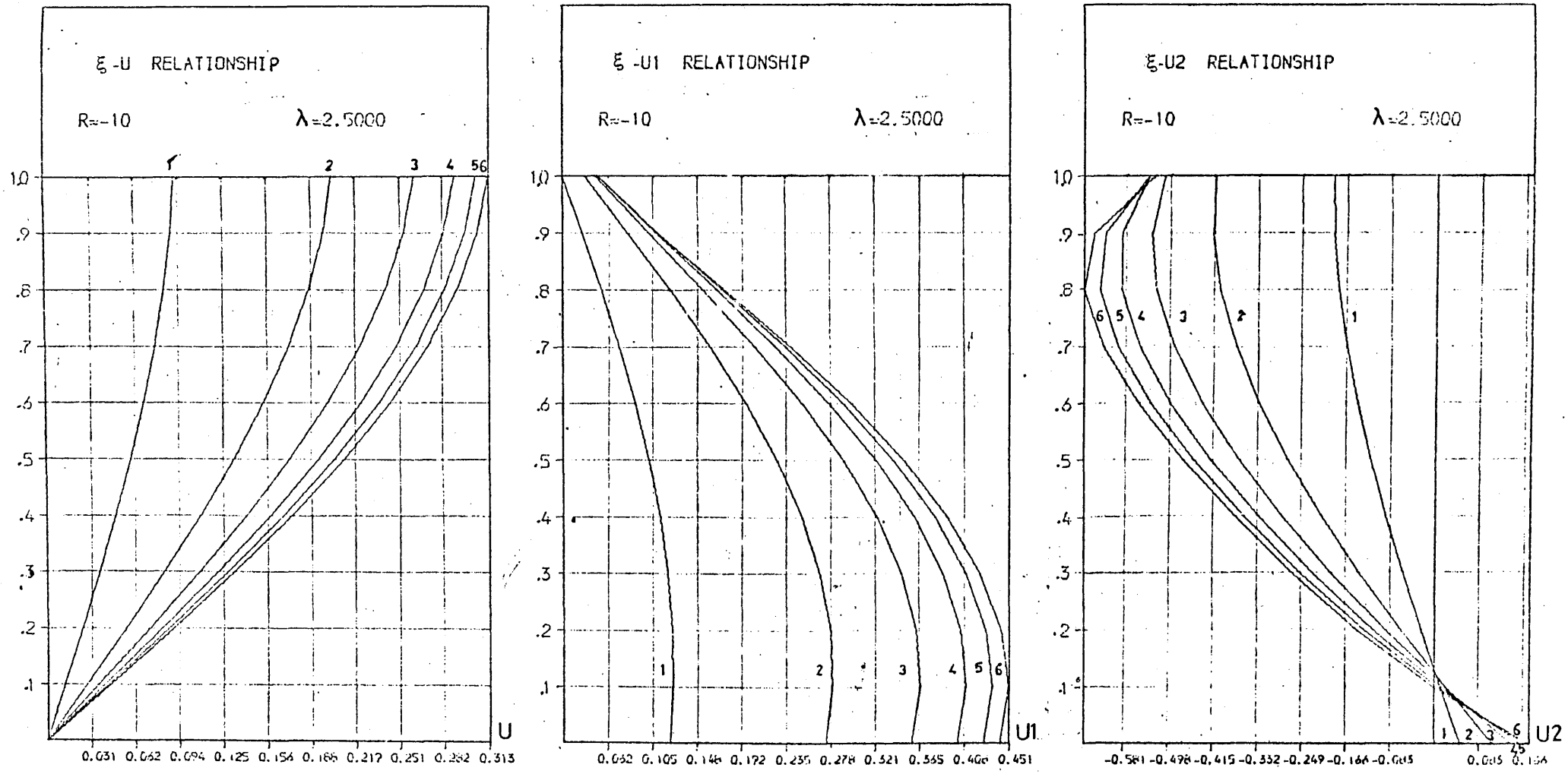
ξ -U RELATIONSHIP
R=-10
λ=2.5000
1
2
3
4
56
1.0
.9
.8
.7
.6
.5
.4
.3
.2
.1
U
0.031 0.062 0.094 0.125 0.156 0.186 0.217 0.251 0.282 0.313
ξ -U1 RELATIONSHIP
R=-10
λ=2.5000
1
2
3
4
5
6
U1
0.062 0.105 0.148 0.192 0.235 0.278 0.321 0.365 0.408 0.451
ξ-U2 RELATIONSHIP
R=-10
λ=2.5000
6
5
4
3
2
1
1
2
3
6
U2
-0.581 -0.498 -0.415 -0.332 -0.249 -0.166 -0.085 0.085 0.154

Fig. B.III.16

APPENDIX C

EFFECT OF REDUCTION IN WALL THICKNESS ON PRIMARY CORE ACTIONS

APPENDIX C

The following graphs show the effects of reducing the thickness of the walls on the primary actions of the particular core example considered in Chapter 4. They are arranged as follows:

Fig. C.1 to Fig. C.5 shows the effect of size of reduction.

Fig. C.6 to Fig. C.10 shows the effect of level of reduction.

Fig. C.11 to Fig. C.15 shows the effect of reduction on restrained core.

Fig. C.16 to Fig. C.20 shows the effect of reduction on elastically supported core.

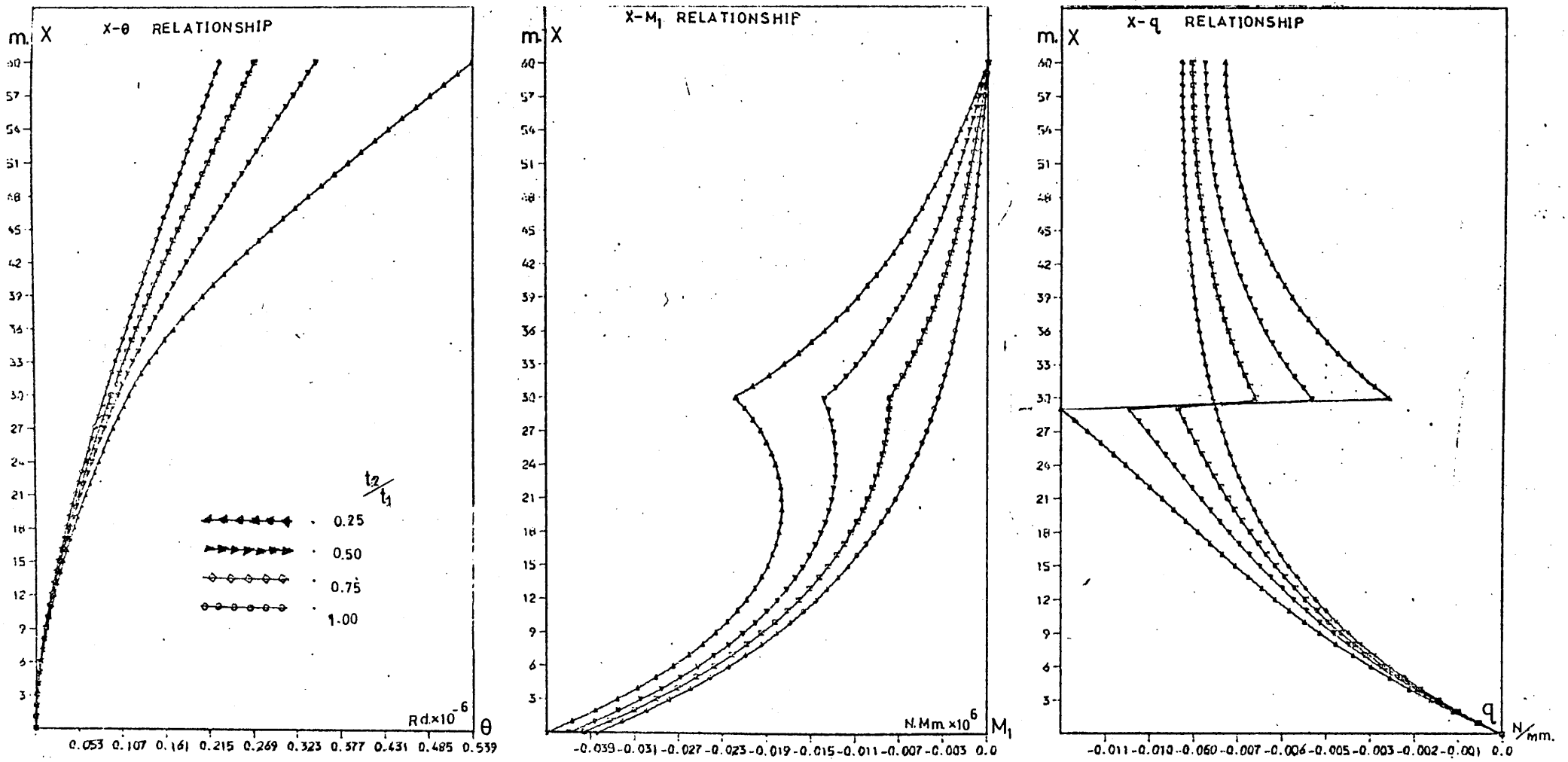

Fig. C.1 Effect of reduction in wall thickness on primary core actions (Doubly-symmetric, Point Torque at the Top)

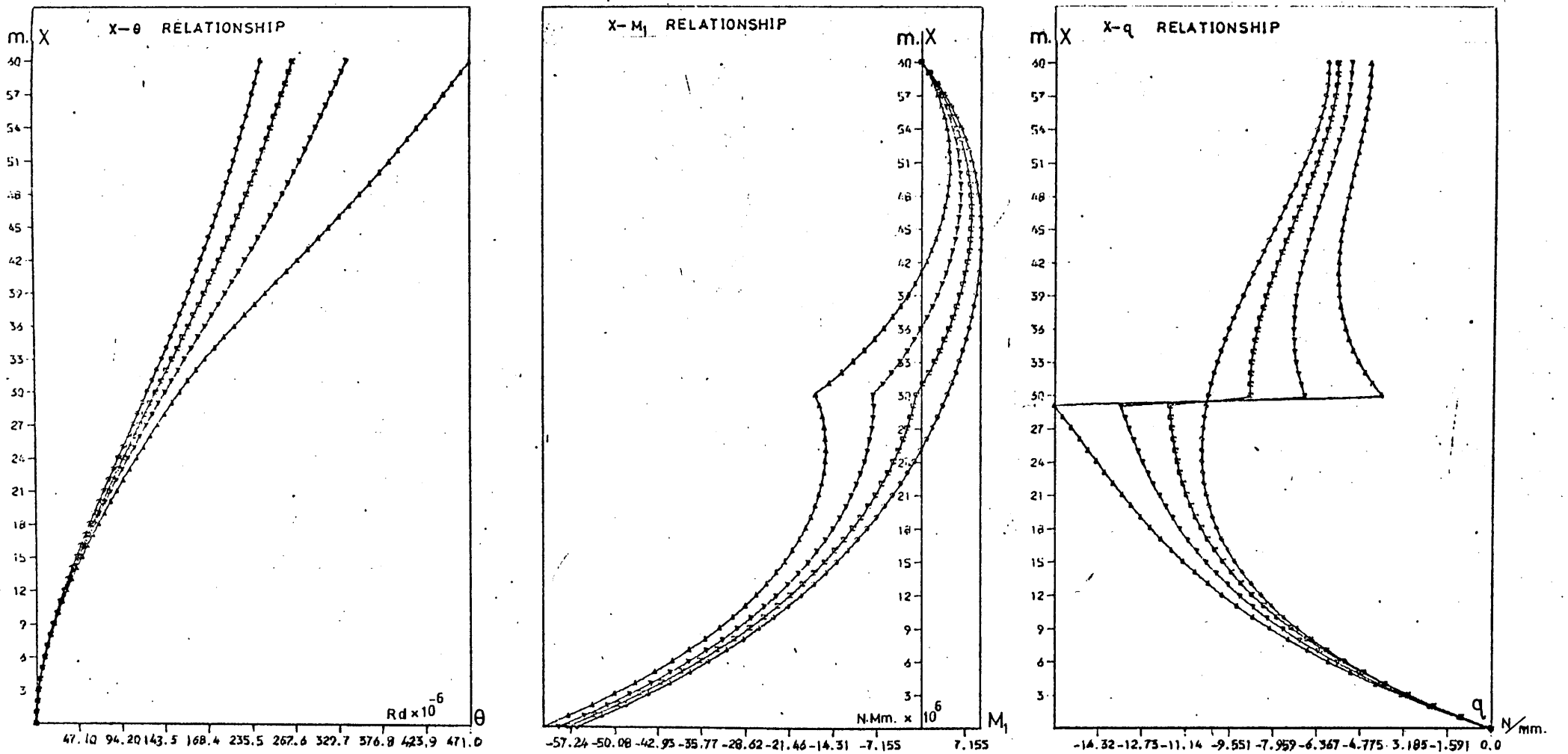

Fig. C.2 Effect of reduction in wall thickness on primary core actions
(Doubly-Symmetric, Triangularly Distributed Torque)

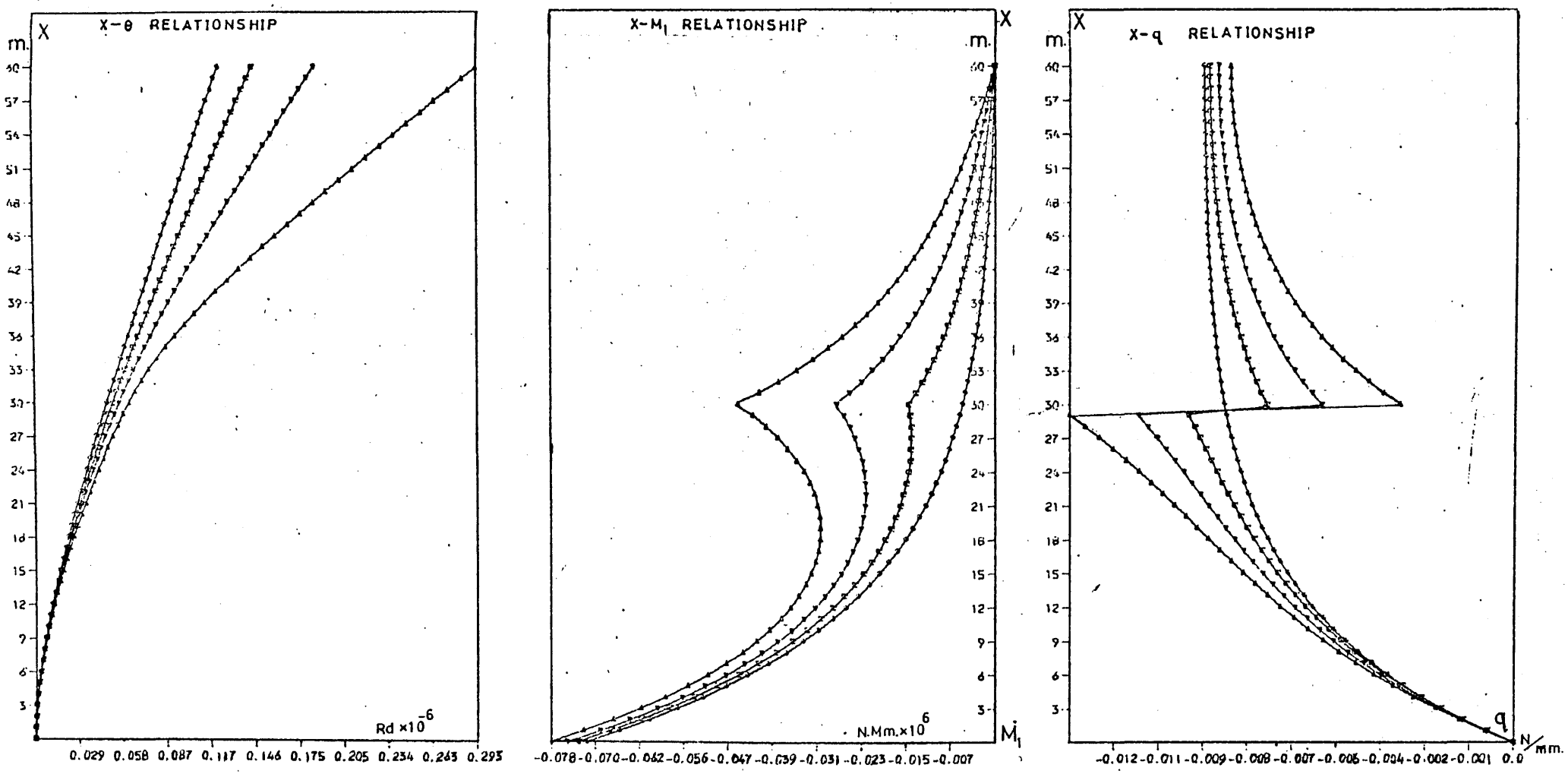

Fig. C.3 Effect of reduction in wall thickness on primary core actions (Singly-Symmetric, Point Torque at the Top)

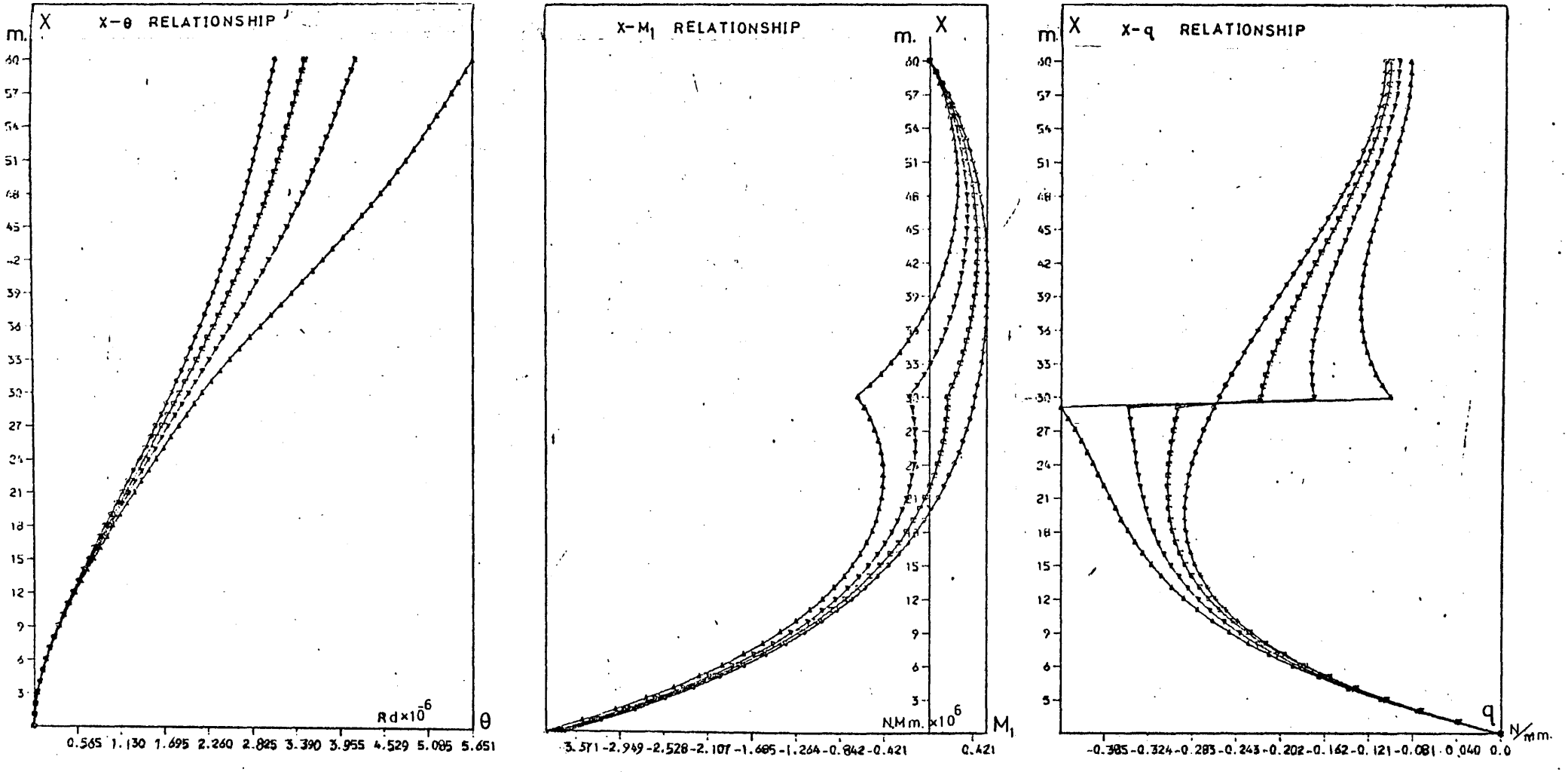

Fig. C.4 Effect of reduction in wall thickness on primary core actions
(Singly-Symmetric, Uniformly Distributed Torque)

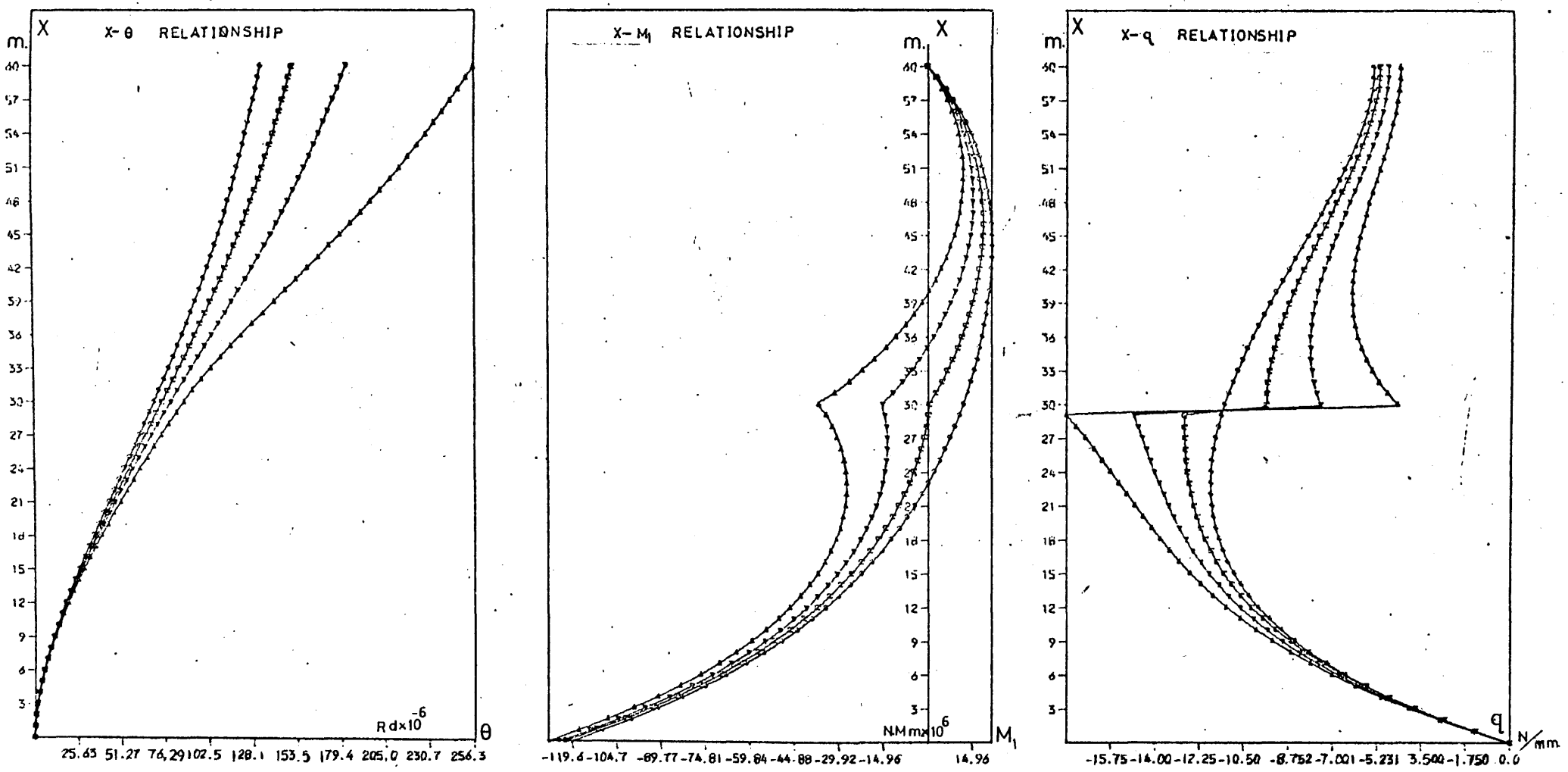

Fig. C.5 Effect of reduction in wall thickness on primary core actions
(Singly-Symmetric, Triangularly Distributed Torque)

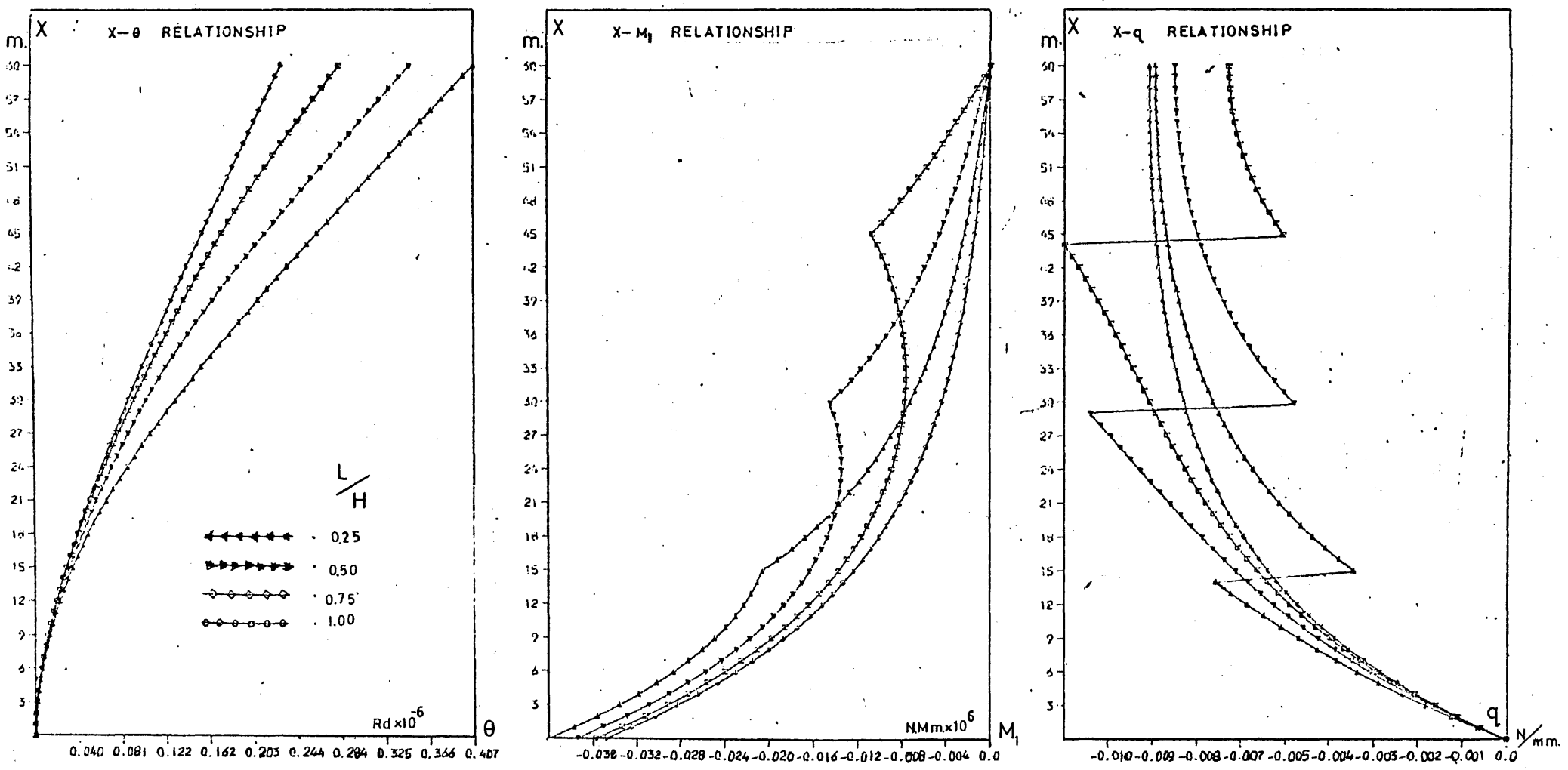

Fig. C.6 Effect of level at which reduction in wall thickness occurs on primary core actions (Doubly-symmetric, Point Torque at the Top)

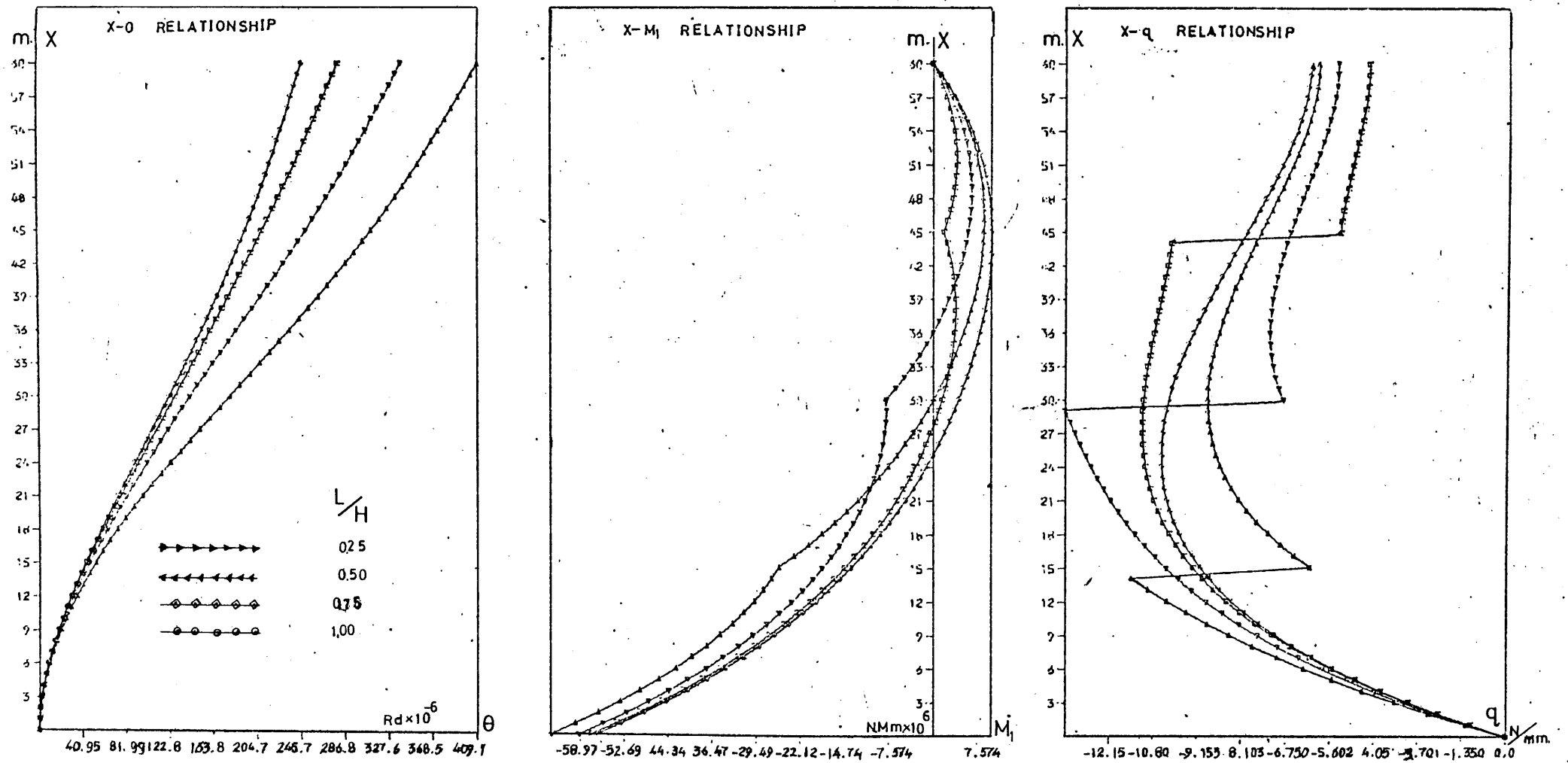

Fig. C.7 Effect of level at which reduction in wall thickness occurs on primary core actions (Doubly-Symmetric, Triangularly Distributed Torque)

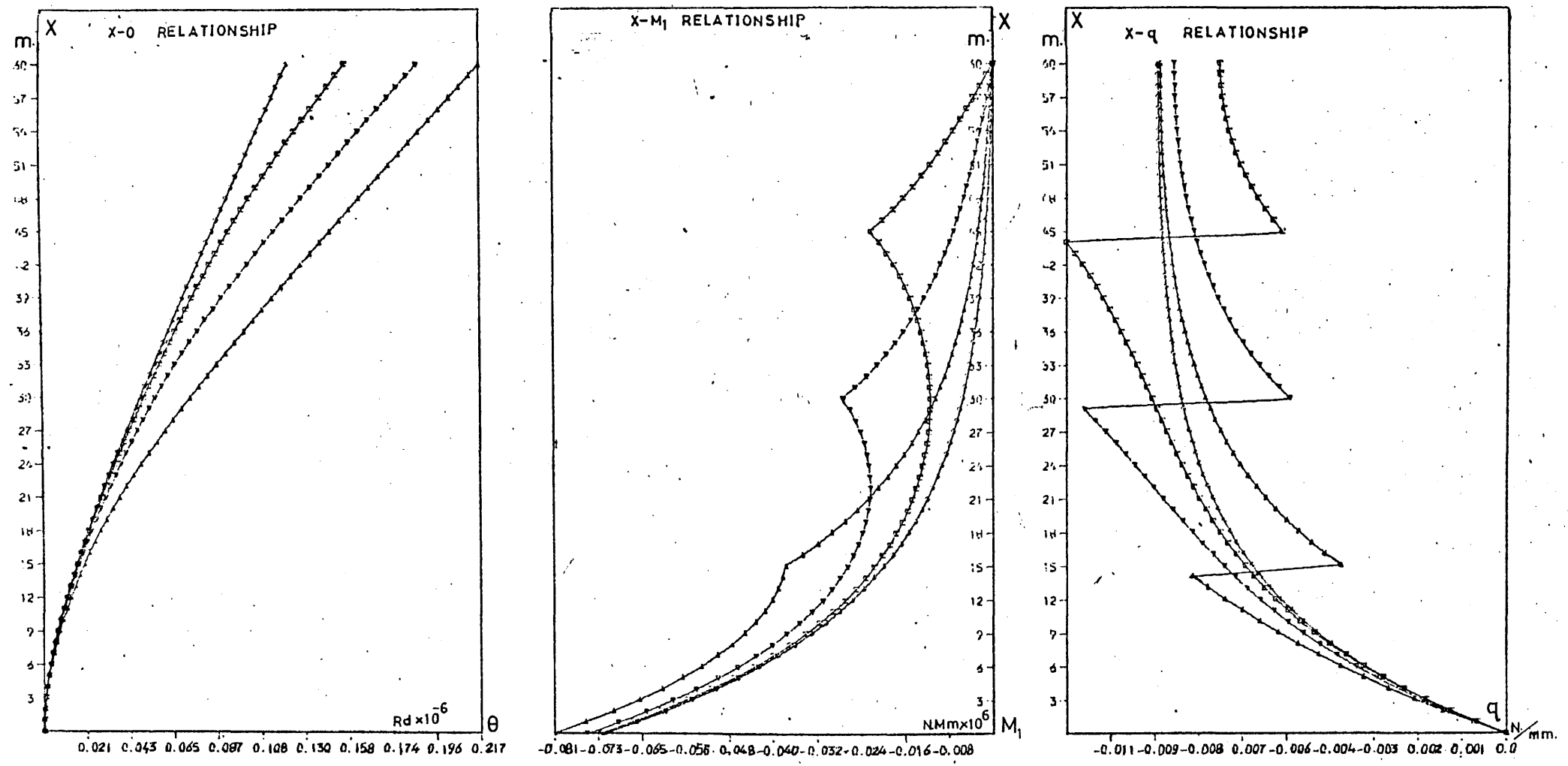

Fig. C.8 Effect of level at which reduction in wall thickness occurs on primary core actions (Singly-Symmetric, Point Torque at the Top)

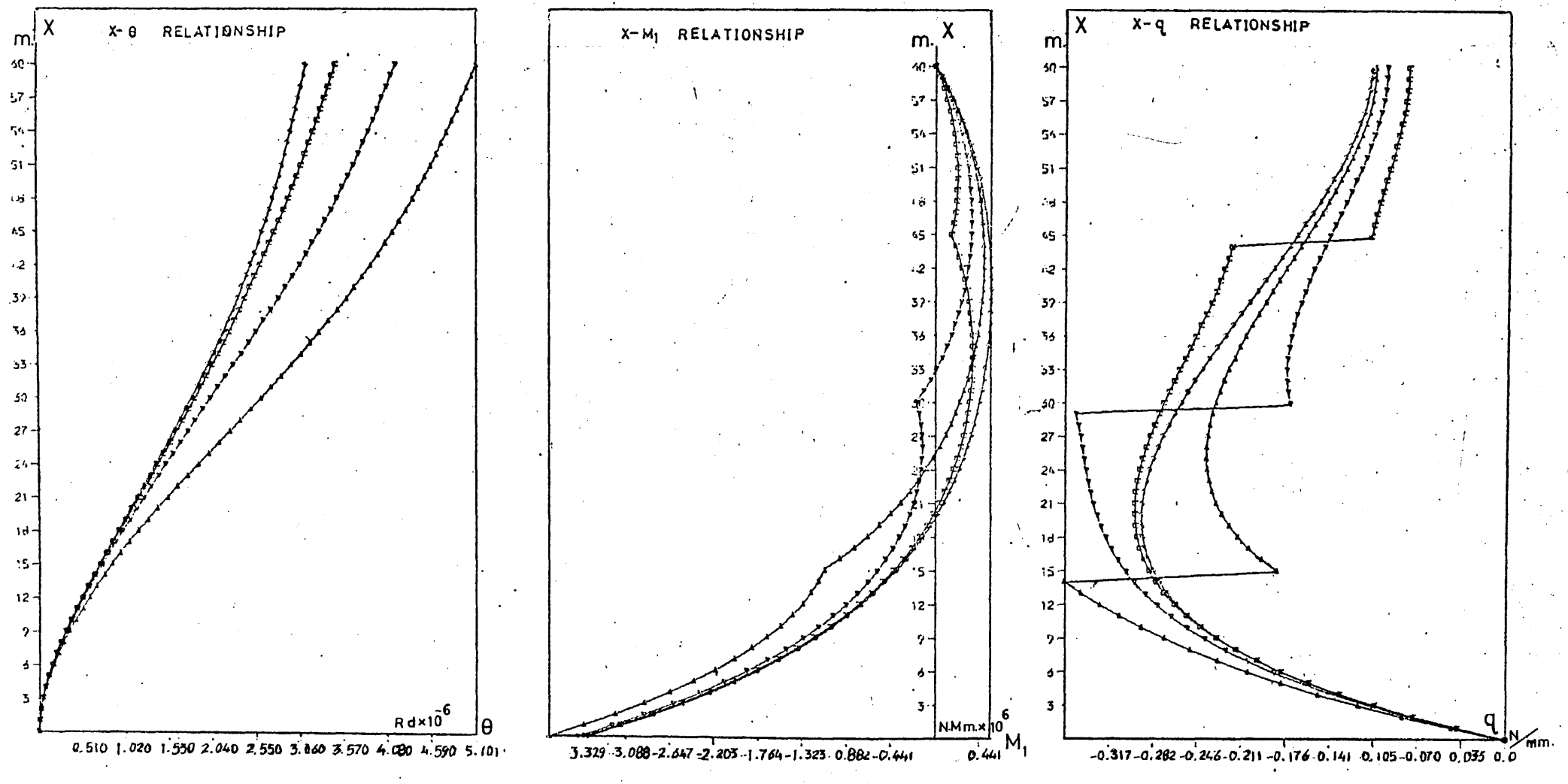

Fig. C.9 Effect of level at which reduction in wall thickness occurs on primary core actions (Singly-Symmetric, Uniformly Distributed Torque)

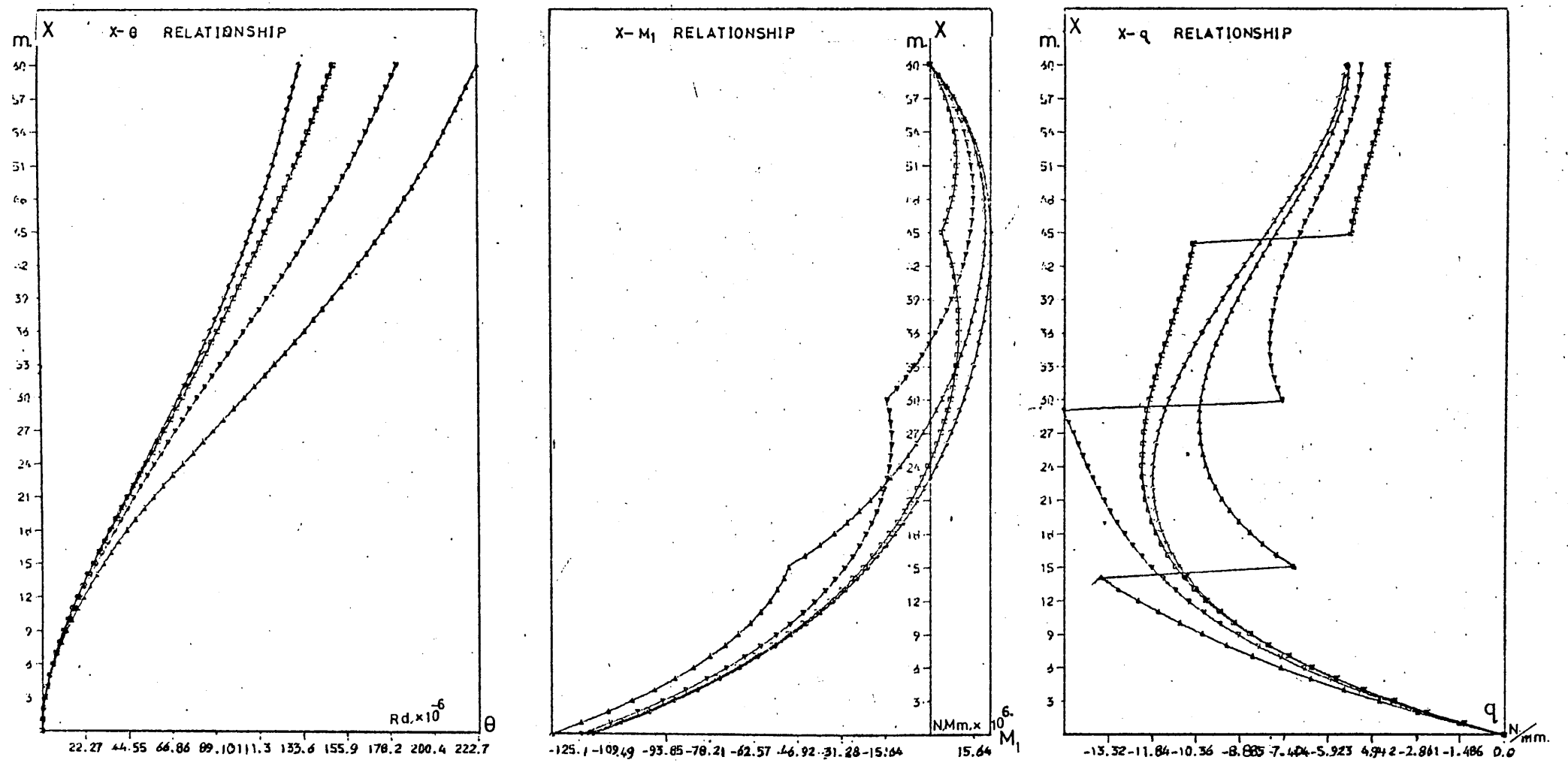

Fig. C.10 Effect of level at which reduction in wall thickness occurs on primary core actions (Singly-Symmetric, Triangularly Distributed Torque)

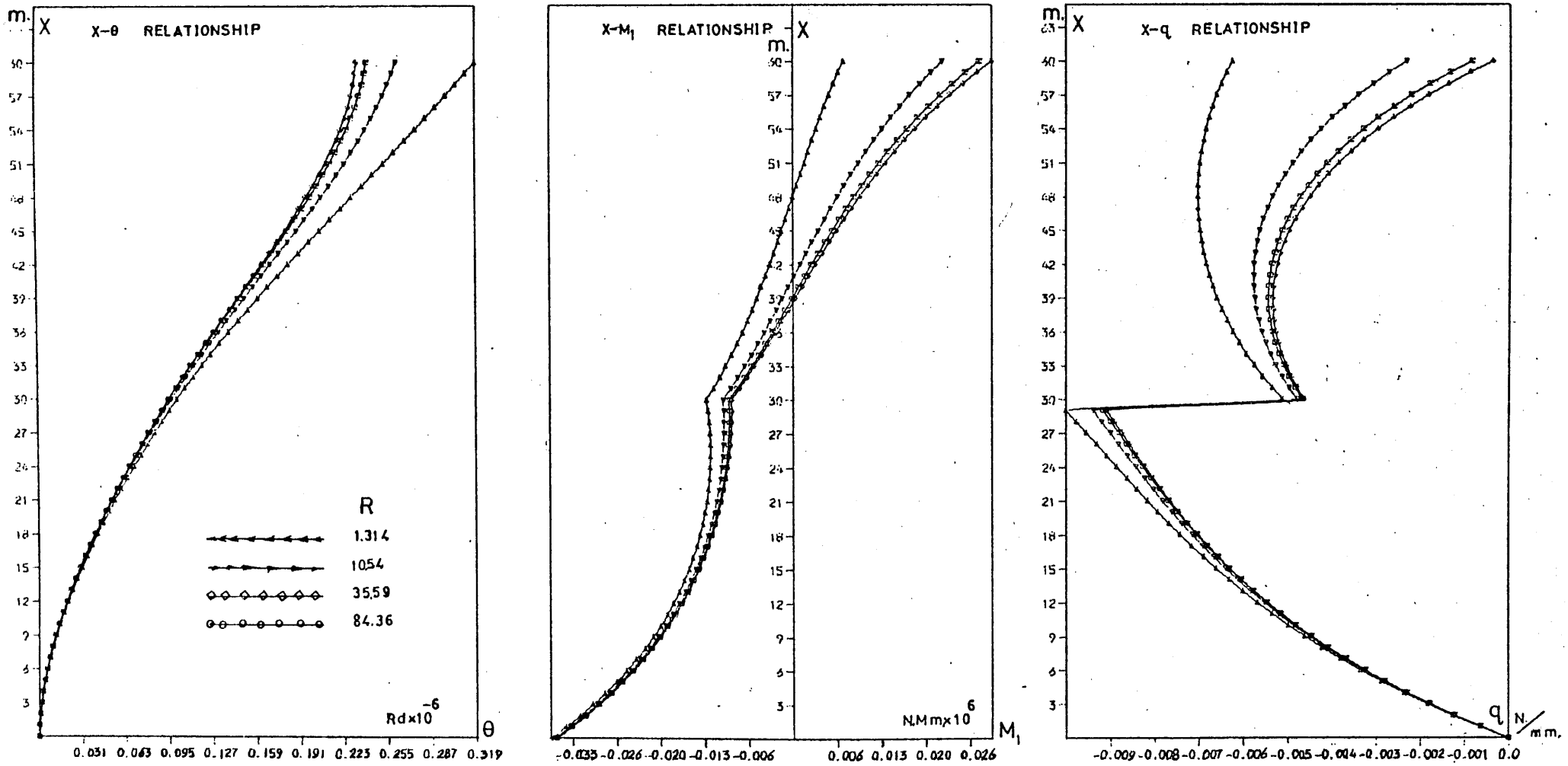

Fig. C.11 Effect of reduction in wall thickness at mid-height on primary actions of stiffened cores (Doubly-Symmetric, Point Torque at the Top)

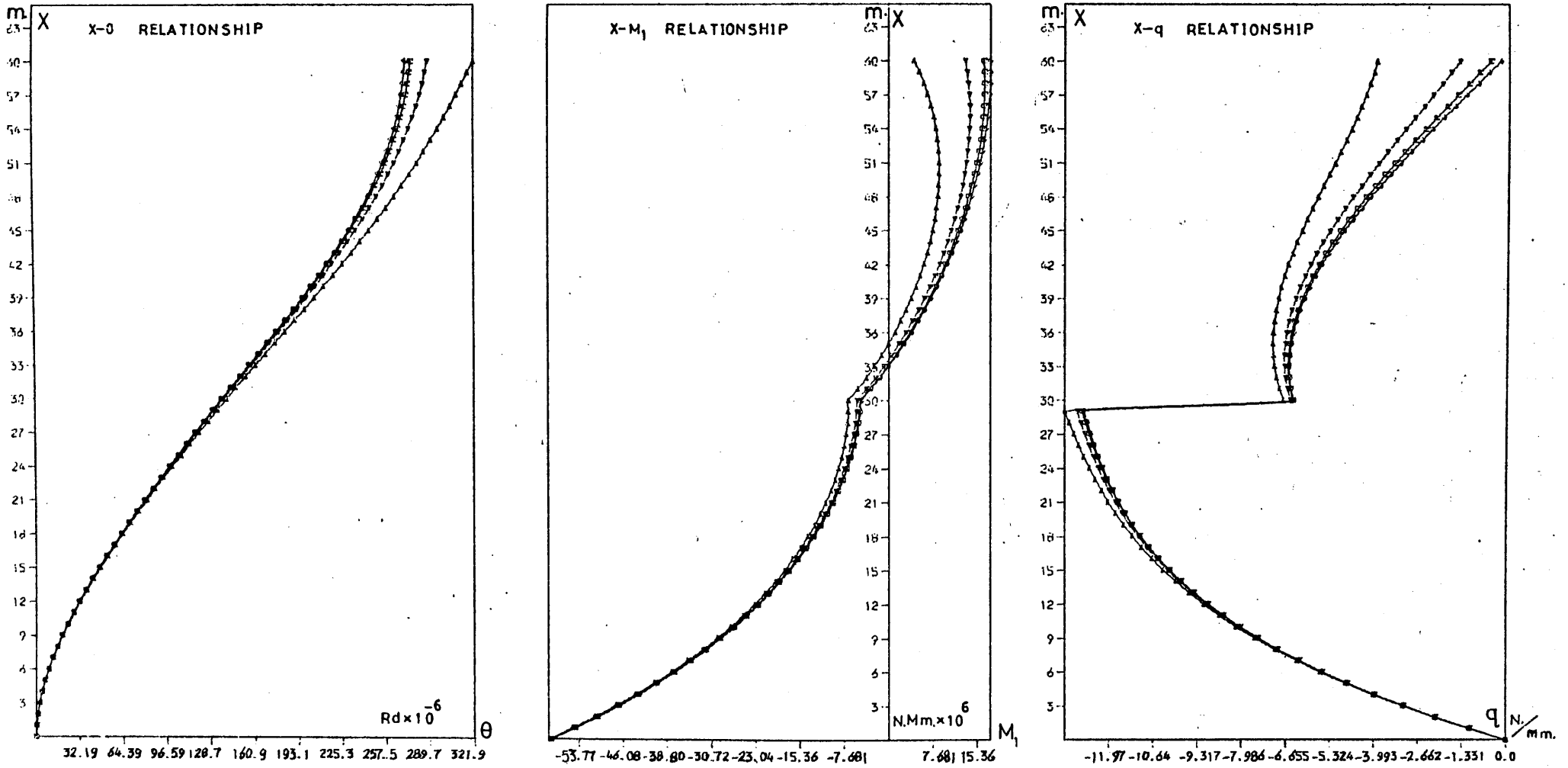

Fig. C.12 Effect of reduction in wall thickness at mid-height on primary actions of stiffened cores (Doubly-Symmetric, Triangularly Distributed Torque)

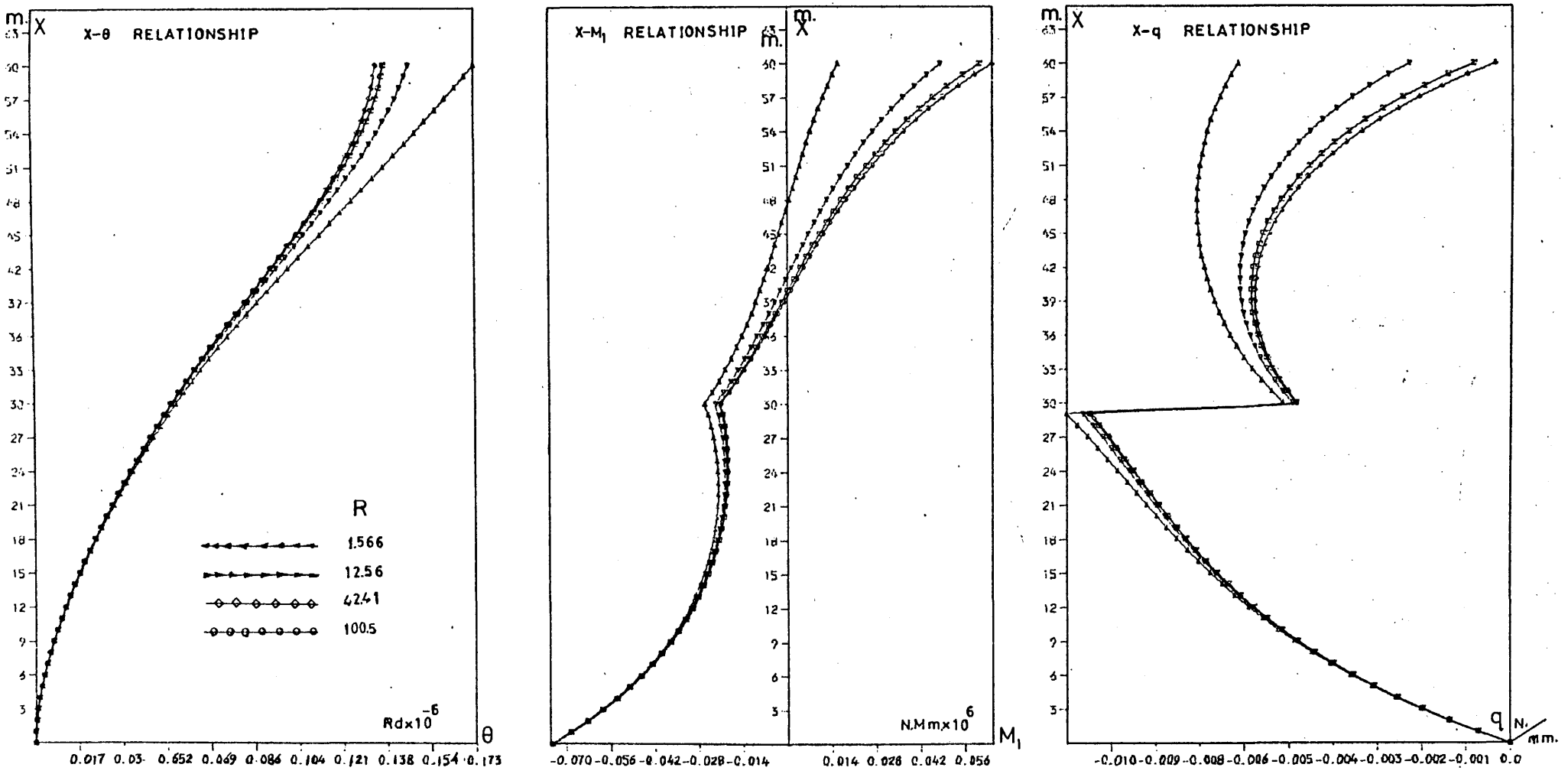

Fig. C.13 Effect of reduction in wall thickness at mid-height on primary actions of stiffened cores (Singly-Symmetric, Point Torque at the Top)

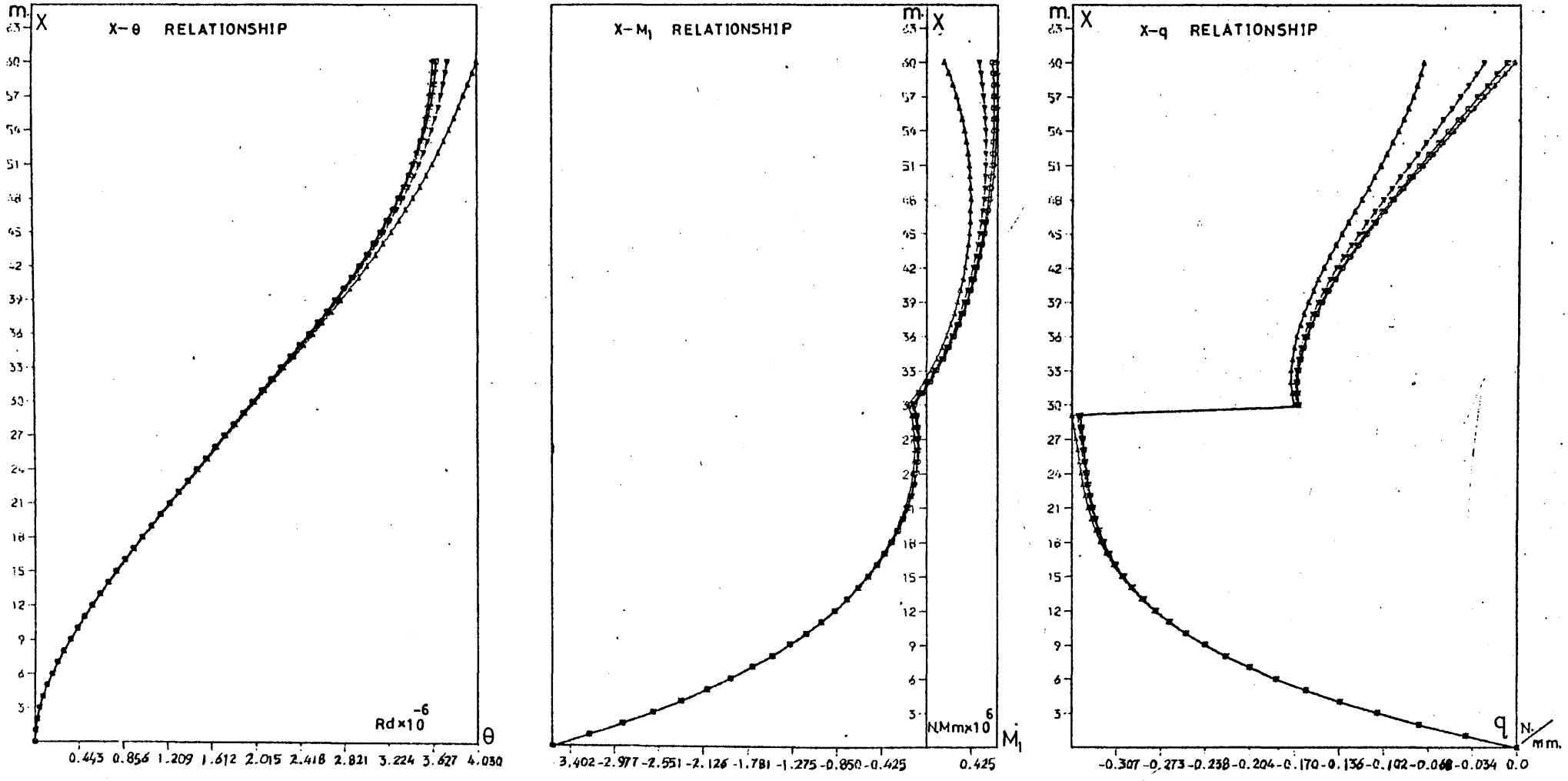

Fig. C.14 Effect of reduction in wall thickness at mid-height on primary actions of stiffened cores (Singly-Symmetric, Uniformly Distributed Torque)

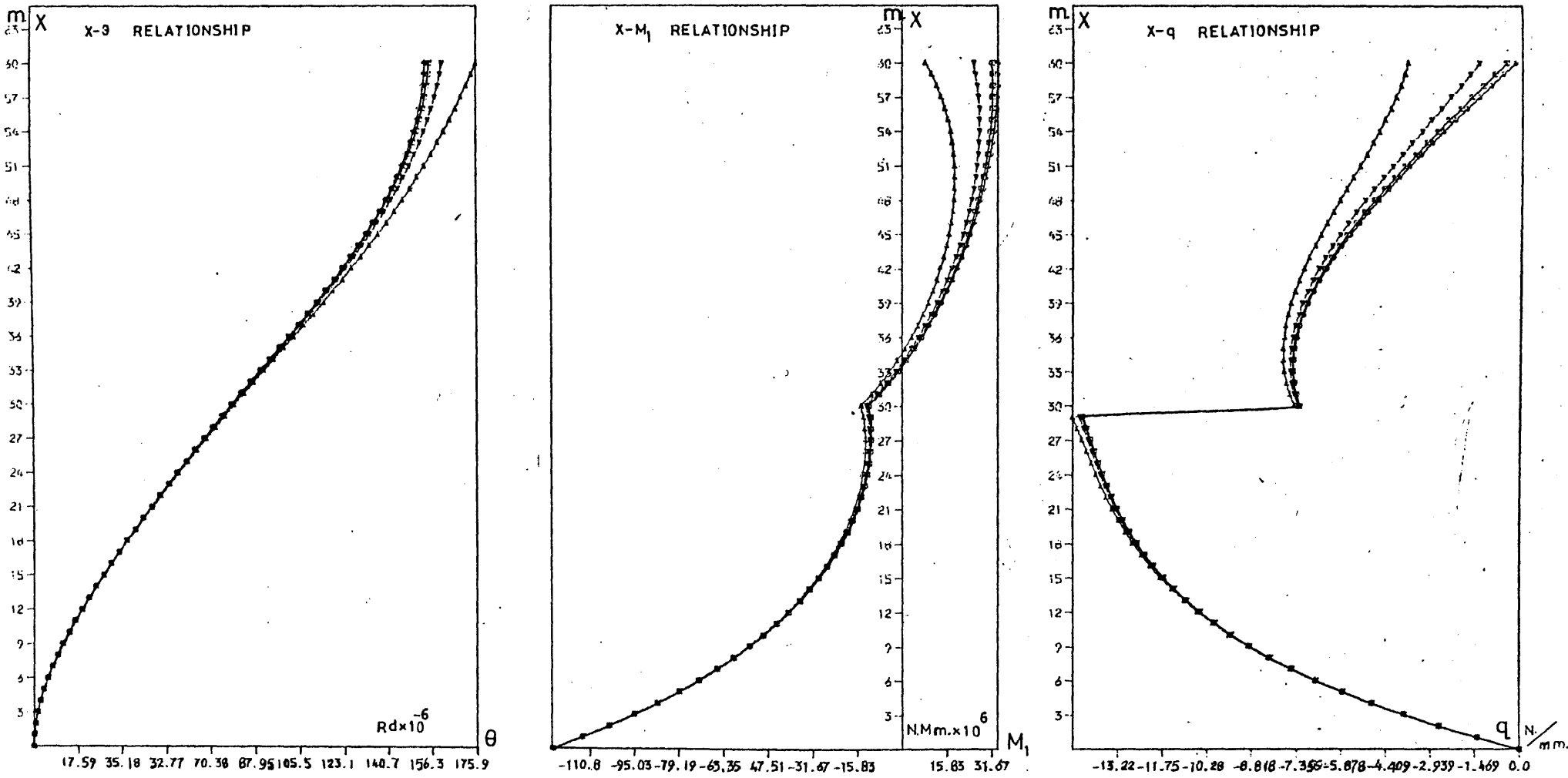

Fig. C.15 Effect of reduction in wall thickness at mid-height on primary actions of stiffened cores (Singly-Symmetric, Triangularly Distributed Torque)

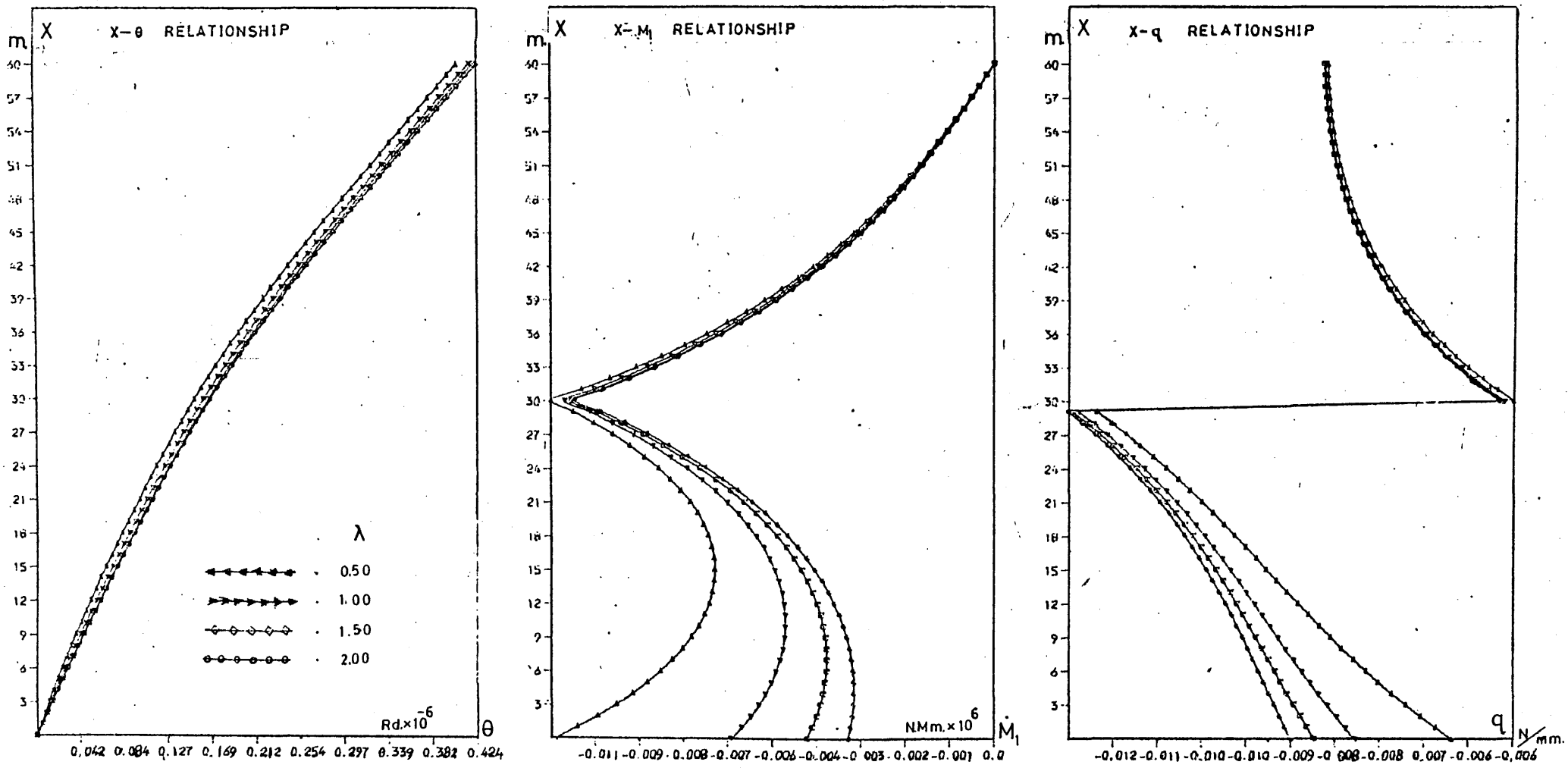

Fig. C.16 Effect of reduction in wall thickness at mid-height on primary actions in elastically supported cores.
(Doubly-Symmetric, Point Torque at the Top)

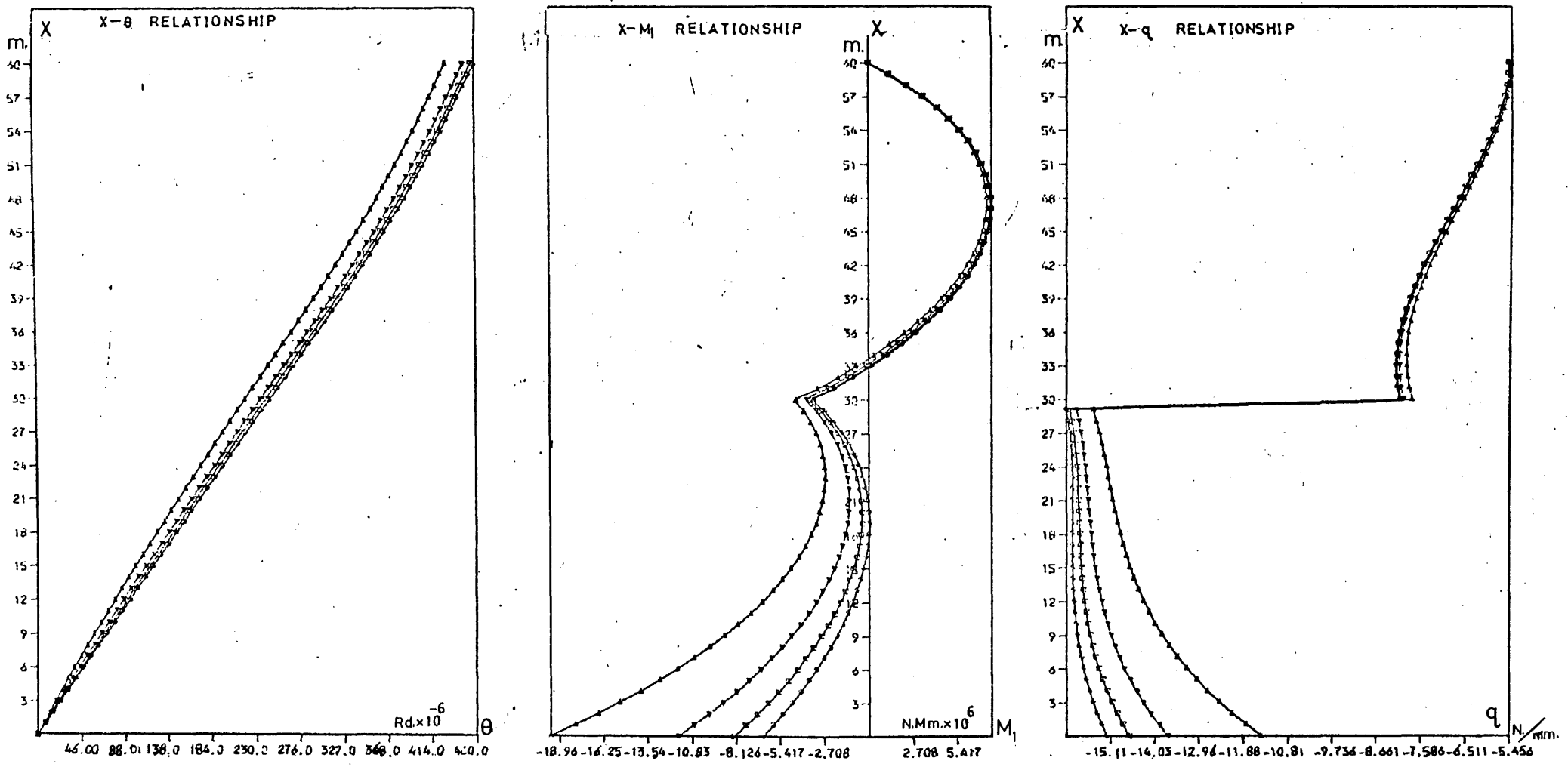

Fig. C.17 Effect of reduction in wall thickness at mid-height on primary actions in elastically supported cores.
(Doubly-Symmetric, Triangularly Distributed Torque)

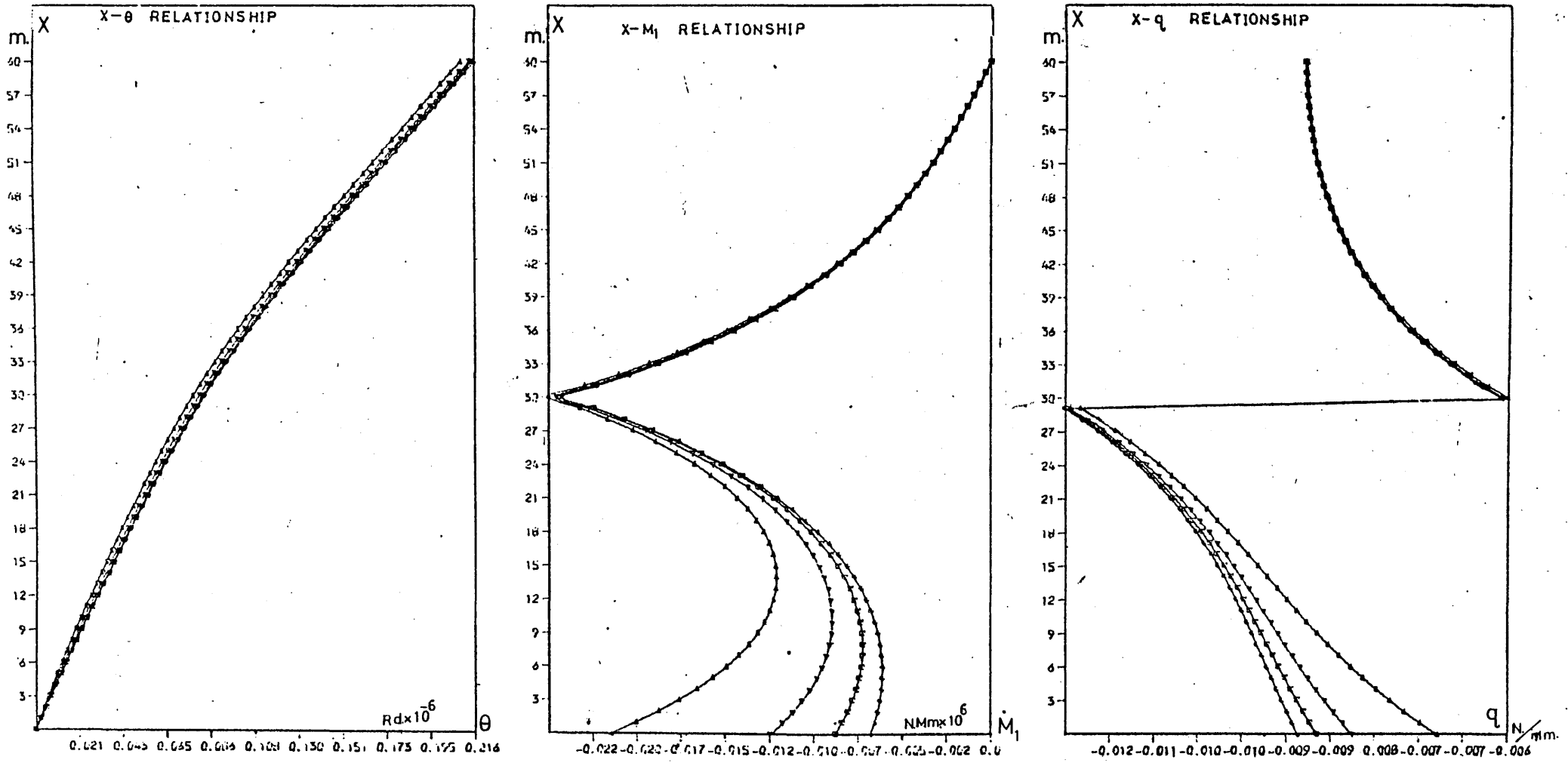

Fig. C.18 Effect of reduction in wall thickness at mid-height on primary actions in elastically supported cores.
(Singly-Symmetric, Point Torque at the Top)

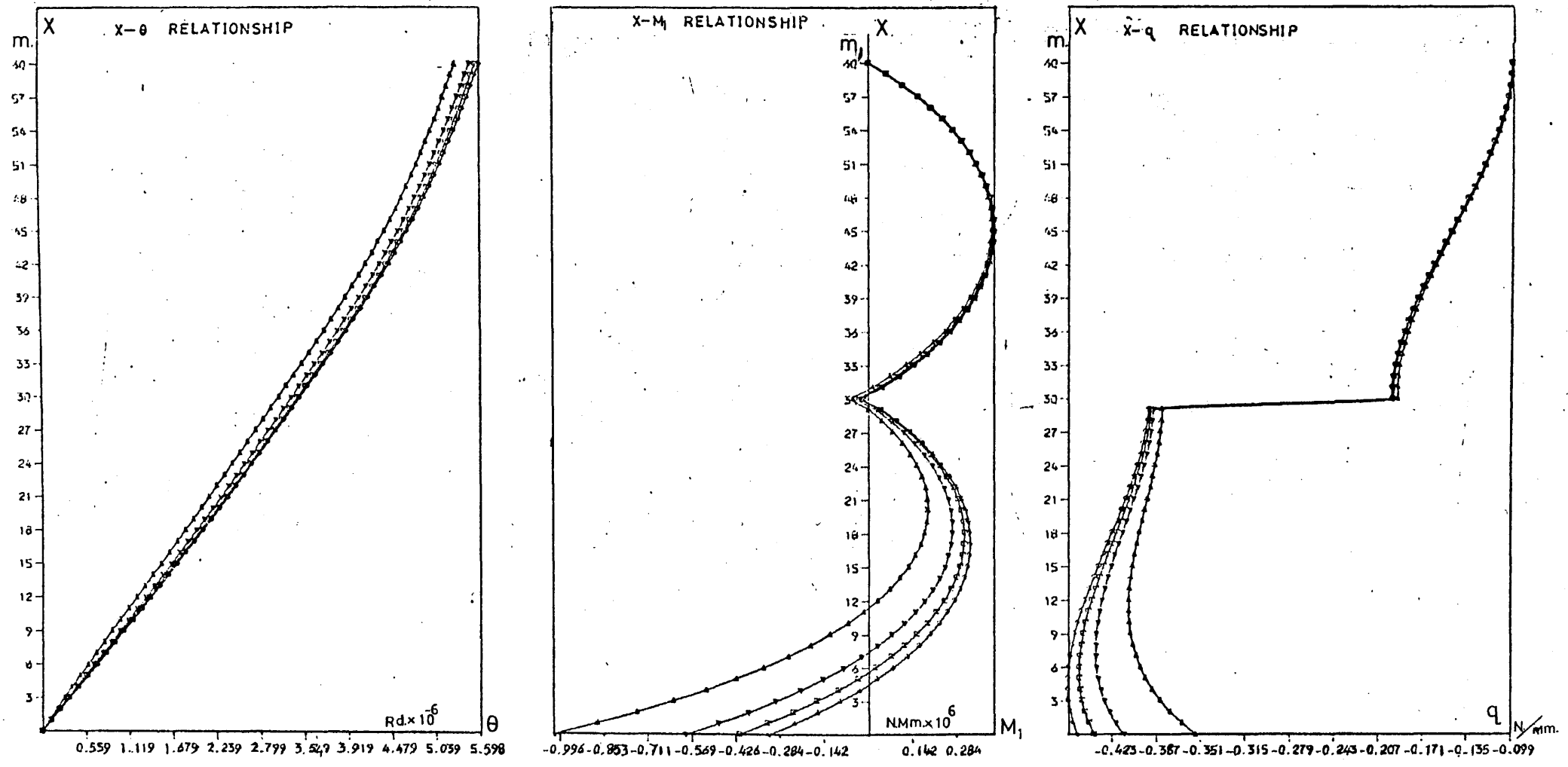

Fig. C.19 Effect of reduction in wall thickness at mid-height on primary actions in elastically supported cores.
(Singly-Symmetric, Uniformly Distributed Torque)

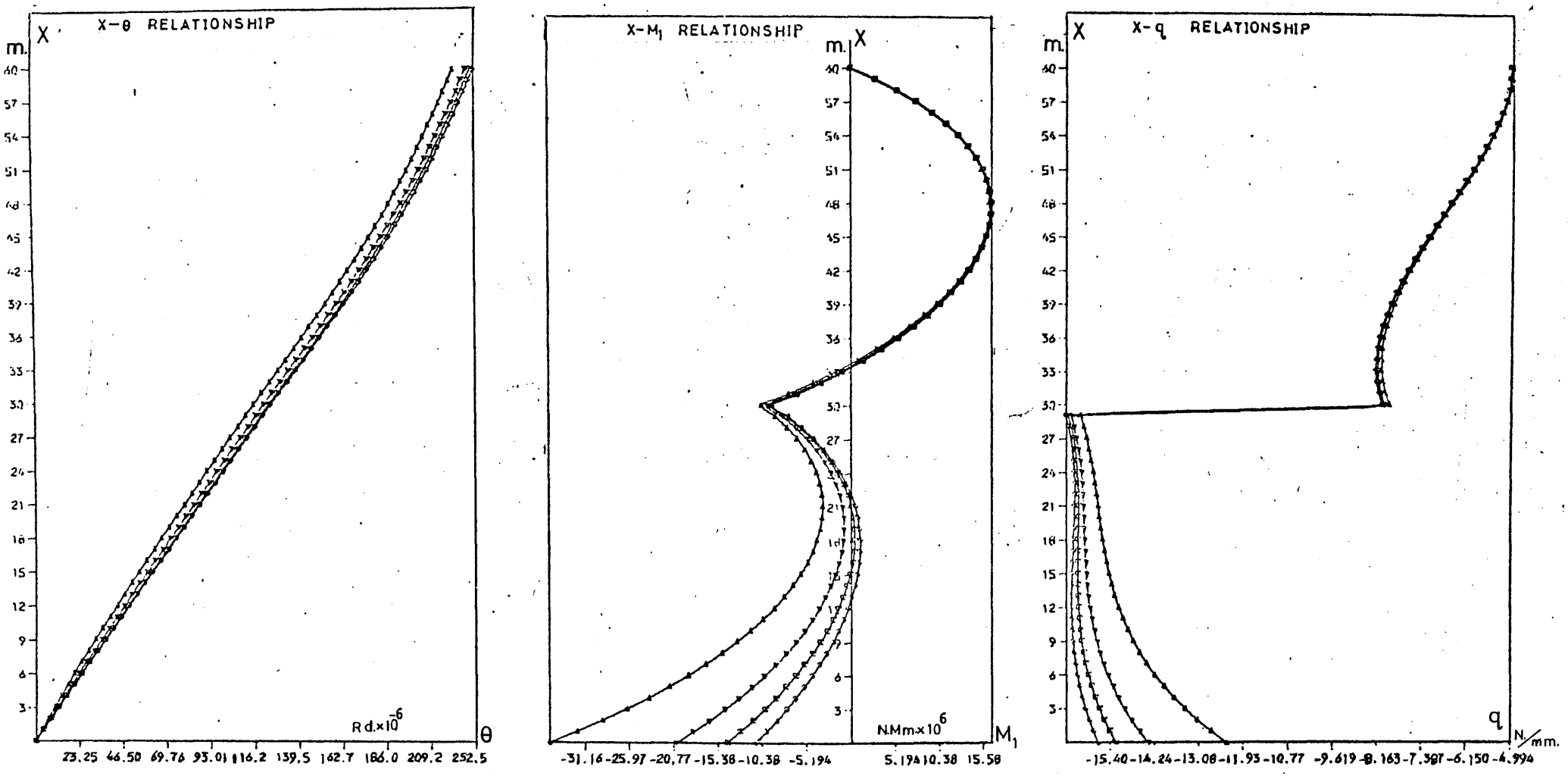

Fig. C.20 Effect of reduction in wall thickness at mid-height on primary actions in elastically supported cores.
(Singly-Symmetric, Triangularly Distributed Torque)

APPENDIX D

FLOW CHART OF THE PROGRAM (PREPS)

APPENDIX D

FLOW CHART OF THE PROGRAM (PREPS)

The following flow chart demonstrates the logic sequence of the computer program used to calculate and plot the primary actions in the elastic and elasto-plastic behaviour of singly and doubly symmetrical core structures. The sequence of the programs are joined through numbers in the following pages.

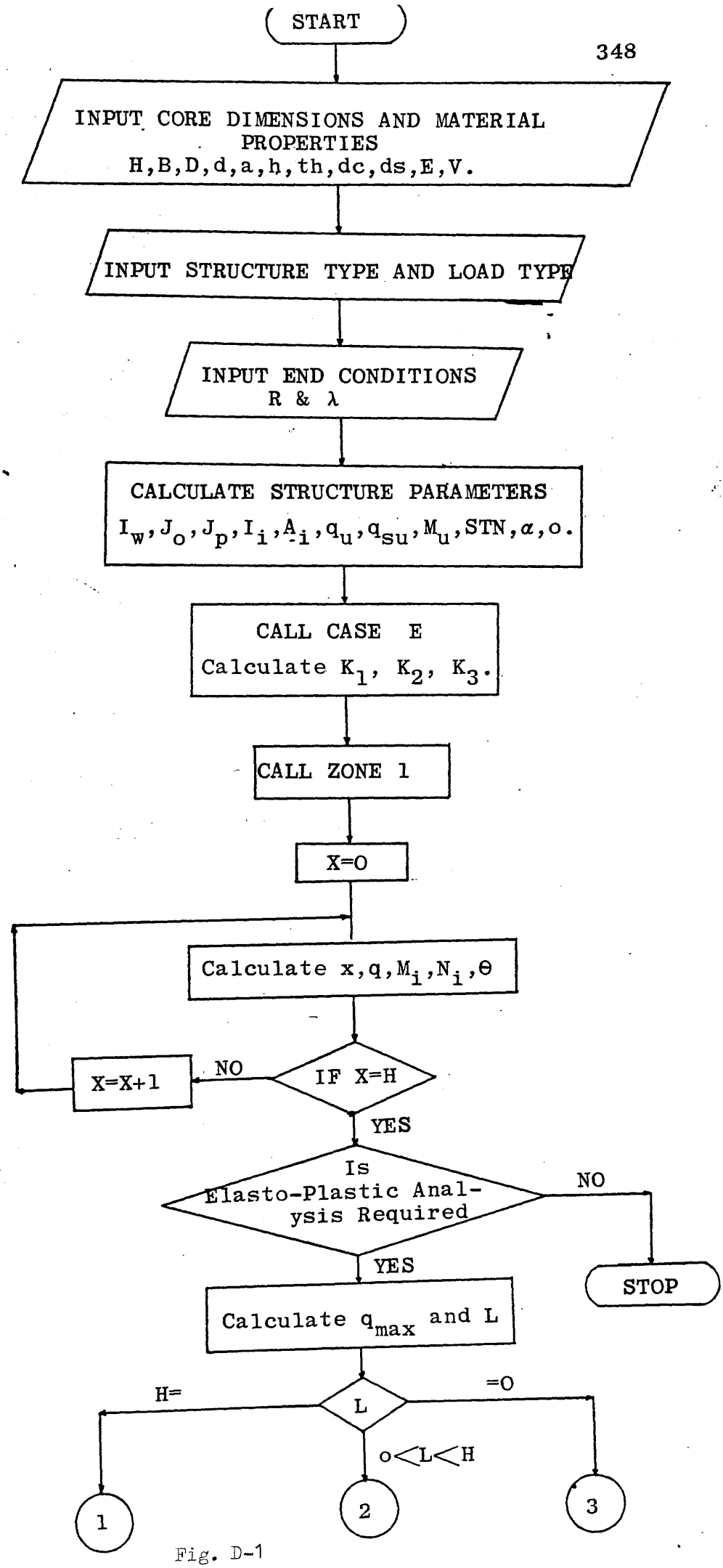
START
INPUT CORE DIMENSIONS AND MATERIAL PROPERTIES
H,B,D,d,a,h,th,dc,ds,E,V.
INPUT STRUCTURE TYPE AND LOAD TYPE
INPUT END CONDITIONS
R & λ
CALCULATE STRUCTURE PARAMETERS
$I_w, J_o, J_p, I_i, A_i, q_u, q_{su}, M_u$, STN, α, o.
CALL CASE E
Calculate K_1, K_2, K_3.
CALL ZONE 1
X=O
Calculate x,q,M_i,N_i,Θ
IF X=H
NO
X=X+1
YES
Is Elasto-Plastic Analysis Required
NO
STOP
YES
Calculate q_{max} and L
L
H=
=O
o<L<H
1
2
3

Fig. D-1

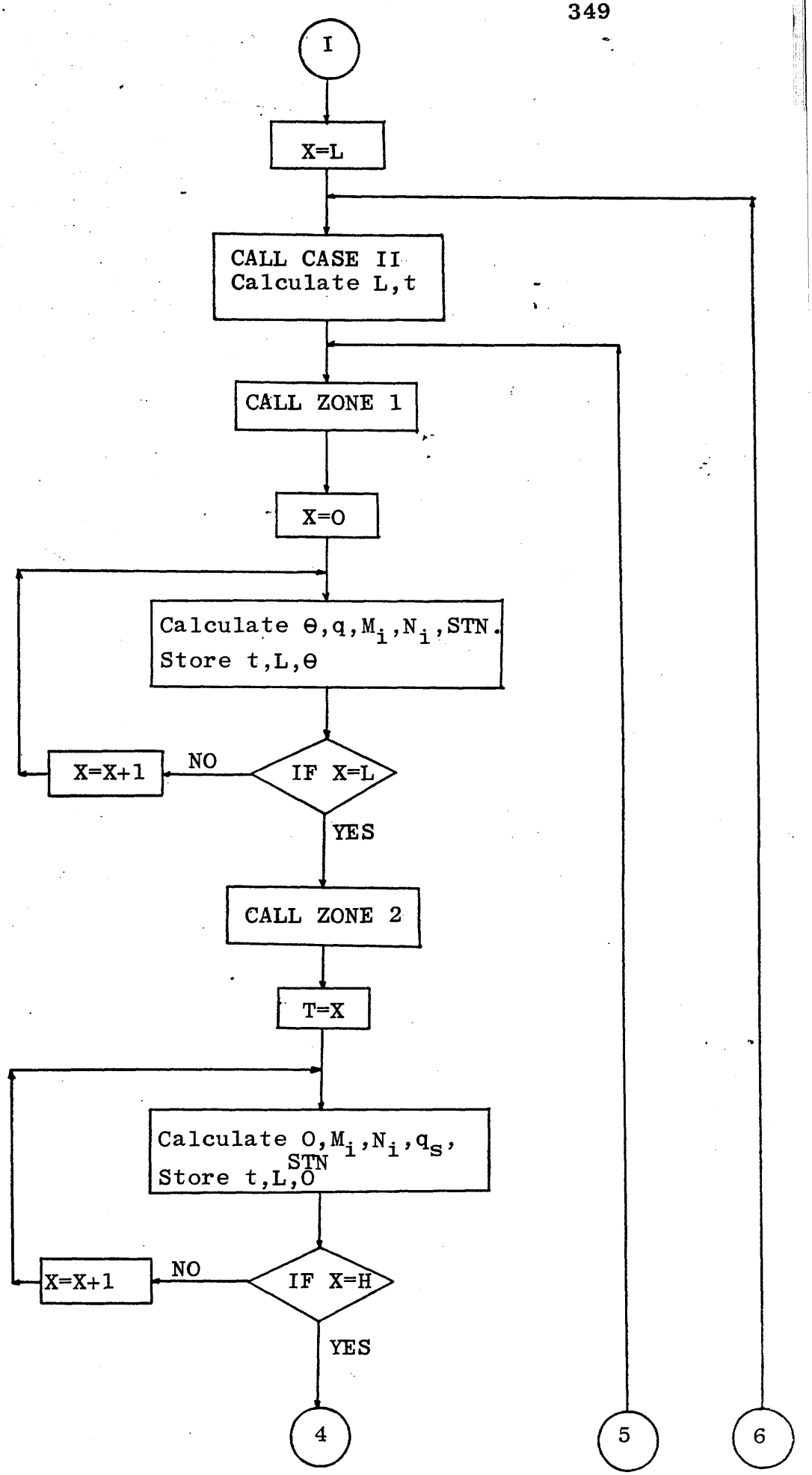
I
X=L
CALL CASE II
Calculate L,t
CALL ZONE 1
X=O
Calculate θ,q,M_i,N_i,STN.
Store t,L,θ
X=X+1
NO
IF X=L
YES
CALL ZONE 2
T=X
Calculate O,M_i,N_i,q_s,
STN
Store t,L,O
X=X+1
NO
IF X=H
YES
4
5
6

Fig. D-2

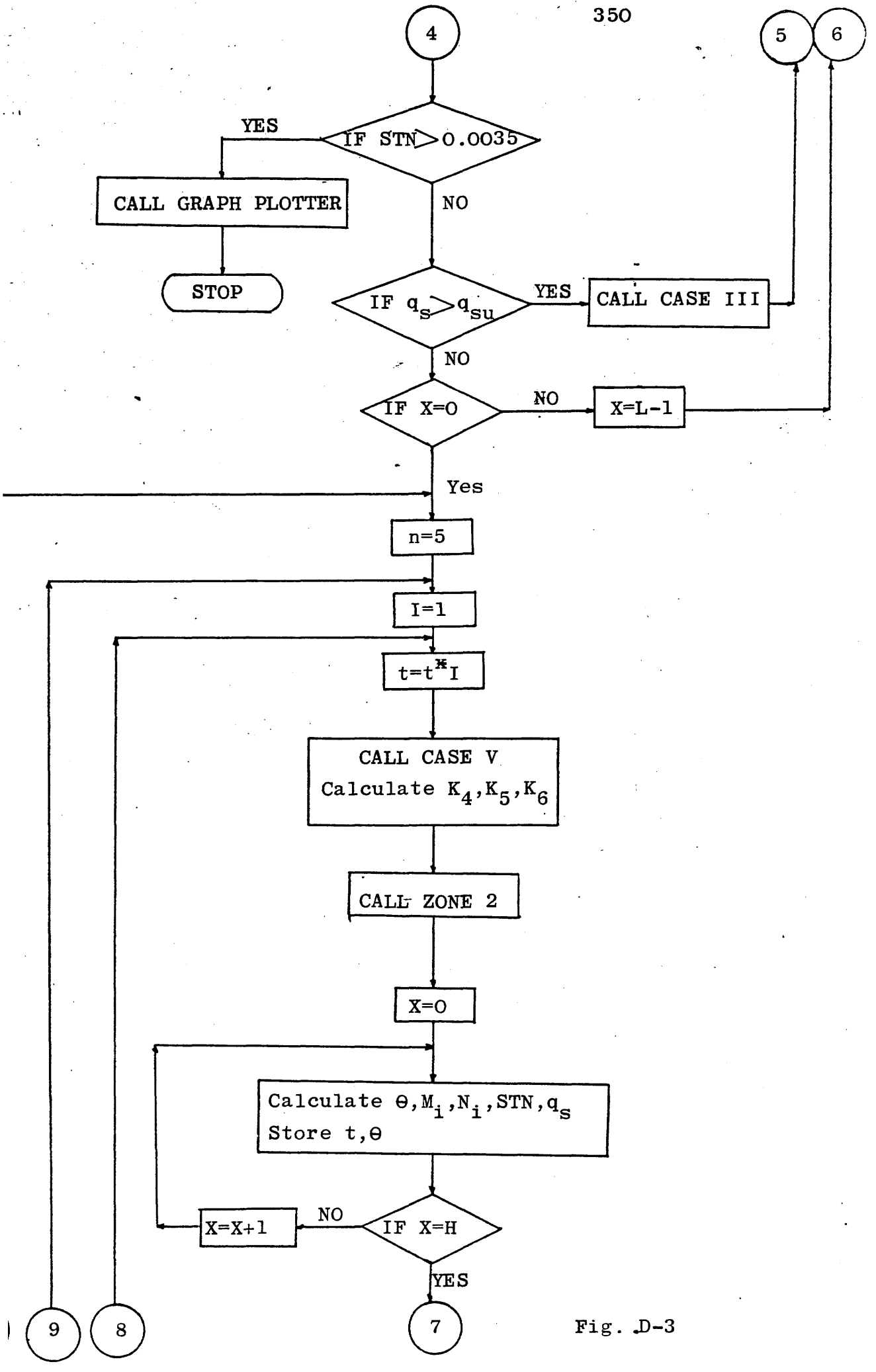
4
5
6
IF STN > 0.0035
YES
NO
CALL GRAPH PLOTTER
STOP
IF $q_s > q_{su}$
YES
CALL CASE III
NO
IF X=0
NO
X=L-1
Yes
n=5
I=1
t=t*I
CALL CASE V
Calculate K_4, K_5, K_6
CALL ZONE 2
X=0
Calculate θ, M_i, N_i, STN, q_s
Store t, θ
X=X+1
NO
IF X=H
YES
9
8
7

Fig. D-3

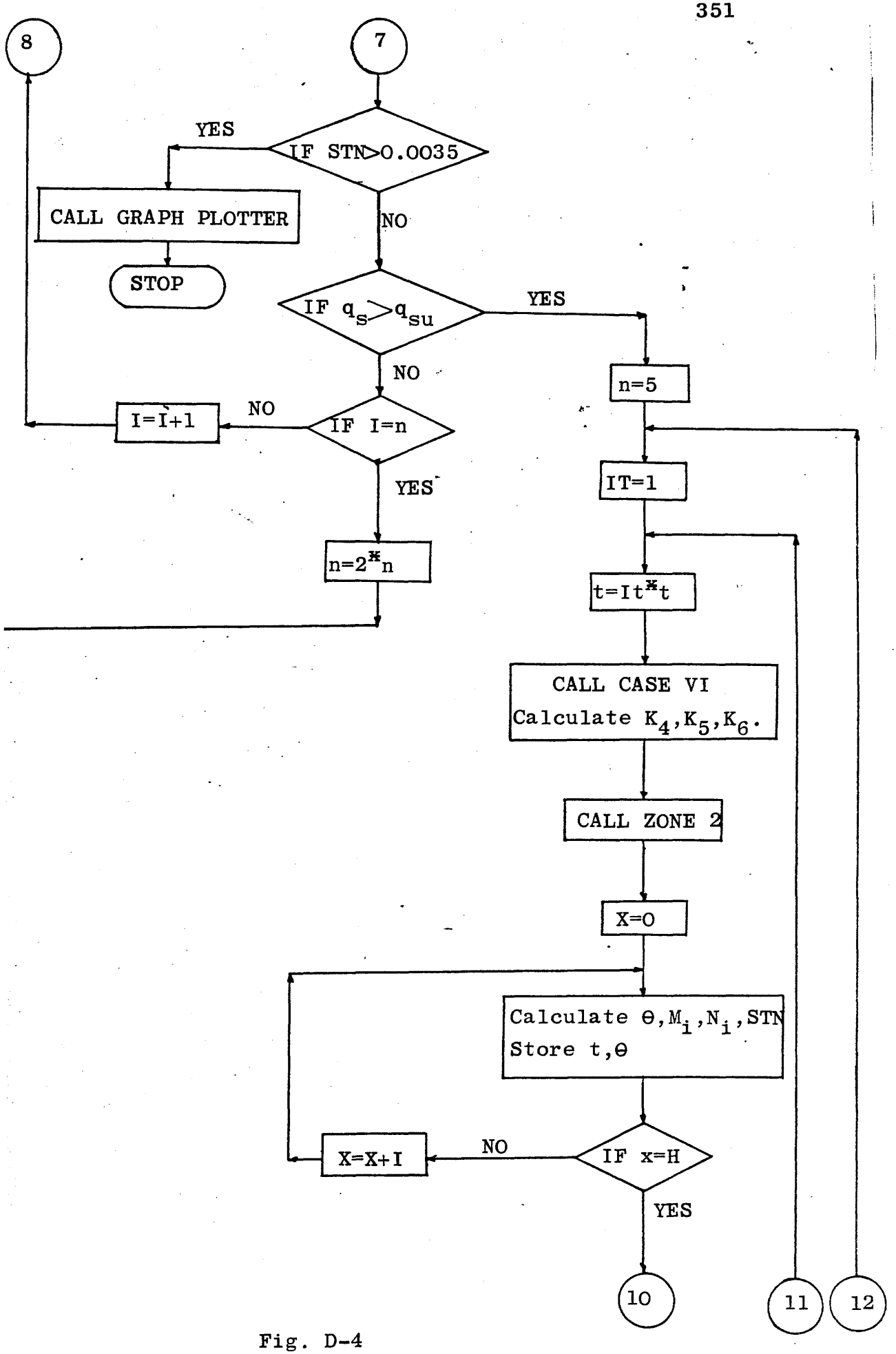
8
7
YES
IF STN>0.0035
CALL GRAPH PLOTTER
STOP
NO
IF $q_s > q_{su}$
YES
NO
n=5
I=I+1
NO
IF I=n
YES
IT=1
$n=2^{*}n$
$t=It^{*}t$
CALL CASE VI
Calculate K_4, K_5, K_6.
CALL ZONE 2
X=0
Calculate θ, M_i, N_i, STN
Store t, θ
X=X+I
NO
IF x=H
YES
10
11
12

Fig. D-4

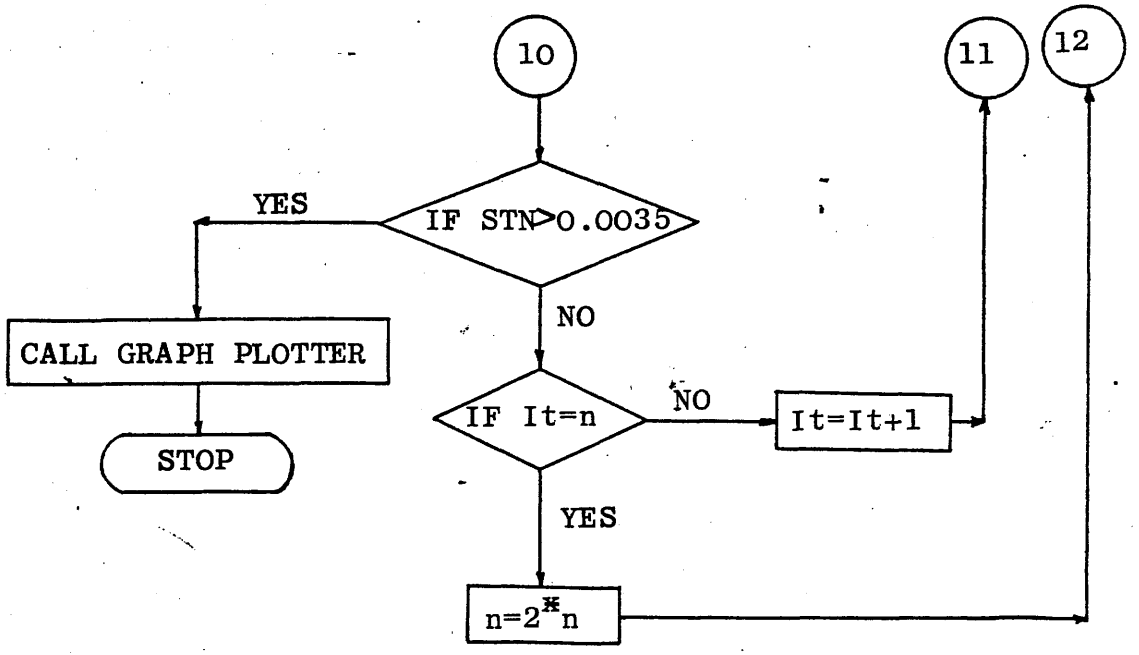
10
11
12
IF STN>0.0035
YES
NO
CALL GRAPH PLOTTER
STOP
IF It=n
NO
It=It+1
YES
n=2*n

Fig. D-5

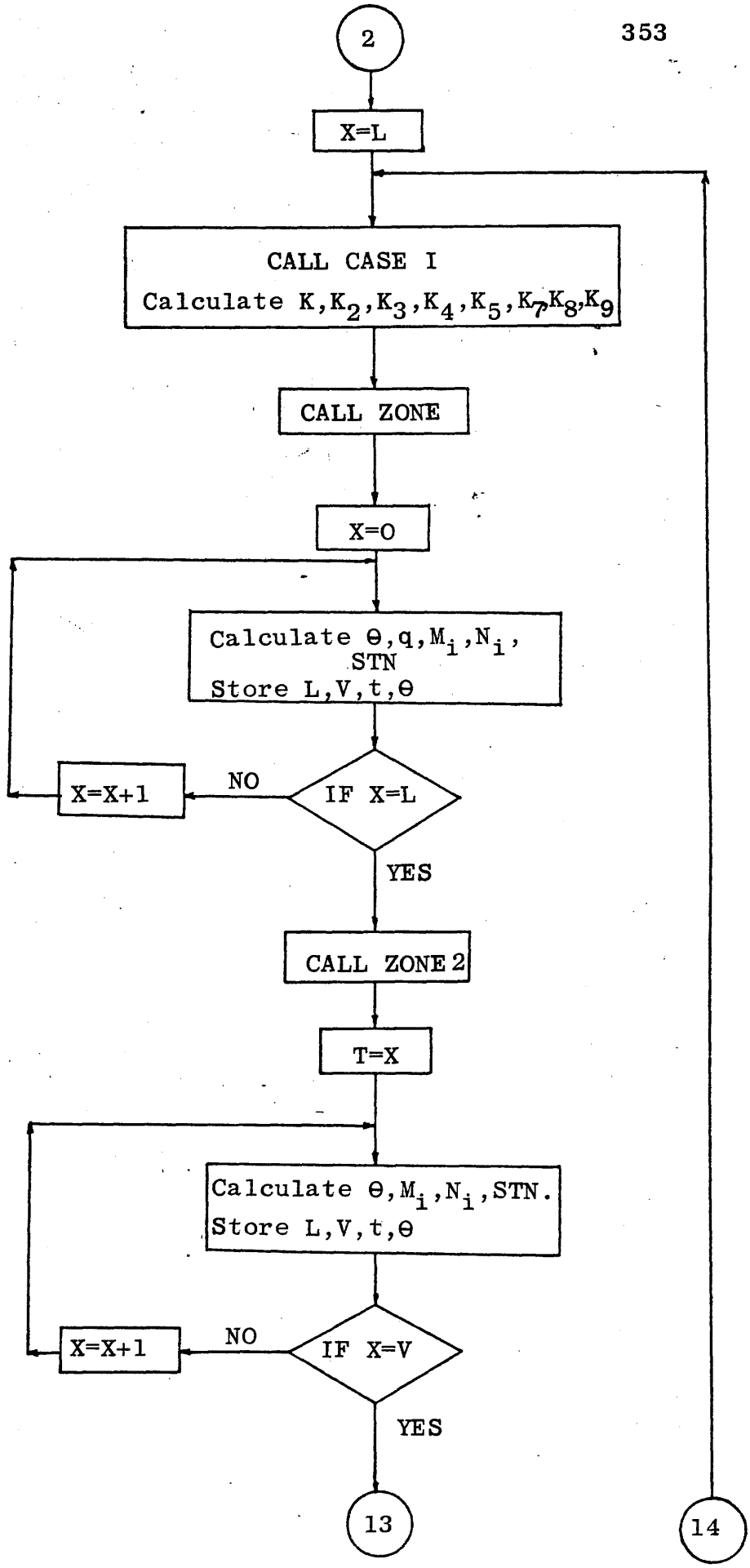
2
X=L
CALL CASE I
Calculate K,K2,K3,K4,K5,K7,K8,K9
CALL ZONE
X=O
Calculate θ,q,Mi,Ni,
STN
Store L,V,t,θ
X=X+1
NO
IF X=L
YES
CALL ZONE 2
T=X
Calculate θ,Mi,Ni,STN.
Store L,V,t,θ
X=X+1
NO
IF X=V
YES
13
14

Fig. D-6

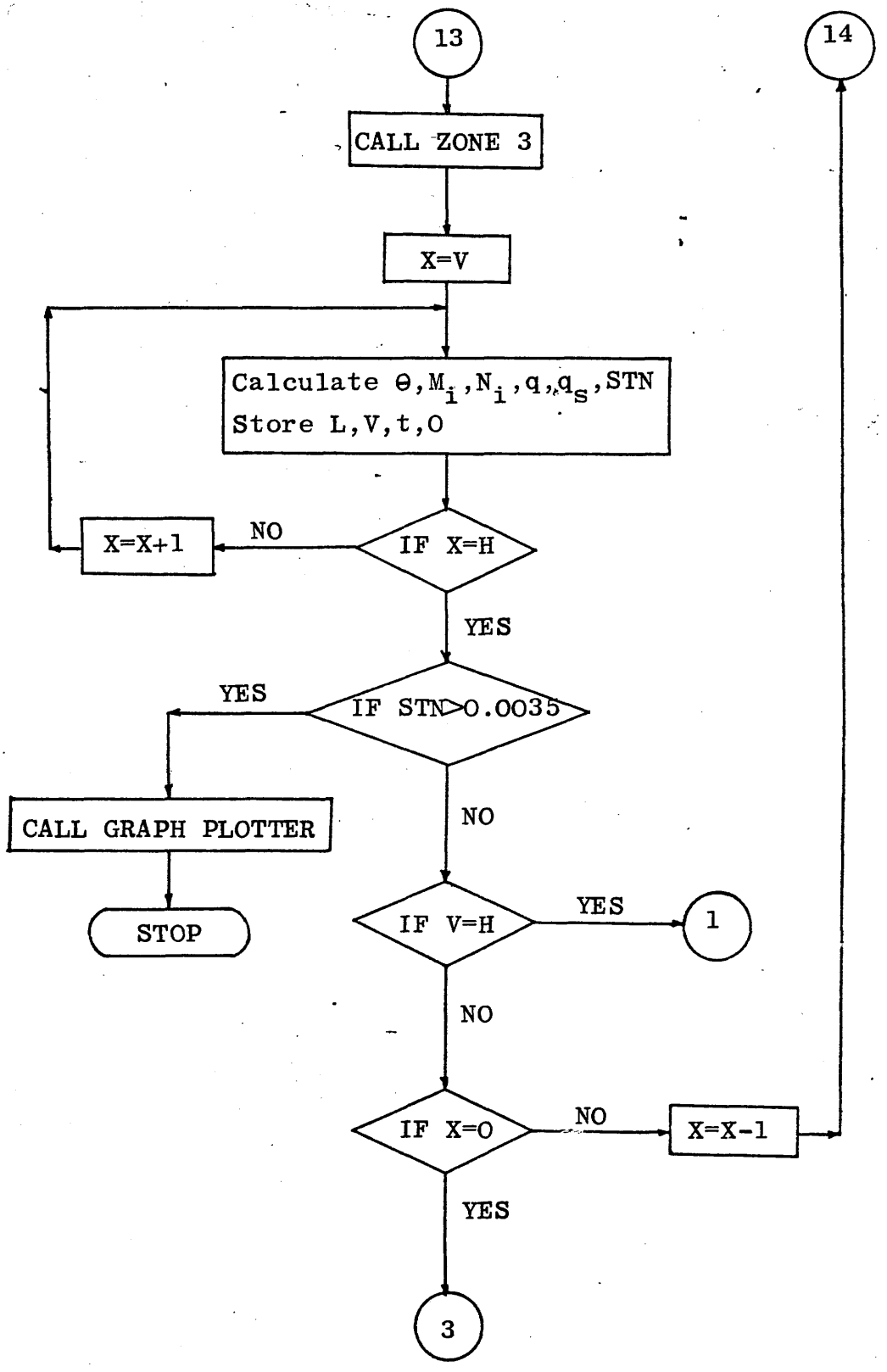
13
14
CALL ZONE 3
X=V
Calculate Θ,M_i,N_i,q,q_s,STN
Store L,V,t,O
X=X+1
NO
IF X=H
YES
YES
IF STN>0.0035
CALL GRAPH PLOTTER
NO
STOP
IF V=H
YES
1
NO
IF X=O
NO
X=X-1
YES
3

Fig. D-7

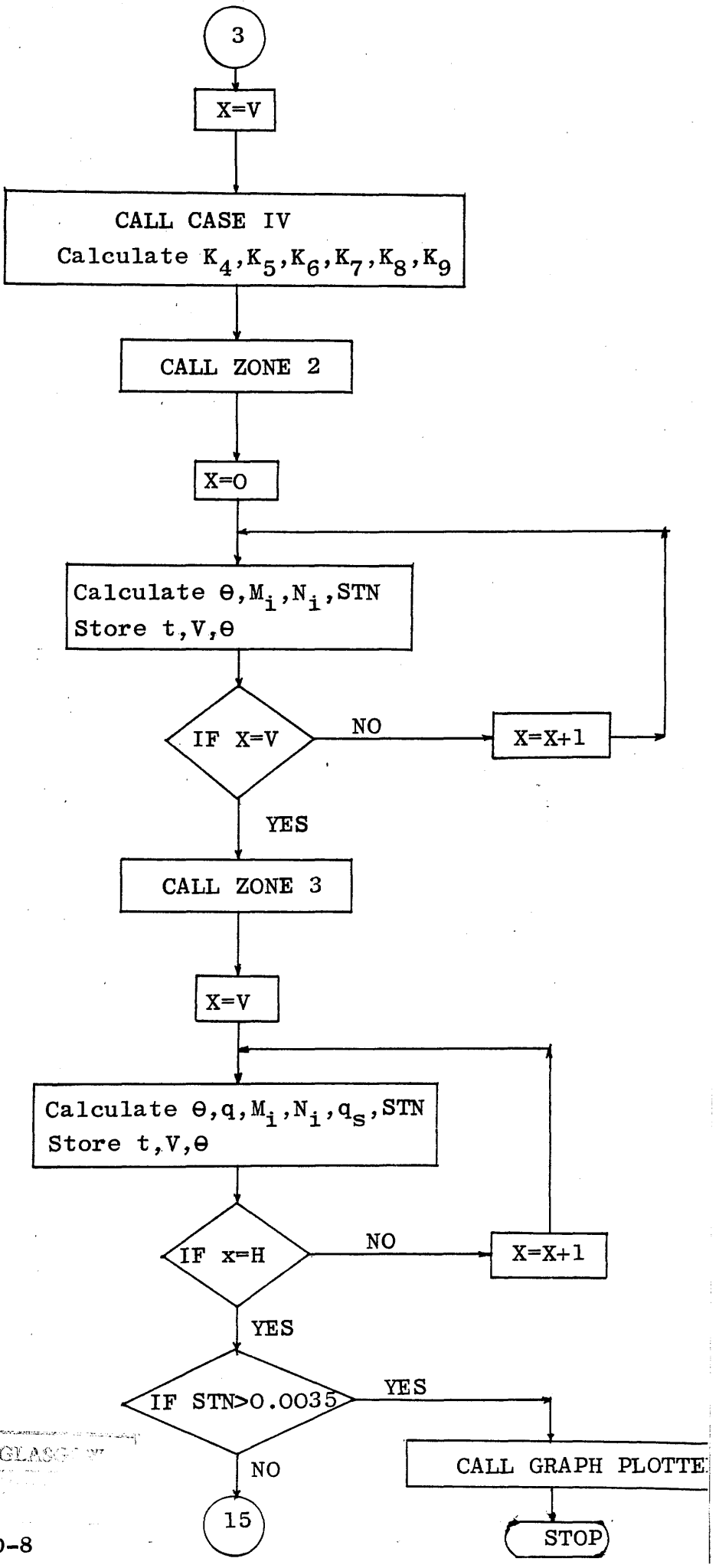
3
X=V
CALL CASE IV
Calculate $K_4, K_5, K_6, K_7, K_8, K_9$
CALL ZONE 2
X=O
Calculate θ, M_i, N_i, STN
Store t, V, θ
IF X=V
NO
X=X+1
YES
CALL ZONE 3
X=V
Calculate θ, q, M_i, N_i, q_s, STN
Store t, V, θ
IF x=H
NO
X=X+1
YES
IF STN>0.0035
YES
NO
CALL GRAPH PLOTTE
15
STOP

Fig. D-8